Identification of Novel Antigens for T Cell Targeting of Prostate Cancer Stem Cells

Amy Codd

Thesis submitted for the degree
DOCTOR OF PHILOSOPHY

Division of Cancer and Genetics
School of Medicine
Cardiff University

2019

Declaration

The work has not been submitted in substance for any other degree or award at this or any other university or place of learning, nor is being submitted concurrently in candidature for any degree or other award.

Signed…… (candidate) Date…….

STATEMENT 1

This thesis is being submitted in partial fulfilment of the requirements for the degree of PhD.

Signed…… (candidate) Date…….

STATEMENT 2

This thesis is the results of my own independent work/investigation, except where otherwise stated.

Other sources are acknowledged by explicit references. The views expressed are my own.

Signed…… (candidate) Date…….

STATEMENT 3

I hereby give consent for my thesis, is accepted, to be available online in the University's Open Access repository and for inter-library loan, and for the title and summary to be made available to outside organisations.

Signed…… (candidate) Date…….

STATEMENT 4: PREVIOUSLY APPROVED BAR ON ACCESS

I hereby give consent for my thesis, is accepted, to be available online in the University's Open Access repository and for inter-library loans after expiry of a bar on access previously approved by the Academic Standards & Quality Committee.

Signed…… (candidate) Date…….

WORD COUNT: 79377

Acknowledgements

Firstly, I would like to thank my PhD studentship sponsor, Tenovus Cancer Care, for funding my research. This project would not have been possible without their support. Tenovus Cancer Care also provided great opportunities for involvement in engagement and science communication events. I am also grateful for funding provided by the Great Britain Sasakawa Foundation to conduct research in Sapporo Medical University, Japan. Another key element of this project was healthy and patient donors, thank you for your participation.

It is impossible to do justice here in thanking my fantastic main supervisor, Dr. Zsuzsanna Tabi. Thank you for all of the guidance and just the right amount of independence that allowed me to learn so much. Thank you to my co-supervisor, Dr. Steve Man, for providing essential support when we needed it the most. Thank you both for encouraging me towards so many opportunities. Thank you also to Professor Aled Clayton and Professor Rachel Errington, particularly for assisting my 'next steps' in applying for the ISSF funding. Thank you to Dr. Jason Webber for lots of helpful advice, particularly with the gene expression experiments.

I was very fortunate to collaborate with many excellent researchers during the course of this project. Firstly, my thanks go to my hosts in Sapporo Medical University, in particular Professor Toshihiko Torigoe, Professor Takayuki Kanaseki, Dr. Emi Mizushima and Ms. Serina Tokita, and the members of the First Pathology Department. This project would not have been the same without the advice and tips on CSC assays and the opportunity to do the HLA ligandome analysis, not to mention all the excellent food, events and trips around Sapporo. This work led to further collaborations in Cardiff University which enhanced my skillset and broadened the focus of my project. The bulk of the immunology work in my final year simply would not have been achieved without the collaborative efforts of Professor David Price, Dr. Kristin Ladell, Ms. Kelly Miners, Ms. Siân Llewellyn-Lacey and Ms. Anzelika Rubina and extended members of the lab. I am so grateful for your help and looking forward to continuing working with you! Thank you to Dr. Pierre

Rizkallah for contributing structural expertise and support, here's hoping for future productive trips to Diamond!

I feel confident in saying that I had the best experience possible in the lab, throughout this project and in Cardiff in general all down to my friends and colleagues here. Thank you to Mr. Mark Gurney, lab and life guide, "Dr." Alex Cocks, Dr. Vincent Yeung, my lab child Ms. Lauren Evans, Dr. Alex Shepard, Ms. Sara Veiga (ASMR queen) and Dr. Kate Milward. My thanks also to the wider TMEG group; Thea, Francesca, Muireann, Andreia, Chris, Marie, Rachel and Dimitris. At Velindre Cancer Centre I would like to thank Ms. Lynda Churchill, particularly for managing blood donors, Dr. Josephine Salimu (especially for staying late on my first every flow cytometry experiment!), Dr. Saly Al Taei, Dr. Lisa Spary, Mr. Hossein Navabi and Ms. Gwyneth Coles and Ms. Sandra Cusack, the staff of the phlebotomy department and the canteen's custard slices. Thank you to the many more friends that contributed help, advice, trips and chats down the pub and occasionally elsewhere, and generally kept somewhat sane- Alex, James, Henry, book club hosts: Hester and Jason. There are too many more people to mention, so at the risk of missing out anyone, I want to thank everyone in Cardiff whose contribution to this work was their friendship- there's more to research than the science. Thanks also to my friends who've known me the longest, it's been lovely to see more of you all this year.

Finally, I want to thank my parents and my sister, who have always supported, encouraged and inspired me, through so many years of education, and in particular, the final leg of this one. I was lucky to spend the unfunded write-up period of this thesis at home, with all the associated benefits, which I am unendingly grateful for.

Summary

Cancer stem cells (CSC) are a subpopulation of tumour cells which are resistant to conventional therapy, such as radiation and chemotherapy, and contribute to tumour progression and relapse. We hypothesised that CSC could be specifically targeted by T cells, in an antigen specific manner. This was investigated in prostate cancer, because it is associated with a relapse rate of 15-40% and progressive disease has poor survival outcomes.

The CSC markers, CD44 $\alpha_2\beta_1$Integrin and CD133 and aldehyde dehydrogenase (ALDH), were compared to optimise CSC isolation in DU145 cells and primary prostate cancer cells. I did not identify a conclusive $CD44^+$ $CD49b^{high}$ $CD133^+$ population, in contrast to previous work on primary prostate cancer cells. ALDH high DU145 cells demonstrated higher clonogenicity and self-renewal *in vitro* and tumorigenicity *in vivo*, than ALDH low DU145 cells. In the DU145 and primary prostate cancer cells, the ALDH high population divided less than the ALDH low population. Gene expression analysis identified genes associated with cell cycling and NOTCH signalling differentially expressed in the ALDH high compared to the ALDH low DU145 and primary prostate cancer cells. I carried out HLA ligandome analysis of the DU145 cells to identify novel antigens. The ligandome dataset was analysed using *in silico* algorithms, PCR and homology modelling to identify therapeutically relevant CSC antigens. Candidate antigens identified include ARHGAP42, XPO1, RLN2 and AKT2, which were also expressed in the primary prostate cancer cells. In preliminary experiments, antigen specific T cell lines were found to produce cytokines in response to cells presenting the target antigen.

This study demonstrated that CSC markers are of varying utility in identifying distinct populations. CSC characteristics were confirmed in prostate cancer cells identified by high ALDH activity. We conclude that prostate CSC are suitable targets for T cell immunotherapy, on the basis of presenting therapeutically relevant antigens.

Publications

1. Hongo, A., Kanaseki, T., Tokita, S., Kochin, V., Miyamoto, S., Hashino, Y., Codd, A., Kawai, N., Nakatsugawa, M., Hirohashi, Y., Noriyuki, S., Torigoe, T. Upstream position of proline defines peptide-HLA class I repertoire formation and CD8+ T cell responses. Journal of Immunology, 2019, vol. 202 no. 10, pages 2849-2855.
2. Codd, AS., Kanaseki, T., Torigo, T., Tabi, Z. Cancer stem cells as targets for immunotherapy. Immunology. 2018 Mar;153(3):304-314.
3. Codd. AS., Al-Taei, S., Tabi, Z. Cross-talk between cancer-initiating cells and immune cells – considerations for combination therapies. *(Commentary)* Annals of Translational Medicine. 2016 Oct; 4(Suppl 1): S56.

Presentations

1. *Attacking the roots of prostate cancer: T cell targeting of cancer stem cell antigens*. Fred Hutch Immuno-Oncology Graduate Student Symposium, Seattle, USA, October 2019.
2. *Targeting prostate cancer stem cells with T cell immunotherapy*. Thermo Fisher 'Cell Culture Heroes' series January 2019. Webinar.
3. *T cell targeting of novel antigens on prostate cancer stem cells*. Cardiff University Division of Infection and Immunity Annual Symposium, Cardiff, 2018. Invited oral presentation, selected 3rd place prizewinner for oral presentation.
4. *Identification of prostate cancer stem cell antigens for T cell immunotherapy by HLA ligandome analysis*. Fourth CRI-CIMT-EATI-AACR International Cancer Immunotherapy Conference, New York, 2018. Poster presentation.
5. *T cell targeting of novel antigens on prostate cancer stem cells*. ECSCRI, Cardiff, 2018. Invited oral presentation.
6. *T cell targeting of novel antigens on prostate cancer stem cells.* Cardiff University Division of Cancer and Genetics Seminar Series, Cardiff, 2018. Invited oral Presentation.
7. *Selection of cancer stem cell epitopes as T cell targets in prostate cancer*. EACR25, Amsterdam, 2018. Poster presentation.

8. *Identification of candidate antigens for T cell targeting of prostate cancer stem cells*. Cardiff University School of Medicine and Dentistry Postgraduate Research Day, 2018. Invited oral presentation.
9. *Identification of candidate antigens for T cell targeting of cancer stem cells.* Defence is the Best Attack: Immuno-oncology Breakthroughs (EACR Conference Series), Barcelona, 2017. Poster presentation.
10. *Are prostate cancer stem cells susceptible to T cell killing?* Sapporo Medical University First Pathology Department, 2017. Invited oral presentation (division seminar).
11. *Establishing a 3D model to study prostate cancer stem cells*. European Cancer Stem Cell Conference, Cardiff, September 2016. Poster presentation.

Funding and Awards

- **2019** Wellcome Trust Institutional Strategic Support Fund 3 (ISSF3) Consolidator Award: £44111 to support a post-doctoral project 'Characterization of T cell responses to novel prostate cancer stem cell antigens.'
- **2018** Cardiff Institute for Tissue Engineering and Repair (CITER) Travel Bursary: £1000 to support attendance of the Fourth CRI-CIMT-EATI-AACR International Cancer Immunotherapy Conference, New York.
- **2018** Tenovus Cancer Care: £200 supporting attendance of EACR25, Amsterdam.
- **2017** M Banfill Fund Travel Bursary, Cardiff University: £415 to support attendance of the Fourth CRI-CIMT-EATI-AACR International Cancer Immunotherapy Conference, New York
- **2017** W M Thomas Fund Travel Bursary, Cardiff University: £200 to support attendance of the Fourth CRI-CIMT-EATI-AACR International Cancer Immunotherapy Conference, New York.
- **2017** Amgen Scholars Travel Bursary, Amgen Foundation: £500 to support attendance of Defence is the Best Attack: Immuno-oncology Breakthroughs, Barcelona.
- **2017** Great Britain Sasakawa Foundation Grant: £3200 to facilitate collaborative work with Sapporo Medical University, Japan.

- **2016** Vitae Three Minute Thesis. Cardiff University's First Place Winner (£250).

Table of Contents

Figures and Tables

Abbreviations

(A)DMEM	(Advanced) Dulbecco's Modified Eagle Medium
(m)CRPC	(Metastatic) Castrate resistance prostate cancer
ABC(B)(G)	ATP binding cassette transporter (subfamily B/G)
ACT	Adoptive cell transfer
ADAM	A disintegrin and metalloproteases
ADT	Androgen deprivation therapy
AKT	Protein kinase B
ALDH	Aldehyde dehydrogenase
AML	Acute myeloid leukaemia
ANN	Artificial neural network
ANOVA	Analysis of variance
AR	Androgen receptor
ARHGAP42	Rho GTPase Activating Protein 42
AS	Active surveillance
ATRA	All trans retinoic acid
BAA	BODIPY-aminoacetate
BAAA	BODIPY-aminoacetaldehyde
BCR	Biochemical relapse
BCRP	Breast cancer resistance protein (AKA ABCG2)
BLCL	B lymphoblastoid cell lines
BP	Base pair
BrdU	Bromodeoxyuridine
BSA	Bovine serum albumin
CAR	Chimeric antigen receptor
CB	Committed basal
CCNA2	Cyclin A2
CDR	Complementarity determining region
CCP4	Collaborative Computational Project Number 4
CEA	Carcinoembryonic antigen
CFSE	Carboxyfluorescein Diacetate Succinimidyl Ester
CK	Cytokeratin
CML	Chronic myeloid leukaemia

CNS	Central nervous system
COOT	Crystallographic Object-Oriented Toolkit
CRC	Colorectal cancer
CSC	Cancer stem cells
CT	Cycle threshold
CTL	Cytotoxic T lymphocyte
D	Diversity
DAMPs	Damage Associated Molecular Patterns
DAVID	Database for Annotation, Visualization and Integrated Discovery
DC	Dendritic cell
DD	Double distilled
DEAB	4-(diethylamino) benzaldehyde
DHT	Dihydrotestosterone
DLL	Delta-like ligand
DMSO	Dimethyl sulfoxide
DNA	Deoxyribonucleic acid
EAU	European Association of Urology
EBV	Epstein Barr virus
ECACC	European Collection of Authenticated Cell Cultures
ECM	Extracellular matrix
EDTA	Ethylenediaminetetraacetic acid
EGF	Epidermal growth factor
EMT	Epithelial to mesenchymal transition
EpCAM	Epithelial cell adhesion molecule
ER	Endoplasmic reticulum
ERAAP	Endoplasmic reticulum aminopeptidase
ERBT	External beam radiation therapy
FACS	Fluorescence activate cell sorting
FBS	Foetal bovine serum
FGF	Fibroblast growth factor
FITC	Fluorescein isothiocyanate
GM-CSF	Granulocyte-macrophage colony stimulating factor
GS	Gleason Score
GTEx	Genotype-Tissue Expression

Gy	Gray (unit of ionizing radiation)
HBV, HCV	Hepatitus B/ C virus
HER2	Human epidermal growth factor receptor 2
HIF	Hypoxia inducible factor
HLA	Human leukocyte antigen
HMGB1	High Mobility Group Box 1
HNSCC	Head and neck squamous cell carcinoma
HPV	Human papilloma virus
hTERT	Huma telomerase reverse transcriptase
ICCS	Intracellular cytokine staining
ICIs	Immune checkpoint inhibitors
IEDB	Immune epitope database
IFN	Interferon
J	Joining
JAK/STAT	Janus Kinase/Signal Transducer and Activator of Transcription
KSFM	Keratinocyte serum free medium
MACS	Magnetic activated cell sorting
MAGE	Melanoma antigen gene
MART-1	Melanoma antigen recognised by T cells
MDSC	Myeloid derived suppressor cells
MEX3A	Mex-3 RNA Binding Family Member A
MFI	Mean fluorescence intensity
MHC	Major histocompatibility complex
MICA/MICB	MHC class-I related chain A and B glycoproteins
MIP1β	Macrophage inflammatory protein
MMP	Matrix metalloproteinase
mOM	Modified organoid media
MUC1	Mucin 1, cell surface associated
NAPSA	Napsin A Aspartic Peptidase
NCI	National Cancer Institute
NFE2L2	Nuclear Factor, Erythroid 2 Like 2
NF-κB	Nuclear factor kappa B
NK cell	Natural Killer cell
NOD	Non-obese diabetic

NPW	Neuropeptide W
NSCLC	Non-small cell lung cancer
NSG	NOD-SCID IL2rγnull
NY-ESO	New York oesophageal squamous cell carcinoma 1
OM	Organoid media
P	Passage
PAMPs	Pathogen associated molecular patterns
PAP	Prostatic Acid Phosphatase
PARP	Polyadenosine diphosphate–ribose polymerase
PBMC	Peripheral blood mononuclear cells
PBS	Phosphate buffered saline
PCa	Prostate cancer
PFA	Paraformaldehyde
PGE	Prostaglandin E2
PI3K	Phosphatidylinositol-3-Kinase
PIN	Prostatic intraepithelial neoplasia
PISA	Protein Interfaces, Surfaces and Assemblies
PKP3	Plakophilin 3
PLC	Peptide loading complex
PNMA2	Paraneoplastic antigen Ma2
PRAME	Preferentially Expressed Antigen In Melanoma
PRRs	Pattern recognition receptor
PSA	Prostate specific antigen
PSCA	Prostate stem cell antigen
PSMA	Prostate specific membrane antigen
RA	Retinoic acid
RAG1/2	Recombination activating gene 1/2
RIN	RNA integrity number
RLN2	Relaxin 2
RNA	Ribonucleic acid
ROS	Reactive oxygen species
RP	Radical prostatectomy
RPKM	Reads per kilobase million
RPMI	Roswell Park Memorial Institute

RT qPCR	Reverse transcription quantitative polymerase chain reaction
RT	Radiation therapy
SC	Stem cells
SCID	Severe combined immunodeficiency
SCM	Stem cell medium
SEM	Standard error of the mean
SEPT9	Septin 9
SEREX	Serological analysis of recombinant tumour cDNA expression libraries
SMM	Stabilized matrix method
SOX11	SRY-Box 11
SSC	squamous cell carcinoma
SSEA-1	Stage-specific embryonic antigen
STEAP	Six-transmembrane epithelial antigen of the prostate-1
TA	Transit amplifying
TAA	Tumour associated antigen
TAP	Transporter associated with antigen processing
TCR	T cell receptor
TdT	Terminal deoxynucleotidyl transferase
TFA	Trifluoroacetic acid
TGF-β	Transforming growth factor beta
mTEC, cTEC	Medullary/ Cortical thymic epithelial cells
TIC	Tumour initiating cells
TIL	Tumour infiltrating lymphocyte
TME	Tumour microenvironment
TNF	Tumour necrosis factor
TOP2A	Topoisomerase 2A
TPX2	Targeting protein for Xklp2
TRAMP	Transgenic adenocarcinoma of the mouse prostate
Tregs	T regulatory cells
UHW	University Hospital Wales
V	Variable
WCB	Wales Cancer Bank
WDR62	WD Repeat Domain 62

Wnt	Wingless-related integration site
WST-8	Water-soluble tetrazolium salt 8
XPO1	Exportin-1
YASARA	Yet Another Scientific Artificial Reality Application
ZEB1/2	Zinc finger E-box-binding homeobox 1/ 2

Chapter 1.
Introduction

1 Introduction

In many cancers, failure of primary treatment is associated with poorer prognosis. This is particularly evident in localised prostate cancer (PCa), where progression beyond a localised tumour shifts the treatment focus from effectively curative to non-curative disease management. Cancer stem cells (CSC) are a treatment resistant subpopulation of tumour cells possessing stem-like characteristics, including self-renewal and the capacity to produce both CSC and non-CSC progeny. As such, CSC are thought to contribute to relapse and thus represent an important therapeutic target in PCa, since preventing relapse could drastically improve survival outcomes. Since CSC are resistant to conventional DNA damaging anti-cancer treatments, immunotherapy could represent a viable alternative, in particular T cell immunotherapy, as this facilitates direct targeting of CSC in an antigen-mediated way. Here, the role of CSC in cancer development and relapse is introduced, in addition to identification and characterisation of CSC, which has been carried out in various types of cancer. The role of the immune system in recognition of cancer, and how CSC may interact with the immune system are discussed. There is a focus on the clinical course of PCa, to consider the available treatments for localised disease, the impact of relapse and the limited therapeutic options for advanced disease. Current literature relating to prostate CSC is then discussed, in particular suitable markers of prostate CSC, since there are various different types of markers and marker combinations used in different studies. Potential and existing immunotherapy approaches to targeting prostate CSC are then discussed, to bring together the rational for my study.

1.1 Models for the development of cancer

There are two models of cancer development, the stochastic/ clonal evolution model and the CSC model (Figure 1.1). The stochastic model of cancer suggests that all cells are equally and randomly predisposed to acquiring a driver mutation e.g. in an oncogene or tumour suppressor gene, which can contribute to carcinogenic transformation (Figure 1.1A) (Greaves and Maley, 2012; Nowell, 1976; Shackleton et al., 2009). According to this model, heterogeneity arises by selection of the most optimal mutations in a clonally transformed lineage. Multiple individual malignant clones may possess

different growth advantages e.g. treatment resistance, promotion of angiogenesis, etc. (Figure 1.1B). Thus, different lineages co-exist in a tumour; however, these lack a hierarchical relationship. According to this theory, cancer treatment must eliminate all the cancer cells as they are essentially independent of each other in their carcinogenic potential. On the other hand, the CSC model suggests that tumours consist of a hierarchy in which only the CSC have carcinogenic potential and drive tumour growth, similar to the hierarchy and development of a healthy tissue (Figure 1.1C) (Kreso and Dick, 2014). CSC give rise to non-CSC which represent the majority of cells in the tumour (Figure 1.1D). These non-CSC contribute to the hallmarks of a tumour but ultimately differ in gene expression and phenotype to CSC. Non-CSC lack self-renewal capacity, thus, are not capable of initiating tumours. Therefore, CSC-specific treatments are required (Valent et al., 2012). This thesis investigates PCa in the context of the CSC hypothesis, specifically focusing on the feasibility of T cell immunotherapy of prostate CSC.

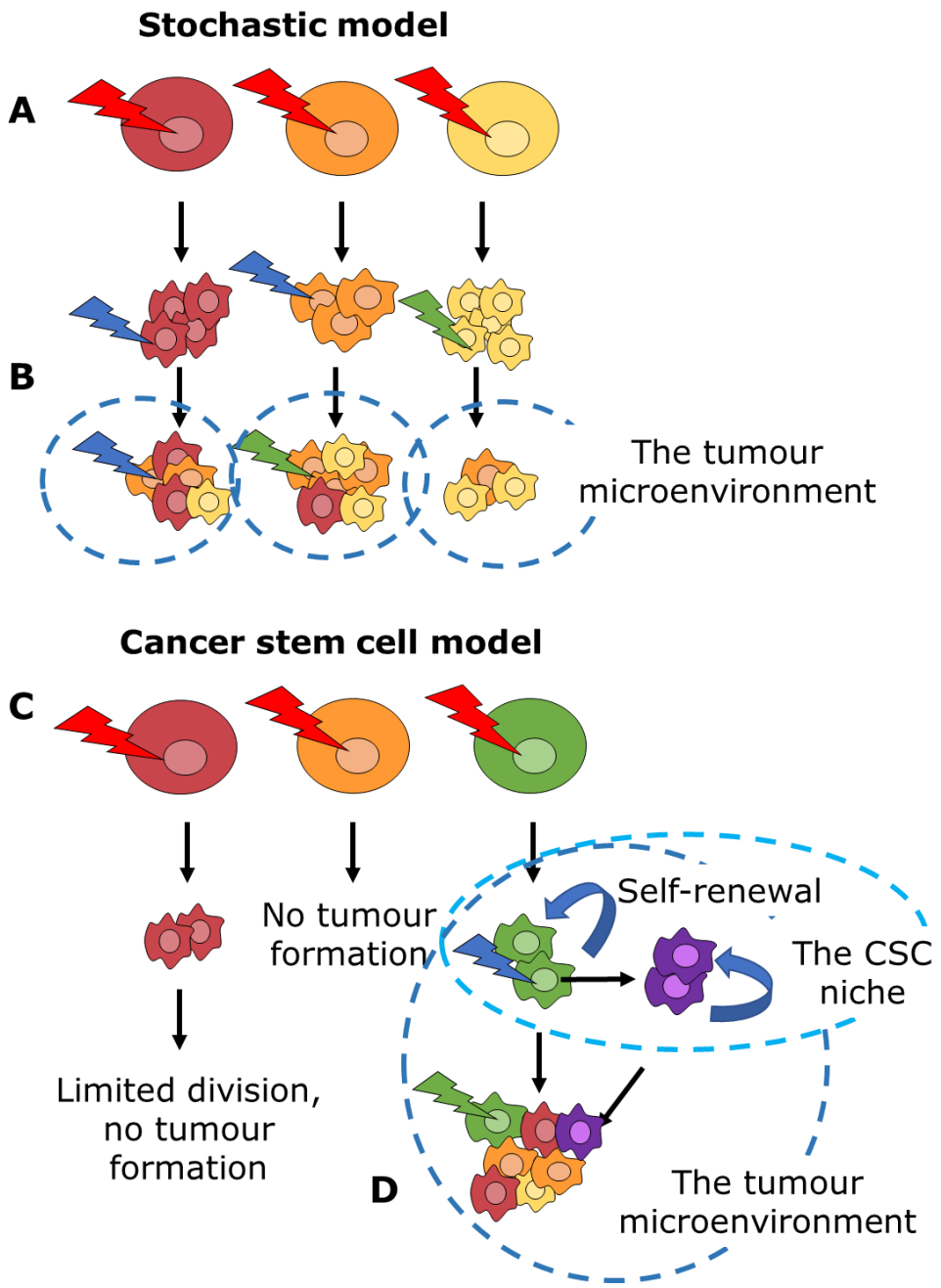

Figure 1.1. Models for the development of cancer. (A) Somatic cells are transformed with equal probability. (B) Further mutations occur e.g. due to genetic instability, further carcinogenic exposure and interactions with the TME. Tumour heterogeneity arises by clonal evolution of mutated lineages. (C) Stem cells acquire mutations and are transformed/ stemness is acquired by transformation. Non-stem cells are less susceptible to transformation owing to a requirement for a mutation to confer limitless replication and multipotency. (D) The tumour is established as a hierarchy, supplied by self-renewing CSC, which occupy a CSC niche within the TME. Heterogeneity arises due to further mutations to the CSC or acquisition of stemness by non-CSC. Lightning bolts indicate mutation events. Adapted from van Vlerken et al., (2012).

The CSC hypothesis has existed since the 1940s (Jackson and Brues, 1941; L. V. Nguyen et al., 2012). Early definitions of CSC proposed the existence of CSC as an explanation for cancer relapse, in that cancer treatment must fail to eradicate treatment resistant cells which have cancer initiating capacity, for tumour re-growth to occur. The CSC hypothesis has also been interpreted to suggest that stem cells (SC) are the source of CSC. It is argued that SC are the most susceptible target for a cancer-causing DNA mutation, and both genetic and epigenetic mutation signatures impacting stemness pathways have been implied in cancer development (Kreso and Dick, 2014; Vogelstein et al., 2013). This is supported by a recent study in mice, in which mutation of SC was a tumour initiating event across a wide range of neonatal and adult organs (Zhu et al., 2016). Cancer is also characterised as a disease of 'unregulated self-renewal' (Reya et al., 2001) which is underpinned by 'perturbed differentiation' (Clarke et al., 2006).

The hypothesis that SC are the source, or most likely source of CSC, is not universally accepted. There are technical limitations in clinically and experimentally demonstrating this proposal, particularly in solid, compared to haematological, cancers. These include selecting markers of SC/CSC and recapitulating an in-situ hierarchy *in vitro*, discussed further below. Consequently, the clonal evolution/ stochastic theory of cancer suggests that any cell type could be transformed if a cancer mutation 'overcomes' the restraints of a differentiated cell; i.e. limited replication and unipotency (Greaves and Maley, 2012; Shackleton et al., 2009). However, it is argued here and elsewhere (Calabrese et al., 2004; Packer and Maitland, 2016) that SC are more susceptible to carcinogenesis, even if SC and differentiated cells have equal probability of acquiring DNA mutations. Due to their longevity, SC accumulate mutations over time and pass these to their progeny, whereas differentiated cells may not persist in the tissue long enough to clonally sustain a cancer initiating mutation. Studies in AML suggest that accrual of passenger mutations occurs in stem cells prior to acquisition of a driver mutation; such that the mutations in the clonal lineage are fixed before cancer initiation driven by a driver mutation (Jan et al., 2012; Welch et al., 2012). Lineage tracing studies also support the SC population as the target for mutation drive cancer initiation (Chen et al., 2012; Cortina et al., 2017;

Driessens et al., 2012; Schepers et al., 2012). However, the clonal evolution and CSC hypotheses may not be mutually exclusive; clonal evolution can occur in a CSC hierarchy, resulting in more than one CSC lineage (Hermann et al., 2007; Stewart et al., 2011). A growing body of evidence supports that SC are most susceptible to cancer initiation, and the resulting CSC drive progression, treatment resistance and relapse.

1.1 Cancer stem cells

CSC are a challenge to define and identify, although the rigid concepts arising from early experimental results in the field are giving way to a more nuanced appreciation of transitional phenotypes and the potential for plasticity (Figure 1.2A) (Batlle and Clevers, 2017). It is generally accepted that CSC reside at the apex of a hierarchy consisting of non-CSC progeny. This hierarchy can include an transitional phenotype which are non-self-renewing and non-tumour initiating but may demonstrate some evidence of stem-like features e.g. limited multipotency and a proliferative contribution to tumour growth (Batlle and Clevers, 2017; Packer and Maitland, 2016). In the prostate CSC hierarchy, this may correspond to transit amplifying (TA) cells (Packer and Maitland, 2016)

The main features of CSC are self-renewal, multipotency and resistance to DNA damaging agents; resulting in survival beyond first line treatment, and contribution to relapse (Batlle and Clevers, 2017; Cojoc et al., 2015a; Kreso and Dick, 2014; Visvader and Lindeman, 2008). Like SC, CSC are capable of both asymmetric and symmetric division, to produce non-CSC or more CSC, respectively (Mukherjee et al., 2015). However, it has been suggested that the cell division and multipotency of CSC are likely deregulated and not exactly similar to that of SC (Kreso and Dick, 2014) and therefore may not entirely recapitulate the tissue hierarchy. For example, while prostate CSC have typically been described with a basal phenotype, the luminal cell type is over-represented in PCa tumours. The differentiated cells in the CSC hierarchy may not be truly differentiated in the physiological sense but are assumed to be shorter lived, contribute less to tumour growth and are not capable of tumour initiation. Each of these respective populations may

possess a degree of plasticity, including the ability to acquire stemness characteristics and 'replenish' the CSC population for example in response to selective pressure in a therapeutic setting; thus, the hierarchy is not unidirectional (Figure 1.2B). This plasticity reconciles the stochastic and CSC models to a certain degree, in suggesting that non-SC could, under certain conditions, acquire stem-like features, including tumour initiation capacity (Plaks et al., 2015; Quail et al., 2012; Vlashi and Pajonk, 2015).

Certain CSC characteristics may be evident *in situ* but not possible to demonstrate experimentally. For example, it has been suggested that *in vivo* tumour initiation experiments may not identify the same CSC population as is present in the original tissue but rather, select for the clone capable of surviving experimental manipulation and propagating xenobiotic growth (Valent et al., 2012). The concept of the CSC niche (Figure 1.1, 1.2) particularly impacts CSC identification and functional assessment, as markers and cell function may be altered by imperfect modelling of the niche under experimental conditions. For these reasons, there is a lack of consistency in the nomenclature associated with CSC. As suggested by Prager and colleagues, this 'lack of rigor [is] born from convenience' (Prager et al., 2019). Many publications refer to CSC as a population expressing stem cell markers, which has been demonstrated *in vitro* and/or *in vivo* to have characteristics including, but not limited to, self-renewal, multipotency, resistance to conventional cancer therapeutics and tumorigenicity. Other publications distinguish between tumour initiating cells (TIC) and CSC. TIC refers to a functional definition in which cells are tumorigenic and may possess some stemness characteristics, but as mentioned above, may not coincide with the tissue CSC population. Since TIC are typically isolated based on stem cell markers, it is suggested that TIC represent the same population as CSC, under specific experimental conditions. For simplicity in this thesis, the term CSC refers to a distinct population of cells, found in a cell line and primary tumours, that possesses stemness characteristics.

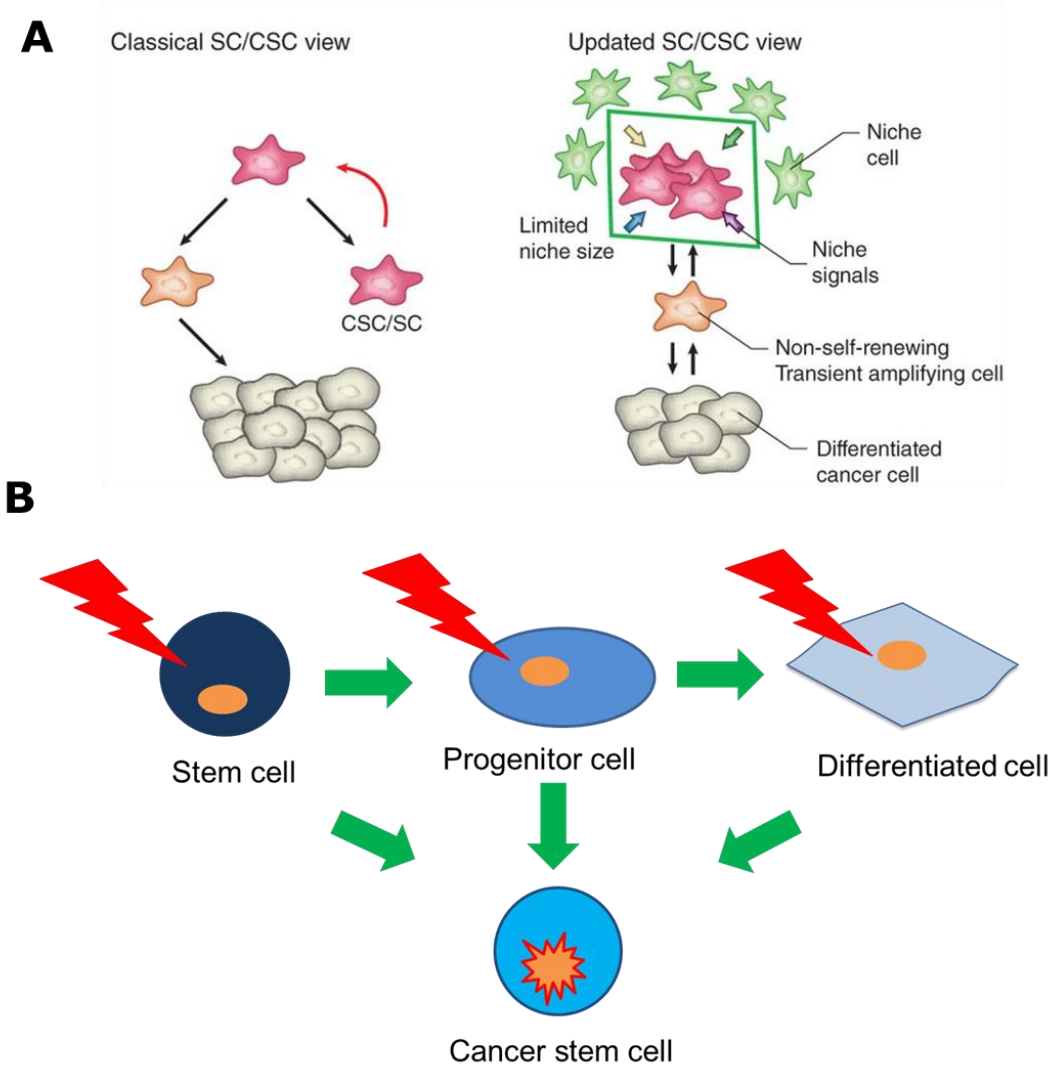

Figure 1.2. Modification of the 'classical' concept of CSC and CSC mediated tumour initiation to reflect transitional cell phenotypes and the contribution of the niche. (A) Left: The classical unidirectional view of the CSC hierarchy. Stemness characteristics are restricted to the CSC population. Right: An update of the CSC hypothesis recognising that CSC are acted upon by the niche they reside in, and in turn interact and remodel their niche. A transient phenotype exists which could acquire plasticity, additionally it could be possible (but less likely) for differentiated cells to acquire CSC characteristics. The hierarchy is preserved; however, if perturbed, possesses bidirectional capacity to reinstate the CSC population. Image reference part A: Batlle and Clevers., (2017). (B) While SC may be the most susceptible cell type to carcinogenic mutation, being long lived and already possessed of a genetic program of unlimited replication and multipotency, it is possible that mutations conferring such stemness features could transform transit amplifying and differentiated cells.

1.1.1 Identification and characterisation of cancer stem cells

Isolation of CSC is performed using magnetic activated cell sorting (MACS; typically beads coated with a single antibody) or fluorescence activated cell sorting (FACS; allowing for multiple simultaneous marker or functional activity-based isolation). CSC may also be enriched by growth in low adherence conditions *in vitro* (sphere culture); however, this is unlikely to produce relatively pure populations of CSC. Thus, it is necessary to validate the putative CSC population by demonstrating functional differences between CSC marker positive and negative populations. This includes *in vitro* testing such as the colony and sphere forming assays (of sorted cells), assessment of drug resistance and gene expression and, *in vivo*, tumour initiation in a xenograft model (Ajani et al., 2015; Clevers, 2011).

CSC have been identified in many types of cancer, including leukaemia, breast, colorectal (CRC), lung, pancreatic, head and neck, PCa, melanoma and glioblastoma (Table 1.1) (K. Chen et al., 2013; Islam et al., 2015; Klonisch et al., 2008; Visvader and Lindeman, 2008). CSC are often identified using the markers which are also used to identify non-malignant stem cells from the same tissue, e.g. haematological, prostate and neuronal stem cells (Günther et al., 2008; Richardson et al., 2004; Wang and Dick, 2005). It is generally hypothesised that CSC arise from the same lineage as non-malignant stem cells within a tissue. Therefore, the use of tissue specific linage markers, which are not necessarily stem cell specific, can focus the search for CSC to a certain lineage in the tissue, for example CD49f, CD49b are markers of basal cells of the prostate. CSC markers include surface and functional markers, however, there are varying degrees of evidence for direct stem cell functions of these markers. Many cell surface proteins expressed by CSC have functional roles in cell-cell adhesion (CD44, CD90, CD49f, CD166, CD29, Lgr5) (Islam et al., 2015; Klonisch et al., 2008). Modulation of adhesion has a key role in cancer progression and angiogenesis (Bendas and Borsig, 2012), therefore high expression may have a functional role in CSC directed metastasis and tumour vascularisation. However, these functions are not specific to CSC and may not be essential to the CSC phenotype, in contrast to, for example, functional biomarkers of the immune system. Additionally, some markers used to identify CSC have functional roles in

certain cell types (e.g. CD20, CD24; immune cells) but are not likely to function in the same way in CSC. The CSC-specific role of other surface markers, including CD133 and CD271, remains the subject of debate (Bidlingmaier et al., 2008; Prager et al., 2019); which is an important consideration in selecting therapeutic targets of CSC. Functional markers of CSC include aldehyde dehydrogenase (ALDH) and the ATP binding cassette (ABC) transporter family of proteins. In contrast to CSC surface markers, these proteins have direct contributions to the CSC phenotype; ALDH catalyses the oxidation of aldehyde, which in CSC has a protective detoxifying effect in metabolising pharmaceutical agents, endogenous waste products and damaging metabolites (Tomita et al., 2015). Similarly, the ABC family of membrane bound transporters efflux molecules from the cell, including chemotherapy drug molecules (Davidson et al., 2008). However, the assay typically used to determine high expression of ABC transporters, known as the side population (SP) assay can cause toxicity in cells (Smalley and Clarke, 2005). The SP assay involves measuring Hoechst 33342 dye efflux as an indicator of ABC transporter activity, however, since Hoechst 33342 dye is toxic to cells, this could introduce bias in downstream functional assays of the sorted cells (SP or main population, MP cells), since the MP cells are likely to have reduced viability due greater intracellular build-up of the dye.

The caveats associated with the markers discussed above caution careful selection of markers used in identifying CSC. Nevertheless, it can be prudent to use a relatively small number of biomarkers rather than designing bespoke panels of biomarkers for each cancer type. In this way, functional characteristics of CSC from different cancers could be compared. One way to improve accuracy could be to use a panel of markers instead of a single marker. It is also important to consider that the suitability of a stem cell marker in different cancer types may be divergent; e.g. $CD24^-$ in breast cancer but $CD24^+$ in CRC and pancreatic cancer. The majority of studies on CSC focus on characterisation of the cells identified based on existing markers, rather than the discovery of novel CSC markers which have a specific functional role. Some studies investigating immune targeting of CSC have identified antigens, DNAJB8 and OR7C1, which functionally contributed to CSC characteristics, including population frequency, tumorigenicity and

expression of stemness genes (*SOX2, LGR5 and POU1F5*) (Morita et al., 2016; Nishizawa et al., 2012). The mechanism of action by which expression of either of these genes contributes to the CSC phenotype is not known and requires further investigation. Additionally, since these antigens are intracellular, they are not suitable for use in isolation of CSC. These studies nevertheless suggest there is scope for discovery of novel CSC markers. In this thesis, I focused on characterisation of CSC using existing markers, because it remains unclear which existing markers for prostate CSC are best suited for use in different *in vitro* models, including different cell lines and primary prostate cancer cells. The markers investigated are discussed further below.

Table 1.1. Tumour types in which CSC have been identified, and markers used to identify the respective CSC. The markers in this table have been previously reviewed (Islam et al., 2015; Klonisch et al., 2008; Visvader and Lindeman, 2008; Wang and Dick, 2005).

CSC marker	Function	Tumour type	Reference
Surface markers			
CD44/ CD44v6^{+}	Hyaluronic acid receptor; pleiotropic function including migration, adhesion, cell survival, interaction with immune cells	Colon, prostate, pancreas, ovarian, breast (specifically CD44v6), head and neck	(Islam et al., 2015; Jaggupilli et al., 2012; Meng et al., 2012; Sahlberg et al., 2014; Senbanjo and Chellaiah, 2017; Thapa and Wilson, 2016)
CD133^{+}	Function not entirely known; suggested to be associated with membrane interactions involved in migration and adhesion. May also be involved in signalling pathways e.g. AKT-Wnt	Lung, pancreas, prostate, glioblastoma, colon	(Beier et al., 2007; Brescia et al., 2013; Chen et al., 2015; Collins et al., 2005; Grosse-Gehling et al., 2013; Kallifatidis et al., 2011; Miyata et al., 2017; Shmelkov et al., 2008)

EpCam	Adhesion and migration, associated with activation of Wnt signalling, tumour associated antigen (TAA)	Prostate, colon, pancreas	(Deng et al., 2015; Gires et al., 2009; Munz et al., 2009; Ni et al., 2018)
CD24	Cell differentiation, B cell proliferation and maturation; modulation of T cell activation when expressed by B cells	Positive expression: colon, pancreas Lack of expression: breast, ovarian	(Islam et al., 2015; Jaggupilli et al., 2012; Kristiansen et al., 2004; Meng et al., 2012)
Human Leukocyte antigen (HLA)	Presentation of peptides at the cell surface for interaction with immune cells	Lack of expression: prostate (HLA Class I), leukaemia (HLA-DR/ Class II)	(Eppert et al., 2011; Meng et al., 2012; Patrawala et al., 2006; Vidal et al., 2014)
CD20	Regulation of B cell differentiation	Melanoma	(Fang et al., 2005; Pinc et al., 2012)
CD166	Cell adhesion	Lung	(Opdenaker et al., 2015; Zakaria et al., 2015)
CD271	Regulation of neuronal cell differentiation	Melanoma	(Boiko et al., 2010)
Functional markers			

ALDH (activity){Citation}	Metabolism of aldehydes	Prostate, pancreas, head and neck, breast	(Croker et al., 2009; Hellsten et al., 2011; Kallifatidis et al., 2011; Kamata et al., 2013; Kim et al., 2013; Magnen et al., 2013; Visus et al., 2007)
Side population/ ABCG protein family gene expression	Membrane bound ABCG proteins efflux small molecules from the cell (side population refers to the population with highest ABCG protein activity)	Glioblastoma, melanoma, lung, breast	(Beier et al., 2007; Gu et al., 2016; Mathew et al., 2009; Patrawala et al., 2005; Sabnis et al., 2017; Smalley and Clarke, 2005; Zhou et al., 2011)
Lineage markers			
$CD34^{+}$ $CD38^{-}$	CD34 is involved in cell adhesion. CD38 is also involved in cell adhesion, and calcium signal transduction. Together this expression pattern typifies haematopoietic stem cells. Gain of CD38 expression occurs as	Leukaemic stem cell	(Bonnet and Dick, 1997; Lapidot et al., 1994)

	haematopoietic stem cells differentiate into progenitor cells.		
Trop2^{+}	Transduction of intracellular calcium signalling. Cell functions associated with this calcium signalling include cell cycling, proliferation, self-renewal and invasion. Trop2 signalling can also modulate EpCam signalling.	Prostate; basal	(Magnen et al., 2013; Shvartsur and Bonavida, 2015)
CD49b (α_2 Integrin) CD29 (β_1 Integrin) CD49f (α_6 Integrin)	Membrane bound integrins; functional in adhesion to the prostate basal membrane.	Prostate; basal	(Collins et al., 2005; Frame et al., 2013; Moad et al., 2017)
NKx3-1	Transcription factor involved in cell fate decisions; in the prostate this includes regulation of prostate cell differentiation.	Prostate; luminal	(Wang et al., 2009)

CD44

CD44 is a cell surface receptor used to identify CSC in breast, prostate, CRC head and neck and pancreatic cancer (Islam et al., 2015; Klonisch et al., 2008). CD44 is the receptor for hyaluronic acid but also binds extracellular matrix components and growth factors (Thapa and Wilson, 2016). It has a multitude of physiological and pathological functions, including adhesion, leukocyte homing, cell migration, growth, survival and epithelial to mesenchymal transition (EMT) (Senbanjo and Chellaiah, 2017; Tsuneki and Madri, 2016). It is widely expressed in healthy tissues, including in the epithelium, on leukocytes and in connective tissue (Chen et al., 2018; Visvader, 2009). CD44 is also expressed by a number of cell types typically present in the TME (stromal, immune and cancer cells). This is an important consideration for CSC identification, as it requires that other lineage markers are included in a staining panel, to remove contaminating cellular fractions (Al-Hajj et al., 2003).

A number of CD44 isoforms exist, including the standard isoform 'CD44s,' and up to 9 possible variant isoforms 'CD44v' in humans (10 in mice), which is due to alternative splicing (Thapa and Wilson, 2016). Notably, CD44v isoform expression is restricted to epithelial cells, and it is these isoforms that are associated with cancer (although variant isoforms can be expressed concurrently to the standard isoform) (Prochazka et al., 2014). CD44v isoforms have been linked to specific functional roles in cancer progression, including EMT and metastasis (Barbour et al., 2003; Mashita et al., 2014). However, CSC were not singled out as the CD44v expressing population in these studies. In breast cancer, CSC enriching mammosphere growth conditions promoted expression of CD44v isoforms, although $ALDH^+$ cells expressed the standard isoform. Different CD44v isoform expression was also identified in different breast cancer subtypes (Olsson et al., 2011). In another study, CD44v5 and CD44v6 mRNA levels were higher in $CD133^+$ CSC in CRC, conferring metastatic ability (Todaro et al., 2014). This adds further complexity to the application of CD44 as a CSC marker beyond expression of standard versus variant isoforms; particularly since most commercial antibodies react with all CD44 isoforms (standard and variant). CD44 is therefore a highly versatile marker of aggressiveness and poor prognosis in

cancer but should be used in combination with other lineage specific and/ or CSC markers to identify CSC and due consideration be given to specifically identifying variant isoforms.

CD133

CD133 (Prominin-1) is a 5 transmembrane glycoprotein, which has been used to identify SC and CSC in many tissues. CD133 has two extracellular and three intracellular loops and is localised to cholesterol microdomains and protrusions such as cilia and microvilli in the cell membrane (Glumac and LeBeau, 2018). CD133 is expressed in healthy tissues (not specifically SC) including the colon, pancreas and kidneys (Fargeas et al., 2006; Wu and Wu, 2009). CD133 has also been used to identify CSC alone, or in combination with other markers in glioblastoma, CRC, prostate, pancreatic and lung cancer (Beier et al., 2007; K. Chen et al., 2013; Collins et al., 2005; Glumac and LeBeau, 2018; Islam et al., 2015; Ricci-Vitiani et al., 2007). The organ-wide applicability of CD133 as an SC and CSC marker was recently tested (Zhu et al., 2016). Organs in which CD133 expression was detected in both neonatal and adult stem cells included the prostate, intestine, stomach and uterus, although notably not the kidneys, pancreas and brain (Zhu et al., 2016). The $CD133^+$ SC were susceptible to cancerous transformation via various different well characterised mutations, including deletion of PTEN, B-catenin or p53, or mutation of KRAS (Zhu et al., 2016). However, some organs (the salivary glands, pancreas, kidney and brain) showed negligible tumour development despite the presence of a $CD133^+$ SC population, which suggests a disconnect between CD133 expression and stemness in these organs (Zhu et al., 2016). The variability in organs in which CD133 can be used to identify SC and CSC may be associated with the functional role of CD133 in these cell populations. However, comprehensive evaluation of the physiological function of CD133 has not yet been achieved. It has been suggested that CD133 plays a role in migration and invasiveness, owing to its cellular localisation (Glumac and LeBeau, 2018). In cancer, CD133 appears to have pleiotropic effects. In $CD133^+$ glioma cells, phosphorylation of CD133 mediated PI3K/AKT pathway activation, which conferred self-renewal *in vitro* and tumour initiation *in vivo* (Wei et al., 2013). CD133 signalling has also been implicated in resistance to radiation and invasion, the latter specifically

by control of matrix metalloproteinase (MMP) and CCL5 expression (Kohga et al., 2010; Li, 2013; Long et al., 2012).

While these functional data mainly support CD133 as a SC and CSC marker, it remains a challenge to use in the experimental setting. A number of studies have demonstrated stemness characteristics in both the $CD133^+$ and $CD133^-$ populations, in the colon, brain and prostate (Shmelkov et al., 2008; Sun et al., 2009; Wu and Wu, 2009; Zhou et al., 2011). Isolation of $CD133^+$ cells for functional characterisation has been hampered by the impact of experimental conditions on the expression or detection of CD133. CD133 expression has been suggested to be affected by culture conditions, including oxygen levels (CD133 is upregulated in hypoxic conditions), cell cycle and serum content (Pellacani et al., 2011). Some studies suggest that CD133 specifically identifies quiescent CSC (Pellacani et al., 2013; Sun et al., 2009), which may explain the effect of cell cycle on identifying CSC. Additionally, Pellacani and colleagues found that CD133 expression is differentially regulated in primary PCa cells compared to established cell lines (Pellacani et al., 2013). Commercial antibodies which recognise the CD133 protein bind different epitopes; including glycosylated and non-glycosylated epitopes and intracellular or extracellular sequences (Glumac and LeBeau, 2018). This has resulted in different studies reporting different patterns of CD133 expression patterns, across multiple tissues, depending on the antibody used (Hermansen et al., 2011). Expression of different splice variants or loss of CD133 expression has been demonstrated upon differentiation of stem cells (Grosse-Gehling et al., 2013; Richardson et al., 2004; Sundberg et al., 2009), however another study found unchanged protein expression but a difference in glycosylation which resulted in lack of CD133 detection (Kemper et al., 2010). CD133 is a widely used marker for identifying CSC, and this is largely borne out by functional and prognostic evidence. However, caution should be taken against over-reliance on this marker due to the large number of factors imparting variability into its detection.

ALDH

ALDH has been used as a functional maker for CSC in breast, prostate, pancreatic, ovarian, and lung cancer and melanoma (Croker et al., 2009; Klonisch et al., 2008; Kryczek et al., 2012; Luo et al., 2012; Miyata et al., 2017; van den Hoogen et al., 2010). The ALDH superfamily consists of 19 enzyme isoforms which catalyse aldehyde metabolism (Pors and Moreb, 2014). The ALDH isoforms have different tissue distribution and functions. The ALDH1 family and ALDH3A1 are associated with SC and CSC while ALDH4A1 and ALDH7A1 may have cancer related functions by interactions with p53 and cell cycle regulation respectively (Ma and Allan, 2011; Marchitti et al., 2008). ALDH has a physiological role in metabolising vitamins, lipids and amino acids and also exogenous substances such as alcohol, and pharmaceutical drugs (Tomita et al., 2015). This has a detoxifying effect and thus provides a protective role in cells; ALDH is highly active in SC as well as CSC. ALDH is also an essential regulatory enzyme in retinoic acid (RA) signalling. RA signalling is involved in development and differentiation; inducing differentiation using all trans retinoic acid (ATRA) to inhibit ALDH has been explored as a CSC therapy (Ma and Allan, 2011). ALDH also contributes to treatment resistance in cancer, including metabolism of reactive oxygen species (ROS) generated by radiation therapy (RT) and of chemotherapy drugs. ALDH based isolation of CSC differs to antibody-based surface marker isolation as ALDH is an intracellular enzyme; it is based on enzyme activity using the ALDEFLUOR assay. Additional discriminatory markers are also required if the ALDEFLUOR assay is used to identify CSC in a co-culture setup, as other cells present may be capable of metabolising the substrate. Different ALDH isoforms have been identified in different types of cancerFor example, as well as ALDH1A1, ALDH1A2, ALDH1A3 and ALDH7A1 have been identified in PCa samples, ALDH1A2 in AML, ALDH4A1 in glioblastoma (Pors and Moreb, 2014). Therefore, it may be additionally important to report the expression of ALDH isoforms in studies of CSC.

1.1.2 Identification of CSC in haematological and solid cancers

CSC were first identified in haematological cancer, designated leukaemia initiating cells, based on $CD34^{+}$ $CD38^{-}$ expression (Bonnet and Dick, 1997; Lapidot et al., 1994). These CSC were identified from AML blasts isolated from patients and demonstrated tumour initiation capacity in SCID and later

NOD/SCID mice and recapitulated the leukemic cell hierarchy *in vivo* (Bonnet and Dick, 1997; Lapidot et al., 1994). Identification of CSC in solid tumours has proved more challenging in some tissues, due to absence of a clear hierarchy or lack of lineage restricted surface markers. Investigation of solid tumours is also complicated by disruption of the proposed CSC niche in the tissue in the preparation of cell suspensions for analysis. The first solid cancer CSC/TIC were identified in breast cancer (Al-Hajj et al., 2003). This study tested tumour initiation in immunocompromised NOD/SCID mice and found that ESA^+ (EpCAM) $CD44^+$ $CD24^-$ Lin^- cells initiated tumours from as low as 100-200 cells. Additionally, the ESA^+ $CD44^+$ $CD24^-$ Lin^- cells gave rise to a heterogeneous hierarchy. This was significant owing to the complexity of the proposed cellular hierarchy in breast development; reconciling the CSC origin of different breast cancer lineages. Subsequent studies have also identified $ALDH^+$ as a marker of breast CSC (Ginestier et al., 2007). Metastasis initiating breast CSC have been identified using the markers ALDH high $CD44^+$ $CD24^-$ and ALDH high $CD44^+$ $CD133^+$ (Croker et al., 2009).

In the colon, CSC have been identified by a number of markers, including $CD133^+$ $Lgr5^+$ $ALDH^+$, $CD44,^+$ in combination, or alone (Holah et al., 2017; Islam et al., 2015; Ricci-Vitiani et al., 2007; Schepers et al., 2012). In contrast to the breast, a clearer tissue hierarchy and physical location of the SC/ CSC niche guides the selection of CSC markers, based on the phenotype of SC in the intestinal crypts (Huels and Sansom, 2015). However, it is possible that distinct CSC phenotypes exist in the colon as CD133 was found to be expressed in both epithelial and differentiated luminal cells in a mouse model (Shmelkov et al., 2008). This study also found that both $CD133^+$ and $CD133^-$ cells derived from human liver metastases were tumorigenic; suggesting that the metastatic CSC phenotype may differ from that of the primary tumour.

CD133 has been used consistently, albeit with varying reliability, to identify glioblastoma CSC. One study suggests that both $CD133^+$ and $CD133^-$ cells represent molecularly distinct but functionally similar CSC populations in glioblastoma. In another study, a novel antibody recognising CD133 was developed, which detected CD133 in a glioblastoma cell line previously

considered CD133 negative (WANG et al., 2015). Glioblastoma CSC have been extensively characterised, due to the successes in generating cell lines from primary samples and optimised *in vivo* models. Bao and colleagues found that $CD133^+$ glioblastoma CSC were enriched in response to radiation and were additionally more efficient at repairing RT induced DNA damage (Bao et al., 2006). Another subset of glioblastoma CSC, characterised by slow cell cycling, has been implicated in recurrence following chemotherapy *in vivo* (Chen et al., 2012).

1.1.3 Characteristics of CSC

Characteristics of CSC, including self-renewal and survival, driving tumour growth and therapeutic resistance occur by activation of signalling pathways such as NOTCH, Wnt, Hedgehog, NF-κB, TGF–β, HIF, JAK-STAT and PI3K/AKT (Cojoc et al., 2015a; Dreesen and Brivanlou, 2007; Reya et al., 2001). CSC characteristics occur by activation of multiple pathways and each signalling pathway can contribute to more than one characteristic. For example, Wnt, NOTCH, Hedgehog and TGF-β are involved in self-renewal, JAK/STAT and PI3K/AKT signalling have pleiotropic contributions to tumorigenesis including proliferation, resistance to apoptosis and immune modulation; NF-κB, PI3K/AKT, HIF, TGF-β and JAK/STAT signalling have all been implicated in various mechanisms of treatment resistance. These pathways have been reviewed elsewhere (Merchant and Matsui, 2010; Prager et al., 2019; Reya and Clevers, 2005; Wang et al., 2012); some are briefly discussed in the context of CSC signalling here (Figure 1.3).

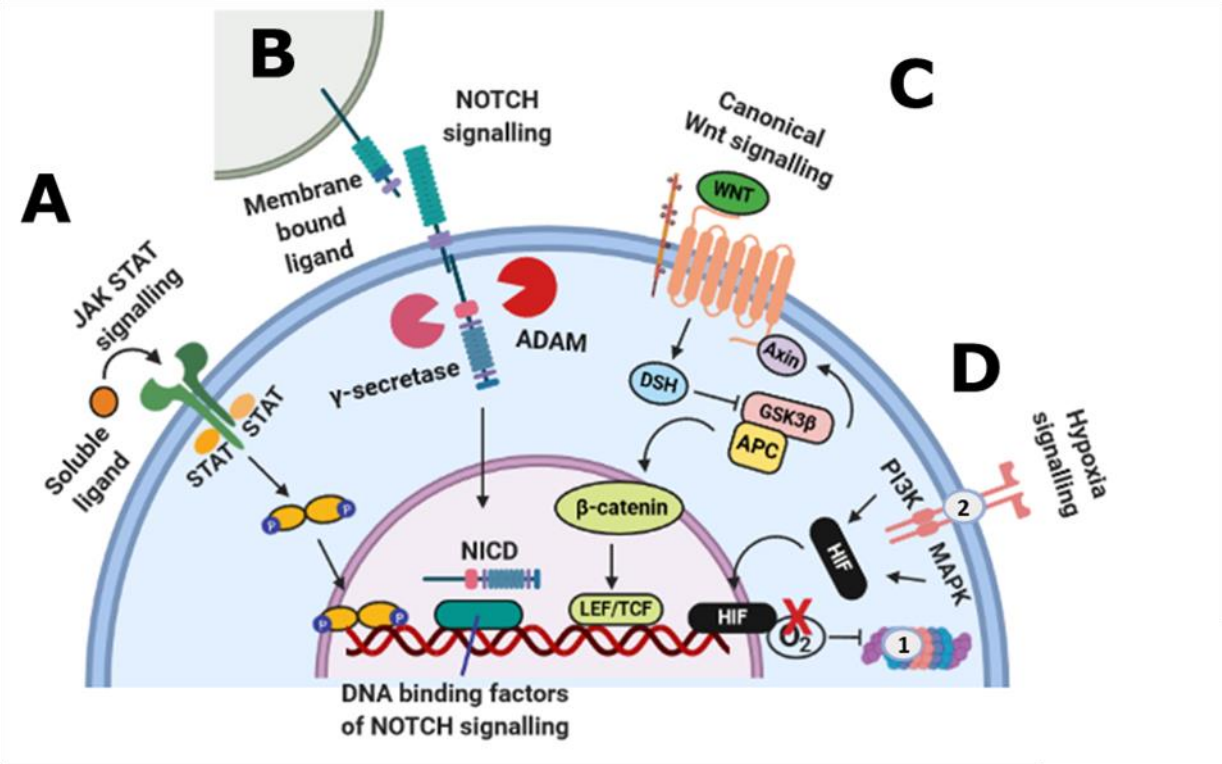

Figure 1.3. Selected signalling pathways and gene targets involved in cellular homeostasis; which if disrupted can contribute to various characteristics of tumours and CSC, including proliferation and survival, stemness, treatment resistance and tumorigenesis. Image adapted from Dreesen and Brivanlou., (2007), to highlight certain pathways which are discussed here. These and further pathways are reviewed in more detail in the original publication. Image was produced using BioRender (https://biorender.com/). (A) Receptor and intracellular mediators of signalling in the JAK-STAT pathway. (B) Mechanism and mediators of NOTCH signalling. (C) The canonical Wnt signalling pathway. (D) Hypoxia signalling: HIF protein synthesis and oxygen mediated regulation of HIF degradation or DNA binding in the absence of oxygen. Pathway graphics also adapted from O' Shea et al., (2015) (JAK-STAT), Matsui, H., (2016) (NOTCH), Reya and Clevers., (2005) (Wnt) and Semenza, G., (2003) (Hypoxia/ HIF).

Tumorigenesis

JAK/STAT signalling

The Janus kinase/signal transducer and activator of transcription (JAK/STAT) pathway is pleiotropic; it has a functional role in apoptosis, growth factor signalling and inflammation and other immune cell signalling. There are 4 JAKs, which interact with different membrane bound receptors, and different STATs, resulting in a large number of ligand-receptor/JAK/STAT combinations which mediate different functional signalling outcomes (O'Shea et al., 2015) (Figure 1.3A). JAK receptors are phosphorylated as a result of ligand binding (example ligands include IL-6, IL-12, GM-CSF, and interferons); this creates a binding site for STATs, which are activated as a result of binding the intracellular tail of the receptor (O'Shea et al., 2015). The STATs (as homo or heterodimers) mediate the signal by translocating to the nucleus and activating gene expression (Quintás-Cardama and Verstovsek, 2013).

Cancer development and progression can occur due to mutations of the receptor, JAKs or the STATs. STAT3, and to a lesser extent, STAT5B mutations occur in up to 40% of T-cell large granular lymphocytic (T-LGL) leukemia patients, a rare and incurable cancer characterised by expansion of $CD3^+$ $CD8^+$ T cells (Shahmarvand et al., 2018). The malignantly expanded T cells have a mature, differentiated effector phenotype in which a dominant monoclonal population persists (Lissina et al., 2018; Teramo et al., 2017). Expansion of the malignant T cell clone is attributed to a combination of chronic antigen exposure, evidence by the differentiated phenotype, and mutated STAT3 signalling, which is downstream of T cell activation signalling (Lissina et al., 2018; Siegel et al., 2011). Mutated STAT3 can contribute to a failure in activation induced cell death, causing T cell persistence (Teramo et al., 2017). JAK/STAT signalling also plays a functional role in CSC. IL-6 signalling, mediated by JAK1/STAT3, has been associated with stemness, including EMT and DNA repair in response to radiation, in $CD133^+$ cells in non-small cell lung cancer (NSCLC) (Chen et al., 2015; S. O. Lee et al., 2016; O'Shea et al., 2015). IL-6 and JAK/STAT signalling is particularly relevant in PCa and may contribute to stemness characteristics in prostate CSC. High serum IL-6 is reported in aggressive disease and is associated with poor prognosis (Culig and Puhr, 2012; Hobisch et al., 2000; Smith et al., 2001).

JAK1 and STAT3 activation is associated with poorer recurrence-free survival following prostatectomy treatment (Xingyan Liu et al., 2012). Additionally, Shroeder and colleagues showed that AR silencing resulted in a gain in CSC functional characteristics such as sphere formation and expression of CD44, Sox2 and MSI-1 (Musashi-1) (Schroeder et al., 2014). This was shown to be associated with increased STAT3 activation, via IL-6 signalling, and blocking IL-6 signalling reduced tumour growth *in vivo* (Schroeder et al., 2014). Components of the JAK/STAT pathway, including IL-6, CSF2 and STAT1 were overexpressed in $CD133^{+}$ $\alpha_2\beta_1 Integrin^{high}$ cell lines derived from primary prostate cancer samples (Birnie et al., 2008). STAT3 activation via IL-6 signalling was shown to be indispensable for CSC tumour initiation *in vivo* (Kroon et al., 2013).

Stemness and self-renewal

NOTCH pathway

NOTCH signalling occurs by cleavage of the receptor intracellular domain upon binding of the membrane bound ligands, Delta-like (DLL) 1-4, Jagged 1, 2 (Figure 1.3B) (Matsui, 2016). Receptor cleavage is mediated by a disintegrin and metalloproteases (ADAM) and γ-secretase; the intracellular domain (NICD) then translocates to the nucleus and binds DNA response elements (Ranganathan et al., 2011). NOTCH signalling plays an essential role in embryonic development and is directly implicated in T cell acute lymphoblastic leukaemia (Ranganathan et al., 2011). Deregulated NOTCH signalling, mediated by ADAMs, is also implicated in a wide number of cancers (Mochizuki and Okada, 2007). Aberrant ADAM activity is implicated in PCa aggressiveness and progression. ADAM15 interacts with Integrins and may contribute to invasion by degrading the ECM and is associated with metastatic PCa (Kuefer et al., 2006).

Wnt signalling

Canonical Wnt signalling is involved in maintaining the SC phenotype and has been implicated in tumorigenesis (Figure 1.3C). The inter-relatedness of these pathways particularly highlights how SC could represent likely targets of tumour initiation and progression. Wnt signalling controls cell fate and

regulates the cellular hierarchy in the colon and also in haematopoietic stem cells (Reya et al., 2003; Reya and Clevers, 2005). Wnt signalling occurs by binding of Wnt ligands to Frizzled receptors (Clevers et al., 2014). Wnt signalling 'rescues' the signalling effector protein β-catenin from destruction by ubiquitination as it inactivates the Axin, APC and GSK3-β complex (Figure 1.3C) (Clevers, 2006). β-catenin can translocate to the nucleus and interact with Tcf/Lef DNA binding proteins, resulting in activation of gene expression (Reya and Clevers, 2005). Mutation of Wnt signalling pathway components is strongly associated with tumorigenesis, particularly mutated APC which is associated with CRC (Phelps et al., 2009). Wnt signalling mediates radiation resistance in ALDH high prostate CSC (Cojoc et al., 2015a; Wetering et al., 2002). Overactive Wnt signalling in prostate cells is suggested to be associated with AR overexpression (Murillo-Garzón and Kypta, 2017). Wnt and CD44 signalling are reciprocally associated; CD44 gene expression is modulated by Wnt while CD44 membrane expression associates with Wnt receptors (Schmitt et al., 2015).

Hypoxia

Hypoxia refers to a state of poor oxygenation resulting in activation of transcription factors called hypoxia inducible factors (HIFs) (McKeown, 2014; Peng and Liu, 2015). In the presence of oxygen, HIFs are hydroxylated and subsequently ubiquitinated by the tumour suppressor protein von Hippel–Lindau (VHL) and degraded by the 26S proteasome (Figure 1.3D (1)) (Semenza, 2003). In the absence of oxygen mediated degradation, HIF1α or HIF2α subunits dimerise with HIF1β and bind hypoxia response regions (HREs) of DNA to regulate gene expression (Semenza, 2003). The actual oxygen levels which define hypoxia varies widely across different tissues (McKeown, 2014). Transient hypoxia is distinguished from pathological hypoxia by the tissue retaining the capacity to revert to normoxic cell signalling (McKeown, 2014). Mutations occurring in signalling pathways regulating HIF expression, including PI3K/AKT signalling via MTOR and RAS/ERK/MAPK signalling, can cause aberrant HIF signalling, resulting in chronic hypoxia (Figure 1.3D (2)) (Semenza, 2003). Hypoxia in tumours represents a major barrier to successful therapeutic outcomes as it reduces the efficacy of RT and chemotherapy. CSC are capable of surviving, and are

enriched, under hypoxic conditions. Upregulation of HIF in CSC further contributes to their resistance to treatment and invasiveness. PCa is one of the most hypoxic cancer types; oxygen levels in PCa have been reported as low as 0.3-0.6% and the healthy prostate also has lower than average organ oxygen levels (2.4-3.9%) (McKeown, 2014). HIF1α expression was found in a high proportion of PCa tissue biopsies and was significantly correlated with higher Gleason Score (GS); stem cell genes NANOG and OCT4 were concurrently expressed in these biopsies (Miyazawa et al., 2014). Prostate CSC can be isolated under hypoxic conditions; HIF1α target genes *Epo* (erythropoietin) and *Redd1* (DNA damage response 1) and *VEGF, GLUT1* and *REDD1* were upregulated in CSC derived from the transgenic adenocarcinoma of the mouse prostate (TRAMP) mouse model and DU145 cell line respectively (Marhold et al., 2015). Expression of these genes suggests hypoxia induced metabolic changes and induced pro-angiogenesis signalling by the CSC, while increased DNA damage repair could enable CSC to survive hypoxic conditions better than non-CSC.

CSC therefore represent a distinct subpopulation of tumour cells, characterised by specific markers and found in most cancer types. Stemness associated signalling pathways are active in CSC; however, clonogenicity and self-renewal capacity is reduced or absent in non-CSC progeny. Additionally, CSC have enhanced activation of signalling pathways associated with cancer and resistance to treatment. Since CSC are key players in tumour development, it follows that CSC are present in the process of immunosurveillance, which is detailed below, and later specific interactions, such as are known, between CSC and the immune system, are discussed.

1.2 Cancer immunology

1.2.1 Cancer Immunosurveillance

Cancer immunosurveillance proposes that the immune system is capable of recognising and engaging with tumours. This is based on the hypothesis that a host defence mechanism must surely exist to control neoplastic growth throughout life (Ehrlich, 1909). Burnet and Thomas coined the term 'immune surveillance,' based on the observation that immunosuppressed transplant recipients had a higher tumour incidence (Burnet, 1970; Thomas, 1982).

However, they acknowledged the challenges of providing experimental evidence with the available mouse models, since early experiments investigating immunosurveillance appeared to disprove the hypothesis. For example, no difference in tumour incidence in the first 'immunodeficient' mouse model was observed (Stutman, 1979, 1974); however these athymic *nu/nu* mice retained NK cells which have since been shown to play a role in controlling developing tumours (Street et al., 2001). Eventually with the use of RAG2 knock out mice (lacking T cells, B cells and NK cells) Shankaran and colleagues demonstrated that these immune system components are required to prevent tumorigenesis (Shankaran et al., 2001). Other studies also provided evidence for critical immune molecules including interferons (Dighe et al., 1994; Dunn et al., 2006; Kaplan et al., 1998) perforin; specifically NK cell derived perforin (Street et al., 2001).

The study by Shankaran and colleagues also critically demonstrated that interactions between the immune system and developing tumours alter the tumours. This manifests in the capacity of tumours to grow even in the presence of a competent immune system (Shankaran et al., 2001). These data and many other relevant studies coalesced into the hypothesis of 'The Three Es of Immunoediting' (Dunn et al., 2004a). The three Es stand for Elimination, Equilibrium and Escape, describing the continuum of interactions between the immune system and tumorigenesis throughout life (Figure 1.4).

1.2.2 Cancer immunoediting

Elimination: tumour recognition and immune effectors

In the elimination stage, the innate and adaptive immune system, including interferons, NK, B and T cells (including NKT cells, αβ and γδ T cells), dendritic cells (DC) and M1 (inflammatory) macrophages engage the transformed cells and successfully eradicate the developing tumour (Figure 1.4A) (Dunn et al., 2004a; Gao et al., 2003; Jaiswal et al., 2010; Ostrand-Rosenberg, 2008; Smyth et al., 2001). The immune response to a transformed cell is not dissimilar to an infection; activation of innate immune cells to bring about antigen-mediated cell killing is required (Chen and Mellman, 2013). Polly Matzinger's 'Danger Theory' (Matzinger, 1994) reconciled the idea that

endogenous 'danger' signals from cells (Damage Associated Molecular Patterns; DAMPs) could activate the immune system. Tumour associated DAMPs include hyaluronic acid, extracellular matrix components and high mobility group box 1 (HMGB1), (Figure 1.4B) (Hernandez et al., 2016; Termeer et al., 2002). Additionally, transformation by specific oncogenes such as EGFR, Ras and BCR-ABL results in expression of NKG2D ligands MHC class-I related chain A and B glycoproteins (MICA and MICB) and ULBP (cytomegalovirus UL16-binding protein) (Figure 1.4B) (Boissel et al., 2006; Corthay, 2014; Groh et al., 1999; X. V. Liu et al., 2012; Raulet and Guerra, 2009; Vantourout et al., 2014). This leads to immune activation via the NKG2D receptor expressed on NK cells.

Danger sensing by immune cells results in the release of pro-inflammatory cytokines (Figure 1.4C). Macrophages are polarised to the pro-inflammatory, anti-tumour M1 phenotype by IFNγ signalling and can release further cytokines and chemokines. DC form the most important bridge between the innate and adaptive immune system for the activation of T cells; DC express pathogen recognition receptors (PRRs), which can recognise the DAMPs produced by tumours (Palucka and Banchereau, 2013). Activated DC phagocytose antigens released by tumour cells killed by NK cells. DC co-stimulation signals, along with antigen presentation, are essential for activation of tumour-antigen specific cytotoxic $CD8^+$ T cells. This is a significant consideration for designing immunotherapies expected to boost the effector arm of the immune response; *ex vivo* generation of T cells must provide activation signals to avoid production of anergic or tolerogenic T cells (Chen and Flies, 2013).

Equilibrium

A successful elimination response can prevent tumour growth, however, throughout the lifespan of the individual, the immune system may re-engage with mutated cells. This stage, involving continued interactions between immune cells and a developing tumour, in which tumour dormancy is maintained, is known as equilibrium (Figure 3.1D) Equilibrium involves dynamic remodelling of the tumour and the immune cells. This period may exist after treatments reduce the tumour to a 'minimal residual disease'

(Bhatia and Kumar, 2011). The mechanisms of tumour immune equilibrium were first demonstrated by Koebel and colleagues, who showed that blocking $CD8^+$ and $CD4^+$ T cells and IFNγ in mice bearing non-progressive sarcomas caused failure of immune constraints on tumour growth (Koebel et al., 2007). Tumour equilibrium is maintained by adaptive immune cells (Bhatia and Kumar, 2011; Mittal et al., 2014; Wu et al., 2013). IFNγ and IL-12 are essential for tumour control (Koebel et al., 2007; Müller-Hermelink et al., 2008), while tumour promoting cytokines, such as IL-10 and IL-4, produced by tumour cells, support pro-tumour immune cells such as T regulatory cells (Tregs), M2 macrophages and myeloid derived suppressor cells (MDSC), resulting a feedforward loop of anti-inflammatory cytokine production (Mittal et al., 2014; Ostrand-Rosenberg, 2008; Stassi et al., 2003; Vence et al., 2007; Wang et al., 2004).

During the elimination phase, genetic instability as well as interactions with the immune system result in elimination of highly immunogenic, and survival of less immunogenic, tumour clones. This is known as immunoediting, described above (Shankaran et al., 2001). Matsushita and colleagues showed that the genetic mutations in tumours grown in immunocompromised mice differed from those in immunocompetent mice and identified antigens involved in rejection of experimental tumours (Matsushita et al., 2012). Another group investigated sarcoma development in immunocompromised and immunocompetent mice, finding that the penetrance and time to tumour development was significantly different in the immunocompromised and immunocompetent mice (DuPage et al., 2009).

Escape

Interactions with the immune system in the equilibrium stage paradoxically remodel tumours towards a state of evading immune recognition and suppressing effector immune cells (Spranger et al., 2013). This occurs in three ways: loss of immunogenicity, downregulation of immune cell ligands such as NKG2D and expression of immune inhibitory receptors and cytokines (Figure 1.3E) (Beatty and Gladney, 2015; Mittal et al., 2014; Schreiber et al., 2011). Tumours become less immunogenic by altering antigen presentation to immune cells; HLA Class I is downregulated or lost (Campoli and Ferrone,

2008; Garrido et al., 1997; Marincola et al., 2000; Speetjens et al., 2008) and components in the antigen processing pathway are dysregulated or mutated e.g. proteasome processing and the transporter for antigen processing (TAP) protein, transporter for antigen processing (TAP) protein, (Ebstein et al., 2016; Seliger et al., 2000). Loss of immunogenic antigens or epitopes has also been described (Cormier et al., 1999; Urban et al., 1984), as immune killing of immunogenic tumour cell clones exerts selective pressure such that only those tumour cells expressing less immunogenic antigens are selected for survival (Khong and Restifo, 2002; Schreiber et al., 2011).

The surrounding stroma is also modified to become cancer promoting; this has been reviewed extensively elsewhere (Dunn et al., 2004b; Mittal et al., 2014; Motz and Coukos, 2013; Schreiber et al., 2011). Production of factors such as IL-4, survivin, VEGF and MMPs remodel the surrounding stroma resulting in establishment of a tumour microenvironment (TME) (Zitvogel et al., 2006). The balance of immune cells in the TME becomes tumour promoting, due to recruitment of regulatory and inhibitory immune cells, including Tregs, MDSC and M2 macrophages (Gajewski, 2007; Gajewski et al., 2011; Woo et al., 2001). Chronic engagement by anti-tumour T cells results in their exhaustion (Wu et al., 2013). Both tumour and immune cells express checkpoint proteins, e.g. PD-1, CTLA-4, Lag-3 (expressed by $CD8^+$ T cells, Tregs and M2 macrophages recruited to the TME) and PD-L1 (expressed by tumours and M1 macrophages), which are normally involved in the control of immune cells following a successful immune response; preventing further healthy cell killing (Figure 1.3F). However, in the case of chronic tumour engagement, checkpoint molecule expression results in inhibition of a still necessary effector immune response (Motz and Coukos, 2013; Moy et al., 2017; Zheng et al., 2013). Inflammation, which can be an anti-tumour response in acute interactions, can also be tumour promoting under chronic conditions (Atsumi et al., 2014; Baniyash et al., 2013).

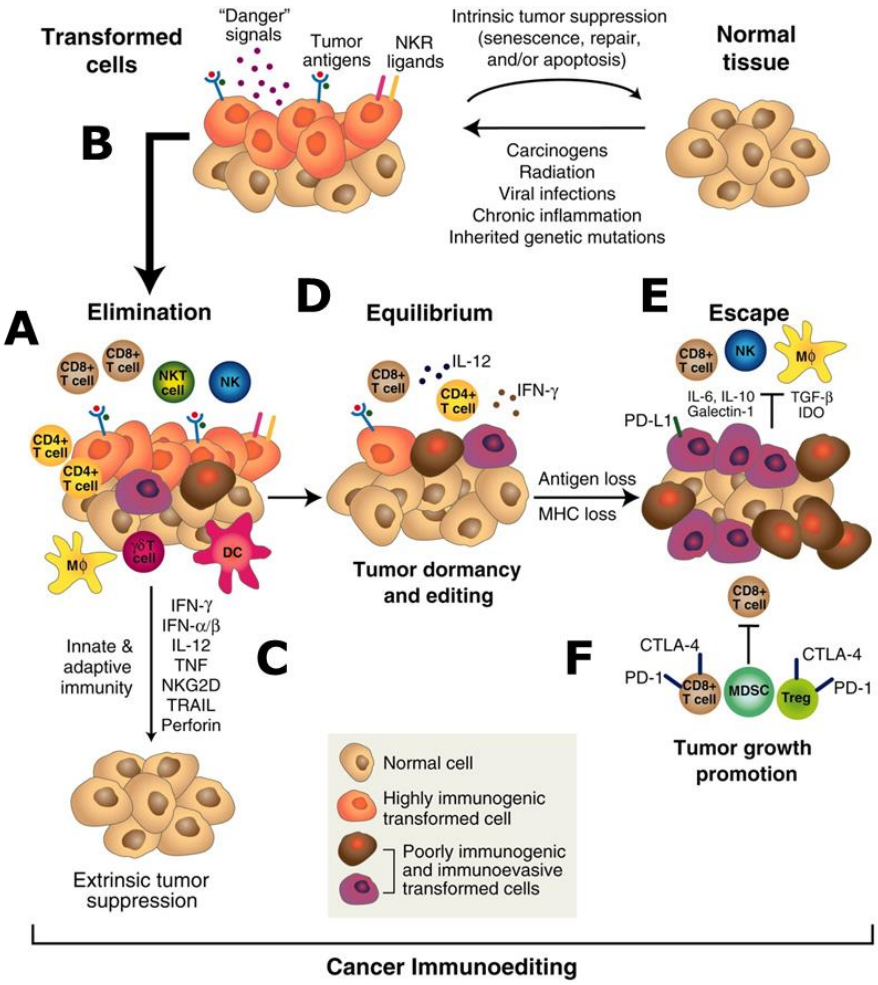

Figure 1.4. Cancer Immunoediting: the ongoing process, throughout life, in which the immune system surveys, identifies and engages with nascent tumours. (A) Successful Elimination of a developing tumour is mediated by anti-tumour innate and adaptive immune cells, including M1 macrophages, NK cells and DC, and $CD4^+$ and $CD8^+$ T cells. This involves (B) sensing of tumour intrinsic signals associated with transformation, including DAMPS and NK ligands. (C) Tumour killing is achieved by production of cytokines and other immune cell signals e.g. IL-12, TNFα and IFNγ. (D) Incomplete or unsuccessful tumour elimination can lead to the continuous Equilibrium stage, categorised by ongoing presence of immune cells in the absence of tumour growth. This stage can last throughout life, without further tumour growth. (E) Tumours may escape due to reduced anti-tumour efficacy of chronically stimulated immune cells, and immune evasive tumour cells are selected due to ongoing immune pressure. (F) Signalling in the tumour microenvironment becomes tumour-promoting; anti-inflammatory M2 macrophages and Tregs are attracted to the tumour. Both these and the chronically activated immune cells express checkpoint inhibitor receptors. This stage is the most well studied of cancer immunoediting as tumour escape presents as a clinical stage. Figure adapted from Schreiber et al., (2011)

1.2.3 $CD8^+$ T cells: key mediators of anti-tumour immunity

$CD8^+$ T cells play a crucial role in each of the stages of immunoediting discussed above, and are often employed in cancer immunotherapy strategies, discussed further below. The role of $CD8^+$ T cells in killing cancer cells based on antigen recognition is a parallel to the original function for which $CD8^+$ T cells were investigated; recognition of foreign antigens and killing infected cells presenting these antigens via HLA Class I. The origin of the $CD8^+$ T cell lineage is a bone marrow derived lymphoid progenitor which is double negative at the early developmental stages (Germain, 2002). T cells develop from this lymphoid progenitor in the thymus (Starr et al., 2003). T cell development occurs most prolifically in early life and declines approximately past the age of 40, although TCR diversity is maintained by long lived memory T cells (Kumar et al., 2018).

T cells begin to express the T cell receptor (TCR) at the double negative developmental stage, before expressing both the CD4 and CD8 co-factor proteins, resulting in a double positive precursor T cell (Germain, 2002; Robey and Fowlkes, 1994). The double positive T cells go through two stages of selection, which also includes determination of the lineage specificity ($CD4^+$ or $CD8^+$). The first stage of selection is known as positive selection, in which T cells expressing functional TCR are activated by antigen-specific interactions with cortical thymic epithelial cells (cTEC), a specialised type of antigen presenting cell (Ziegler et al., 2009). The cTEC present self-antigens, via HLA Class I or HLA Class II to the T cells (which are still double positive). Therefore, T cells which are activated in response to the self-antigens are 'saved' and unresponsive T cells in which TCR recombination as resulted in a non-functional TCR 'die of neglect' due to lack of TCR activation (Gascoigne et al., 2016; Singer et al., 2008; Ziegler et al., 2009). Only approximately 5% of T cells are retained through positive selection as there is a large scope for recombination events in the TCR (discussed below) to yield non-functional sequences which do not interact with peptide-HLA (Kyewski and Klein, 2006). Responses which are positively selected are of low affinity (Palmer, 2003; Ziegler et al., 2009) This first step in T cell selection creates a repertoire which is functionally responsive, however, negative selection is required to eliminate highly self-responsive T cells. The process by which T cells become

single positive ($CD4^+$ or $CD8^+$) is not entirely clear, but is essentially controlled by the HLA molecule the TCR and co-receptor interacts with, i.e. a HLA Class I signalling through the TCR and interaction with the $CD8^+$ co-receptor will preserve a single positive cells of the $CD8^+$ lineage and a HLA Class II signalling through the TCR and interaction with the $CD4^+$ co-receptor results in differentiation into CD4 expressing single positive T cells (Germain, 2002; Singer et al., 2008). Positive selection is necessary as the random combinatorial nature of TCR α chain rearrangement imparts a high possibility of generating unresponsive TCR that do not recognise any HLA-peptide combination.

Both the positive and negative selection process involve presentation of self-antigens; however, these developmental stages achieve different purposes. Negative selection of $CD8^+$ T cells is biased towards producing a T cell repertoire containing T cells expressing a TCR with a higher affinity for foreign, rather than self-antigens. Negative selection is facilitated by presentation of peptides to the single positive T cells by medullary thymic epithelial cells (mTEC), mTEC are spatially distinct from cTEC there remains some debate as to the contribution of cTEC to negative selection (Gascoigne et al., 2016; Klein et al., 2014; Palmer, 2003; Ziegler et al., 2009). DCs also present peptides in the medullary cortex. Most studies have shown the mTEC and medullary resident DC to be essential to negative selection, in comparison to cTEC (Palmer, 2003). mTEC or DC in the medullary thymus express tissue restricted antigens and present peptides which could be presented by peripheral tissues (Derbinski et al., 2001). Expression of these proteins in mTEC is mediated by the autoimmune regulator (AIRE) gene (Peterson et al., 2008). It appears a paradox that presentation of similar peptide sequences from the same self-antigen could control positive selection and negative selection and the precise mechanism for this remains unclear, however, it is generally accepted that high affinity TCR – peptide-HLA interactions result in negative selection. This may be mediated by a different set of signals activated by a longer interaction between the TCR and peptide-HLA complex, which characterises a high affinity response (Palmer, 2003). It has also been suggested that cTEC and mTEC express structurally distinct HLA proteins, which bind to and present different peptide repertoires (Ziegler et al., 2009). Following negative selection, the resulting naïve $CD8^+$ T cell

repertoire is poised to respond to foreign antigens by distinction of the removal of high affinity self-reacting T cells.

In the context of cancer immunology, this can partly explain the 'hierarchy' in affinity responsiveness to tumour antigens, discussed in more detail later; virus associated cancers presenting viral peptides and neoantigens, i.e. peptides occurring as a result of a mutation or splicing event would not have been presented to T cells during developmental selection typically have the highest affinity responses, followed by germline antigens and other self-antigens which due to their developmentally restricted expression may not have been presented during T cell selection, or which are presented at a sufficiently high cell surface density to activate T cells, respectively. However, it remains a challenge to identify (e.g. novel neoantigens) or design tumour antigen targets (based on prediction of self-protein sequences) since other factors such as the co-receptor complex and environmental stimuli contribute to T cell activation. Many of the peptides identified from commonly targeted (public; discussed below) tumour antigens e.g. MART-1 and NY-ESO are associated with weak TCR affinity (Stone and Kranz, 2013), since these are derived from self-proteins, thus high affinity TCR recognising peptide sequences from these proteins are likely to have been deleted during negative selection.

The TCR

The TCR is the crucial structure at the centre of the T cell selection process. The TCR is comprised of an α (light) and a β (heavy) chain. The chains are linked at the constant regions by cysteine disulphide bonds (Miles et al., 2011). The α chain consists of variable (V) and joining (J) regions and the β chain consists of variable, joining and diversity (D) regions (Bassing et al., 2002; Davis and Bjorkman, 1988; Miles et al., 2011). It is in these regions that the broad variety in the T cell repertoire is generated. This is achieved through germline variety and recombination. The germline variety refers to the possible combinations of V (47 genes) and J (57 genes) regions of the α chain and the V (54 genes), J (13 genes) and D (2 genes) regions of the β chain (Miles et al., 2011; Rosati et al., 2017). Additional diversity is introduced randomly by recombination. It is this stage that makes analysis of

TCR highly complex and almost impossible to predict based on known sequences, since the genomic sequence is not directly related to the translated protein. Recombination involves introduction of double stranded DNA breaks into the sequences encoded by the V, J and D genes, which is mediated by the RAG1 and RAG2 (recombination activating gene 1/2) genes and directed by recombination signal sequences expressed at the V, J and D loci (Bassing et al., 2002; Krangel et al., 1998; Schatz, 2004). The gene segments are then rearranged into functional sequences, which includes random insertion or deletion of nucleotides, mediated by the enzyme terminal deoxynucleotidyl transferase (TdT) (Bassing et al., 2002; Krangel et al., 1998; Schatz, 2004). The V, J and D regions contribute to the site of the TCR that interacts with the peptide-HLA complex and mediates recognition. This site consists of six complementarity determining region (CDR) loops (3 from each chain). CDR1 and CDR2 are encoded by germline V genes from each chain while the CDR3 region, which mediates peptide recognition, is an assembly of the V, J and D regions/ V and J regions of the β and α chain respectively and is thus highly variable as it is a result of the above described recombination and rearrangement process (Miles et al., 2011; Schrama et al., 2017). Accordingly, there is no existing technical approach which can determine the cognate peptide sequence, based on the CDR3 peptide recognition region of a TCR.

The TCR α and a β chains are rearranged separately (sequentially). The TCR β chain D and J gene segments are firstly recombined, then the variable gene segment is joined to the DJ segment and the resulting sequence is expressed in the double negative stage of T cell development in the thymus (Livák et al., 1999; Schrama et al., 2017). Each single cell has an unique Vβ chain, however, controlled by successful binding outcomes to this 'template' α chain recombination can give rise to the same α chain in different T cell clones (Rosati et al., 2017). Expression of a precursor α chain occurs concurrent to expression of co-receptors and it is the precursor α chain - β chain structure that interacts with HLA peptide complexes presented by cTEC during positive selection (Fehling et al., 1995; Starr et al., 2003). It has been suggested that more than one $\alpha\beta$ combination is 'tested' with a peptide-HLA complex expressed by cTEC, since expression of recombination genes at the α chain

locus persists upon interaction with the complex, therefore giving T cells more than one 'opportunity' for positive selection (Brändle et al., 1992; Germain, 2002; Starr et al., 2003). Recombination of the TCR α chain involves rearrangement and joining of the V and J segments (Schrama et al., 2017). Downregulation of recombination genes at the α chain locus occurs following successful signalling through interaction with a peptide-HLA complex. The $\alpha\beta$ TCR expressing T cells then become single positive, as described above, and undergo negative selection.

Recombination and random nucleotide insertion explain how the immune system can produce receptors capable of recognising and protecting against the extensive diversity of potentially harmful insults encountered throughout life, since this would not be possible through simple genomic expression. However, the theoretical TCR diversity estimated based on analysis of these processes is vastly greater than experimentally observed TCR repertoire diversity (Arstila et al., 1999; Miles et al., 2011). Therefore there is a high degree of redundancy and cross-reactivity in the T cell repertoire (Mason, 1998; Wooldridge et al., 2012). These features present both advantages and disadvantages to development of T cell-based cancer immunotherapy. Repertoire analysis would be next to impossible if receptor diversity was as extensive as predicted, which would greatly decrease the possibility of identifying the T cell clones contributing to an immune response or developing TCR products for use in patients. Due to factors including sample availability and differences between peripheral blood, intratumoral and normal tissue T cell repertoires, T cell repertoire analysis techniques only characterise a small portion of TCRs in a given individual (Schrama et al., 2017). Some applicable techniques are discussed in the next section.

TCRs which are found in multiple individual's immune repertoires are known as 'public' TCRs (Venturi et al., 2008). Antigen targeting in cancer immunotherapy has largely focused on identification of the corresponding public antigens which can be targeted in multiple patients (Bethune and Joglekar, 2017; Venturi et al., 2008). However, public TCR are likely to be of lower affinity as they are the result of negative selection in the thymus i.e. elimination of high affinity self-responding T cells (Bethune and Joglekar,

2017). Strategies to increase the affinity of a public TCR introduce the risk of cross-reactivity and has led to off target toxicity in previous studies (Holler et al., 2003; Linette et al., 2013). On the other hand, 'private' TCR, which are found in only one individual and typically recognise novel neoantigens which are not presented by TEC during the process of T cell development (Klein et al., 2014), could have higher affinity responses and less likelihood of cross-reactivity, but involve a more labour intensive approach to identify (requiring TCR repertoire analysis and exome sequencing) and in the translational sense, are highly patient specific. As discussed below, some T cell therapy approaches e.g. TIL therapy, may inherently involve targeting neoantigens by private TCR, however the composition of the T cell product is not necessarily analysed to identify the TCR present.

In addition to identifying target peptides and TCR which recognise them with an optimal affinity response, development of T cell based cancer immunotherapies must consider the optimal way to activate T cells against cancer antigens, and which T cell subset represents the best choice for therapeutic design. For this, the mechanism of T cell activation and the progression of a T cell response *in situ* must be considered.

Activation and responses of mature, naïve CD8$^+$ T cells in the periphery: implications for therapeutic design

Mature native T cells circulate through peripheral blood vessels and lymphoid organs following exit from the thymus. While T cells may encounter antigens in circulation, it is interactions with antigen presenting DCs (in secondary lymphoid organs) that is necessary for T cell activation as DCs express the necessary co-stimulatory receptors (e.g. CD80, CD86,) and produce cytokines (e.g. IL-12, IFNγ) which constitute the necessary signal for activation (antigen, co-receptor and cytokines are known as the three signals of T cell activation) (Alegre et al., 2001; Gardner and Ruffell, 2016; Mescher et al., 2006). T cells which respond to antigens in the absence of these signals become anergic (Constantino et al., 2017). Thus, the importance of DC derived signalling in activating cytotoxic T cells drives the DC vaccine therapeutic strategy. CD4$^+$ T cells are also involved in CD8$^+$ T cell activation

both by priming DC toward a primary (cytotoxic) response and by providing stimuli to activate T cells for a secondary (memory) response (Bennett et al., 1997; Janssen et al., 2003). Naïve DC which have not been activated by $CD4^+$ T cells can induce tolerance in T cells; thus, strategies to mature DC as part of an *ex vivo* therapeutic design are important. Additionally, it has been shown that concurrent activation of $CD4^+$ T cell responses can improve responses in immunotherapy strategies designed to activate $CD8^+$ T cells (Moeller et al., 2005). Notably, the natural activation of T cells by DCs in lymphoid organs in response to infection, after which T cells are attracted by other signals produced by e.g. innate immune cells and damage signalling from target cells may also present a target or challenge for cancer immunotherapy. Impaired T cell homing to tumours contributes to failures in treatment (Sackstein et al., 2017). Infiltration of solid tumours by $CD8^+$ T cells is a prognostic factor in many cancers (Brambilla et al., 2016; Yang et al., 2010).

Naïve $CD8^+$ T cells which are activated by antigen and other signals from mature DC differentiate into effector (cytotoxic) T cells and proliferate rapidly. The function of cytotoxic $CD8^+$ T cells in the classical immune response is to clear infection, followed by apoptosis of most of the cytotoxic T cell population (Kumar et al., 2018). The functional response of cytotoxic T cells is production of perforin and granzymes, resulting in cell lysis, and ligation of Fas ligand on target cells, resulting in activation of apoptosis (Russell and Ley, 2002). This response has been studied in greater detail in the context of infection, rather than tumour cells and it has been suggested that the production of cytokines by cytotoxic T cells plays a greater role alongside lytic enzymes in tumour cell killing (Martínez-Lostao et al., 2015). Cytotoxic T cells produce inflammatory cytokines such as IFNγ and TNFα, they also produce IL-2, which promotes further expansion of both $CD4^+$ and $CD8^+$ T cells (Seder et al., 2008). Other effector molecules produced by some cytotoxic T cells which have recently gained interest are MIP1β and CD107a. MIP1β is a chemokine receptor and involved in attraction of macrophages in the context of an inflammatory response and CD107a is a marker of de-granulation. T cells capable of producing a greater range of effector molecules than perforin and granzymes, known as 'polyfunctional' T cells, have been shown to be effective in anti-viral

and anti-tumour responses (Perales et al., 2008; Precopio et al., 2007; Saunders et al., 2011).

Activation of T cells is also associated with upregulation of proteins designed to control cessation of the effector immune response, i.e. checkpoint proteins. As previously mentioned, DC provide activation signalling via CD80 and CD86, which bind to the CD28 activating receptor on T cells. However, T cells also express the checkpoint inhibitor CTLA-4, for which CD80 and CD86 have a higher affinity than CD28 (Linsley et al., 1994). It has been suggested that blocking of CTLA-4 has different effects on $CD4^+$ and $CD8^+$ T cells as CTLA-4 is more highly expressed on $CD4^+$ T cells, thus improved tumour killing outcomes may be achieved indirectly by re-activation of $CD4^+$ T cells providing activation signals to $CD8^+$ T cells. The other most commonly targeted checkpoint inhibitor expressed by T cells is PD-1. PD-1 is expressed as a delayed response to T cell activation, however its ligand is expressed on epithelial and haematopoietic tissue to preserve bystander tissue from excessive damage during an immune response; and thus co-opted to protect tumour cells from T cell killing (Topalian et al., 2015; Wei et al., 2017).

Effector T cells represent terminally differentiated $CD8^+$ T cells, however some antigen- activated $CD8^+$ T cells persist as memory T cells. Memory T cells are a crucial part of lifelong immune protection as they can persist for long periods in the absence of antigen stimulation but are more responsive to restimulation with lower levels of antigen, providing a faster secondary immune response than the initial antigen encounter. While the generation of a memory T cell response is an implicit aim of cancer immunotherapy, responses to 'tumour re-challenge,' i.e. a tumour antigen specific secondary immune response have not yet been widely measured beyond *in vivo* models (Moeller et al., 2005). Durable immune responses which have been observed in clinical settings (Rosenberg et al., 2011) may be indicative of immune memory controlling re-emergent tumour growth however it is difficult to assess this *in situ* or track as a long term clinical outcome. There are a number of different subsets of memory $CD8^+$ T cells, central memory (T_{CM}), effector memory (T_{EM}) and stem memory (T_{SCM}) (Gattinoni et al., 2011; Lin et al., 2009; Mescher et al., 2006; Wherry et al., 2003). It is not entirely clear

whether memory subsets are derived directly from naïve T cells or effector T cells (prior to replicative senescence) (Kumar et al., 2018). Memory T cell have differing primary functions; T_{EM} persist in peripheral tissues and produce more effector cytokines in response to restimulation, compared to lymphoid-homing T_{CM} which proliferate more in response to restimulation (Kumar et al., 2018; Sallusto et al., 1999; Willinger et al., 2005). The more recently described T_{SCM} do not produce cytokines but have self-renewal capacity and are capable of differentiating into T_{EM} and T_{CM} cells (Gattinoni et al., 2011). Both naïve and memory T cells have been suggested as the optimal 'product' in the T cell lifecycle to manipulate for therapeutic purposes. Memory T cells may be more easily activated and expanded *ex-vivo*, however, it has been shown that this is not necessarily an advantage; as less-differentiated T cells which have undergone fewer rounds of expansion persist for longer and mediate therapeutic responses (Chapuis et al., 2017; Klebanoff et al., 2012). Nevertheless, there is still much work to be done to best mimic the activation mechanism of naïve T cells discussed above to deliver an optimal T cell product. Details of the spectrum of existing cancer immunotherapy approaches, different forms of T cell immunotherapy and strategies to identify antigens for these different modalities is discussed further below.

1.3 Cancer immunotherapy

1.3.1 Types of immunotherapy

Immunotherapy is the term usually used to describe cancer therapy that is based on the use of the immune system. Successful immunotherapy must activate appropriate immune effector cells, inhibit or eliminate suppressive immune cells and overcome the suppressive effects of tumour cells. The main types of immunotherapy are: monoclonal antibodies, including immune checkpoint inhibitors (ICI), modified antibody products e.g. bi-specific antibodies or ImmTacs; cytokines, vaccines (cellular and non-cellular); oncolytic viruses, and adoptive cell transfer (ACT), including tumour infiltrating lymphocytes (TILs), chimeric antigen receptor (CAR) T cells and adoptive T cell therapy using endogenous or engineered TCR, some of which are discussed below. These approaches may also be used in combination; e.g. ICI and ACT (Houot et al., 2015). Non-immunotherapy approaches could also augment immunotherapy. RT can be used to induce immunogenic

tumour cell death, releasing antigens, DAMPs and promoting inflammation (Burnette and Weichselbaum, 2013; Salimu et al., 2015; Spary et al., 2014a). Chemotherapy can be used to deplete Tregs; this is often an essential priming strategy in the introduction of cellular immunotherapies (Ghiringhelli et al., 2007).

There is a vast number of clinical and pre-clinical studies of immunotherapy for different types of cancer, although few have been licenced for treatment, as the clinical outcomes are highly variable. Reasons for this include the introduction of immunotherapy at late stage disease, after the failure of other treatments, at which point due to disease factors (tumour aggressiveness) and immune factors (suppression and exhaustion of tumour associated effector immune cells) it is particularly difficult to have an effect. There is also great variation in the receptiveness of different cancer types to immunotherapy treatments, in that tumours considered immunologically 'hot' are expected to respond better to immunotherapy due to the presence of effector immune cells (T cells, NK cells etc.) and a relative lack of regulatory or suppressive immune cells (Tregs, MDSC etc.) in the TME (Fridman et al., 2012). Additional factors include the mutational burden, which can be a source of neoantigens and inflammation, which has a multifaceted contribution to the development of cancer, and the responses of immune cells in the TME (Alexandrov et al., 2013; Baniyash et al., 2013; Schumacher and Schreiber, 2015). Increased understanding of factors influencing successful immunotherapy outcomes means that the use of immunotherapy in different types of cancers, and the possibility of focusing on specific targets in a tumour, e.g. CSC, is a viable strategy.

ICIs reactivate tumour specific T cells (Hargadon et al., 2018). As discussed above, the two checkpoint protein targets of currently licenced ICIs are expressed in response to T cell activation, resulting in downregulation of the immune response which is intended as a control mechanism following clearance of infection. However, in context of chronic tumour associated T cell activation, T cell inhibition occurs. ICIs are largely reliant on the presence of antigen-experienced/ memory T cells in the TME, although it has been suggested that anti-CTLA4 therapy can effect T cells in secondary lymphoid

organs (Topalian et al., 2015). Additionally the quality of the 're-activated' T cell response requires that immunogenic antigens have been presented by the tumour cells (Houot et al., 2015; Pitt et al., 2016). Therefore this type of immunotherapy has shown the most effective results in cancers in which there is a higher burden of more immunogenic antigens (typically neoantigens), e.g. melanoma (Alexandrov et al., 2013). ICIs targeting the checkpoint proteins CTLA-4, PD-1 and PD-L1 have been approved for the treatment of melanoma, NSCLC and head and neck squamous cell carcinoma (HNSCC) (Hargadon et al., 2018). These tumours, particularly melanoma, are well suited to immunotherapy approaches in that there is typically an effector immune cell infiltrate that can be 'rescued' (i.e. reactivated) by ICIs.

The alternative to the various forms of antibody or viral immunotherapies is cellular therapy. This consists of indirect or direct activation of T cells. DC vaccination is an indirect approach aiming to activate T cells in an antigen-specific way. DC with optimal co-stimulatory signals activate naïve T cells in the lymph nodes followed by migration to the tumour site (Constantino et al., 2017; Melero et al., 2014). Antigens can be provided to DC in the form of viral vectors, peptides, or cell lysates. Another challenge of DC therapy is the myriad number of ways it can be administered; determining the optimal DC *ex vivo* production or *in* vivo targeting and peptide loading approach results in a complex journey to translational clinical research. There is a lack of consensus on the optimal protocol for DC generation (Constantino et al., 2017); resulting in essentially the use of different DC subsets in immunotherapy (monocyte or $CD34^+$ haematological precursor-derived), with antigen presentation characteristics potentially differing between these (Bol et al., 2016; Gardner and Ruffell, 2016). A DC vaccine, Sipuleucel-T, has been licenced to treat advanced PCa, which is discussed in more detail in later sections.

ACT involves an infusion of T cells to treat cancer, a direct approach to delivering activated T cells. The different types of ACT have different characteristics, for example the specificity and source of the infusion product, making them applicable to different types of cancer (Figure 1.5). The most basic type of ACT is TIL therapy; involving harvesting and expansion of

intratumoral T cells (Figure 1.5A). The infusion product is polyclonal, and the antigen specificity of the T cells is not known, as there is no clonal selection carried out and the activation protocol is non-antigen specific (e.g. anti-CD3 and IL-2). This works on the assumption that that the starting T cells are tumour specific, based on their location, thus it requires a sizeable population of memory T cells to be effective. TIL therapy has shown the most success in treating melanoma, which has a favourable 'immune contexture' for immunotherapy, in that there is typically high T cell infiltration into tumours, a high neoantigen burden and limited immune inhibition (Alexandrov et al., 2013; Andersen et al., 2016; Besser et al., 2013; Fridman et al., 2012; Rosenberg et al., 2011).

Other direct types of T cell therapy include endogenous/ engineered TCR T cell therapy and CAR-T cells (Figure 1.5 B-D). Unlike TIL therapy, the production process involves selecting T cells of a particular antigen specificity, from peripheral blood mononuclear cells (PBMC), instead of intratumorally. Thus the infusion product can be clonal; alternatively it could be polyclonal, containing multiple clonal populations recognising different (known) antigen targets, to reduce the possibility of antigen loss mediating tumour immune escape (Leung and Heslop, 2019). Clonal or polyclonal T cell infusions can also lead to epitope spreading, resulting in responses to antigens not targeted by the infusion (Rooney et al., 2014). Both endogenous and engineered TCR therapy (Figure 1.5 B, C) involve recognition of endogenously processed short peptide sequences presented by HLA Class I, which can be sampled from proteins localised anywhere within the cells or cell surface (Hinrichs and Restifo, 2013; Rooney et al., 2014). Excepting in the case of cancers which have an infectious aetiology, peptides presented to T cells are generally derived from self-protein TAAs. The interaction between endogenous TCR and self-epitopes is generally weaker than the same interaction with viral epitopes (Bollard et al., 2014; Rooney et al., 1995; Stone and Kranz, 2013). However, due to the greater frequency of self-TAAs, there is a large focus, and undeniable success thus far in the use of endogenous T cells to target tumour cells. Some self-TAAs include NY-ESO, MART, WT1 and MUC, many more have been described, and the categories of TAA are discussed further below (Cheever et al., 2009; Hinrichs and Restifo, 2013; Olsen et al., 2017; Stone and Kranz, 2013). The role of the endogenous T cell repertoire in responding

to tumour antigens is also evident, indirectly, in the mechanism of action of tumour vaccines (Melero et al., 2014). The vaccine approach mimics the immune response *in situ* by introducing tumour peptides 'upstream' of T cells; this typically involves priming and activating dendritic cells *ex vivo* against a tumour peptide. As mentioned briefly above, the most prominent example of this approach is the use of Sipuleucel-T in treating metastatic prostate cancer; however simple peptide-based vaccines have also demonstrated significantly improved survival outcomes in melanoma (Hodi et al., 2010).

CAR T cells possesses the antigen recognition capacity of an antibody/ B cell receptor, as the recognition domain is constructed from the single-chain variable fragment of an antibody (Figure 1.5D). CAR T cells thus recognise conformational, as opposed to endogenously processed epitopes and are only capable of recognising cell surface antigens. Effective CAR T cell stimulation also requires a high density of antigen expression on the cell surface compared to the affinity of TCR for HLA-peptide complexes (Harris and Kranz, 2016; Sadelain et al., 2013). The other crucial difference between endogenous/engineered TCR T cell therapy and CAR T cells is that the former is HLA Class I restricted, while the latter recognises antigen in an interaction independent of HLA Class I. This has implications in the widespread application of TCR therapies as it may be more difficult to find matched donors for infrequent HLA alleles. While T cells could be obtained from the peripheral blood of patients, it may be advantageous to isolate the T cells from healthy donors, as the T cells from patients may be dysfunctional and obtaining sufficient blood to isolate T cells may be detrimental to patients. The development of expansion protocols enables the generation of large numbers of cells from TAA specific T cells which are likely to be infrequent in healthy donors. CAR T cell therapy has been approved for the treatment of ALL by targeting surface expressed CD19 (Brentjens et al., 2013; Lee et al., 2015). Other CAR T cell targets under investigation in clinical trials include CD20 (to treat lymphoma), CD33, CD123 (each for treating AML) and solid tumour targets EFGRvIII, HER2 and CEA (Gomes-Silva and Ramos, 2018).

In this thesis, peptides were identified as potential epitopes for targeting by endogenous T cells/ TCR. Endogenous T cells, instead of engineered TCR,

were investigated for targeting CSC for several reasons. The use of engineered TCR is a relatively new area of T cell immunotherapy, and as such presented practical considerations relating to the development of novel antigen specific transgenic TCR in the timeframe of the project. Engineered TCR are disadvantaged in terms of co-stimulation signals, by concurrent expression of endogenous TCR which compete for CD3 binding (Comoli et al., 2019). Additionally, endogenous TCR could recognise off-target epitopes, and expression of multiple (i.e. endogenous and engineered) TCR α and β chains in a single T cell can lead to unpredictable antigen-recognition combinations (Comoli et al., 2019). Engineered TCR are aimed at overcoming the challenges presented by low affinity interactions between endogenous TCR and non-viral tumour TAA as a result of thymic deletion of strongly self-reactive T cells (Klein et al., 2014). However, since engineered TCR are not be subject to negative selection in the thymus this presents a greater possibility of off-target damage. High affinity TCR responses have been shown to have off-target responsiveness (Holler et al., 2003; Linette et al., 2013; Stone et al., 2015). However, it is acknowledged that the capacity of endogenous T cells to interact with a low density of HLA-peptide complexes, and the relatively 'broad' reactivity of TCR, means that the potential for off-target reactivity also exists with the use of endogenous T cells. Endogenous T cells have been tested in humans to target NY-ESO in melanoma and synovial cell sarcoma, hTERT and survivin in myeloma and NY-ESO, survivin, PRAME, SSX2 and MAGE-A4 in Hodgkin's and non-Hodgkin's lymphoma (Gerdemann et al., 2011; Hunder et al., 2008; Rapoport et al., 2011). Autoimmune responses by endogenous T cells to melanocytes expressing MelanA/MART-1 (Mandelcorn-Monson et al., 2003) nevertheless highlights the importance of careful selection of target antigens/ epitopes. In this thesis, expression of antigens of interest were compared to healthy tissue expression, to reduce the possibility of off-target damage (detailed in Chapter 4).

Endogenous peptide targets were investigated instead of evaluating potential CAR targets, due to the challenges of identifying a surface antigen suitable for CAR T cell therapy. Since most surface markers of CSC are also expressed by SC or other tissues in the body, these are not suitable CAR T cell targets. It was also not considered feasible within the time and funding constraints of

the project to both identify a novel antigen, expressed at a sufficiently high density and tumour exclusivity for CAR targeting, and develop the CAR. Additionally, the limited responses thus far demonstrated in CAR therapy of solid tumours (Hinrichs and Restifo, 2013; Sadelain et al., 2013) suggests that this approach does not have a clear advantage to T cell therapy using endogenous/ engineered TCR for treatment of solid tumours.

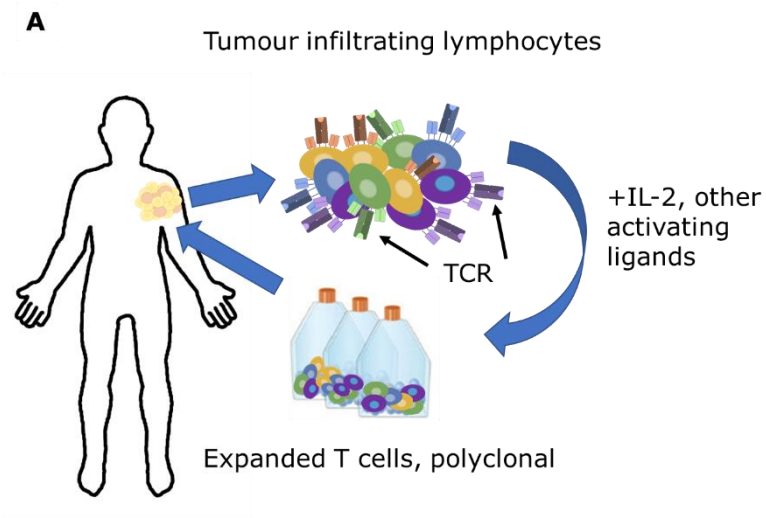

Specificity	Polyclonal
Receptor	Naturally occurring TCR
Target recognition	Intracellular epitopes
HLA restriction	Implicit HLA matching as product is derived from patient. Matching required to 'donate' TILs
Source	Patient: intratumoral

Figure 1.5 Types of immunotherapy involving direct manipulation of T cells. (A) TIL therapy involves extracting lymphocytes from the tumour site followed by *ex-vivo* expansion using cytokines that activate $CD8^+$ T cells. The resulting product is polyclonal as there is no selection involved. This approach has been particularly successful in melanoma, owing to the presence of antigen-specific T cells in the TME. Continued overleaf: (B, C) T cell therapy includes endogenous TCR/ engineered TCR. This involves harvesting PBMC and isolating T cells that recognise specific antigens. (B) Antigen specific T cells expressing endogenous TCR are activated and expanded using peptide stimulation and cytokines. (C) Engineered TCR involve analysis of TCR affinity to select a high affinity TCR, or modifications to an endogenous TCR to improve affinity for the epitope. Endogenous high affinity TCR are likely to be rare to due to negative selection in the thymus. The TCR is then transduced into peripheral T cells (which may express endogenous TCR not necessarily of the same antigen affinity) which are expanded for infusion. (D) CAR T cells consist of a synthetic receptor transduced into primary peripheral T cells. Determining the antigen specificity of the endogenous TCR expressed by the transduced T cells is not required. Antigen recognition is mediated by the scFV domain from an antibody and is not HLA Class I restricted. Second and third generation CAR designs have included co-stimulatory molecules such as CD28 and 4-1BB, and suicide genes to control the CAR response. TCR/ CAR depictions are adapted from Coulie et al., (2014)

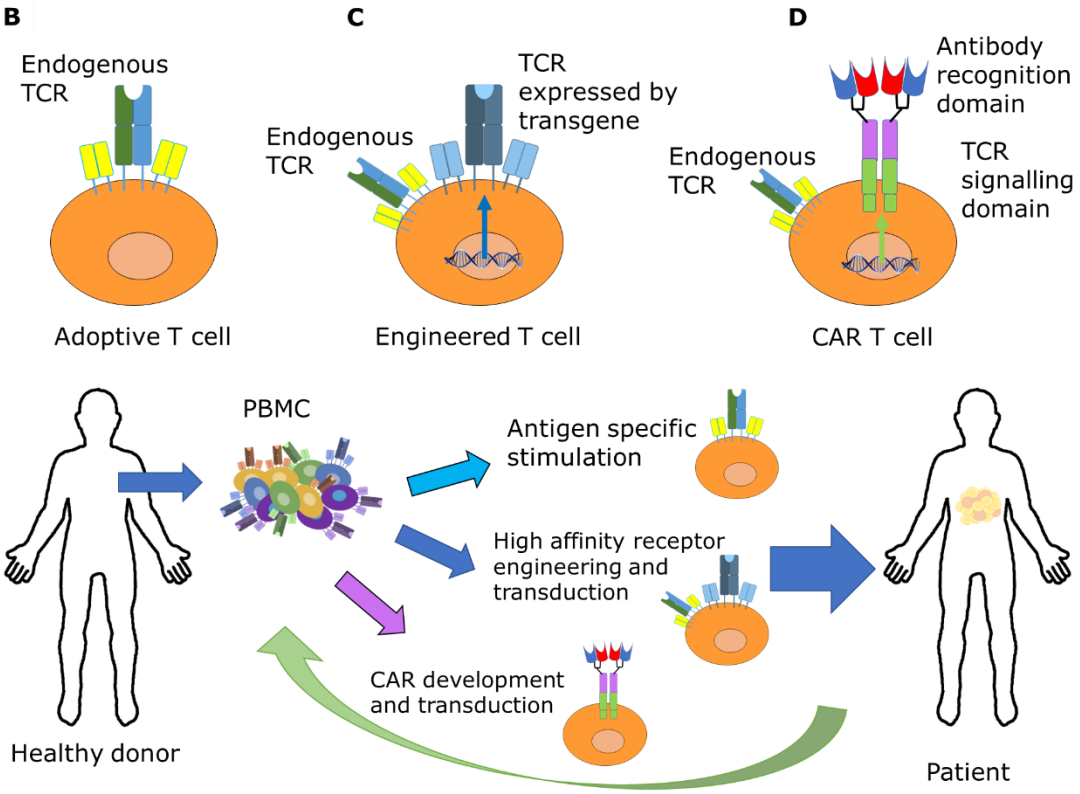

Type of T cell therapy	Naturally occurring T cells	TCR engineered T cells	CAR T cells
Specificity	Clonal/ polyclonal	Clonal/ polyclonal	Clonal/ polyclonal
Receptor	Naturally occurring TCR	T cell transduced to express specific TCR (may also express native TCR)	Engineered receptor consisting of modified BCR recognition domain combined with modified TCR signalling domain
Target recognition	Intracellular epitopes	Intracellular epitopes	Surface antigens
HLA restriction	HLA matching required	HLA matching required	Not HLA restricted
Source	Healthy donor/ patient PBMC	Healthy donor/ patient PBMC	Healthy donor/ patient PBMC

1.3.2 Tumour associated antigens

With the exception of cytokines and virus mediated cell lysis, immunotherapy requires antigen specific immune responses for effective tumour elimination (even if the antigen targeted is not known e.g. TIL therapy). Antigens are the way by which the adaptive immune system recognises cancer cells (and pathogens) (Coulie et al., 2014). $CD8^+$ (cytotoxic) T cells that recognise tumour antigens have the most potent cell killing capacity, as well as the potential for immune memory (Houot et al., 2015). Production of cytokines and chemokines, such as IFNγ, TNFα and MIP1β, by polyfunctional T cells also contributes to tumour cell elimination and recruitment of other anti-tumour immune cells (Dunn et al., 2006; Seder et al., 2008). The different types of tumour antigens are detailed in Table 1.2.

Table 1.2 The different types of tumour antigen. Source, healthy and malignant tissue distribution, examples. Adapted from (Coulie et al., 2014; Dunn et al., 2004b; sFinn, 2017; Ilyas and Yang, 2015)

Antigen type	**Source**	**Distribution**	**Example**
Neoantigen	Mutated self-protein	Specific to individual tumour/ clone	KRAS
	Spliced self-protein	Some cancers may be driven by oncogenes activated by spliced proteins, meaning multiple patients have the same 'mutation'	BCR/ABL (spliced gene) PMEL17 (spliced amino acid sequence)
Overexpressed	Non- mutated self- protein	Healthy tissues and tumours (differing	MUC1 HER2 hTERT

		expression levels)	
Differentiation	Non- mutated self-protein	Healthy (differentiated) tissues and tumours	MART1 CEA Tyrosinase PSA PAP
Cancer testis/ oncofoetal (lineage restricted)	Non-mutated self- protein	Tumours and specific lineages	MAGE family NY-ESO 5T4
Viral antigen	Virus	Tumours caused by viruses	HPV (cervical cancer) EBV

Viral antigens are the most immunogenic type of antigen as they represent both foreign antigens and pathogen associated molecular patterns (PAMPs). Viral antigens may be expressed by tumour cells in the cases of cancers which have an infectious pathology (~15% of all cancers), including human papilloma virus (HPV; cervical and other genitourinary cancers), Epstein-Barr virus (EBV; some types of lymphoma and stomach cancer) and Hepatitis B and C (HBV, HCV; liver cancer) (Stewart and Kleihues, 2003). Viral antigens can be targeted by prophylactic vaccination, eliciting an antibody response to prevent infection, rather than therapeutic vaccination targeting T cells to infected tumour cells presenting processed viral antigens, for example the HPV vaccine (Tumban et al., 2015).

Self-antigens are typically less immunogenic than viral antigens, owing to thymic deletion of highly self-reactive T cells during development of the T cell repertoire (Klein et al., 2014; Stone and Kranz, 2013). Nevertheless, self-antigens are currently the main antigen targets in cancer immunotherapy. Of the self-antigens, neoantigens would be expected to be the most

immunogenic as these are non-native peptide sequences arising as a result of mutations including gene translocations or splicing at the protein translation stage; proteasomal splicing can result in amino acid sequences not derived from a native protein sequence (Schumacher and Schreiber, 2015; Vigneron et al., 2004). While there are some known gene mutation hotspots leading to predicted neoepitopes e.g. KRAS (Finn, 2017); neoantigens are largely patient specific, requiring a personalised rather than widely applicable therapeutic approach. There is also a wide range in mutation burden across the different types of cancer (Alexandrov et al., 2013), making neoantigen load and discovery more or less likely depending on the cancer type (Schumacher and Schreiber, 2015). Cancer testis and oncofoetal antigens are expressed only in the testis or embryonic tissues respectively. These tissues are immune privileged and/ or the proteins may be only temporally expressed, thus the immune system does not become tolerant to them. Differentiation and overexpression antigens are common to both tumour and healthy tissues. Differentiation antigens, which are expressed in certain lineages of a tissue, have been identified in melanoma and the prostate, although spontaneous T cell responses against these antigens have only been demonstrated in melanoma (Coulie et al., 2014). Overexpression antigens are more highly expressed in cancer tissue, resulting in a differential threshold for T cell activation between healthy and tumour tissue due to the difference in antigen density (Buonaguro et al., 2011).

$CD8^+$ T cells recognise endogenously processed peptides in complex with HLA Class I (Figure 1.6). HLA Class I is expressed by all nucleated cells, including tumour cells, although tumour cell mutations may result in downregulated HLA Class I expression (Dunn et al., 2004b). HLA Class I presents peptides typically 8-14 (most commonly 9) amino acids in length (Mester et al., 2011). The peptides are derived by a multi-step processing mechanism. Proteins are degraded by the proteasome cleavage complex (Figure 1.6A). The different protease subunit activities of the proteasome can cleave acidic, basic and hydrophobic residues in proteins to derive peptides (Adams, 2003; Dick et al., 1998). There are two different proteasomes, the standard proteasome and the immunoproteasome (Guillaume et al., 2010). The immunoproteasome is expressed in immune cells and cells responsive to IFNγ and has subunits with different proteasomal activity, thus different

degradation processes result in the production of different peptide sequences (Figure 1.6B). Another specialised proteasome (the 'thymoproteasome') is expressed by thymic epithelial cells that mediate T cell selection during development, controlling the repertoire of peptides 'shown' to T cells (Klein et al., 2009; Murata et al., 2007). The availability of substrates, i.e. whole proteins, for the proteasomal degradation is influenced by protein-half life; additionally, more peptides are produced from proteins with a longer amino acid sequence (Bassani-Sternberg et al., 2015). The proteasome can also splice protein sequences to produce non-continuous peptides (Liepe et al., 2016). These proteasomes each produce peptides both smaller than possible to bind to HLA (<8 peptides in length) and larger than those eventually presented by HLA Class I; thus further processing occurs in the endoplasmic reticulum (ER) (Cascio et al., 2001; Kanaseki et al., 2006; Kisselev et al., 1999; Serwold et al., 2002). Translocation of peptides into the ER is controlled by the transporter for antigen processing (TAP) protein, which is located in the ER membrane (Figure 1.6C). TAP allows entry into the ER of degraded peptides ranging from 8-16 amino acids in length, in an ATP dependent mechanism (Androlewicz et al., 1993; Chang et al., 2005; Endert et al., 1994). Mutations in TAP commonly occur in cancer, resulting in immune evasion due to reduced peptide presentation (Evans et al., 2001). Further processing in the ER involves modification of the N-terminus of the peptide, the C-terminus sequence is typically determined by proteasomal processing. Processing in the ER is mediated by the Endoplasmic reticulum aminopeptidase associated with antigen processing (ERAAP) protein (Figure 1.6D) (Serwold et al., 2002). ERAAP displays both length and substrate preferences; peptides between 8-16 amino acids in length bind the cleavage site optimally however the presence of certain residues including a charged C terminal chain and upstream proline (Chang et al., 2005; Hongo et al., 2019; Kanaseki et al., 2006).

The HLA Class I protein-peptide complex is assembled in stages (Figure 1.6E). The partly folded α chain enters the ER and is bound to calnexin, which prevents aggregation of individual α chains (Bouvier, 2003). The association of β microglobulin with the α chain results in disassociation of calnexin (Williams et al., 2002). The HLA Class I protein is then associated with a complex of chaperone proteins, calreticulin and ERp57, and is anchored to

TAP via tapasin (Figure 1.6F) (Bouvier, 2003; Cresswell et al., 1999; Grandea and Van Kaer, 2001). These proteins are known as the peptide loading complex (PLC). Calreticulin and ERp57 provide an enclosure type complex which promotes the correct conformational refolding of the HLA Class I α chain and β microglobulin (Bouvier, 2003). In addition to bridging the folded HLA protein to TAP, tapasin is involved in the recruitment of the components of the PLC (Williams et al., 2002). Peptides produced by ERAAP can then bind the HLA protein, within the ER (Figure 1.G). Peptide binding results in completion of folding of the HLA complex which is then exported from the ER and shuttled to the cell surface via the golgi complex, and can then interact with the cognate TCR (Figure 1.6H) (Williams et al., 2002). High affinity binding between peptide and HLA Class I in the binding pocket is correlated with stability of the complex at the cell surface, which may increase likelihood of interaction with T cells, however this is not necessarily a predictor of immunogenicity (Calis et al., 2013; Harndahl et al., 2012). As discussed above, different types of antigens may be more likely to elicit an immune response based on development of the T cell repertoire which selects or deflect TCR which will recognise the antigens; however, antigen processing exerts a strong influence on whether peptides from more immunogenic antigens may ever be shown to the T cells. Thus both T cell recognition and antigen processing must be considered in approaches to discovering novel antigens (Akram and Inman, 2012; Müller et al., 2017).

As well as immunogenicity and tissue specificity, the importance of an antigen for clinical investigation is ranked by the National Cancer Institute (NCI) based on: the evidence for its therapeutic function, the oncogenic role of the antigen, the number of cells expressing the antigen in a tumour, the frequency of antigen expression in patients, the cellular localisation of the antigen and evidence for antigen expression in cancer stem cells (Cheever et al., 2009). Of the 75 antigens reviewed by the study, just over 60% (46/76) were found to be immunogenic in a clinical setting. This could be due to several factors, including patients expressing the antigen at a low level or not at all, or lack of responsive T cells. Therefore, there is still a large scope for antigen discovery.

Figure 1.6 Antigen processing and peptide presentation, to $CD8^+$ T cells in the HLA Class I pathway. (A) Proteins are degraded by the proteasome, which has subunits with differing protease activities, enabling catabolism of different polypeptide residues. (B) The immunoproteasome is a comparable structure which is expressed in cells responsive to IFNγ. (C) Polypeptides, which are longer than the peptides eventually loaded onto HLA Class I are translocated to the ER by the TAP transporter. (D) ERAAP performs further processing to trim peptides to the optimal length to stably bind HLA; different HLA Class I alleles have different preferences in both length and binding motifs, of the peptide sequences which eventually bind. ERAAP processes the N-terminal end of the polypeptide and is influenced by both the sequence length of the polypeptide, in terms of fitting into the enzyme's two active sites, and in terms of the amino acids present in the N-terminus of the polypeptide, preceding the peptide which is eventually loaded into HLA. (E) HLA Class I alleles are partly assembled in two stages prior to peptide loading. (F) The HLA Class I α chain is initially bound to chaperone protein calnexin, followed by association with the chaperone proteins calreticulin and ERp57 which promote correct refolding with β microglobulin. The additional accessory protein in the PLC is tapasin, which anchors the HLA to TAP. (G) Peptides generated by ERAAP can then be bound to the re-folded HLA Class I protein. 'Empty' HLA proteins are instable and are not presented at the cell surface. (H) HLA Class I - peptide complexes are shuttled to the cell surface from the ER, via the golgi apparatus and can interact with the cognate TCR at the cell surface. The affinity of peptide binding in the HLA binding pocket influences the stability of the complex, which may impact cell surface expression.

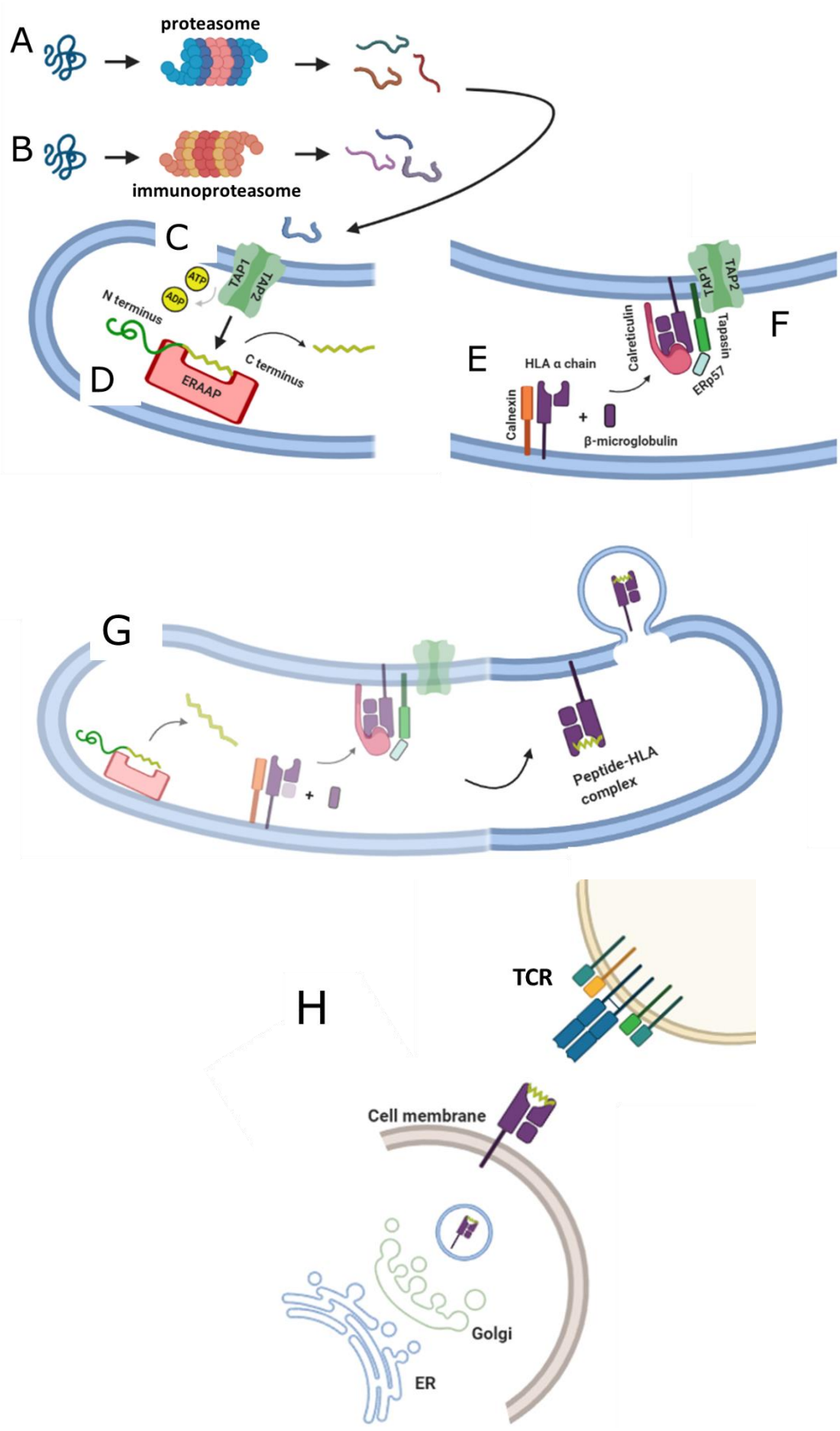
A
proteasome
B
immunoproteasome
C
TAP1
TAP2
ATP
ADP
N terminus
C terminus
D
ERAAP
E
HLA α chain
Calnexin
+
β-microglobulin
Calreticulin
TAP1
TAP2
Tapasin
ERp57
F
G
+
Peptide-HLA complex
H
TCR
Cell membrane
Golgi
ER

1.3.3 Identification of antigens/ epitopes for cancer immunotherapy

TAA can be identified experimentally or by predictive methods. Some of the stages of antigen processing investigated to derive potential tumour epitopes are shown in Figure 1.7. The first characterised antigen, MAGEA3, was identified in melanoma by screening T cell responses to a panel of sub-cloned melanoma cell lines, and establishing the line harbouring the 'rejection antigen' based on T cell killing or lack thereof (Figure 1.7A) (van der Bruggen et al., 1991). Serological analysis of expression cDNA libraries (SEREX) is another technique based on gene expression analysis to identify a potential antigen (Figure 1.7B). SEREX was used to identify the NY-ESO antigen based on B cell recognition (antibody responses) (Chen et al., 1997). $CD8^+$ T cell epitopes from the NY-ESO protein were later identified, and form the basis of TCR therapy targeting NY-ESO (Gnjatic et al., 2006; Jäger et al., 2000, 1998).

HLA ligandome analysis, also known as immunopeptidomics, involves direct analysis of peptides presented in the context of HLA molecules, most commonly HLA Class I (Figure 1.7C). This is the method used in this thesis to identify antigens of PCa cells, which was combined with other techniques to identify potential CSC antigens. It involves immunoprecipitation of HLA-peptide complexes, and analysis of the eluted peptides by mass spectrometry. This approach does not require screening using patient derived T cells or serum. Therefore, it may be more relevant for identifying antigens in cancer types for which there are less frequently described immune responses. This method is high throughput, although labour intensive and technical and requires a high volume of sample input (tumour tissue or cells).

HLA ligandome analysis typically identifies self-peptides, as the annotation of spectral sequences uses existing self-protein databases. Identification of neoantigens by HLA ligandome analysis requires generation of a *de novo* protein database that includes mutated proteins. This approach was taken in a recent study of melanoma by Kalaora and colleagues, in which whole exome sequencing and RNAseq performed on melanoma samples was used to generate a reference library to annotate the peptide mass spectrometry data (Kalaora et al., 2018). Perhaps surprisingly, considering the typical

mutational load in melanoma (Schumacher and Schreiber, 2015) the number of neoantigens was a tiny fraction of the peptides presented; only 5 neoantigens were identified. However, the neoantigen TAA reactive T cells comprised a much greater fraction of the overall TIL than the self-TAA reactive TIL (64.6% vs 16.4%). An important contrast between HLA ligandome analysis and the T cell rejection antigen or SEREX methods is that the latter integrates testing of the immunogenicity of the antigen, as the peptides are identified based on immune cell responses. Additional analysis is required to identify peptides of an HLA ligandome dataset that elicit T cell responses.

Many other studies have carried out HLA ligandome analysis to investigate the endogenous self-antigen repertoire of tumour cells, including leukaemia, glioblastoma, CRC, and ovarian cancer (Berlin et al., 2016; Bilich et al., 2019; Löffler et al., 2018; Neidert et al., 2018; Schuster et al., 2017). The changes in the peptide repertoire in response to IFNγ, attributable to expression of the immunoproteasome, which has altered catalytic subunits, has also been investigated, showing that some antigens are processed exclusively by one of the proteasomes (Chong et al., 2018; Guillaume et al., 2010). Non-mutated, tumour specific TAA are likely to be important for the development of T cell immunotherapy to treat cancers with a low mutational burden, e.g. AML and CML (Alexandrov et al., 2013). Several immunopeptidomics studies show clinical relevance of these antigen datasets by demonstrating the immunogenicity of the self-TAA identified. Specific responses to peptides from AML $CD8^+$ T cells compared to those from healthy $CD8^+$ T cells were observed by Berlin and colleagues, while a novel cancer testis antigen, *SUV39H2,* was also discovered by Kochin and colleagues which elicited a $CD8^+$ T cell response from healthy donors PBMC (Berlin et al., 2016; Kochin et al., 2017).

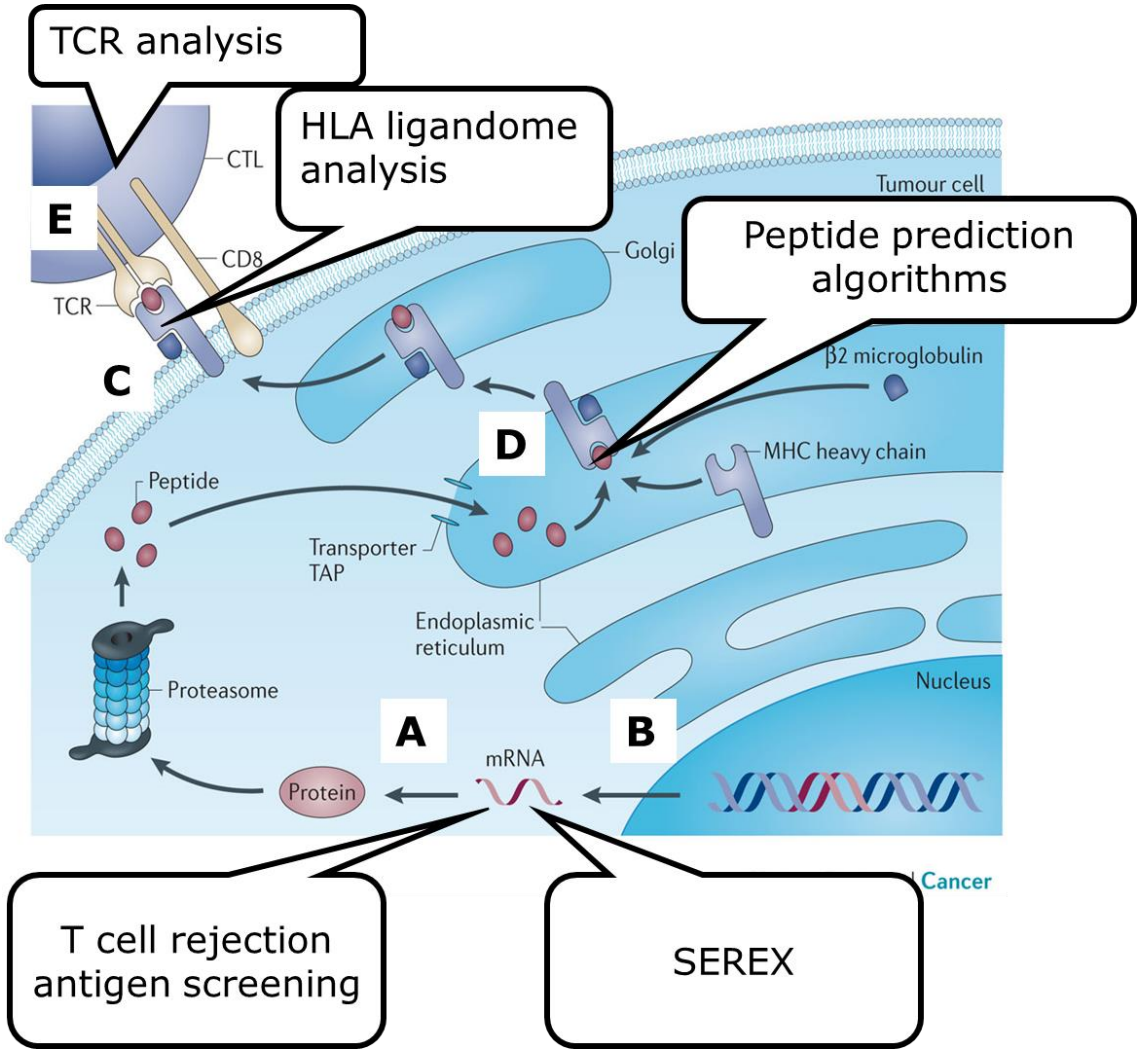

Figure 1.7. Methods for the identification of prospective epitopes based on stages of antigen processing. (A, B) The T cell screening of rejection antigens and SEREX methods involve cloning cDNA into vectors and expressing the DNA in tumour cells or *E.coli*, to produce peptide or protein targets respectively. Target recognition is tested by T cell killing of transfected tumour cells or antibody production by patient serum, respectively. (C) HLA ligandome analysis involves analysing peptides presented by HLA at the cell surface. Current methods for isolation involve immunoprecipitation, previously HLA-peptide complexes were isolated by acid elution. Recovery of HLA-peptide complexes by either method has a low return, therefore the peptides identified represent a 'snapshot' of the cell ligandome. (D) Prediction algorithms suggest potential peptides based on HLA binding data; some prediction tools also incorporate protein processing prior to HLA loading (TAP transporter and ERAAP chaperone modifications and proteasomal cleavage). Different algorithms make predictions based on experimental affinity data, structural data and ligand datasets. Figure adapted from Coulie et al., 2014.

Antigen/ peptide prediction algorithms have been developed to complement experimental approaches. Databases hosting such algorithms include the Immune Epitope Database (IEDB), RANKPEP, HLAPred, NetMHCpan, NetMHC, SYFPEITHI and BIMAS (Bhasin and Raghava, 2007; Guan et al., 2003; Nielsen et al., 2007; Rammensee et al., 1999; Soria-Guerra et al., 2015; Vita et al., 2019). Peptide prediction (IEDB) was used in this thesis to interrogate the HLA ligandome of the DU145 cells. Prediction of potential epitopes involves identifying which peptide sequences from a protein could be presented to T cells, based on binding to HLA molecules, such that high binding affinity peptides are suggested as candidate epitopes (Figure 1.7D). There are few available algorithms for modelling of HLA Class II interactions, as the prediction of peptide binding to HLA Class II is more complex than predicting HLA Class I-peptide interactions, owing to the greater peptide length of the former. These algorithms integrate experimental binding affinity data and/ or data from eluted ligands for epitope prediction. The IEDB also has an integrated tool for predicting proteasomal cleavage sites, TAP transport and binding affinity to HLA Class I. However, it remains that predictive methods naturally lack the accuracy of direct identification of antigens presented by tumour cells, as an epitope predicted from a whole protein sequence may not be processed *in vivo*.

Nevertheless, predictive algorithms have an advantage of being far less labour intensive than experimental methods to identify potential epitopes from antigens. In this thesis, prediction algorithms were applied to peptides known to be processed and presented by HLA Class I, since the HLA-peptide complexes were captured by immunoprecipitation. Therefore, the uncertainty as to whether the peptides were naturally presented was greatly reduced. Predictive methods also reduce the experimental labour required to test peptide immunogenicity as it narrows down the number of peptides tested (to those predicted to undergo antigen processing and HLA presentation). Several clinically relevant epitopes have been identified by the application of prediction methods to previously identified antigens. This includes a HLA-A*02 epitope from MAGEA3 (van der Bruggen et al., 1994); the first epitope identified from this TAA was HLA-A*01 restricted and was identified by the T cell recognition of a rejection antigen method (van der Bruggen et al., 1991). Additionally, an epitope from the leukaemia oncogene BCR-ABL was identified

(Bosch et al., 1996). Antigen prediction databases have a reciprocal relationship with *de novo* HLA ligandome generated data, as the data deposition helps improve prediction algorithms while predictive tools can be used to simplify the analysis pipeline or enable selection of HLA-allele specific targets. Algorithms could also be used to investigate immunogenicity; an algorithm has recently been developed based on immunisation data in mice, which suggests that the amino acids at positions p4-6, and whether these amino acids have large side chains particularly contribute to the immunogenicity score (Calis et al., 2013). Considering the shape of the HLA-peptide binding pocket, the amino acids in these positions are most likely to protrude out of the cleft and contact the TCR; this may be augmented by the side chain of the amino acids in this position (ibid). This could be useful for selecting targets from large antigen datasets, however, evaluation of T cell responses *in vitro* and pre-clinical models remains essential for selecting epitopes for clinical evaluation.

There are a small number of approaches which instead analyse the TCR with the aim of identifying the cognate peptide (Figure 1.7E). The complexities of this approach are evident in the genetics of TCR expression and the promiscuity of TCR-peptide binding (Morris and Allen, 2012; Newell and Becht, 2018; Wooldridge et al., 2012). As previously discussed, T cell development involves random recombination of segments of the TCR β and α chain, a physiological phenomenon as yet not deconvoluted by computational prediction algorithms, although this technology is rapidly improving (Lanzarotti et al., 2019; Ogishi and Yotsuyanagi, 2019). TCRs can be analysed using flow cytometry using antibodies against the α and β chains, however this only provides basic information as to the expressed α and β chains in a given sample, limited to antibody availability (Miles et al., 2011). This approach can provide information as to the clonality of a T cell response (many TCRs vs. few predominant TCR), which may be useful in the clinical setting, however, it does not provide information as to the TCR, in particularly the CDR3 (peptide recognition domain) sequence. Analysis of the TCR is performed by high through-put sequencing, which can be carried out on a bulk T cell population or single clones. The former can give a measure of the diversity of receptor chains present in a sample while the latter allows for analysis of TCR α and β chain pairs (Rosati et al., 2017). Some approaches

involve sequencing only the β chain as the Vβ gene locus has a greater capacity for diversity than the Vα chain locus, as discussed previously in the context of T cell development (Miles et al., 2011; Rosati et al., 2017). Single cell TCR analysis requires high-fidelity flow cytometry sorting of clonal T cell populations and a PCR-based pre-amplification step using primers for regions of the TCR α and β chains, prior to sequencing (Miles et al., 2011). In this way, the full TCR sequence and CDR3 region sequence can be determined, although this does not yet allow for accurate prediction of a cognate antigen sequence (Bridgeman et al., 2012). However, detection and measurement of the clonality of a T cell infusion product, or analysis of the receptor diversity in a patient that responds to immunotherapy represent important clinical applications of TCR analysis (Schrama et al., 2017). T cell receptor Vβ sequencing of two different ACT therapeutic protocols by Chapuis and colleagues showed that a polyclonal infusion product persisted in patients and was associated with better therapeutic responses, compared to a monoclonal infusion product, despite the polyclonal product giving rise to a low number of dominating clones (Chapuis et al., 2017). TCR β-chain repertoire analysis can also be used to diagnose T-LGL, since malignant clonal expansion of T cells is a characteristic indicator (Qiu et al., 2015). In prostate and pancreatic cancer, both considered 'cold' or poorly immunogenic, TCR sequencing revealed T cell infiltration and clonal expansion, suggesting that both these tumours could perhaps only be considered 'cold' due to failure of current therapeutic strategies to activate the T cells *in situ*, rather than primary failure of the immune system to engage the tumours (Poschke et al., 2016; Sfanos et al., 2009).

Crystallisation and structural analysis can also provide in insight into 3D interactions between TCR and HLA-peptide complexes, which may not be evident based on analysis of 2D sequences, however, production of TCR crystal structures also relies on sequencing of the TCR. The constant development and improvement in techniques for analysing and interpretation data pertaining to TCR has enabled the collection of datasets of TCR with known peptide specificities, for example 'VDJdb' (https://vdjdb.cdr3.net/) (Shugay et al., 2018). This has likely influenced the development of predictors of peptide sequences from TCR sequence data, such as the recently developed 'TCRex' (https://tcrex.biodatamining.be/) (Gielis et al., 2019).

Peptide library and yeast display techniques can provide a systematic approach to identifying the cognate peptide of a TCR which measure TCR responses rather than determining the cognate peptide based on analysing the TCR sequence or structure (Bijen et al., 2018; Gee et al., 2018). By testing the responses of TCR to each possible amino acid in a 9mer sequence, these approaches also provide the capacity to engineer higher affinity TCRs (S. N. Smith et al., 2015).

1.4 CSC immunosurveillance and immunotherapy

1.4.1 Interactions between CSC and the immune system

The CSC hypothesis of cancer development and the Immunoediting theory of cancer development have been discussed extensively above. These hypotheses arose largely independently of each other, because CSC experiments, particularly *in vivo* tumorigenesis, are performed in immunocompromised animals, out of necessity, using minimal cell numbers to demonstrate the efficiency of cancer initiation. On the other hand, immunosurveillance and immunotherapy experiments involve testing the immune system's response to tumour growth, which is induced by larger cell numbers without identifying CSC in immunocompetent animals. It is not known when, in the course of tumour development, that CSC-immune system interactions become important.

Many of the immunomodulatory characteristics of CSC, including production of inhibitory cytokines, recruitment of suppressive immune cells, downregulated antigen presentation and modulation of the TME have been described in unfractionated tumour cell populations (Campoli and Ferrone, 2008; Stassi et al., 2003; Wang et al., 2004). Additionally, experiments comparing immunomodulatory characteristics are conducted using matched numbers of CSC and non-CSC, which does not reflect the typical frequencies of these populations in an *in-situ* tumour. Therefore, it is important to consider CSC immunomodulation as relative to the immunosuppressive effects of non-CSC and the tumour as a whole. Nevertheless, at an individual

level, enhanced inhibition and evasion capacity of CSC compared to non-CSC, and the existence of an even more immunosuppressive niche, the CSC niche, within the TME, impacts on therapeutic targeting of CSC.

It has been suggested that CSC reside in a niche in tumours (Figure 1.8), although this has not been elucidated in most tumours. The characteristics of the CSC niche are considered similar to the SC niche, which is well established for most organs (Kise et al., 2016). Autocrine and paracrine signalling in the SC niche maintain the SC phenotype (Figure 1.8A), including expression of stemness genes and control of differentiation; it is assumed that differentiation is in part a gene expression program but is also influenced by the SC progeny leaving the niche and its signalling factors (Cabarcas et al., 2011; Voog and Jones, 2010). As well as maintaining the stemness phenotype, the SC niche is immunosuppressive, as a tissue protective mechanism. This immunosuppression occurs by inhibition of immune effector cells by signals from the SC and stromal cells of the SC niche (Kim et al., 2009; Krampera et al., 2006). Various SC have also been shown to express low levels of HLA Class I (Le Blanc et al., 2003). A study that investigated immunosurveillance of stem cells demonstrated that quiescent stem cells evaded the $CD8^+$ T cells by downregulating antigen processing and presentation (Agudo et al., 2018), while also evading killing by NK cells. This mechanism was reversed upon entry into the cell cycle, and cycling SC were subject to immunosurveillance by T cells (Figure 1.8B). This suggests that slow cycling stem cells could accumulate mutations over time, without being subject to immunosurveillance and elimination. Thus, immunoediting of CSC may occur over a prolonged equilibrium stage (Figure 1.8C). This is supported by evidence of mutations acquired in leukemic SC prior to transformation by a driver mutation (Welch et al., 2012). It has been suggested that the transformative mutation required to generate CSC from SC should confer niche independence, or result in transformation of the SC niche (Figure 1.8D) (Packer and Maitland, 2016). Therefore, CSC may have superior immunosuppressive characteristics than even SC, as they have adapted to evading the immune system following transformation.

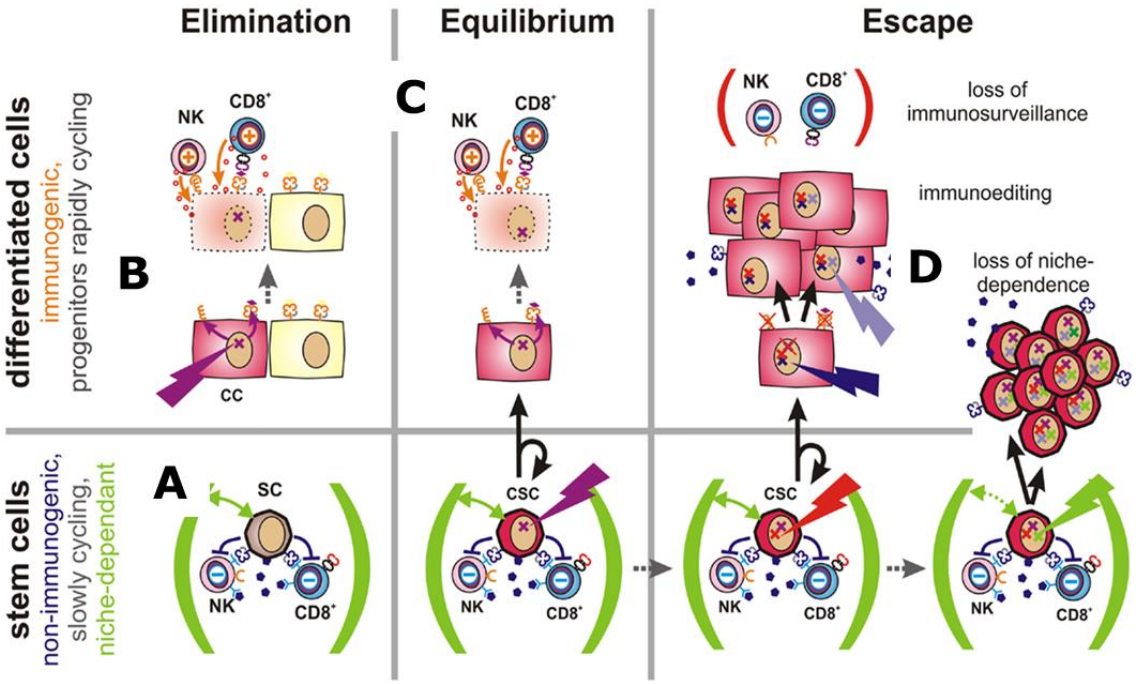

Figure 1.8. How CSC could fit into the immunoediting hypothesis. (A) In the SC niche, SC are protected from immunosurveillance, by various mechanisms including immune inhibition (NK and T cell), downregulated HLA Class I and potentially slow cycling. (B) Upon acquisition of an oncogenic mutation, stress related upregulation of immune signalling receptors e.g. NKG2D receptors, production of DAMPS, alerts the immune system, and elimination occurs. (C) SC, being susceptible to transformation, accrue mutations over their lifespan, and interact with the immune system in an equilibrium state. This resulting in selective pressure which could, in the lifespan of the individual, result in CSC and/ or their progeny acquiring mutations enabling the CSC lineage to evade the immune system, resulting in tumour development. Once a TME is established, reciprocal signalling between CSC and the TME maintains the CSC niche. The CSC niche may be less immunogenic and possess additional capacity for immune inhibition owing to distinct characteristics of the CSC within. Figure modified from Bruttel and Wischhusen., 2014.

There are varying degrees of evidence suggesting CSC possess unique or enhanced immune inhibition or evasion capacity compared to non-CSC. These data suggest that conditions in the TME and CSC niche could simultaneously benefit CSC and inhibit immune cells, respectively. As previously mentioned, CSC respond to hypoxia by upregulated HIF1α, resulting in downstream signalling conferring apoptosis resistance, proliferation and migration; (Corzo et al., 2010). Contrastingly, hypoxia can inhibit an anti-tumour immune response in a number of ways. Dysfunctional vasculature induced by hypoxia impairs immune cell infiltration (Vaupel and Harrison, 2004). Hypoxia has also been shown to upregulate PD-L1 expression in DCs and breast and PCa cells (Barsoum et al., 2014; Peng and Liu, 2015). On the other hand, HIF1 signalling is required in $CD8^+$ T cells to maintain the glycolytic metabolism associated with effector functions such as perforin and granzyme production (Finlay et al., 2012). HIF1α signalling in $CD8^+$ T cells is also advantageous under conditions of chronic antigen-specific activation (viral infection) (Doedens et al., 2013). Despite this anti-tumour effect of hypoxia, $CD8^+$ T cells are not highly effective in the TME, which may be due to competition for glucose between T cells and cancer cells which restricts T cell differentiation and cytotoxicity.

CSC signalling (Section 1.1.3 Characteristics of CSC) may have an inhibitory effect on immune cells, however, targeting these pathways may also inhibit immune cells (Figure 1.9) (Codd et al., 2018). For example, TGF–β produced by stromal cells contribute to the stemness phenotype, however TGF–β has an immunosuppressive effect by recruiting Tregs and also T helper 17 (T_H17) cells (Plaks et al., 2015). IL-6 signalling occurs in CSC by paracrine and autocrine mechanisms and is an important contributor to tumorigenicity of CSC. In breast cancer, CSC can produce IL-6 which recruits mesenchymal stem cells (MSC) which produce IL-6, creating a signalling loop which increases tumorigenicity of the CSC (Liu et al., 2011). MSC have a wide range of immunosuppressive effects, including inhibiting maturation of DCs and inhibition of proliferation by T cells and NK cells (Zhao et al., 2010). The effects of IL-6 signalling on immune cells in the CSC niche are diverse; IL-6 is an inflammatory cytokine, but it has been shown to skew T cells towards a $CD4^+$/ Th2 T cell phenotype (Rincón et al., 1997), which is considered mainly tumour promoting (Ellyard et al., 2007). Another way in which an

inflammatory immune response may inadvertently promote CSC survival is by activation of the NF-κB signalling pathway. NF-κB signalling is activated by cytokines including IL-1, TNFα and IL-6, produced by cytotoxic T cells, M1 macrophages, activated stroma and CSC; and also, by hypoxia and ROS. However, NF-κB mediated gene expression in CSC results in proliferation, apoptosis resistance, EMT and remodelling of the ECM. Genes under the control of NF-κB relating to these outcomes include cyclins, Bcl-2 and Bcl-xL, MMPs, Twist, Snail and Slug (Rinkenbaugh and Baldwin, 2016). NF-κB has been shown to be upregulated in CSC compared to non-CSC; in leukaemia, PCa, glioblastoma, breast and pancreatic cancer (Garner et al., 2013; Guzman et al., 2001; Murohashi et al., 2010; Rajasekhar et al., 2011; Vazquez-Santillan et al., 2015). The role of NF-κB signalling in CSC may highlight an important early interaction between CSC and the immune system. NF-κB mediated CSC survival and proliferation induced in response to inflammatory anti-tumour immune responses could represent a mechanism by which CSC escape immunosurveillance.

CSC may also recruit inhibitory and regulatory immune cells, furthering the production of immunosuppressive cytokines and mediating direct inhibition of effector immune cells. Melanoma CSC were found to express CD86 more highly than non-CSC; this induced a $CD4^+$ $CD25^+$ $FoxP3^+$ Treg phenotype from naïve PBMC, which produced IL-10 (Schatton et al., 2010). CSC may evade effector immune cells by disrupting optimal antigen presentation, by downregulation of HLA Class I and low expression of antigen processing machinery, as in glioblastoma CSC (Di Tomaso et al., 2010). CSC have also been suggested to express higher levels of the inhibitory receptors CD200 (Kawasaki et al., 2007). CSC have been shown to produce IL-4 and express the IL-4 receptor, which was protective against apoptosis induced by chemotherapy in CRC CSC (Todaro et al., 2007). Inhibition of apoptosis by IL-4 signalling is mediated by upregulation of cFLIP and BCL-x_L and downregulation of FasL (Conticello et al., 2004) which could also be protective against T cell killing.

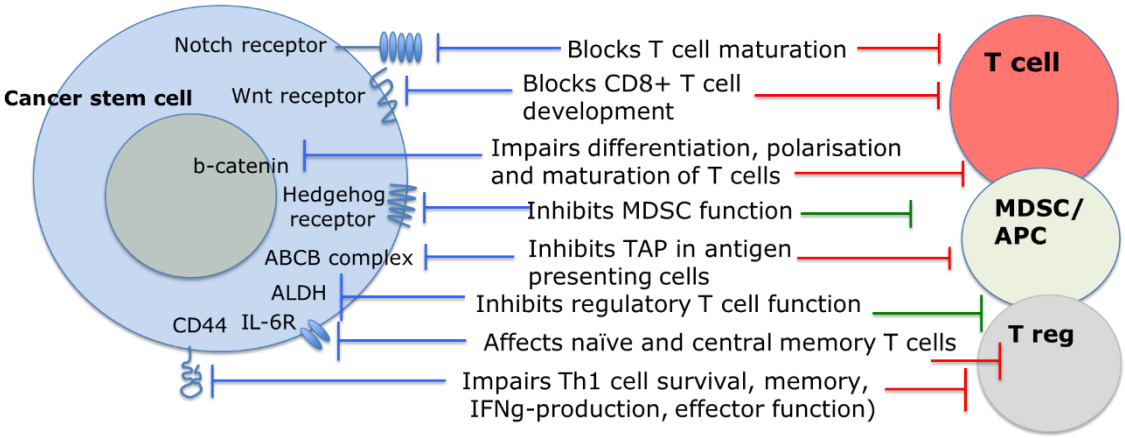

Figure 1.9. The potential impact on immune cells, of targeting CSC associated signalling pathways or markers. In addition to modulating the immune system as a collective population, exogenous modulation of CSC by therapeutic approaches could have off-target effects on an immune response, some of which could be detrimental to anti-tumour immunity. Red/ green arrows indicate therapeutic approaches against CSC that may have a correspondingly positive/ negative effect respectively on immune responses, if blocked in immune cells. For example, some markers of CSC; CD44 and ALDH have functional roles in Th1 responses, although blocking ALDH could also block Treg function. SC signalling pathways, including some previously discussed in the context of CSC, function in the development and effector responses of T cells (NOTCH, Wnt). Adapted from Codd et al., 2018.

1.4.2 Targeting CSC with immunotherapy

The interactions between CSC and the immune system suggest there may be additional challenges in designing immunotherapy to specifically eliminate CSC. Immunotherapy of CSC could be effectively combined with targeting of the CSC niche e.g. using RT (Ogawa et al., 2013). Thus far, anti-CSC preclinical immunotherapy strategies have mainly involved cellular therapies, as this allows for antigen specific targeting (there is currently no available clinical data on treating CSC). Antigen specific targeting of CSC requires deciding whether to target a CSC specific or shared (also present on non-CSC) antigen. Hirohashi and colleagues suggest that the optimal effector: target ratio of T cells to CSC occurs by directing the T cells against a CSC specific antigen rather than a shared antigen (Hirohashi et al., 2012). Targeting a CSC specific or shared antigen has shown that targeting the CSC specific antigen afforded significantly greater tumour control (Morita et al., 2016; Nishizawa et al., 2012).

Targeting markers also expressed by SC may risk off-target damage. Some CD44 isoforms are specifically associated with CSC, which may allow safe targeting. However, a phase I clinical trial testing CD44v6 targeting with an immunoconjugate consisting of anti-CD44v6 antibody and antimicrotubule agent had to be halted due to severe skin toxicities (Riechelmann et al., 2008). To counteract off target toxicities, a preclinical study in leukaemia engineered a suicide gene into a CAR for T cell therapy targeting CD44v6. This was shown to have anti-tumour effects *in vivo* and adverse monocyte depletion effects could be rescued by activation of the suicide gene (Casucci et al., 2013, 2012). Therefore, the greater control of targeting afforded by this therapeutic design could represent a safer way to target CD44v6 CSC. Several studies have investigated ALDH-based CSC targeting. One preclinical study demonstrated CSC specific targeting *in vivo,* resulting in effective tumour immune control in melanoma and squamous cell carcinoma (SCC) (mouse models) (Hu et al., 2016). The CSC therapy consisted of DC activated by ALDH high CSC lysates and was given after surgical resection (SCC) or in the minimal residual disease state (melanoma). The CSC targeting strategy in SCC prevented relapse and increased survival, while lung metastasis was inhibited in the melanoma model. These effects were accompanied by

reduced CSC in the tumour, and ALDH high specific cytotoxic T lymphocyte CTL activation (tested *in vitro* at the end of the treatment). The disease settings are particularly interesting as they demonstrate the success of CSC targeting to prevent disease relapse, compared to most other models which investigate the targeting of CSC to prevent primary tumour growth or treat a tumour *in situ*. This approach warrants investigation for PCa, as it could reduce relapse occurring following successful first line treatment for localised disease. Relapse followed by progression is the main cause of mortality in PCa, discussed below. An ALDH antigen has also been targeted by $CD8^+$ T cells, in HNSCC, and breast cancer, including secondary lung metastasis *in vivo* (Visus et al., 2011). The ALDH target was identified as a naturally presented antigen by mass spectrometry analysis of an immunogenic HNSCC cell line (Visus et al., 2007), which is a novel way of identifying endogenously presented CSC antigens. Crucially this study also evaluated safety aspects of targeting ALDH, finding that endogenous ALDH antigen presentation was not sufficient to activate specific CTLs. Targeting this antigen led to not only primary tumour control but prevented lung metastasis in a primary resection breast cancer model *in vivo* (Visus et al., 2011). ALDH-directed CSC therapy is also currently being investigated in clinical trials. Patient derived ALDH high or ALDH low CSC are being used to load DC to test for *in vitro* T cell cytotoxicity in lung cancer (NCT02084823) and CRC (NCT02176746).

Other studies have used antigen identification techniques as described above, to identify novel CSC antigens. The aim of this is to identify TAAs and avoid targeting antigens shared with SC. The same immunogenicity and safety considerations exist for selecting a CSC antigen as any other prospective TAA. The additional challenge of verifying a therapeutically useful CSC antigen is evaluating both T cell killing and tumour control, to determine if specific targeting of CSC influences tumour growth or relapse. Targeting lineage restricted or neoantigens, for which tolerance may not exist, may result in a more immunogenic T cell response and may have a greater safety profile. It has also been suggested that CSC preferentially express cancer testis antigens, compared to the other types of antigens (Yamada et al., 2013). This was found in an antigen identification study in glioblastoma, in which HLA ligandome analysis was carried out on glioblastoma stem cells and non-stem cells (Neidert et al., 2018). Other novel CSC antigens include DNAJB8

and OR7C1, identified in renal and colon CSC (Morita et al., 2016; Nishizawa et al., 2012).

1.5 Prostate cancer

In this thesis, the possibility of targeting CSC with T cell immunotherapy was investigated using PCa as a model. This was prompted by a relative lack of successful immunotherapy treatments available for PCa. In this study, *in* vitro models of both localised and metastatic PCa (primary tissue derived cells and an established cell line, respectively) were used. Most immunotherapies being investigated to treat PCa focus on metastatic PCa, as this has a very poor prognosis. However, this stage represents a greater challenge for immunotherapy due to immunosuppression. However, due to the efficacy of treatments available for localised PCa, it is difficult to investigate immunotherapy as a viable alternative, despite the potential for preventing progression to metastatic disease which could be achieved with a durable immune response. In the context of targeting prostate CSC with immunotherapy, it may be particularly advantageous to intervene at the localised disease stage, with the aim of preventing CSC-driven relapse. This is likely to be most effective in combination with other therapies, for example the existing PCa treatments (detailed below), to de-bulk the tumour. Targeting prostate CSC in advanced disease also warrants investigation, as few therapeutics under clinical investigation have greatly extended survival or shown durable responses.

PCa is globally the most common cancer diagnosed in men, although there is significant variation in incidence and mortality across the world (Pernar et al., 2018). In the UK, PCa is the most common type of cancer and the second most common cause of cancer related death in males ("Prostate cancer incidence statistics," 2015). The majority of PCa-associated deaths occur from advanced metastatic disease. PCa has a high survival rate up to TNM Stage 3 (McPhail et al., 2015). In the UK, essentially all men diagnosed at Stage 1 (GS ≤6) survive a further 5 years. Five year survival rates then decrease slightly based on a diagnosis of grade 2 or 3 (99% and 93%) before sharply decreasing with a diagnosis of stage 4 which has a 30% 5 year relative survival ("Prostate cancer mortality statistics," 2015).

The diagnosis, staging and resulting treatment course for PCa is complex, owing to the heterogeneity of disease pathology and lack of factors predicting the clinical course. PCa is diagnosed based on tissue histology i.e. the GS, the TNM Classification of Malignant Tumours and prostate specific antigen (PSA) levels (EAU risk stratification) (Heidenreich et al., 2014; Mottet et al., 2017). The PSA test measures serum PSA levels, a protein uniquely produced by the prostate. Increased release of PSA into circulation occurs as a result of disrupted prostate tissue architecture, and increased PSA levels correlate with risk of PCa. However, PSA secretion also increases with ageing, infection or inflammation (prostatitis) and an enlarged prostate, which is not always associated with PCa. Therefore systematic PSA screening is not globally implemented, because there is some controversy and a lack of consensus as to its benefit in the management of PCa in all men (Heidenreich et al., 2014). PSA testing is also used in post-treatment management of PCa, as detectable or rising PSA levels are indicative of disease recurrence known as biochemical relapse (BCR).

1.5.1 Treatment of PCa

A high proportion of men are diagnosed with localised, compared to metastatic PCa (Figure 1.10A). Localised PCa can be treated by active surveillance (AS), a non-interventional monitoring strategy, radical prostatectomy (RP), and/or radiation therapy (RT). Both interventional treatments are highly effective; 10 year cancer specific survival rates for RP have been reported as greater than 90% (Boorjian et al., 2011; Han et al., 2001; Roehl Kimberly A. et al., 2004). At three years, BCR free survival was 92% in the most favourable cohort in one study (Zelefsky et al., 2002), while in another recent trial comparing two different types of ERBT, the BCR free survival at 5 years was 95.4% and 94.3% respectively (no significant difference between the types of RT) (Viani et al., 2016). Additionally a first of its kind trial comparing each of these treatments (the ProtecT trial), demonstrated no significant difference in cancer specific mortality (Hamdy et al., 2016).

Thus, a large proportion of men treated successfully for localised PCa can expect to live for at least a further 10 years. However, BCR following treatment of localised PCa is not uncommon (Figure 1.10B) (Artibani et al., 2018). BCR is a rise in PSA levels following anti-cancer treatment and is associated with an increased risk of PCa-specific mortality (Van den Broeck et al., 2018). However, it is particularly difficult to identify the optimal conditions for therapeutic intervention if BCR occurs, as it often precedes clinical progression (the emergence of locally advanced or metastatic PCa) by many years or may not lead to clinical progression at all. PCa specific death following BCR has been reported as 17% (Freedland et al., 2005) and 18.3% (Trock et al., 2008).

However, if PCa progresses beyond localised recurrence, treatment is not curative (Figure 1.10C). The standard approach for treating advanced PCa involves blocking androgen production and androgen receptor (AR) signalling, using androgen deprivation therapy (ADT) and anti-androgen therapy respectively (Paller and Antonarakis, 2013). However, PCa almost inevitably becomes resistant to these treatments, characterised by androgen independent growth. This stage is known as castration resistant prostate cancer (CRPC) and it occurs in the majority of patients within 1-2 years of ADT, followed by evidence of metastases (mCRPC) (Gravis et al., 2016; Karantanos et al., 2015; Merseburger et al., 2016; Nuhn et al., 2019). CRPC is treated with ADT, chemotherapy, radiation and immunotherapy to extend survival and mitigate symptoms of metastases. Additionally, zoledronic acid and denosumab is given to manage osteolytic effects of bone metastasis. Docetaxel (chemotherapy) was the first treatment shown to improve survival in mCRPC (Tannock et al., 2004). Other first line therapeutics for mCRPC include Abiraterone, a CYP17 inhibitor (CYP17 is involved in testosterone biosynthesis) which also reduces AR expression (Merseburger et al., 2015) and enzalutamide, which binds the AR with higher affinity than bicalutamide and acts on a molecular level to reduce AR mediated DNA expression (Nuhn et al., 2019; Tran et al., 2009).

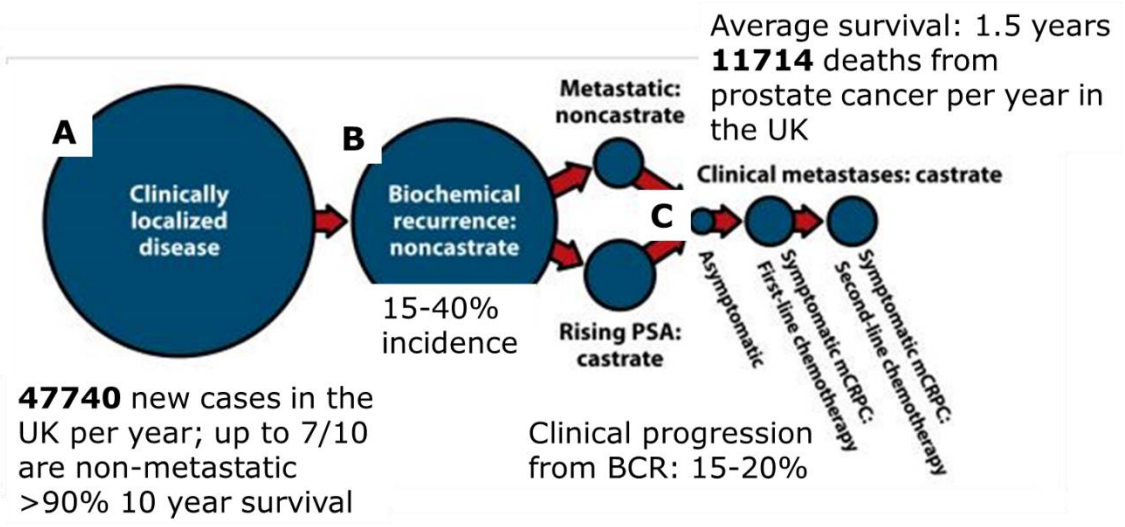

Figure 1.10. The clinical course of PCa. It is difficult to report a linear statistical relationship between cases of PCa and eventual mortality owing to the discrepancy in stages at which PCa is diagnosed and the relative mortality at each stage. Disease progression also depends on multiple factors. (A) Despite the lack of screening program implementation, over half of men diagnosed with PCa present with tumours that do not extend beyond the prostate, and have a high rate of successful treatment (reduction of PSA to castrate levels). (B) BCR is reported across a wide range from various studies. Recurrence is reported at similar rates for interventional treatments (RT and RP). However, ≤20% of men who experience BCR demonstrate clinical progression, which is reported as extracapsular growth and/ or rising PSA (depending on the primary treatment). (C) Clinical progression following BCR has a high rate of metastatic progression and is treatment refractory. Treatments for localised PCa are not suitable for treating metastatic PCa, however the primary mode of treatment, anti-hormonal therapy, is not curative. Therefore, the proportion of patients that experience clinical metastasis and treatment resistance is close to linear and has a poor prognosis. Figure adapted from: Paller and Antonarakis, 2013. Statistics from: Cancer Research UK (diagnosis and survival case numbers, 10 year survival rate), Hamdy et al., 2016 (localised survival), Artibani et al., 2018 (BCR incidence) Kirby et al., 2011 (Clinical progression) Karantanos et al., 2015 (CRPC survival).

Apart from immunotherapy (discussed below), there are a number of other novel agents in development for the treatment of mCRPC, including polyadenosine diphosphate–ribose polymerase (PARP) inhibitors, specifically for patients with mutations in DNA homologous recombination genes (Nuhn et al., 2019). In a phase II trial, 16/50 patients had mutations in DNA repair genes, and in these patients there was a high response rate (50% PSA level reduction or reduction in circulating tumour cells) (Mateo et al., 2015). However, it remains that the available agents for treatment of mCRPC only extend survival by relatively short periods, which may be accompanied by a poor quality of life.

1.5.2 Immunotherapy for Prostate Cancer

PCa is paradoxically considered optimal for treating with immunotherapy, yet a cancer type in which immunotherapy is less likely to succeed (Bilusic et al., 2017). Reasons why immunotherapy could succeed in PCa include the expression of tissue-specific antigens and the potential for activating an immune response at an early stage of disease, in which the tumour burden may be more effectively eliminated by immunotherapy. BCR also represents a window of opportunity for immunotherapy, prior to the development of immunosuppression associated with metastatic disease (Drake, 2010). On the other hand, PCa is considered an immunologically 'cold' cancer; despite PCa development being associated with inflammation and inflammatory pre-malignant conditions such as prostatic intraepithelial neoplasia (PIN), immune tolerance to tumours may be established even in localised disease. It has been shown that DC mediate suppression of $CD4^+$ cells in the TRAMP mouse model (Valent et al., 2012). The prostate TME is characterised by infrequent effector T cell infiltration; in the cases that TIL are present in the TME, they are often dysfunctional (Bronte et al., 2005; Vitkin et al., 2019). Additional factors contributing to the immunosuppressive TME include TGF-β producing M2 macrophages and Treg cells (Lundholm et al., 2015; Strasner and Karin, 2015). The stroma also contributes to immunosuppression, for example, cancer activated myofibroblasts have been shown to impair DC-mediated antigen presentation to T cells and also upregulated PD-L1, inducing PD-1 by T cells (Spary et al., 2014b).

There is currently only one FDA-approved immunotherapy for PCa; Sipuleucel-T (Provenge) a DC vaccine therapy which is indicated for mCRPC. This treatment demonstrated modest but significantly improved survival outcomes in a phase III clinical trial (Small et al., 2006) and was first approved in 2010. However, Sipuleucel-T has not been widely implemented for mCRPC and the manufacture of Sipuleucel-T has encountered financial difficulties (Nuhn et al., 2019). Sipuleucel-T consists of PBMC obtained from the patient and activated towards a DC phenotype by treatment with a GM-CSF fusion protein that incorporates prostatic acid phosphatase (PAP), a prostate-specific antigen. While the DC generation method only results in an 18% frequency of $CD14^+$ DCs, these are sufficient to activate T cells, evidenced by detection of antigen-specific T-cell proliferation and IFNγ production (Sheikh et al., 2013). The high cost of the treatment is due to the use of individual patient derived cells to produce DC, and the time-consuming process involved in DC maturation and peptide loading.

Many other forms of immunotherapy are under investigation for the treatment of cancer. The majority unsurprisingly focus on mCRPC, due to the lack of effective treatments available, although few single agent immunotherapies have thus far shown promising results applicable to the majority of patients. A number of trials investigating anti-CLTA4 treatment for mCRPC have failed to improve OS but demonstrated improved PFS (Beer et al., 2016; Kwon et al., 2014). Notably, the study by Kwon and colleagues demonstrated increased overall survival in patients with more favourable prognostic features (e.g. lacking lung metastases) (Kwon et al., 2014). Preliminary results from an ongoing Phase II clinical trial show that checkpoint inhibition (Anti-PD-1; pembrolizumab) is effective in chemotherapy resistant CRPC for a specific subset of patients; those with microsatellite instability (MSI) PCa (Hempelmann et al., 2018). MSI represents a relatively small subset of PCa patients; approximately 1% of primary tumours and up to 12% of metastatic tumours have mismatch repair mutations which lead to increased mutational load due to low fidelity DNA repair. This treatment shows promise for a small subset of patients and highlights the importance of molecular profiling for patient selection.

A number of vaccines are currently under clinical evaluation to treat mCRPC. PROSTVAC consists of vaccinia and fowlpox vectors which express PSA and three co-stimulatory molecules; it is delivered as a prime boost protocol in which the vaccinia vector activates the immune system and fowlpox boosts the response. In a phase II trial for mCRPC, after three years follow up, a significant proportion of men had greater OS compared to the control (empty vector) (Kantoff et al., 2010), which was associated with greater PSA specific T cell responses (Gulley et al., 2010). However, this improved OS was not observed in a phase III trial recently completed (Gulley et al., 2018). GVAX is a different form of vaccine, comprising whole tumour cells; LNCaP and PC3 metastatic PCa cell lines, which are transduced to secrete GM-CSF (aimed at maturing DCs and potentially also stimulating M1 inflammatory macrophages). This vaccine showed benefits in a phase II clinical trial (Simons and Sacks, 2006), but further investigation in a phase III trial was terminated early due to lack of efficacy and high mortality rates (Comiskey et al., 2018).

Antigen-specific targeting in PCa has mainly focused on PAP, PSA, PSMA and PSCA, in preclinical and clinical trials. Preclinical responses include tumour cell lysis *in vitro* based on simultaneous targeting of PSCA and PSMA using T cells (Arndt et al., 2014). Another study investigated immunogenic epitopes of PSCA by testing T cell responses from PCa patients; 8 peptides binding HLA-A*02:01 were identified from the PSCA protein sequence however only two of these caused T cell activation in patient derived cells (Kiessling et al., 2002). Antigen-specific T cell responses, indicated by TCR analysis of clonal populations in samples from patients with localised disease, have also been observed, however this is concurrent with high immunosuppressive PD-1 expression (Sfanos et al., 2009). Other antigens investigated for the treatment of PCa include MUC-1, which has been tested *in vitro* in CAR-T cell format; the CAR-T cells were shown to lyse PCa cell lines expressing the antigen, although non-MUC-1 escape variants were observed, suggesting a multi-antigen strategy may be more effective (Sanchez et al., 2013). However, there is little clinical data on targeting antigens using CAR T cells in PCa; there are currently only 7 active studies in the NIH clinical trials database searched using the keywords ‘prostate cancer’, ‘T cell’ and ‘CAR.’ The antigen targets in these studies are PSMA, PSCA and EpCAM. Phase I

clinical trials investigating CAR-T cells targeting PSMA are ongoing (Junghans et al., 2016; Narayan et al., 2019); successful engraftment and PSA reductions in some patients have been demonstrated (Junghans et al., 2016). The cancer testis antigen NY-ESO has also been evaluated in a phase I clinical trial, in which patients were vaccinated with recombinant NY-ESO protein (and CpG adjuvant), which activated antibody responses in some patients (Karbach et al., 2011). Additionally, in a Phase I/II clinical trials, a MUC-1 DC vaccine was safely tolerated and significantly reduce PSA doubling time in patients with non-metastatic CRPC (Scheid et al., 2016).

Conventional treatments for PCa are also suggested to have a beneficial synergistic effect when with immunotherapy. For example, ADT can improve T cell infiltration ($CD4^+$ T cells) (Mercader et al., 2001). ADT was also shown to increase maturation of DCs in mice, although co-stimulation of T cells depended on the T cells having already encountered the antigen (PSCA delivered by DNA vaccine) (Koh et al., 2009). Importantly, ADT does not have a negative effect; there was no impairment of MUC-1 CAR T cell function when combined with ADT (Sanchez et al., 2013). PCa patients may also benefit from a combination of RT and immunotherapy, although the immunomodulatory effects of radiation depend on the dosage (fractionation and total dosage). Pro-immunogenic effects of radiation include upregulated antigen expression and release of DAMPs from dying cells (Park et al., 2014), although radiation can also deplete effector immune cell subsets while sparing Tregs at higher doses (Kachikwu et al., 2011). The data on optimal immune-modulating radiation dosage is conflicting; it has been suggested that low dose per fraction radiation is immunosuppressive (Lee et al., 2009) while others have observed activation of an effector immune response after low dose per fraction RT *in vitro* (Spary et al., 2014a). A hypofractionated dose (7.5 Gy per fraction) given *in vivo* was found to impart maximal benefits in increasing the tumour reactive T cells while maintaining low Treg numbers (Schaue et al., 2012). Clinical studies with vaccines also demonstrate different effects; RT (3Gy/ day up to a total of 30 Gy) combined with Sipuleucel T did not improve immune responses (Twardowski et al., 2018). However, RT (external beam radiation therapy (EBRT); 1.2 Gy-2Gy to a total of 70 Gy) combined with GVAX improved tumour cell killing (Gulley et al., 2005). Thus, differences in the radiation protocol may impact efficacy.

Nevertheless, since RT is a standard treatment for localised PCa, it is particularly worthwhile to investigate the effects of combining RT and immunotherapy.

There is no doubt that treating metastatic PCa with immunotherapy could improve survival outcomes, based on the outcomes observed in other late state cancers and preliminary results from clinical trials in PCa. It is suggested here that there is also cause to implement immunotherapy at an earlier stage of treating PCa, owing to the high mortality and treatment failure rate of recurrent PCa. Immunotherapy for localised PCa is being investigated in a small number of clinical studies. A phase III clinical trial is evaluating the combination of oncolytic virus 'ProstAtak' with standard external beam radiation therapy (EBRT); which is typically delivered in low dose fractions (2-3Gy to a total of 74-80 Gy), to treat high risk localised PCa (NCT01436968). In addition to metastatic disease, PROSTVAC is also currently being tested (Phase II) to treat localised PCa which is naïve to other forms of interventional therapy (i.e. patients undergoing AS) (Parsons et al., 2018). Patients are assigned to AS based on weighing up the risks of treatment versus disease progression; approximately one third of patients progress to requiring interventional treatment (Klotz et al., 2010). GVAX is also being evaluated in combination with RP and cyclophosphamide (NCT01696877), in which the limited results available suggest that immunotherapy increased both $CD8^+$ T cells and Treg densities in the tumour (evaluated upon resection) (Antonarakis et al., 2017). These studies suggest that the use of immunotherapy to treat localised PCa, despite the availability of conventional treatments, is recognised as an intervention which could reduce mortality for advanced disease. Therefore, the potential to prevent relapse by treating prostate CSC with immunotherapy warrants investigation.

1.5.3 Prostate stem cells

The tissue structure of the healthy prostate consists of glandular subunits of pseudostratified epithelia comprised of basal and luminal cells with rare neuroendocrine cells (Shen and Abate-Shen, 2010; Strand and Goldstein, 2015). The glands are supported by a stromal network. Signalling from the stroma directly influences functional epithelial development (Lang et al.,

2001). The basal cells are in contact with the basement membrane and are characterised by expression of cytokeratin (CK) 5 and 14, and p63 (Figure 1.11A) while luminal cells express CK8 and 18 (Figure 1.11B) (Niranjan et al., 2012). The basal compartment also consists of transit amplifying cells (TA) and committed basal (CB) cells (Packer and Maitland, 2016). The intermediate phenotype expresses CK 5, 8, 14, 18 and 19 may correspond TA or CB cells, which in a stepwise fashion give rise to terminally differentiated luminal cells (Niranjan et al., 2012) (Figure 1.11B). Luminal cells express the AR and their growth is androgen sensitive in the healthy prostate. Basal cells express low to negligible levels of the AR (Strand and Goldstein, 2015). Androgen dependent growth and the lineage relationships of the prostate were originally demonstrated by castration of rats, where it was shown that castration caused significantly greater regression of luminal cells than basal cells (English et al., 1987). Reinstating androgen signalling caused regeneration of basal, but mainly luminal cells. As a result, it was hypothesised that the basal compartment contained stem cells capable of regenerating the luminal lineage (multipotency) (Isaacs, 1987). Prostate stem cells have been identified with a basal phenotype, $CD44^{+}$ $\alpha_2\beta_1 Integrin^{high}$ $CD133^{+}$, at a frequency of 1%, from human tissue derived samples (Collins et al., 2001; Packer and Maitland, 2016; Richardson et al., 2004). These cells were capable of reproducing differentiated epithelial prostate acini *in vivo* (Richardson et al., 2004). TA and CB cells can be distinguished by their expression profiles $CD44^{+}$ $\alpha_2\beta_1 Integrin^{high}$ $CD133^{-}$ and $CD44^{+}$ $\alpha_2\beta_1 Integrin^{low-}$ respectively (Figure 1.10) (Collins et al., 2005).

Other markers used to distinguish basal and luminal cells include $CD49f^{+}$ (α Integrin) $CD26^{-}$ and $CD49f^{-}$ $CD26^{+}$ respectively (Figure 1.11 A, C) (Karthaus et al., 2014; Moad et al., 2017). DLK1 has also been suggested as a prostate stem cell marker in a basal phenotype panel of markers ($CD49f^{+}$ $CD26^{-}$ $DLK1^{+}$) (Ceder et al., 2008; Moad et al., 2017). Single basal stem cells have been shown to give rise to clonal hierarchies which are maintained across the span of the prostate in a unidirectional way from proximal paraurethral ducts to distal acini (Moad et al., 2017). Lineage tracing has also demonstrated that basal and luminal cells have a single clonal cell of origin (Blackwood et al., 2011). These data suggest a linear decline in stemness capacity in the basal to luminal cell hierarchy. However, luminal stem cells have also been

described in cultures established from human tissue-derived samples (Karthaus et al., 2014). Therefore, the terminally differentiated luminal phenotype must be subject to a certain degree of plasticity, enabling luminal cells to acquire stemness characteristics under certain conditions.

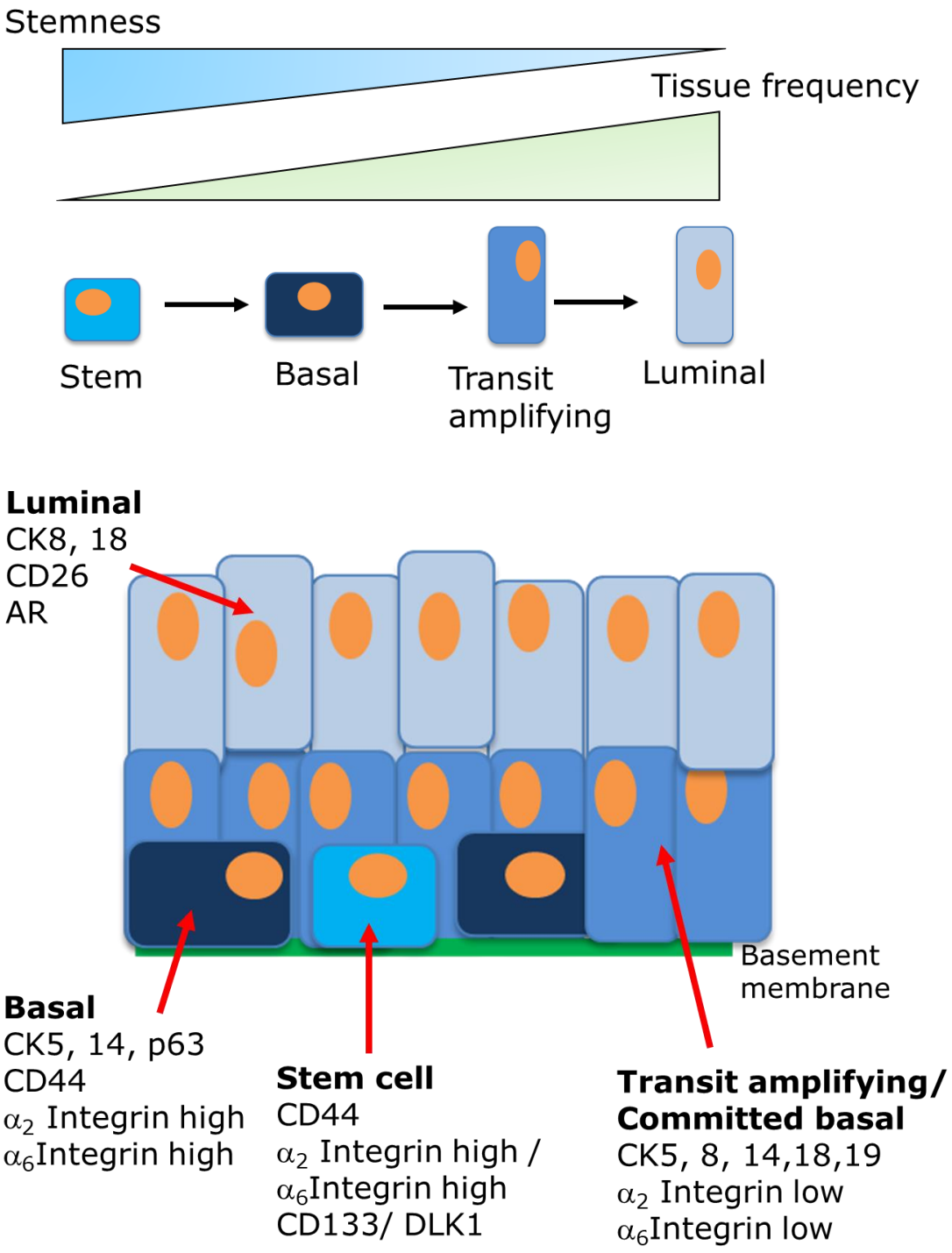

Figure 1.11. Phenotype markers for the cell lineages of the healthy prostate. SC reside at the top of a linear hierarchy in the healthy prostate and are part of the basal compartment. Stemness capacity is reduced in the intermediate transit amplifying / committed basal cells and luminal cells represent the most frequent, terminally differentiated cell type. As part of the basal compartment, SC can be identified using markers common to basal cells, along with specific SC markers. Transit amplifying cells express cytokeratins common to both basal and luminal cells. Luminal cells are AR positive and express cytokeratins distinct to basal cells. Adapted from Niranjan et al., 2012.

1.5.4 Prostate cancer stem cells

PCa is characterised by overgrowth of the luminal cell compartment, and reduction or loss of the basal population. For this reason, it appears that prostate CSC would originate from luminal cells. However, most evidence suggests that prostate CSC are derived from basal SC (Figure 1.12A). Primary prostate CSC were first identified using the same basal markers as prostate SC; $CD44^+$ $\alpha_2\beta_1Integrin^{high}$ $CD133^+$ (Collins et al., 2005). While prostate SC are present at a frequency of 1% in the healthy prostate, luminal cell proliferation in PCa disrupts the luminal basal ratio; prostate CSC were found at a frequency of 0.1% (Figure 1.12B) (Packer and Maitland, 2016). In primary PCa cells, the CSC had greater colony forming efficiency *in* vitro, than $CD44^+$ $\alpha_2\beta_1Integrin^{high}$ $CD133^-$ (TA) and $CD44^+$ $\alpha_2\beta_1Integrin^{low}$ (CB) cells, respectively (Collins et al., 2005). Several studies have used different combinations of these markers to identify prostate CSC (Kerr and Hussain, 2014). The existence of different CSC subpopulations has been suggested by Liu and colleagues, based on different gene expression profiles. The $CD44^+$ and $\alpha_2\beta_1Integrin^{high}$ populations differed in their expression of ABCG2 and SOX1, compared to the respective negative populations ($CD44^-$ and $\alpha_2\beta_1Integrin^{low}$) (Liu et al., 2015).

Other surface markers for the identification of prostate CSC have largely been investigated using PCa cell lines or xenograft derived models, which may not recapitulate the lineages present in primary prostate tissue. HLA^- cells found in DU145 and 22RV1 cell lines were AR^-, suggesting a basal phenotype, however these cells additionally did not express either of basal or luminal cytokeratins (CK 5, 14 or CK18, 19 respectively) (Domingo-Domenech et al., 2012). Functional markers, such as ALDH and ABCG2/ side population (mediated by the ABC transporter family) have also been used to identify prostate CSC (Chen et al., 2016; Huss et al., 2005; Liu et al., 2015; Patrawala et al., 2005; van den Hoogen et al., 2010). ALDH high cells (in modified PC3 cell lines) have been shown to express significantly higher CD44, EpCAM and integrins $\alpha5$ and $\alpha6$, suggesting a basal phenotype (van den Hoogen et al., 2010). Gene expression profiling has been performed on a number of different prostate CSC models. Basal and luminal transcriptomes were compared in one study, in which distinct characteristics, such as stem cell

and EMT-related genes were upregulated in the basal cells, concurrent with greater clonogenicity and sphere formation by basal cells *in vitro* (Zhang et al., 2016). A notable exception to the basal prostate CSC phenotype was demonstrated by Wang and colleagues. This study identified Nkx3.1 as a marker of cells which survived castration in a *Pten* PCa model *in vivo* (Wang et al., 2009). The Nkx3.1^{+} had a luminal CK18^{+}, AR^{+} phenotype and did not express basal markers p63 and CK14 and were targets of transforming mutations *(Pten* deletion). However, developmental, anatomical and phenotypic differences between the mouse and human prostate must be taken into consideration when interpreting these results, such that luminal cells could represent a target for transformation in mice but not in humans. Therefore, the selection of markers must consider whether it is optimal to use lineage-restricted (surface) or lineage-independent (functional) markers for identifying prostate CSC, taking into consideration the *in vitro* or *in vivo* model under investigation. It may be possible that a cell from each lineage in the prostate could be transformed to become a CSC, albeit with different likelihood based on the existing transcriptional program in the cell (Figure 1.12C).

Activation of signalling pathways associated with stemness has been identified in prostate CSC. This includes NF-κB, which was constitutively activated in a subset of PCa cells (xenograft derived and cell lines), identified by a novel panel of CSC markers; TRA-1-60, CD151 and CD166 (Rajasekhar et al., 2011). These prospective CSC also demonstrated high IL-6 signalling, and there was evidence of resistance to apoptosis by high expression of Bcl-2. NF-κB inhibition abrogated sphere formation and *in vivo* tumour initiation. Another study similarly found an upregulated NF-κB and IL-6 gene signature in prostate CSC, identified by the markers CD133^{+}/$\alpha_2\beta_1^{high}$ (Birnie et al., 2008). NF-κB was co-expressed with CD133 in primary PCa samples and NF-κB inhibition resulted in preferential apoptosis in the CD133^{+} population. In the HLA^{-} population (DU145 and 22RV1 PCa cell lines) docetaxel resistance was associated with Notch and Hedgehog stem cell pathway signalling (Domingo-Domenech et al., 2012). In the study by Cojoc and colleagues, the ALDH high cells (DU145 cells) were enriched by radiation treatment and upregulated expression of CD133, ABCG2 and NANOG (Cojoc et al., 2015b).

Radiation resistance was associated with enhanced PI3K/AKT and Wnt/β-catenin signalling and the ALDH high cells had lower baseline ROS.

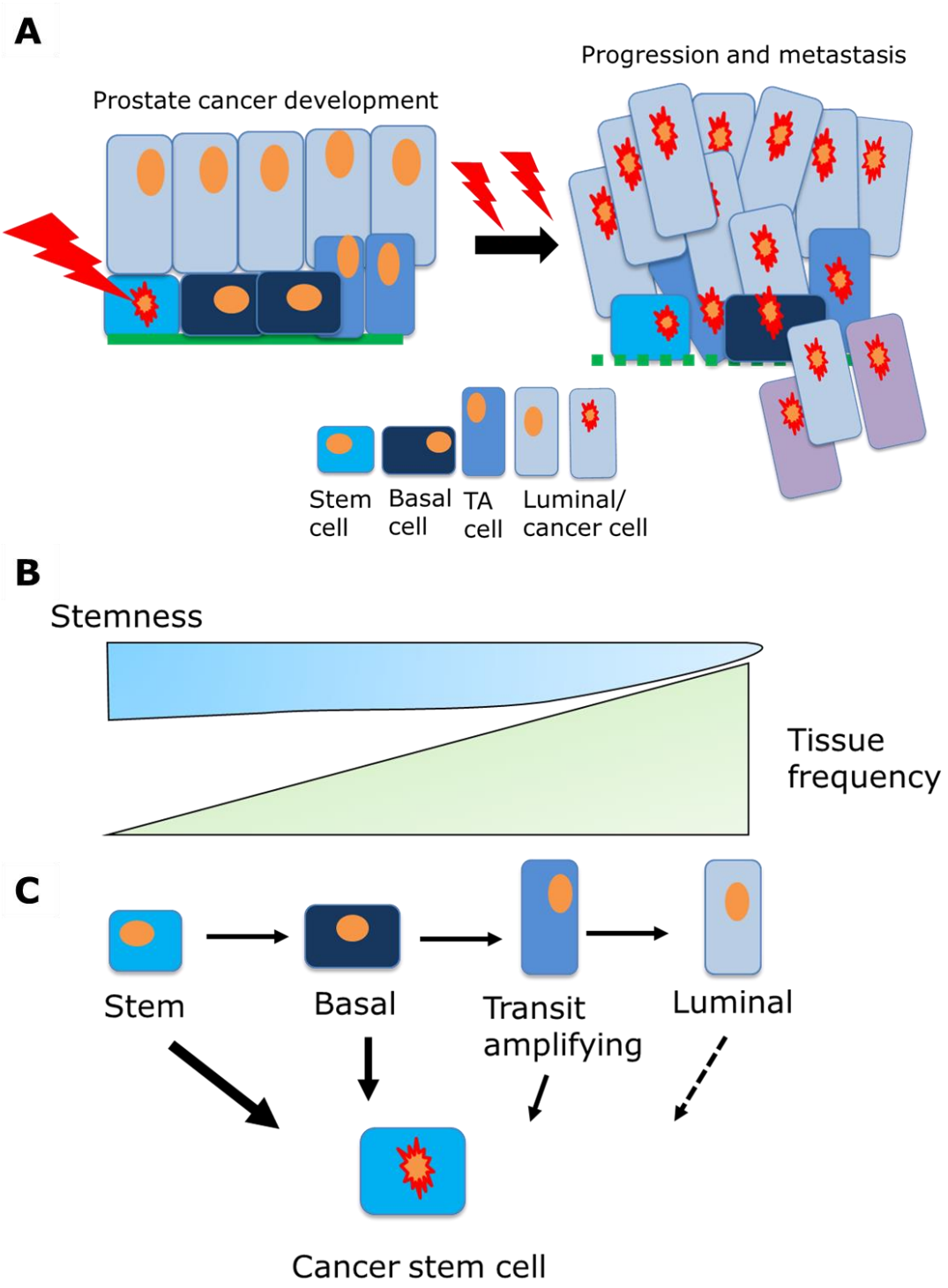

Figure 1.12. Prostate CSC in the development of PCa. (A) SC acquire mutations to become CSC**,** however extensive proliferation occurs mainly in the luminal cells, further accumulation of mutations in the CSC lineage results in cancer progression and metastases. (B, C) The lineage hierarchy of the tissue is disrupted. While SC may be the most susceptible to transformation, mutations in differentiated cell conferring stem-like characteristics could occur. The balance of evidence suggests prostate CSC have a basal phenotype, however luminal cells with tumour initiating capacity have been described.

As previously mentioned, a key characteristic of CSC is tumour initiation *in vivo*. This has been investigated in a variety of PCa cells, using different markers. These include $CD44^+$ $\alpha_2\beta_1$Integrin$^+$ (various human cell lines), $CD133^+$ (CD133/2 epitope) $CD44^+$ (DU145 cells), (Rybak et al., 2014) and HLA^- (DU145 and 22RV1 cells) (Domingo-Domenech et al., 2012). $CD44^+$ cells isolated from xenograft tumours (initiated by cell lines) have also been shown to have tumorigenic properties (Patrawala et al., 2006). Tumorigenic PCa cells, from cell lines, have also been identified using functional CSC markers ALDH and ABCG2. ALDH high cells were significantly more tumorigenic *in vivo* and also initiated significantly more bone metastases (metastatic bone-trophic cell lines were used) (van den Hoogen et al., 2010). The radiation resistant ALDH high cells were also capable of initiating tumours (Cojoc et al., 2015b). ABCG2 has been shown to identify tumorigenic prostate CSC in a number of cell line models (Liu et al., 2015; Sabnis et al., 2017).

It is necessary to use PCa cell lines to investigate *in vivo* tumorigenicity owing to the technical challenges of engrafting primary PCa cells *in vivo* (X. Chen et al., 2013). Indirect analysis of human primary prostate CSC *in vivo* tumorigenicity was performed by grafting unsorted primary tissue into NOD-SCID IL2rγnull (NSG) mice and isolating CD44, CD133 and CD24 from the resulting tumours (with mouse lineage depletion), although the precise methodology was poorly described (Maitland et al., 2011). This revealed that both $CD133^+$ and $CD24^+$ (luminal) cells were tumorigenic *in vivo*, although the $CD24^+$ cells generated fewer tumours, with a greater latency period. Another study provides evidence that $CD44^+$ primary PCa cells are tumour-initiating, when co-injected with stromal cells in NSG mice (Liu et al., 2015).

While the identification of prostate CSC based on a single panel of surface markers is difficult due to the variable expression of these markers in different experimental models, these challenges apply to the identification of CSC in many types of cancer. Due to the limited number of broadly applicable CSC markers, it is thus possible to validate such markers in the best available *in vitro* and *in vivo* models and determine a panel which could be uniformly applied and allow for better comparable analyses of CSC. This could further lead to clearer distinctions between potential CSC subpopulations which are

otherwise unclear due to inconsistent use of CSC markers in different experimental models. Isolation based on functional markers could also confirm the phenotype of the cells used in experimental models and may represent a way of identifying the prostate CSC lineage in a less biased way. For each identification method ultimately the marker(s) used are best supported by further detailed characterisation of cells with the putative CSC phenotype.

1.5.5 Immunotherapy of prostate CSC

Immunotherapy of prostate CSC has been investigated in a limited number of studies. CSC, established by a neurosphere assay from a TRAMP mouse model, were found to express PAP, PSCA and Six-transmembrane epithelial antigen of the prostate-1 (STEAP) (Jachetti et al., 2013; Mazzoleni et al., 2013). Cytokine responses to CSC were observed *in vitro* and *in vivo* (lysis by splenocytes from CSC-DC vaccinated WT mice). WT mice vaccinated with TRAMP-CSC loaded DC and challenged with TRAMP cells showed delayed tumour growth compared to unpulsed DC (Jachetti et al., 2013). However, the CSC antigen(s) mediating tumour rejection were not identified in these experiments, and it was further shown that DC vaccination with CSC, compared to STEAP, was more effective in delaying tumour growth in TRAMP mice, suggesting that this antigen was not responsible for CSC targeting tumour regression outcomes. This may be due to the observation that STEAP was not exclusively expressed by the CSC but was also expressed in a differentiated TRAMP cell line, although vaccination with DC pulsed with the differentiated cells did not improve tumour protection. Antigen-specific vaccination has been tested in another study (Garcia-Hernandez et al., 2008). In this study, DCs were loaded with PSCA cDNA in a prime and viral vector boost model in TRAMP mice, which conferred significantly improved survival compared to unvaccinated mice.

However, since these studies investigated responses to antigens expressed in a mouse model, the epitopes targeted may not be applicable to human tumours. Additionally, owing to differences in the development of the prostate in mice compared to humans, the CSC population could be different, thus it may not be an accurate model of the effects of targeting CSC in the human

prostate. Therefore, identification of human antigens expressed by prostate CSC, and testing the effects of targeting these *in vivo* is warranted. An example of this is the study by Deng and colleagues, using EpCAM CAR T cells against tumours grown *in vivo* from PC3M cells, a subline of the metastatic human PCa cell line PC3 (Deng et al., 2015). As previously discussed, CAR T cells are targeted against surface proteins; optimal targets are typically highly expressed on the cell surface. EpCAM was originally identified in colon cancer tissue, and is also expressed on prostate CSC (Gires et al., 2009; Herlyn et al., 1979; Munz et al., 2009). EpCAM has been found to be expressed in a wide range of cancers (Went et al., 2004), thus the EpCAM CAR T cell based CSC targeting approach could be tested in further cancers which express the same CSC markers. While EpCAM is widely expressed by epithelial tissues, the expression pattern of EpCAM is localised differently in healthy compared to cancer tissue; EpCAM is specifically localised cell surfaces at tight junctions in healthy cells whereas it is homogenously expressed in cancer tissue; additionally EpCAM is more highly expressed in cancer tissue (Munz et al., 2009, 2004; Schnell et al., 2013). Munz and colleagues further suggest that this expression pattern in which EpCAM is sequestered at the tight junctions in healthy tissue may have a protective effect in the context of anti-cancer therapies targeting EpCAM (Munz et al., 2009). EpCAM is functionally involved in cell-cell adhesion however, EpCAM associated adhesion has a negative regulatory effect on cadherin mediated adhesion (Went et al., 2004). EpCAM is thus suggested to be associated with modulating, rather than maintaining cell-cell junctions, which presents a potential functional link to loss of cell polarity and deregulated morphology and cell motility associated with tumorigenesis. EpCAM expression is also recognised as a marker of SC and CSC (Imrich et al., 2012; Ni et al., 2018). There are a number of immunotherapy approaches under clinical investigation for targeting EpCAM in solid tumours. EpCAM targeting therapies include CAR-T cells, an antibody-drug conjugate (Tucotuzumab celmoleukin) and a bi-specific antibody combining anti-EpCAM targeting with CD3 activation (MT110) (Clara et al., 2019)

Previous studies investigating the use of antibody based anti-EpCAM cancer therapies demonstrated that targeting this cancer antigen was largely well tolerated although off-target toxicity occurred in healthy tissue was

associated with the use of high-affinity antibodies (Schwartzberg, 2001). Further clinical evaluation failed to show a significant therapeutic effect (Punt et al., 2002) however it has been suggested that other immunotherapy modalities could be effective (Went et al., 2004). In the study by Deng and colleagues, EpCAM CAR T cells were effective at controlling tumour growth *in vivo* but more interestingly, also prevented metastasis in a model of tumorigenesis driven by the parent PC3 cell line, which has lower and heterogenous EpCAM expression (Deng et al., 2015). Since human EpCAM is highly conserved between humans and mice (Schnell et al., 2013), this suggests that EpCAM targeting was highly specific to tumour cells in this *in vivo* model. The results from this study highlighted two key concepts. First, immune targeting of CSC antigens can control metastatic tumour growth. Second, CSC antigens can be shared between different prostate cancer cell types. This suggests that immune targeting of CSC in human prostate cancer is a valid approach and that identification of novel CSC antigens could form the basis of effective immunotherapies; this forms the motivation for this thesis.

1.6 Hypothesis and Aims

I hypothesise that prostate CSC (a) are a distinct population of cells found in PCa cell lines and primary samples which can be identified by specific markers, (b) express antigens, uniquely or in common with prostate non-CSC, and (c) presentation of these antigens by CSC can activate a T cell response.

To investigate this, the aims of this thesis are:

1. Identify CSC using primary PCa samples and PCa cell lines using optimal markers.
2. Characterise the CSC *in vitro* and *in vivo.*
3. Identify novel antigens of prostate CSC.
4. Test T cell responses to prostate CSC antigens.

Chapter 2.
Materials and Methods

2 Materials and Methods

2.1 Cell culture

2.1.1 Cell lines and primary samples

All cells used in this project were maintained at 37°C in an atmosphere of 5% CO_2 in a humidified incubator. Mycoplasma testing was carried out regularly using a MycoAlert Mycoplasma Detection Kit (Lonza). All tissue culture work was carried out in a class II biosafety cabinet. Authentication of cell lines was carried out by the supplier and visual inspection of the cells' morphology was regularly carried out for the duration of the *in vitro* culture period.

The DU145 cell line is a PCa cell line originally isolated from CNS metastases, and was obtained from ATCC (ATCC HTB-81) (Stone et al., 1978). The DU145 cells were used in the lab up to passage (p) 59. The LNCaP cell line is a PCa cell line originally isolated from lymph node metastases, and was obtained from the European Collection of Authenticated *Cell* Cultures ECACC) (Horoszewicz et al., 1983). The LNCaP cells were used from p8-p11.

B lymphoblastoid cell lines (BLCL) were prepared according a previously described method, by infecting PBMC with EBV-containing B95.8 cell supernatant and PHA (Louie and King, 1991).

Ethical approval for the project was obtained from the School of Medicine Research Ethics Committee (Ref no. 17/52). Informed consent to provide peripheral blood samples was obtained from healthy donors. Consent was obtained from healthy donors by research staff trained in 'Valid Informed Consent in Research' by Health and Care Research Wales. Whole blood was sampled by trained phlebotomists at the Velindre Cancer Centre or University Hospital Wales (UHW).

Ethical approval specifically pertaining to the collection and use of PCa tissue was held by the Wales Cancer Bank (WCB) (WCB 16/002 and WCB 17/021). Consent for the sampling of PCa tissue was obtained from patients by WCB

staff. PCa tissue was obtained from patients undergoing prostatectomy surgery; the sampling was performed by pathologists in University Hospital Wales (UHW). Relevant clinical information was obtained from the WCB.

2.1.2 Cell culture and passaging

The cell culture media and conditions for each cell type are summarised in Table 2.1. Details of the media supplementation, culture and passaging protocols are provided below.

Table 2.1. Summary of in vitro culture conditions for the cell types used in this project.

Cell type	**Culture conditions**	**Media**	**Passaging**
DU145	Adherent plasticware	10% RPMI	Trypsin
LNCaP	Adherent plasticware	10% RPMI	Trypsin
Primary PCa samples	Adherent plasticware	Collection: SCM Culture: SCM/ OM /mOM	Accutase
BLCL	Suspension in adherent plasticware	10% RPMI	Dilute/ divide suspension cells
PBMC	Suspension in adherent plasticware	10% RPMI or 10% AB RPMI Additional supplements depending on experimental conditions	Dilute/ divide suspension cells

PCa cell lines

The DU145 and LNCaP PCa cell lines were cultured in Roswell Park Memorial Institute (RPMI)-1640 media (Lonza) in Cellstar TC-treated adherent cell culture flasks (Greiner Bio-One). RPMI-1640 was supplemented with 100 U/ ml penicillin and 100 µg/ ml streptomycin (Lonza), 2 mM $_{L}$-glutamine (Gibco Thermo Fisher Scientific) 25 mM HEPES buffer (Sigma Aldrich) and 1 mM Sodium Pyruvate (Sigma Aldrich). This basal media was additionally supplemented with 10% foetal bovine serum (FBS) (Gibco Thermo Fisher Scientific). This media is referred to as 10% RPMI throughout the text.

To passage the PCa cell lines, the culture media was removed, and the cell monolayer was washed with PBS not containing Ca^{2+} and Mg^{2+} (Lonza). Trypsin/EDTA solution (Lonza) was added as required to cover the base of the culture flask. Trypsin is a protease enzyme that cleaves cell-cell and cell-matrix adhesions, causing detachment of the cells from the culture surface. EDTA acts as a chelating agent, sequestering any Ca^{2+} and Mg^{2+} ions present which otherwise act as trypsin inhibitors. The flasks were incubated at 37°C for 8-10 min followed by neutralisation using FBS at ≥2 times the volume of Trypsin/EDTA used. FBS inhibits trypsin as it contains protease inhibitors. The detached cells were collected and centrifuged for 3 min at 354 *x g* (1300 x RPM) in a Heraeus Megafuge 1.0. This centrifuge was used for all live cell centrifugations. The cell pellet was resuspended in media for counting and once counted, re-plated or used in experiments as required. The PCa cell lines were passaged when 90-100% confluent to maintain stocks or at 70-80% confluent for use in experiments.

Doubling time of the DU145 cell line was determined by plating the cells at a range of concentrations: 10^4, 10^5 and 10^6 cells per well in a 6-well adherent Cellstar TC-treated adherent cell culture plate (Greiner Bio-One). Cell counts were performed using a Millipore Guava EasyCyte TM8 flow cytometer at 3 days, 5 days and 7 days, by detaching the cells and staining with Guava ViaCount reagent for counting (counting protocol detailed below). The doubling time of the DU145 cells was calculated using the formula: time x log2/ log2(final concentration) - log2(initial concentration).

Primary PCa sample processing and culturing

The primary PCa biopsies were collected in sterile universal tubes containing 5 ml 'Stem cell media' (SCM) (Frame et al., 2013), consisting of Keratinocyte SFM media (KSFM) kit supplemented with the included EGF and BPE (Gibco Thermo Fisher Scientific). This basal media was additionally supplemented with 1X Antibiotic-Antimycotic (Gibco Thermo Fisher Scientific), 2ng / ml stem cell factor (First Link UK), 100ng / ml cholera toxin (Sigma Aldrich) and 1ng / ml recombinant GM-CSF (Molgramostim; distributed by Sigma Aldrich for European Pharmacopoeia (EP) Reference Standards). The biopsies were washed briefly in PBS followed by dissection using a scalpel. The biopsies were dissected about 1 mm^3 pieces and transferred to a solution of 200 U / ml Collagenase I (Worthington Biochemicals, distributed by Lorne Laboratories UK) or 5 mg / ml Collagenase II (Life Technologies Thermo Fisher Scientific) additionally containing 10 µm Y-27632 2HCL (ROCK inhibitor) (Selleck Chemicals, supplied by Stratech Scientific Ltd.). The pieces were enzymatically digested by overnight incubation with rotation on a MACSmix Rotator (Miltenyi Biotech) at 37°C. The efficacy, in terms of cell viability and cell numbers recovered from biopsy digestion, using Collagenase I or Collagenase II, was compared for consecutive PCa biopsies. Following the overnight step, the solution was passed through an 18 G needle 3 times to break up any remaining pieces and the solution was centrifuged at 838 *x g* for 5 min. The supernatant was discarded, and the pellet was resuspended in 10 ml PBS and centrifuged again at 838 *x g* for 5 min. This step was repeated one further time. The sample was then resuspended in the culture media for counting. Once counted, the cells were plated at 1.5- $2x10^5$ cells per well in a 6-well plate; lower cell numbers were plated in single wells in 12- or 24-well plates (Cellstar TC-treated adherent multi-well plates from Greiner Bio-One). The cells were grown without disturbing them, until growth became evident, up to a maximum of 3 weeks, before passaging. The cultures were passaged or used in experiments at approximately 80% confluency.

To passage primary PCa cell lines, the cell monolayer was washed with PBS not containing Ca^{2+} and Mg^{2+} (Lonza). Accutase Enzyme Cell Detachment Medium (Thermo Fisher Scientific), was added as required to cover the base

of the well in the cell culture plate and the plates were incubated at 37°C for 15 min. Accutase was used as part of a primary prostate passaging protocol previously established in the lab. This is because accutase is considered a gentler alternative for cell detachment than trypsin, which may be more suitable for cells not adapted to *in vitro* cell culture (i.e. cell lines). Accutase is a solution containing both protease and collagenolytic enzymes. The cells were washed with PBS to aid detachment (unlike Trypsin, Accutase does not require neutralisation) and the detached cells were collected and centrifuged for 3 min at 471 *x g*.

Several different media were tested for the optimal growth of primary PCa cells. The first medium tested was SCM, to which 10 nM Dihydrotestosterone (DHT) (Sigma Aldrich) was later added to some individual cultures (DHT stimulates the androgen receptor). The basal media (KSFM) is suitable for culturing epithelial cells and keratinocytes and does not support the growth of fibroblasts (product technical data; CC2v3 SFM brochure, available at https://www.thermofisher.com/order/catalog/product/17005075?SID=srch-srp-17005075). Contaminating fibroblasts in a primary epithelial culture could out-grow the epithelial cells and confound the measurement of responses to treatment (Dollner et al., 2004; Luo et al., 2011). Additionally, it has been found using a different basal media, WAJC-404, that EGF and BPE have an important contribution to prostate epithelial cell proliferation (Sutkowski et al., 1992). This media was supplemented with Stem Cell Factor, GM-CSF and Cholera Toxin. Frame and colleagues suggest that KSFM can be used without these supplements for culturing healthy primary prostate epithelial cells, if the selection of subpopulations is not required (Frame et al., 2016). Therefore, these supplements are considered an important factor in promoting the distinct growth of prostate stem, transit amplifying and committed basal cells.

Following the publication of a dedicated 'organoid medium' (OM), designed for the growth of primary prostate and PCa cells by Drost and colleagues, this medium was tested in my study (Drost et al., 2016). Supplementation of the OM is detailed in Table 2.2. OM was developed to support growth of basal and luminal prostate and PCa cells under non-adherent conditions (sphere/

organoid culture); however for the purpose of expanding cell numbers for use my experiments, PCa cells were grown under adherent conditions (Cellstar TC-treated adherent multi-well plates from Greiner Bio-One). The factors influencing the choice of supplements in the medium developed by Drost and colleagues are discussed in accompanying publications by Karthaus and colleagues and Gao and colleagues (Gao et al., 2014; Karthaus et al., 2014). Growth factors EGF, Noggin and R-spondin constituted a "generic" medium for the growth of organoids, which was previously successfully used for the long term growth of organoids from colon cancer and various intestinal tissues (Sato et al., 2011). TGF-β and DHT were also included, to prevent a proliferative block and to encourage luminal cell growth, respectively (Karthaus et al., 2014). Additional supplements, PGE_2, FGF-10, FGF-2, Nicotinamide and p38 inhibitor were added specifically for the culture of human prostate organoids (the basal media could be used successfully to culture mouse prostate organoids) (ibid).

Table 2.2. Basal media formulation and supplementation used to make Organoid media.

Organoid media:

Basal media consisting of ADMEM/F12 (Gibco Thermo Fisher Scientific), additionally supplemented with 100 U/ ml penicillin+ streptomycin (Lonza), 2 mM L-glutamine (Gibco Thermo Fisher Scientific), 10 mM HEPES buffer (Sigma Aldrich).

Additional supplements:

Supplement	**Manufacturer**	**Media concentration**
FGF-10	Peprotech	10 ng / ml
FGF-2 (FGF basic)	Peprotech	5 ng / ml
EGF	Peprotech	5 ng / ml
NOGGIN	Peprotech	100 ng / ml

R-spondin	Peprotech	500 ng / ml
P38 inhibitor	Sigma Aldrich	10 µM
B27	Life technologies	1 X
Y-27632 dihydrochloride (ROCK inhibitor)	Selleck Chemicals/ Stratech	10 µM
N-acetylcysteine	Sigma Aldrich	1.25 mM
TGF–β inhibitor (A83-01	Tocris	500 nM
PGE_2	Tocris	1 µM
Nicotinamide	Sigma Aldrich	10 mM
DHT	Sigma Aldrich	1 nM

The extensive supplementation required to culture the human organoids is suggestive of the inherent difficulty in successful growth of human prostate and PCa tissue *in vitro*. Drost and colleagues provide comparison to previous studies including novel media formulations in which short term culture, or a lower success rate in culturing heathy prostate tissue was achieved; however culturing PCa tissue remained unsuccessful (Höfner et al., 2015; Niranjan et al., 2013; Xin et al., 2007). The contribution of the basal growth factors to various aspects of the cell culture was investigated by Karthaus and colleagues and it was found that Noggin and Wnt signalling were not essential for, but greatly enhanced prostate organoid formation (Karthaus et al., 2014). EGF was an essential supplement while TGF-β was required for passaging the spheres. These data were used to further optimise a media for adherent culture of primary PCa cells in my study, as the use of organoid media did not result in particularly long *in vitro* culture lifespans. This step was also taken as the extensively supplemented organoid media was not cost-effective. The novel medium used in this study was denoted 'modified organoid medium,' (mOM) consisting of the same basal medium as used in the organoid medium formulation and supplemented by a combination of reagents used in both of SCM and OM. The supplements used in mOM are detailed in Table 2.3.

Table 2.3. Basal media formulation and supplementation used to make modified Organoid media.

Modified Organoid Media

Basal media consisting of ADMEM/F12 (Gibco Thermo Fisher Scientific), additionally supplemented with 100 U/ ml penicillin+ streptomycin (Lonza), 2 mM L-glutamine (Gibco Thermo Fisher Scientific), 10 mM HEPES buffer (Sigma Aldrich).

Additional supplements:

Supplement	**Manufacturer**	**Media concentration**
FGF-2 (FGF basic)	Peprotech	5 ng / ml
EGF	Peprotech	5 ng / ml
B27	Life technologies	1X
TGF–β inhibitor (A83-01)	Tocris	500 nM
PGE_2	Tocris	1 μM
Nicotinamide	Sigma Aldrich	10 mM
DHT	Sigma Aldrich	10 nM
Stem cell factor	First link UK	2 ng / ml
Cholera toxin	Sigma Aldrich	100 ng / ml
GM-CSF	Molgramostim; distributed by Sigma Aldrich for European Pharmacopoeia (EP) Reference Standards	1 ng / ml

Immune cell isolation and culturing

Venous blood was collected by trained phlebotomists into 'Vacutainer' blood collection tubes containing EDTA as an anti-coagulation agent (BD). The blood was layered onto Histopaque-1077 (Sigma Aldrich) at approximately a 2:1 ratio and centrifuged at 838 *x g* for 30 min (with the break off for a gradual decrease in rotation speed at the end of the centrifugation step). In this way, the blood was separated into the different components by density gradient centrifugation. Due to their higher density, the red blood cells sedimented below the Histopaque layer. The PBMC were isolated from the buffy coat (separated between the Histopaque and plasma layers) and centrifuged two more times with PBS to wash the cells. The cells were washed for a final time in 10% RPMI and suspended in this media for counting. PBMC were cultured in adherent multi-well plates or flasks (upright/ tilted as required) (Cellstar TC-treated adherent plasticware from Greiner Bio-One), with cytokines or peptides, or further cell populations were isolated as required (details of specific experimental protocols are given below).

BLCL were cultured in adherent flasks orientated in an upright position (Cellstar TC-treated adherent plasticware from Greiner Bio-One), in 10% RPMI. BLCL were passaged routinely, typically upon observation of a colour change in the media (red to yellow) indicating acidic conditions as a result of excessive waste products. BLCL were passaged weekly in a 1:10 ratio by removing 9 parts of the cell suspension and adding 9 parts fresh 10% RPMI to the remaining cells. The cells were passaged in a lower ratio if large numbers were required for experimental use.

2.1.3 Cell counts and viability measurements

The cells were counted manually, using a Neubauer haemocytometer in conjunction with the trypan blue exclusion assay, or using the ViaCount Assay reagent (Merck Millipore) on a Guava EasyCyteTM8 flow cytometer (EMD Millipore). Manual cell counting was typically carried out for passaging of cells, and for counting PBMC. The cell suspension was diluted 1:10 in 0.1% trypan blue and 10 µl of the stained suspension was counted in a quadrant of known volume. The number of cells was determined by the following formula: mean

number of cells per quadrant (count of 4 quadrants) x dilution factor x 10^4 = number of cells/ ml.

The Guava ViaCount Assay is another type of cell viability and counting assay based on dye uptake or exclusion. The assay stains non-viable cells based on their permeability to the DNA-binding dyes in the ViaCount Reagent. The Guava EasyCyte TM8 flow cytometer was set up by running a cleaning protocol using the Instrument Cleaning Fluid (ICF) (EMD Millipore) and double distilled water (ddH_2O). The instrument was calibrated using the Guava Check Kit (EMD Millipore). To count cells using the ViaCount assay, an aliquot of the total cell suspension was stained by addition of the Guava ViaCount Reagent, in a 1.5 ml microfuge tube (STARLAB). The dilution factor of cells to dye was determined by estimating the cell count and following the manufacturer's recommended dilution factor, given below:

Table 2.4. Cell suspension concentration and recommended dilution factor of Guava ViaCount reagent for cell count and viability analysis on a Guava EasyCyte flow cytometer.

Cell Suspension concentration	Dilution Factor
$1x10^5$ to $1x10^6$ cells/ ml	10
$1x10^6$ up to $1x10^7$ cells/ ml	20
$>1x10^7$ cells/ ml Further dilution of the cell suspension is recommended if > than this concentration	40

The cells were incubated for 5 min and analysed using the Guava EasyCyte TM8 flow cytometer (Millipore). The data were visualised in the form of flow cytometry dot plots and viable cells were enumerated automatically based on placement of inclusion/ exclusion gates on the FSC/SSC and viability dye dot plots respectively (Figure 2.1A, B; DU145 cells, C,D: freshly digested primary PCa cells and E, F: cultured primary PCa cells at p5).

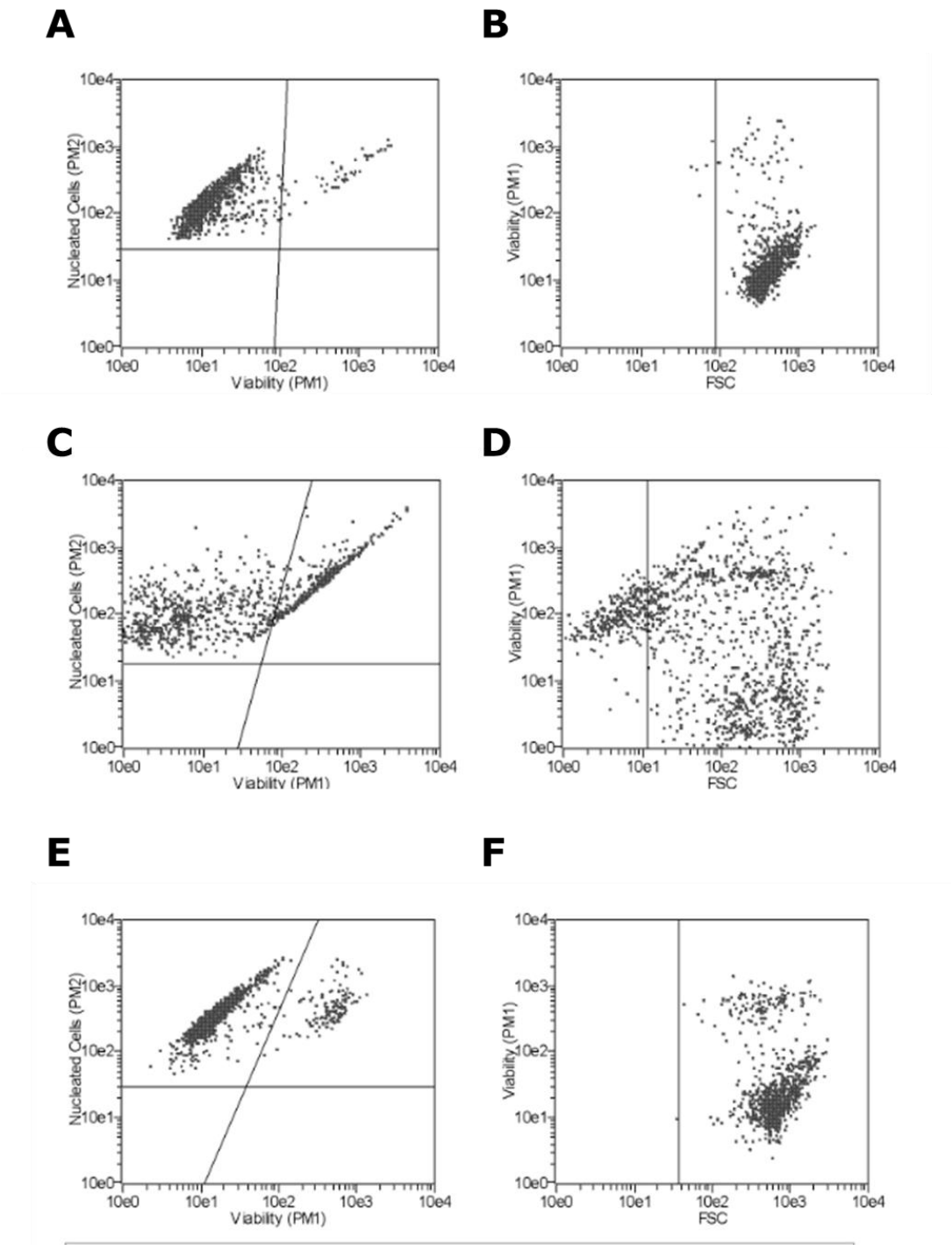

Figure 2.1 Dot plots generated by Guava EasyCyte flow cytometer for cell counting and viability analysis. (A) DU145 Cells are gated based on size and debris are excluded (B) DU145 Live cells are gated based on low ViaCount dye uptake. (C) Freshly processed (Collagenase I digestion) primary PCa cells at passage '0'. (D) Viability analysis for the same primary PCa sample. (E, F) The same primary PCa sample as shown in C, D at p5 of *in vitro* culture; (E) counting and (F) viability measures. Automated calculation of the cell number (both viable and total cell numbers are provided) based on the dot plot gating.

2.1.4 Cryopreservation, storage and recovery

Freezing media for storing cell lines and PBMC consisted of 10% RPMI, further supplemented with 20% FBS and 10% dimethyl sulphoxide (DMSO) (Sigma Aldrich). DMSO reduces the formation of large ice crystals in the course of a slow freezing process, which could otherwise puncture cells and cause cell death. The freezing media was prepared fresh and cooled on ice for use. Cells were counted, and then centrifuged at 354 *x g* for 3 min. The supernatant was removed, and cells re-suspended in freezing media and transferred to pre-chilled cryogenic vials ('CryoPure,' Sarstedt) (1 ml cell suspension per vial). The vials were placed into CoolCell alcohol-free cell freezing containers (Biocision) to ensure controlled cooling at -1 °C/min in a -80 °C freezer. The vials were transferred to vapour phase liquid nitrogen (-180 °C) for long-term storage within 2-3 days. Primary PCa cells, if sufficiently expanded in culture, were frozen for storage in Recovery Cell Culture Freezing Medium (Gibco Thermo Fisher Scientific). This is a pre-made cryopreservation solution that is suggested to improve recovery of cryopreserved mammalian cells (technical data). This solution is indicated by Drost and colleagues for cryopreservation of primary PCa cells grown in organoid media (Drost et al., 2016). This solution is used in the same way as hand-made freezing media; 1 ml of the cooled solution is added to a cell pellet and transferred to a cryovial. The cryovials were cooled in the -80 °C freezer and transferred to vapour phase liquid nitrogen as described above.

To recover cryopreserved cells, the cryovials were removed from liquid nitrogen and placed into a 37 °C water bath, for 2-3 min, until partially thawed. 0.5 ml 10% RPMI was added to the cryovial, 1 ml of the cell suspension was retrieved from the vial and added dropwise to a 15 ml falcon tube containing 10 ml pre-warmed (37 °C) 10% RPMI. This large volume is intended to dilute the DMSO, which is toxic to live cells. This was repeated until all of the cell suspension had been added to the media. The cell suspension was centrifuged at 354 *x g* for 3 min. The media supernatant was discarded, and the cells were resuspended in fresh media for counting. Defrosting of primary PCa cells from the Recovery Cell Culture Freezing Medium proceeded in the same way.

2.2 Flow cytometry

Antibodies and fluorescent dyes used in flow cytometry experiments are summarised in Table 2.5. Cell staining was performed in 5 ml sterile non-pyrogenic FACS tubes (BD Bioscience) except for Aldehyde dehydrogenase (ALDH) incubations and Cell Trace staining, which were carried out 15 ml CELLSTAR polypropylene tubes (Greiner Bio-One). A BD FACSVerse 8 colour flow cytometer operated by BD FACSuite v1.2.1 software was used to analyse the cells. BD FACS-DIVA software version 6.1.2 (BD Bioscience) was used to analyse the data. Cell sorting was carried out using a special-order system BD FACSAria II cell sorter flow cytometer (tetramer sorting of T cells) or a BC FACSAria III flow cytometer cell sorter (tumour cell sorting for CSC/non-CSC populations).

Table 2.5. Details of antibodies used in flow cytometry analysis. The use of T cell phenotyping antibodies for tetramer sorting experiments were kindly provided by Professor David Price (Cardiff University).

Antibody	Clone, Isotype	Manufacturer	Test concentration/ volume
CD44	IM7 Rat IgG_{2b}	eBioscience Thermo Fisher	0.05 µg / test
CD49b α_2Integrin	AK7 Mouse IgG_1	Bio-Rad	0.5 µg / test
CD133	AC133 Mouse IgG_1	Miltenyi Biotech	0.01925 µg / test
	EMK08 Mouse IgG_{2b}	eBioscience Thermo Fisher Scientific	0.0125 µg / test
CD49f	G0H3 Rat IgG_{2a}	Biolegend	2.5 µg / test

CD26	M-A261 Mouse IgG_1	BD Biosciences	2.5 µg / test
CD3	UCHT1 Mouse IgG_1	eBioscience Thermo Fisher	Flow cytometry 0.25 µg / test
	SK7 Mouse IgG_1	Biolegend	FACS tetramer sorting 1 µl / test
CD8	RPA-T8 Mouse IgG_1	eBioscience Thermo Fisher	Flow cytometry 0.0625 µg / test
	RPA-T8 Mouse IgG_1	Biolegend	FACS tetramer sorting 1 µl / test
CD4	RPA-T4 Mouse IgG_1	Biolegend	Flow cytometry 0.75 µg / test
	S3.5 Mouse IgG_{2a}	Invitrogen Thermo Fisher Scientific	FACS tetramer sorting 0.5 µl / test
CD14	63D3 Mouse IgG_1	Biolegend	Flow cytometry 1.5ul/test
	M5E2 Mouse IgG_{2a}	BD Biosciences	FACS tetramer sorting 1.5 µg / test
CD19	HIB19 Mouse IgG_1	BD Biosciences	FACS tetramer sorting 1.5 µg / test
TNFα	MAB11 Mouse IgG1	eBioscience Thermo Fisher	0.2 µg / test

CD107a	eBioH4A3 Mouse IgG1	eBioscience Thermo Fisher	7.5 µg / test
MIP1β	24006 Mouse IgG_{2b}	R&D Systems	1 µl / test
IFNγ	4S.B3 Mouse IgG1	eBioscience Thermo Fisher	0.75 µg / test
IL-2	MQ1-17H12 Mouse IgG_{2a}	eBioscience Thermo Fisher	2.5 µl / test
Isotype control antibody Isotype control antibodies were used where indicated in specific protocols; where an appropriate isotype control was not available, unstained cells were used instead.			
Mouse IgG_{2a}	MOPC-173	Biolegend	Matched to test antibody concentration
	eBM2a	eBioscience Thermo Fisher Scientific	Matched to test antibody concentration
Mouse IgG_1	P3.6.2.8.1	eBioscience Thermo Fisher Scientific	Matched to test antibody concentration
Mouse IgG_{2b}	eBMGb2	eBioscience Thermo Fisher Scientific	Matched to test antibody concentration
Mouse IgG_1	IS5-21F5	Miltenyi Biotech	Matched to test antibody concentration
Rat IgG_{2a}	eBR2a	eBioscience Thermo Fisher Scientific	Matched to test antibody concentration

Rat IgG_{2b}	eB149/10H5	eBioscience Thermo Fisher Scientific	Matched to test antibody concentration
Fluorescently conjugated goat anti mouse IgG (H+L) Alexa fluor 633	Polyclonal Goat IgG	eBioscience Thermo Fisher Scientific	1:200
Other fluorescent dyes			
Fixable viability dye	N/A	eBioscience Thermo Fisher	1:1000
Aqua viability dye	N/A	Thermo Fisher Scientific	1:40
ExtrAvidin PE	N/A	Sigma Aldrich	4:1 monomer: ExtrAvidin molar ratio

2.2.1 General gating strategy

The forward and side scatter voltages were adjusted depending on the size and granularity respectively of the cells under investigation; generally, the PCa cells (cell lines and primary cells) were larger than the immune cells. PBMC contained multiple populations of differing size and granularity. The general gating strategy applied before the investigation of populations expressing specific markers was as follows: doublet cells and debris were excluded by gating the population of cells observed with the x-axis set to FSC-A and the y-axis set to FSC-H (Figure 2.2A). Plotting cells on the FSC-A and FSC-H axes identifies single cells as the area correlates to the height; for doublet cells this is not a direct correlation therefore doublet cells can be excluded off the diagonal representing the single cells. This was followed by gating the population observed with the x-axis set to FSC-A and the y-axis set to SSC-A (Figure 2.2B). This gate encompasses the majority of the population except in the analysis of BLCL and PBMC; for consistency this gating was also used in the analysis of tumour cells. Cells were stained with

Fixable Viability Dye (eBioscience Thermo Fisher Scientific), so that dead cells (positive for the stain) could be gated out (Figure 2.2C). The remaining live cells were then gated as required (details given below for specific experiments).

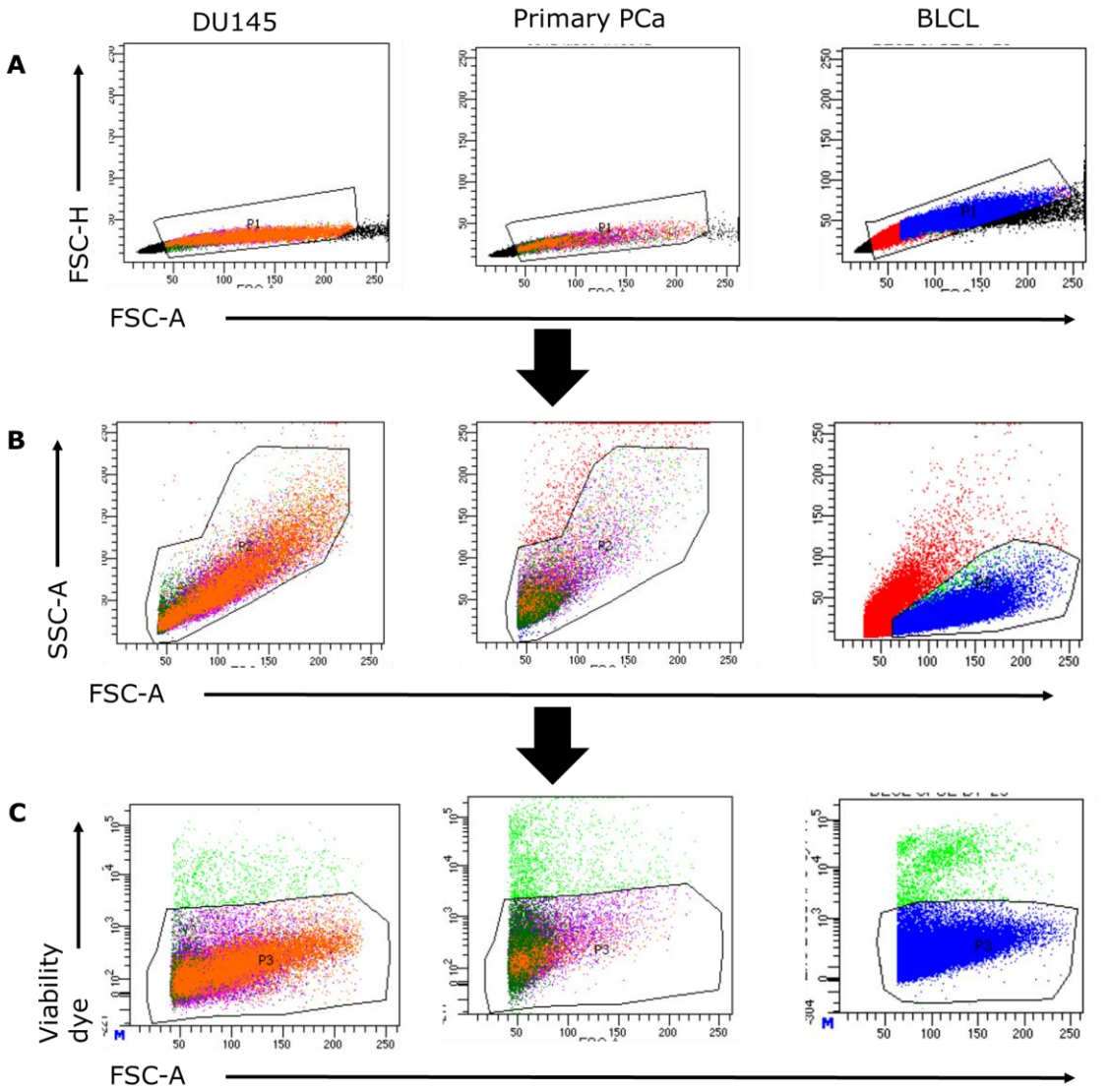

Figure 2.2 General gating strategy for flow cytometry analysis. Example dot plots are shown for DU145 cells, Primary PCa cells and BLCL, to illustrate some differences in cell size and granularity. (A) The first gate was placed to exclude doublets; the cells were arranged on a dot plot where the x-axis was set to FSA-A and the y-axis was set to FSC-H. The debris (on the extreme left of the x-axis) were also excluded in this way. (B) Setting the dot plot axes to FSC-A on the x-axis and SSC-A on the y-axis was intended to allow discrimination of size and granularity, which was mainly relevant for immune cell experiments. Increased granularity was also observed in samples containing higher frequencies of dead cells therefore this gate added to the dead cell exclusion strategy. (C) Viability gating: the viability stain (Fixable Viability dye; Thermo Fisher Scientific) binds to intracellular amines in cells which are permeable due to cell death; a high fluorescent signal on the y-axis thus indicates dead cells; live cells are gated for analysis at the lower end of the y-axis.

2.2.2 Cell surface marker staining

Cells were washed with PBS and stained for 30 min on ice in the dark with Fixable Viability dye 1:1000 in 200 µl PBS. At the end of the incubation, 2 ml PBS was added to the cells and the cells were centrifuged at 354 *x g* for 3 min followed by removal of the supernatant, to remove excess dye. This step was repeated one more time. The cells were stained with appropriate volumes of antibody or isotype control antibody (determined by titration) in the residual volume of PBS for 40 min on ice in the dark followed by 2x 2 ml PBS washes to remove unbound antibodies.

The gating strategy for analysis of prostate CSC surface markers was as follows: live single cells were gated as described above (general gating strategy), followed by gating the $CD44^+$ α_2Integrin $(CD49b)^+$ double positive population using a quadrant gating strategy. Positive staining was based on the respective isotype control gating. From this double positive population, the $CD133^+$ cells were identified by a quadrant gating strategy that was based on the isotype control antibody. These gates are shown in the results figures (Figure 3.4 and Figure 3.5).

For analysis of the prostate phenotyping markers CD49f (basal) and CD26 (luminal), the general gating strategy was followed and the respective single positive ($CD49f^+$ or $CD26^+$) or double positive $CD49f^+$ $CD26^+$ populations were gated using quadrant gates. The placement of the quadrant gates was guided by isotype control antibody staining. These gates are shown in Figure 3.3.

HLA levels in ALDH high and ALDH low DU145 and primary PCa cells were investigated with the use of an unconjugated pan HLA Class I antibody (W6/32), kindly provided by Dr Stephen Man. The staining thus required two steps: incubation with the primary antibody and with the fluorescent conjugated secondary antibody. Following the ALDEFLUOR assay and viability staining, the cells were incubated with 50 µl of the pan HLA Class I antibody for 20 min, on ice. The cells were then washed twice by centrifugation with 2 ml PBS and incubated with AlexaFluor633 anti-mouse secondary antibody

(Invitrogen Thermo Fisher Scientific) at 1:200 dilution, resuspending the cells in PBS for analysis. Gating to determine a positive pan-HLA Class I signal was determined by unstained cells and also compared to cells stained only with the fluorescently conjugated secondary antibody, this is shown in Figure 5.11.

2.2.3 Intracellular cytokine staining (ICCS)

T cells were co-incubated with antigen presenting target cells in 10% RPMI for 1 hr followed by addition of 1 µl / ml Golgi Plug (BD Biosciences) and 0.7 µl / ml Golgi Stop (BD Biosciences). Golgi Plug contains brefeldin A and Golgi Stop contains monensin. The addition of Golgi Plug and Golgi Stop blocks intracellular protein transport, resulting in retention of cytokines and other granules, produced in response to stimulation, in the Golgi apparatus (Dinter and Berger, 1998; Mollenhauer et al., 1990). This accumulation enables improved measurements by increasing the antibody staining signal detected by flow cytometry analysis (O'Neil-Andersen and Lawrence, 2002). The CD107a antibody was also added to the cells at this point. The cells were then incubated for 12 hr at 37 °C. This incubation time was selected as a result of determining the optimal incubation time (6 hr or 12 hr) for detection of IL-2, TNFα, IFNγ, MIP1β and CD107a. The incubation was stopped by washing the cells in cold PBS. This was followed by staining using the Fixable Viability dye, carried out as described above. The cells were washed to remove excess live dead stain and incubated with 100 µl fixation buffer (eBioscience Thermo Fisher Scientific) for 15 min at room temperature. The cells were then washed with 2 ml PBS and followed by addition of 100 µl permeabilisation buffer (eBioscience Thermo Fisher Scientific) for 40 min at room temperature in the dark. Antibodies for T cell phenotyping (CD3, CD4 and CD8) in addition to T cell functional markers (IL-2, TNFα, IFNγ and MIP1β) were added to the cells in the permeabilisation solution. The cells were then washed with 2 ml PBS and resuspended in PBS for analysis.

To investigate cytokine production by cytotoxic T cells ($CD8^+$), the general gating strategy described previously was first applied. The next discriminatory marker applied was CD3. From the $CD3^+$ cells the $CD4^+$ cells were distinguished from the $CD8^+$ cells by quadrant gating; $CD4^+$ $CD8^+$ T cells

were also identified in this way. The phenotype staining gating was determined based on the signal from samples that did not contain T cells. Cytokine production by these different T cell populations was measured by gating an unstained control.

2.2.4 ALDEFLUOR assay

The ALDEFLUOR assay measures the activity of the ALDH enzyme, by providing an uncharged substrate for the ALDH enzyme, BODIPY-aminoacetaldehyde (BAAA), which is oxidised to BODIPY-aminoacetate (BAA). BAA is fluorescent, and is retained in cells due to its negative charge (Ma and Allan, 2011). BAA is excited and detected in the green channel on a flow cytometer (488 nm excitation and 537/ 32 filter on the BD FACS Verse 8 laser configuration used in this study). This corresponds to the same channel in which the fluorescent conjugate Fluorescein isothiocyanate (FITC) (494 nm to 518 nm) is measured. Accumulation of BAA is proportional to ALDH activity, therefore ALDH high and ALDH low populations can be identified based on the fluorescence intensity. Generally, the ALDH high population can be gated from the 10-20% most highly fluorescent cells and the ALDH low population from the 10-20% lowest fluorescence cells (Ma and Allan, 2011; Nishida et al., 2012; van den Hoogen et al., 2010), however, since the frequency of ALDH high cells can vary by cell type, gating is specifically guided by the use of 4-(diethylamino) benzaldehyde (DEAB), an inhibitor of ALDH1 isoforms. As an additional measure for the stringent isolation of putative CSC and non-CSC populations, a gate identifying an intermediate population of cells representing 'ALDH medium' was created (Figure 3.6) and these cells were not investigated. The A549 cell line was used as a positive control for optimisation of the ALDFLUOR assay.

The ALDEFLUOR reagent was prepared according to the manufacturer's protocol. The reagent was reconstituted at room temperature by adding 25 µl DMSO, mixing (using a pipette) and incubating for 1 min. Next, 25 µl of 2N HCL (provided in the kit) was added, mixed and incubated (at room temperature) for 15 min. Finally, 360 µl of the ALDEFLUOR buffer was added and mixed. The ALDEFLUOR reagent and DEAB were kept on ice during usage.

The ALDH assay was carried out by washing detached/ suspension cells with PBS and preparing a cell suspension in 1ml of ALDH buffer, which contains efflux inhibitors to prevent active efflux of the BAA metabolite. The ALDH substrate was added to the cell suspension and mixed, followed by the removal of 300 µl of the cell suspension to a different tube containing 3 µl DEAB inhibitor. This is a modification of the manufacturer's recommended protocol (removal of 500 µl cell suspension to a tube containing 5 µl DEAB) to retain a greater cell number in the ALDH incubation for analysis and cell sorting. The cells were incubated at 37°C (in a water bath) for 45 min. The substrate was added at 5 µl per 1 x 10^6 cells for flow cytometry analysis, and the cell number was scaled up to 7 x 10^6 cells in 1 ml, with corresponding addition of 35 µl ALDH substrate (and 21 µl DEAB) for cell sorting. The number of cells and ALDH reactions (at 7x10^6 per reaction) required to yield sufficient cells for downstream experiments was calculated based on the following factors: frequencies of ALDH high and ALDH low cells recorded in the optimisation experiments, loss of cells to the control DEAB condition and expected viability of the sorted cells, estimated at 40-50%. For ordinary flow cytometry staining the ALDH substrate was adjusted to the available cell number/ based on the size of the experiment (e.g. 2.5 µl per 5x10^5 cells, 0.5 µl per 10^5 cells) and is indicated for individual experiments. At the end of the incubation, the cells were washed in PBS three times and resuspended in PBS for analysis or further antibody staining. The cells were kept on ice once the ALDH incubation was completed to reduce active efflux of the fluorescent metabolite. Thus, live dead and surface antibody staining were carried out on ice after completion of the ALDH incubation. Additionally, ALDH staining is not compatible with intracellular staining as permeabilisation of the cells results in loss of ALDH fluorescent signal.

Although the technical data regarding the ALDH assay suggests that ALDH staining can simultaneously identify live cells (as ALDH enzyme activity is confined to live cells, in contrast to the potential for antibodies to bind to dead cells), the fixable viability live dead stain (eBioscience Thermo Fisher Scientific) was incorporated into the ALDH staining protocol. Thus, the gating strategy for ALDH high and ALDH low cell analysis first consisted of the

general gating strategy as described above. Optimisation of the ALDH gating strategy is described in the Chapter 3.

2.2.5 CFSE and Cell Trace staining

Carboxyfluorescein Diacetate Succinimidyl Ester (CFSE) is a molecule that can be used to track cell divisions. CFSE is membrane permeable and once intracellular is rendered fluorescent by the action of intracellular esterases and membrane impermeable by covalently binding to certain amino acids (Lyons, 2000; Lyons and Parish, 1994). Upon cell division, the fluorescent signal is divided equally between daughter cells. This enables tracking of multiple sequential divisions per single cell, specifically the division 'history' of a single cell can be analysed retrospectively by flow cytometry analysis of the cells following *in vitro* or *in vivo* cell culture. The CFSE dye signal is measured at a fluorescent wavelength of excitation 491 nm emission 518 nm (in the green channel of BD FACS Verse 8 laser configuration used in this study).

BLCL and DU145 cells were stained with CFSE (eBioscience Thermo Fisher) as follows: the cells were prepared (detached as required, counted and washed) in a suspension of up to 10^7 cells per 1 ml in PBS, in a 15 ml CELLSTAR polypropylene tube (Greiner Bio-One). 10 µl CFSE, reconstituted in DMSO to a concentration of 50 µM was added to the cell suspension, the tube(s) were covered in aluminium foil (to protect against light exposure) and incubated for 8 min in at 37 °C in a water bath. The cells were then washed by adding 10 ml PBS, centrifuged at 354 *x g* for 3 min and the supernatant was removed. The cells were resuspended in 10% RPMI and incubated for 30 min at 4 °C (in the fridge). The cells were then plated according to the normal cell culture conditions for the specific cell type. The DU145 cells were plated at 5 x 10^5 cells in a 75 cm^2 flask for analysis after 3 days of growth and at 10^5 cells in a 75 cm^2 flask for analysis after 7 days of growth. The BLCL were plated at the same cell numbers and cultured upright in 25 cm^2 flasks. The flasks were covered in aluminium foil to protect against light exposure. Separate flasks of cells were stained at the same Day 0 and grown for analysis after three or seven days respectively. The cell division was then analysed by

flow cytometry (including viability staining using Fixable Viability Dye). Events were acquired at a low flow rate. The general gating strategy, including selection of live cells, was used to analyse the CFSE labelled cells. To analyse cell division, the CFSE fluorescence, was analysed by 'High,' 'Medium' and 'Low' gates, the placement of which was guided by analysing the fluorescence of separate cells stained the same day as flow cytometry analysis ('High') or unstained cells plated the same day as the stained cells were plated in culture ('Low'); the 'Medium' fluorescence/ proliferation was placed between the high and low gates. Fluorescence inversely correlated with to cell proliferation (High fluorescence/ low proliferation, medium fluorescence/ medium proliferation and low fluorescence/ high proliferation).

Cell Trace (Violet) (Thermo Fisher Scientific) is an alternative dye to CFSE for measuring cell divisions. Improved dyes for measuring cell division have been developed to address some of the disadvantageous aspects of CFSE, including toxicity, dye longevity and 'leakage' in measuring divisions (CFSE can measure up to 7 cell divisions) and fluorescence channel in which the dye is measured (Quah and Parish, 2012). Cell Trace is available in a number of fluorescent labels, including blue, violet, yellow and far red, corresponding to excitation by UV, 405 nm, 532 nm or 561 nm and 633 nm or 635 nm lasers respectively. These dyes can measure a range of cell divisions, up to 8-10 divisions (Cell Trace Violet), and are considered to be less toxic than CFSE, although improvements to staining protocols have reduced the cytotoxic effects of CFSE staining (Quah and Parish, 2012). Similarly to CFSE, Cell Trace can diffuse into cells, bind to amino acids and is cleaved by intracellular esterases to yield a fluorescent compound that is divided equally between new daughter cells. In my study, Cell Trace Violet was used as an alternative dye to CFSE for tracking cell divisions in ALDH high and ALDH low cells as both CFSE and ALDH are analysed in the same fluorescent channel (green). CFSE and Cell Trace labelling were compared using DU145 cells and BLCLs (without carrying out the ALDEFLUOR assay on the cells), to compare the dyes for tracking cell divisions before the Cell Trace dye was used to stain DU145 and primary PCa cells in combination with the ADLEFLUOR assay to measure division of the ALDH high and ALDH low populations.

Cell trace staining was carried out according to the manufacturer's instructions, following titration of the optimal dye concentration. The Cell Trace stock solution was prepared by adding 20 µl DMSO to the lyophilised powder (for the 20-assay kit). The cell suspension for labelling was prepared by detaching the cells (where applicable) counting and washing the cells. The cell suspension was prepared at 1 x 10^6 / ml in PBS, in a 15 ml falcon tube (CELLSTAR polypropylene tubes (Greiner Bio-One). 0.5 µl Cell Trace Violet was added (for a 2.5 µM working concentration of the dye) to the cell suspension, which was mixed by pipetting. The tube was covered using aluminium foil and incubated at 37°C, in a water bath for 20 min. Then 5 ml 10% RPMI was added and the tube was incubated for 5 minutes at 37 °C. The cells were centrifuged (at 354 *x g* for the DU145 cells and BLCL and 471 *x g* for the primary PCa cells), resuspended in 5 ml 10% RPMI an incubated at room temperature for 10 min, followed by plating the cells according to the normal cell culture conditions for the specific cell type: The DU145 cells were plated at 5 x 10^5 cells in a 75 cm^2 flask for analysis after 3 days of growth and at 10^5 cells in a 75 cm^2 flask for analysis after 7 days of growth. The primary prostate cancer cell lines were plated at 5 x 10^5 cells per well in a 6-well plate for analysis after 3 days of growth and at 2 x 10^5 cells per well in a 6-well plate for analysis after 7 days of growth. The flasks were covered in aluminium foil to protect against light exposure. Separate flasks of cells were stained at the same Day 0 and grown for analysis after three or seven days respectively. Cell division of the ALDH high and ALDH low populations was analysed on days 3 and 7 by detaching the cells and performing the ALDEFLUOR assay as described above, followed by viability staining using Fixable Viability Dye. Events were acquired at a low flow rate. The general gating strategy, including selection of live cells, was used to analyse the Cell Trace labelled cells. The same gating strategy that was used to analyse cell division based on CFSE staining was used to measure the cell divisions tracked by Cell Trace Violet: High, Medium and Low fluorescence gates were applied to the histogram plots, corresponding to Low, Medium and High division respectively; however these gates were applied to each of the ALDH high and ALDH low populations, which were gated as described above; based on the fluorescence observed in the DEAB inhibitor condition. The placement of the Cell Trace gates was guided by analysing the fluorescence of separate cells stained the same day as flow cytometry analysis ('High') or unstained

cells plated the same day as the stained cells were plated in culture ('Low'); the 'Medium' fluorescence/ proliferation was placed between the high and low gates (Figures 3.11 and 3.20)

The gating strategies used to analyse the CFSE and Cell Trace signal differ from the technical data provided with each product; in which individual peaks are gated, denoting successive generations of cells. It was not possible to apply this gating strategy to the tumour cells investigated in this study. The more distinct peaks observed in T cell assays in which CFSE or Cell Trace is used to measure activation of proliferation may be associated with co-ordinated activation of the population by a mitogen.

2.3 Microscopy

Live imaging of *in vitro* cell culture to record morphology was performed using a Zeiss axio observer z1 microscope (Zeiss, Germany), operated by Zen Blue Software or a Zeiss Axiovert 100 microscope, operated by Metamorph Software. The scale was calculated automatically and applied to the images using the Zen Blue software program for images recorded using the Zeiss axio observer z1 microscope. The scale was manually calculated for images taken using the Zeiss Axiovert 100 microscope, by imaging a reference length (a haemocytometer grid) and calculating the pixel: μm ratio. Scale bars were added using ImageJ for images recorded using the Zeiss Axiovert 100 microscope.

Imaging of fluorescent stained cells was performed using a Zeiss axio observer z1 microscope, enabled with ApoTome Optical Sectioning, operated by Zen Blue Software. The ApoTome is a form of structural illumination which introduces an evenly spaced grid through which light is focused. This enables the removal of out of focus light by acquiring three images of the specimen in which the grid is shifted by one third; the resulting image is a composite in which blurred regions are removed, resulting in improved resolution, comparable to that of confocal imaging. The scale was calculated automatically and applied to the images using the Zen Blue software

program. The antibodies used for fluorescent microscopy are detailed in Table 2.6.

Table 2.6. Details of antibodies used in fluorescence microscopy analysis			
Antibody	Clone, Isotype	Manufacturer	Test concentration (µg / ml)
Primary antibodies			
CK8	E-12 Mouse IgG_{2a}	Santa Cruz Biotechnology	2
CK5	Polyclonal Rabbit IgG	Invitrogen Thermo Fisher Scientific	4.95
CD44	DF1485 Mouse IgG_1	Santa Cruz Biotechnology	2
α-actin	1A4 Mouse IgG_{2a}	Santa Cruz Biotechnology	2
ALDH1A1	B-5 Mouse IgG_{2a}	Santa Cruz Biotechnology	2
ALDH3A1	B-8 Mouse IgG_1	Santa Cruz Biotechnology	2
ALDH7A1	EP1935Y Rabbit IgG	Abcam	2.36
ARHGAP42	Polyclonal Rabbit IgG	Sigma Aldrich	1
TPX2	18D5-1 Mouse IgG_1	Abcam	1
XPO1	Polyclonal Rabbit IgG	Abcam	1
SEPT9	Polyclonal Rabbit IgG	Novus Biologicals	1
TOP2A	TOP2A/1361 Mouse IgG_{2b}	Novus Biologicals	1
NFE2L2	Polyclonal Rabbit IgG	Sigma Aldrich	4

RLN2	Fred Mouse IgG_1	Santa Cruz Biotechnology	4
AKT2	F-7 Mouse IgG_1	Santa Cruz Biotechnology	4
Isotype control antibodies			
Mouse IgG_1	P3.6.2.8.1	eBioscience Thermo Fisher Scientific	Matched to test antibody concentration
Mouse IgG_{2a}	eBM2a	eBioscience Thermo Fisher Scientific	Matched to test antibody concentration
Mouse IgG_{2b}	eBMG2b	eBioscience Thermo Fisher Scientific	Matched to test antibody concentration
Rabbit IgG	EPR25A	Abcam	Matched to test antibody concentration
Secondary antibodies			
Goat anti-mouse IgG (H+L) conjugated to Alexa fluor 488 or Alexa fluor 594	Polyclonal Goat IgG	eBioscience Thermo Fisher Scientific	1:200
Goat anti-Rabbit IgG (H+L) conjugated to AF488 or AF594	Polyclonal Goat IgG	eBioscience Thermo Fisher Scientific	1:200

Protein expression was investigated by fluorescence microscopy. The cells were plated in 8-well imaging chamber slides (Thermo Fisher Scientific) or 96-well black walled glass bottom plates (Greiner Bio-One) at 10^4 cells per well and grown until they were 90% confluent. The cells were fixed for staining using either a mixture of methanol and acetone, or paraformaldehyde (PFA). The fixation method was determined by the antibody manufacturer's recommendation, or both methods were compared if no method was recommended. For methanol/acetone fixation, a 1:1 mixture of methanol and acetone was produced and stored in the -20°C freezer. The mixture was used to fix and permeabilise cells by removing the media from the cells and washing with PBS, followed by addition of cold acetone: methanol mixture, taken directly from the freezer; 200 µl per well was added to the 8 well chamber slides while 100 µl per well was added for the 96-well plate. The plates were incubated at room temperature for 10 min followed by removal of the methanol: acetone mixture. The plates were air dried. For fixation using PFA, the media was removed and the cells were washed in PBS followed by addition of 4% PFA (room temperature) (200 µl per well was added to the 8 well chamber slides while 100 µl per well was added for the 96-well plate). The working concentration of 4% PFA was made by diluting 16% PFA (Thermo Fischer Scientific) using PBS. The cells were incubated at room temperature for 30 min followed by removal of the PFA. The cells were then permeabilised by addition of 10% Triton X-100 (Sigma Aldrich) for 10 min. The plates were air dried following removal of the Triton X-100.

Prior to antibody staining, the plates were blocked for 2 hr at room temperature using 1% BSA, made by diluting 10X BSA (R&D Systems) in PBS 1:10. Antibodies were prepared at the recommended dilution (or a range of recommended dilutions were tested) in 0.1% BSA-PBS. The isotype control antibodies were diluted to match the concentration of the respective antibodies in 0.1% BSA-PBS. Antibodies and isotype controls used for fluorescence microscopy are detailed in Table 2.3. The antibody or isotype controls were added to the chamber slides at 200 µl per well for the 8 well chamber slides or 100 µl per well for the 96-well plate. The plates were incubated at room temperature for 45 min. The primary antibody was

removed, and the plates were then washed with 200 µl PBS for 3 x 5 min. The fluorescent conjugated secondary antibody was diluted 1:200 in 0.1% BSA-PBS, added to the cells and incubated for 45 min at room temperature. The secondary antibody was removed, and the plates were then washed with 200 µl PBS for 3 x 5 min. The plates were then stained with DAPI (a nuclear stain), diluted 1:100,000 for 2 minutes, followed by removal of the stain and washing by adding 200 µl PBS for 5 min. For microscopy visualisation, 200 µl PBS was added to the well.

2.4 *In vitro* assays

2.4.1 Colony formation assay

The colony formation assay was carried out based on an established protocol, with some modifications (Franken et al., 2006). DU145 cells were sorted by FACS into ALDH high and ALDH low populations and seeded at 50 cells/ cm^2 per well of a 6-well adherent cell culture plate (450 cells per well) (Cellstar TC-treated adherent cell culture plate) (Greiner Bio-One). The cells were grown in 10% RPMI and until the colonies were ≥50 cells (determined by visualisation with a light microscope, typically 7-10 days). The optimal seeding density was determined by testing a range of cell concentrations: 25 cells/ cm^2, 50 cells/ cm^2 and 100 cells/ cm^2. The colonies were fixed by removing the culture media and washing with PBS, followed by addition of 1 ml per well 10% Neutral Buffered Formalin (VWR International). The cells were incubated for 30 min at room temperature. The colonies were stained using a 5% w/v solution of crystal violet, made up in ddH_2O for 1 hr at room temperature. The concentration of crystal violet was increased from the recommendations of the established protocol to enable visualisation and quantification of the colonies. The stained colonies imaged using a DSLR camera. Where possible, the colonies were quantified using the ColonyArea plugin for ImageJ (Guzmán et al., 2014). To do this, the images were converted to 8-bit type images, then cropped and rotated to straighten the orientation of the plate in the image, so that only the plate was visible, to enable detection by the plugin of the plate and individual well edges. The ColonyArea plugin was then run according to the published instructions. A

threshold (in pixels) was applied to the image for detection of stained colonies (stained colonies measured a pixel value higher than that of unstained plate surface). Size exclusion criteria for areas above the pixel threshold were applied to exclude colonies <50 cells and measures from the edge of an individual well were excluded, based on the recommendations of the protocol (Guzmán et al., 2014). The analysis was then executed to quantify the number of colonies and the total colony area.

2.4.2 Sphere formation assay

Sphere formation was measured by culturing the cells in the basic ADMEM/F12 media described for prostate organoid culture by Drost and colleagues, however the only supplements added were with 5 ng / ml EGF and 5 ng / ml bFGF (Drost et al., 2016). This media was selected by investigating the minimal supplement conditions required to support sphere formation (by unsorted DU145 cells), and a search of the literature also suggested the chosen supplements as being commonly used in sphere formation assays (Beier et al., 2007; Moore et al., 2012; Nishida et al., 2012).

Sphere formation by ALDH high and ALDH low cells (DU145 cells and primary PCa cells) was measured by seeding the FACS isolated populations into cell-repellent 96-well U bottom plates (CELLSTAR cell repellent surface plate, Greiner Bio-One) at 1000 and 100 cells per well. Blank wells containing an equal volume of media (180 µl) were included for use in the Orangu assay. Addition of blank wells at the same time as seeding the cells is important so that the blank measurements are taken from media at the same approximate temperature and pH as the cell containing wells, as this can affect the Orangu measurements. The cells were grown in the sphere formation media for 7 days, including a change of media for wells containing both cells and blank wells (100 µl from the total volume of 180 µl) after 3 days. The analysis parameters were sphere size (area um^2) and proliferation/ viability, measured by microscopy and the Orangu assay (Cell Guidance Systems), respectively. The spheres were imaged using a Zeiss axiovert 100 microscope and sphere area was calculated using Metamorph Software. The Orangu assay is based on the measurement of WST-8 metabolism as an indicator of cell proliferation

and viability. WST-8 is a tetrazolium salt that is reduced to formazan by mitochondrial dehydrogenases (not ALDH), using NADH as an electron donor (Präbst et al., 2017). Formazan is a coloured metabolite (orange) that can be measured using a spectrophotometer. Increased absorbance measurements correlate to greater production of formazan and higher proliferation/ a greater number of viable cells. WST based assays can be used to quantify the cell number in adherent *in vitro* culture. However, the nutrient and oxygen gradients occurring in larger spheres, leading to differences in cell turnover at the peripheral zone core, precludes the same quantification capacity of WST assays in non-adherent *in vitro* culture. Nevertheless, the use of a different tetrazolium salt (WST-1) to measure viability in large spheres suggests WST based assays are suitable for measuring viability and proliferation in sphere culture (Zanoni et al., 2016). The Orangu assay was carried out according to the manufacturer's protocol: 10 µl of the Orangu reagent was added to each well (including blank wells) and mixed by gentle pipetting (to avoid creating bubbles). The cells were then incubated for 2 hr at 37 °C. Absorbance at 450 nm was measured using a PHERAstar FS Microplate Reader (BMG Labtech, Aylesbury, UK). A protocol was created on the microplate reader specifically for analysis of U bottom plates. The absorbance was determined by subtracting the averaged measurements from the blank (media only) wells to which Orangu was added, from the readouts of the wells containing spheres to which Orangu was added.

2.5 Gene expression analysis

RNA extraction and gene expression analysis were performed on surfaces kept free of contaminating genomic material using RNAzap (Thermo Fisher Scientific) and 70% ethanol. RNAse and DNAse free pipette tips and plasticware and decontaminated pipettes were used (separate pipettes and pipette tips were used for working with RNA and DNA). Pipettes, tips and plasticware were decontaminated after use by UV light in a Labcaire Vertical Laminar Airflow Cabinet with UV Sterilisation PCR workstation.

2.5.1 RNA extraction

RNA was extracted from FACS isolated ALDH high and ALDH low DU145 or primary PCa cells using the Trizol method (Chomczynski, 1993). This involves liquid phase separation of the cellular material, which is homogenised in the Trizol/ Tri-reagent, which contains phenol and guanidine thiocyanate. Genomic material: DNA, RNA and protein are each separated into the interphase, aqueous phase and organic phase respectively. To extract RNA, the cells were pelleted by centrifugation and the supernatant was removed. The cell pellets were resuspended in 1ml Tri-reagent (Sigma Aldrich), and transferred to a RNAse and DNAse free 1.5 ml Eppendorf tube (STARLABS). The tubes were plated in a -80 °C freezer overnight. The solution was thawed at room temperature and 200 µl chloroform was added to the tubes. The tube was shaken vigorously for 15 sec and placed on ice for 5 min. The tube was centrifuged at 16,000 *x g* for 20 minutes at 4 °C, to allow the separation of the aqueous and phenol (organic) phases using a MSE *Sanyo Hawk 15/05* Refrigerated Centrifuge The aqueous layer was retrieved using a pipette, without removing any of the organic layer, and added to a new 1.5 ml RNAse and DNAse free Eppendorf tube containing 500 µl ice-cold molecular grade isopropanol (Fisher Scientific). The tubes were inverted 3 times and placed in a -20 °C freezer overnight, to allow RNA precipitation to occur. The samples were centrifuged at 16,000 *x g* for 20 minutes at 4 °C. The isopropanol was removed by inverting the tubes into a waste container and the RNA pellet was resuspended in 1 ml ice-cold 70% molecular grade ethanol (Fisher Scientific). The tubes were centrifuged at 16000 *x g* for 20 minutes at 4 °C. The ethanol was removed by inverting the tubes into a waste container and the ethanol wash step was repeated one more time. The RNA pellets were then air dried at room temperature and dissolved in 11 µl HyClone™ Water, Molecular Biology Grade (nuclease free) (Fisher Scientific). RNA concentration and quality were measured using NanoDrop™ 2000 Spectrometer (ThermoFisher Scientific). The NanoDrop was first blanked with 1 µl of the HyClone™ Water, then 1 µl of the RNA sample was measured. In addition to providing a readout of the RNA concentration, the NanoDrop obtains a ratio of absorbance measured at 260 nm and 280 nm. RNA and DNA absorb at 260 nm, they will contribute to the total absorbance of the sample. A ratio >1.7 is generally accepted as 'pure' RNA and used for analysis. If the ratio is considerably

lower, it may indicate the presence of protein, phenol or other contaminants that absorb strongly near 280nm. Samples for which the $_{A}$260/280 ratio was lower than 1.7 were not used for gene expression analysis.

2.5.2 RT-qPCR

Expression of pre-selected CSC associated genes was investigated in the ALDH high and ALDH low DU145 cells using the RT^2 Profiler™ PCR Array Human Cancer Stem Cells (Qiagen). The array format consisted of a 96-well plate containing pre-loaded primers, to which cDNA was added. The array consisted of 84 genes associated with CSC signalling, and 5 housekeeping genes (Appendix 2.1). The remaining wells included experimental controls; genomic DNA control, 3 X reverse transcription controls and 3 X positive PCR controls. This PCR array uses SYBR green detection, a method of detecting amplified DNA based on the binding of a fluorescent dye (SYBR green) to double stranded DNA. dsDNA produced as a result of primer amplification is bound by SYBR green dye, enabling quantification of gene expression proportionate to the dye fluorescence. This method of quantifying gene expression is less specific than TaqMan probes as the reporter dye is not probe specific. For this reason, this method can be more cost effective for larger scale arrays.

The RT² Profiler™ PCR Array was used in combination with the RT^2 First Strand kit to produce cDNA by reverse transcription of RNA. cDNA was produced according to the manufacturer's instructions. The contents of the RT^2 First Strand were thawed at room temperature and stored on ice during usage. The genomic DNA elimination reaction was prepared by making up a reaction volume of 10 µl, containing 2 µl Buffer GE, 0.5 µg of RNA and nuclease free H_2O as required. The reaction was prepared in 0.2 ml PCR tubes (MicroAmp™ Reaction Tube with Cap, Applied Biosystems from Thermo Fisher Scientific). The reaction was prepared on ice. The mixture was pipetted to mix and briefly centrifuged. The mixture was incubated for 5 min at 42 °C using a S1000 Thermal Cycler (BioRad) then immediately placed on ice for 1 min. The reverse transcription mix was prepared as follows (in a 0.2 ml PCR tube):

Table 2.7. Reagents and volumes for a Reverse Transcription reaction using the RT2 Profiler First Strand kit (Qiagen)	
Reagent	Volume per 1 reaction (µl)
5X Buffer BC3	4
Control P2	1
RE3 Reverse transcriptase mix	2
Nuclease free H_2O	3
Total volume	10

The reverse transcription mix was added to the genomic DNA elimination reaction and mixed by pipetting. The 20 µl reverse transcription reaction was incubated at 42 °C for 15 min, then at 95 °C for 5 min, using the S1000 Thermal Cycler. The reaction was placed on ice and 91 µl nuclease free H_20 was added.

The PCR reaction mix was prepared at room temperature (as it contains HotStart DNA Taq polymerase which is activated only after heating). The reaction was prepared in a RNAse and DNAse free 50 ml falcon tube (Greiner Bio-One). The PCR reaction was prepared as follows:

Table 2.8. PCR reaction master mix reagents and volumes for the RT2 Profiler CSC Array (Qiagen)	
Component	Volume (µl)
2X RT^2 SYBR Green Master mix	1350
cDNA	102
Nuclease free H_2O	1248
Total	2700
Volume per well/ reaction	25

The remaining 9 µl of cDNA was retained and stored at -20 °C, as recommended by the manufacturer for any arising quality control requirements. The PCR reaction was mixed by pipetting and dispensed into the RT^2 Profiler Array plate (pre-loaded with the relevant primers). 25 µl of the PCR reaction was added to each well. The plate was sealed with the supplied Optical Adhesive Film and centrifuged at 1000 *x g* for 1 min. The plate was kept on ice from this point onwards. The PCR reaction was carried out using an Applied Biosystems StepOnePlus™ Real-Time PCR System Thermocycler (ThermoFisher Scientific). The cycling conditions and data collection was performed as follows:

Table 2.9. Cycling conditions for the PCR reaction for the RT2 Profiler CSC Array (Qiagen).

Cycles	Duration	Temperature	Process
1	10 min	95 °C	Activation of the Taq polymerase
40	15 sec	95 °C	
	1 min	60 °C	Data collection

The raw data was processed on the StepOnePlus Thermocycler; a cycle number baseline was applied to exclude noise and a threshold line was applied in the linear phase of the fluorescence amplification plot, to calculate the cycle threshold (CT) values of the individual genes (example; Figure 2.3. The CT value is the threshold cycle number where amplification is in the linear range of the amplification curve. Data analysis was carried out using a pre-formatted Microsoft Excel file obtained from Qiagen and statistical testing was performed in an ordinary Microsoft Excel file. The pre-formatted Excel file contained the gene list and automatically calculated quality control tests using the CT values of from the control wells in the array. The comparative CT method was used for relative quantification of target gene expression (Schmittgen and Livak, 2008). The normalised CT values (ΔCT) were calculated in the pre-formatted file by subtracting the averaged CT values of the housekeeping genes from the CT value of each gene in the ALDH high

and ALDH low samples. Of the five housekeeping genes, 4 were selected to compute the average, based on the lowest variation across n=3 replicate PCR reactions. The fold change was calculated manually by transferring the normalised CT values to the blank excel file. The fold change was calculated by the formula $2^{-\Delta\Delta CT}$ = (ΔCT ALDH high gene of interest)- (ΔCT ALDH low gene of interest). Statistical analysis was carried out by performing a Student's T test on the ΔCT values of each individual gene from the ALDH high and ALDH low samples. The fold change cut off was set at ≥1.5, p≤0.05.

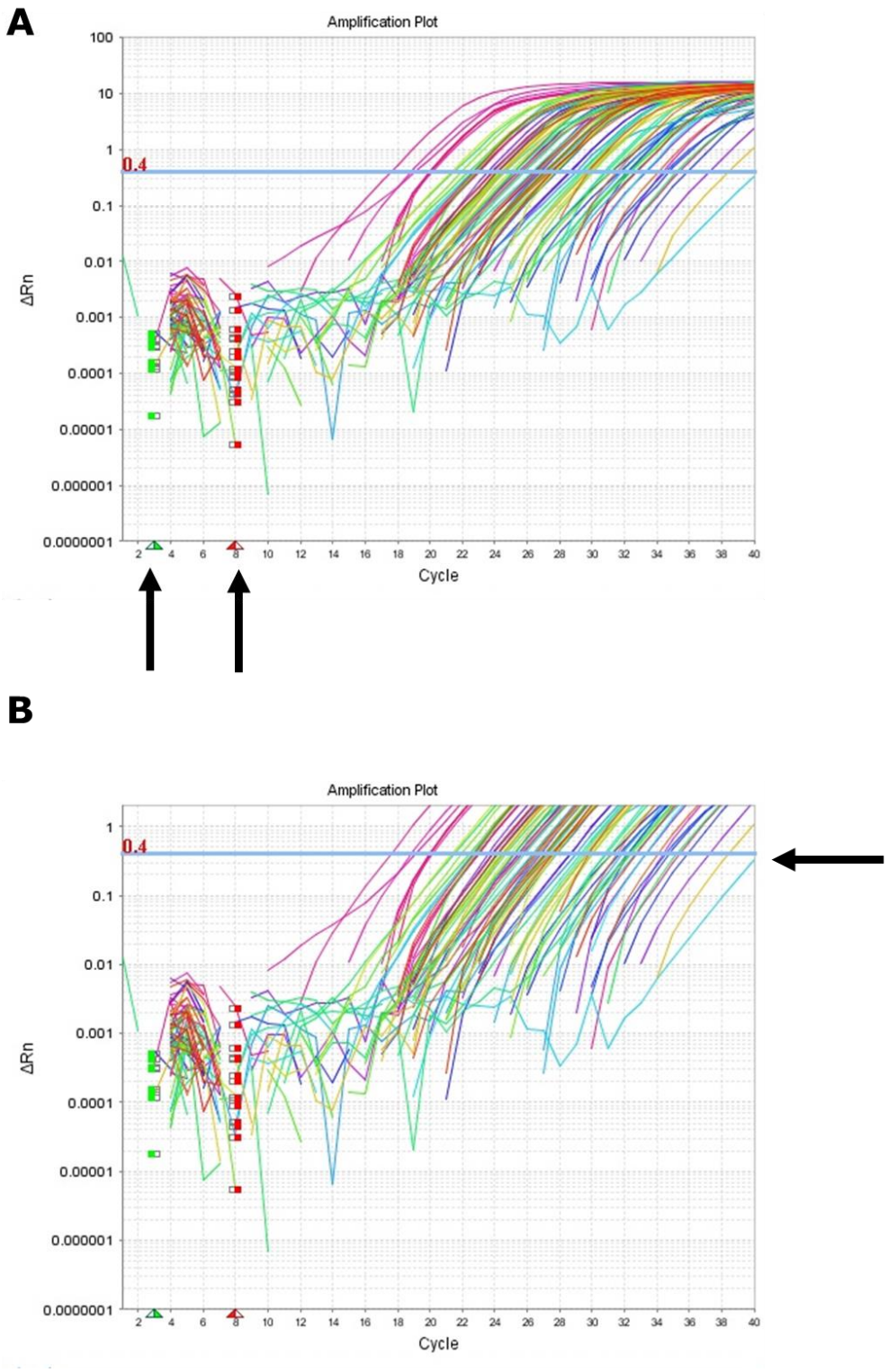

Figure 2.3 Analysis of Qiagen RT2 Profiler qRT-PCR amplification plot raw data. Application of (A) a baseline to exclude noise and (B) a cycle threshold in the linear region of the amplification plot to identify the cycle threshold of individual genes. The same baseline and cycle threshold were applied to all of the genes analysed as the layout of the plate did not allow for programming individual baselines or cycle thresholds.

Expression of certain genes identified as a result of HLA ligandome analysis of the DU145 cells was measured in ALDH high and low DU145 and primary PCa cells. The aim was to identify if any of the genes were more highly expressed in ALDH high cells, suggesting greater processing and presentation of sequences derived from the translated protein by HLA. The genes investigated were selected by bioinformatics methods detailed below. The gene expression was investigated on an individual basis, using TaqMan primer-probes. The primers were purchased from Thermo Fisher Scientific by selecting the 'Best Coverage' primer for each gene, where available. If no primer was recommended, the selection was made based on minimising the possibility of amplification of genomic DNA; the different primers available from Thermo Fisher Scientific include primers that span an exon junction (excluding the possibility of amplifying genomic DNA) or primers that map within a single exon (possibility of amplifying genomic DNA). The primers used are detailed in Table 2.10. TaqMan primer-probe based gene expression quantification differs from SBYR green in that the fluorescent signal is coupled to the primer. Therefore, the signal is more specific as fluorescence occurs due to the quencher molecule being displaced from proximity to the fluorescent reporter dye by cleavage by TaqMan polymerase, in the process of extending the primer sequence. This can be more expensive and prohibitive towards larger scale analysis (the expression of 42 genes was compared between ALDH high and ALDH low DU145 cells and a selected subset was compared in primary PCa cells).

Table 2.10. Gene and primer list for qRT-PCR analysis of genes for which the peptides were identified in the HLA ligandome analysis as having low or absent global healthy tissue expression and high allele specific HLA binding affinity.

CRBN	Hs00372266_m1
SEPT9	Hs00246396_m1
XPO1	Hs00185645_m1
ZNF14	Hs00221420_m1
ARHGAP42	Hs00611831_m1

FGD6	Hs00217947_m1
STIL	Hs00161700_m1
EGFR	Hs01076090_m1
SMARCB1	Hs00268260_m1
AKT2	Hs01086099_m1
HIF1A	Hs00153153_m1
NFE2L2	Hs00232352_m1
NPW	Hs00405318_g1
SHCBP1	Hs00226915_m1
BRCA1	Hs01556193_m1
TRAIP	Hs00183394_m1
TOP2A	Hs01032137_m1
KRAS	Hs00932330_m1
MAGED4	Hs01017371_m1
RLN2	Hs00366471_m1
CENPE	Hs01068241_m1
ASAH2B	Hs04185427_m1
MEX3A	Hs00863536_m1
TPR	Hs00162918_m1
TP53	Hs01034249_m1
KIF14	Hs00978236_m1
CBL	Hs01011446_m1
MTR	Hs00165188_m1
MYH8	Hs00267293_m1
CCDC127	Hs00299171_m1
TACSTD2	Hs01922976_s1
RIPK4	Hs01062501_m1

TPX2	Hs00201616_m1
HIST1H4A	Hs00747492_s1
ABL1	Hs01104728_m1
MTOR	Hs00234508_m1
RRM1	Hs00168784_m1
MSH6	Hs00943000_m1
WDR62	Hs00543464_m1
THADA	Hs00152982_m1
SOX11	Hs00846583_s1
ATP9B	Hs01015711_m1

RNA extracted from the ALDH high and ALDH low cells was reverse transcribed to cDNA using a High Capacity cDNA Reverse Transcription Kit (Applied Biosystems Thermo Fisher Scientific). A negative control for the RT reaction was produced by substituting nuclease free H_2O instead of RNA in the reaction. The reaction was prepared on ice, in an RNAse and DNAse free 1.5 ml Eppendorf tube. The volumes given are for one reaction however the reaction was typically prepared as a scaled-up master mix for multiple reverse transcription reactions for ALDH high and ALDH low RNA and negative control nuclease free H_2O.

Table 2.11. Reagents and volumes for a Reverse Transcription reaction using the High Capacity cDNA Reverse Transcription Kit (Applied Biosystems Thermo Fisher Scientific.

Kit component	Volume (µl) per 1 reaction
10 X RT buffer	2
2X dNTP Mix (100 mM)	0.8
10X RT Random Primers	2
MultiScribe Reverse Transcriptase	1

RNAse Inhibitor (not included in the kit; also supplied by Thermo Fisher Scientific)	1
Nuclease free H_2O	3.2
Total	10

A single reverse transcription mix (10 µl) was added to 1 µg of RNA sample (or negative control), which was prepared in a 0.2 µl PCR tube (details as previously described) to a total volume of 10 µl (volume of RNA based on the individual concentration with addition of nuclease free H_2O as required for a total of 10 µl). The reverse transcription and RNA was mixed by pipetting and placed on ice. Reverse transcription was carried out using an s1000 Thermal Cycler (BioRad); the samples were incubated at 25 °C for 10 min (annealing), then 37 °C for 120 min (primer extension), followed finally by incubation at incubating at 85 °C for 5 min (deactivation of the reverse transcriptase). The thermocycler was programmed to incubate the samples at 4°C to preserve the cDNA integrity when the reverse transcription reaction was completed. The resulting cDNA sample was diluted by addition of 80 µl nuclease free H_2O.

The PCR reaction was prepared on ice, by making a master mix in an RNAse and DNAse free 1.5 ml Eppendorf tube as follows:

Table 2.12. PCR reaction master mix reagents and volumes for TaqMan qRT=PCR of genes identified by HLA ligandome analysis. For each plate, 8 individual master mixes were produced, containing 7 different gene specific primer probes. GAPDH was used as a housekeeping control gene in each plate thus the 8th tube for each plate always contained the GAPDH gene specific primer-probe.

Reagent	Volume (µl) per 1 reaction
TaqMan Master Mix	10
Gene specific primer-probe	1
Nuclease free H_2O	4

Total	15

The PCR reaction (15 µl) was added to each well of a MicroAmp™ Optical 96-Well Reaction Plate (Thermo Fisher Scientific). 5 µl of cDNA from the ALDH high, ALDH low or negative control reverse transcription reactions was then added to individual well. Nuclease free H_2O was added to some wells in lieu of cDNA, as a negative control for the PCR reaction. The plate additions were made on ice. The plates were sealed using MicroAmp™ Optical Adhesive Film (Thermo Fisher Scientific) and centrifuged at 1000 *x g*. The plates were kept on ice prior to running the PCR reaction. The PCR amplification was performed in a StepOnePlus™ Real-Time PCR System Thermocycler (ThermoFisher Scientific). Samples were amplified by heating them to 50 °C for 2 minutes, then at 95 °C for 15 seconds and 60 °C for 1 minute, for a total of 40 cycles.

The data was analysed similarly to that of the PCR array described previously; a baseline and threshold was applied to the raw data to obtain the gene specific CT values (Figure 2.4: A, B). Due to the differences in setup (i.e. individual primers instead of an array), different thresholds and baselines could be set for individual genes within each plate. The same threshold and baseline were applied for a specific gene analysed across three replicate cDNA samples. The fold changes were calculated by the comparative CT method, as described previously. The fold change cut off was set at ≥ 1.5, $p \leq 0.05$. Statistical analysis was carried out by performing a Student's T test on the ΔCT values of each individual gene from the ALDH high and ALDH low samples. Additionally, the most abundant genes were of interest in relation to antigen processing and presentation. Gene transcript abundance was calculated as $2^{-\Delta CT}$. Gene abundance in the ALDH high and ALDH low samples were not compared as the most highly abundant genes shared in both ALDH high and ALDH low samples were of interest.

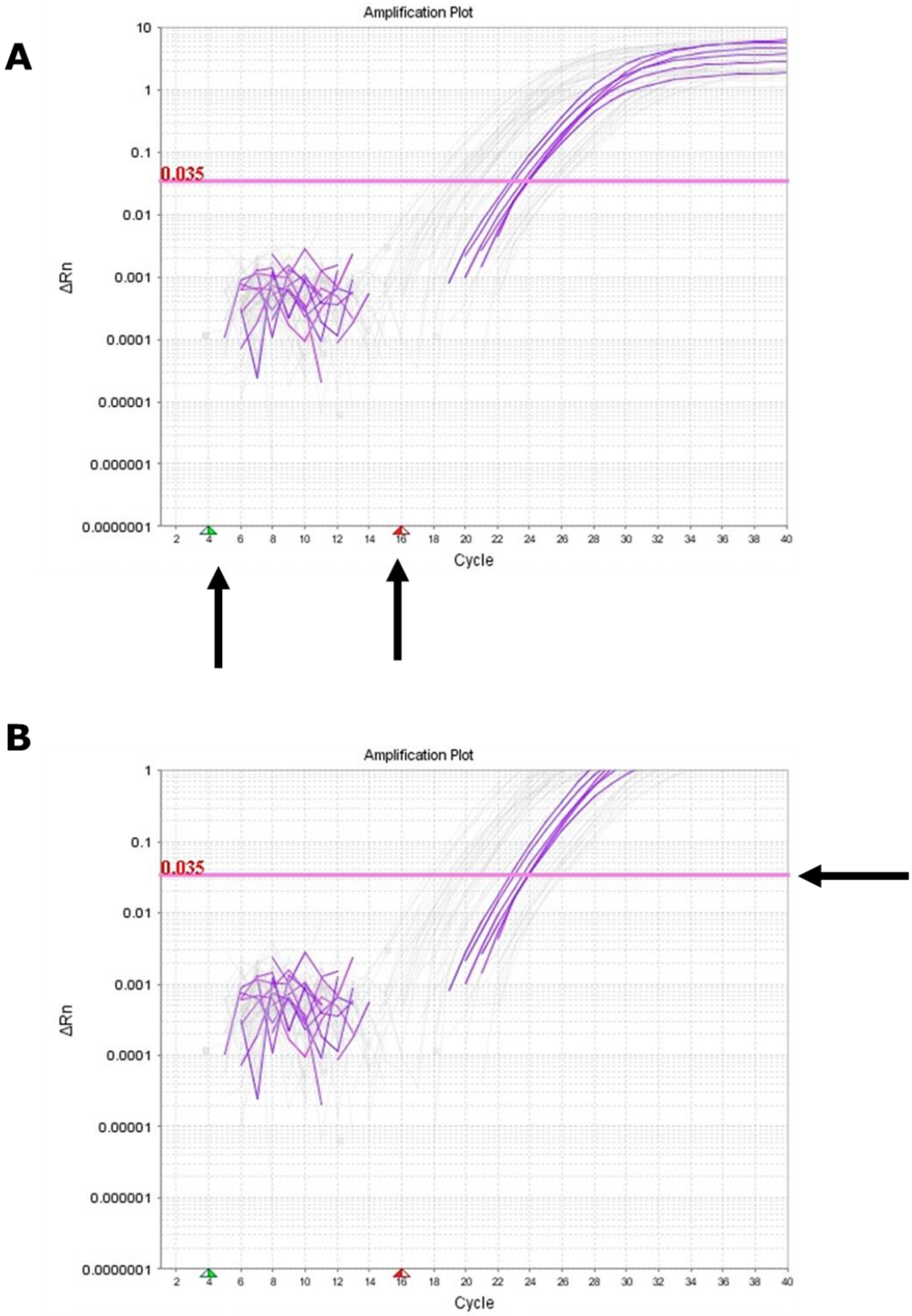

Figure 2.4 Analysis of Taqman qRT-PCR amplification plot raw data. Application of (A) a baseline to exclude noise and (B) a cycle threshold in the linear region of the amplification plot to identify the cycle threshold of individual genes. Individual baselines and cycle thresholds were applied to each gene; the same baseline and cycle thresholds were used to analyse the same gene across ALDH high and ALDH low samples.

2.5.3 Nanostring

Gene expression was also investigated using the Nanostring platform, a non-amplification based method of analysing gene expression (Geiss et al., 2008). This method was selected as it was of interest to investigate gene expression in primary PCa cells, from which low amounts of genomic material were recovered. The Nanostring platform is optimised for quantification of gene transcripts from 50 ng RNA.

As a requirement of carrying out the Nanostring gene expression, quality control analysis of the RNA intended for the gene expression analysis was performed using an Agilent 2100 Bioanalyzer (Agilent Technologies). The Bioanalyzer measures RNA degradation by electrophoresis and returns a measure of the level of RNA degradation, the RNA Integrity Number (RIN) (higher RIN indicates less degradation, more optimal for Nanostring gene expression analysis). Other QC measures including the percentage of ≥200 base pair (bp) RNA fragments in the sample can also be determined. The Bioanalyser also returns the RNA concentration; it was this concentration rather than the NanoDrop derived concentration that was used to produce aliquots of RNA for Nanostring analysis. The RNA obtained from ALDH high and ALDH low DU145 and primary PCa cells was analysed according to the manufacturer's protocol. The RNA ladder and electrophoresis gel were prepared in advance. The RNA ladder was prepared by aliquoting the ladder into a 0.2 ml PCR tubes (MicroAmp™ Reaction Tube with Cap, Applied Biosystems from Thermo Fisher Scientific), which was incubated at 70 °C for 2 min in a Thermal Cycler, then immediately placed on ice. The denatured ladder was stored at -80 °C. The electrophoresis gel was prepared by pipetting 550 µl gel matrix into a spin filter (supplied) and centrifuging the gel at 1500 *x g* for 20 min at room temperature, then aliquoted for single use and stored at 4 °C. On the day of analysis, one aliquot (65 µl) of gel was prepared by equilibrating at room temperature then adding 1 µl of RNA dye concentrate to the gel. The gel was vortexed to mix then centrifuged at 13000 *x g* for 10 min at room temperature. A new single use RNA Nano chip (containing lanes for simultaneous analysis of 12 RNA samples) was placed in the chip priming station. 9 µl of the gel-dye mix was added to the well marked **G**. The plunger of the attached syringe was then positioned at 1 ml,

the chip priming station closed securely, and the plunger was pressed down until held by the clip, for 30 sec, to disperse the gel evenly through the chip. The clip was then released and after a further 5 sec the plunger was returned to the 1 ml mark. 9 µl of the gel dye mix was then pipetted into the two wells marked **G.** 5 µl of the RNA marker was added to each of the sample wells and the well marked for the ladder. 1 µl of the pre-made RNA ladder was added to the well marked for the ladder. 1 µl of RNA sample was added to each sample well, and the chip was removed from the chip priming station and vortexed for 1 min at 2400 rpm, using the designated vortex. The chip was then analysed using the Agilent 2100 Bioanalyzer. The RIN and RNA concentration were returned automatically and the percentage of ≥200 bp RNA fragments was measured by placing gates on the x-axis (nucleotide) size of the fragmentation profiles from 200 bp to the maximum.

Nanostring analysis was carried out at Bristol University, UK. The RNA samples were prepared for analysis by aliquoting 50 ng into a 0.2ml PCR tube and making up the final volume to 5 µl using HyClone™ molecular grade water. Sample hybridization and gene expression analysis was carried out according to the manufacturer's instructions. The Reporter CodeSet and Capture ProbeSet components were thawed at room temperature, inverted to mix and centrifuged at 1000 *x g* for 30 sec. 70 µl of the hybridization buffer was added to the Reporter CodeSet tube, and mixed by inverting, then centrifuged briefly to bring the liquid to the base of the tube. 8 µl of the hybridization buffer/ Reporter CodeSet master mix was added to 0.2 µl PCR tubes. The 5 µl RNA samples were each added to the hybridization reaction tubes. The Capture ProbeSet was inverted to mix and centrifuged briefly, then 2 µl was added to the hybridization reaction tubes. The tubes were mixed by flicking the tubes, centrifuged briefly and incubated at 65°C for 16 hr. The following day the samples were retrieved from the thermal cycler and 15 µl ddH_20 was added to each tube. The samples were then added to the Nanostring cartridge and the cartridge was sealed and loaded onto the Nanostring SPRINT. The gene expression analysis program was run for 6 hr.

The Nanostring data was analysed by transferring the raw data (counts) to a Microsoft Excel file. Analysis was carried out based on guidelines from both

the Nanostring technical bulletin 'Gene Expression Data Analysis Guidelines' and a study by Prokopec and colleagues, in which different medium-throughput platforms for analysing gene expressing using RNA as the starting material are compared (Prokopec et al., 2013). The samples were analysed on a pairwise basis; ALDH high and ALDH low DU145 samples (n=2 independent FACS) experiments were investigated, and each pair of primary PCa samples were analysed separately due to the large variation in transcript counts. To determine the fold change between ALDH high and ALDH low samples, the counts below the threshold ≤30 were first eliminated. The in-built positive control counts were summed, averaged and the sum was divided by the to derive the positive normalisation factor. The counts were multiplied by the positive normalisation factor (each sample was normalised by its own specific normalisation factor). The housekeeping genes were selected according to the results in each pairwise analysis; based on the correlation between the housekeeping counts for the ALDH high and ALDH low samples (tested by dividing the ALDH high counts by the ALDH low counts). To apply a housekeeping gene normalisation, the geometric mean of each individual housekeeping gene, for the ALDH high and ALDH low samples, was calculated. The counts for each housekeeping gene per individual sample was summed, and the sum was divided by the geometric mean to derive the housekeeping normalisation factor. The counts were then multiplied by the housekeeping normalisation factor. The normalised counts were then $\log_2$ transformed, followed by calculation of the $\log_2$ ratio by subtracting the $\log_2$ transformed ALDH low counts from the $\log_2$ transformed ALDH high counts. The fold change was derived from the $\log_2$ ratio by the formula $2^{\log 2}$ ratio.

Pathway analysis was performed using the Functional Annotation Tool at the Database for Annotation, Visualization and Integrated Discovery (DAVID) online bioinformatics resource https://david.ncifcrf.gov/ (Huang et al., 2009a, 2009b). The genes up- or downregulated were compared to a reference list; for this the gene list provided with the assay was used. This gene list was converted to entrez_gene_ID naming format using the UniProt ID mapping tool https://www.uniprot.org/uploadlists/, as the official gene symbol naming format is not accepted as the format for a reference list. The

up- or downregulated genes were input in the naming format 'official gene symbol' and compared to the reference list using the default settings. The resulting Annotation Clusters were investigated for specific pathways in which the up or downregulated genes were significantly enriched.

2.6 *In vivo* analysis of tumorigenicity

Demonstrating the *in vivo* tumour initiating capacity is an essential characteristic of a proposed CSC population (Visvader and Lindeman, 2008). ALDH high and ALDH low DU145 cells were injected subcutaneously into NOD/SCID gamma (NSG) mice to assess tumour growth. NSG mice were purchased from The Jackson Laboratory, USA, and maintained in the animal facility of Sapporo Medical University. All procedures and animal care were performed in accordance with the institutional animal care guidelines. DU145 cells were isolated by FACS based on the ALDEFLUOR assay. The sorted cells were resuspended in PBS and kept on ice prior to the injections. Tumour initiation was investigated under limiting dilution conditions, using two starting cell numbers. For expected viable injected cell numbers of 10^2 cells and 10^3 cells, suspensions of 10^3 cells and 10^4 cells in 100 µl PBS respectively were prepared, for n=5 mice per group. The mice were prepared for subcutaneous injections by shaving a small area of fur on the flank, which was sterilised using ethanol-soaked cotton swabs. Immediately prior to injecting, each individual cell suspension was mixed 1:1 with Matrigel (BD Biosciences) which had also been stored on ice to prevent solidifying. This mixture was slowly injected subcutaneously, and the needle slowly withdrawn, and pressure applied. Tumour growth was detected by palpating the injection site. Once the masses were of a sufficient size the tumour area was measured using a digital calliper. The tumour volume (mm^3) was calculated using the *formula* V = ((W (2) × L)/2 (W= width, L= length). Tumour growth was monitored weekly up to 43 days, followed by a final measurement at 64 days. The animals were sacrificed by vertebral cervical dislocation after the final measurements at 64 days. The *in vivo* experimental procedures were carried out by Ms Serina Tokita of Sapporo Medical University, Japan.

2.7 Analysis of the DU145 HLA ligandome

2.7.1 Identification of HLA presented peptides by mass spectrometry

Analysis of the peptide sequences from DU145 cells by mass spectrometry was carried out according to the protocol by Kowalewski and Stevanovic, with some modifications (Kowalewski and Stevanovic, 2013). This analysis was carried out in Sapporo Medical University, with assistance from Ms Serina Tokita and Professor Takayuki Kanaseki. DU145 cells were shipped from Cardiff University and cultured as described previously, in Sapporo Medical University. The cell culture was scaled up with the aim of analysing peptides derived from approximately 10^9 cells. The DU145 cells were cultured in 175 cm^2 and 225 cm^2 surface area cell culture flasks (Corning), continuously for approximately 4 weeks (a balance between continued expansion of the cells and obtaining aliquots for the ligandome analysis was maintained). The cells were snap frozen by detaching and pelleting the cells as described previously. The pellets were stored on ice and snap frozen by immersing the tube in liquid nitrogen. The pellets were then stored at -80 °C. Additional aliquots of snap frozen cells, obtained from 18 T175 flasks which were 80% confluent, were provided by Saly al Taei (shipped on dry ice from Cardiff University to Sapporo Medical University). The cell pellets (approximately 10^9 total cells) were homogenised by sonification, in lysis buffer containing 0.6% CHAPS (Dojindo Molecular Technologies) and 1 × complete protease inhibitor (Roche) in PBS. The rotor dishes of the ultrasonic homogeniser were pre-cooled by placing in liquid nitrogen for 3-5 min. The cell pellets were distributed evenly between the two rotor dishes of the ultrasonic homogeniser which was run for 1 min @ 30% pulse length per second. The rotors were unscrewed from the homogeniser and kept at room temperature for 5-10 min (so as not to freeze the solubilisation buffer). The solubilisation buffer was added to the rotors (containing the cell pellets) to approximately the same volume as the cell pellets (5 ml). The rotors were placed on the homogeniser which was then run for 1 minute @ 15% pulse length per sec. The lysate was collected in a new 50 ml falcon tube, which was rotated on a slow rotor setting for 60 min. The rotors were additionally rinsed with solubilisation buffer to retrieve remaining lysate. The lysate was centrifuged @ 2000 *x g* for 20 minutes at 4 °C. From this, the supernatant was retained and transferred to a new falcon tube, with washing during tube transfer using the solubilisation buffer (the

pellet was discarded). Following this, the lysate was subjected to ultracentrifugation, at 150,000 × g and 4°C for 70 min. The supernatant from ultracentrifugation was syringe filtered, firstly through a 0.45 µm filter, into a falcon tube. This filtered supernatant was then passed through a 0.2 µm filter. The lysate was filtered into a conical flask containing a stirrer. The falcon tube was rinsed with solubilisation buffer during filtering step. The extensive rinsing steps are aimed at maximising the retention of HLA-peptide complexes within the cell lysate, for which the affinity chromatography retrieval efficiency is extremely low. The filtered lysate was transferred into a sterile beaker.

HLA-peptide complexes were isolated from the cell lysate by affinity chromatography. The affinity chromatography reaction was prepared by adding pre-prepared antibody coupled sepharose to the chromatography spin column (Pierce™ Spin Columns - Screw Cap, Thermo Fisher Scientific). The affinity chromatography step was carried out in a 4° C cold room. The antibody was prepared at 1 mg + 200 ul cyanogen bromide–activated Sepharose 4B (GE Healthcare). Two aliquots of sepharose-coupled antibody were added to column for a total of 2 mg of antibody in the column; further details on antibody coupling to sepharose are detailed in the chapter by Kowalewski and Stevanovic (Kowalewski and Stevanovic, 2013). The antibody used was the pan HLA-I antibody (clone W6.32). The column and pump setup were flushed with PBS at a flow rate of 4 ml / min for 30 min. At this stage the pumping configuration was connected to a waste container for the PBS used for flushing the system (linearised setup). The pumping was stopped, and the PBS was replaced with lysate. The system was then aspirated linearly with lysate at a flow rate of 2 ml / min until it completely displaced the PBS in the void volume of the system (i.e. the lysate was present in all parts of the tubing of the affinity chromatography apparatus pump system, instead of the PBS used for flushing). The pumping configuration was altered through the beaker containing the lysate such that lysate was continuously circulated through the system. The beaker was placed on a magnetic stirrer which enabled continuous gently stirring. The lysate was recirculated through the system overnight at a flow rate of 2 ml/min. The next day the system was again linearised and flushed with PBS

at a flow rate of 4 ml/min. The remaining lysate was collected in the beaker and stored at -20 °C (this would enable repeated affinity chromatography if required). The system was flushed with PBS for 30 min. The system was then flushed with ddH_2O for 60 min at a flow rate of 4 ml / min. The system was then air dried by connecting the tubing to a 50 ml syringe and flushing through with air. The column was removed and stored on ice in aluminium foil.

The bound HLA Class I-peptide complexes were isolated from the affinity chromatography columns by acid elution. The required pipette tips (molecular grade), microcentrifuge tubes and centrifugal filter (Amicon Ultra-4 Centrifugal Filter Unit, 10 KDa membrane, 4 ml capacity; Merck Millipore) were washed prior to usage with 0.2% Trifluoroacetic acid (TFA). The centrifugal filter was washed through by adding 4 ml 0.2% TFA and centrifuging at 4640 *x g* for 20 min. 300 µl 0.2% TFA + 7.5 ul 10% TFA was prepared in the pre-washed microcentrifuge tube. The affinity chromatography spin column was prepared for elution by fitting a stopcock to the base and removing the filter that was packed on top of the sepharose. The 300 µl 0.2% TFA + 10% TFA was then added the chromatography column which was shaken vigorously for approximately 1 min. The chromatography column was plated on a rotor and run on slow rotation at 4 °C (in the fridge) for 20 minutes. The chromatography column was briefly spun down using a benchtop centrifuge to collect the eluate in the base. The stopcock and screw top lid were removed from the chromatography column and the eluate was eluted into the centrifugal filter by flushing with 50 ml of air using a syringe fitted to the column. The addition of TFA to the column followed by 20 min rotation at 4 °C and flushing into the centrifugal filter (which was stored on ice throughout the process) was repeated 7 more times, with the use of 300 µl 0.2% TFA instead of the 10% / 0.2% TFA mixture. The eluate was then filtered by centrifuging the 15 ml tube containing the centrifugal filter for 30 min at 4650 *x g*. The centrifugal filter was then removed from the tube and the eluate, containing proteins <10 KDa i.e. the eluted peptides, was distributed evenly between two 0.2% TFA pre-washed microcentrifuge tubes (1.2 ml per tube). The retained eluate that did not pass through the 10 KDa filter contains the HLA α and β chains. The filtrate volume was then reduced

to approximately 100 µl by placing the tubes in a vacuum centrifuge (Thermo Fisher Scientific) for 3 days at room temperature, (running for approximately 8 hr per day, not overnight).

The peptides were desalted and pre-concentrated using a ZipTipµ-$_{C18}$ (Merck Millipore). 7 microcentrifuge tubes were prepared by washing with 1ml 0.2% TFA, using pre-washed pipette tips. The TFA was removed then the tubes were washed with molecular grade H_2O. The 7 tubes were prepared as follows:

1. Desalting solution= 1.5 ml LC-MS grade H_20 + 15 µl Formic acid (1%) (FA)
2. ZipTip Elution buffer= 750 µl LC-MS grade H_20 + 750 µl acetonitrile (ACN) + 15 µl FA (=50% (v/v) ACN + 1% (v/v) FA in LC-MS grade H_20).
3. Waste liquid
4. Pipetting for buffer
5. Pipetting for sample
6. Keep used ZipTip
7. Keep post-ZipTip sample.

The final container, the autosampler vial (used to input the peptide sample into mass spectrometer) was also washed with (a) 100 µl 0.2% TFA, followed by (b) 100 µl H_20, followed by (c) 100 µl elution buffer. 10 µl elution buffer was added to the autosampler. The ZipTip was washed by aspirating and dispensing to waste (Tube 3) 10 µl of elution buffer x 10 times. The ZipTip was equilibrated by aspirating 10 µl of desalting solution, which was pipetted up and down on the inside of tube 4, x10 times. The final wash was discarded in tube 4. 10 µl of eluate was then aspirated into the ZipTip. This was pipetted up and down (without the introduction of air) on the side of tube 5, x 30 times. The eluate was then transferred to tube 7, which was kept on ice. This was repeated a further 4 times, to transfer all of the eluate to tube 7; at this stage the peptides were bound to the ZipTip. The ZipTip was washed by aspirating 10 µl desalting solution and pipetting up and down 5 times on the side of tube 4; the desalting solution was then discarded in tube 4. The elution solution prepared in the autosampler vial was then aspirated and pipetted up and down 5 times followed by dispensing the solution into the autosampler vial. In this way the peptides were eluted from the ZipTip. The ZipTip was stored in tube 6 and tube 7 was also retained, both were stored at -20°C.

The autosampler was placed in the vacuum centrifuge (with a balance vial) for 1.25 hr at the same settings as described previously. A solution of 5% ACN 0.1% TFA in molecular grade H_20 was prepared in a 15 ml falcon tube: 4745 µl H_20+ 250 µl ACN + 5 µl TFA. 5ul 5% ACN+ 0.1% TFA was added to the autosampler vial to resuspend the lyophilised peptides. The peptide solution was sonicated for 1 min to fully mix the suspension.

The mass spectrometer was calibrated prior to commencing the final peptide desalting step. Data from the calibration run was confirmed to only contain low confidence sequences. The peptide sample was loaded into a nanoflow liquid chromatograph (Easy-nLC 1000 system; Thermo Fisher Scientific) online-coupled to an Orbitrap mass spectrometer, equipped with a nanospray ion source (Q-Exactive Plus; Thermo Fisher Scientific). The samples were separated using a 75 µm × 20 cm capillary column with a particle size of 3 µm (NTCC-360, Nikkyo Technos) by applying a linear gradient ranging from 3% to 30% buffer B (100% acetonitrile and 0.1% formic acid) at a flow rate of 300 nL/minute for 80 minutes. For the mass spectrometry analysis, survey scan spectra were acquired at a resolution of 70,000 at 200 *m/z* with a target value of 3e6 ions, ranging from 350 to 2,000 *m/z* with charge states between 1+ and 4+. A data-dependent top 10 method was applied, which generates high-energy collision dissociation (HCD) fragments for the 10 most intense precursor ions per survey scan. MS/MS resolution was 17,500 at 200 *m/z* with a target value (signal threshold) of 1e5 ions. These running and analysis conditions are identical to a previously developed published protocol (Miyamoto et al., 2018). The MS/MS spectra were annotated using the Proteome Discoverer 2.1 software (Thermo Fisher Scientific). This software used embedded algorithms Sequest HT (Thermo Fisher Scientific) and Mascot version 2.6 (Matrix Science). The mass spectrometry peak lists were searched against the UniProt/ Swiss-Prot human databases with a tolerance of precursor ions at 10 ppm and fragment ions at 0.02 Da, and the false discovery rate was set at 0.01.

2.7.2 Analysis of the DU145 HLA ligandome

The spectral annotation data was collated into a Microsoft Excel file. For each peptide sequence identified, the data entry also included sequence length,

protein, protein sequence, gene, reads per kilobase million (RPKM) (RNA-Seq readout), 'cancer panel' chromosome, biological process, cellular component and molecular function; these data were derived from the gene entry in the UniProt/ Swissprot database, which was automatically searched by the Proteome Discoverer 2.2 software. The UniProt / SwissProt entry for each gene is cross-referenced from multiple databases for specific readouts e.g. genome annotation (i.e. cellular component and molecular function) data is derived from the KEGG (https://www.genome.jp/kegg/), ENSEMBL (https://www.ensembl.org/index.html) and GENEID (https://www.ncbi.nlm.nih.gov/gene) databases, sequence information is derived from databases including the nucleotide archive (https://www.ebi.ac.uk/ena) and GenBank nucleotide sequence databank (https://www.ncbi.nlm.nih.gov) databases and gene expression data is obtained from Bgee (https://bgee.org) and EMBL-EBL Expression Atlas (https://www.ebi.ac.uk/gxa) databases. Descriptive statistics for the data were produced using excel functions, including counting the number of peptides identified and partitioning the data based on sequence length. Contaminating peptides, including those flagged as contaminants by the Proteome Discoverer 2.2 software, and peptides derived from contaminating sources; enzymes used in sample processing such as catalase and cellular sources other than the samples analysed (e.g. keratins) were excluded from these statistics. Proportional representation of each amino acid at locations in each peptide sequence was analysed by researchers at Sapporo Medical University, by inputting selected 9-11mer sequences into the logo sequence generator at https://weblogo.berkeley.edu/ Logo.cgi, and has been published (Hongo et al., 2019).

The steps for analysing the dataset to identify potential CSC epitopes were as follows: select peptides representing viable therapeutic targets; for which the genes that have low or limited expression in heathy tissues, next select high affinity HLA -binding peptides, as these are expected to be more stability presented at the cell surface, increasing the possibility of interacting with the T cell receptor TCR). These steps were carried out *in silico*. This approach allowed for selection of a relevant and feasible number of peptides of interest to investigate experimentally.

To determine which peptides might not be presented by healthy tissues, I queried the expression of each gene that encoded the protein the peptides were derived from. The aim was to identify genes which had low or absent expression in healthy tissues. The healthy tissue gene expression and tissue distribution data was obtained from the Genotype-Tissue Expression (GTEx) database (https://GTExportal.org). This was used as an independent gene expression source to the databases used by the Proteome Discoverer. This database was chosen as it a purpose-built repository of human gene expression ("The Genotype-Tissue Expression (GTEx) project," 2013), therefore it was expected the same quantity of expression data (in terms of tissues and numbers of donors tested) would be available for each gene queried. In contrast, the expression data associated with each gene in the UniProt/ SwissProt database is a composite of various databases; therefore the amount of data available for each gene differs depending on the studies referenced in the database. In the GTEx portal, gene expression information was obtained from living and post-mortem donors, from surgically derived tissue and peripheral blood donations and autopsy procedures respectively ("The Genotype-Tissue Expression (GTEx) project," 2013). The methodology described in this publication indicates the gene expression data is derived from parallel RNA sequencing ("The Genotype-Tissue Expression (GTEx) project," 2013). At the time of searching, the GTEx database contained gene expression data from 42 healthy human tissues and 2 cultured cell lines: cultured fibroblasts and EBV-transformed lymphocytes (i.e. BLCL), which was obtained from n=449 donors (https://gtexportal.org/home/releaseInfoPage) ("Genetic effects on gene expression across human tissues," 2017). Thus the healthy tissue expression of the genes of interest was investigated by searching for the gene entry in the database and examining the gene expression entry, in the form of a RPKM or transcripts per million (TPM; an updated value provided in later versions of the database) plot. The criteria of the genes from the HLA ligandome dataset which were investigated using the GTEx portal was based on the RPKM values for each gene which were included in the entry for each peptide generated by the Proteome Discoverer analysis.

The healthy tissue gene expression analysis was carried out for genes for which the median RPKM = 1, or the RPKM was denoted ≤5, and for genes flagged in the ligandome dataset as 'cancer panel.' The gene expression plot result for each gene searched was visually inspected, and the decision of whether to further investigate the peptide as a therapeutically relevant target was based on the gene having low expression across most healthy tissues, or expression in immune privileged tissues (e.g. testis). Peptides excluded from further analysis included those for which the source gene was widely/ highly expressed across many healthy tissues, or highly expressed in a limited number of immune-accessible tissues.

Since the immunoprecipitation step was carried out using a pan-HLA-I antibody, it was necessary to determine which HLA alleles expressed by the DU145 cell line that the peptides identified bound to. The HLA type of the DU145 cells was obtained from the Tron Cell Line Portal (TLCP) http://celllines.tron-mainz.de/ (Scholtalbers et al., 2015). The cognate HLA allele for each peptide and the peptide-HLA binding affinity were predicted using the IEDB Epitope Analysis Resource for HLA-I binding http://tools.iedb.org/mhci/. Based on the guidelines from the IEDB website, the threshold for meaningful binding was set at the first percentile rank. Some of the binding predictions were also confirmed using the binding prediction algorithm hosted at the NetMHCpan server *www.cbs.dtu.dk/services/NetMHCpan*.

The next steps in the analysis of the DU145 HLA ligandome focused on specifically identifying peptides that could be presented by CSC. For this, gene and protein expression of the source genes or proteins associated with the peptides were investigated, by the previously described methods (TaqMan qRT-PCR and fluorescence microscopy, respectively).

2.7.3 Homology modelling and quantification of peptide-HLA interfaces

The peptides selected for further investigation based on gene and protein expression analysis were investigated for the capacity to activate T cells from bulk PBMC of HLA matched donors. This protocol is detailed in the below

section, 'Immunological Assays'. Based on these results, homology modelling of the peptide-HLA interfaces was undertaken to rank the remaining peptides of interest for tetramer production. Tetramer production was required to isolate and enrich the rare peptide responsive T cell populations, so that a detectable level of functional response (cytokine/ chemokine production or degranulation) could be measured. However, due to time and financial constraints it was not possible to produce tetramers to investigate the T cell response to each of the remaining peptides. Homology modelling was carried out to model the peptide-HLA interface and determine the best predicted interactions, which could inform successful HLA monomer re-folding with the peptide of interest. This analysis was carried out in collaboration with Pierre Rizkallah (Cardiff University).

Homology models of HLA-A*33:03 and HLA-B*50:01 were generated using solved crystal structures obtained from the Protein Data Bank https://www.rcsb.org. The structures used were HLA-A*02 (Protein databank structure '2p5e') and HLA-B*15 (structure '5txs') respectively. The HLA-A*02 model was also used, without altering the HLA structure, to analyse the interface interactions between HLA-A*02 XPO1 sequences identified by a collaborative study (Hongo et al., 2019). The HLA-A*02 model consisted of HLA complexed with a peptide and TCR; therefore the TCR part of the structure was removed using Pymol (Schrödinger, LLC, 2015). For both models, sequence alignment was carried out to identify the residues that differed between the HLA allele of solved crystal structure and the HLA allele of interest intended for modelling. This involved inputting the sequences into the Clustal Omega Multiple Sequence Alignment tool (https://www.ebi.ac.uk/Tools/msa/clustalo/) (Madeira et al., 2019). These residues were then substituted using Crystallographic Object-Oriented Toolkit (COOT) software (Emsley et al., 2010; Emsley and Cowtan, 2004). The structures were then regularised using the REFMAC program within in the Collaborative Computational Project Number 4 (CCP4) software suite, and submitted to the Yet Another Scientific Artificial Reality Application (YASARA) server (http://www.yasara.org/minimizationserver.htm) for energy minimisation (Krieger et al., 2009). To model the HLA-peptide interface for each of the peptides of interest, the specific peptide sequence was substituted

for the peptide sequence in the HLA homology model. Each HLA-peptide sequence was regularised and submitted for energy minimisation as described previously. The interfaces of the final structures received from the YASARA server were quantified using Protein Interfaces, Surfaces and Assemblies (PISA) software (Krissinel and Henrick, 2007).

2.8 Immunology assays: verification of T cell responses to peptides from the DU145 HLA ligandome

2.8.1 Testing T cell activation in response to peptides

Activation of T cells in response to peptides, prior to tetramer based isolation, was measured by incubating PBMC with each individual peptide followed by culturing the cells for 7 days and re-stimulating using surrogate antigen presenting cells (BLCL). The PBMC were incubated with peptides that matched the HLA type of the donor i.e. HLA-A*33 or HLA-B*50, or a positive control viral peptide pool: CEF Peptide Pool (MABtech) (Currier et al., 2002). Addition of 10 µl DMSO was used as a negative/ background control, as the peptide pool, and other peptides used were dissolved in DMSO to prepare stock solutions. The PBMC were plated at 8 x 10^5 cells per well in 10% AB RPMI a 48-well plate. The viral peptides were added to the cells at 5 µg / ml while the HLA ligandome peptides were added at 10 µg / ml. Each well was supplemented with 1000 U / ml IFNα, 20 ng / ml IL-1β and 500 U / ml IL-6. The cells were cultured for 6 days in the 48-well plate at a 45° angle at 37° C. On day 7, autologous BLCL were incubated with 10 ug/ ml peptide or 2.5 µg / ml viral peptides or DMSO (1ul/ ml) for 4hr at 37 °C in 10% RPMI. Excess peptide at the end of this incubation was washed off by adding 5 ml PBS to the cells, centrifuging for 3 min at 354 *x g* and removing the supernatant. The BLCL were then incubated with the PBMC which had been previously exposed to the respective peptide, in 5 ml sterile non-pyrogenic FACS tubes at a ratio of 20:1 (PBMC: target cells), and the protocol for ICCS as described previously was followed.

The production of different activation markers by $CD8^+$ T cells was compared using PBMC from a donor previously observed to have immune memory to various viral antigens. The HLA type of the donor was HLA-A*1, A*11, B*55, B*15(62). A custom peptide pool was designed to test immune responses to viral peptides. The HLA restricted peptides included in the custom pool are detailed in Table 2.13. The peptides were synthesised by Severn Biotech Ltd. (UK) at >85% purity and dissolved in DMSO to prepared stock solutions. The peptides were selected from the IEDB database of previously described ligands, or for less frequent alleles, predicted using the IEDB HLA-I binding prediction tool. The 7-day peptide incubation and re-stimulation process was carried out in the same way as described previously. Production of the T cell functional markers CD107a, MIP1β, IFNγ, TNFα and IL-2, in accordance with the previously described ICCS protocol. Optimal incubation times for the detection of CD107a and MIP1β were investigated by carrying out a 6 hr and a 12-hr co-incubation; it was found that the longer incubation period resulted in detection of increased MIP1β. Selected functional markers were then used to measure the response to peptide by tetramer enriched T cell lines.

Table 2.13. HLA restricted peptides custom synthesised to prepare a pool of viral peptides of a wide variety of HLA restrictions, to test donor T cell activation responses.

HLA restriction (obtained/ predicted from IEDB)	Peptide sequence	Antigen reference
A*01:01	CTELKLSDY	Influenza A (PR8) NP 44-52
A*01:01	VSDGGPNLY	Influenza A PB1 591-599
A*02:01	GILGFVFTL	Influenza A MP 58-66
A*02:01	NLVPMVATV	HCMV pp65 495-504
A*02:01	FLYALALLL	EBV LMP-2 356-364
A*03:01	ILRGSVAHK	Influenza A (PR8) NP 265-274
A*03:01	RLRAEAQVK	ENV EBNA 3A 603–611
A*11:01	ATIGTAMYK	EBV BRLF1 134-142
A*33; A*50	LQHYREVAAAK	EBV BZLF1 197-208
B*07:02	QPEWFRNVL	Influenza A PB1 329-337

B*07:02	QPRAPIRPI	EBV EBNA-3C 881-889
B*07:02	TPRVTGGGAM	HCMV pp65 418-427
B*08:01	RAKFKQLL	EBV BZLF1 190-197
B*08:01	QAKWRLQTL	EBV EBNA-3A 158-166
B44	EFFWDANDIY	HCMV pp65 512-521
B*44:05	EENLLDFVRF	EBV EBNA 3C 281-290
DRB1*01:01	TSLYNLRRGTALA	EBV EBNA1 15-527
DRB1*07:01	EPDVYYTSAFVFPTK	CMV pp65 177-191
DRB1*15:01	MSIYVYALPLKMLNI	CMV pp65 109-123
DRB1*04:01	AEGLRALLARSHVER	EBV EBNA1 482-496
DRB1*01:01++	PKYVKQNTLKLAT	Influenza A HA1 307-319
DRB1*07:01	PDDYSNTHSTRYVTV	CMV gB 215-229
DRB1*11:01	VSIDKFRIFCKALNPK	TT 1084-1099
MULTIPLE	AAFEDLRVLSFIKGTK	Influenza A NP 336-351

2.8.2 Production of tetramers

Monomers were produced by Sian Llewellyn-Lacey (Cardiff University), according to an established protocol. Biotin tagged HLA Class I heavy chains and human $\beta_2$microglobulin were expressed as insoluble inclusion bodies in IPTG-induced E. Coli Rosetta DE3 plysS strain (Novagen 71401-4). Resulting bacterial pellets were resuspended in lysis buffer (Bugbuster Protein Extraction Reagent Novagen 70584-4) with DNase (Sigma DN25). Proteins were then washed with Triton wash buffer (50mM Tris, 0.5% Triton X-100 Sigma T9284) with 2 mM DTT and further cleaned with repeat freeze/thaw cycles and centrifugation. Finally, protein preparations were resuspended in 6M-guanidine buffer. Purity of the protein preparations were confirmed with SDS page electrophoresis and determination of concentrations by nanodrop protein absorbance at $_A$280 nm and the molecular mass and extinction coefficients of chains from protein sequences.

The process of re-folding the HLA allele α chain, β_2 microglobulin and the peptide of interest, to produce a monomeric HLA-peptide complex is

proprietary. Peptides were synthesised by Severn Biotech Ltd. (UK), at >95% purity. In brief, the re-fold protocol involves denaturing the α chain, and β_2 microglobulin chains separately, then combining the denatured chains with the peptide and re-folding by dialysis. The refolded protein was recovered by anion exchange. The fractions containing protein recovered from the chromatography column were pooled and biotinylated.

Biotinylated HLA-peptide monomers were conjugated by addition of ExtrAvidin-R-phycoerythrin (PE) (Sigma Aldrich) HLA-peptide: streptavidin molar ratio of 4:1 to produce a tetrameric complex of fluorescently conjugated HLA-peptides, for use in flow cytometry. The tetramerization process was carried out to produce 50 tests of tetramer, using 50 µg tetramer. The tetramerization process was carried out on ice. The volume for 50 µg of monomer was added to an Eppendorf tube (STARLABS). 1.5 µl proteinase inhibitor was added to the tube. The total volume for the 4:1 monomer: streptavidin ratio relating to 50 µg monomer was calculated and added in 5 increments (with mixing by pipetting up and down), with 20 min incubations on ice after each addition.

2.8.3 Tetramer staining and isolation of T cells

A pre-stimulation protocol was used to isolate tetramer specific T cells. $CD8^+$ cells were isolated using an EasySep™ Human CD8 Positive Selection Kit II, according to the manufacturer's instructions (STEMCELL Technologies. PBMC were isolated from whole blood as described previously and a suspension was prepared in 1ml buffer consisting of 2% FBS 1 mM EDTA in PBS, in a 5ml polystyrene round-bottom tube (BD Biosciences). The manufacturer's protocol was followed for isolation of $CD8^+$ cells from $\leq 1 \times 10^8$ PBMC. 100 µl of the selection cocktail reagent was added to the cells, mixed by pipetting and incubated for 3 min at room temperature. The RapidSpheres reagent was vortexed for 30 sec in the final stages of the 3 min incubation, then 50 µl RapidSpheres was added to the cell suspension, mixed and incubated for 3 min at room temperature. 1.5 ml media was added to the tube and which was then placed in an EasySep magnet (STEMCELL Technologies) and incubated for 3 min at room temperature. The supernatant

was then poured off into a 15 m falcon tube (Greiner Bio-One). The addition of 1.5 ml media followed by incubating for 3 min was repeated twice more, and the isolated $CD8^+$ T cells where then retrieved by washing removing the tube from the magnet and washing the tube using RPMI containing 10% AB serum (Sigma Aldrich); the wash media containing the isolated cells was retained for plating the cells. The $CD8^+$ T cells were plated in 10% AB RPMI at 2 x 10^6 per 1 ml in a 24-well adherent cell culture plate (Greiner Bio-One). The $CD8^-$ fraction, (retained in the 15 ml tube) was irradiated at 40 *x g* and used as feeder cells for the $CD8^+$ cells. 10 µg / ml of peptide and 10 U / ml IL-2 (Peprotech) were added to the $CD8^+$cells. The cells were incubated for 3 days at which point a further 1 ml 10% AB RPMI containing 40 U / ml IL-2 was added (for a final concentration of 20 U/ ml IL-2). At day 6 (the first day of plating being counted as day 0), 1ml of media was removed and replaced with fresh media, 10% AB RPMI, containing 40 IU IL-2. At day 7, the peptide stimulation process was repeated; any remaining $CD8^-$ feeder cells previously cryogenically stored were used as feeder cells; if no $CD8^-$ cells were available then fresh/ frozen non-autologous PBMC were used. 20 U / ml UL-2 was added. Further addition of IL-2 accompanied with changing the media, as for days 3 and 6, were carried out at days 10 and 13, and finally on day 14 the cells were sorted using the respective tetramers.

For tetramer-based T cell sorting, the $CD8^+$ cells were collected from the 24 well plate and transferred to 5ml polystyrene round-bottom tubes (BD Biosciences). The staining protocol was optimised with use of 1 test of tetramer (1 µg) to stain 5 x 10^6 $CD8^+$ cells; thus, the cell suspension was prepared at 5 x 10^6 cells/ tube, in 10% RPMI. Where greater numbers of PBMC or $CD8^+$ T cells were present, multiple tubes containing a suspension of 5 x 10^6 cells were prepared. The cell suspension was washed with 2 ml 10% RPMI and the supernatant was removed after centrifugation. The cells (in residual volume) were incubated with 50 nM dasatinib (Axon Medchem, Reston, VA, USA) for 30 min at 37 °C (in an incubator). Dasatinib is a protein kinase inhibitor that has been found to prevent TCR recycling from the cell surface upon tetramer binding (Wooldridge et al., 2009). Next, the streptavidin-PE conjugated tetramer was added to the cells and incubated for 20 min at 37 °C (in an incubator). Following this incubation, the cells were

washed by adding 2 ml of PBS and centrifuging at 354 *x g* for 3 min. The PBS was removed, and the cells were stained in residual volume with 8 µl Aqua viability stain (Invitrogen Thermo Fisher Scientific) at 1:40 dilution for 5 min at room temperature followed by addition of the primary antibodies (without washing off the viability stain). The cells were incubated with the primary antibodies for 20 min at 4 °C (on ice) followed by washing twice with 2 ml PBS and resuspending the cells in PBS for sorting. The collection media for FACS was 10% RPMI, stored on ice. The gating strategy for tetramer sorting involved combining the viability, CD14 and CD19 staining fluorophores as a 'dump channel;' in which cells staining positive for any of these were excluded. A sample of cells, which were not stained with the tetramer, was used to guide the placement of a tetramer positive gate in which to sort the cells. The antibodies used for tetramer FACS were optimised for use on a special-order system BD FACSAria II cell sorter flow cytometer and were kindly provided by collaborators (David Price, Cardiff University). Tetramer frequency of sorted cells was tested by flow cytometry using a BD FACSVerse; using the antibodies indicated in Table 2.5. $CD14^+$ cells were excluded although this was not combined with a dump channel. The general gating strategy used for tetramer sorting consisted of excluding doublets and selection of the T cell population based on size and granularity (Figure 2.5A-C) followed by identification of viable $CD3^+$ cells, combined with exclusion of $CD14^+$ or $CD19^+$ cells (dump channel) (Figure 2.5D). Gates used to isolate tetramer positive $CD8^+$ T cells are shown in the results figures.

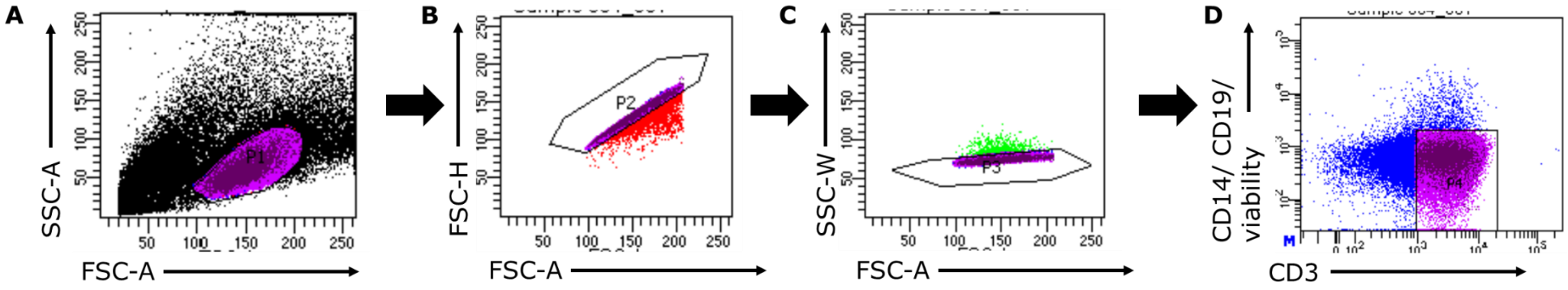

Figure 2.5 General gating strategy for tetramer-based T cell FACS. (A) Activated T cells were isolated based on size. The dot plot shown is from the second sort of expanded HLA-B*50 T cells, thus exclusion of remaining feeder cells was required. Activated lymphocytes have a medium forward scatter and low side scatter (B, C) Doublets were excluded by gating cells as those which had a higher FSC-A than FSC-H, and also cells with a greater SSC-W profile. (D)Live $CD3^+$ cells were selected while dead/ CD14/ CD19 cells were excluded when the CD3 fluorescent signal was shown on the x-axis, while the 'dump channel;' CD14, CD19 and viability staining (dead cells) were shown on the y-axis.

The sorted cells were expanded by plating the cells in a 25 cm^2 tissue culture flask, along with 15 x 10^6 feeder cells: PBMC irradiated with 40 Gy, from 3 different donors (5 x 10^6 PBMC from each donor), 1 µg / ml PHA (Sigma Aldrich), in T cell media consisting of 10% AB RPMI supplemented with 25 ng / ml IL-15 (Peprotech) and 200 U/ ml IL-2 (Peprotech), for a total volume of 20 ml. The flask was incubated at 37 °C at an angle (tilted on the flask short end) for 5 days. Half of the media was then changed without disturbing the cells, and fresh T cell media was added (not containing new feeder cells or PHA). The flask was thereafter incubated upright, and half the media replaced every 2-3 days. The phenotype and tetramer positive frequency was investigated at day 14.

2.8.4 Testing T cell responses to peptide presentation by target cells

Tetramer sorted T cells were incubated with HLA matched peptide loaded or unloaded target cells, to measure the functional response to the peptides. The target cells were incubated with 10 µg peptide for 4 hr at 37 °C in an incubator. The cells were then centrifuged at 354 *x g* and the supernatant removed. The cells were then resuspended in fresh media (10% AB RPMI).

Tetramer enriched T cell line	**Target**
REHQNFYEA HLA-B*50 T cells	HLA-B*50 BLCL + peptide HLA-B*50 BLCL no added peptide
	DU145 cells+ peptide DU145 cells no added peptide
KLFEFMHET HLA-A*02 T cells from Donor 1	HLA-A*02 BLCL + peptide HLA-A*02 BLCL no added peptide
	Primary PCa cells #5042 + peptide Primary PCa cells #5042 no added peptide
	HLA-A*02 BLCL + peptide

KLFEFMHET HLA-A*02 T cells from Donor 2	HLA-A*02 BLCL no added peptide
	Primary PCa cells #5042 + peptide Primary PCa cells #5042 no added peptide

The T cells were co-incubated with the target cells at a ratio of 10:1 (10 T cells to every 1 target cell), in 5 ml sterile non-pyrogenic FACS tubes (BD Biosciences). Thereafter the protocol for ICCS was followed, as described previously. The functional responses tested were IFNγ (cytokine) and MIP1β (chemokine), and the reactive T cells were also stained for phenotyping surface markers CD3, CD4 and CD8.

2.9 Data presentation and statistical analysis

Calculations relating to raw data were performed using Microsoft Excel (RT-qPCR CT analysis and statistical testing, *in* vivo tumour volume analysis and quantification of HLA ligandome data). The rest of the data analysis, including statistical testing, was performed using GraphPad Prism 5 software. The Student's T test was used to compare two groups (paired or unpaired analysis is denoted in the results). One-way ANOVA was used to compare >2 groups for the difference between one condition of interest while the two-way ANOVA was used to compare the variation in two conditions for ≥2 groups. The first primary PCa sample study (n=21) did not have a normal distribution therefore the Mann Whitney U test was used to investigate the difference in viability associated with the use of Collagenase I or Collagenase II in biopsy processing.

Appendix 2.1

RT² Profiler™ PCR Array Human Stem Cell Gene list

Gene symbol	Gene name
ABCB5	ATP-binding cassette, sub-family B (MDR/TAP), member 5
ABCG2	ATP-binding cassette, sub-family G (WHITE), member 2
ALCAM	Activated leukocyte cell adhesion molecule
ALDH1A1	Aldehyde dehydrogenase 1 family, member A1
ATM	Ataxia telangiectasia mutated
ATXN1	Ataxin 1
AXL	AXL receptor tyrosine kinase
BMI1	BMI1 polycomb ring finger oncogene
BMP7	Bone morphogenetic protein 7
CD24	CD24 molecule
CD34	CD34 molecule
CD38	CD38 molecule
CD44	CD44 molecule (Indian blood group)
CHEK1	CHK1 checkpoint homolog (S. pombe)
DACH1	Dachshund homolog 1 (Drosophila)
DDR1	Discoidin domain receptor tyrosine kinase 1
DKK1	Dickkopf homolog 1 (Xenopus laevis)
DLL1	Delta-like 1 (Drosophila)
DLL4	Delta-like 4 (Drosophila)
DNMT1	DNA (cytosine-5-)-methyltransferase 1
EGF	Epidermal growth factor

ENG	Endoglin
EPCAM	Epithelial cell adhesion molecule
ERBB2	V-erb-b2 erythroblastic leukemia viral oncogene homolog 2, neuro/glioblastoma derived oncogene homolog (avian)
ETFA	Electron-transfer-flavoprotein, alpha polypeptide
FGFR2	Fibroblast growth factor receptor 2
FLOT2	Flotillin 2
FOXA2	Forkhead box A2
FOXP1	Forkhead box P1
FZD7	Frizzled family receptor 7
GATA3	GATA binding protein 3
GSK3B	Glycogen synthase kinase 3 beta
HDAC1	Histone deacetylase 1
ID1	Inhibitor of DNA binding 1, dominant negative helix-loop-helix protein
IKBKB	Inhibitor of kappa light polypeptide gene enhancer in B-cells, kinase beta
CXCL8	Interleukin 8
ITGA2	Integrin, alpha 2 (CD49B, alpha 2 subunit of VLA-2 receptor)
ITGA4	Integrin, alpha 4 (antigen CD49D, alpha 4 subunit of VLA-4 receptor)
ITGA6	Integrin, alpha 6
ITGB1	Integrin, beta 1 (fibronectin receptor, beta polypeptide, antigen CD29 includes MDF2, MSK12)
JAG1	Jagged 1
JAK2	Janus kinase 2
KIT	V-kit Hardy-Zuckerman 4 feline sarcoma viral oncogene homolog
KITLG	KIT ligand

KLF17	Kruppel-like factor 17
KLF4	Kruppel-like factor 4 (gut)
LATS1	LATS, large tumor suppressor, homolog 1 (Drosophila)
LIN28A	Lin-28 homolog A (C. elegans)
LIN28B	Lin-28 homolog B (C. elegans)
MAML1	Mastermind-like 1 (Drosophila)
MERTK	C-mer proto-oncogene tyrosine kinase
MS4A1	Membrane-spanning 4-domains, subfamily A, member 1
MUC1	Mucin 1, cell surface associated
MYC	V-myc myelocytomatosis viral oncogene homolog (avian)
MYCN	V-myc myelocytomatosis viral related oncogene, neuroblastoma derived (avian)
NANOG	Nanog homeobox
NFKB1	Nuclear factor of kappa light polypeptide gene enhancer in B-cells 1
NOS2	Nitric oxide synthase 2, inducible
NOTCH 1	Notch 1
NOTCH 2	Notch 2
PECAM1	Platelet/endothelial cell adhesion molecule
PLAT	Plasminogen activator, tissue
PLAUR	Plasminogen activator, urokinase receptor
POU5F1	POU class 5 homeobox 1
PROM1	Prominin 1
PTCH1	Patched 1
PTPRC	Protein tyrosine phosphatase, receptor type, C

SAV1	Salvador homolog 1 (Drosophila)
SIRT1	Sirtuin 1
SMO	Smoothened, frizzled family receptor
SNAI1	Snail homolog 1 (Drosophila)
SOX2	SRY (sex determining region Y)-box 2
STAT3	Signal transducer and activator of transcription 3 (acute-phase response factor)
TAZ	Tafazzin
TGFBR1	Transforming growth factor, beta receptor 1
THY1	Thy-1 cell surface antigen
TWIST1	Twist homolog 1 (Drosophila)
TWIST2	Twist homolog 2 (Drosophila)
WEE1	WEE1 homolog (S. pombe)
WNT1	Wingless-type MMTV integration site family, member 1
WWC1	WW and C2 domain containing 1
YAP1	Yes-associated protein 1
ZEB1	Zinc finger E-box binding homeobox 1
ZEB2	Zinc finger E-box binding homeobox 2
ACTB	Actin, beta
B2M	Beta-2-microglobulin
GAPDH	Glyceraldehyde-3-phosphate dehydrogenase
HPRT1	Hypoxanthine phosphoribosyltransferase 1
RPLP0	Ribosomal protein, large, P0

Appendix 2.2

Nanostring nCounter Stem Cell Panel Gene list

ABCG2	ATP-binding cassette, sub-family G (WHITE), member 2
ACTC1	actin, alpha, cardiac muscle 1
ADAM17	ADAM metallopeptidase domain 17
ADAR	adenosine deaminase, RNA-specific
ALDH1A1	aldehyde dehydrogenase 1 family, member A1
ALDH2	aldehyde dehydrogenase 2 family (mitochondrial)
APC	adenomatous polyposis coli
APH1A	anterior pharynx defective 1 homolog A (C. elegans)
ASCL2	achaete-scute complex homolog 2 (Drosophila)
AXIN1	axin 1
BMP1	bone morphogenetic protein 1
BMP2	bone morphogenetic protein 2
BMP3	bone morphogenetic protein 3
BTRC	beta-transducin repeat containing
CCNA2	cyclin A2
CCND1	cyclin D1
CCND2	cyclin D2
CCND3	cyclin D3
CCNE1	cyclin E1
CD3D	CD3d molecule, delta (CD3-TCR complex)
CD4	CD4 molecule
CD44	CD44 molecule (Indian blood group)
CD8A	CD8a molecule
CD8B	CD8b molecule
CDC2	cell division cycle 2, G1 to S and G2 to M

CDC42	cell division cycle 42 (GTP binding protein, 25kDa)
CDH1	cadherin 1, type 1, E-cadherin (epithelial)
CDH2	cadherin 2, type 1, N-cadherin (neuronal)
CIR1	corepressor interacting with RBPJ, 1
COL1A1	collagen, type I, alpha 1
COL2A1	collagen, type II, alpha 1
CREBBP	CREB binding protein
CSNK1A1	casein kinase 1, alpha 1
CSNK1A1L	casein kinase 1, alpha 1-like
CSNK1D	casein kinase 1, delta
CSNK1E	casein kinase 1, epsilon
CSNK1G1	casein kinase 1, gamma 1
CSNK1G2	casein kinase 1, gamma 2
CSNK1G3	casein kinase 1, gamma 3
CSNK2A1	casein kinase 2, alpha 1 polypeptide
CTBP1	C-terminal binding protein 1
CTBP2	C-terminal binding protein 2
CTNNA1	catenin (cadherin-associated protein), alpha 1, 102kDa
CTNNB1	catenin (cadherin-associated protein), beta 1, 88kDa
CXCL12	chemokine (C-X-C motif) ligand 12 (stromal cell-derived factor 1)
DHH	desert hedgehog homolog (Drosophila)
DLL1	delta-like 1 (Drosophila)
DLL3	delta-like 3 (Drosophila)
DLL4	delta-like 4 (Drosophila)
DTX1	deltex homolog 1 (Drosophila)

DTX2	deltex homolog 2 (Drosophila)
DTX3	deltex homolog 3 (Drosophila)
DTX3L	deltex 3-like (Drosophila)
DTX4	deltex homolog 4 (Drosophila)
DVL1	dishevelled, dsh homolog 1 (Drosophila)
DVL2	dishevelled, dsh homolog 2 (Drosophila)
DVL3	dishevelled, dsh homolog 3 (Drosophila)
EP300	E1A binding protein p300
FBXW11	F-box and WD repeat domain containing 11
FBXW2	F-box and WD repeat domain containing 2
FGF1	fibroblast growth factor 1 (acidic)
FGF2	fibroblast growth factor 2 (basic)
FGF4	fibroblast growth factor 4
FGFR1	fibroblast growth factor receptor 1
FOSL1	FOS-like antigen 1
FOXA2	forkhead box A2
FRAT1	frequently rearranged in advanced T-cell lymphomas
FOXD3	forkhead box D3
FURIN	furin (paired basic amino acid cleaving enzyme)
FZD1	frizzled homolog 1 (Drosophila)
FZD10	frizzled homolog 10 (Drosophila)
FZD2	frizzled homolog 2 (Drosophila)
FZD3	frizzled homolog 3 (Drosophila)
FZD5	frizzled homolog 5 (Drosophila)
FZD6	frizzled homolog 6 (Drosophila)
FZD7	frizzled homolog 7 (Drosophila)
FZD8	frizzled homolog 8 (Drosophila)

FZD9	frizzled homolog 9 (Drosophila)
GAS1	growth arrest-specific 1
GDF3	growth differentiation factor 3
GJB1	gap junction protein, beta 1, 32kDa
GLI1	GLI family zinc finger 1
GLI2	GLI family zinc finger 2
GLI3	GLI family zinc finger 3
GSK3B	glycogen synthase kinase 3 beta
HDAC1	histone deacetylase 1
HDAC2	histone deacetylase 2
HES1	hairy and enhancer of split 1, (Drosophila)
HHIP	hedgehog interacting protein
IGF1	insulin-like growth factor 1 (somatomedin C)
IHH	Indian hedgehog homolog (Drosophila)
ISL1	ISL LIM homeobox 1
JAG1	jagged 1 (Alagille syndrome)
JAG2	jagged 2
JUN	jun oncogene
KAT2A	K(lysine) acetyltransferase 2A
KRT15	keratin 15
LDLR	low density lipoprotein receptor
LFNG	LFNG O-fucosylpeptide 3-beta-N-acetylglucosaminyltransferase
LOC400927	TPTE and PTEN homologous inositol lipid phosphatase pseudogene
LOC652788	PREDICTED: Homo sapiens similar to dishevelled 1 isoform a

LRP2	low density lipoprotein-related protein 2
MAML1	mastermind-like 1 (Drosophila)
MAML2	mastermind-like 2 (Drosophila)
MAML3	mastermind-like 3 (Drosophila)
MAP3K7	mitogen-activated protein kinase 7
MAP3K7IP1	mitogen-activated protein kinase 7 interacting protein 1
MAPK10	mitogen-activated protein kinase 10
MAPK9	mitogen-activated protein kinase 9
MFNG	MFNG O-fucosylpeptide 3-beta-N-acetylglucosaminyltransferase
MME	membrane metallo-endopeptidase
MYC	v-myc myelocytomatosis viral oncogene homolog (avian)
MYOD1	myogenic differentiation 1
NANOG	Nanog homeobox
NCAM1	neural cell adhesion molecule 1
NCOR2	nuclear receptor co-repressor 2
NCSTN	nicastrin
NLK	nemo-like kinase
NOTCH1	Notch homolog 1, translocation-associated (Drosophila)
NOTCH2	Notch homolog 2 (Drosophila)
NOTCH3	Notch homolog 3 (Drosophila)
NOTCH4	Notch homolog 4 (Drosophila)
NUMB	numb homolog (Drosophila)
NUMBL	numb homolog (Drosophila)-like
PAFAH1B1	platelet-activating factor acetylhydrolase, isoform Ib, subunit 1 (45kDa)

KAT2B	K(lysine) acetyltransferase 2B
PDX1	pancreatic and duodenal homeobox 1
PLAU	plasminogen activator, urokinase
POU5F1	POU class 5 homeobox 1
PPARD	peroxisome proliferator-activated receptor delta
PPARG	peroxisome proliferator-activated receptor gamma
PPP2CA	protein phosphatase 2 (formerly 2A), catalytic subunit, alpha isoform
PPP2R5C	protein phosphatase 2, regulatory subunit B', gamma isoform
PPP2R5E	protein phosphatase 2, regulatory subunit B', epsilon isoform
PRKACA	protein kinase, cAMP-dependent, catalytic, alpha
PRKACB	protein kinase, cAMP-dependent, catalytic, beta
PRKACG	protein kinase, cAMP-dependent, catalytic, gamma
PRKCA	protein kinase C, alpha
PRKCB	protein kinase C, beta
PRKCD	protein kinase C, delta
PRKCE	protein kinase C, epsilon
PRKCG	protein kinase C, gamma
PRKCH	protein kinase C, eta
PRKCI	protein kinase C, iota
PRKCQ	protein kinase C, theta
PRKCZ	protein kinase C, zeta
PRKD1	protein kinase D1
PRKX	protein kinase, X-linked
PRKY	protein kinase, Y-linked
PSEN1	presenilin 1
PSEN2	presenilin 2 (Alzheimer disease 4)

PSENEN	presenilin enhancer 2 homolog (C. elegans)
RAB23	RAB23, member RAS oncogene family
RAC1	ras-related C3 botulinum toxin substrate 1 (rho family, small GTP binding protein Rac1)
RB1	retinoblastoma 1
RBPJ	recombination signal binding protein for immunoglobulin kappa J region
RFNG	RFNG O-fucosylpeptide 3-beta-N-acetylglucosaminyltransferase
RHOA	ras homolog gene family, member A
S100B	S100 calcium binding protein B
SFRP4	secreted frizzled-related protein 4
SHH	sonic hedgehog homolog (Drosophila)
SMAD4	SMAD family member 4
SMO	smoothened homolog (Drosophila)
SNW1	SNW domain containing 1
SOX1	SRY (sex determining region Y)-box 1
SOX2	SRY (sex determining region Y)-box 2
STK36	serine/threonine kinase 36, fused homolog (Drosophila)
SUFU	suppressor of fused homolog (Drosophila)
T	T, brachyury homolog (mouse)
TCF7	transcription factor 7 (T-cell specific, HMG-box)
TERT	telomerase reverse transcriptase
TLE1	transducin-like enhancer of split 1 (E(sp1) homolog, Drosophila)
WIF1	WNT inhibitory factor 1
WNT1	wingless-type MMTV integration site family, member 1

WNT10A	wingless-type MMTV integration site family, member 10A
WNT10B	wingless-type MMTV integration site family, member 10B
WNT11	wingless-type MMTV integration site family, member 11
WNT16	wingless-type MMTV integration site family, member 16
WNT2	wingless-type MMTV integration site family member 2
WNT2B	wingless-type MMTV integration site family, member 2B
WNT3	wingless-type MMTV integration site family, member 3
WNT3A	wingless-type MMTV integration site family, member 3A
WNT4	wingless-type MMTV integration site family, member 4
WNT5A	wingless-type MMTV integration site family, member 5A
WNT5B	wingless-type MMTV integration site family, member 5B
WNT6	wingless-type MMTV integration site family, member 6
WNT7A	wingless-type MMTV integration site family, member 7A
WNT7B	wingless-type MMTV integration site family, member 7B
WNT8A	wingless-type MMTV integration site family, member 8A
WNT8B	wingless-type MMTV integration site family, member 8B
WNT9A	wingless-type MMTV integration site family, member 9A
WNT9B	wingless-type MMTV integration site family, member 9B
ZIC2	Zic family member 2 (odd-paired homolog, Drosophila)
CLTC	clathrin, heavy chain (Hc)
GAPDH	glyceraldehyde-3-phosphate dehydrogenase
GUSB	glucuronidase, beta
HPRT1	hypoxanthine phosphoribosyltransferase 1
PGK1	phosphoglycerate kinase 1
TUBB	tubulin, beta

Chapter 3. Identification and characterisation of prostate cancer stem cells

3 Identification and characterisation of prostate cancer stem cells

3.1 Introduction

This chapter focuses on identification and characterisation of prostate CSC, in order to investigate prostate CSC antigens in subsequent chapters. Prostate CSC were first identified in PCa samples using the surface markers $CD44^+$ $\alpha_2\beta_1Integrin^{high}$ $CD133^+$ (Collins et al., 2005). Functional markers of CSC, such as high aldehyde dehydrogenase (ALDH) activity and ATP-binding cassette super-family G (ABCG2) expression have also been used to identify prostate CSC (Huss et al., 2005; van den Hoogen et al., 2010). In these studies, the prostate CSC population was investigated using xenograft derived cells or cell lines. Further studies have confirmed the existence of prostate CSC by using both functional and surface markers ($ALDH^+$ $\alpha_2\beta_1Integrin^{high}$ $CD44^+$ PSA^{low}), in PCa cell lines (Chen et al., 2016; Qin et al., 2012). Additionally, distinct and overlapping CSC populations have been identified in different cell lines, using markers such as CD44 and $\alpha_2\beta_1$Integrin together or individually (Liu et al., 2015). This suggests that prostate CSC can be identified using various CSC markers, the suitability of which may be associated with the *in vitro* model used.

Therefore, I set out to compare surface and functional markers in identifying prostate CSC, using both cell lines and primary PCa cells. Studies of PCa CSC rely heavily on cell lines, few of which are established from primary, rather than metastatic lesions (van Bokhoven et al., 2003). Establishing primary cultures of PCa samples in *in vitro* cell culture is particularly challenging (Niranjan et al., 2012), thus primary prostate CSC remain poorly investigated. In this chapter, primary PCa culture conditions are optimised to establish whether primary prostate CSC may be identified using the same markers used in the cell line. Many of the surface and functional markers used in the identification of prostate CSC are also widely used to isolate CSC from other tissues (Bao et al., 2006; Ricci-Vitiani et al., 2007; Yasuda et al., 2013). However, some studies have reported comparable stemness characteristics

such as clonogenicity and tumour initiation in cells negative for some of these CSC markers (Beier et al., 2007; Patrawala et al., 2005; Zhou et al., 2011). Therefore, it is important not only to investigate suitable CSC markers in the context of this study but also to demonstrate distinct stemness characteristics of the CSC marker positive, compared to the CSC marker negative cells. The CSC and non-CSC populations isolated using the chosen markers are compared in *in vitro* and *in vivo* assays previously described in the literature (Franken et al., 2006; Moore et al., 2012; Pastrana et al., 2011; Prager et al., 2019). Novel assays for characterising CSC are also described in this chapter.

Question

Which CSC markers can be used to identify and isolate a CSC population in prostate cancer?

Specific Aims

1. Select and characterise a suitable cell line in which to investigate prostate CSC.
2. Compare surface markers and functional markers in identifying prostate CSC in the selected cell line.
3. Isolate and characterise the potential CSC population in the cell line using the optimised CSC markers.
4. Develop a suitable *in vitro* culture protocol for the growth of primary PCa cells.
5. Investigate potential primary prostate CSC using the markers established in the PCa cell line.

3.2 Selection and characterisation of a prostate cancer cell line for the identification of prostate CSC

The selection of the PCa cell line for this study was based on the aim of identifying CSC which expressed prostate CSC surface markers $CD44^{+}$ $CD49b^{high}$ (α_2Integrin) and $CD133^{+}$ (Collins et al., 2005). These markers were first used in a primary PCa model; however few studies have rigorously investigated and confirmed this combination of markers for the identification of CSC in PCa cell lines (Wei et al., 2007). Other studies have investigated single or double marker positive populations as potential CSC in PCa cell lines (Liu et al., 2015; Patrawala et al., 2006; Pfeiffer and Schalken, 2010). As a first step, both cell lines were assessed for the expression of CD44. LNCaP cells did not express CD44 (Figure 3.1A); while DU145 cells were positive for CD44 (Figure 3.1B). The absence of CD44 expression is in agreement with previous findings by (Liu et al., 2015). Since no $CD44^{+}$ cells were present in LNCaP, I proceeded with further characterisation of the DU145 cells.

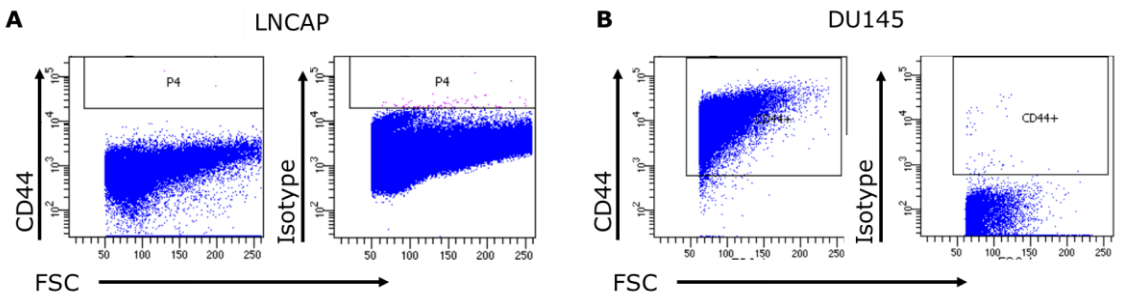

Figure 3.1 Determining the expression of the CSC marker CD44 in PCa cell lines. Flow cytometry was used to measure the proportion of cells expressing CD44 (A) Flow cytometry dot plot of CD44 antibody staining of LNCaP cells and isotype control. (B) Flow cytometry dot plot of CD44 antibody staining of DU145 cells and isotype control staining. A,B: Positive gating is determined by the isotype control. The LNCaP experiment is representative of n=2 experiments and the DU145 cells were stained in more than three experiments.

3.2.1 Characteristics of the DU145 prostate cancer cell line

The growth and phenotype of the DU145 cell line was investigated, to provide baseline data on the expected characteristics of *in vitro* culture, and verify that these characteristics were similar to those previously described (Cunningham and You, 2015). The DU145 cell line was cultured in adherent *in vitro* culture in normoxic (atmospheric oxygen) conditions, in RPMI media containing 10% FBS and standard supplements described in Materials and Methods). These conditions have been previously described (Yan et al., 2014). In the basic conditions, the cells grew with a characteristic 'cobblestone' epithelial morphology (Figure 3.2A). The growth and doubling time of the DU145 cells were noted in order to optimise the cell culture conditions specifically for CSC isolation and characterisation. It was expected that cell culture would have to be scaled up to isolate sufficient cell numbers for downstream assays, based on previous studies in which CSC have comprised a relatively infrequent population; 0.01%- ≤10% (Collins et al., 2005; Patrawala et al., 2007; Pfeiffer and Schalken, 2010; Qin et al., 2012). The doubling time of the DU145 cells was 37.15 hr (28.79 to 52.35 hr 95% CI), This was calculated based on the exponential growth curve equation of the cells seeded at 10^5 (Figure 3.2B). This is in agreement with previous findings (Cunningham and You, 2015).

I investigated the phenotype of the DU145 cells to provide comparison to the primary PCa cells used in this study. The DU145 cell line was originally isolated from the CNS metastasis of a PCa adenocarcinoma. In contrast, the primary samples in this study were obtained from men undergoing prostatectomies, an effective treatment for localised disease, in which it may be expected that a greater proportion of luminal cells are present (Liu et al., 1999; van Leenders et al., 2001). Expression of the basal cytokeratin CK5 was not detected in the DU145 cells however, CD44 was readily detected (Figure 3.3A), confirming previous flow cytometry results (Figure 3.1B). CK8, a cytokeratin expressed by both intermediate and luminal prostate cells in the healthy prostate and PCa (Niranjan et al., 2012) was detected (Figure 3.3A). Taken together the expression of CD44 and CK8 suggest that the DU145 cells consist of basal and intermediate phenotypes. This was further investigated by flow cytometry using markers which specifically discriminated

Chapter 3. Identification and characterisation of prostate cancer stem cells between the basal; CD49f (α_6 Integrin) and luminal; CD26 (dipeptidyl peptidase) populations, since CK8 was not a sufficiently discriminatory marker for the latter (Karthaus et al., 2014; Moad et al., 2017). The phenotype of the DU145 cells was predominantly basal cell (70.69% $CD49^+$ $CD26^-$) whereas luminal cells were rare (0.125% $CD49f^-$ $CD26^+$) (Figure 3.3B). The remainder of the cells (28.63%) had an intermediate phenotype; $CD49^+$ $CD26^+$ (Figure 3.3B). DU145 cells have been shown to be CD49f positive and CD26 negative in a previous study, however the relative frequency of the single or double positive populations was not investigated in that study (Liu, 2000). The DU145 cells were next investigated for the expression of CD44 CD49b (α_2Integrin) and CD133, which identify CSC within the basal cell population.

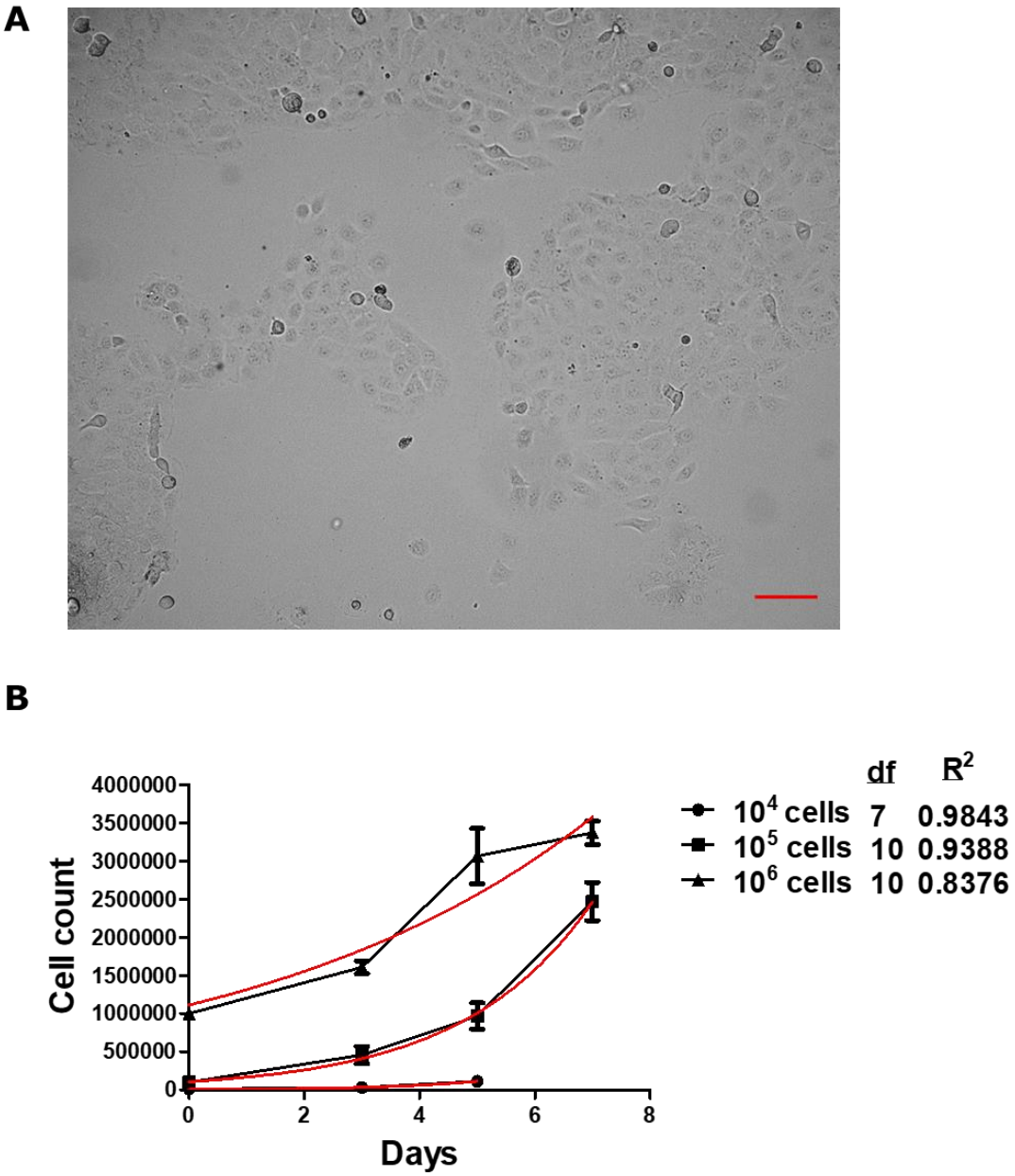

Figure 3.2 Growth characteristics of the DU145 cell line in adherent *in vitro* culture conditions. (A) DU145 cell 'cobblestone' morphology (brightfield). Imaged using a Zeiss axio observer z1 microscope. Scale bar represents 100 μm. (B) Kinetics of DU145 cell growth (black lines). DU145 cells were plated at 10^4, 10^5 or 10^6 cells per one well of a 6 well plate, in triplicate. Viable cells were enumerated by staining with ViaCount Reagent and counting using a Millipore Guava Flow Cytometer. Data points and error bars represent triplicate counts. The growth curve was analysed by calculating the non-linear regression exponential growth equation (red lines) of the data points, using GraphPad Prism. Doubling time was calculated from the equation of the growth curve line of 10^5 cells as this was the best fit line (R^2) which had the most degrees of freedom (df).

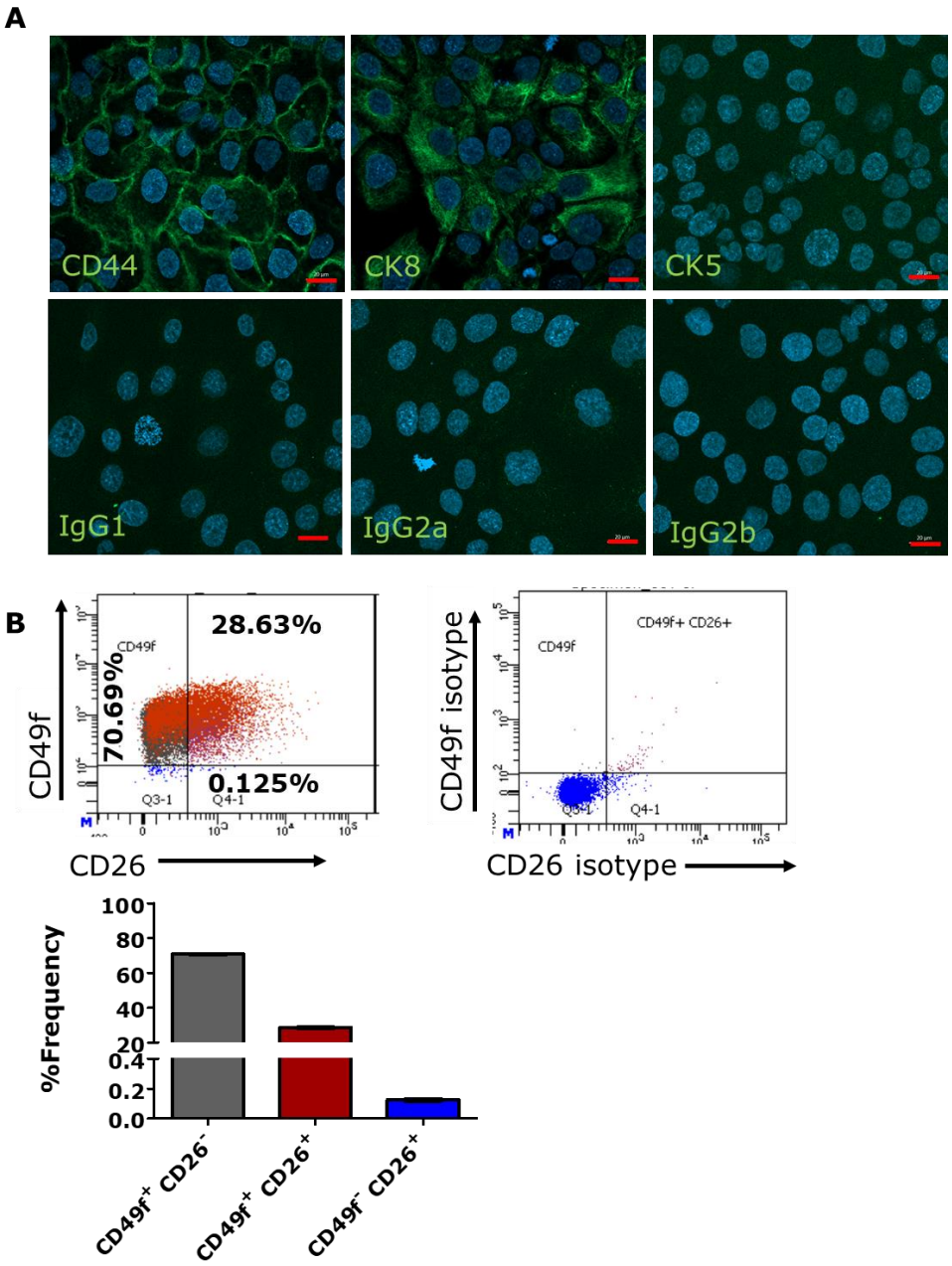

Figure 3.3 Phenotyping of DU145 cells. (A) DU145 cells were plated at 10^4 in 8 well chamber slides and grown to 90% confluency, fixed and stained with the indicated antibodies or isotype controls as described in Materials and Methods. The cells were imaged using a Zeiss axio observer z1 microscope. Scale bar represents 20μm. Positive staining was determined at the same exposure as the isotype control stained cells. Images are representative of triplicate samples in which at least 5 random fields of view were imaged. (B) Flow cytometry dot plot of basal and luminal antibody staining of DU145 cells. Isotype control staining was used to determine the placement of quadrant gates. Population frequencies correspond to the representative staining shown and the mean ± SEM frequency of triplicate samples is given in the bar graph.

3.3 Identification and characterisation of DU145 CSC based on expression of surface markers

I carried out flow cytometry analysis of the DU145 cells to identify potential CSC based on $CD44^+$ $CD49b^{high}$ $CD133^+$ expression. A population expressing these markers was identified, which comprised <0.1% of the total cells (Figure 3.4A). This population frequency was lower than the frequency of the $CD44^+$ $CD49b^{high}$ $CD133^+$ cells identified in primary samples (Collins et al., 2005). Additionally, the CD133 staining of DU145 cells in this study did not conclusively identify a $CD133^+$ population. The CD133 expression did not differ significantly from the isotype control, based on mean fluorescence intensity (MFI) (Figure 3.4B, C). This differs from CD133 staining which was used to define positive populations in other studies. CD133 populations have previously been identified based on higher fluorescent signal, shown by FACS dot plots and/or isotype control staining (Bao et al., 2006; Birnie et al., 2008; Pfeiffer and Schalken, 2010; Richardson et al., 2004).

Studies that have described inconsistencies in the use of CD133 as a CSC marker have suggested that the expression of different epitopes may occur owing to cell culture conditions or cell phenotype (more or less differentiated) (Angelotti et al., 2010; Kemper et al., 2010). The antibody used for the aforementioned experiments recognises the AC133 (CD133/1) epitope of CD133 (Miltenyi Biotech). Therefore, I tested the identification of $CD44^+$ $CD49b^{high}$ $CD133^+$ DU145 cells using the antibody clone EMK08 (Thermo Fisher eBioscience), which recognises a different epitope (Figure 3.5A). However, the CD133 fluorescence intensity was not significantly higher than the isotype control (Figure 3.5B, C). I concluded that these data did not provide enough supporting evidence for a $CD44^+$ $CD49b^{high}$ $CD133^+$ population in the DU145 cells. Therefore, I did not isolate CSC based on these surface markers, and instead proceeded to investigate if DU145 CSC could be isolated by alternative markers; in the absence of previously described alternative prostate CSC surface markers I next investigated the CSC functional marker ALDH.

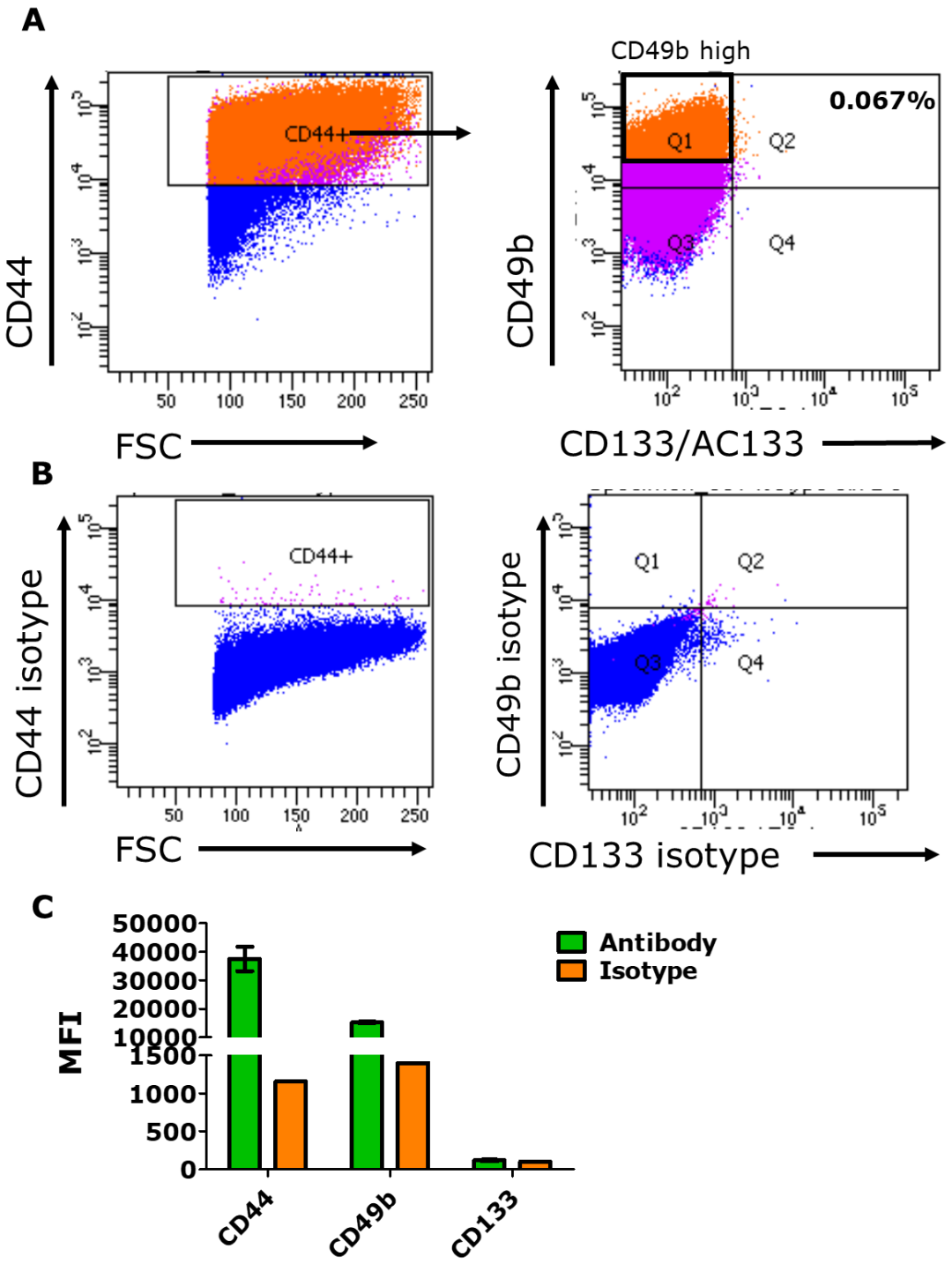

Figure 3.4 Investigation of a CD44$^+$ CD49b^{high} CD133$^+$ population in the DU145 cell line. (A) Identification of CD44$^+$ CD49b^{high} CD133$^+$ DU145 cells by flow cytometry, using a CD133 antibody recognising the AC133 epitope. (B) Isotype control staining for each of the three markers. 1.5x10^6 cells were stained for each antibody or isotype stain. (C) MFI for each antibody and isotype. Single marker 'box' gating (CD44) and quadrant gating in each experiment was determined with the use of an isotype control antibody. Error bars represent triplicate measurements. The experiment was repeated at least three times.

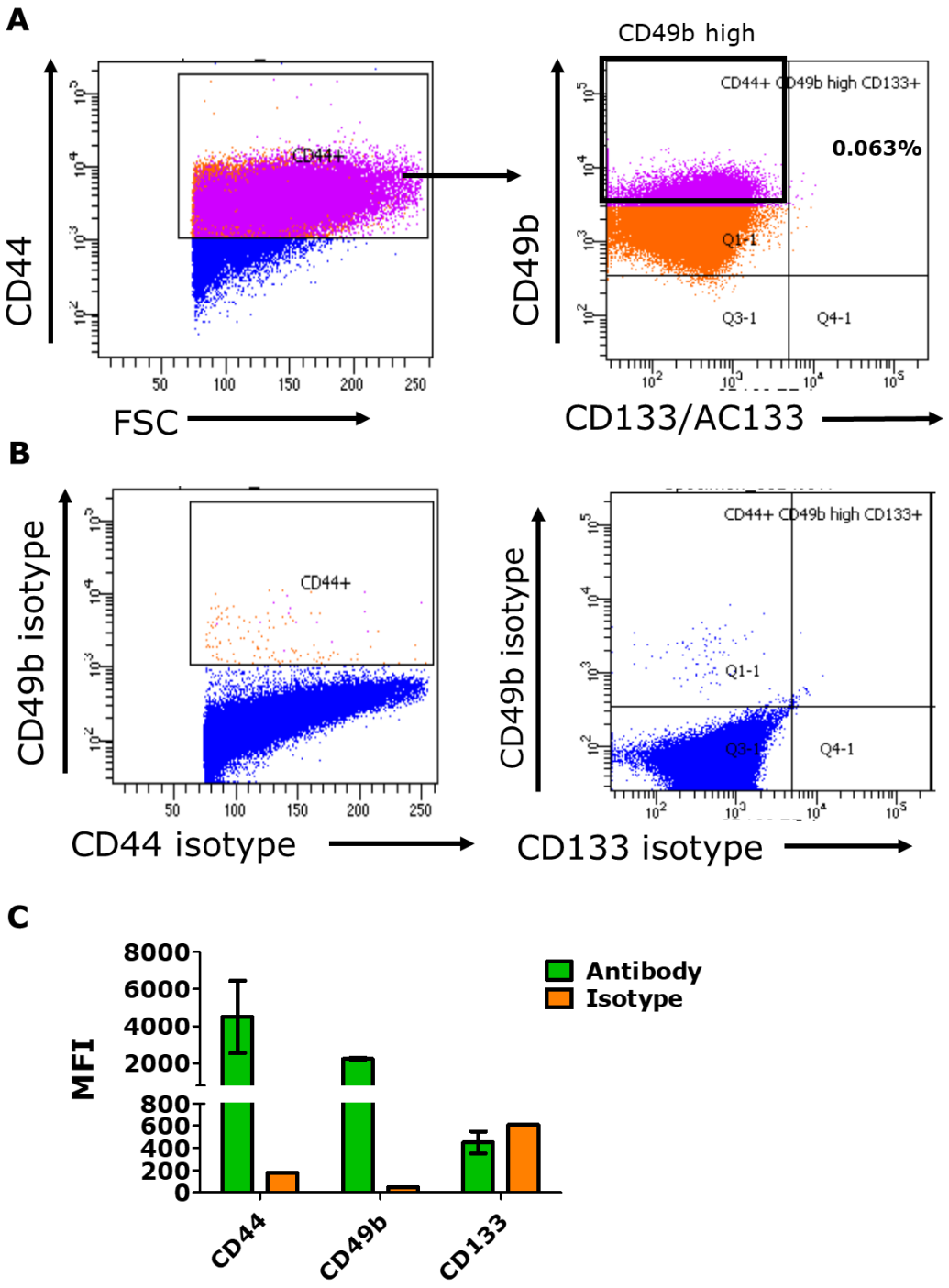

Figure 3.5 Investigation of an alternative epitope for CD133 staining in the identification of a CD44$^+$ CD49b^{high} CD133$^+$ population in the DU145 cell line. (A) Identification of CD44$^+$ CD49b^{high} CD133$^+$ DU145 cells by flow cytometry, using a CD133 antibody recognising the EMK08 epitope. (B) Isotype control staining for each of the three markers. 5x 10^5 cells were stained for each antibody or isotype stain. (C) MFI for each antibody and isotype. Single marker 'box' gating (CD44) and quadrant gating in each experiment was determined with the use of an isotype control antibody. Error bars represent triplicate measurements and the experiment was repeated twice.

3.4 Identification and characterisation of DU145 CSC based on the functional marker ALDH

ALDH activity has been used to identify CSC in PCa cell lines including DU145, PC3 and LNCaP (Doherty et al., 2011; van den Hoogen et al., 2010). ALDH expression has also been detected in primary PCa samples and has been shown to correlate with poor prognosis (Magnen et al., 2013). Based on this previous work, the ALDH CSC marker was selected to investigate CSC in the DU145 cell line.

3.4.1 Optimisation of the ALDEFLUOR assay for DU145 cells

High ALDH activity is characteristic of CSC (Ma and Allan, 2011). Expression of ALDH isoforms ALDH1A1, ALDH3A1 and ALDH7A1 was detected in the DU145 cells by fluorescence microscopy (Figure 3.6A). ALDH activity in the DU145 cell line was investigated using the ALDEFLUOR assay, which primarily measures the activity of ALDH1 isoforms, although the contribution of other isoforms to ALDH activity has also been described (Morgan et al., 2015; Zhou et al., 2019). Preliminary experiments tested the A549 lung cancer cell line, which has high ALDH activity, as a positive control (Moreb et al., 2007). The A549 cell line had a frequency of 11.1% ALDH high cells, while the DU145 cells had 5.63% ALDH high cells, (Figure 3.6B). The ALDEFLOUR incubation protocol was optimised and the substrate concentration scaled up with increasing cell numbers for FACS experiments. The dot plot gating strategy was modified to obtain a more stringent separation of ALDH high (blue) and ALDH low (green) cells. The cells in the gate placed in the presence of DEAB (red population) to guide the identification of the ALDH high population, which could be considered ALDH 'medium,' were not further analysed (Figure 3.6C). This is based on the gating described by Nishida and colleagues for the analysis of ALDH high and low populations in PCa cell lines (Nishida et al., 2012). The ALDH high frequency in three independent FACS experiments was 7.81% ± 1.12 SEM (Figure 3.6D).

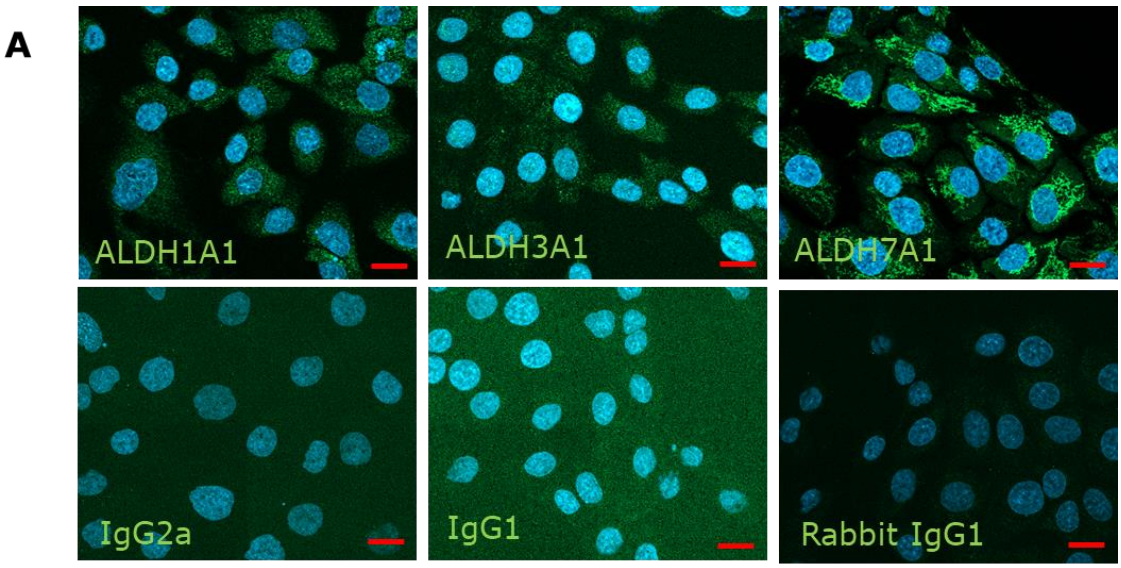

Figure 3.6. Optimisation of the ALDEFLUOR assay in DU145 cells. (A) DU145 cells were plated at 10^4 in a glass bottomed, black walled plate and grown to 90% confluency, fixed and stained with the indicated antibodies or isotype controls as described in Materials and Methods. The cells were imaged using a Zeiss axio observer z1 microscope. Each exposure setting was determined based on the staining at the highest antibody concentration (different for each antibody). Scale bar represents 20 µm. Figure continued overleaf: (B, C) Flow cytometry: The A549 cell line was used as a positive control to compare ALDH activity DU145 cells. The ALDH high gate was positioned to the right of the DEAB inhibitor gate; the ALDH high and low frequencies for each cell line are given in the graph, based on the manufacturer's recommended gating strategy. A549 and DU145 cell numbers of 2 x 10^5 and 5x10^5, with the appropriate volume of ALDH substrate, were tested for ALDH activity, each incubated for 30 minutes without any resuspension. Data shown is 2x10^5 cells, for each cell line. (D) Optimised gating strategy (cells from the middle gate are not analysed). 10^6 cells were incubated with the appropriate volume of ALDH substrate and incubated for 45 minutes, with resuspension of the cells by gentle shaking at 15 minute intervals. (E) An optimised incubation and scaling up protocol resulted in comparable ALDH high and ALDH low frequencies across three independent FACS experiments. The DU145 cells were stained with 5 µl ALDH substrate per 10^6 cells. Input on the optimisation of the ALDEFLOUR assay was provided by group members of the First Pathology Dept., Sapporo Medical University, in particular Dr. Emi Mizushima.

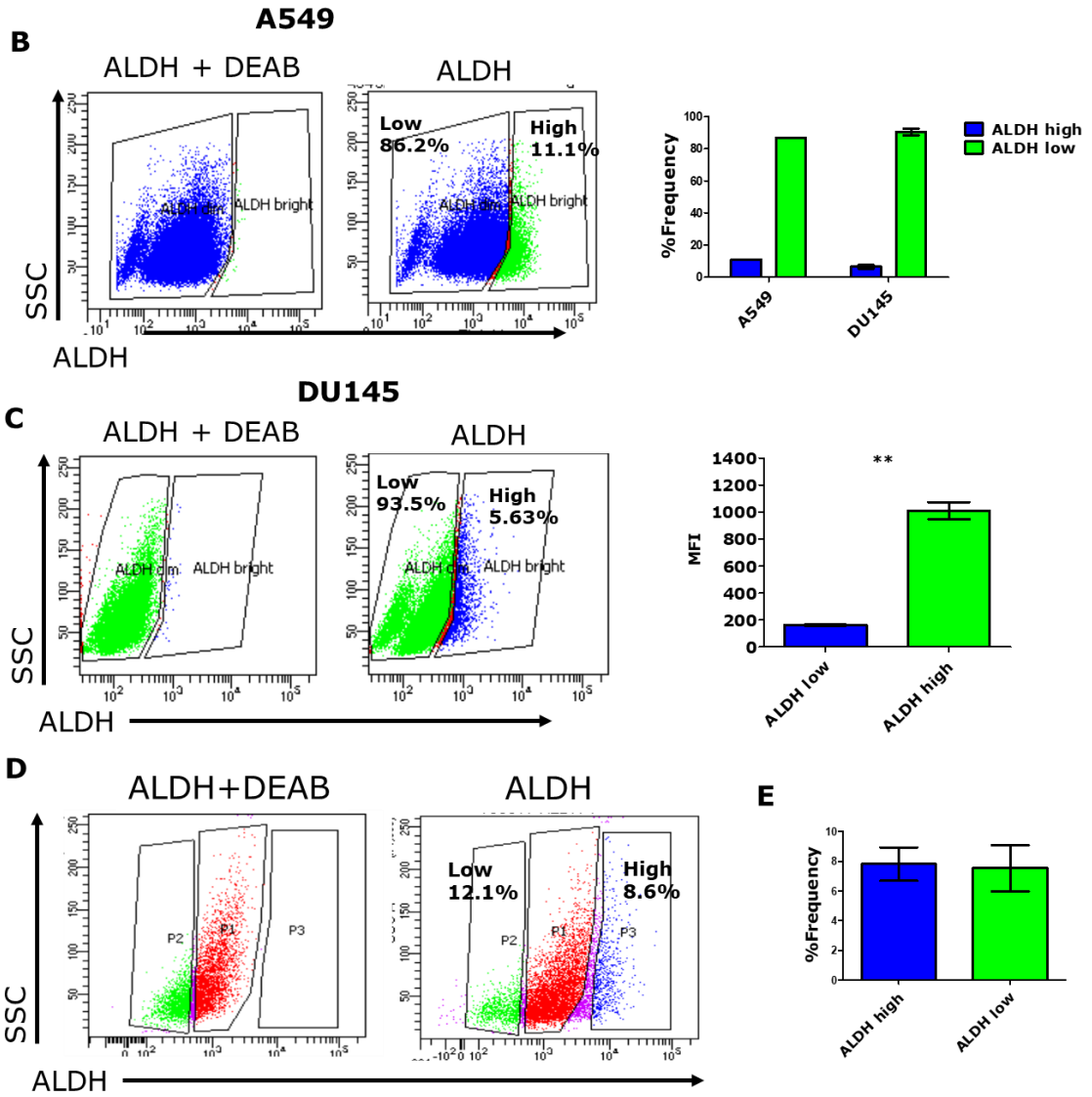
A549
B
ALDH + DEAB
ALDH
Low
86.2%
High
11.1%
ALDH dim
ALDH bright
SSC
ALDH
%Frequency
ALDH high
ALDH low
A549
DU145
DU145
C
ALDH + DEAB
ALDH
Low
93.5%
High
5.63%
ALDH dim
ALDH bright
SSC
ALDH
MFI
**
ALDH low
ALDH high
D
ALDH+DEAB
ALDH
Low
12.1%
High
8.6%
P1
P2
P3
SSC
ALDH
E
%Frequency
ALDH high
ALDH low

3.4.2 Characterisation of ALDH high and ALDH low DU145 cells

Having optimised the ALDH assay and sorting strategy, I performed *in vitro* analysis of the sorted ALDH high and ALDH low populations. I found that the viability of the sorted cells was greatly reduced after sorting, and the viability of the sorted populations differed not only from each other but from experiment to experiment (Figure 3.7). The sorted cells were plated for all downstream assays based on the viable cell count.

The aim of these assays was to investigate the CSC characteristics of clonogenicity and self-renewal. Colony formation is used as a measure of clonogenicity, or the fraction of cells of a population capable of multiple population divisions to sustain the growth of a colony of cells (Franken et al., 2006). The ALDH high cells gave rise to a larger number of colonies than the ALDH low cells, (Figure 3.8A and B; two representative experiments shown). The Colony Area software, which detects and enumerates colonies and total colony area based on pixel values (Figure 3.8C), was a useful application to measure colonies which were sufficiently distinct, as was the case in Figure 3.8B. This enabled quantification of the colonies, shown in Figure 3.8D and 3.8E. The ALDH high DU145 cells produced a significantly larger number of colonies and the surviving fraction (colonies formed/ cells seeded) was significantly higher. The reason for the different ALDH colony characteristics across replicate experiments is not clear.

Sphere formation is considered a measure of self-renewal in CSC. Self-renewal is indicative of the capacity of CSC to maintain their own population, in addition to producing more proliferative non-CSC progeny. Sphere formation is suggested to represent this by modelling a renewing 'colony' in 3D, compared to modelling the linear formation of a clonally-derived colony in 2D. Sphere formation can be used to select for CSC from a bulk population, or to characterise populations which have been isolated from a bulk population using CSC markers (Kryczek et al., 2012; Nishida et al., 2012; Portillo-Lara and Alvarez, 2015; Rybak et al., 2011). Sphere formation is typically assessed in non-adherent conditions in media containing growth factors and lacking serum, as the latter can induce differentiation (Lee et al.,

2006; Ricci-Vitiani et al., 2007). Sphere formation was tested under limiting dilution conditions; 1000 and 100 initially plated cells (Figure 3.9 A and B, two representative experiments shown). The ALDH high DU145 cells grew significantly larger spheres than the ALDH low DU145 cells from both of 1000 and 100 initial starting cell numbers (Figure 3.9C and D). The size of the spheres from both ALDH high and low cells varied in experimental repeats, which may be due to the differences in viability of the sorted populations. Larger spheres may have a necrotic core due to reduced penetration of nutrients and oxygen with an increase in size. Therefore, proliferation and viability of the spheres was also measured using the Orangu assay. Proliferation in the ALDH high spheres was significantly higher than ALDH low spheres grown from 1000 cells (Figure 3.9E and F). Despite the apparent sphere size differences across replicate experiments, the absorbance in the ALDH high spheres grown from 100 cells was not consistently higher than the ALDH low spheres. This may be due to the differences in viability in the sorted cells or that the spheres were too small to reliably detect the Orangu reagent.

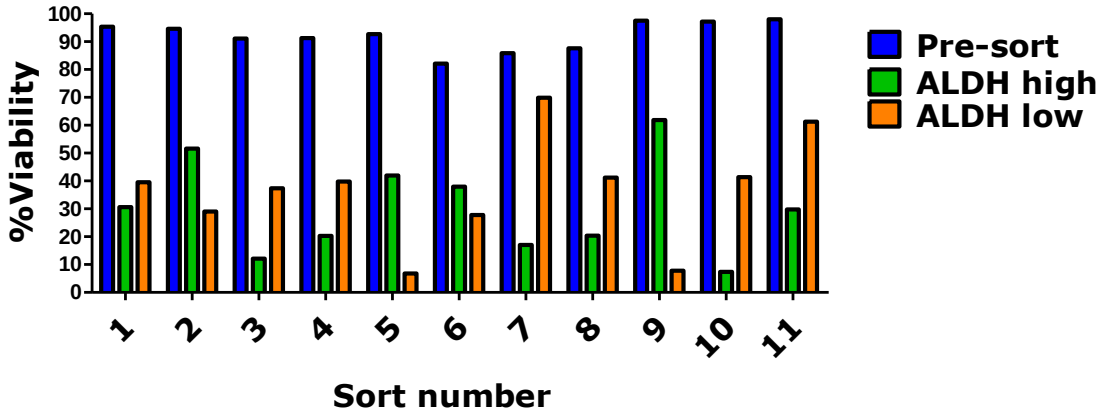

Figure 3.7 Viability of DU145 cells before and after FACS to isolate the ALDH high and ALDH low populations. Prior to carrying out the ALDEFLUOR assay for sorting, the DU145 cell suspension (prepared from trypsinising the adherent cells) was counted and the viability measured by staining with ViaCount Reagent with analysis using the Millipore Guava Flow Cytometer. The flow cytometry staining protocol involved incubating 7 x 10^6 cells/ ml with 35 µl of the ALDH substrate followed by removal of 300 µl of the cell suspension to a tube containing 21 µl DEAB. The number of ALDH reactions required to yield sufficient cells for downstream experiments was pre-determined as described in the Materials and Methods; briefly the cell number required for downstream assays was calculated and worked back from, to include considerations of viability, cell loss to controls in the ALDEFLUOR assay and expected frequency of the ALDH high and ALDH low populations. Typically, 28-35 million cells were prepared (4-5 ALDH reactions at 7 x 10^6). The cells were re-stained following sorting and the same measurements carried out. Note: the DU145 ALDEFLUOR sorts carried out in collaboration with Sapporo Medical University are not included as the pre- and post-sort cell counts and viability investigations were carried out in a different way, using a Countess (Thermo Fisher) which involves automated visual assessment of stained cells rather than flow cytometry readouts.

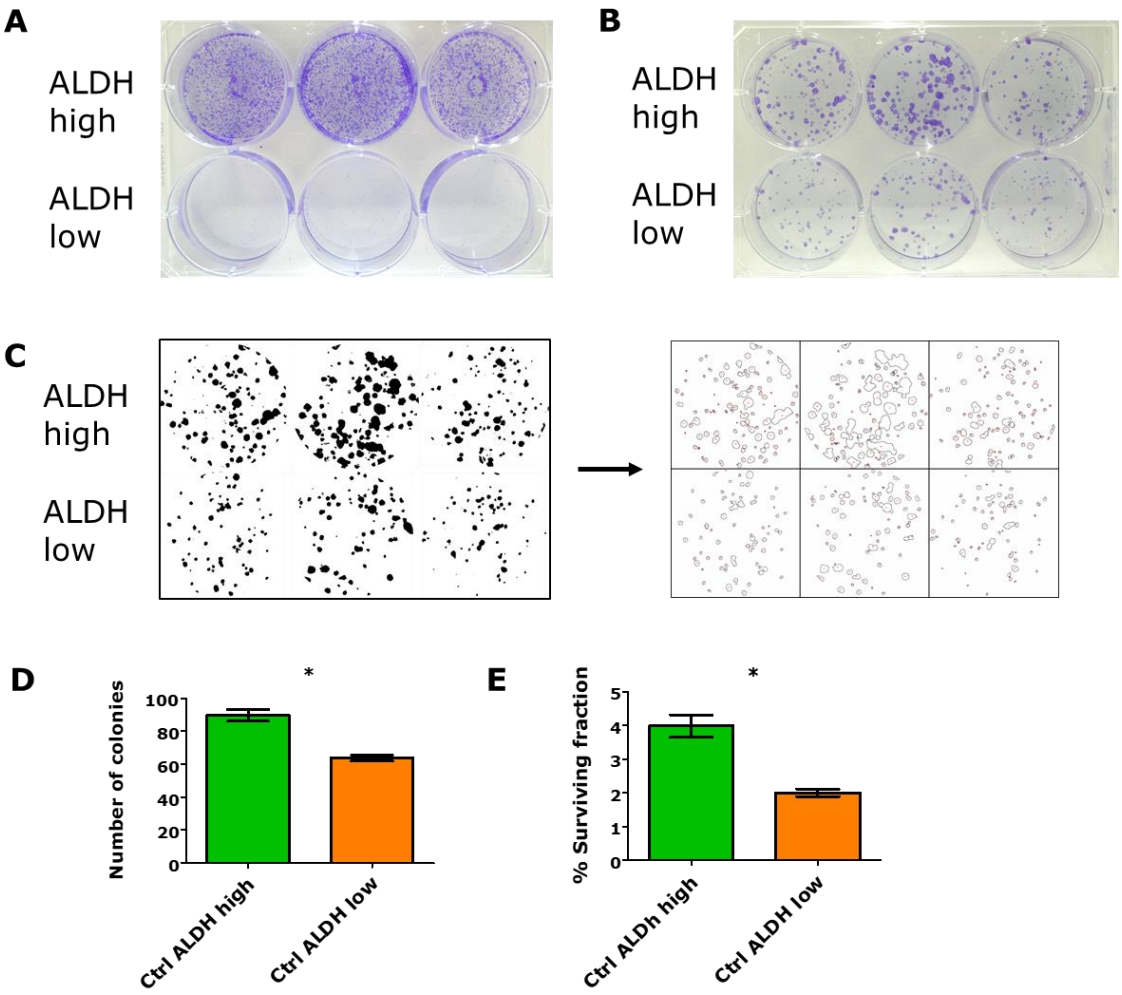

Figure 3.8 Clonogenicity of ALDH high and ALDH low DU145 cells. (A,B) ALDH high and ALDH low DU145 were plated at 50 cells/ cm^2 (450 cells/ well in a 6 well plate) and colonies were stained with 5% crystal violet. Plates were photographed using a Canon 350D DSLR camera. (C): Colonies in (B) were analysed using the Colony Area plugin for ImageJ. The colonies were identified by setting the pixel value threshold above that of the background, which enabled the software to enumerate the colonies and also analyse the colony size. (D) Colony number in ALDH high and ALDH low DU145 cells (* $p<0.05$; Student's T test). (E) The surviving fraction was calculated by first calculating the plating efficiency (colonies formed/ cells seeded). The surviving fraction was calculated as (colonies formed/ (cells seeded x plating efficiency)) Significance was determined by the paired T test * $p<0.05$. Colonies in (A) were not enumerated; the crystal violet colony formation assay was repeated three times.

Figure 3.9 Sphere formation of ALDH high and ALDH low DU145 cells. DU145 cells were sorted by FACS into ALDH high and ALDH low populations and seeded at 1000 or 100 initial cell numbers, in cell-repellent 96-well plates, for non-adherent sphere formation conditions. (A,B) Sphere formation by ALDH high and ALDH low DU145 cells was investigated in serum free ADMEM/F12 media containing EGF and FGF. After 7 days, the spheres were imaged using a Zeiss axoivert 100 microscope. Scale bars represent 200 μm. Cell numbers were not estimated at this time. Two representative experiments shown in A and B (Sphere setup from 1000 cells was repeated a total of 3 times and from 100 cells twice, owing to the technical difficulties in consistent detection of Orangu levels from ALDH high and ALDH low spheres. Black arrows indicate dead cells collected at the base of the well which were not incorporated into the sphere.

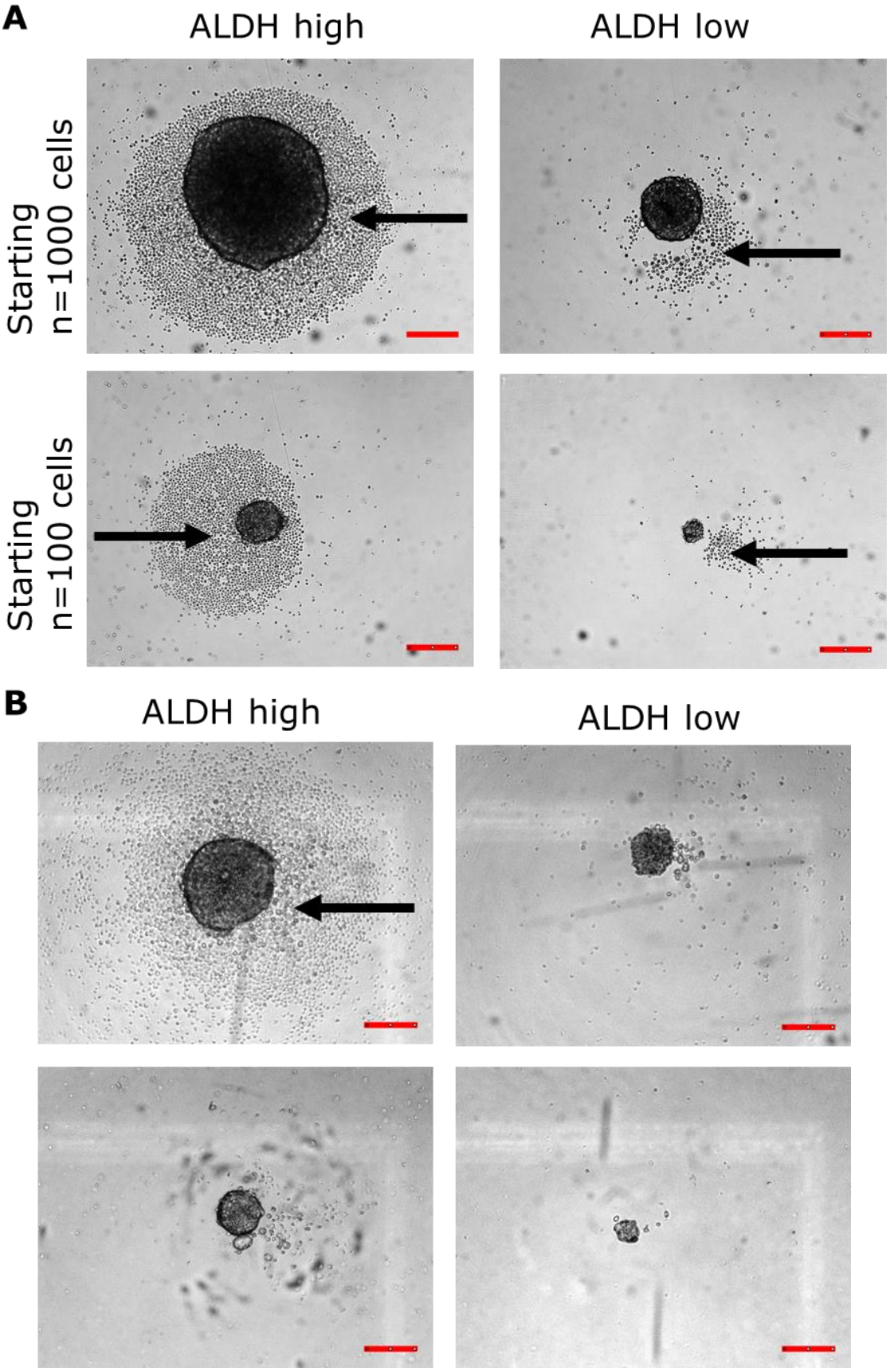
A
ALDH high
ALDH low
Starting n=1000 cells
Starting n=100 cells
B
ALDH high
ALDH low

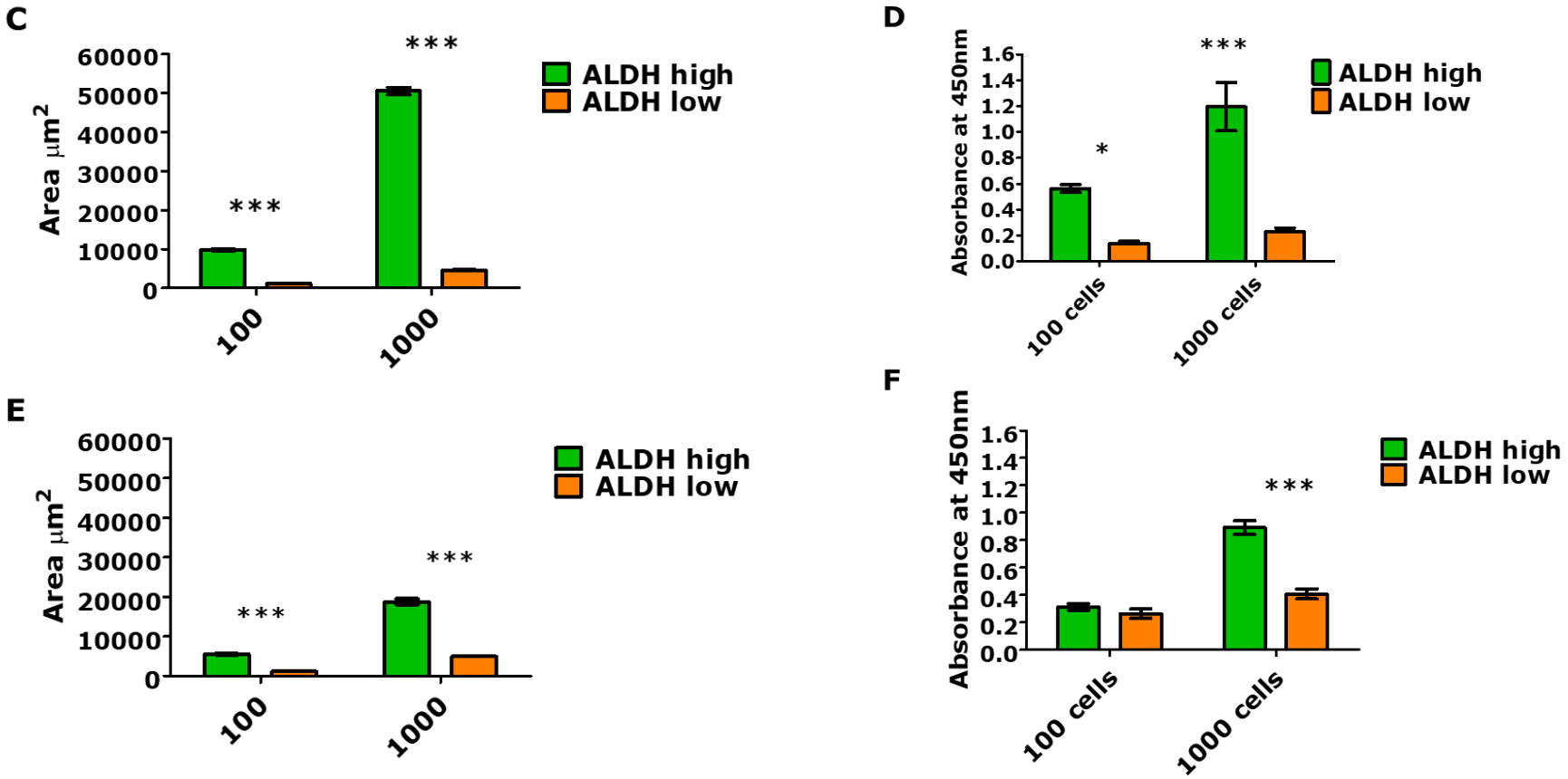

Figure 3.9 continued (C, E) The sphere area was measured using the MetaMorph microscopy image analysis program. (D, F) The spheres were incubated with orange reagent for 2 hr and the absorbance was measured to determine proliferation and cell viability in the spheres. Error bars represent n=5 spheres. Statistical analysis of sphere size and orange absorbance was investigated by a 2 way ANOVA;* $p<0.05$ *** $p<0.001$. Sphere size measures and Orangu assay absorbance in (C, D) correspond to experiment (A) and (E, F) correspond to (B).

3.4.3 Cellular division of ALDH high and ALDH low DU145 cells

Cancer cells typically grow more quickly than healthy cells; it is on this basis that cancer treatments such as chemotherapy and radiation therapy are used to treat tumours by causing DNA damage while minimising off target damage to healthy tissues. However, it has been suggested that CSC divide less frequently than non-CSC, which reduces the susceptibility of CSC to DNA damaging agents (Dembinski and Krauss, 2009; Moore et al., 2012; Patrawala et al., 2006). Therefore, we compared division and proliferation in the ALDH high and ALDH low DU145 and primary PCa cells.

Labelling of cells with DNA or protein binding dyes, such as Bromodeoxyuridine (BrdU) or carboxyfluorescein succinimidyl ester (CFSE), has identified slow cycling (less frequently dividing) cells which have CSC characteristics (Deleyrolle et al., 2012; Ma et al., 2014). The Cell Trace Violet reagent (Thermo Fisher Scientific) was used as an alternative to CFSE. CFSE fluorescence is measured in the same emission channel as FITC and is not compatible with ALDEFLUOR analysis. To optimise this approach, Cell Trace Violet and CFSE staining and dye dilution over time was compared for DU145 cells (without performing the ALDEFLUOR assay). High, medium and low dye retention (representing low, medium and high proliferation, respectively) gating for each dye was determined by measuring autofluorescence of non-stained DU145 (low) or cell trace fluorescence of DU145 cells stained immediately before analysis (high), (Figure 3.10 A and B). The fluorescence of the Cell Trace dye decreased less over a short time than that of the CFSE dye, demonstrated by the significantly higher MFI of Cell Trace high than CFSE high at Day 3 (Figure 3.10C). After 7 days the proportion of high dye retention was not significantly different between Cell trace and CFSE. However, the DU145 Cell Trace medium and low gates had a higher frequency of cells than the respective CFSE gates, suggesting better retention of the Cell Trace dye over a longer time period (enabling tracking of more cell divisions) (Figure 3.10D).

The Cell Trace dye was then used to measure the division and proliferation of ALDH high and ALDH low DU145 cells. ALDH high DU145 cells contained a

significantly higher proportion of Cell Trace high cells than ALDH low DU145 cells after 3 days of culture (Figure 3.11A). The frequency of ALDH high Cell Trace high cells decreased over time and was not significantly higher than ALDH low cell trace high cells after 7 days (Figure 3.11B). However, the cell trace MFI of the ALDH high cells was significantly higher than the ALDH low cells (Figure 3.11C), suggesting the fluorescence signal was less diluted due to less cell divisions in the total ALDH high population. This demonstrates that the ALDH high DU145 cells divide at a lower rate than the ALDH low DU145 cells.

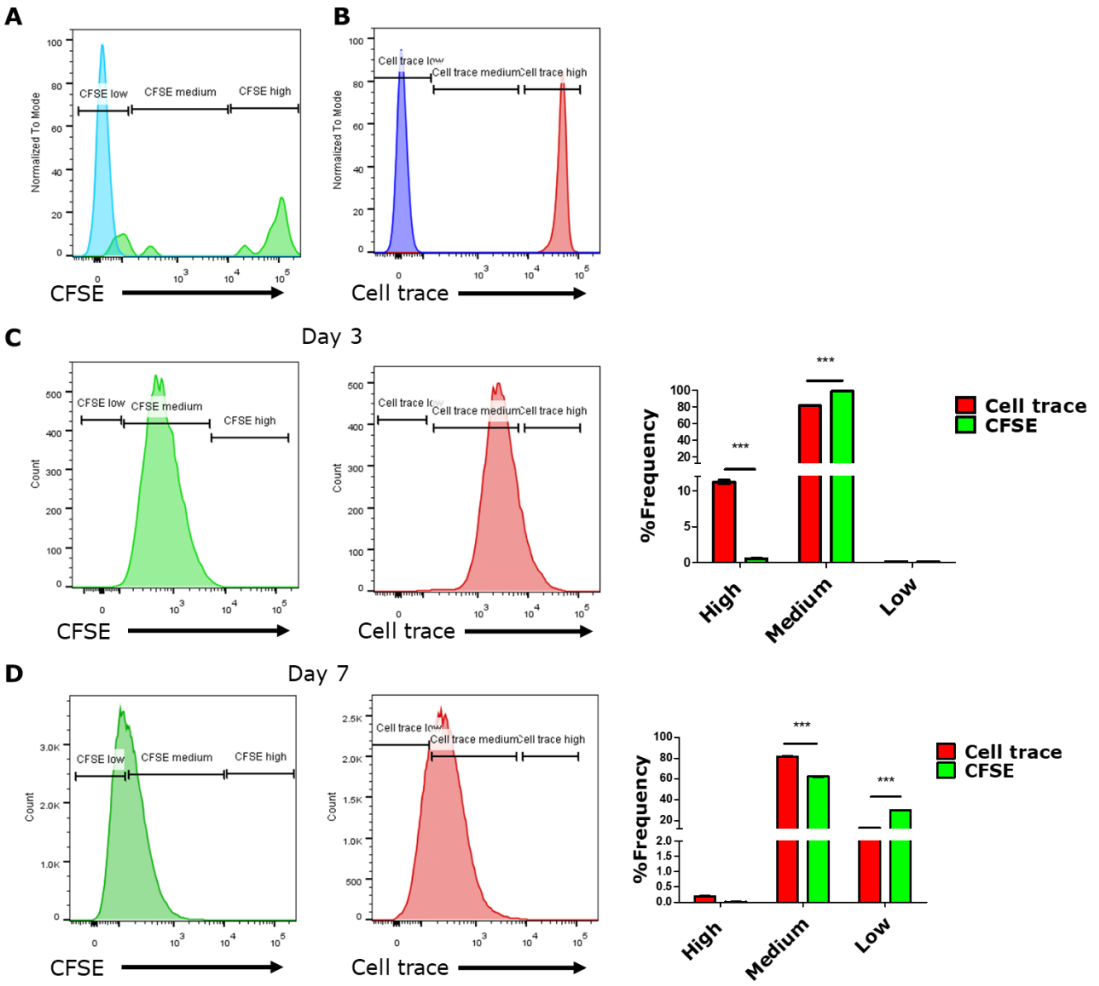

Figure 3.10 Optimisation of Cell Trace dye staining of DU145 cells. The cellular dyes CFSE and Cell Trace were compared for use in tracking proliferation in successive generation of DU145 cells. Both cell types were stained with 2.5μM or 50 μM CFSE respectively at day 0. The DU145 cells were plated at 5 x 10^5 cells in a 75 cm^2 flask for analysis after 3 days of growth and at 10^5 cells in a 75 cm^2 flask for analysis after 7 days of growth. The BLCL were plated at the same cell numbers and cultured upright in 25 cm^2 flasks. (A and B) The staining was divided into high, low and medium fluorescence for each of CFSE (A) and Cell Trace (B), to represent low, medium and high proliferation respectively. This was based the principle that the dye fluorescence signal is reduced upon subsequent cell division of a labelled population. (C) The high medium and low fluorescence populations for each dye were investigated after 3 days in 2D culture. The population frequencies are graphed and represent triplicates. *** $p<0.001$, analysis by 2-way ANOVA. (C) The high, medium and low fluorescence populations for each dye were investigated after 7 days in 2D culture. The population frequencies are graphed and represent triplicates. *** $p<0.001$, analysis by 2-way ANOVA. Analysis was performed using FlowJo flow cytometry software so that overlay histograms could be generated.

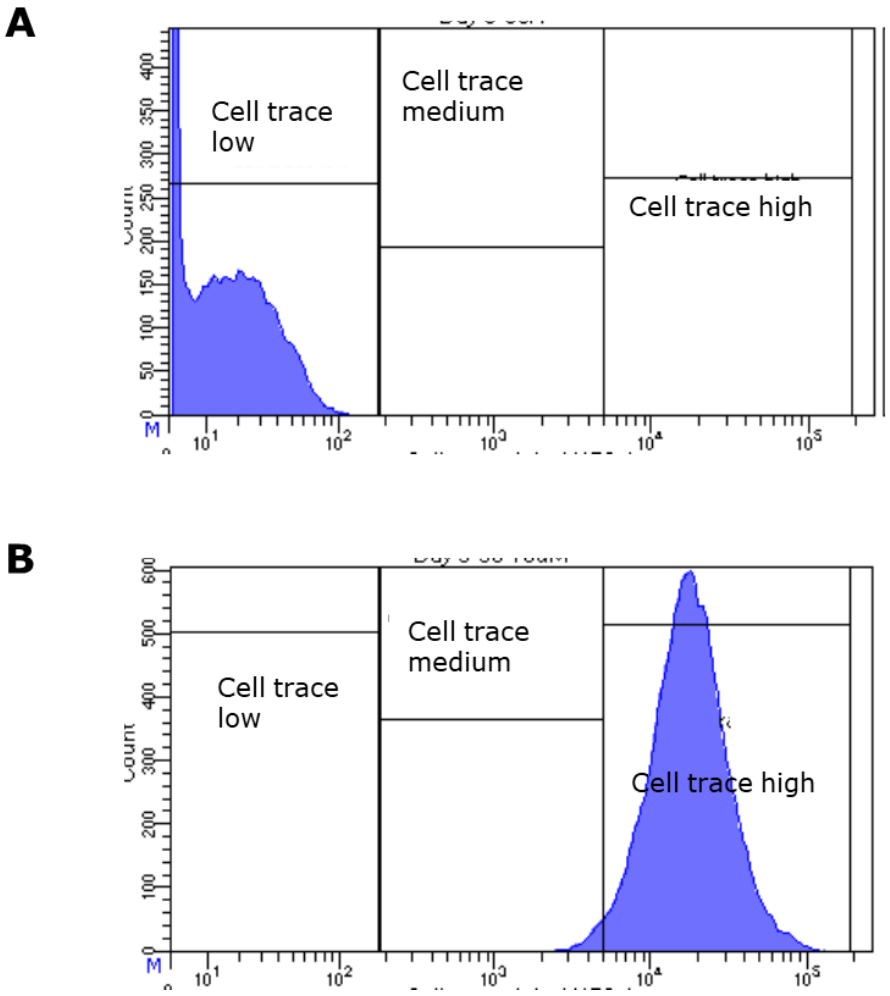

Figure 3.11 Measurement of division and proliferation of ALDH high and ALDH low populations in DU145 cells. A bulk (unsorted) population of DU145 cells was stained with Cell Trace dye and plated in 2D culture. The DU145 cells were plated at 5 x 10^5 cells in a 75 cm^2 flask for analysis after 3 days of growth and at 10^5 cells in a 75 cm^2 flask for analysis after 7 days of growth. (A) Unstained cells autofluorescence, used to gate 'cell trace low' (B) Cells stained immediately prior to analysis, used to gate 'cell trace high.' Continued overleaf: (C) After 3 days the ALDEFLUOR assay was performed and the proliferation and division of the ALDH high and low DU145 cells was measured. (D) Proliferation and division of the ALDH high and low DU145 cells was measured in the same way after 7 Days. The different frequencies of Cell Trace staining in the ALDH populations was assessed by 2-way ANOVA; *** $p<0.001$. (E) Cell trace fluorescence MFI of the ALDH high and ALDH low populations after 7 days. MFI was analysed by paired T test; ** $p<0.01$. The high and low gates for each timepoint were set using DU145 cells stained immediately prior to analysis and unstained cells respectively. Error bars represent triplicates and this experiment was repeated twice.

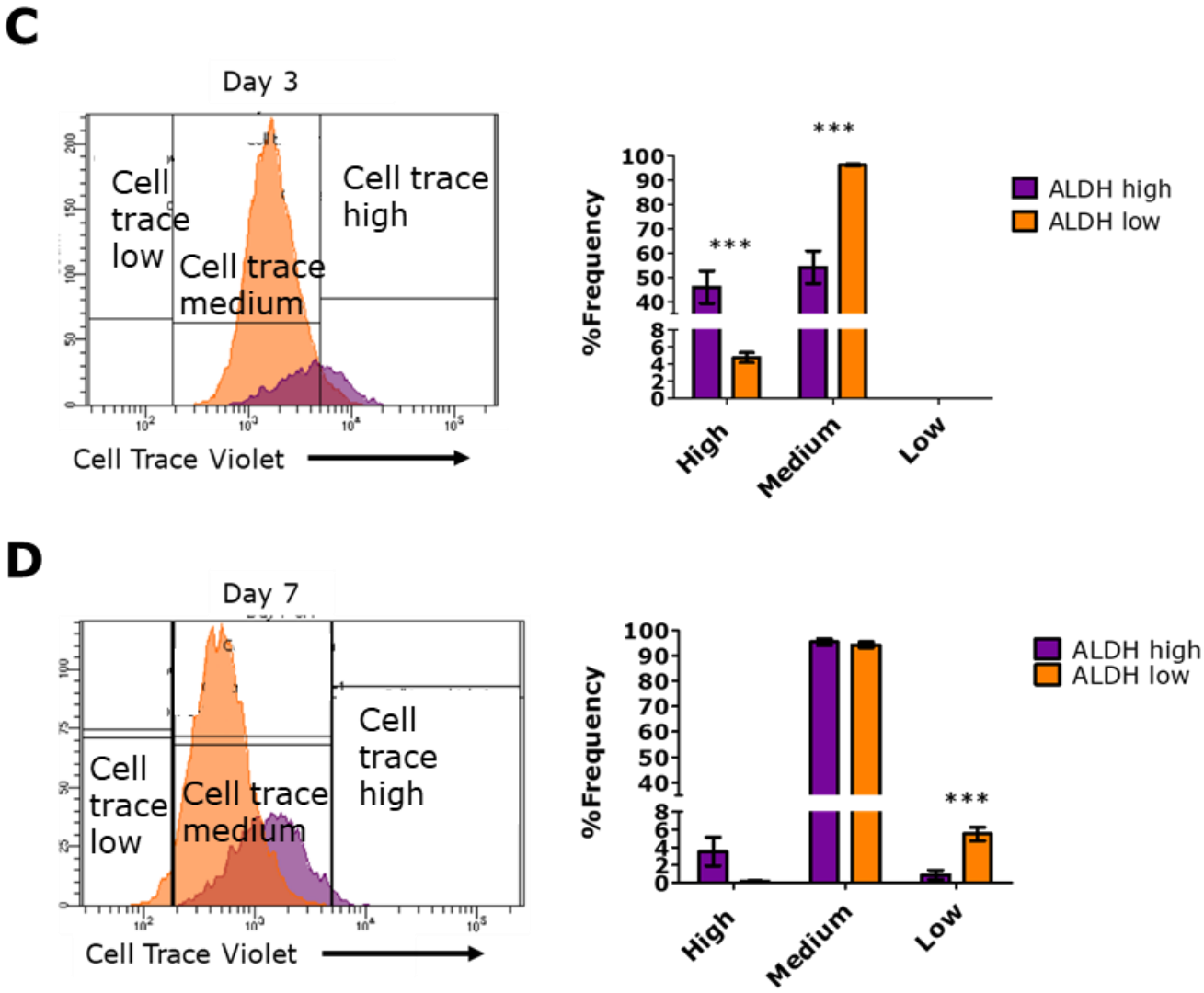
C
Day 3
Cell trace low
Cell trace medium
Cell trace high
Cell Trace Violet
%Frequency
***
***
ALDH high
ALDH low
High
Medium
Low
D
Day 7
Cell trace low
Cell trace medium
Cell trace high
Cell Trace Violet
%Frequency
***
ALDH high
ALDH low
High
Medium
Low
E
Cell trace MFI
**
ALDH high
ALDH low

3.4.4 Gene expression in ALDH high and ALDH low DU145 cells

Investigation of the gene signature of CSC has previously been performed in a small number of studies, which focused either on a limited number of pre-selected CSC associated genes or large scale non-targeted array data (Birnie et al., 2008; Nishida et al., 2012; B. A. Smith et al., 2015). In addition to *in vitro* functional characteristics, I investigated gene expression using RT-qPCR and Nanostring. These assays employ different methods while providing a similar throughput to measure gene expression; RT-qPCR measures cDNA while Nanostring measures mRNA transcripts. Gene expression RT-qPCR analysis was performed using the RT2 Profiler CSC Gene Array. This array contained primers for over 80 genes associated with CSC (details in Chapter 2 Materials and Methods). For the Nanostring analysis, differential gene expression was analysed using the Stem Cell Panel, which contained 195 genes. There were 19 genes in common between the RT2 Profiler CSC Gene Array and the Stem Cell Panel (gene lists provided as appendices to Chapter 2 Materials and Methods).

In the RT-qPCR analysis, the genes which were >1.5 fold significantly greater in expression in the ALDH high compared to the ALDH low DU145 cells were DLL1 (+4.69 fold), MUC1 (+2.32 fold), WEE1 (+1.68 fold) and JAG1 (1.5 fold) (Figure 3.12A). This cut-off was selected rather than the traditional 2-fold difference since the fold changes >1.5 were significant over three repeated experiments. The selection of a fold change threshold in gene expression data is the subject of debate and it has been argued that the use of different cut-offs can change the interpretation of data (Dalman et al., 2012). However, there is no specific biological rational for the 2-fold threshold, and there is precedent for the use of 1.5 fold or 1.3 fold upregulation, in addition to significance testing, to identify biologically relevant differences in gene expression (Huggins et al., 2008; Peart et al., 2005; Raouf et al., 2008). Additionally, upregulation of JAG1 and WEE1, although below 2-fold, were of interest and could be linked to other experimental results. DLL1 and JAG1 are both ligands for NOTCH signalling (Matsui, 2016), while WEE1 is a cell cycle (G_2) checkpoint kinase, with a role in regulating cell cycling in response to genomic stress (Do et al., 2013). Altered cell cycling between ALDH high and ALDH low cells, demonstrated by

differences in dilution of the Cell Trace dye, and, as discussed later, also observed in gene expression analysis using the Nanostring platform, may suggest an under-explored novel characteristic of prostate CSC. MUC1 is a membrane associated protein involved in a wide variety of intracellular signalling pathways, which is overexpressed in lung, stomach, breast and colorectal cancer and PCa (Genitsch et al., 2016; Nath and Mukherjee, 2014; O'Connor et al., 2005). MUC1 is also a highly expressed cell surface cancer antigen (Kiessling et al., 2012). The genes which were ≤0.5 fold significantly lower in the ALDH high DU145 cells compared to the ALDH low DU145 cells were ZEB1 and MS4A1 (CD20), with ZEB2 fold change also approaching significance (Figure 3.12B). ZEB1 and ZEB2 are positive regulators of epithelial-mesenchymal transition (EMT), (Hanrahan et al., 2017).

Nanostring analysis was performed on DU145 ALDH high and low cell-derived mRNA from two independent FACS experiments. This was not sufficient to carry out statistical analysis, therefore the genes which showed a fold change ≥1.5 are shown in Figure 3.12C, to provide an overview of genes of interest which could inform future directed analysis. The 1.5-fold change threshold was selected as the Nanostring SPRINT is sensitive to detection of fold changes >1.5 fold when there are greater than 5 copies of a gene transcript per cell (platform specifications https://www.nanostring.com/products/ncounter-systems-overview/ncounter-sprint-profiler). The genes for which the fold change was above this threshold were: CDK1 (+2.15 fold), CDH1 (+1.99 fold), JUN (+1.85 fold), CCNA2 (+1.75 fold), TUBB (+1.733 fold), PPARD (+1.54 fold), NOTCH3 (+1.535 fold) FOSL1 (+1.53) and PLAU (+1.52 fold). These genes were not associated with any significant pathway enrichment, when analysed using the DAVID bioinformatics platform (Huang et al., 2009b). However, it remains of interest that genes associated with cell cycling were upregulated and the lack of significant enrichment with this pathway could be due to the low number of genes which were significantly upregulated in the Nanostring analysis. Cyclin A2 (CCNA2) and CDK1 are expressed in the S phase, peaking in the G_2 phase of the cell cycle, with a contribution to mitosis regulation (Yam et al., 2002). Cyclin A2 has also been identified as a cancer testis antigen in PCa (based on antibody responses detected in patient sera) and

Chapter 3. Identification and characterisation of prostate cancer stem cells has been shown to elicit high avidity T cell responses in a number of peptide pulsed cell lines (melanoma, CRC) (Kondo et al., 2009; Shi et al., 2005). There were no genes for which the fold change was ≤0.5 compared to the gene expression in ALDH low DU145 cells. Additionally, none of the genes in common in the two assays were differentially expressed in the ALDH high DU145 cells. These data may suggest that relatively few genes, or genes other than those investigated in these assays, contribute to the CSC phenotype demonstrated in the previous functional assays. Genes of interest, which require further analysis for validation, include NOTCH signalling and cell cycle regulation.

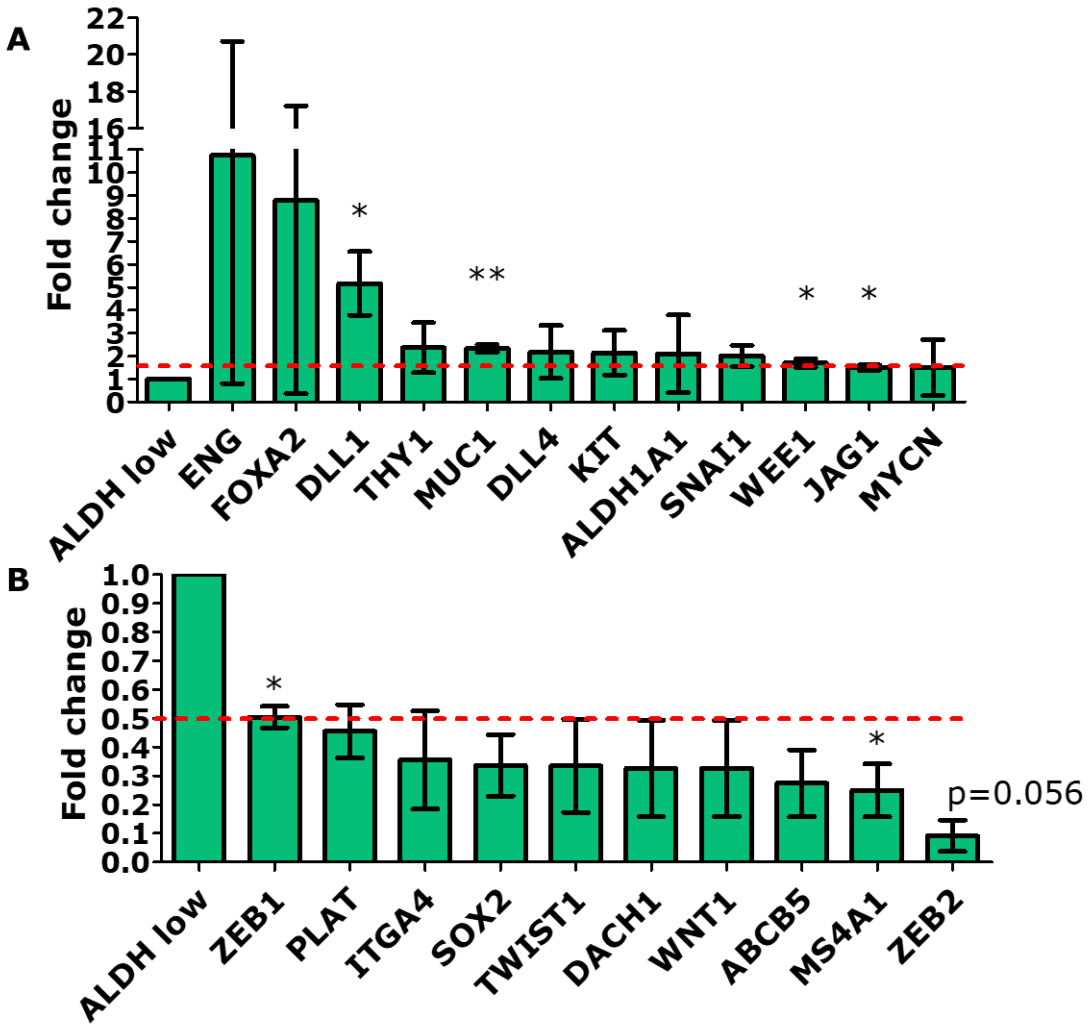

Figure 3.12 Gene expression analysis of ALDH high and ALDH low DU145 cells by RT-qPCR. In the RT-qPCR array (A and B), differential gene expression was calculated by the $2^{-}\Delta\Delta CT$ (comparative CT) method. Genes upregulated >1.5 fold, for which the fold change was statistically significant across three replicate experiments, were considered of interest. The red dashed lines indicate the fold change threshold. The error bars indicate the 95% confidence interval. (A) Genes for which the fold change in gene expression was ≥1.5 greater in the ALDH high compared to the ALDH low DU145 cells in the CSC PCR array. (B) Genes for which the fold change in gene expression was ≤0.5 less in the ALDH high compared to the ALDH low DU145 cells in the CSC PCR array. Statistical significance shown is based on paired T test of housekeeping gene- normalised cycle thresholds (ΔCT) for ALDH high and ALDH low DU145 cells; fold change data ($2^{-}\Delta\Delta CT$) is shown on the graph. Error bars represent fold changes from n=3 repeated experiments (i.e. RNA isolated from 3 individual ALDH FACS sorts).

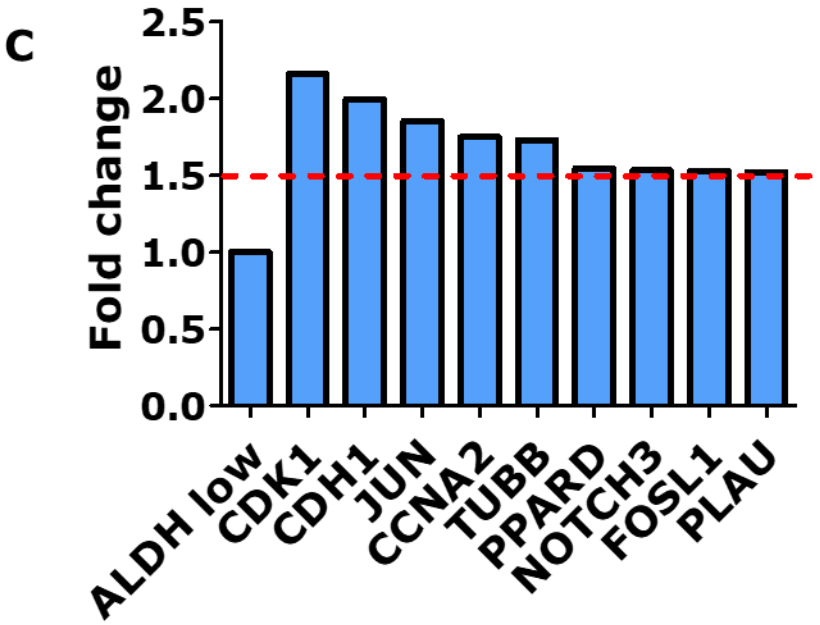

Figure 3.12 Gene expression analysis of ALDH high and ALDH low DU145 cells using the Nanostring platform (continued). (C) Differential gene expression ≥1.5 fold in ALDH high compared to ALDH low DU145 cells measured by Nanostring. The fold change was measured from n=2 individual ALDEFLUOR sorting experiments. The fold change was manually calculated from the log ratio of normalised Nanostring count data which was derived from the raw count values according to the protocol by Prokopec and colleagues (2013). The red dashed lines indicate the fold change threshold (>1.5 fold). Genes upregulated >1.5 fold were considered of interest however the sample number was too small to carry out statistical testing.

3.4.5 Investigation of *in vivo* tumorigenicity of DU145 CSC

An essential characteristic of CSC is the capacity to initiate tumours *in vivo* (Prager et al., 2019). The tumour initiating capacity of FACS- sorted ALDH high and ALDH low DU145 cells was investigated by injecting 10^2 or 10^3 cells, in Matrigel, subcutaneously into individual NSG mice. NSG mice (NOD/SCID gamma) are a highly immunocompromised mouse model which lack mature T cells, B cells and NK cells and also have defective DCs, macrophages and complement signalling (Shultz et al., 2005). Tumours arose more quickly in mice injected with 10^3 ALDH high cells compared to matched numbers of ALDH low cells and after 64 days the size of tumours initiated by either of 10^3 or 10^2 ALDH high DU145 cells was significantly larger than matched numbers of ALDH low DU145 cells (Figure 3.13A). Additionally, individual tumours from 4/5 mice injected with 10^3 ALDH high cells, and 3/5 mice injected with 10^2 ALDH high cells, were larger than the 10^3 ALDH low recipient mice (Figure 3.13B). This demonstrates that ALDH high DU145 cells have greater tumour initiating capacity.

These *in vivo* data support the *in vitro* demonstration of increased clonogenicity and self-renewal of ALDH high DU145 cells in the CFA and sphere formation assays. Furthermore, ALDH high DU145 cells had a lower rate of cell division, and enrichment for stemness defining genes compared to ALDH low DU145 cells. Overall, these data suggest that ALDH high cells represent a CSC population in the DU145 cell line, and this warranted further investigation of the ALDH high cells in primary PCa samples.

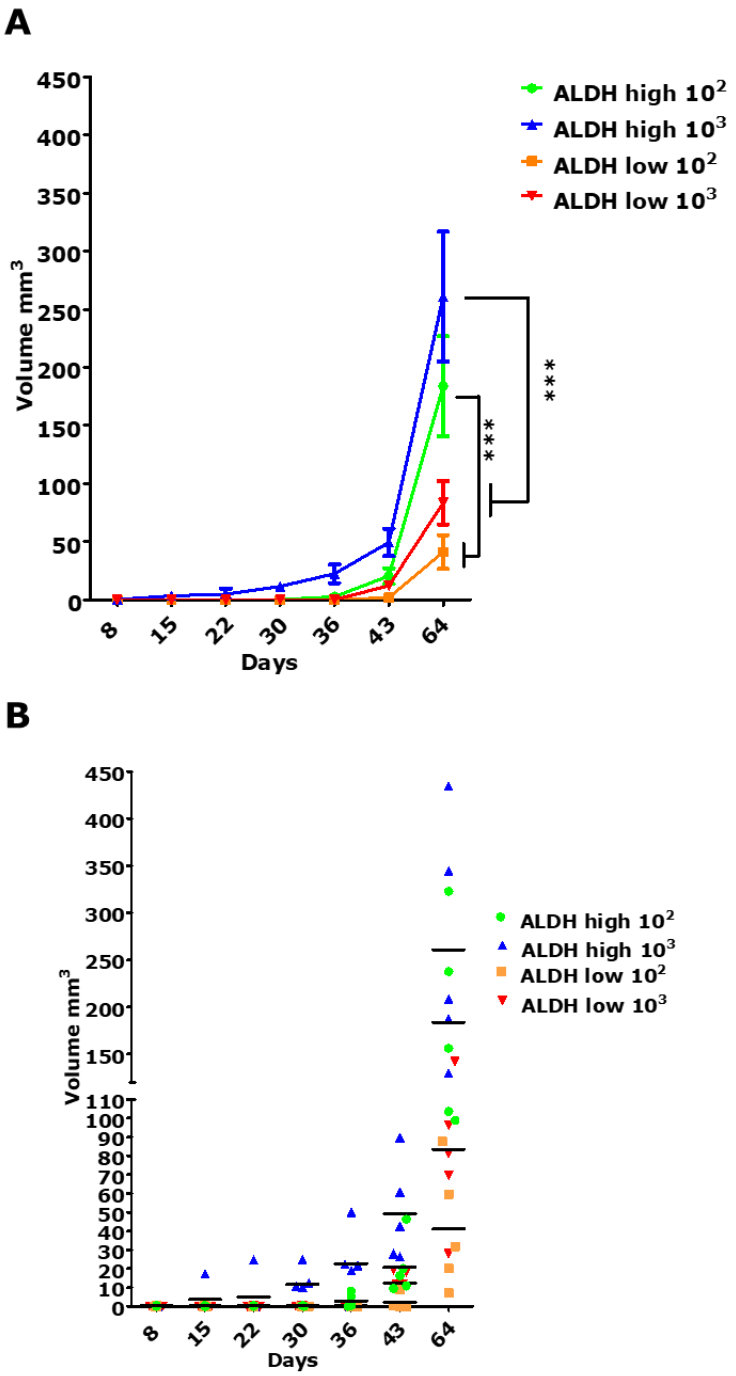

Figure 3.13 *In vivo* tumour initiation by ALDH high and ALDH low DU145 cells. 10^3 or 10^4 ALDH high and ALDH low DU145 cells were injected subcutaneously into individual NSG mice. Tumour growth was detected by palpation until the tumours could be measured using digital callipers. (A) Tumour size over time. Data points and error bars represent mean ±SEM, n=20, 5 per ALDH/count condition; *** $p<0.001$ calculated by 2way ANOVA. (B) Tumour size in individual mice. This work was carried out in collaboration with Sapporo Medical University, Japan: this experiment was performed with the assistance of Dr. Emi Mizushima (FACS) and Ms Serina Tokita (in vivo assay).

3.5 Growth and characterisation of primary prostate cancer cells

As previously discussed, the challenges of establishing primary PCa cell lines *in vitro* has limited investigations of primary prostate CSC. However, the use of primary samples is an important confirmatory step in studies relying on the use of cell lines, particularly a single cell line, to appreciate possible biological heterogeneity and to improve the potential clinical application of the study. Therefore, having characterised CSC using the DU145 cell line, I next investigated CSC in primary PCa samples. The aim was to optimise primary prostate culture conditions, investigate the phenotype of the primary cells in comparison to the DU145 cells, and characterise primary prostate CSC using methods developed using the cell line.

3.5.1 Characteristics of primary prostate biopsies and optimisation of processing methods

Establishing primary PCa cultures consisted of processing biopsies obtained from men undergoing prostatectomies, then optimising media conditions for sufficient cell growth to investigate the CSC population. The patient characteristics are described in Appendix 1. The first study sample (Study 1: N=21 samples, from 19 patients) was obtained with the aim of optimising the biopsy processing protocol, testing media conditions for optimal growth and investigating the CSC markers previously characterised in the DU145 cells. This was followed up by a second study (Study 2: N=8), in which optimised media and CSC markers were used to isolate and characterise primary prostate CSC. The characteristics of the samples obtained in the two studies are detailed in Table 1.

The biopsies were mechanically dissected into ~1mm^3 pieces (Figure 3.14A) followed by enzymatic digestion using Collagenase I or Collagenase II. Collagenase I was indicated by a previous protocol developed in our lab, and Collagenase II was indicated in the protocol by Drost et al., (2016), therefore these reagents were compared. The use of Collagenase I resulted in recovery of a higher yield of cells from the biopsies than Collagenase II (Figure 3.14B).

Additionally, the biopsies digested using Collagenase I were more viable than those digested using Collagenase II (Figure 3.14C). Following this comparison, the remainder of samples received in Study 1 and all samples received in Study 2 were enzymatically digested using Collagenase I (Figure 3.14D). The average viability in Study 1 was 77.46% and 45.75% for samples digested using Collagenase I and Collagenase II respectively, and the average viability in Study 2 was 52.95%.

Table 3.1 Characteristics of prostatectomy biopsies

Study Identifier	**Study 1**	**Study 2**
Number of samples	21	8
Number of patients	19	8
Sample type	N=18 needle core N=3 tissue slice	N=8 needle core
Time from operation to sample receipt	16/21 same day 5/21 next day	8/8 same day
Average age	61.9 years	53.5 years
Gleason Score	7 (n=19)	7 (n=7/8) 9 (n=1/8)
Diagnosis	Adenocarcinoma (n=19)	Adenocarcinoma (n=8)

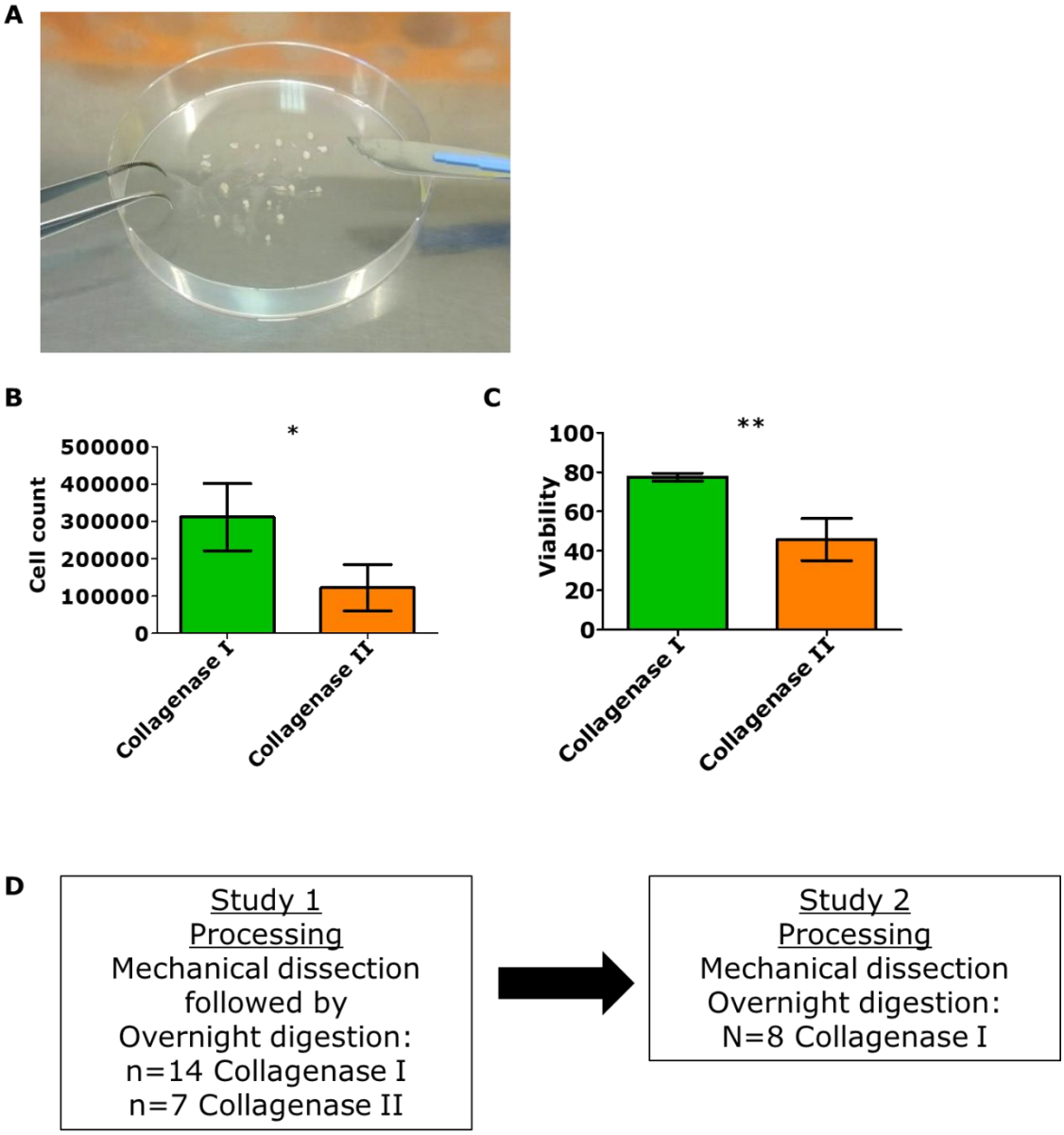

Figure 3.14 Optimisation of mechanical and enzymatic processing of primary prostate biopsies. (A) Primary prostate biopsies were dissected into 1mm^3 pieces using a scalpel. (B) The first n=10 samples received as part of Study 1 were enzymatically digested using Collagenase I, followed by n=7 samples which were digested using Collagenase II. This was discontinued following reduced cell count (B) and viability (C). Error bars = SEM; differences assessed by Mann Whitney U test; * $p<0.05$, ** $p<0.01$.

3.5.2 Optimisation of a growth medium for primary prostate cancer cells

In Study 1, the growth of primary PCa cells was investigated in adherent (2D) and non-adherent (3D; spheres) conditions. The cells grown in adherent culture were grown in the 'SCM' medium described by Frame and colleagues, but without the inclusion of irradiated stromal feeder cells (Frame et al., 2013). The reason for this was to minimise undefined xenobiotic factors; however certain components of the supplements used, e.g. B27, are not disclosed by the manufacturer. DHT (10 nM) was added to surviving adherent cultures to stimulate proliferation by activating the AR, however this did not improve the survival of the cells. Sphere cultures were established according to the protocol by Drost and colleagues (Drost et al., 2016) using OM. The details of the media conditions tested are given in Figure 3.15A. Adherent culture was prioritised, as it was found that spheres were not compatible with fluorescent microscopy and could not be dissociated completely to perform flow cytometry analysis. Of the 21 samples received, 19 (90%) grew from the initial plating. However only 57% of the samples reached passage 2 in culture, with only 5 (34%) of the samples reaching passage 6 or more (Figure 3.15B). The morphology of an adherent culture in SCM, and a sphere culture, is shown in Figure 3.15 C and D. It was noted that in long term 3D culture, spheres adhered to the plates used (despite these being cell repellent) (Figure 3.15E).

Therefore, in Study 2, SCM and OM were compared, for adherent growth of the primary PCa samples. In a comparison of SCM and OM, the lifespan of the sample was 2 passages (Figure 3.16A). The OM was then further modified, based on the relative importance of individual supplements which were determined by Karthaus and colleagues, for the culture of sphere/ organoids (Karthaus et al., 2014). This is denoted as modified organoid media (mOM); further detailed in Chapter 2, Materials and Methods. This greatly improved the lifespan of the subsequent samples (Figure 3.16B); 100% of the subsequent 6 samples reached passage 2 and 5/6 (83%) of the samples reached passage 6, enabling further experiments to be carried out. The

morphology of the primary PCa cells grown in mOM, in adherent culture plates, is shown in Figure 3.16C.

3.5.3 Investigation of the lineage phenotype of primary prostate cancer cells

The phenotype of the primary PCa cells was compared to that of the DU145 cells in two separate studies. Study 1 samples were investigated by fluorescence microscopy due to insufficient cell numbers for flow cytometry (Figure 3.17). The primary PCa cells were found to have a similar phenotype to that observed in the DU145 cells; the phenotype was basal/ intermediate; $CD44^+$ $CK8^+$ $CK5^-$. The primary samples were also negative for fibroblast marker α-actin (Figure 3.17A). The primary PCa samples were also negative for AMACR and AR (data not shown). For Study 2, samples were investigated by flow cytometry. Fluorescence microscopy could not be used in this study because the cells grown in mOM did not grow well in the plates used for microscopy staining (8 well plastic chamber slides or 96 well glass bottomed black walled plates. Staining failed in the few samples successfully grown in these plates which appeared to be due to lack of permeabilisation as fluorescence was observed in non-specific patterns around the outside of the cell membrane. It is suggested that differences in the media composition altered adherence protein expression. This may also have contributed to the differences in morphology observed between the cells grown in SCM and mOM. The samples investigated by flow cytometry showed some differences to the phenotype of the DU145 cells (approximately 75% basal, 25% intermediate and negligible luminal cells); the primary PCa cells were found to consist almost entirely of basal $CD49f^+$ cells (97%) (Figure 3.17B).

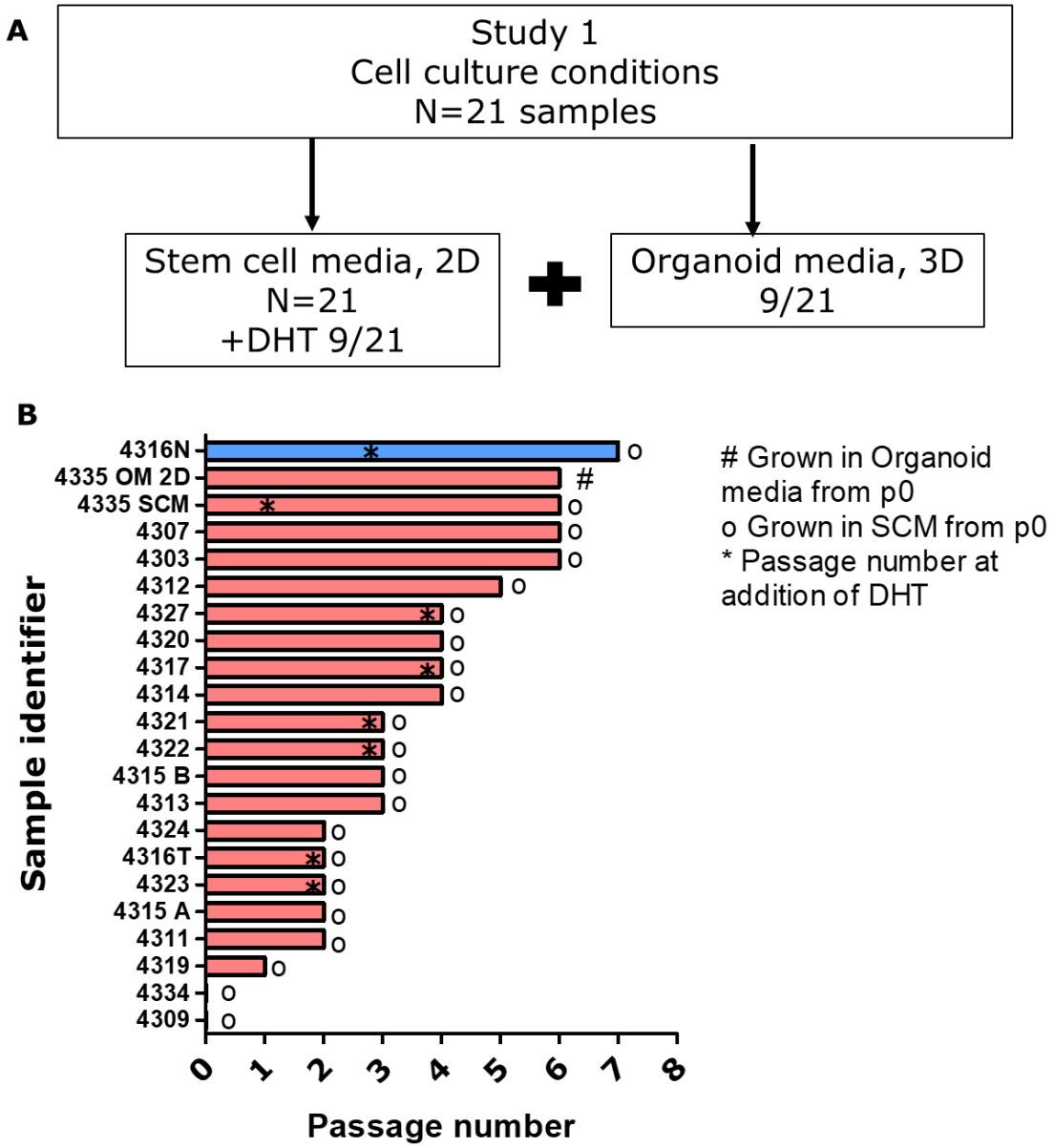

Figure 3.15 Optimisation of growth conditions for primary prostate cancer cells. (A) Schematic of the media and adherent/non-adherent conditions tested in Study 1 and the number of samples in which each condition was tested. Adherent cultures (SCM) were established for all samples. DHT (10 nM) was added to prolong sample lifespan (but was unsuccessful). Spheres were grown when sufficient cell numbers were obtained from biopsy processing. (B) Lifespan of samples from Study 1, with media conditions. Tumour samples are indicated by red bars, one adjacent normal sample which was provided with the corresponding numbered tumour sample is indicated by a blue bar. The y-axis indicates the sample number; samples were received in numerical order but are arranged by highest passage number achieved in culture (the x-axis). The symbol(s) associated with each bar indicate the media conditions each sample was grown in o for SCM from p0, * indicating the passage at which DHT was added and # for organoid media from p0.

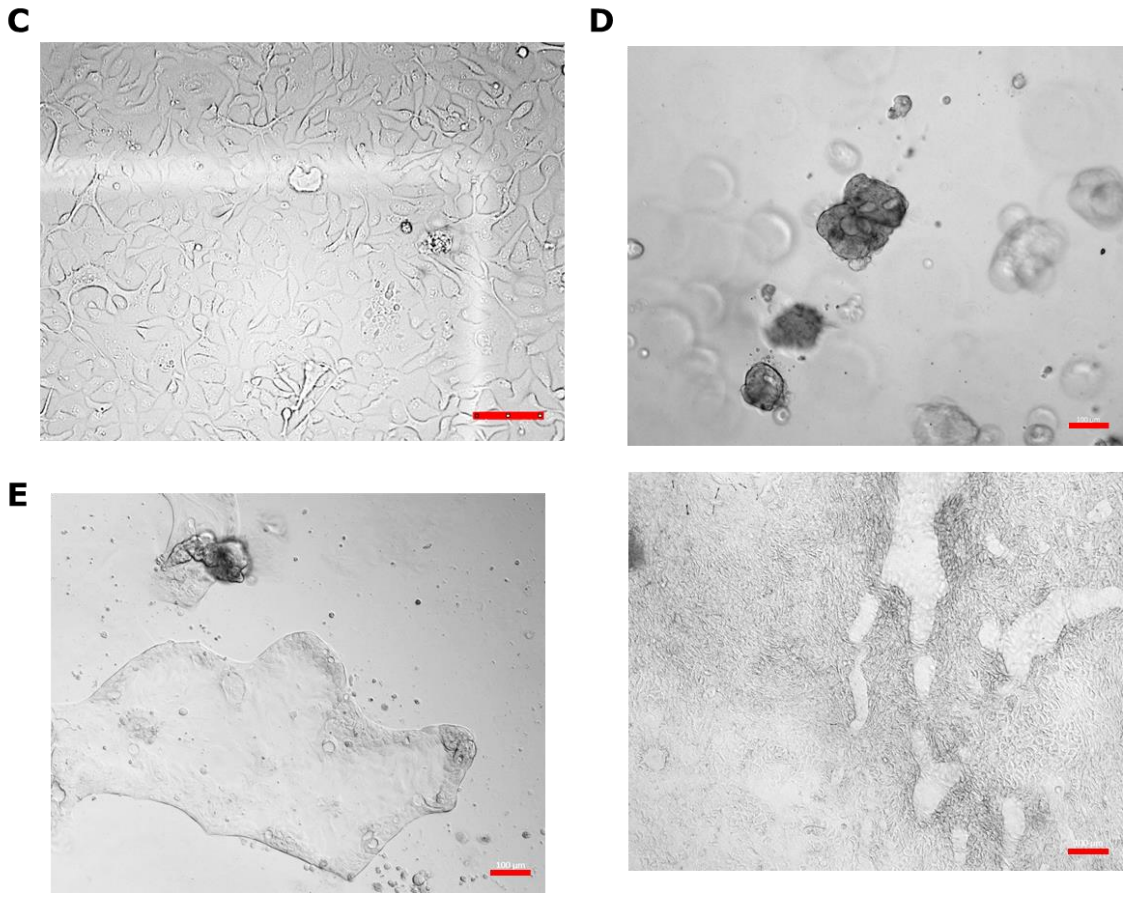

Figure 3.15 Continued optimisation of growth conditions for primary prostate cancer cells. Adherent cells were grown in a 6-well plate and re-seeded at approximately 2.5 x 10^5 cells per well at each passage. Cell numbers and plate size was adjusted for lower cell numbers. The spheres were grown from cells seeded at 40000 cells per well in a 24 well non-adherent plate. Morphology of (C) Adherent cells in SCM (Scale represents 20 μm). (D) Spheres in OM (Scale represents 100 μm). (E) Cells grown as spheres in OM which became adherent over time (Scale represents 100μm).

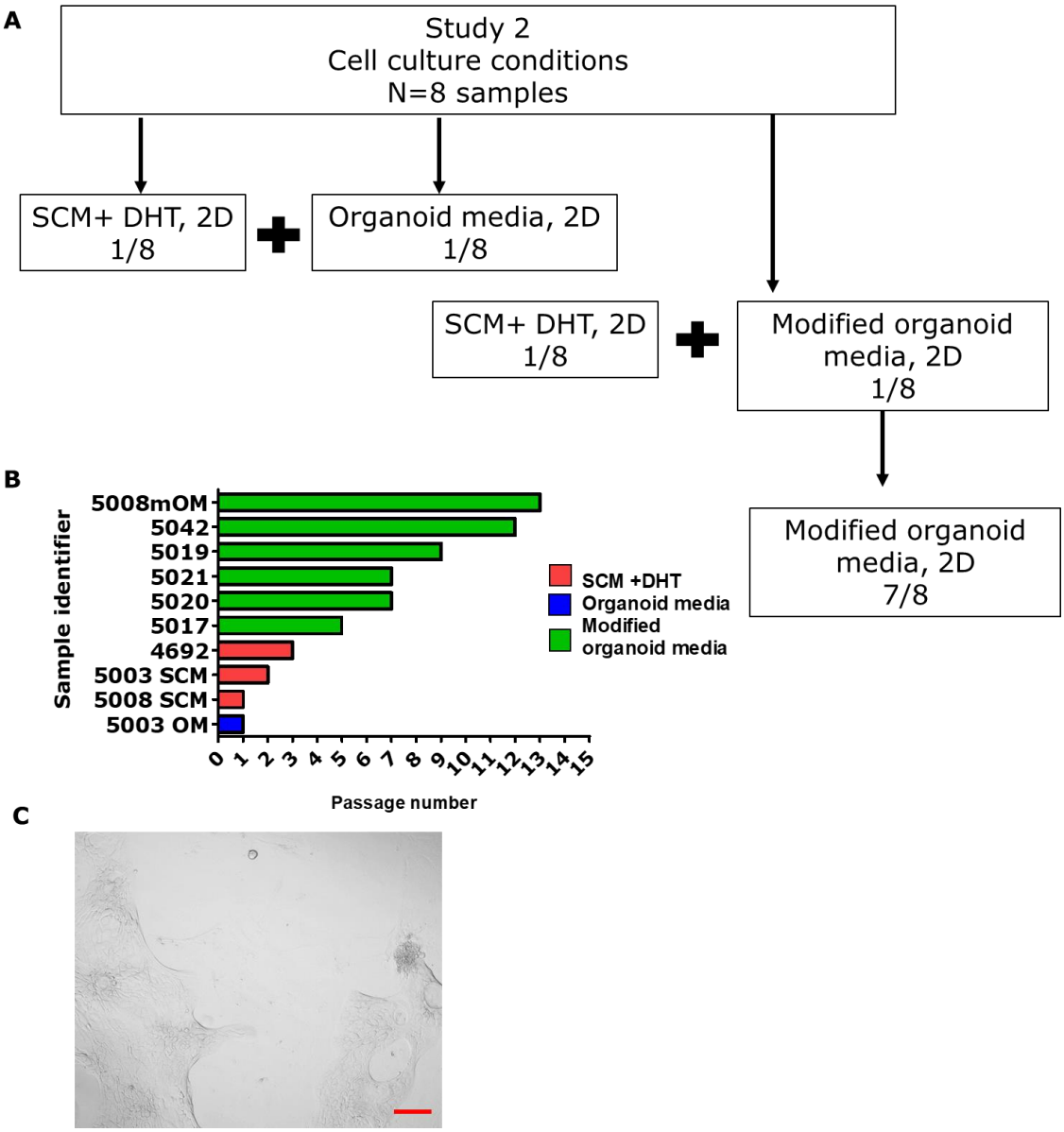

Figure 3.16 Investigation of novel media conditions for the growth of primary prostate cancer cells. (A) Schematic of the media and adherent/non-adherent conditions tested in Study 2 and the number of samples in which each condition was tested. Based on the previous study, SCM +DHT and OM were compared for 2D culture of primary prostate cancer cells. For the subsequent sample, the OM supplementation was altered; making modified Organoid media (mOM). The comparison of SCM to mOM demonstrated improved growth and mOM was used to culture all subsequent samples. (B) The lifespan of all samples received in Study 2, with media conditions: Red: SCM+DHT from p0 '*', Blue: OM from p0 '#', Green: mOM from p0 '##'. (C) Morphology of primary prostate cancer cells grown in mOM on an adherent plate. Scale represents 100 µm.

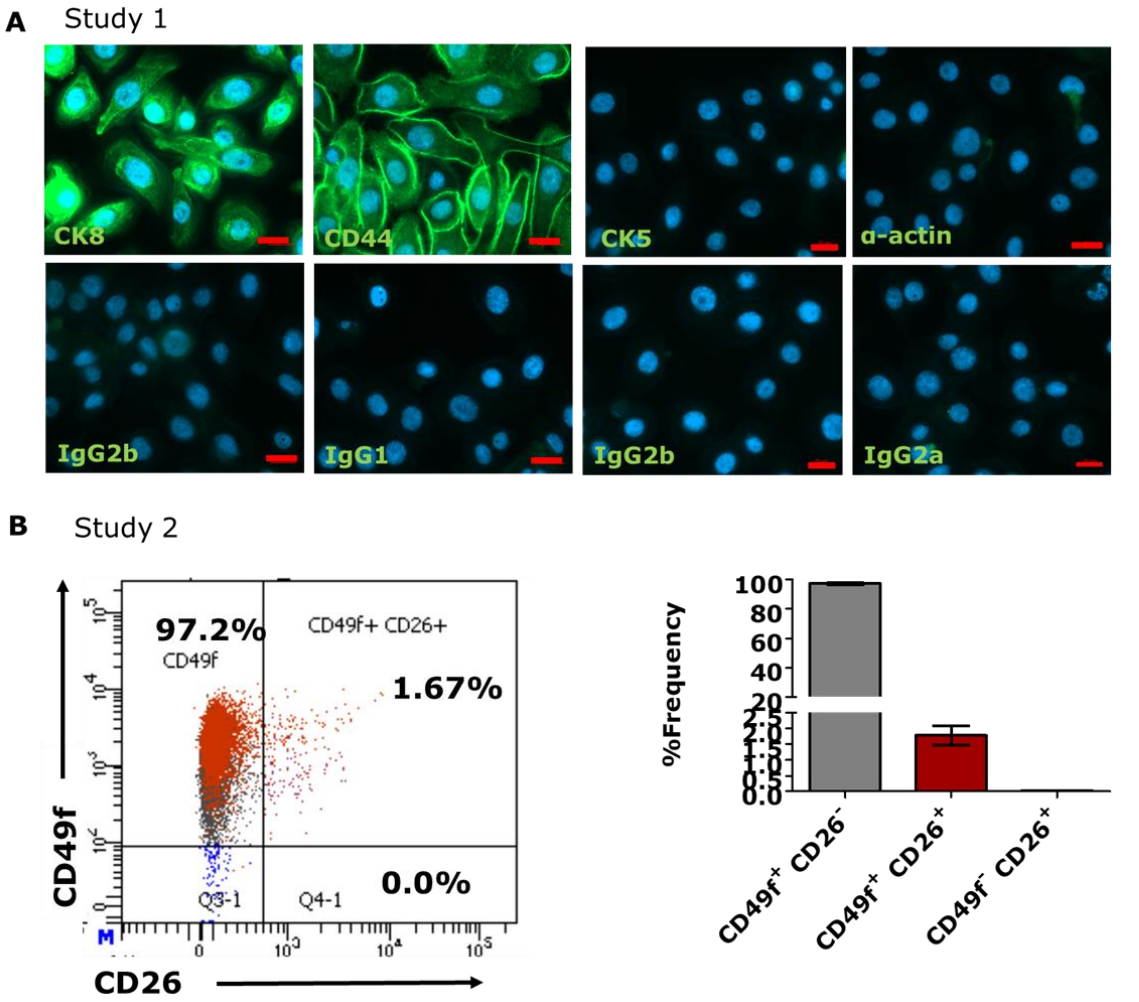

Figure 3.17 Phenotype of primary prostate cancer cells in *in vitro* culture. (A) Cells grown from biopsy samples in Study 1 cells were plated at 10^4 in 8 well chamber slides and grown to 90% confluency, fixed and stained with the indicated antibodies or isotype controls as described in Materials and Methods. This staining was performed for each sample from which sufficient cell numbers could be obtained. The cells were imaged using a Zeiss axio observer z1 microscope. The phenotype was investigated by fluorescence microscopy using luminal/intermediate and basal markers CK8 and CD44 respectively. The cells were also stained with anti-α-smooth muscle actin antibody to distinguish contaminating fibroblasts. Scale bar represents 20 μm. (B) (Left) The cells grown from biopsies received in Study 2 were characterised by flow cytometry (data is representative of n=2) as fluorescence microscopy did not work, owing to differences in the morphology of the cells. The markers used were basal and luminal: CD49f (α6 Integrin) and CD26 respectively. Right; graph of the frequency of $CD49f^+$ and $CD26^+$ single positive and $CD49f^+$ $CD26^+$ double positive populations.

3.6 Identification of CSC in primary prostate cancer cells

3.6.1 Investigation of a CD44$^+$ $\alpha_2\beta_1$Integrin^{high} CD133$^+$ population

As shown earlier, the DU145 cell line lacked a conclusive CD44$^+$ $\alpha_2\beta_1$Integrin^{high} (CD49b^{high}) CD133$^+$ population, due to negative CD133 staining. However, it is possible that these markers are less suitable for use in PCa cell lines as these markers were first used to characterise CSC in primary prostate samples. Therefore, the CD44$^+$ $\alpha_2\beta_1$Integrin^{high} CD133$^+$ phenotype was investigated in the primary PCa *in vitro* cultures, to determine whether the CD44$^+$ $\alpha_2\beta_1$Integrin^{high} CD133$^+$ subpopulation is more distinct in primary PCa cells versus the DU145 cell line.

Two primary samples were sorted by FACS (Figure 3.18A). The CD44$^+$ CD49b^{high} CD133$^+$ population frequency was 0.1%. The MFI of the CD133 staining was higher in the CD44$^+$ CD49b^{high} CD133$^+$ than in the CD44$^-$ CD49b^{low} CD133$^-$ population or the isotype control (Figure 3.18C). However, despite the selection of CD133$^+$ cells in the sort, post-sorting analysis showed that the CD44$^+$ CD49b^{high} CD133$^+$ sorted population consisted of two distinct clustered CD133$^+$ populations (Figure 3.18B). This suggests that the CD133 staining did not select for a homogenous positive population. This could have affected the comparison of the CD44$^+$ CD49b^{high} CD133$^+$ and CD44$^-$ CD49b^{low} CD133$^-$ populations in downstream assays; however due to the low cell numbers obtained in the sort it was not possible to further characterise these populations. Three further primary PCa samples were analysed by flow cytometry to identify the CD44$^+$ $\alpha_2\beta_1$Integrin^{high} CD133$^+$ population, with a view to further expanding the cells for sorting. The populations identified by the staining are shown in Figure 3.18D. Each primary PCa sample showed different frequencies of the CD44$^+$ $\alpha_2\beta_1$Integrin^{high} CD133$^+$ population (Figure 3.18E). However, the CD133$^+$ population staining was not higher than the isotype, in comparison to the CD44 and CD49b staining (Figure 3.18F). Similarly to the findings in the DU145 cells, the CD133 staining did not demonstrate a high positive population, which could be used to isolate CD44$^+$ $\alpha_2\beta_1$Integrin^{high} CD133$^+$ cells. As discussed previously, CD133$^+$ cells in other publications have higher fluorescence, enabling conclusive identification of the population. The data from the sorted samples suggests that the sorted

$CD44^+$ $CD49b^{high}$ $CD133^+$ population was not a pure population, or that the CD133 antibody additionally bound non-specific targets. This is further supported by the data from the samples investigated by FACS, in which the $CD133^+$ staining was not significantly higher than the isotype control. These data agree with previous results in the DU145 cell line. In the absence of conclusive data for the expression of CSC surface markers which would enable potential CSC population sorting, I investigated ALDH as an alternative CSC marker in the primary PCa cells.

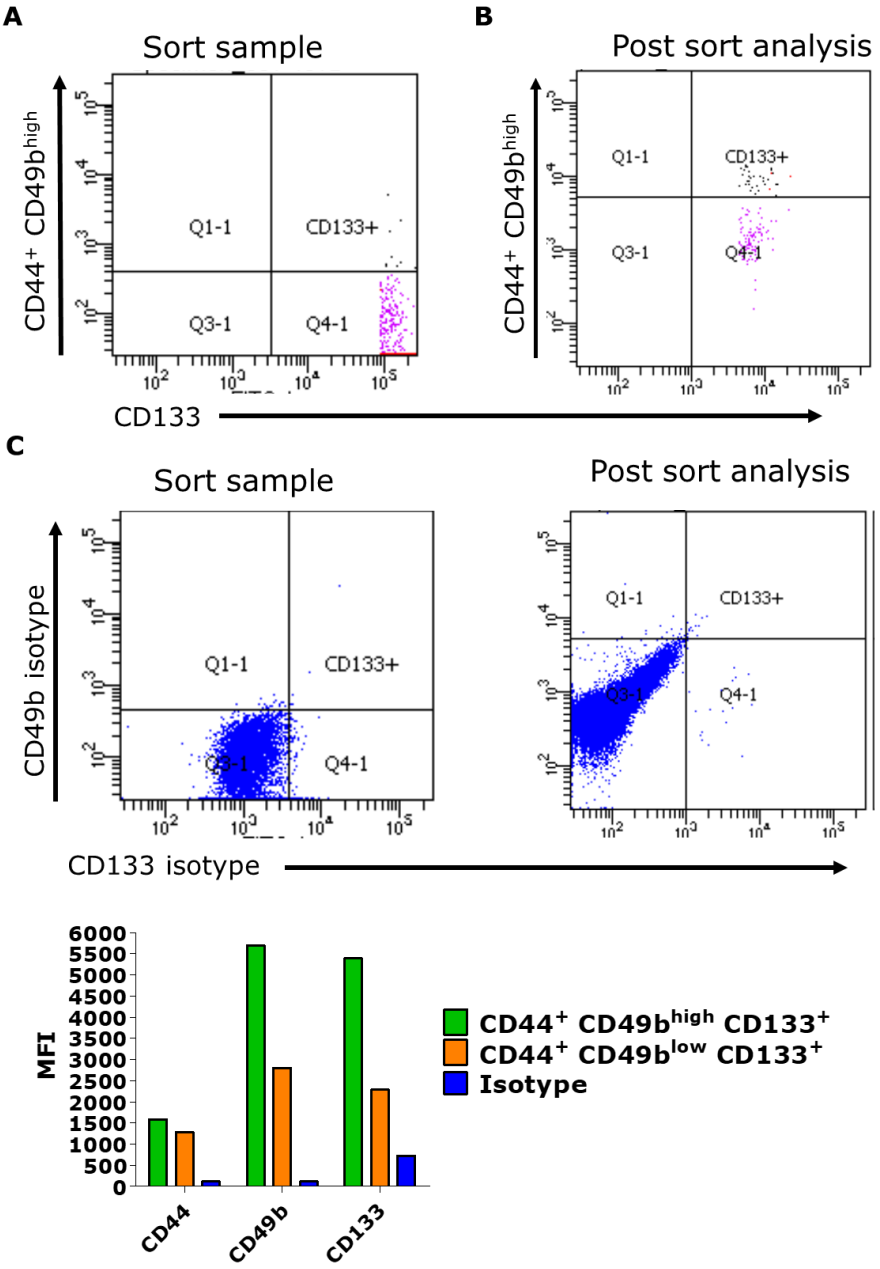

Figure 3.18 Investigation of a CD44$^+$ $\alpha_2\beta_1$Integrin^{high} CD133$^+$ population in primary prostate cancer cells. (A) The CD44$^+$ CD49b^{high} CD133$^+$ and CD44$^-$ CD49b^{low} CD133$^-$ populations from two (different) primary PCa samples were sorted using a FACS Aria 3.2x10^6 cells were sorted from the first sample and 3.65x10^6 cells were sorted from the second sample. Antibody staining was scaled up x5 for CD133 and CD49b and x2.5 for CD44. Representative dot plots shown (B) A sample of the CD44$^+$ CD49b^{high} CD133$^+$ and CD44$^-$ CD49b^{low} CD133$^-$ populations were immediately analysed using a FACS Verse, and unsorted cells were stained with the relevant isotype control antibodies. (C) The MFI of the antibody staining for the sorted populations and unsorted isotype is shown (representative of n=2 biological replicates).

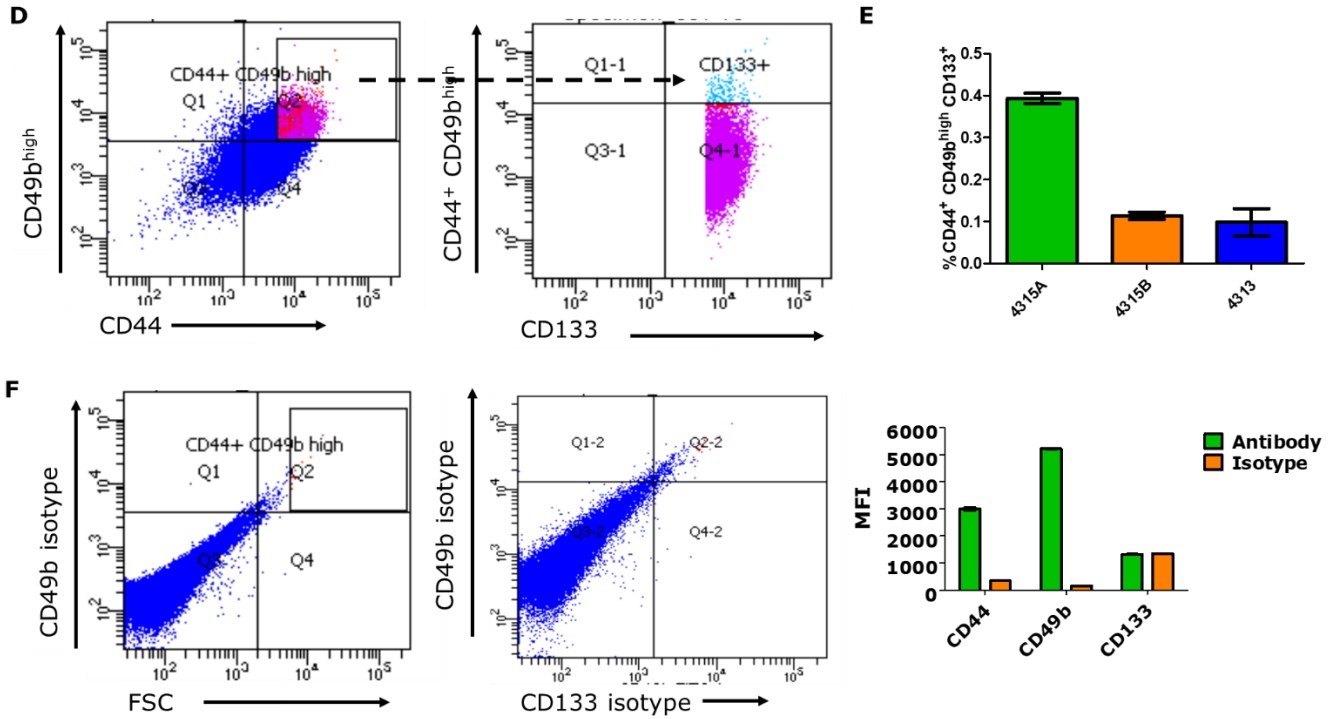

Figure 3.18 Investigation of a CD44$^+$ $\alpha_2\beta_1$Integrin^{high} CD133$^+$ population in primary prostate cancer cells. (D) continued overleaf) Flow cytometry was used to identify the CD44$^+$ CD49b^{high} CD133$^+$ population in three further primary PCa samples ($3x10^5$ cells were stained with each antibody or isotype control) (different biological replicates). The isotype controls were used to set the gating. The samples used were received as tissue slices, rather than needle core biopsies, which provided sufficient cell numbers for the analysis and further FACS experiments were anticipated based on confirming the CD44$^+$ CD49b^{high} CD133$^+$ population at an early passage (p2) (E) The frequency of the CD44$^+$ CD49b^{high} CD133$^+$ population in n=3 primary prostate cancer samples. (F) MFI of antibody and isotype staining for the CSC markers (representative of staining shown in (D).

3.6.2 Identification and characterisation of ALDH high cells in primary PCa *in vitro* culture

The ALDH assay was carried out on the primary PCa cells according to the approach optimised for the DU145 cell line (Figure 3.19A). The average frequency of ALDH high cells from all samples sorted was 7.2% (Figure 3.19B), a similar proportion to that of the DU145 cells (Figure 3.5E). The optimised cell culture conditions for the primary PCa cells enabled most of the samples in the study to be expanded sufficiently to perform FACS. The viability of the sorted cells was highly variable (Figure 3.19C), limiting the characterisation of the sorted populations. ALDH high cells produced more colonies than ALDH low cells in a colony formation assay (n=1) (Figure 3.19D). Sphere formation was investigated in two sorted samples, in which the ALDH high cells grew larger spheres than the ALDH low cells (Figure 3.19E), although the absorbance of the spheres was below the limit of detection in the Orangu assay (data not shown). In further experiments, colonies and spheres did not form in either of the ALDH high or ALDH low populations, despite confirming the sphere formation capacity of the cells prior to sorting (data not shown). Owing to poor survival of the primary PCa cell lines *in vitro* after sorting, further characterisations of ALDH high and ALDH low primary PCa cells were performed by using assays which did not require sorting or post-sort *in vitro* culture of the cells.

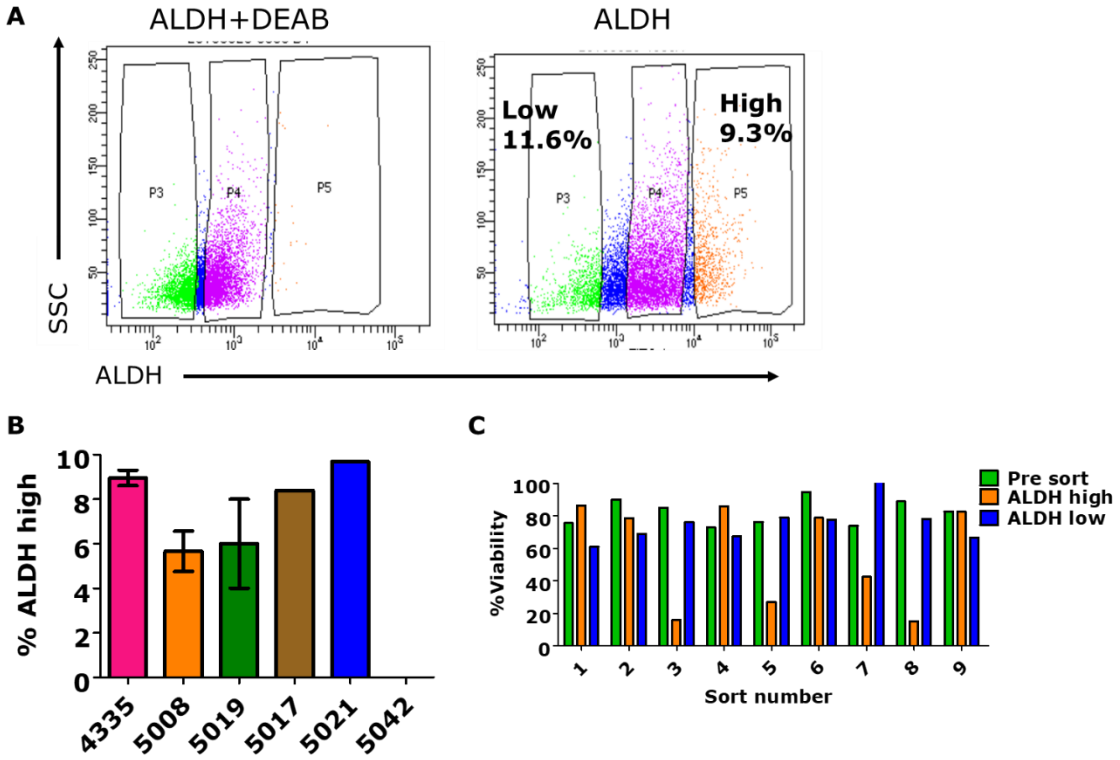

Figure 3.19 Identification and characterisation of ALDH high primary prostate cancer cells. (A) The ALDEFLUOR assay was used to sort the primary prostate cancer cell lines. The ALDH high and ALDH low populations were sorted from the gating strategy optimised using the DU145 cells. Sorting was typically performed from 10^6 cells which were incubated with 5 µl of ALDH substrate, as the samples did not grow sufficiently to perform the reaction with the same cell numbers as used for the DU145 cells. (B) The frequency of ALDH high cells from primary prostate cancer cell lines; error bars refer to samples which were sorted more than once. (C) Viability of primary prostate cancer cells prior to sorting and when sorted into ALDH high and low populations.

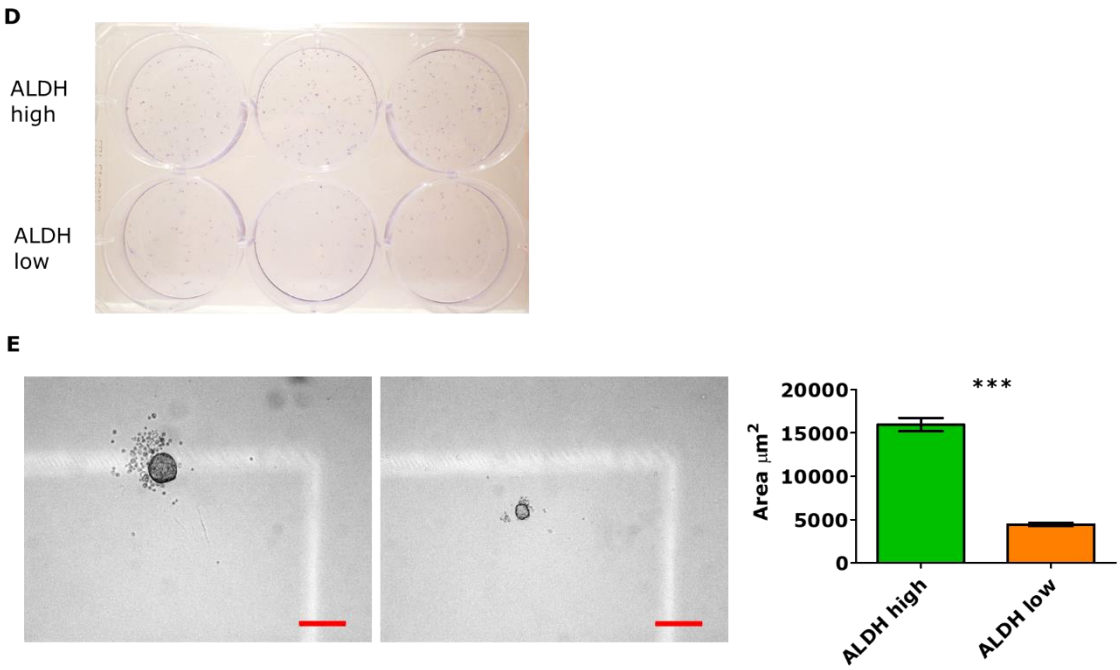

Figure 3.19 Continued identification and characterisation of ALDH high primary prostate cancer cells. (D) Colony forming assay (n=1): the sorted cells were plated at 50 cells/ cm^2 i.e. 450 cells per well in a 6-well plate and fixed and stained when colonies contained >50 cells (visualised by light microscopy). The plate was imaged using a Canon 350D DSLR. (E) ALDH high and ALDH low cells were seeded at 1000 or 100 cells per well and sphere formation from these initial cell numbers was measured in mOM media in cell repellent plates. Representative of n=2 biological replicates. The cells were imaged using a Zeiss axoivert 100 microscope and (F) sphere area size was measured using Metamorph software. Scale bar represents 200 µm. Mean ± SE was calculated from n=5 spheres and significance testing was done by a paired T test; *** $p<0.001$.

3.6.3 Cellular division of primary prostate cancer cells

I investigated cell division and proliferation of the ALDH high and ALDH low unsorted primary PCa cells using the Cell Trace assay. In the same was as for the DU145 cells, High, medium and low dye retention (representing low, medium and high proliferation respectively) gating for each dye was determined by measuring fluorescence of unstained primary PCa cells (autofluorescence in the 450 nm channel) (low dye/ high proliferation) or cell trace fluorescence of primary PCa cells stained immediately before analysis (high), (Figure 3.20 A and B). After 3 days in adherent culture, the frequency of Cell Trace high cells was significantly greater in the ALDH high compared to the ALDH low cells (Figure 3.20C). This is similar to the results observed in the DU145 cells. The Cell Trace high population decreased over time but at 7 days remained significantly higher in the ALDH high (23.4%) compared to ALDH low cells (3.2%) (Figure 3.20D). This may suggest that primary prostate ALDH high cells divide more slowly than DU145 ALDH high cells, however it may also be attributable to the slower turnover of the total primary PCa cell population. The growth of the primary PCa cells was highly variable within the same sample at different passage numbers and between different samples; as a result, it was not possible to estimate the doubling time of these cultures. In another primary PCa cell line there was greater proliferation/ Cell trace dye dilution in both ALDH high and ALDH low populations. However, at Day 7 there was a significantly higher proportion of Cell Trace medium ALDH high cells (but not Cell Trace high) compared to Cell trace medium ALDH low cells (data not shown). This is similar to the dye dilution associated with proliferation observed in the DU145 cells. Therefore, this assay is effective in identifying differences in cell division in the ALDH high and ALDH low primary PCa cells and provides a useful measurement for CSC which does not require sorting the cells and reducing viability.

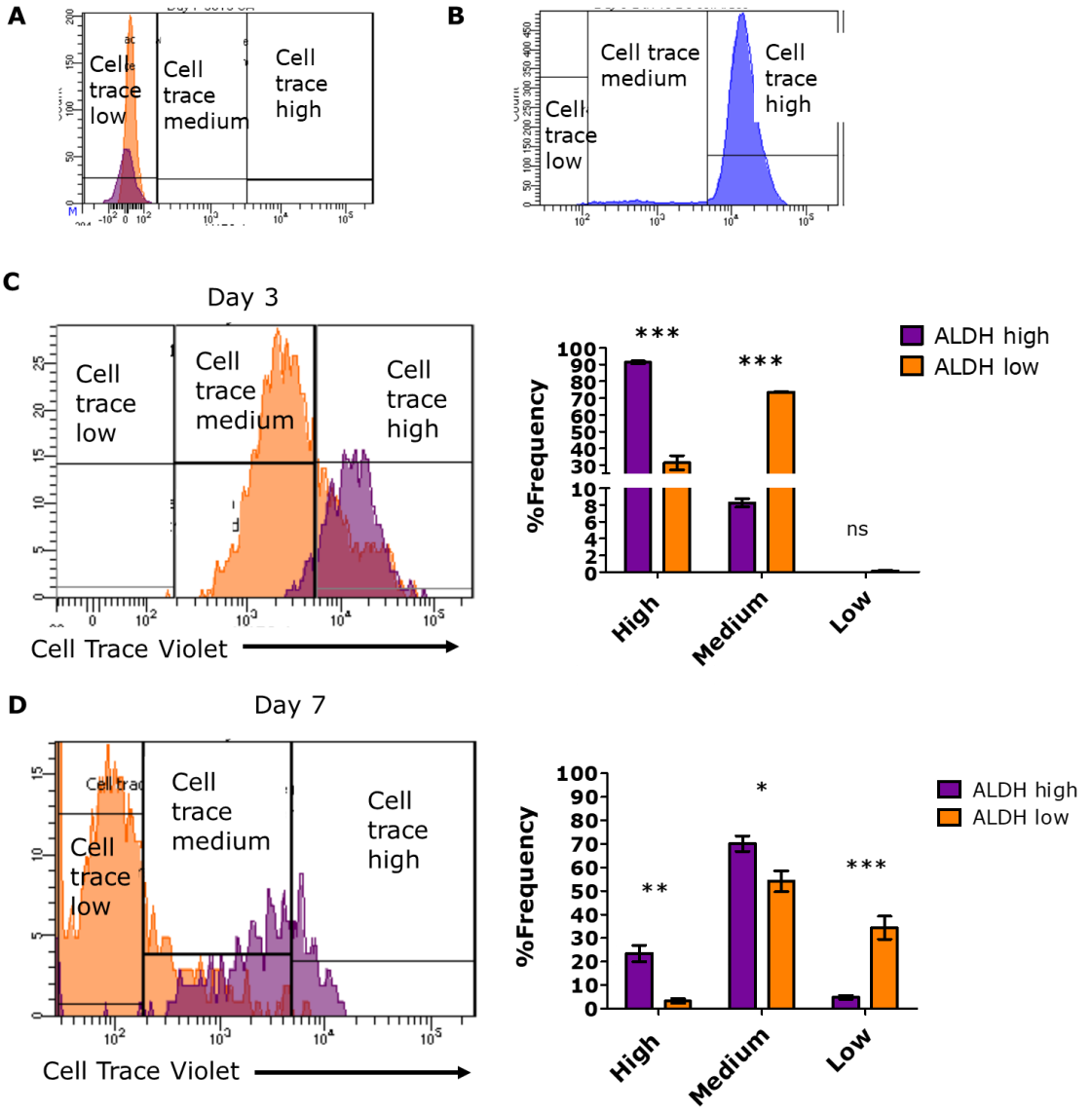

Figure 3.20 Cell Trace assay of cell division in ALDH high and ALDH low primary prostate cancer cells. Primary prostate cancer cells (unsorted) were stained with Cell Trace dye at 2.5 μM and plated in 2D culture. The cells to be measured after 3 days were plated at 5 x 10^5 cells per well in a 6 well plate and the cells to be measured at 7 days were plated at 2 x 10^5 cells per well in a 6 well plate. (A) Unstained cells autofluorescence, used to gate 'cell trace low' (B) Cells stained immediately prior to analysis, used to gate 'cell trace high.' (C) After 3 days the ALDEFLUOR assay was performed and the proliferation and division of the ALDH high and low primary prostate cancer cells were measured. (B) Proliferation and division was measured in the same way after 7 Days. The different frequencies of Cell Trace staining in the ALDH populations was assessed by 2-way ANOVA; * $p<0.05$ ** $p<0.01$, *** $p<0.001$ Error bars represent triplicates, this experiment was repeated in two primary PCa cell lines (biological replicates).

3.6.4 Gene expression of ALDH high and ALDH low primary prostate cancer cells

Gene expression in ALDH high and ALDH low primary PCa cells was investigated using the Nanostring platform, using the same gene panel as was used to investigate the DU145 cells, the Stem Cell Panel. While the sensitivity of qPCR and Nanostring are considered comparable (Prokopec et al., 2013), the Nanostring array is suggested to be better suited to analysis of the primary PCa cells; this assay does not require pre-amplification of low amounts of genetic material prior to analysis, and it suggested to be tolerant of poorer quality material as the technology was developed for analysis of FFPE samples (Veldman-Jones et al., 2015). The mRNA counts obtained from the Nanostring analysis were spread across a large range; in the ALDH high samples the coefficient of variation (%CV) for mRNA counts of an individual gene in the three biological repeats was 7.53%- 160.58%, similarly in the ALDH high cells the %CV was 1.48%-139.46%. There is not a recommended %CV given by Nanostring within which samples can be combined for analysis. Due to this variation, the fold changes in each primary PCa sample pair (ALDH high and ALDH low) was analysed individually (without statistical comparisons between replicates). The highest ranked fold change differences in either direction are shown in Figure 3.21 for the three biological replicates analysed. Full details of fold changes are given in Appendix 2. There were 45 and 111 genes for which the ALDH high cells showed a fold change ≥2 compared to the ALDH low cells respectively; the top 10 highest fold changes are shown in (Figure 3.21 (A; #4335) and (B; #5017)). Full details of all the fold changes >2 for #4335 and #5017 are detailed in Appendix 2. There were one and two genes for which the expression was 0.5-fold lower in the ALDH high compared to the ALDH low cells in Figure 3.21A and Figure 3.21B respectively. Contrastingly, there were 35 genes for which the expression was 0.5-fold lower in the ALDH high compared to the ALDH low cells in the third primary PCa cell line (#5008). The 10 lowest expressed genes in ALDH high compared to ALDH low cells are shown in Figure 5.21C; full details are given in Appendix 2. Only one gene was >2 fold higher expressed in ALDH high compared to ALDH low cells in this sample; thus genes >1.5 were also considered, these are show on the same graph in Figure 3.21C. There were two genes commonly upregulated (>1.5 fold or >2 fold) across all three

samples (Figure 3.21) and also in common with the DU145 cells (Figure 3.11C); CDK1 and CCNA2/Cyclin A2.

The functional relationships between the up and down regulated genes in the Nanostring analysis were investigated by functional annotation clustering using the DAVID Bioinformatics Resource (Huang et al., 2009b). Genes which were ≥2 fold increased in the ALDH high populations of #4335 and #5017 were significantly enriched for the NOTCH pathway (Figure 3.21A, C). Of the genes upregulated in the ALDH high cells of #4335 and #5017, 30.8% were associated with the NOTCH pathway; the fold enrichment was 1.39, $p = 0.0024$. Genes upregulated >2 fold were also significantly enriched for cell cycle signalling; 14.1% of the genes were involved in this pathway (Figure 3.21B, D). The fold enrichment was 1.46, $p = 0.021$. Conversely, it was the 0.5-fold decreased genes in primary PCa cells #5008 which were significantly enriched for NOTCH pathway function. The fold enrichment of the downregulated genes was 1.64, $p = 0.042$, 37.14% of the genes were associated with NOTCH signalling. This indicates that the ALDH high cells from the primary cell lines #4335 and #5017 had a different phenotype, involving upregulation of NOTCH signalling, compared to the #5008 primary PCa cell line (Figure 3.22 A, B). These data indicate that ALDH high and ALDH low primary PCa cells have different gene signatures, which may contribute to functional differences, including those observed in experimental replicates in this study. While further investigation is required, these data suggest that ALDH can be used as a suitable marker for stem-like population in primary PCa cells.

Figure 3.21 Differential gene expression in ALDH high compared to ALDH low primary prostate cancer analysed by Nanostring. The samples in the Nanostring analysis met the criteria for quality control in terms of RNA integrity number (RIN) and fragment size (number of base pairs) (data not shown). This was determined using a Bioanalyzer (Agilent). (A, B, C) Fold change in gene expression of ALDH high compared to ALDH low cells in three different primary prostate cancer cell lines. The 10 genes with the greatest fold change differences (up-regulated or down-regulated; where applicable) are shown and the full details of fold changes are given in Appendix 2. To assess relevant gene expression differences, a fold change threshold of >2 or <0.5 was chosen for samples (A) and (B); this upper threshold was >1.5 fold greater expression in ALDH high compared to ALDH low cells in (C), owing to the low number of genes with a fold change >2. The lower fold change threshold was 0.5. The fold change thresholds applied are denoted by dashed red lines.

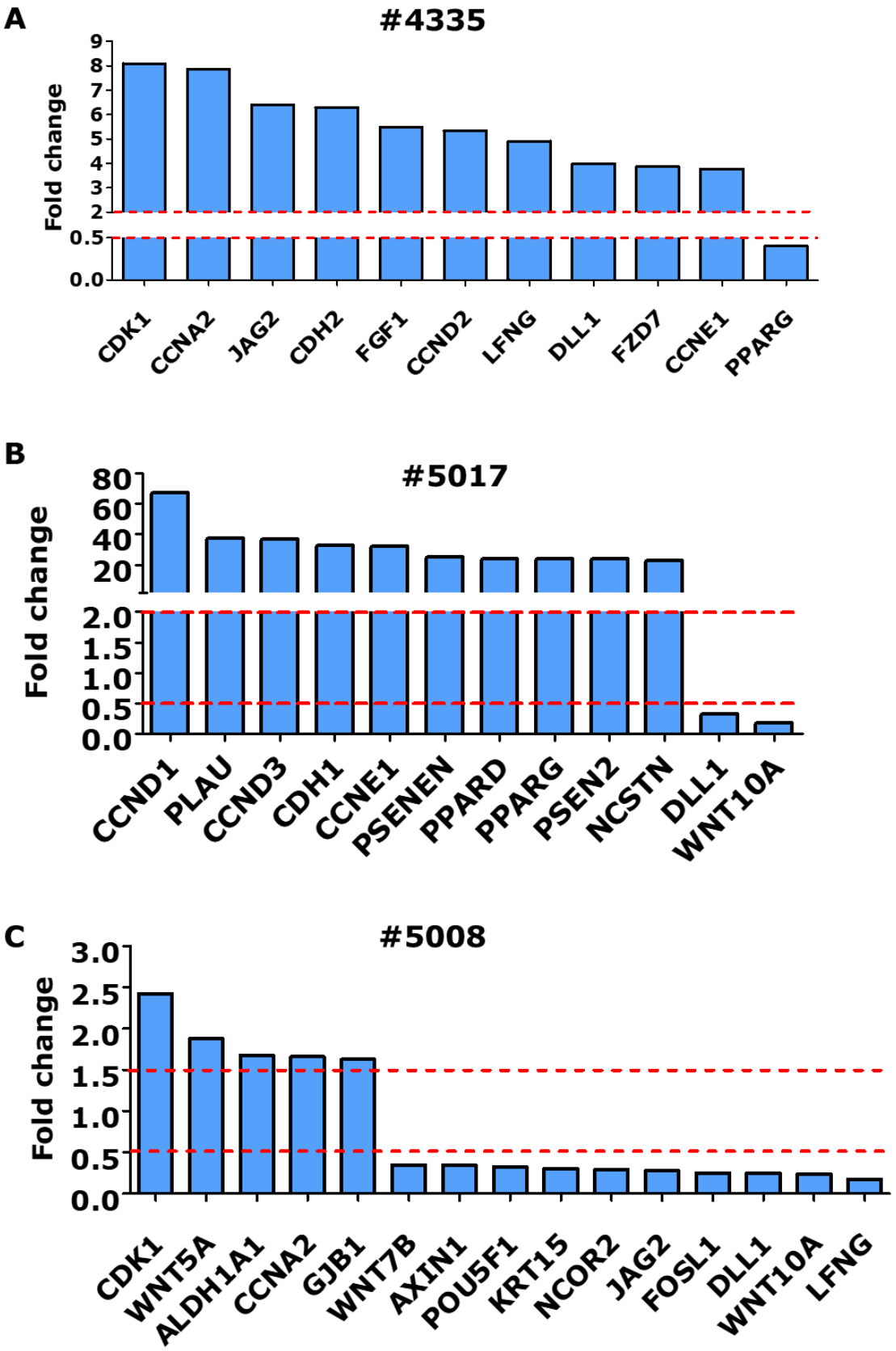
A
#4335
Fold change
9
8
7
6
5
4
3
2
0.5
0.0
CDK1
CCNA2
JAG2
CDH2
FGF1
CCND2
LFNG
DLL1
FZD7
CCNE1
PPARG
B
#5017
Fold change
80
60
40
20
2.0
1.5
1.0
0.5
0.0
CCND1
PLAU
CCND3
CDH1
CCNE1
PSENEN
PPARD
PPARG
PSEN2
NCSTN
DLL1
WNT10A
C
#5008
Fold change
3.0
2.5
2.0
1.5
1.0
0.5
0.0
CDK1
WNT5A
ALDH1A1
CCNA2
GJB1
WNT7B
AXIN1
POU5F1
KRT15
NCOR2
JAG2
FOSL1
DLL1
WNT10A
LFNG

A

EP300	CCNE1
RB1	CDK1
SMAD4	GSK3B
CCNA2	HDAC1
CCND1	HDAC2
CCND2	MYC
CCND3	

B

ADAM17	DVL1	NOTCH1	DTX2	NOTCH3
CTBP1	DVL2	NOTCH2	HDAC1	NCOR2
CTBP2	DVL3	NUMB	HDAC1	PSEN1
EP300	HES1	RFNG	HDAC2	PSEN2
LFNG	MAML1	SNW1	JAG1	PSENEN
NUMBL	MAML2	APH1A	JAG2	RBPJ
DTX3L	MAML3	CIR1	KAT2A	
DTX4	NCSTN	DLL1	KAT2B	

Figure 3.22 Functional annotation clustering of >2 fold upregulated genes in ALDH high primary prostate cancer cells. Functional annotation clustering was performed using the DAVID Bioinformatics Resource Functional Annotation Tool. The tool was used to analyse a list of pre-selected genes, the genes >2 fold upregulated in the #4335 and #5017 primary PCa cell lines. Clustering was performed by mining the text (the fold change values were not included) for upregulated genes common to each sample. The fold enrichment and pathway annotation were determined by comparing the upregulated genes to the full gene list from the Nanostring assay (as a reference list). (A) The upregulated genes which were enriched for NOTCH pathway signalling. (B) The upregulated genes which were enriched for Cell Cycle Pathway signalling. (C) The NOTCH pathway (D) The Cell Cycle pathway. The red stars indicate genes identified in the enrichment analysis which are directly involved in the pathway or associated with genes in the pathway. DAVID uses a modified Fisher's Exact test (EASE statistic) to determine significantly enriched genes. Image credit Kanehisa Laboratories accessed by link provided from the DAVID results.

C

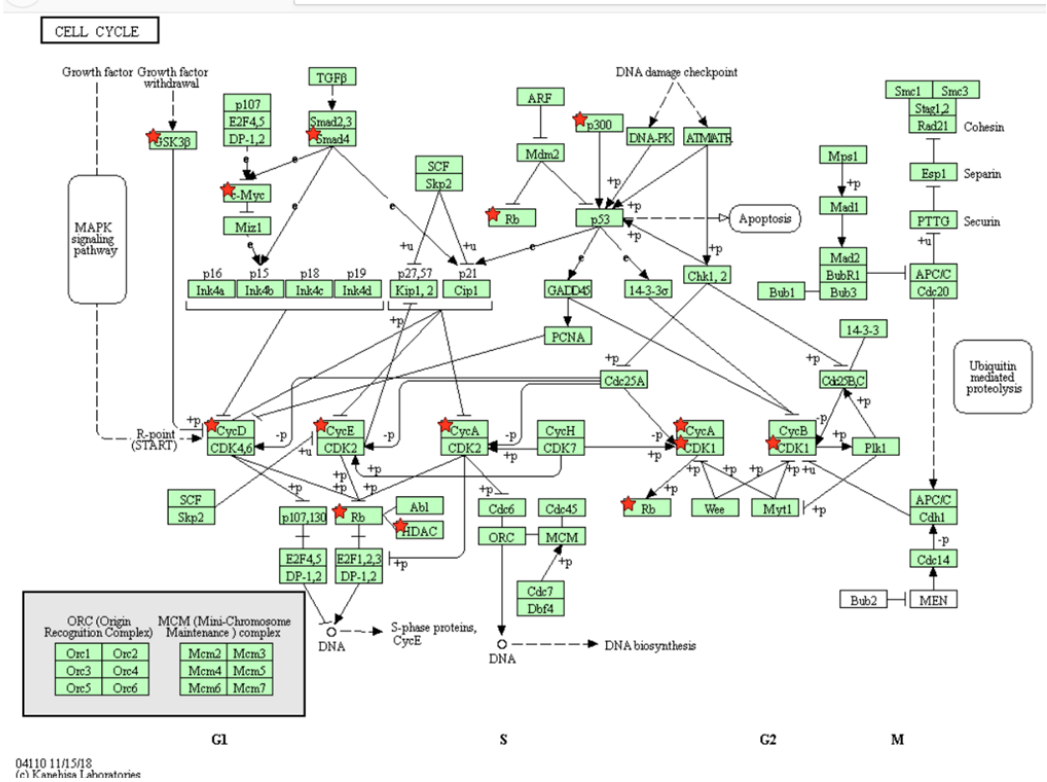

D

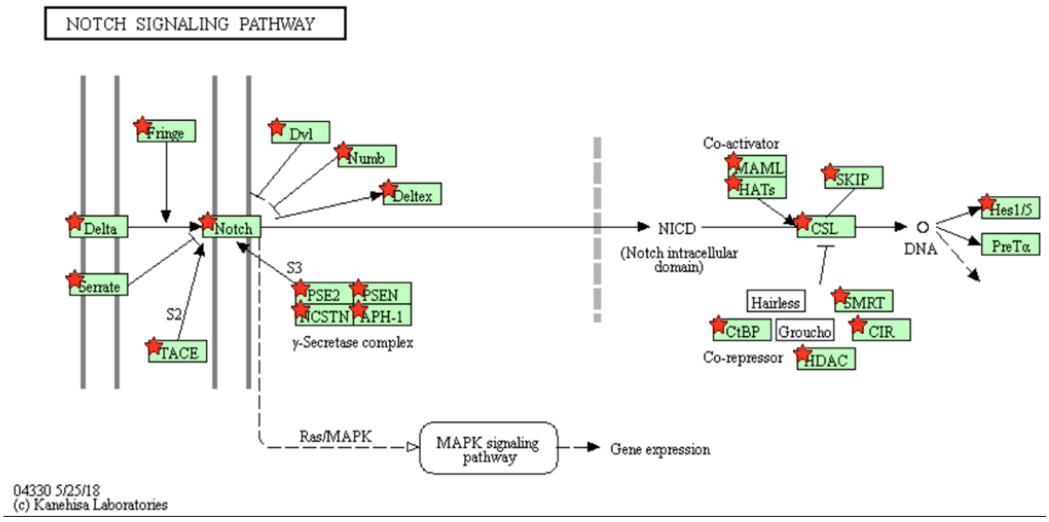

Figure 3.22 Continued: functional annotation clustering of >2 fold upregulated genes in ALDH high primary prostate cancer cells. (C) The NOTCH pathway (D) The Cell Cycle pathway. The red stars indicate genes identified in the enrichment analysis which are directly involved in the pathway or associated with genes in the pathway. DAVID uses a modified Fisher's Exact test (EASE statistic) to determine significantly enriched genes. Image credit Kanehisa Laboratories accessed by link provided from the DAVID results.

A

CTBP1	DTX4	MAML2
CTBP2	DVL2	MAPK10
CD44	FRAT1	NOTCH1
FOSL1	FZD5	NCOR2
LFNG	FZD6	PGK1
POU5F1	FURIN	PLAU
WNT10A	JAG2	PRKCD
WNT7B	LDLR	PRKCI
AXIN1	KAT2A	MYC
CSNK1E	KAT2B	
DLL1	MAML1	

Figure 3.23 Functional annotation clustering of 0.5-fold decreased genes in ALDH high cells in primary prostate cancer cells. Functional annotation clustering was performed for the primary PCa cell line #5008 separately, owing to the different gene signature observed to that of the other primary PCa cell lines investigated by in the Nanostring assay. Functional annotation clustering was carried out in the same way, by in putting the pre-selected genes; 0.5 fold downregulated, and comparing this to the reference gene set, the Nanostring gene list. (A) The downregulated genes which were enriched for the NOTCH signalling pathway. (B) The NOTCH signalling pathway. The red stars indicate genes identified in the enrichment analysis which are directly involved in the pathway or associated with genes in the pathway. DAVID uses a modified Fisher's Exact test (EASE statistic) to determine significantly enriched genes. Image credit Kanehisa Laboratories accessed by link provided from the DAVID results.

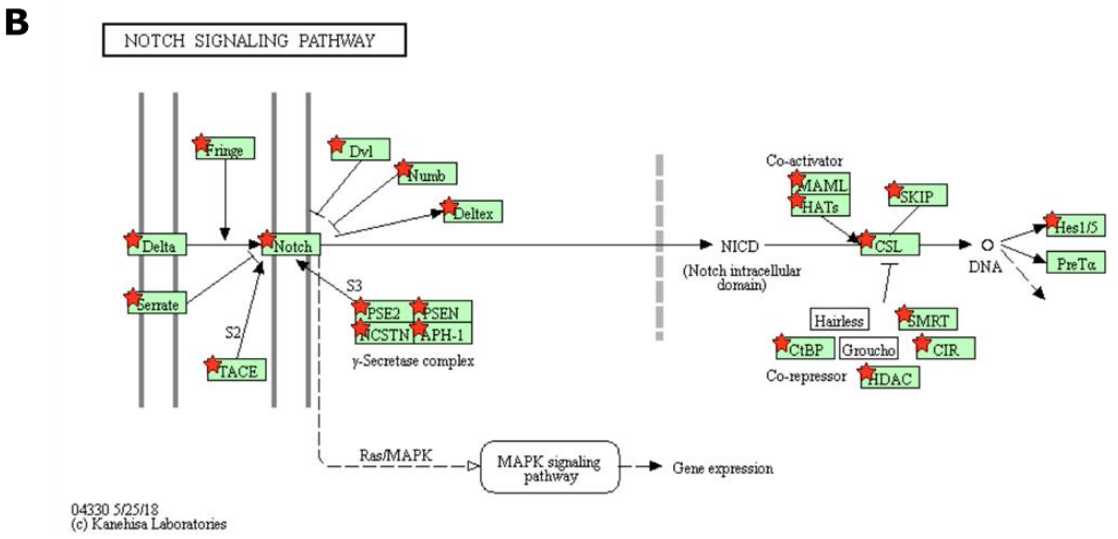

Figure 3.23 Continued functional annotation clustering of 0.5-fold decreased genes in ALDH high cells in primary prostate cancer cells. (B) The NOTCH signalling pathway. The red stars indicate genes identified in the enrichment analysis which are directly involved in the pathway or associated with genes in the pathway. DAVID uses a modified Fisher's Exact test (EASE statistic) to determine significantly enriched genes. Image credit Kanehisa Laboratories accessed by link provided from the DAVID results.

3.7 Discussion

3.7.1 Identification of prostate CSC

In this chapter, I investigated which CSC markers were suitable for isolation of a distinct population of CSC in both established and primary PCa cell lines. The LNCAP and DU145 PCa cell lines were compared for suitability in terms of CSC marker expression. Primary PCa cells cultures were established to investigate primary prostate CSC. The prostate CSC surface markers CD44, $\alpha_2\beta_1$Intergin and CD133 were investigated in the DU145 cell line and in the primary PCa cells, in addition to the functional marker ALDH. DU145 and primary PCa cells isolated based on ALDH activity were investigated for stemness characteristics.

The earliest studies describing prostate CSC used different makers to identify the putative CSC populations. Patrawala and colleagues characterised prostate CSC using a functional approach; by using the side population assay, independent of ABCG2 expression, to isolate putative CSC, (Patrawala et al., 2005). Huss and colleagues identified prostate CSC which were AR^-, in combination with positive expression of ABCG2 (breast cancer resistance protein; aka ABCG2) (Huss et al., 2005). Collins and colleagues used the surface markers $CD44^+$ $\alpha_2\beta_1Integrin^{high}$ $CD133^+$ (Collins et al., 2005).

The study by Collins and colleagues is the most highly cited investigation of prostate CSC, which may be attributable to the investigations being carried out using primary PCa cells (the two other studies used cell lines and xenograft-derived cells). This has influenced the use of the surface markers CD44, $\alpha_2\beta_1$Integrin and CD133 as the most common standard for identifying prostate CSC. CD44 alone or CD44 and β_2Integrin together have been used to identify tumorigenic CSC in PCa cell lines (Patrawala et al., 2007, 2006). However, few studies have characterised CSC from established PCa cell lines based on $CD44^+$ $\alpha_2\beta_1Integrin^{high}$ $CD133^+$ expression. One study showed that the $CD44^+$ $\alpha_2\beta_1Integrin^{high}$ $CD133^+$ population in DU145 cells was more clonogenic *in vitro* but did not provide clear outcomes in the *in vivo* tumorigenicity assay (Wei et al., 2007). Prostate CSC isolated from cell lines based on functional markers ABCG2/ side population, or ALDH, have been to

be tumorigenic *in vivo* (Guzel et al., 2014; Li et al., 2010; Patrawala et al., 2005; Sabnis et al., 2017; van den Hoogen et al., 2010; Yan et al., 2014). However, these markers have only been evaluated in primary PCa tissue using immunohistochemistry.

It is therefore unclear which, if any, CSC markers can be used to identify a prostate CSC population in both established and primary prostate cancer cell lines. This is an important consideration for developing cancer treatments targeting CSC, to demonstrate that a consistent CSC population is the therapeutic target in different experimental models. To our knowledge this study is the first to compare the use of prostate CSC markers, and characterise the resulting populations of the selected marker, using an established cell line and primary PCa cells.

I compared the DU145 and LNCaP cell lines to identify a suitable cell line model in which to investigate prostate CSC (Horoszewicz et al., 1983; Stone et al., 1978). These cell lines were each established from PCa metastases; however, are typically used as contrasting models of PCa as the LNCaP cells are AR^+ while the DU145 cell are AR^-. These cell lines have been widely used in studies of prostate CSC, using various markers or enrichment methods (Liu et al., 2015; Portillo-Lara and Alvarez, 2015; Wang et al., 2013). My aim was to investigate if the surface markers $CD44^+$ $\alpha_2\beta_1 Integrin^{high}$ $CD133^+$ could identify potential CSC in these cell lines. I firstly investigated the expression of CD44 in the DU145 and LNCaP cells, as previous studies have not reached a consensus on the frequency of $CD44^+$ cells in these cell lines. In the DU145 cells, I found that CD44 was expressed in almost all of the DU145 cells, determined by flow cytometry (>90% positive) and fluorescent microscopy. This is higher than the $CD44^+$ population frequency described by previous studies, which ranged from 2.8%-28% (Liu et al., 2015; Patrawala et al., 2006; Wang et al., 2013). There is conflicting evidence for CD44 expression in LNCaP cells (Hurt et al., 2008; Li et al., 2013; Liu, 2000; Liu et al., 2015). The LNCaP cells used in this study did not express CD44. While LNCaP CSC have previously been investigated using other prostate CSC surface markers, the focus of my study was on the use of the combination of surface markers

$CD44^+$ $\alpha_2\beta_1$Integrin^{high} $CD133^+$. Therefore, the DU145 cells were used for further CSC experiments in this study.

3.7.2 The phenotype of *in vitro* models used to investigate PCa

The majority of established PCa cell lines, including the DU145 cells, are derived from metastases, rather than localised tumours (Sobel and Sadar, 2005). While the development of PCa is associated with the outgrowth of luminal cells, the phenotype of metastases-derived PCa cell lines has not been well studied (Sobel and Sadar, 2005). As the primary PCa cells used in this study were obtained from localised tumours, the phenotype of the DU145 cells and the primary PCa cells were compared. In this study, DU145 cells were already confirmed to express the basal marker CD44; however, did not express the basal cytokeratin CK5, and were additionally positive for the intermediate marker CK8. There is a lack of consensus in the literature for CK5 expression in DU145 cells (Liu, 2000; Pfeiffer and Schalken, 2010; Sobel and Sadar, 2005; van Bokhoven et al., 2003). Therefore I further investigated the expression of CD49f and CD26 as markers for basal and luminal cells respectively (Blackwood et al., 2011). This analysis revealed a predominant population of basal cells ($CD49^+$ $CD26^-$) and a substantial population of cells with an intermediate phenotype ($CD49^+$ $CD26^+$). This intermediate population may correspond to transit amplifying cells, which feature in the prostate hierarchy as part of the basal cell population, but represent lineage committed, rather than stem cells (Packer and Maitland, 2016; Taylor et al., 2012). It is also possible that the *in vitro* culture conditions select for the survival of the basal and intermediate cells over the luminal cells, although both basal and luminal cells have been described in previous studies (using the markers CK5 and CK18) in which similar culture conditions were used (Pfeiffer and Schalken, 2010; van Leenders et al., 2001).

The primary prostate cell lines also had a predominantly basal phenotype, and a minor proportion of intermediate cells. Notably the primary PCa cells lacked a luminal population, despite supplementation of the media with DHT, the ligand for AR, which is expressed by luminal cells. The conditions for the successful growth of primary prostate cancer cells in my study differed to

those described previously by Frame and colleagues and Drost and colleagues (Drost et al., 2016; Frame et al., 2013). The use of stromal feeder cells is a likely a contributing factor to the successful establishment of primary PCa cultures by Frame and colleagues. These were not used in this study as it was deemed of greater importance to maintain conditions defined solely by the media composition and supplements added, rather than undefined factors contributed by xenobiotic feeder cells which may have an impact on phenotype or antigen expression. The study by Frame and colleagues described an epithelial hierarchy in the primary PCa cultures, of $CD133^{+}$ $\alpha_2\beta_1Integrin^{high}$ (stem-like cells), $CD133^{-}$ $\alpha_2\beta_1Integrin^{high}$ (transit-amplifying cells) and $\alpha_2\beta_1Integrin^{low}$ (committed basal cells), however the presence of luminal cells was not investigated. The media described by Drost and colleagues was shown to support the growth of organoids derived from both basal and luminal prostate cells; and the capacity of both lineages to give rise to a heterogenous lineage phenotype. In my study this media was adapted to establish adherent primary PCa cultures, which may account for the lack of luminal cells observed. The lack of systematic use of culture conditions for primary PCa cells could result in differences in phenotype, lineage hierarchy and gene expression across different studies. However, establishing optimal culture conditions could be confounded by sample heterogeneity across different studies. The samples used in this study had broadly similar clinical characteristics; all but one sample was GS=7, and there was no significant difference in the average patient age. Therefore, it was not apparent that patient characteristics had any correlation with success in establishing *in vitro* culture.

This study showed that the phenotypes of the established cell line and primary PCa cells used as models to identify prostate CSC did not recapitulate the expected proportions that occur in cancer; in which the luminal cells overgrow and the basal cells are infrequent (Packer and Maitland, 2016). This phenotype, and lack of complete lineage hierarchy, is an important consideration for the identification and characterisation of CSC. In identifying CSC, the use of surface markers $CD44^{+}$ $\alpha_2\beta_1Integrin^{high}$ $CD133^{+}$ select for CSC which have a basal phenotype. This aligns with the hypothesis that prostate stem cells, and consequently cancer stem cells, have a basal phenotype. On

the other hand, the use of functional markers to identify prostate CSC does not specifically consider the lineage of the CSC. Therefore, it is an important consideration for this and other studies of prostate CSC, that the use of media conditions which do not support the growth of PCa luminal cells specifically select for a CSC population in the basal lineage independent of the markers used.

3.7.3 Identifying prostate CSC using the markers CD44, $\alpha_2\beta_1$Integrin and CD133

The DU145 and primary PCa cells were investigated for the presence of a $CD44^+$ $\alpha_2\beta_1Integrin^{high}$ $CD133^+$ potential CSC population. In both the DU145 cells and primary samples tested, the frequency of $CD44^+$ $CD49b^{high}$ (β_1Intergin) $CD133^+$ cells was comparable (0.176% DU145 and 0.098%-0.039% from n=3 samples) to the population identified in primary PCa cells by Collins and colleagues (Collins et al., 2005). Therefore, it appeared that my results were in agreement regarding the use of these markers to identify prostate CSC. However, this low population frequency presented challenges to the downstream analysis required to demonstrate CSC characteristics of a putative population, an important aspect of identifying a CSC population (Clevers, 2011). Additionally, I determined that the staining did not convincingly or consistently identify a $CD133^+$ population, in either of the DU145 cells or primary PCa cells. This was specifically attributed to the antibody staining of the CD133 population, which was not significantly higher than the isotype control staining, whereas the staining for the CD44 and CD49b were significantly higher than the isotype control. However, there is a lack of clarity around the use of CD44 and/ or CD49b without the addition of CD133 to identify prostate CSC. Some studies distinguish 'high' from 'positive' expression of CD49b in selecting the prostate CSC population (Collins et al., 2005; Frame et al., 2013), while other studies, including those from Chen and colleagues and Lin and colleagues, consider the entire CD49b positive population (Chen et al., 2016; Liu et al., 2015). Therefore, it is unclear if these differences result in isolation of different CSC populations. Having shown in this study, using markers independent of the CSC marker panel, that the DU145 cells and primary samples consisted of a high

proportion of basal cells, I expected to identify a high frequency of $CD44^+$ $CD49b^{high}$ cells. Due to this high frequency, these markers alone were not sufficient to isolate a potential CSC population. Therefore, I was unable to conclude that the combination of CD44 CD49b CD133 staining was suitable to identify a potential CSC population in the DU145 cells for further characterisation.

The lack of consistency in the positive CD133 staining in this study, in both the DU145 and primary PCa cells, may be attributed to technical and biological aspects of antibody-based assessment of CD133 expression. Inconsistent identification of $CD133^+$ populations has previously been attributed to a number of factors, including loss of glycosylated epitopes, recognised by some of the most commonly used CD133 antibodies, or downregulation of CD133 expression entirely upon differentiation (Bidlingmaier et al., 2008; Kemper et al., 2010). One of the antibody clones used in this study recognises a glycosylated epitope (AC133; Miltenyi Biotech) (Grosse-Gehling et al., 2013); however the epitope recognised by the other antibody used is not stated by the manufacturer (Thermo Fisher Scientific/ eBioscience). The CD133 staining was negative with both antibodies based on isotype controls. Such controls are not strongly supported for use in flow cytometry experiments (Keeney et al., 1998), due to the possibility for higher non-specific binding than the antibody specific binding. This is particularly due to the identification of a rare population with low expression, which may lead to false negative staining. Nevertheless, isotype control antibodies can be of use when the population of interest is not well defined or can be distinguished by multiple markers, as is the case in prostate CSC. In the literature, the publication of such controls is not consistent. Additionally, distinguishing positive CD133 staining even with the use of an isotype control is not completely reliable (Gameiro et al., 2016; SONER et al., 2014; Tirino et al., 2008). High CD133 staining has been demonstrated by comparing conditions that functionally affect CD133 expression, for example radiation, or serum-free media (Bao et al., 2006; Fan et al., 2012; Portillo-Lara and Alvarez, 2015; Soeda et al., 2009; Wang et al., 2013). Therefore, confirming positive CD133 staining should not blindly rely on the use of an isotype control as a threshold, but should consider the appearance and degree of positive

staining, in comparison to the isotype control. It is possible that the culture conditions employed were not conducive to CD133 expression. Serum free conditions are associated with maintenance of a stemness phenotype (Kemper et al., 2010; Litvinov et al., 2006; Ricci-Vitiani et al., 2007; Wang et al., 2013). However, these conditions were only suitable for the culture of the primary PCa cells, as DU145 cells require serum for growth, and nevertheless the serum-free conditions were still insufficient to upregulate expression levels adequately for identification the primary PCa $CD133^+$ population.

3.7.4 Identifying prostate CSC using the marker ALDH

I therefore investigated the CSC functional marker ALDH, in the DU145 and primary PCa cell lines. Some studies have investigated ALDH activity in PCa cell lines although ALDH activity in primary prostate CSC is not well characterised (Doherty et al., 2011; Han et al., 2014; van den Hoogen et al., 2010). There are advantages and disadvantages to the ALDEFLUOR assay. Importantly, ALDH also has a direct functional contribution to CSC characteristics, including resistance to ROS induced DNA damage and radiation therapy (Cojoc et al., 2015b; Xu et al., 2015). This is not the case for some CSC surface markers, e.g. CD133, for which the function in the context of stemness is not well elucidated. A disadvantage of the ALDEFLUOR assay is that it is not amenable to combining with intracellular staining, as fixation causes loss of ALDH fluorescent signalling, and it is also not suitable for simultaneous analysis of cell cycling by annexin/ PI staining (which requires a different buffer).

In comparison to the use of isotype controls for antibody staining, the ALDEFLUOR assay uses a functional inhibitor, N,N-diethylaminobenzaldehyde (DEAB), which is incorporated into each replicate in which the assay is performed. However, DEAB is primarily an inhibitor of the ALDH1 isoform family; and since other ALDH isoforms have been identified in PCa cells (Cojoc et al., 2015b; van den Hoogen et al., 2011; Yan et al., 2014), the contribution of different isoforms to the ALDH activity measured by the assay is unknown. This could result in incorrect estimates of the ALDH high

population frequency if ALDH high cells are identified due to the activity of other ALDH isoforms, even when DEAB is used as a control.

ALDH activity varies in different cell types, for example, the A549 cell line used in this study had a higher ALDH high population frequency (11.1%) than the DU145 cell lines (7.81%). In brain and lung cancer the ALDH high population can constitute up to 30% of the cells (Choi et al., 2014; Ucar et al., 2009). The frequency of ALDH high cells compared to that of the $CD44^{+}$ $CD49b^{high}$ $CD133^{+}$ population observed in this study (approximately 0.1%) and others, raises the question of which is the more accurate estimate of CSC in these models. It may suggest that the identification of ALDH high cells is not the most stringent assay for identifying CSC, although the converse of this is that these surface markers underestimate the CSC fraction. However, the frequency of a CSC population is not considered a defining characteristic. CSC frequency should be considered in the context of methodologically similar studies, due to the difficulties in systematically reporting the frequency of cells possessing stem-like characteristics in assays of widely varying techniques and culture conditions.

There are also differences in selecting the potential CSC population identified by ALDH activity, compared to antibody staining to detect the presence or absence of protein expression. For the preliminary experiments conducted in my study, the cells were divided into two populations ALDH high and ALDH low (Figure 3.6C). However, the populations isolated using this gating strategy did not consistently demonstrate significantly different characteristics *in vitro* (e.g. colony formation assay; data not shown). This could be attributable to the activity of other ALDH isoforms, e.g. ALDH3A1 and ALDH7A1, which were detected by fluorescence microscopy in unsorted cells (Figure 3.6A). Thus, it was thought that ALDH activity in some cells in the 'ALDH low' population, contributed to stem-like characteristics. Therefore, the gating strategy shown in Figure 3.6D was used to isolate ALDH high and ALDH low cells with a much greater difference in ALDH activity. As previously mentioned, this gating strategy was based on the study by Nishida and colleagues, although strategies to isolate ALDH high and low cells vary across different studies (Chen et al., 2016; Liu et al., 2015; Nishida et al., 2012;

van den Hoogen et al., 2010). These different approaches could be associated with differences in the apparent hierarchy between surface and functional markers, as have been described in a number of studies (Chen et al., 2016; Liu et al., 2015). Chen and colleagues showed that CD44 and $\alpha_2\beta_1$Intergin can further enrich for potential CSC within the ALDH high population, however, Liu and colleagues found that the ALDH high population does not entirely overlap with potential CSC populations identified by other surface or functional markers. Therefore, it would be of interest in future work to compare the *in vitro* and *in vivo* characteristics of ALDH high, ALDH medium and ALDH low cells.

3.7.5 Characterisation of ALDH high and low DU145 and primary PCa cells

In my study, ALDH high DU145 cells had significantly higher clonogenicity than ALDH low DU145 cells. Additionally, ALDH high cells grew larger spheres compared to ALDH low cells. While the ALDH low cells were viable, as shown by the Orangu assay, the larger size of the ALDH high spheres suggests a self-renewing population driving sphere growth and production of new progeny in the event of cell turnover. These data are in agreement with previous studies investigating colony formation of ALDH high DU145 cells (Cojoc et al., 2015b; Hellsten et al., 2011; van den Hoogen et al., 2011), and also sphere formation in ALDH high cells (in DU145 and other PCa cell lines) (Cojoc et al., 2015b; Liu et al., 2015; Nishida et al., 2012). The colony and sphere formation characteristics of the ALDH high DU145 cells is also similar to studies of other phenotypically defined CSC (Beier et al., 2007; Collins et al., 2005; Kryczek et al., 2012; Patrawala et al., 2006; Rybak et al., 2011). Overall these findings on the characteristics of ALDH high DU145 cells support this as a CSC marker.

Characteristics of the primary PCa cells identified by ALDH activity were also investigated. However, these experiments were limited by the capacity to sort viable cells. The viability of the sorted primary PCa cells was more variable than the DU145 cells, and lack of cell adherence in the colony formation assay was noted in some samples despite recording viability of >50%. Therefore, it

was not possible to conclude that ALDH high primary PCa cells have greater clonogenicity. In two samples, the of ALDH high primary PCa cells gave rise to significantly larger sphere

s than ALDH low cells. This suggests greater self-renewal or anchorage independent clonogenic growth in the ALDH high compared to the ALDH low primary PCa cells, however further investigation using a larger sample size is needed. Data in the literature on functional characteristics of ALDH high primary PCa cells is limited. Previous investigations on primary PCa cells demonstrated an association of ALDH isoform expression with disease stage and prognosis, and limited assessment of ALDH activity in primary samples has been described (Magnen et al., 2013; van den Hoogen et al., 2011, 2010; Yan et al., 2014). With a larger number of primary PCa samples, different assay or media conditions could be investigated to improve viability in downstream assays and technical aspects of the flow cytometry sorting protocol be compared, e.g. event rate and nozzle size (as the primary PCa cells and DU145 cells are relatively large. Nevertheless, these data represent promising preliminary findings that extend previous findings on prostate CSC.

It is suggested that proliferation that contributes to larger colony and sphere growth mainly occurs in the intermediate or transit amplifying progeny of CSC (Packer and Maitland, 2016), while CSC, in common with SC, are thought to have a slower rate of division compared to non-CSC. I investigated this characteristic by combining the Cell Trace dye with the ALDEFLUOR assay. I found that ALDH high cells retained more dye than ALDH low cells. This assay merits improvement to the gating strategy to reflect dye dilution over time, since there was a significant difference in ALDH high cell trace high populations after 3 days but the cell trace high population was not significantly different between the ALDH high and ALDH low cells after 7 days for the DU145 cells and one of the primary PCa cell lines. Additional modifications to the protocol, such as increasing the number of timepoints in the experiment could better distinguish generations of cell divisions. This represents a novel use for the Cell Trace dye (Thermo Fisher), which could be combined with other markers of CSC such as surface markers or sphere formation. Hu and colleagues investigated primary prostate cells and found that sphere forming cells retained the label (BrdU/ CFSE); this coincided with

high CD49f expression and activation of SC associated pathways NFκB and PI3K/AKT (Hu et al., 2017). Bragado and colleagues found that the ALDH high and CD49f high populations overlapped with label retaining HNSCC cells which possessed greater tumour initiating capacity (Bragado et al., 2012). The Cell Trace data also demonstrate presence of slow cycling prostate CSC, which complements the finds in primary prostate cells by Hu and colleagues.

In this study, both qPCR and the Nanostring platform were used to interrogate medium scale targeted gene sets, of stemness and CSC associated genes. Methodologically, a crucial difference is the reverse transcription of mRNA and cDNA amplification involved in qPCR, compared to direct detection of mRNA transcripts in Nanostring. This step, in qPCR, is suggested to introduce bias, for example towards differentially weighted gene transcript counts (Geiss et al., 2008). Data collection in both assays involves detection of fluorescence, however the detection of SYBRgreen fluorescence is a measure of the total amplified DNA (qPCR), while microscopic visualisation of the multi-colour fluorescent probes returns the direct counts of specific mRNA transcripts (Nanostring). The data generated, and as a result, the method of analysis is different; being cycle thresholds of detection compared to discrete transcript counts. It is suggested here that the nature of the results is a point in which misinterpretation can occur for the Nanostring platform, as it is more difficult to compare replicate data ranging in the thousands of counts, compared to cycle threshold data, as was observed in this study. Nevertheless, it has been shown that analysis of the same genes provides a strong correlation between fold change results (Prokopec et al., 2013). Therefore, the use of both assays could be considered a way to expand the total number of genes analysed. Finally, an important consideration is that neither product provides the capacity for technical replicates per reaction. The pre-mixed primer and plate set-up for the RT2 Profiler Array incorporates one different primer per well; thus, individual qPCR reactions constitute replicate analysis. While the Nanostring cartridge does allow for technical replicates, correlation data on technical replicates suggests that this is not required (Geiss et al., 2008), and moreover the maximum number of samples per reaction from 6/12 to 2/4 (assumed paired or single analysis) would greatly increase the analysis cost per sample.

The DU145 cells were analysed for differential gene expression using assays incorporating both stem cell signalling and the CSC phenotype. Therefore, it could be expected that the putative CSC population identified by ALDH activity would have a high number of genes more highly expressed than the ALDH low population. Notably, higher expression of ALDH1 was not observed in the DU145 cells; however, having detected ALDH3A1 and ALDH7A1 expression by fluorescence microscopy it is possible that these isoforms contributed to the ALDH activity observed in this study; these isoforms were not included in the gene sets analysed. In particular, the inhibitor used in the ALDEFLUOR assay has also been shown to be a substrate for ALDH3A1 (Morgan et al., 2015). Further analysis of specific isoform expression is warranted to determine the relative contribution to the ALDH activity and to investigate if other isoforms are more highly expressed in ALDH high compared to ALDH low cells.

Unexpectedly there were few genes more highly expressed in the DU145 ALDH high compared to the ALDH low cells, as measured by qPCR and Nanostring. The predetermined gene set investigated in this study differs from large scale, non-targeted array analysis performed previously (Birnie et al., 2008; Zhang et al., 2016), in which larger differential gene signatures were identified between cells identified by CSC markers; different to those used in this study. These studies identified inflammatory and basal gene signatures in CSC. In another study, microarray analysis identified DLL1 and JAG1 are upregulated in DU145 cells in response to HGF, which stimulates a stem-like gene signature incorporating CD49f, CD44 and CD44b expression (van Leenders et al., 2011). Liu and colleagues investigated gene expression in DU145 cells identified by the markers CD44 or $\alpha_2\beta_1$, using a similar qPCR array (Liu et al., 2015). Heatmap data in this study suggests higher expression of JAG1, but similar expression levels of DLL1, in the $\alpha_2\beta_1^+$ population, however neither of these genes are upregulated in the $CD44^+$ population. In my study the PCR data suggests an additional possible phenotype, based on the upregulation of both DLL1 and JAG1, which suggests that NOTCH signalling is important to the CSC phenotype in ALDH high DU145 cells.

There was a lack of consistency in the gene expressing relating to EMT, in the qPCR analysis and Nanostring. In the qPCR analysis ZEB1 and ZEB2, positive regulators of EMT (Hanrahan et al., 2017), were downregulated. This may suggest that the ALDH low cells have a more mesenchymal phenotype than the ALDH high cells. This is also supported by the expression of MUC1, an epithelial marker (Serrano-Gomez et al., 2016), in the ALDH high cells. The increased expression of N-Cadherin (CDH2) detected by Nanostring is in contrast with the findings of decreased expression of ZEB1 and ZEB2 in the ALDH high DU145 cells in the PCR array. N-Cadherin is associated with a mesenchymal phenotype (Wheelock et al., 2008), which is not suggested by the fold downregulation of ZEB1 and ZEB2 expression. However, as none of these genes were common to both assays it was not possible to draw further correlations on the combined effect on the DU145 ALDH high EMT phenotype. Nevertheless, these data could be used to inform further investigation on novel pathways which contribute to the CSC phenotype; this would be complemented by the use of function assays to measure invasion and migration of ALDH high and low DU145 cells.

In the primary PCa ALDH high and low cells, two distinctly different gene signatures emerged in the Nanostring analysis. There was a large differential expression gene signature; which was upregulated in two samples (156 genes) and downregulated in one sample (35 genes). NOTCH and Cell cycling signalling were upregulated in the former while NOTCH signalling was downregulated in the latter. Notably, this sample was the only one in which ALDH1A1 was upregulated; contrastingly the CSC marker CD44 was downregulated. Therefore, ALDH high cells in the latter sample could be suggested to express genes potentially important for stemness which were not covered by this assay.

NOTCH signalling is involved in cell fate determination, and is upregulated in cancer and CSC (Ceder et al., 2008; Grudzien et al., 2010; Wang et al., 2012). NOTCH signalling was found to be enriched in the study by Zhang and colleagues (Zhang et al., 2016). Pathway analysis demonstrated that NOTCH

signalling was regulated at many levels from transmembrane to intracellular signalling, including upregulation of some inhibitors of the pathway (NUMB, NUMBL). Some components of the NOTCH signalling pathway have additional signalling roles which are associated with cancer and CSC. HDAC genes have been associated with radioresistance in primary prostate CSC (Frame et al., 2013). The NOTCH pathway is also associated with MAPK signalling, which has additionally been shown to have a role in radioresistance, in DU145 cells (Kyjacova et al., 2015). ADAM17 is associated with cell cycle progression in prostate cancer via EGFR/ PI3K/ AKT2 signalling (Lin et al., 2012). While the downregulated gene signature in the ALDH high cells of the third primary PCa sample was enriched for NOTCH signalling components, some differences were observed in the genes downregulated, in particular HDAC genes and ADAM17. This may suggest that these genes retained treatment resistance characteristics.

The cell cycle pathway was also significantly enriched in two of the ALDH high primary PCa samples. Cell cycling genes Cyclin A2 (CCNA2) and CDK1 were also upregulated in the ALDH high cells of the third primary PCa sample and the DU145 cells. This common upregulation of cell cycling components in all samples investigated further supports the concept that ALDH high PCa cells have altered cell cycling compared to ALDH low PCa cells. Cyclin expression and subsequent degradation regulates progression through the cell cycle (Vermeulen et al., 2003). D Cyclins promote progression through the G_1 phase and later, CDK1 and CCNA2 regulate the G2-M transition. Cyclins A and D upregulation is associated with PCa (Aaltomaa et al., 1999). Upregulation of cyclin expression suggests that ALDH high prostate CSC are not senescent. Regulation of cell cycle progression controls cell fate determination and can also mediate treatment resistance (Lim and Kaldis, 2013; Vermeulen et al., 2003). Loss of cyclin expression has also been shown to inhibit proliferation and tumorigenesis (Gopinathan et al., 2014). Cell cycle duration in embryonic stem cells differ from those of differentiated cells, mediated by rapid cycling through the G1 and G2 phases (White and Dalton, 2005). Cell cycling of CSC is not expected to match that of embryonic stem cells, and cell cycle proteins are often deregulated in cancer. Nevertheless, these data warrant further validation of cell cycling, and potential resistance

to treatment. Overall the novel gene signatures described here in ALDH high primary prostate CSC represent promising avenues for further investigation.

The final CSC characteristic that was investigated in the ALDH high cells was tumour initiating capacity. This was investigated in the DU145 cells only; as primary PCa cells have previously been shown to be poorly tumorigenic even in bulk (X. Chen et al., 2013). While our study and others on primary PCa cells have demonstrated numerous stem-like characteristics associated with the populations identified by the selected CSC markers, it was not possible to characterise the tumour initiating capacity of the primary prostate CSC. Here it was demonstrated that the ALDH high DU145 cells were significantly more tumorigenic than the ALDH low DU145 cells. It was noted that the ALDH low cells also initiated tumours, although these tumours were significantly smaller and developed more slowly than the ALDH high tumours. Notably, even at a 10-fold lower cell number inoculation, the ALDH high cells grew larger individual tumours in 4/5 mice than the ALDH low cells (10^2 cells compared to 10^3 ALDH high and low respectively). As previously discussed, the ALDH high compartment of prostate CSC does not have a complete overlap with of CSC identified based on expression of other surface markers. The tumorigenicity of the ALDH high CSC population in DU145 cells has not previously been investigated under limiting dilution conditions in NSG mice. In the study carried out by Liu and colleagues, ALDH high DU145 cells were over 60 times more tumorigenic than ALDH low DU145 cells (based on tumour initiation frequency) (Liu et al., 2015). In this study, the ALDH high and low DU145 populations harboured the greatest degree of difference in tumour initiating capacity, compared to the other CSC markers investigated. This suggests that ALDH could be a highly suitable CSC and non-CSC discriminating marker for prostate CSC. In this study, NOD/SCID mice were used, which are deficient in B and T cells but retain NK cells, in comparison to the B, T and NK cell deficient NSG mice used in our study. The greater degree of immunocompromise could also be a factor in the success of ALDH low cell engraftment in our model. Other studies of tumorigenicity of ALDH high prostate cancer cells have used different cell lines, e.g. PC3, LNCaP, 22RV1 and PC-3luc (osteotrophic) or less immunocompromised animal models than those used in our study (e.g. *nu/nu*, NOD/SCID) (Cojoc et al.,

2015b; Hellsten et al., 2011; Nishida et al., 2012; van den Hoogen et al., 2010). Therefore, our study expands the body of knowledge on the tumorigenicity of prostate CSC identified by ALDH enzyme activity.

3.7.6 Summary

In summary, ALDH activity can be used as a marker of prostate CSC in the DU145 cell line and identifies cells which have stem-like characteristics in primary PCa cells. Comparative investigation of prostate CSC characteristics using both an established prostate cancer cell line and primary PCa cells is a key point of this study. Poor growth of primary PCa cells in *in vitro* culture in previous studies has resulted in limited data comparing prostate CSC in a model more representative than long-established cell lines, which are predominantly derived from metastatic tumours. It is important to note that in 2D culture, both cell types grow as a predominantly basal population. Thus, neither accurately recapitulate the lineage hierarchy in the prostate. This may impact studies which have used lineage specific markers to identify prostate CSC as it does not allow for the possibility of transformed luminal prostate CSC. While markers of basal prostate cells have been widely used in previous studies (Collins et al., 2005; Liu et al., 2015; Patrawala et al., 2006), the marker panel tested in this study, $CD44^{+}$ $\alpha_2\beta_1 Integrin^{high}$ $CD133^{+}$, was not suitable for the isolation of DU145 or primary PCa CSC.

Using ALDH as a functional (not lineage restricted) CSC marker, characteristics of CSC were shown in the DU145 cell line and novel preliminary characterisation of ALDH activity in the putative CSC population was carried out. ALDH was shown to be a suitable marker of DU145 CSC based on downstream assays, which demonstrated that ALDH high DU145 cells have greater clonogenicity and self-renewal than ALDH low DU145 cells and are more tumorigenic *in vivo*. Novel characteristics of cell division and gene expression were also demonstrated. Primary prostate CSC had similar cell division properties to the DU145 cells; this was observed across individual donors which had different growth rates in *in vitro* culture. The gene expression data obtained from primary PCa cells supported these functional observations from the DU145 cells and may suggest that stemness-

associated signalling (i.e. NOTCH pathway genes) and cell cycling, could represent a potential prostate CSC gene signature. Preliminary data also suggests primary prostate ALDH high cells could form spheres, indicative of self-renewal capacity, while ALDH low cells did not form spheres, although this warrants further investigation. Overall this study demonstrates the possibility of addressing the relative lack of data on primary cells in studies of prostate CSC, by the development of novel *in vitro* culture conditions and preliminary data demonstrating characteristics similar to those observed in prostate CSC from the DU145 cell line. This provides supporting data for the use of ALDH activity as a prostate CSC marker and forms the basis of a strategy to identify prostate CSC antigens suitable for targeting by T cells.

Appendix 3.1

Patient characteristics Study 1

Sample identifier	Age At Operation	Diagnosis	Gleason Score Total	Gleason Score X	Gleason Score Y	PSA Value (ng/ml)
RWMBV0004303	50	Adenocarcinoma	7	4	3	3.4
RWMBV0004307	51	Adenocarcinoma	7	4	3	23.1
RWMBV0004309	67	Adenocarcinoma	7	4	3	7.1
RWMBV0004311	69	Adenocarcinoma	7	4	3	12.1
RWMBV0004312	65	Adenocarcinoma	7	4	3	10.4
RWMBV0004313	61	Adenocarcinoma	7	4	3	13
RWMBV0004314	69	Adenocarcinoma	7	4	3	5.7
RWMBV0004315#	60	Adenocarcinoma	7	4	3	9
RWMBV0004316#	53	Adenocarcinoma	7	4	3	7.9
RWMBV0004317	57	Adenocarcinoma	7	4	3	4
RWMBV0004320	74	Adenocarcinoma	7	4	3	9.6
RWMBV0004322	54	Adenocarcinoma	7	4	3	6.5
RWMBV0004324	65	Adenocarcinoma	7	4	3	5.1
RWMBV0004319	68	Adenocarcinoma	7	4	3	
RWMBV0004327	70	Adenocarcinoma	7	4	3	8.9
RWMBV0004321	57	Adenocarcinoma	7	4	3	5.7
RWMBV0004323	62	Adenocarcinoma	7	4	3	4.8
RWMBV0004334	60	Adenocarcinoma	7	4	3	7.4
RWMBV0004335	64	Adenocarcinoma	7	4	3	5.5

Two biopsies were received in the case of patient RWMBV0004315, from contralateral regions of the tumour.

Two biopsies were received in the case of patient RWMBV0004316, one tumour biopsy and one adjacent normal biopsy.

Appendix 3.2

Patient characteristics Study 2

Sample identifier	Age At Operation	Diagnosis	Gleason Score Total	Gleason Score X	Gleason Score Y	PSA Value (ng/ml)
RWMBV0004692	59	Adenocarcinoma	7	3	4	Not available
RWMBV0005003	64	Adenocarcinoma	7	4	3	Not available
RWMBV0005008	68	Adenocarcinoma	7	3	4	Not available
RWMBV0005019	61	Adenocarcinoma	9	4	5	Not available
RWMBV0005021	66	Adenocarcinoma	7	3	4	Not available
RWMBV0005020	62	Adenocarcinoma	7	4	3	Not available
RWMBV0005017	48	Adenocarcinoma	7	3	4	Not available
RWMBV0005042	67	Adenocarcinoma	7	4	3	Not available

Appendix 3.3

Primary #4335		Primary #5008		Primary #5017	
Gene	**Fold change**	**Gene**	**Fold change**	**Gene**	**Fold change**
CDK1	8.0913346	CDK1	2.4267058	CCND1	66.929442
CCNA2	7.8453192	WNT5A	1.8792326	PLAU	37.157571
JAG2	6.4044649	ALDH1A1	1.6765703	CCND3	36.951441
CDH2	6.2876674	CCNA2	1.6576793	CDH1	32.40446
FGF1	5.4708582	GJB1	1.6258832	CCNE1	32.082976
CCND2	5.3456056	FBXW2	0.4996837	PSENEN	24.769945
LFNG	4.9142145	MAPK10	0.4992998	PPARD	24.107343
DLL1	3.976313	PRKCD	0.4957341	PPARG	24.060233
FZD7	3.85962	PRKCI	0.4927443	PSEN2	24.02751
CCNE1	3.7720128	FZD5	0.4856272	NCSTN	23.011897
WNT10A	3.7284526	FURIN	0.482138	PSEN1	22.182605
GAPDH	3.7264801	PGK1	0.4760515	TLE1	21.853622
KRT15	3.6354025	LOC652788	0.4758266	FZD3	21.448563
HPRT1	3.1772679	KAT2B	0.4694397	DTX3L	20.845121
CD44	3.163801	MAML2	0.4634116	PRKCH	20.042955
TUBB	3.1609588	MYC	0.4564407	CTNNA1	19.182069
PGK1	2.9322954	CD44	0.4500836	MAML1	19.173398
MAML2	2.72291	FZD6	0.4484081	CDC42	19.059287
PSEN2	2.7074946	FRAT1	0.4418624	TUBB	17.869263
WNT7B	2.6094554	MAML1	0.4364014	HDAC2	17.717548
PRKCI	2.5715388	CTBP2	0.4334547	PRKCZ	17.499805
BMP2	2.5324835	CTBP1	0.4334112	PPP2CA	17.390348
FZD5	2.5295655	DVL2	0.4279008	NLK	17.187309
APC	2.4776225	NOTCH1	0.421292	CLTC	17.120162
FOSL1	2.4182453	DTX4	0.4143648	AXIN1	17.07697
BMP1	2.4093941	CSNK1E	0.4096901	GUSB	16.696243
SMO	2.3994992	LDLR	0.3982248	CSNK1G2	16.416955
CCND3	2.3395117	KAT2A	0.3880063	RHOA	16.36473
LDLR	2.3239244	PLAU	0.3758704	MAML3	16.010933
FGFR1	2.2933267	BMP1	0.3568753	APC	15.967564
CTNNB1	2.2388137	WNT7B	0.349659	DTX4	15.948018
PLAU	2.2377938	AXIN1	0.3436969	RAC1	15.792122
PPP2R5C	2.2149224	POU5F1	0.3256647	LDLR	15.765604
SNW1	2.2018934	KRT15	0.3031538	NOTCH2	15.76442
RHOA	2.1989931	NCOR2	0.2915495	NUMB	15.680381
FBXW2	2.1497776	JAG2	0.2773231	MAML2	15.665611
TCF7	2.1295556	FOSL1	0.2493361	LOC652788	15.490024
NCSTN	2.1223534	DLL1	0.2469543	DVL1	15.40763
CCND1	2.1049575	WNT10A	0.2386665	ADAR	15.356562
PRKACB	2.1041762	LFNG	0.176745	KAT2B	15.112444
PRKACA	2.0953465			APH1A	15.082574

NOTCH2	2.0669972			DVL3	14.823409
PRKCZ	2.0395743			RFNG	14.722058
CSNK1G1	2.0118878			CSNK2A1	14.541338
RB1	2.0008423			PAFAH1B1	14.254943
PPARG	0.401994			PPP2R5C	14.240913
				EP300	14.126649
				CTNNB1	13.924237
				GSK3B	13.772204
				FBXW11	13.761334
				CSNK1D	13.689834
				RBPJ	13.688737
				CIR1	13.63806
				PRKCD	13.637059
				MAPK9	13.592441
				BTRC	13.54286
				CDK1	13.212841
				CTBP1	13.133678
				KAT2A	12.709669
				PPP2R5E	12.557032
				MAP3K7	12.513485
				FBXW2	12.35436
				PRKCI	12.144353
				SNW1	12.086886
				CCNA2	11.935894
				CTBP2	11.454516
				PGK1	11.174291
				CCND2	11.123794
				PRKACB	10.739704
				HDAC1	10.706791
				DTX2	10.671523
				PRKACA	10.647398
				RB1	10.523732
				FZD6	10.380166
				FGF2	10.185072
				DVL2	10.138776
				CSNK1G3	10.075582
				FZD5	10.034976
				MAPK10	9.8957232
				SMAD4	9.6550324
				CSNK1G1	9.5884568
				WNT7A	9.4479943
				GAPDH	9.3698707
				NCOR2	9.1580535
				FOSL1	9.136111
				ADAM17	9.113701
				FURIN	9.0784246
				FZD1	8.9002577

				FRAT1	8.8610125
				PRKD1	8.6037054
				BMP2	8.5172663
				HPRT1	8.3985993
				ALDH2	8.1913982
				CSNK1E	7.9524951
				CSNK1A1	7.7661173
				JUN	7.4767686
				NOTCH3	7.4104637
				HES1	7.3104418
				NUMBL	6.9597991
				PRKX	6.7959014
				CD44	6.5682019
				WNT5A	6.5550078
				WNT7B	5.5615853
				BMP1	5.451239
				MYC	5.3180625
				GLI3	4.5215546
				JAG1	4.2096738
				FZD7	3.8933259
				TCF7	3.7769641
				SMO	3.5063362
				NOTCH1	2.269816
				LFNG	0.5610803
				DLL1	0.3180237
				WNT10A	0.1857278

Chapter 4.

Identification of antigens of prostate cancer cells

4 Identification of antigens of prostate cancer cells

4.1 Introduction

This chapter focuses on the identification of antigens presented by prostate CSC, specifically the selection of therapeutically relevant, potentially immunogenic targets. As previously discussed, CSC have been shown to be resistant to DNA damaging cancer treatments, such as chemotherapy and radiation therapy (Bao et al., 2006; Chen et al., 2015; Cojoc et al., 2015b; Ying et al., 2015). It has been suggested that CSC could be specifically targeted by immunotherapy (Pan et al., 2015). While some resistance mechanisms of CSC, including overexpression of anti-apoptotic proteins and decreased HLA expression could represent a barrier to immunotherapy (Bruttel and Wischhusen, 2014), a number of studies have nevertheless investigated the use of vaccines to induce T cell responses, antibodies against CSC markers and adoptive T cell transfer or CAR T cells (Hu et al., 2016; Ning et al., 2012; Ying et al., 2015). Activation of the adaptive immune system has the potential for durable responses to tumours by the development of immune memory to tumour antigens (Finn, 2012); this could be particularly relevant in the targeting CSC to prevent tumour relapse. In this study, the focus was on T cells as a mode of CSC immunotherapy, as this could be used to target intracellular and extracellular antigens, as presented by HLA-I. This requires selecting antigens known to be expressed by CSC, so that the outcome on tumour growth of specifically targeting CSC can be evaluated.

Some studies have investigated how CSC could be targeted by identifying epitopes from proteins expressed in common with SC, including ALDH, SOX2 and CD133 (Ji et al., 2014; Schmitz et al., 2007; Visus et al., 2011). It has been suggested that quiescent SC can evade immune recognition (Agudo et al., 2018), however it is not known how the immune system can distinguish between more actively cycling healthy SC (e.g. intestinal SC) and CSC. Targeting these antigens could cause off-target damage in some tissues.

Therefore, I set out to identify novel TAAs of prostate CSC, and potential epitopes of these antigens. As previously discussed, (Chapter 1. Introduction), there are a number of ways to identify antigens and epitopes of specific HLA restrictions, including experimental and *in silico* (predictive) approaches. I performed HLA ligandome analysis of the DU145 cells, which was combined with *in silico* analysis of the experimental dataset to select antigens of interest. This was performed on the entire DU145 cell population, rather than on individually sorted populations of ALDH high and ALDH low DU145 cells (which could directly determine the peptides presented by the respective populations) due to the large number of cells required for the analysis (10^9 cells). HLA analysis involves direct identification of peptides presented at the cell surface (Figure 4.1A, B). The peptides identified represent a snapshot of the total ligandome, as immunoprecipitation is estimated to recover only 0.5-3% of the peptides present in the lysate (Figure 4.1C, D). The poor ligand complex recovery necessitates the large number of cells analysed, in addition to the sample input requirements for detection by mass spectrometry. Mass spectrometry analysis of the eluted peptides results in spectral data which is annotated based one or more proteomics databases to generate the peptide sequence data (Figure 4.1 E). This allowed for a relatively unbiased investigation (reliant on proteomics databases) of prostate TAAs, in comparison to pre-selection of antigens from which to predict potential epitopes. In this chapter, a large dataset of novel antigens and potential epitopes, many of which were not previously associated with PCa, are identified.

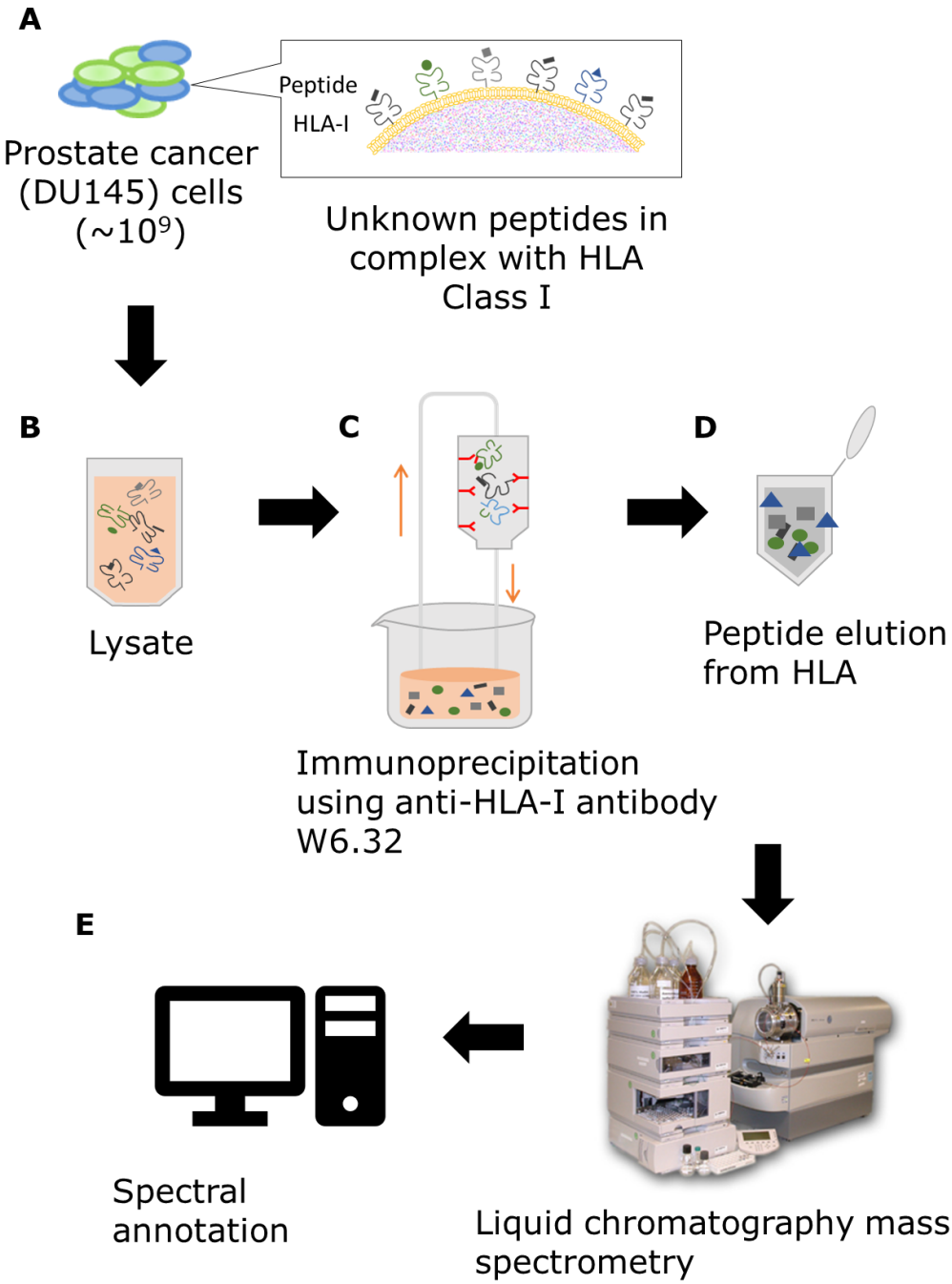

Figure 4.1 HLA ligandome analysis. (A) Approximately 10^9 DU145 cells were grown and snap frozen in liquid nitrogen. (B) The cells were lysed in a buffer containing protease inhibitors. (C) The pan-HLA-I antibody was used to capture HLA-peptide complexes by immunoprecipitation. (D) The peptides were separated from the HLA proteins by acid elution. (E) The amino acids comprising the peptide sequences were identified by mass spectrometry and the peptide, protein and gene information corresponding to the amino acids was derived by spectral annotation of the mass spectrometry peaks and matching these data to proteomics databases. This figure is adapted from a design provided by Ms Serina Tokita, Sapporo Medical University.

Question

Do prostate CSC express antigens which could be therapeutically targeted by T cells?

Specific Aims

4.2 Identify peptides that are processed and presented by the HLA molecules expressed on the DU145 cell line (the 'HLA ligandome').

4.3 Select peptides of the DU145 ligandome which are suitable for potential therapeutic targeting, based on low or absent antigen tissue expression.

4.4 Identify high HLA binding affinity peptides of the DU145 ligandome.

4.6 Identification of peptides presented by DU145 cells

4.6.1 HLA Class I expression in the DU145 cell line

HLA ligandome analysis involves the capture of HLA-peptide complexes from the surface of cells by immunoprecipitation. As previously discussed, analysis of HLA Class II peptide interactions is more complex owing to the greater length of peptides, although some studies have previously isolated HLA Class II ligands (Kowalewski et al., 2015; Nelde et al., 2018). However, the HLA ligandome analysis in my study was focused on identifying potential tumour targets for $CD8^+$ T cells, therefore I analysed the peptides presented by HLA Class I. This required sufficiently high levels of HLA Class I expression, in addition to the use of specific high affinity antibodies, to allow capture of sufficient material for mass spectrometry. To test this, the HLA Class I expression of the DU145 cell line was compared to the SW480 cell line. HLA Class I ligandome analysis of the SW480 cell line was previously successful (Kochin et al., 2017), therefore this served as an indicator of sufficiently high HLA Class I expression that provide an indicator of successful HLA-peptide complex immunoprecipitation. The DU145 cells were found to express comparable HLA levels to the SW480 cells (Figure 4.2A); above that of the isotype control (Figure 4.2B). The HLA Class I type of the DU145 cells was determined from the TRON Cell Line Portal (TLCP), (http://celllines.tron-mainz.de/) (Scholtalbers et al., 2015). The HLA Class I type of the DU145 cells recorded in the TLCP, is HLA-AA*33:03 (homozygous), HLA-B*50:01, HLA-B*57:01, and HLA-C*06:02. In the interest of capturing a large dataset which allowed for further refinement, rather than limiting the peptide output to specific alleles (for which the relative surface expression was not known), immunoprecipitation was performed using a pan-HLA Class I antibody.

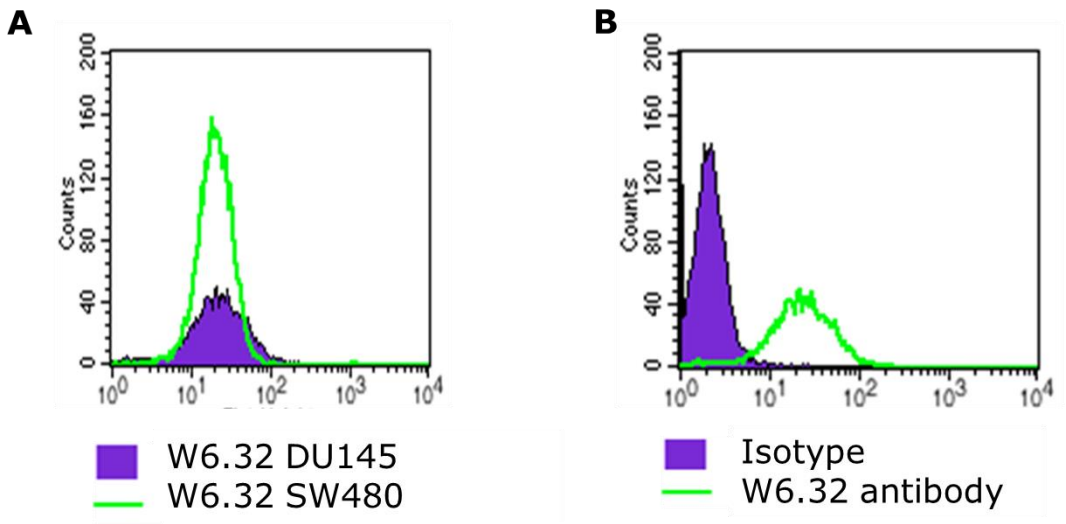

Figure 4.2 Flow cytometry analysis of HLA expression in DU145 cells. (A) HLA Class I expression in DU145 cells was compared to SW480 colorectal cancer cells using the pan HLA Class I antibody clone W6.32. (B) W6.32 staining in the DU145 cells compared to the isotype control. This was performed in duplicate.

4.6.2 Characteristics of the DU145 HLA ligandome

HLA ligandome analysis of the DU145 cell line identified a total of 1933 sequences at the 0.01 confidence level, a further 843 sequences at 0.05 confidence and 17937 sequences at a confidence level of 1. The analysis of the mass spectrometry data was carried out using the Proteome Discoverer software (performed by Serina Tokita, Sapporo Medical University). The mass spectra were converted into peak lists using the Sequest HT and Mascot algorithms and the peak lists were searched against the SwissProt database to identify the peptide sequences and annotate the corresponding proteins (these functions were integrated into the software). The resulting data were categorised as follows: sequence data, sequence length, protein, protein sequence, gene, reads per kilobase million (RPKM) (RNA-Seq readout), 'cancer panel' chromosome, biological process, cellular component and molecular function. Only the sequences at the 0.01 confidence level were considered for further analysis. After the removal of contaminated sequences (user or reagent derived peptides e.g. from keratin, catalase) there were 1763 sequences at a confidence level of 0.01 for which the source gene could be identified. The sequences, gene and protein information are detailed in Appendix 4.1, which is provided as an electronic resource owing to its length. The peptides in the ligandome were derived from 1206 unique proteins. The length of the sequences ranged from 8-14 amino acid monomers (8-14mers); the most common peptide length was 9mer (45.15%) followed by 10mer (14.8%) and 11mer (14.63%) (Figure 4.3A). A total of 1374 sequences of lengths ranging 9-11mer from the DU145 ligandome were further examined by Hongo and colleagues (for a collaborative publication focusing on upstream determinants of epitope presentation). Logo sequence analysis identified conservation of glutamic acid (E) and arginine (R) at anchor positions p2 and conservation of arginine (R), lysine, alanine (A), valine (V) and tryptophan (W) (in descending order of frequency) at p9 Figure 4.3B, adapted from Hongo et al., 2019, Figure 1C. HLA binding motif data from the NetMHC 4.0 Motif Viewer indicated that conservation of arginine at p9 is indicative of HLA-A*33 superfamily binding (data was available for HLA-A*33:01 but not HLA-A*33:03) and tryptophan conservation at p9 is associated with HLA-B*57:01 (http://www.cbs.dtu.dk/services/NetMHC/logos.php). Arginine at p2 is an HLA binding motif for HLA-C*06:02.

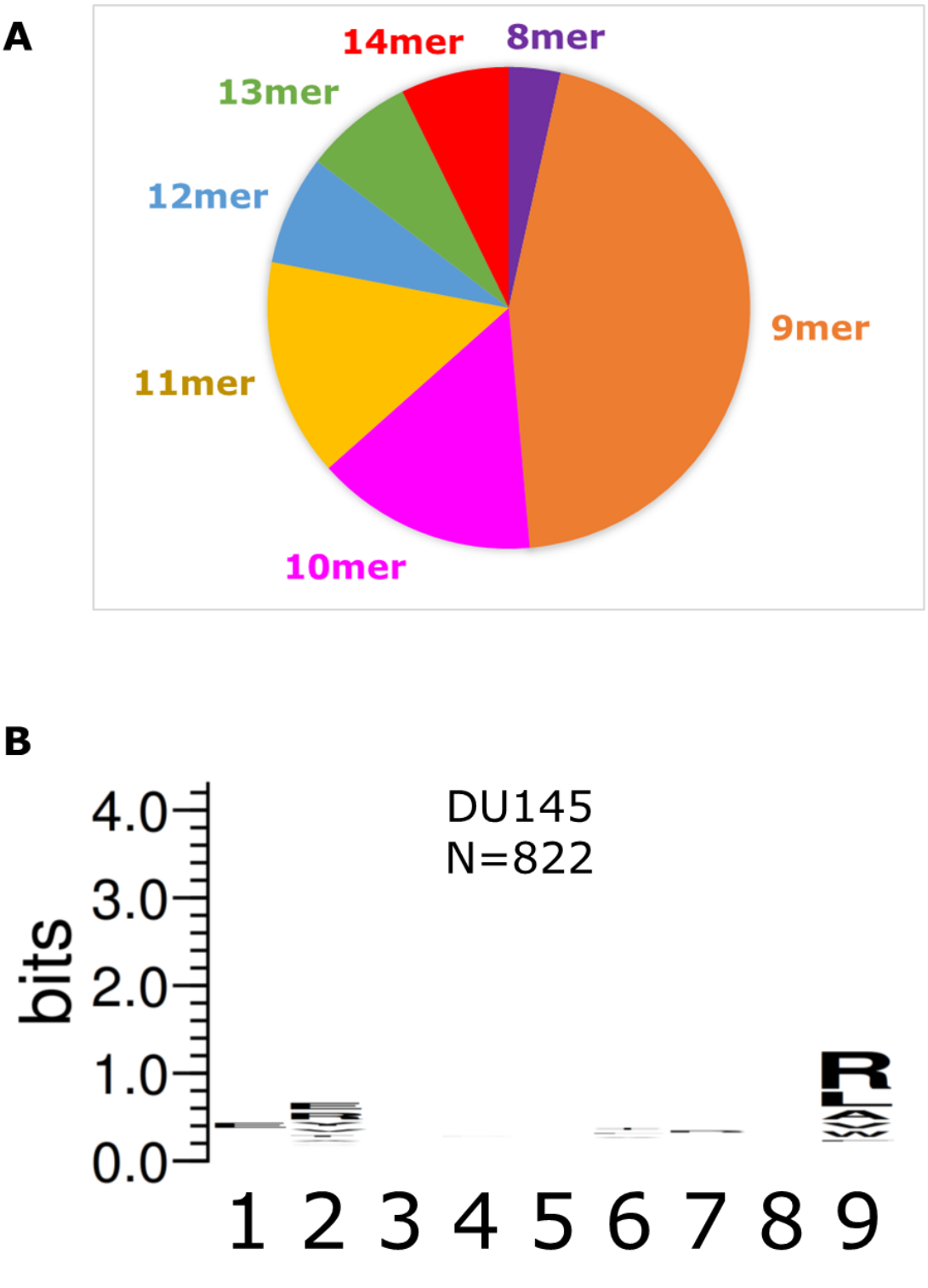

Figure 4.3 Length distribution and HLA binding motifs of the peptides identified in the HLA ligandome analysis of 10^9 DU145 cells. (A) The proportions of peptides of differing lengths in the DU145 HLA ligandome, ranging from 8mer- 14mer. (B) Analysis of the HLA binding motifs of the 9-11mers in the ligandome dataset, adapted from Hongo et al., 2019.

4.7 Selection of therapeutically relevant peptides

4.7.1 Source gene expression in healthy tissue

Selection of therapeutically relevant potential epitopes required exclusion of peptides derived from genes expressed at high levels in healthy tissues, to minimise the possibility of off-target damage by activated epitope specific T cells. In other studies in which therapeutic antigens were identified using ligandome data, multiple peptide datasets have been generated from cancer and healthy tissue or cell lines, to provide a comparison of genes expressed (Berlin et al., 2015; Schuster et al., 2017). In the absence of an available healthy prostate cell line, I used the Genotype Tissue expression (GTEx) database (GTExportal.org) to search for suitable peptides for which the source gene was not highly expressed in healthy tissue, or was expressed in a limited number of tissues ("The Genotype-Tissue Expression (GTEx) project," 2013). The investigation was limited to genes in the ligandome dataset for which the median RPKM = 1, or the RPKM was denoted ≤5, to reduce the time required in this interrogation step. The highest median value for the RPKM ≤5 antigens was 3.139 (UQCC3). RPKM <1 was been previously used to denote absence of tissue expression (Kryuchkova-Mostacci and Robinson-Rechavi, 2017), therefore values in excess of 1 were expected to show increasing tissue expression that would correspond to increased possibility of off-target tissue damage. An exception to this was made for genes denoted 'cancer panel'; for which the RPKM values ranged from 0.012935 (SOX11) to 301 (HSP90AA1).

A total of 194 genes fitted these RPKM criteria. The genes of interest, the median RPKM/ RPKM ≤5 and cancer panel categories, and the selection decisions are detailed in Table 4.1. Examples of gene tissue expression levels and/ or distribution which guided selection of the peptides of interest are shown in Figure 4.4. Selections were made if the overall tissue expression was low; (Figure 4.4 A, B) or if the genes had previously been defined as oncogenes (Figure 4.4 C, D). Genes for which the tissue distribution denoted a potential cancer testis antigen were also identified (Figure 4.4 E, F). Examples of peptides which were not selected due to high gene expression in certain tissues (which included genes which had RPKM values <1) are shown

in Figure 4.3 G, H, I. A total of 142 antigens of interest were selected for further analysis based on the absence of gene expression in healthy tissues.

Table 4.1 Selection of peptides which have the potential for therapeutic targeting, based on limited/ low tissue expression. Peptide sequences, sequence length and the gene the peptides are derived from are shown, for genes which fulfilled the criteria: median RPKM <1 or RPKM≤5 or 'cancer panel.' The inclusion in further analysis as a 'potential therapeutic target (yes/no) was determined by inspection of the tissue expression graphs obtained from the GTEx database (examples in Figure 4.3).

Sequence	Sequence length	Gene	Median RPKM	RPKM≤ 5	Cancer panel	Potential therapeutic target
RFQSSAVMAL	10	HIST1H3A	0	✔		Yes
RFQSSAVMALQE	12	HIST1H3A	0	✔		Yes
KTDLRFQSSAVMAL	14	HIST1H3A	0	✔		Yes
RFQSSAVMALQEA	13	HIST1H3A	0	✔		Yes
VMALQEASEAYL	12	HIST2H3A	0	✔		Yes
VMALQEASEAYLVG	14	HIST2H3A	0	✔		Yes
AVMALQEASEAYL	13	HIST2H3A	0	✔		Yes
IDALDILEE	9	MAGEB10	0	✔		Yes
DYKKIPIKR	9	MAGED4	0	✔		Yes
EAVLWEALR	9	MAGED4	0	✔		Yes
SRFGKFIRI	9	MYH8	0	✔		Yes
ETYLLEKSR	9	MYH8	0	✔		Yes
IFERIASEASRLAH	14	HIST1H2BL	0.01275	✔		Yes
ERIASEASRLAHY	13	HIST1H2BL	0.01275	✔		Yes
SEGTKAVTKYTSSK	14	HIST1H2BL	0.01275	✔		Yes
ERIASEASRLAHYN	14	HIST1H2BL	0.01275	✔		Yes
ERIASEASRL	10	HIST1H2BL	0.01275	✔		Yes
VNDIFERIASEAS	13	HIST1H2BL	0.01275	✔		Yes
IFERIASEAS	10	HIST1H2BL	0.01275	✔		Yes
EGTKAVTKYTSSK	13	HIST1H2BL	0.01275	✔		Yes
RIASEASRLAHYN	13	HIST1H2BL	0.01275	✔		Yes
DYPDYKYRPR	10	SOX11	0.012935	✔	○	Yes
YVPEHVRKL	9	LRRC8E	0.018985	✔		Yes

ENFDKFFTR	9	PRKCG	0.035495			No
AEIAKLKAA	9	KIF14	0.04104			Yes
YAERVGAGAPVYL	13	HIST2H2AB	0.045825	✔		Yes
TEYLNFEKS	9	ESRP1	0.04685			No
EFKKLIRNR	9	RLN2	0.058405	✔		Yes
HRFQQTQYL	9	DLX6	0.061615			Yes
RKTVTAMDVVYALK	14	HIST1H4A	0.069195	✔		Yes
RDNIQGITKPAIR	13	HIST1H4A	0.069195	✔		Yes
KTVTAMDVVYALK	13	HIST1H4A	0.069195	✔		Yes
VTAMDVVYALKR	12	HIST1H4A	0.069195	✔		Yes
TVTAMDVVYALK	12	HIST1H4A	0.069195	✔		Yes
NIQGITKPAIR	11	HIST1H4A	0.069195	✔		Yes
RKTVTAMDVVYAL	13	HIST1H4A	0.069195	✔		Yes
VTAMDVVYALK	11	HIST1H4A	0.069195	✔		Yes
ENVIRDAVTYTEHA	14	HIST1H4A	0.069195	✔		Yes
MDVVYALKRQGRTL	14	HIST1H4A	0.069195	✔		Yes
VVYALKRQGRTLYG	14	HIST1H4A	0.069195	✔		Yes
ALKRQGRTLYGFGG	14	HIST1H4A	0.069195	✔		Yes
LKRQGRTLYGFGG	13	HIST1H4A	0.069195	✔		Yes
HYVEAEKLRGR	11	SIX1	0.070265			Yes
DVMVMCLLPK	10	UNC79	0.07147			No
EDKGINVFR	9	MKI67	0.07477			Yes
KSYLGSEADVW	11	MELK	0.07526			Yes
EVLEAIRVTR	10	MISP	0.10465			No
AEIKVKLIEA	10	NCAPG	0.1251			No
EVKSITKER	9	CENPE	0.12845			Yes
WYKHVASPR	9	NPW	0.1312	✔		Yes
DYLPPEMIEGR	11	AURKB	0.13585		○	Yes
DYLEETHLKFR	11	IQGAP3	0.1563	✔		Yes

IRAPAVRTL	9	PKP3	0.18165			No
KVIHEQVNHRW	11	TOP2A	0.1832			Yes
EYFADMKRHR	10	TOP2A	0.1832			Yes
YFADMKRHR	9	TOP2A	0.1832			Yes
MKRKELIPLVVF	12	C15orf48	0.19455			Yes
VSREAVALV	9	MYO15A	0.21935			Yes
EILEKIRSA	9	DLGAP3	0.22135			No
YRHEKRVKL	9	RAB3B	0.2257			Yes
GEFTGWEKV	9	RIPK4	0.24655			Yes
KVRLLRLR	8	CAPN12	0.28935			Yes
TSTVPLVGR	9	WDR62	0.30445	✔		Yes
TSDRHIRIW	9	CDC20	0.30915			No
AADETLRLW	9	CDC20	0.30915			No
AEHFSMIRA	9	MEX3A	0.31575	✔		Yes
YSYKGLRSV	9	DDX43	0.3606	✔		Yes
ESFPGSFRGR	10	CDCA7	0.47945			No
NSREKIYNR	9	CDCA7	0.47945			No
HEFMTWTQV	9	RASGEF1A	0.4934			No
NRISHAQKF	9	TNNT1	0.50895			No
FTQEPLHLVSPSFL	14	HPSE	0.5519			No
HRFDPKASSSF	11	NAPSA	0.56825			No
ETLLRLLLR	9	ASAH2B	0.58625	✔		Yes
VLLPKKTESHKAK	13	HIST2H2AC	0.6763	✔		Yes
AVLLPKKTESHKA	13	HIST2H2AC	0.6763	✔		Yes
VLLPKKTESHKA	12	HIST2H2AC	0.6763	✔		Yes
MAAVLEYLTAE	11	HIST2H2AC	0.6763	✔		Yes
YAERVGAGAPVYM	13	HIST2H2AC	0.6763	✔		Yes
AIRNDEELNKL	11	HIST2H2AC	0.6763	✔		Yes
AIRNDEELNKLL	12	HIST2H2AC	0.6763	✔		Yes
AEILELAGNAARDN	14	HIST2H2AC	0.6763	✔		Yes
SSRAGLQFPVGR	12	HIST2H2AC	0.6763	✔		Yes
AGLQFPVGRVHRLL	14	HIST2H2AC	0.6763	✔		Yes
VLPNIQAVLLPK	12	HIST2H2AC	0.6763	✔		Yes

GGVLPNIQAVLLPK	14	HIST2H2AC	0.6763	✔		Yes
GVLPNIQAVLLPK	13	HIST2H2AC	0.6763	✔		Yes
ELAGNAARDNKKT	13	HIST2H2AC	0.6763	✔		Yes
AAVLEYLTAE	10	HIST2H2AC	0.6763	✔		Yes
GLQFPVGR	8	HIST2H2AC	0.6763	✔		Yes
NRADLIRHF	9	ZNF805	0.68065	✔		Yes
TRALMVVSL	9	CLDN7	0.7299			No
EEIQKKLEAA	10	STMN2	0.78895			No
NYWDKFVKR	9	RYR2	0.848			No
RRTAQVRYL	9	PNMA2	0.8516			No
AEINRKIINQRLIL	14	C16orf87	0.87555	✔		Yes
KLMPGRIQLW	10	RBM47	0.8955			No
EVFVGKIPR	9	RBM47	0.8955			No
REHQNFYEA	9	ARHGAP42	0.9899	✔		Yes
FRAPDLKRM	9	TRIM6	1.035	✔		Yes
TRIPKVQKL	9	HSPA6	1.0725			No
TVFDAKRLIGR	11	HSPA6	1.0725			No
VYIDKVRSL	9	LMNB1	1.0815			No
SLEDEPRLVL	10	ADGRG6	1.0985			No
DIINGDAIHKR	11	SCAI	1.1455	✔		Yes
VERSFILSA	9	FGD6	1.429	✔		Yes
YKAQPVIQF	9	AGO3	1.5065	✔		Yes
SSYFRIHER	9	ZNF14	1.8895	✔		Yes
EFEAVLTER	9	CCDC127	2.083	✔		Yes
SAFPEVRSL	9	THADA	2.205	✔		Yes
AEFATDDEVSRF	12	TNRC6B	2.2605	✔		Yes
LSQLPQIPQFQLA	13	TNRC6B	2.2605	✔		Yes
LSQLPQIPQFQL	12	TNRC6B	2.2605	✔		Yes
VSEGPLRPVLEY	12	ZNF451	2.326	✔		Yes
VSEGPLRPVLE	11	ZNF451	2.326	✔		Yes
FFSSFMKKR	9	ABL2	2.3755		○	Yes
RFPEHVREI	9	ATR	2.5985		○	Yes
DYHTLPRAR	9	ATP9B	2.955	✔		Yes
MDSLRKMLIS	10	UQCC3	3.149	✔		Yes
MDSLRKML	8	UQCC3	3.149	✔		Yes
EYMTPSSR	8	CBL	3.285		○	Yes

TRIDLIQKL	9	SOCS6	3.5345			No
RRFPDLNRL	9	MSH2	3.614		○	Yes
ENWQPRAR	8	RPTOR	3.935			No
DYFHNGNPR	9	RPTOR	3.935			No
EYLEKQRNR	9	MSH6	3.948		○	Yes
EALNKDKIKR	10	MSH6	3.948		○	Yes
EYEYMNRRR	9	ERBB3	4.528		○	Yes
QIEAIQQAEDGL	12	SYNE1	4.6955		○	No
SRPTFNVQV	9	LPP	5.1675		○	No
KSFEDIHHY	9	KRAS	5.3555		○	Yes
ETLAKEKGMNR	11	MTOR	5.5285		○	Yes
EYVEFEVKR	9	MTOR	5.5285		○	Yes
EINAILQKR	9	MTR	6.1535		○	Yes
FRYNPYLK	8	NBN	6.34		○	Yes
FRIEYEPLV	9	NBN	6.34		○	Yes
STFDSPAHW	9	EGFR	6.799		○	Yes
NYLEDRRLVHR	11	EGFR	6.799		○	Yes
FYGIIRNV	8	PRKDC	7.394		○	Yes
FRPYAKHWL	9	PRKDC	7.394		○	Yes
EYIKNWRPR	9	AKT3	7.445		○	No
DYLHSGKIVYR	11	AKT3	7.445		○	No
KTLERSYLL	9	RRM1	7.9975		○	Yes
EYFTLQIRGRER	12	TP53	8.141		○	Yes
LGIPKDPRQW	10	ETS1	8.398		○	Yes
DIRTPPLQSER	11	FZR1	9.4045		○	Yes
VDITQEPVLDTML	13	NUP98	9.624		○	Yes
SRSVIIREL	9	UBR5	11.185		○	Yes
DFKPGDLIFAK	11	PSIP1	12.34		○	Yes
VAQQGTMWQGRN	12	ARID1A	12.53		○	No
RESPFSTSA	9	XPO1	12.625		○	Yes
EVAQVESLRYR	11	TPR	12.81		○	Yes
EAKAPILKR	9	TPR	12.81		○	Yes
KFNFKTSLW	9	PARP1	13.115		○	Yes
LQDVSASTKSLQEL	14	PARP1	13.115		○	Yes
IVYDIAQVNLKYL	13	PARP1	13.115		○	Yes
DIAQVNLKYL	10	PARP1	13.115		○	Yes
IVYDIAQVNLKY	12	PARP1	13.115		○	Yes
LKLKFNFKTS	10	PARP1	13.115		○	Yes
IAQVNLKYLLKL	12	PARP1	13.115		○	Yes
IAQVNLKY	8	PARP1	13.115		○	Yes

LQDVSASTKSLQE	13	PARP1	13.115		○	Yes
REAQFGTTA	9	CRBN	13.24		○	Yes
TLPSVVRLL	9	BCL3	13.935		○	Yes
EYIKTWRPR	9	AKT2	14.4		○	Yes
MTNLPAVGR	9	ARID1A	15.105		○	No
DYLHSQGVVHR	11	RPS6KA2	16.53		○	No
WVKPIIIGR	9	HEL-S-26	16.96		○	No
REMIPFAVV	9	SEPT9	17.07		○	Yes
YSIRGQLSW	9	SMARCB1	17.765		○	Yes
EYLEKKNFIHR	11	ABL1	19.885		○	Yes
HTWNGIRHL	9	SDHC	21.27		○	Yes
EMREMLTHR	9	HIF1A	21.825		○	Yes
MEDIKILIA	9	HIF1A	21.825		○	Yes
PDLTMFPPFSE	11	ARNT	21.83		○	No
EILKGGVLIQR	11	ERBB2	21.83		○	No
EYKPHSIPLR	10	KDM5C	21.83		○	No
ARAELEMRL	9	NUMA1	24.34		○	Yes
IRNQIIREL	9	MAP2K2	33.635		○	Yes
TVGLIRNL	8	CTNNB1	41.92		○	Yes
WEQGFSQSF	9	CTNNB1	41.92		○	Yes
RRNDKIIVF	9	ERCC3	48.44		○	No
NYAAPPSTR	9	MYC	48.44		○	No
WVKPKDMLGPK	11	FH	48.44		○	No
EWVKPKDMLGPK	12	FH	85.405		○	No
NVNEVISNR	9	FH	85.405		○	No
KSKLDAEVSKW	11	CTNNA1	85.405		○	No
EYMGNAGRKER	11	CTNNA1	140.3		○	No
EYAQVFREH	9	CTNNA1	140.3		○	No
KEAIETIVA	9	GNAS	140.3		○	No
DIIQRMHLR	9	GNAS	301		○	No
FRVDYILSV	9	GNAS	301		○	No
DKSVKDLVILL	11	HSP90AA1	301		○	No
DILEKKVEK	9	HSP90AA1	301		○	No

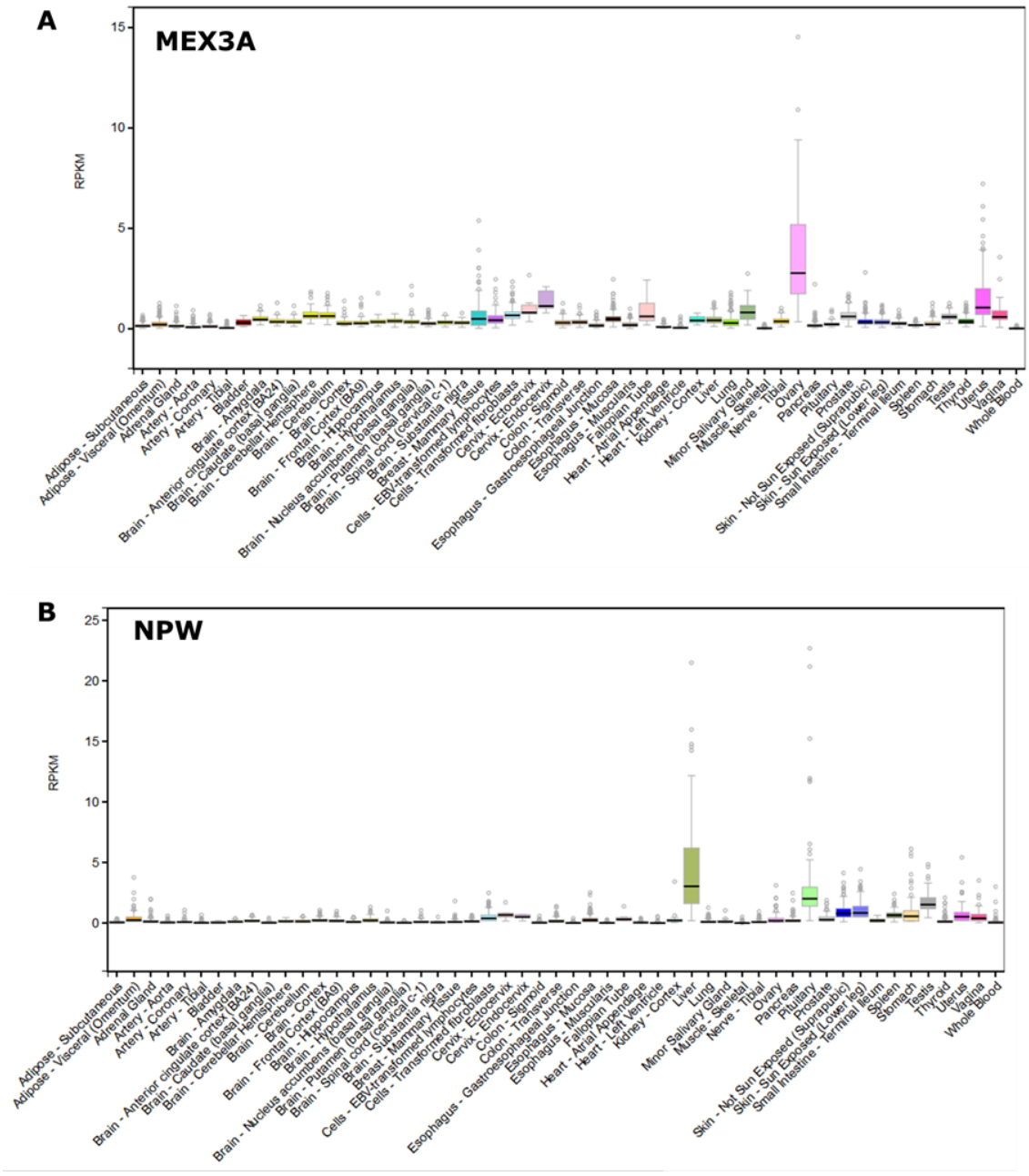

Figure 4.4 Gene expression (RNAseq data) in healthy tissues of peptides identified in the DU145 HLA ligandome. (A, B) Examples of peptides for which the tissue gene expression and distribution was low, MEX3A and NPW. RNAseq data was obtained from the GTEx portal (www.GTEXprotal.org).

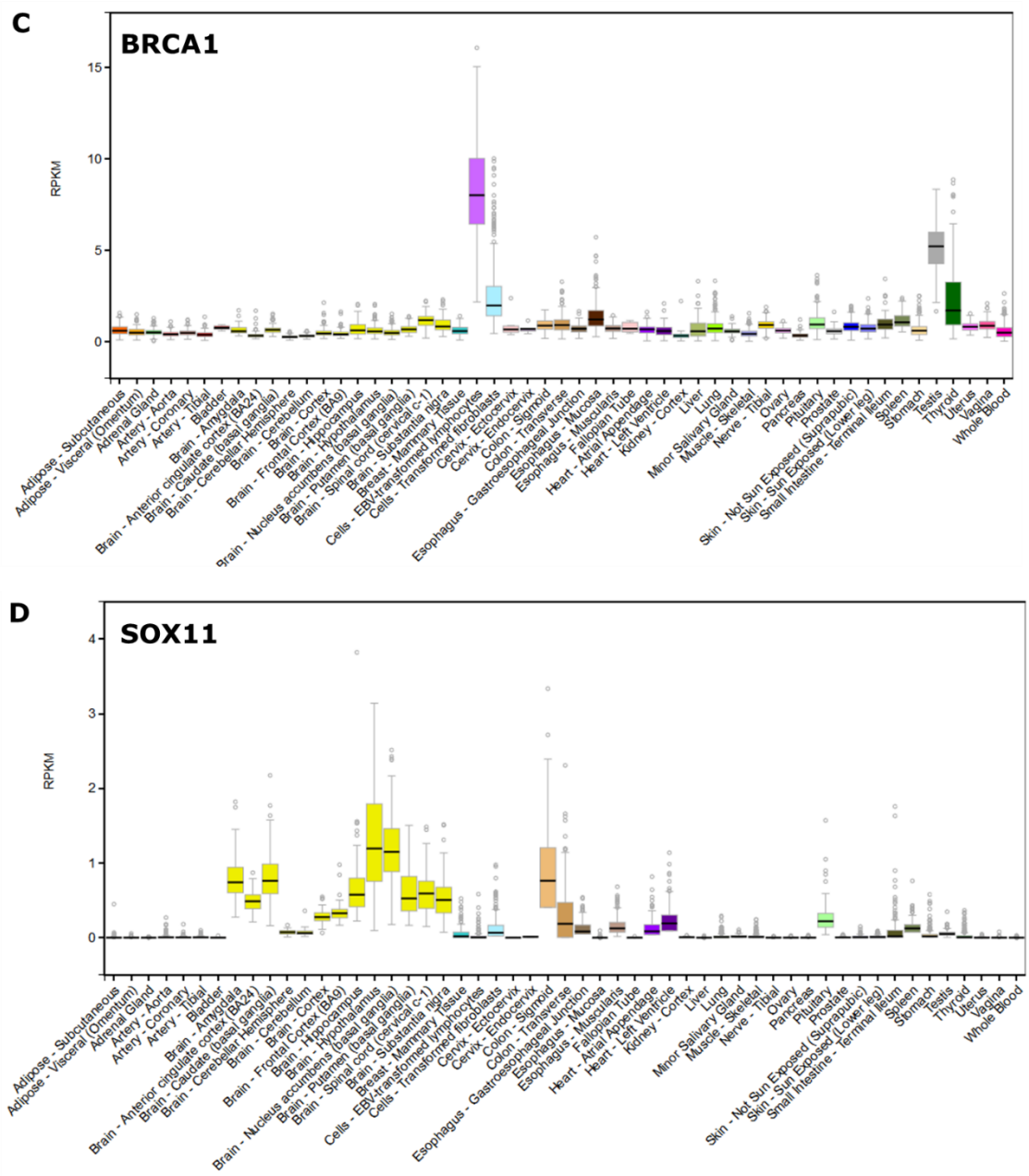

Figure 4.4 (continued) Gene expression (RNAseq data) in healthy tissues of peptides identified in the DU145 HLA ligandome. (C, D) Examples of tissue expression and distribution of genes oncogenes (designated 'cancer panel' in the ligandome dataset) BRCA1 and SOX11.

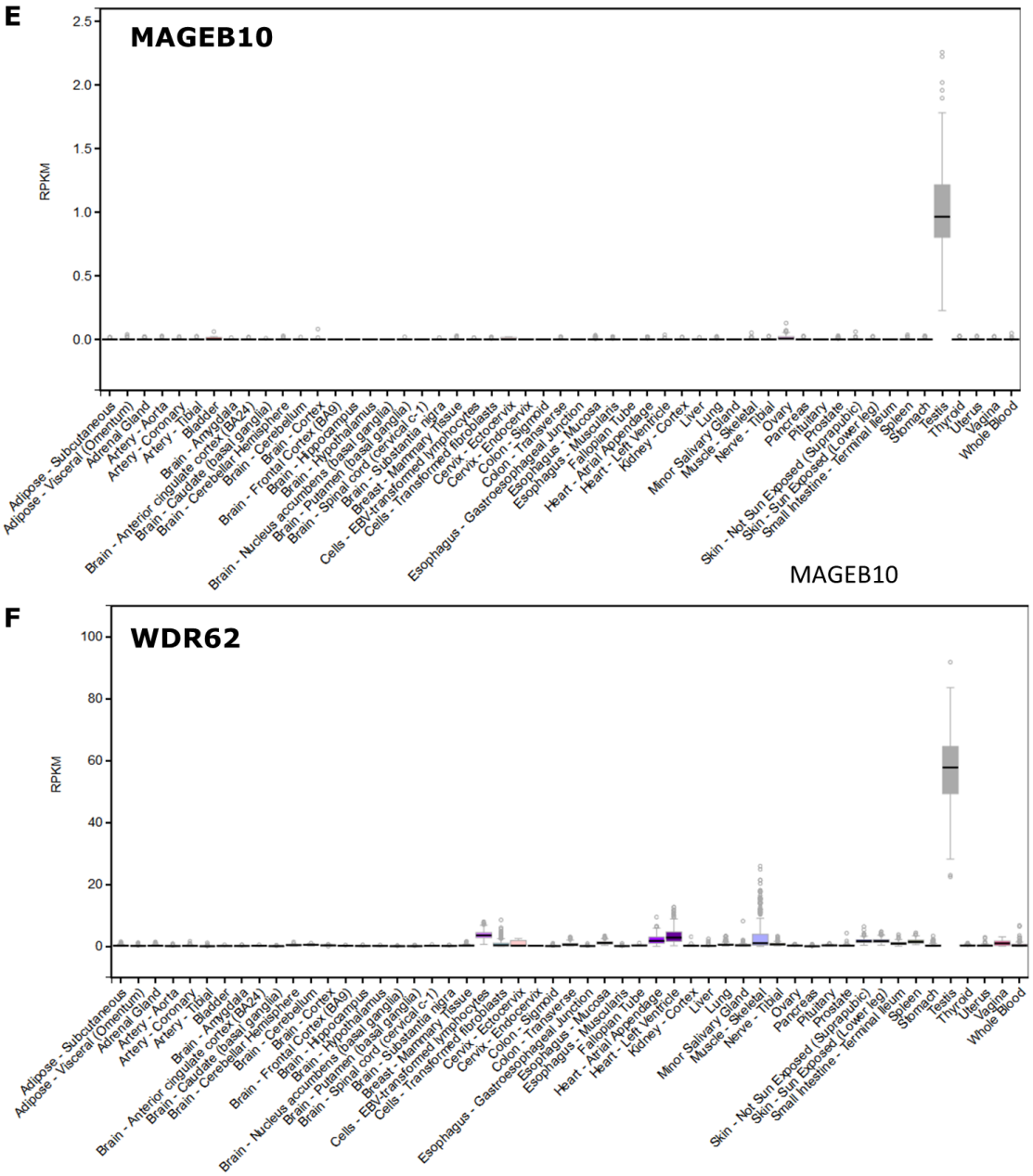

Figure 4.4 (continued) Gene expression (RNAseq data) in healthy tissues of peptides identified in the DU145 HLA ligandome (E, F) Examples of cancer testis antigens, MAGEB10 and WDR62.

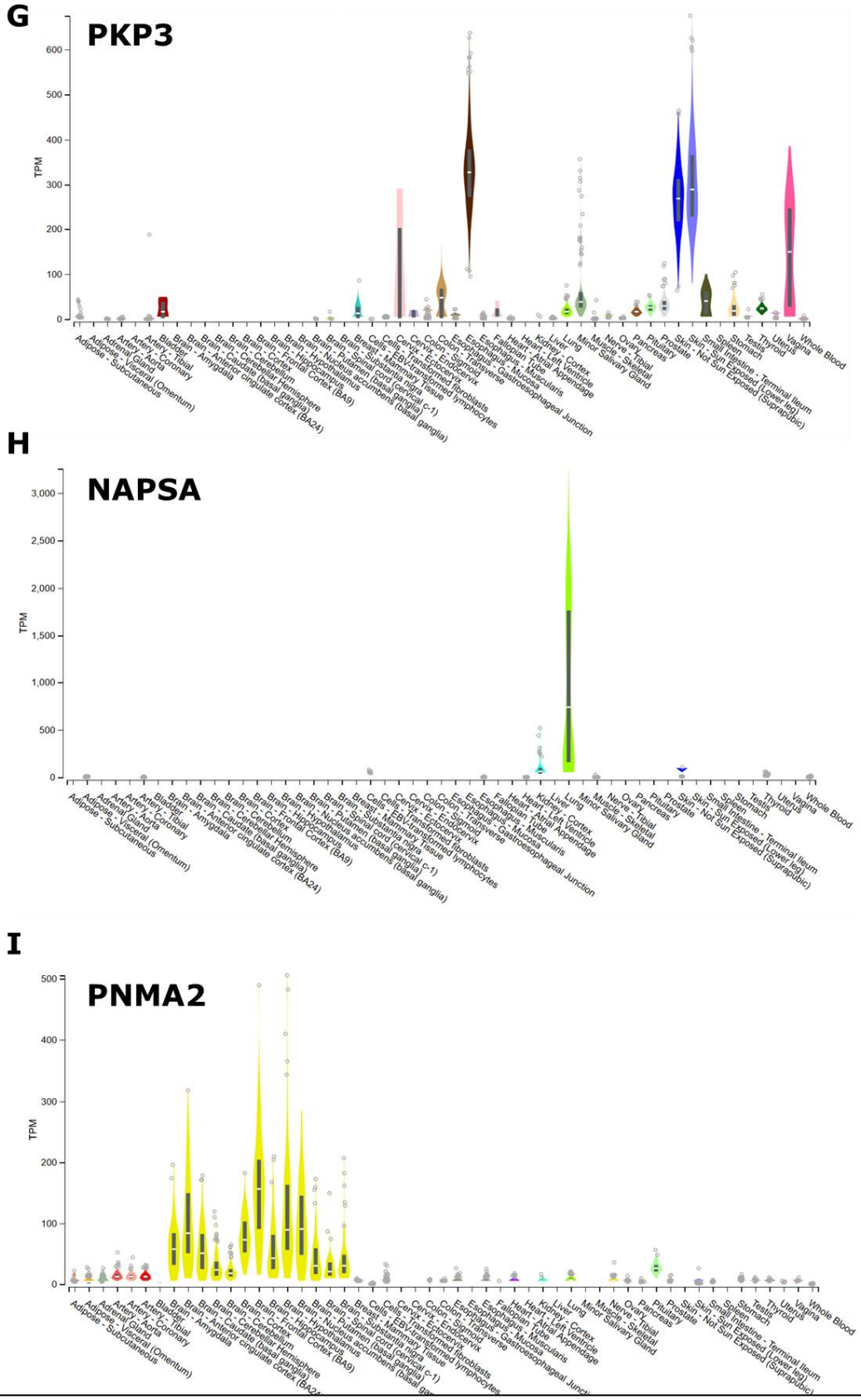

Figure 4.4 (continued) Gene expression (RNAseq data) in healthy tissues of antigens identified in the DU145 HLA ligandome (G, H, I) Examples of peptides excluded based on high gene expression; PKP3, NAPSA, PNMA2.

4.7.2 HLA allele binding assignment and selection of high binding affinity peptides

As previously mentioned, the HLA ligandome analysis was carried out using a pan-HLA Class I antibody. The allele specific binding of the identified sequences was therefore not known. HLA-peptide binding affinity is a contributing factor to T cell stimulation (Reichstetter et al., 1999), and can be directly measured *in vitro* using soluble synthetic peptides and recombinant HLA molecules (Sette et al., 1994). Alternatively, *in silico* methods can be used to predict peptide binding affinities to HLA Class I. This involves the use of algorithms which are trained to make predictions based on available experimental data. This predictive approach was used to (a) to determine the cognate HLA allele of the peptides of interest, and (b) to identify high affinity binding sequences. The HLA-C alleles were not included in the affinity binding analysis as the HLA-C alleles of the healthy donors recruited to this study were not determined.

The HLA binding affinity was determined using the Immune Epitope Database (IEDB) Analysis Resource (https://www.iedb.org/) (Vita et al., 2019). The 'netmhcpan' binding predictor was used to predict the peptides expected to bind HLA-A*33:03 and HLA-B*50:01 and the consensus artificial neural network (ANN)/ Stabilized matrix method (SMM) predictor was used to assign binding for HLA-B*57:01, as recommended by the IEDB site. It must also be noted that inconsistencies regarding the HLA type of the DU145 cells were encountered in the course of assigning allele specific peptide binding. The database used in this study, the TLCP, (Scholtalbers et al., 2015), indicates the DU145 cells are HLA-A*33:03 homozygous. However, another web directory of cell line information, Cellosaurus (https://web.expasy.org/cellosaurus/) (Bairoch, 2018), indicates DU145 cells to be positive for HLA-A*03:01 and HLA-A*33:03. The source of the DU145 HLA type data are studies by Boegel and colleagues, published in 2014 and Adams and colleagues, published in 2005, for the TLCP and Cellosaurus, respectively (Adams et al., 2005; Boegel et al., 2014). The study by Boegel and colleagues collected publicly available next generation sequencing (NGS) RNASeq data to determine the HLA types of the cell lines investigated, while Adams and colleagues used Sequence Based typing, an approach combining

PCR based amplification and sequencing (Adams et al., 2004), therefore the discrepancy could be attributed to the results generated by different technical approaches. The HLA type of DU145 cells used in a previous study in our lab, analysed by PCR (by the Wales Blood Transfusion service) indicated the cells to be positive for HLA-A*03:01 and HLA-A*33:03. The DU145 cells used to generate the ligandome data were newly purchased from ATCC specifically for the ongoing project and were used at passages ranging from approximately p24 to p35 to generate the DU145 HLA ligandome data. HLA typing was not experimentally determined, due to the assumptions of the HLA type based on the previously used cells. Nevertheless, initial HLA allele specific binding predictions for the DU145 HLA ligandome dataset were based on assumptions from the TLCP. A comparison of the 9mer peptides in the DU145 dataset, (independent of the RPKM cut-offs), (n=422), showed that 250/251 of the peptides in the 1st percentile binding rank were assigned specific binding to HLA-A*33:03. The identification of so few HLA-A*03:01 ligands from the DU145 cells may suggest that HLA-A*03:01 expression is downregulated during *in vitro* culture. This is an important consideration for studies using this cell line to investigate potential epitopes for immunotherapy in PCa.

The affinity binding results, based on the DU145 HLA type being HLA-A*33:03 (homozygous), HLA-B*50:01, HLA-B*57:01 are shown in Table 4.2. Not unexpectedly, the 9mer sequences represented the greatest proportion within the 1st percentile binding rank. It has been shown that antigen processing machinery within cells preferentially trims peptides to 9mer lengths (Chang et al., 2005), although some longer peptides are produced, as suggested by allele specific preferential binding of greater length peptides (e.g. HLA-A*01:01; >12 amino acid peptides) (Gfeller and Bassani-Sternberg, 2018). Of the 142 peptides selected based on absence or low healthy tissue expression of the associated antigen, 45 peptide sequences occurred within the 1st percentile binding rank or had netmhcpan IC50 value <500nM. These were then experimentally evaluated as potential CSC antigens, which is described in the next chapter. The selection process arriving at the antigens which will be tested for CSC expression is summarised in Figure 4.5.

Table 4.2. HLA Class I-peptide binding affinity prediction using the IEDB database. Binding affinity of peptides to either of HLA-A*33:03 and HLA-B*50:01 was determined by the netmhcpan predictor and by the Consensus (ann/ smm) predictor for HLA-B*57:01. The prediction method used was determined automatically by selecting the 'IEDB recommended' option, which selects the predictor based on the existing data of the effective performance of a particular predictor for a particular allele. The cut-off for optimal affinity, based on guidelines from the IEDB, was 1st percentile rank, or IC50<500 nM, where applicable (i.e. HLA-A*33:03 and HLA-B*50:01). Peptides within the 1st percentile binding rank/ IC50< 500nM; arranged in increasing percentile rank.

Percentile rank	Allele	Sequence	Sequence Length	Gene	netmhcpan_ic50
0.1	HLA-B*50:01	REAQFGTTA	9	CRBN	65
0.1	HLA-B*50:01	REMIPFAVV	9	SEPT9	61
0.2	HLA-B*50:01	RESPFSTSA	9	XPO1	132.1
0.2	HLA-A*33:03	SSYFRIHER	9	ZNF14	11.2
0.2	HLA-B*50:01	REHQNFYEA	9	ARHGAP42	177.4
0.2	HLA-B*50:01	VERSFILSA	9	FGD6	140.3
0.2	HLA-B*50:01	AETEFFSKA	9	STIL	200.2
0.25	HLA-B*57:01	STFDSPAHW	9	EGFR	-
0.25	HLA-B*57:01	YSIRGQLSW	9	SMARCB1	-
0.3	HLA-A*33:03	EYIKTWRPR	9	AKT2	15.1
0.3	HLA-A*33:03	EMREMLTHR	9	HIF1A	15.3
0.3	HLA-A*33:03	EVFDFSQRR	9	NFE2L2	21.3
0.3	HLA-A*33:03	WYKHVASPR	9	NPW	27.5
0.3	HLA-A*33:03	SYRKFLNLR	9	SHCBP1	22.9
0.3	HLA-A*33:03	ESQDRKIFR	9	BRCA1	24.1
0.3	HLA-B*50:01	KEYENLKEA	9	TRAIP	218.3
0.3	HLA-A*33:03	EYFADMKRHR	10	TOP2A	50
0.35	HLA-B*57:01	KSFEDIHHY	9	KRAS	-
0.4	HLA-A*33:03	EAVLWEALR	9	MAGED4	36.7
0.4	HLA-A*33:03	EFKKLIRNR	9	RLN2	32.6

0.4	HLA-A*33:03	EVKSITKER	9	CENPE	36
0.4	HLA-A*33:03	ETLLRLLLR	9	ASAH2B	32.1
0.4	HLA-B*50:01	AEHFSMIRA	9	MEX3A	332.5
0.4	HLA-A*33:03	EYFTLQIRGRER	12	TP53	177.7
0.5	HLA-A*33:03	YFADMKRHR	9	TOP2A	40.5
0.5	HLA-B*50:01	AEIAKLKAA	9	KIF14	343.9
0.6	HLA-A*33:03	EYMTPSSR	8	CBL	617.6
0.6	HLA-A*33:03	EINAILQKR	9	MTR	49
0.6	HLA-A*33:03	ETYLLEKSR	9	MYH8	55.7
0.6	HLA-A*33:03	EFEAVLTER	9	CCDC127	49.1
0.6	HLA-A*33:03	EIKELGELR	9	TACSTD2	49.2
0.7	HLA-B*50:01	GEFTGWEKV	9	RIPK4	469
0.7	HLA-A*33:03	DFHFRTDER	9	TPX2	61.6
0.7	HLA-A*33:03	NYLEDRRLVHR	11	EGFR	468.8
0.7	HLA-A*33:03	EYLEKKNFIHR	11	ABL1	505.3
0.7	HLA-A*33:03	VTAMDVVYALKR	12	HIST1H4A	471.9
0.8	HLA-A*33:03	EYVEFEVKR	9	MTOR	84.3
0.8	HLA-B*57:01	KTLERSYLL	9	RRM1	-
0.8	HLA-A*33:03	NIQGITKPAIR	11	HIST1H4A	539.1
0.9	HLA-A*33:03	EAKAPILKR	11	TPR	98
1.2	HLA-A*33:03	EYLEKQRNR	9	MSH6	145.1
1.3	HLA-A*33:03	TSTVPLVGR	9	WDR62	169.2
1.45	HLA-B*57:01	SAFPEVRSL	9	THADA	-
1.5	HLA-A*33:03	DYKKIPIKR	9	MAGED4	200.4
1.6	HLA-A*33:03	DYPDYKYRPR	10	SOX11	272.1
1.7	HLA-A*33:03	DYHTLPRAR	9	ATP9B	273.1

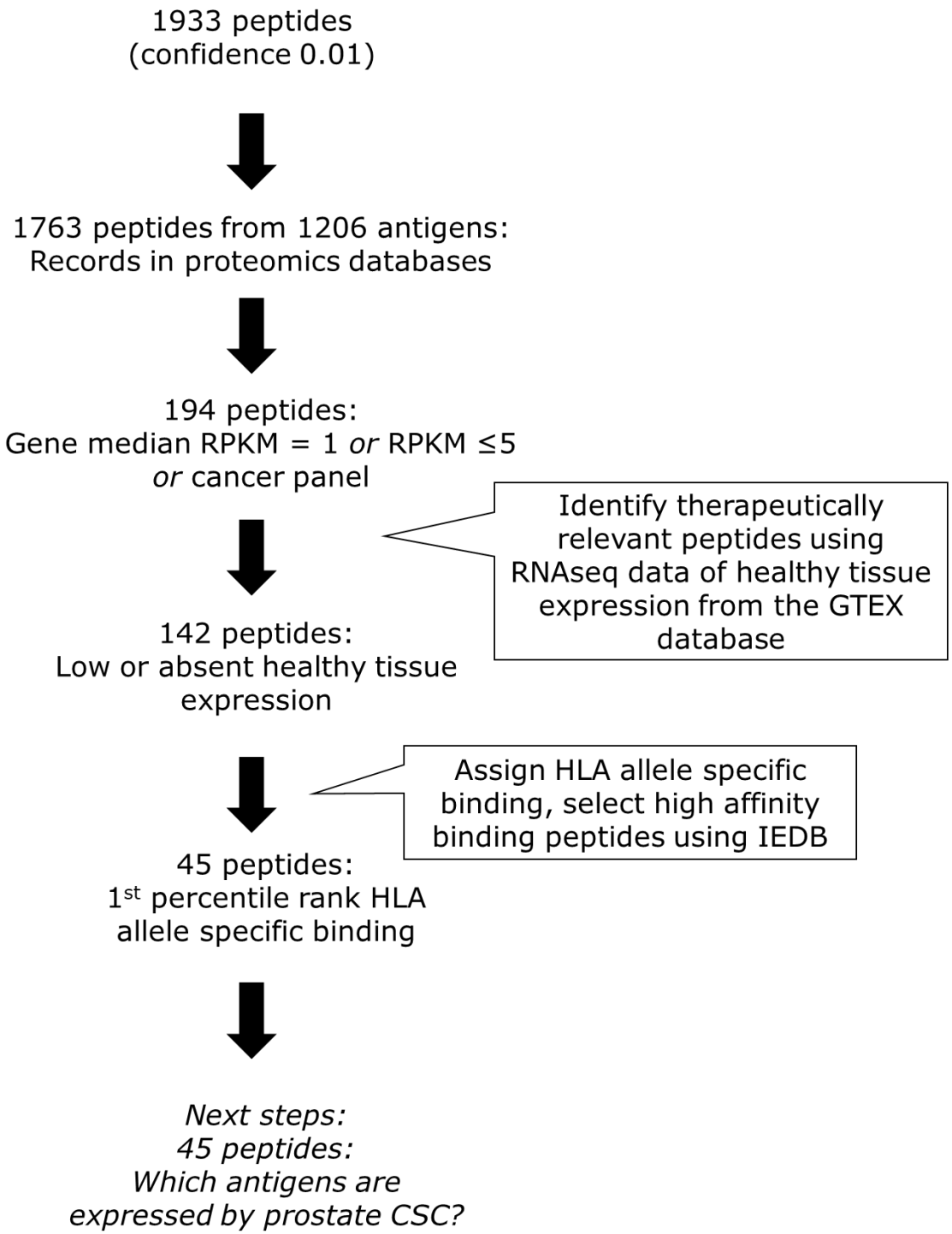

Figure 4.5 Summary of bioinformatic analysis of the DU145 HLA ligandome.

4.8 Discussion

Large scale investigation of the HLA ligandome by peptide elution and mass spectrometry was developed in the early 1990s (Hunt et al., 1992). In this way, viral and endogenous peptides processed intracellularly and presented in the context of HLA were confirmed as the means by which T cells recognise antigens (Rötzschke et al., 1990; Van Bleek and Nathenson, 1990). Further studies using this technique identified the contribution of different HLA alleles in shaping the presented peptide repertoire and the corresponding peptide motifs associated with certain HLA alleles (Falk et al., 1991). Additionally, mass spectrometry was used to identify an epitope recognised by patient derived melanoma specific cytotoxic T cells (Cox et al., 1994). Currently, more than 100,000 HLA ligands have been described by mass spectrometry analysis of the peptides presented by HLA at the cell surface; this has recently surpassed the number of peptide sequences derived by predictive methods (Gfeller and Bassani-Sternberg, 2018). While these data do not all represent peptides for which the allele-specific interactions have been elucidated, nor has the immunogenicity of the peptides been widely established, these data are an important resource which could be exploited for epitope and antigen discovery for therapeutic applications.

The data described in this chapter represent an important addition to the total set of known HLA ligands, specifically in the context of the cell source of ligands (PCa), and the HLA alleles investigated. HLA ligandome analysis has been carried out using cells (primary or cell lines) from a number of cancer types, including melanoma, leukaemia (CLL and AML), colorectal cancer, renal cancer and ovarian cancer, in many cases resulting in the identification of novel epitopes (Berlin et al., 2015; Kochin et al., 2017; Kowalewski et al., 2015; Pritchard et al., 2015; Schuster et al., 2017; Stickel et al., 2009). Few studies have directly investigated peptides presented by PCa cells. Peptides derived from histone antigens have been identified in a mouse model of PCa (Savage et al., 2008). A limited number of short peptides (5-6mer) obtained by acid elution from the LNCaP cell line were analysed by mass spectrometry (Kamata et al., 2013). Acid elution of HLA bound peptides was used prior to the development of immunoaffinity purification of HLA-peptide complexes;

this method is considered highly susceptible to contamination by peptides that are not bound to HLA molecules (Mester et al., 2011). The length of the peptides in the study by Kamata and colleagues is attributed to acid degradation of the peptides (Kamata et al., 2013). Low yield of peptides may also be due to the low levels of HLA expression which have previously been described in LNCaP cells (Carlsson et al., 2007). In another study, PC3 cells were transfected to produce soluble HLA Class I from which eluted peptides were analysed (Barnea et al., 2002). This method is considered particularly susceptible to misrepresentation of the natural HLA ligandome, as transfection of the cells leads to artificially high HLA Class I expression (Mester et al., 2011). Therefore, to our knowledge, this study is the first description of a large-scale HLA ligandome, derived by immunoprecipitation, from PCa cells.

While the identification of peptides presented by prostate CSC is a primary aim of my study, it was not possible to specifically analyse peptides presented by CSC by mass spectrometry, owing to the large number of cells required to perform the experiment (approximately 10^9 cells). It was not possible to achieve this cell number of the CSC and non-CSC populations by FACS. Different strategies employed by the few studies which have directly analysed CSC HLA ligandomes are discussed in Chapter 5. Therefore, in this chapter, analysis of the HLA ligandome dataset of the DU145 cells focuses on identifying peptides derived from therapeutically relevant antigens and assigning HLA allele binding specificity. Analysis of my ligandome data largely followed the approach taken in the aforementioned studies, with some modifications that related to differences in the cellular material used and the HLA alleles investigated.

Firstly, to determine which peptides were derived from proteins that could potentially be effective therapeutic targets, I investigated gene expression in the GTEx database of RNAseq data. The majority of HLA ligandome data published has identified peptides from non-mutated, self-proteins, as the mass spectrometry data is annotated from databases of normally expressed proteins. Identification of neoepitope peptides requires de novo generation of

proteomic data from mutated cells to compare to the mass spectrometry data. This approach is best suited to cancers that have a high mutational burden; and has recently been carried out in melanoma (Bassani-Sternberg et al., 2016; Kalaora and Samuels, 2019). Nevertheless, self-antigens remain important potential immunotherapy targets. Other studies that investigated the HLA ligandome of primary tumour tissues carried out comparative analyses of corresponding healthy primary tissues or cell lines, to determine antigens which were exclusively expressed in the tumour tissue (Berlin et al., 2015; Kowalewski et al., 2015; Schuster et al., 2017). Primary material from prostate tumours is very limited; even more so biopsy material from healthy prostate, owing to the invasiveness of obtaining the material. This necessitated the use of the DU145 cell line which was characterised in Chapter 3. A healthy prostate cell line was not readily available in my study; therefore, the database search represents a surrogate for investigating healthy tissue expression of candidate antigens. Since the prostate is a non-essential organ, it is also suggested that comparative analysis of benign prostate tissue may not be prioritised to the same degree that is required of essential tissues to identify therapeutically applicable antigens. The GTEx portal has previously been used in studies which investigated tissue matched HLA ligandomes, to more widely explore the tissue distribution of the antigens of interest (Löffler et al., 2018; Schuster et al., 2017).

The use of the GTEx portal in my study was a subjective approach to identifying potential therapeutic antigens, compared to quantitative comparison of healthy and disease stage HLA ligandomes. Therefore, it is acknowledged that this could exclude potential antigens, or incorrectly include antigens which have the potential to cause off-target damage despite limited healthy tissue expression. However, the recent case of cardiotoxicity resulting from cross-reactivity to an epitope from a confirmed tumour antigen (MAGEA3) (Linette et al., 2013; Raman et al., 2016), highlights a situation in which despite every care taken to limit targeting to tumours, off-target damage remains a risk in immunotherapy. Manual examination of gene expression and tissue distribution is not particularly suitable for large scale studies of multiple patient derived samples or of multiple different tissue types. However, inspection of the GTEx portal data also provided the

opportunity to identify tissue enhanced antigen expression, which was not immediately evident from ranking the median RPKM data incorporated into my analysis. Examples identified in this study were cancer testis antigens WDR62, DDX43 and TRIP13. Similarly, high antigen expression, which was limited to one to two tissues, which had an otherwise low median RPKM (e.g. RYR2, NAPSA) could be excluded by this manual approach. Therefore, this approach could be applied as a first step in small scale HLA ligandome analyses, for which comparative healthy samples are limited.

The next stage was assigning HLA allele specificity to the peptides in the dataset. HLA Class I-peptide complexes have been isolated using either allele specific or pan-HLA Class I antibodies previously. The use of an allele specific anti-HLA antibody for immunoprecipitation is mainly suitable for cells transduced to express high levels of a single HLA allele. Isolating ligands from a single HLA allele removes the requirement for, and potential bias introduced by *in silico* prediction of allele specific binding (Kochin et al., 2017). Investigation of the HLA ligandome of a single HLA allele for therapeutic antigen discovery is best applied for alleles for which there is a high population distribution, such that the peptides identified could be tested in a large population e.g. HLA-A*02 and HLA*A24. HLA-A*02 has a population frequency of >25% population frequency in North and South America, Europe, Russia and China. HLA-A*24 is found in >25% of the population Japan and Malaysia, 10-25% population frequency in South America, Mexico, India and 10% in Europe (these data are from the HLA allele frequency database http://www.allelefrequencies.net/ (Gonzalez-Galarza et al., 2011)).

The use of a pan-HLA Class I antibody results in capture of a larger number of HLA-peptide complexes than immunoprecipitation of a single allele specific antibody and is suitable for HLA ligandome analysis of both frequent and rarer HLA alleles. The population frequency of the HLA alleles expressed by the DU145 cells is HLA-A*33: 10-25% of the population in studies from North East Asia, South Asia, South East Asia, Indonesia and USA (Asian populations) (<10% in other regions). Globally HLA-B*50 positive population frequency is <10% in all regions with the exception of populations in Western

Asia (Saudi Arabia) and in Tunisia; similarly HLA-B*57 positive frequency is <10% globally, with the exception of small sized studies in the Venezuelan and Indian populations (10-25%) (all allele frequency data obtained from the HLA Allele frequencies database http://www.allelefrequencies.net/) (Gonzalez-Galarza et al., 2011). Therefore, the pan-HLA Class I antibody was the most suitable approach for immunoprecipitation.

There are a number of algorithms which can be used to predict HLA allele specific binding. The SYFPEITHI database is widely used in HLA ligandome studies (Berlin et al., 2015; Kamata et al., 2013; Kowalewski et al., 2015; Stickel et al., 2009). This was the first established database of HLA/ MHC motifs; it hosts a prediction algorithm which is based on binding data of peptides eluted from mono-allelic cells (Rammensee et al., 1999). Predictions for HLA-A33:03 binding were not available from this database, so it was not suitable for use with the DU145 cell ligandome. Instead, the IEDB database (www.iedb.org) was used (Vita et al., 2019). This database provides a range of algorithm options, including the facility to make predictions based on the NetMHCpan algorithm (another commonly used prediction database (Hoof et al., 2009)). Guidance from the IEDB ranks the performance of the difference predictions as Consensus > ANN (artificial neural network) > SMM (stabilised matrix network) > NetMHCpan > CombLib (combinatorial libraries). The consensus method indicates the agreement of ANN, SMM and CombLib in making a prediction. The Consensus method was used to assign peptide binding to HLA-A*33:03 and HLA-B*50:01 and the NetMHCpan method was used to predict binding to HLA-B*57:01.

ANN and SMM predict binding affinity based on the binding energy contributed by the amino acid at each position (Nielsen et al., 2003). In general, the difference between ANN and SMM is that ANN considers interactions between amino acids in the different positions of a peptide sequence in predicting the contribution to binding, while SMM considers the contribution of the amino acids in the different positions independently, without accounting for steric interactions (Nielsen et al., 2003; Peters et al., 2003). These algorithms are trained to consider the binding contribution of each amino acid in the context

of affinity data derived from HLA ligand binding assays, and can integrate recognition of patterns and motifs within the ligand dataset to predict the expected binding of ligands for which there is no affinity binding data. The most recent update of the NetMHCpan algorithm is trained on affinity data from experimental HLA ligand binding assays and also on data from elution assays (i.e. ligands identified in mass spectrometry studies) (Jurtz et al., 2017).

However, the performance of the different predictors is also based on the data availability for training. Allele binding predictions can be biased towards making the most accurate predictions only for HLA alleles which are well represented in ligandome or binding affinity datasets, or have well characterised binding motifs (Antunes et al., 2018; Freudenmann et al., 2018). Training algorithms based on HLA ligandome data can facilitate binding predictions of a wider range of alleles, compared to the laborious process that would be required to achieve the same coverage of allele predictions by production of synthetic peptides and performing binding affinity assays. Algorithms that are trained using HLA ligandome data are also more likely to encounter a wider range of peptide lengths, and have the benefit of recognising sequences which occur as the end result of antigen processing, compared to binding affinity data obtained from synthetic peptides which may not be biologically occurring.

As previously mentioned, the different algorithms used to make the binding predictions for HLA-A*33:03, HLA-B*50:01 and HLA-B*57:01 respectively were based on automatic selections by the 'IEDB recommended' prediction method option. Since the NetMHCpan algorithm makes predictions based on both experimental binding assay and eluted ligand data, this suggests that there is a greater availability of these data for HLA-B*57:01 than for HLA-A*33:03 and HLA-B*50:01. A comparison of the 1st percentile predictions for HLA-A33*:03 and HLA-B*50:01 binding made by the IEDB consensus approach with the NetMHCpan predictions, showed no difference in the alleles assigned to the peptides. The NetMHCpan prediction algorithm provides data on the 'distance' from the training data used to make a binding affinity

prediction. The HLA-B*50:01 and HLA-B*57:01 predictions were made using training data from the same alleles, while the HLA-A*33:03 predictions were made based on training data from HLA-A*33:01. While it has been suggested that extrapolating binding predictions to alleles, for which there is no experimental data, may result in inaccuracies; the agreement of binding specificities predicted by two separate methods suggests that both structural data and experimental binding affinity could be used to assign binding for the alleles used in this study. Ultimately, there is less 'risk' associated with the use of predictive algorithms to assign HLA allele specific binding to eluted ligands, i.e. sequences which are known to be produced as the end products of antigen processing, compared to using such algorithms to generate *de novo* peptide sequences for experimental testing.

While not the focus of this study, HLA-C*06:02 ligands which may be present in the DU145 dataset could also represent novel tumour targets. HLA-C typically has lower cell surface expression than other HLA-I alleles, and has been associated with the presentation of self-peptides which are recognised by autoimmune T cells (Mobbs et al., 2017). The level of population data on this allele is lower than the other alleles of the DU145 cell line, however is expressed in 10-25% of the population surveyed in certain regions of North and Sub-Saharan Africa, Western, South and Northern Asia and also in Asian populations in North America (http://www.allelefrequencies.net). HLA-C alleles have dual functionality; in addition to peptide presentation, HLA-C molecules are ligands of Killer immunoglobulin-like receptors (KIRs), expressed mainly by NK cells but also by some subsets of T cells (Littera et al., 2017). HLA-C activation of receptors may serve a protective role by inhibiting NK cell recognition of tumour cells; however T cells recognising HLA-C epitopes of tumour antigens have been isolated from melanoma patients (Zhu et al., 2012), which suggests that the T cell response is also relevant to elimination of tumour cells by HLA-C mediated antigen presentation.

The *in-silico* methods described here to interrogate the DU145 HLA ligandome dataset represent a basic bioinformatics toolkit for analysing peptide data.

Given the benefit of more time, this dataset could yield further insight by manual examination; additionally there are a number of strategies more in-depth analysis in future. This dataset was compiled from n=1 experiment due to the large number of cells (and associated cell culture resources) required to generate the raw data. However, preliminary validation using the IEDB (https://www.iedb.org/) (Vita et al., 2019), showed that 23/45 (51%) of the predicted high affinity peptides listed in Table 4.2, have been previously described in at least one publication. The DU145 HLA ligandome could be further validated by repeated analysis and selection of only those peptides recurring in at least three repeated experiments.

Further descriptive analysis of the dataset that could be carried out *in-silico* includes saturation analysis, which gives a measure of the coverage of the total human proteome represented by the source proteins in the dataset (Meyer et al., 2011; Walz et al., 2015). This could be used to identify proteins from which peptides are more commonly presented, which could focus future antigen discovery efforts. Gene ontology analysis could also be carried out on the DU145 HLA ligandome database. An example of a bioinformatics tool suitable for this is the PANTHER pathway database algorithm (http://www.pantherdb.org/) (Mi and Thomas, 2009); this functions similarly to the DAVID pathway database (Huang et al., 2009b) used in Chapter 3 (Figure 3.32) however the former is more suited to analysis of larger datasets. The use of the PANTHER database in previous studies of the HLA ligandome found diverse enrichment results in the respective datasets (Löffler et al., 2018; Müller et al., 2017). Löffler and colleagues identified enrichment of genes associated with Wnt, TGF-β p53 and Pi3K signalling in the HLA ligandome of CRC samples compared to non-malignant colon samples (Löffler et al., 2018). In contrast, Müller and colleagues identified enrichment of general cellular processes, including ribosome, cytoskeleton, endosome, Golgi apparatus and nucleus (Müller et al., 2017). However, these terms were derived from a broader ligandome dataset which included both tumour and non-malignant lymphocyte samples. Since PCa is a heterogeneous disease, it may be necessary to analyse further samples e.g. cell lines derived from different pathological sites, to determine if there are any disease-associated pathways from which peptides are sampled in the respective HLA ligandomes.

It would also be informative, particularly due to the rare HLA alleles analysed in the DU145 HLA ligandome, to analyse the peptide motifs in more depth; this could be achieved with the use of the computational approach described by Bassani-Sternberg and colleagues (Bassani-Sternberg et al., 2017). In their study they developed an algorithm to assign peptide motifs to specific HLA alleles, based on available data in the IEDB. Motifs are mapped by comparing peptides obtained from samples which express the same HLA allele (Bassani-Sternberg et al., 2017).

As previously discussed, due to lack of available healthy prostate cell models, it was not possible to perform a comparative HLA ligandome analysis of healthy tissue to allow for comparative analysis of peptides presented in cancer vs healthy cells, such as those carried out by previous studies (Bilich et al., 2019; Kowalewski et al., 2015). An alternative bioinformatics approach could involve querying the peptides from the DU145 HLA ligandome dataset against a database of peptides presented by healthy cells, such as the recently developed 'HLA Ligand Atlas' (https://hla-ligand-atlas.org), which was compiled from multiple studies in which HLA ligandome analysis of healthy tissues was carried out for comparative analysis purposes (Marcu et al., 2019).

In summary, HLA ligandome analysis of DU145 cells identified a large dataset of novel HLA-presented peptides and associated antigens. These data could be used to improve allele binding prediction algorithms and for the development of PCa immunotherapy strategies. The ligands described represent a significant expansion of the data relating to alleles which are under-represented in the IEDB database (Mester et al., 2011). The dataset was interrogated to identify potential therapeutic targets, based on absence of or low expression in healthy tissues, and high affinity peptides were selected for further analysis. This subset of antigens will be further investigated, experimentally, to identify potential CSC antigens.

Chapter 5.

Validation of CSC antigens and investigation of T cell responses to CSC peptide epitopes

5 Validation of CSC antigens and investigation of T cell responses to CSC peptide epitopes

5.1 Introduction

In this study, the aim was to identify antigens which were specifically expressed by CSC, so that T cell targeting of CSC could be investigated. As previously discussed, CSC-presented peptides were not directly analysed by mass spectrometry due to the prohibitively large number of cells (10^9) required. Therefore, this chapter focuses on identifying and validating candidate CSC antigens selected from the DU145 ligandome (Chapter 4). To achieve this, I used ALDH, the prostate CSC marker defined in Chapter 3, to sort DU145 cells into sub-populations (ALDH high/CSC and ALDH low/non-CSC) to investigate expression of individual antigens. It has been suggested that T cell targeting of CSC antigens, compared to antigens shared between CSC and non-CSC, may be more efficient, due to the more favourable T cell: target ratio (Hirohashi et al., 2012). However, targeting 'shared' antigens could also be beneficial to achieve greater tumour clearance, and potentially reduce immune inhibitory signalling in the TME that reduces the efficacy of T cell treatments. Therefore, both CSC and shared (between CSC and non-CSC) antigens were investigated.

In this chapter, T cell recognition of selected CSC antigens was investigated with T cells from healthy donors. These donors were not expected to have pre-existing exposure to the peptides tested, as the antigens selected were tumour associated and was expressed at low levels in healthy tissue. However the naïve T cell repertoire, containing infrequent T cells that collectively recognise a vast variety of peptides could be expected to include T cells capable of recognising the peptides of interest (Houghton and Guevara-Patiño, 2004). CSC immune evasion was also considered; therefore, the expression of HLA by CSC was investigated. Following isolation of T cells using from the healthy donor PBMC using HLA-peptide tetramers, T cell

responsiveness to the peptides presented by model target cells and CSC was investigated.

Question

Can T cells recognise and respond to CSC antigens based on peptide presentation by relevant target cells?

Aims

- Identify antigens from the DU145 HLA ligandome peptide dataset which are expressed by prostate CSC
- Isolate T cells specific for peptides from candidate CSC antigens
- Test the capacity of peptide specific T cells to recognise and respond to peptides presented by target cells

5.2 Validation of candidate antigen expression by prostate CSC

Analysis of the DU145 ligandome defined 45 gene products as candidate antigens (Chapter 4). To identify potential CSC antigens, the expression of the 45 genes was investigated by qRT-PCR in both ALDH high (CSC) and ALDH low (non-CSC) DU145 cells. Candidate CSC antigens were selected as those for which the statistically significant gene upregulation was >1.5 fold in ALDH high compared to ALDH low DU145 cells obtained from at least 2 out of 3 repeated FACS experiments. The fold change data from cells obtained in n=1 of the FACS sorts is shown in Figure 5.1A (some genes on this graph were upregulated in only 1 out of 3 repeated FACS experiments thus were not considered 'CSC antigens'). The fold change and significance values for all of the genes investigated are detailed in Table 5.1. The CSC antigens fitting the criterion for significance were ARHGAP42 and SHCBP1. As there were so few antigens upregulated in the ALDH high DU145 cells, 'shared antigens' were selected from the most abundant genes in both the ALDH high and ALDH low cells, based on calculating the number of transcripts (Figure 5.1B). The selected antigens ranked within the highest abundance in at least 2 out of 3 FACS experiments. These were SEPT9, NFE2L2, XPO1, TOP2A, AKT2, and TPX2. Additionally, while not consistently upregulated in ALDH high cells, the RLN2 was further investigated due to its prostate tissue gene restriction (indicated by data from GTEx database (www.GTExportal.org)).

Antigen expression was also investigated by qRT-PCR in ALDH high and ALDH low primary PCa cells, to determine the possibility of peptide presentation by primary PCa CSC. It was not possible to investigate all of the genes analysed in the DU145 cells due to the limited cell numbers obtained from FACS of the primary PCa cells. Therefore, it was only the genes found to be upregulated in CSC or selected as abundant shared antigens, in the DU145 cells, for which the gene expression was also investigated in primary PCa cells. In the primary PCa cells, TPX2, SCHBP1 and TOP2A were significantly upregulated >1.5 fold in the ALDH high compared to the ALDH low cells (Figure 5.2A; showing data from one of the 3 biological replicates investigated). The abundance of these

antigens was also investigated; SEPT9 and XPO1 were highly abundant (Figure 5.2B).

Figure 5.1. Selection of antigens upregulated in ALDH high DU145 cells (CSC antigens) and antigens highly abundant in ALDH high and ALDH low cell (shared antigens). Gene expression data shown consist of the fold changes observed for each of the 42 genes in PCR reactions carried out using the cDNA produced from cells sorted in n=1 FACS experiment (3 FACS experiments were carried out). (A) Identification of CSC antigens by PCR. Gene expression for myosin 8 (MYH8) was not detected across 3 separate FACS sorts and is not shown. The genes coloured green were significantly upregulated >1.5 fold in sorted ALDH high cells from 2/3 independent FACS experiments. Statistical significance is not shown for genes that did not meet this criterion. Statistical analysis of the gene expression was by paired T test. (B) Selection of 'shared' antigens; i.e. expressed by both CSC and non-CSC, identified as the most abundantly expressed genes in both the ALDH high and ALDH low DU145 cells. Data shown corresponds to the abundance data from the same experiment shown in (A). In both (A) and (B), error bars represent mean ±SEM of technical replicates from one PCR reaction (of cDNA from one FACS experiment).

A

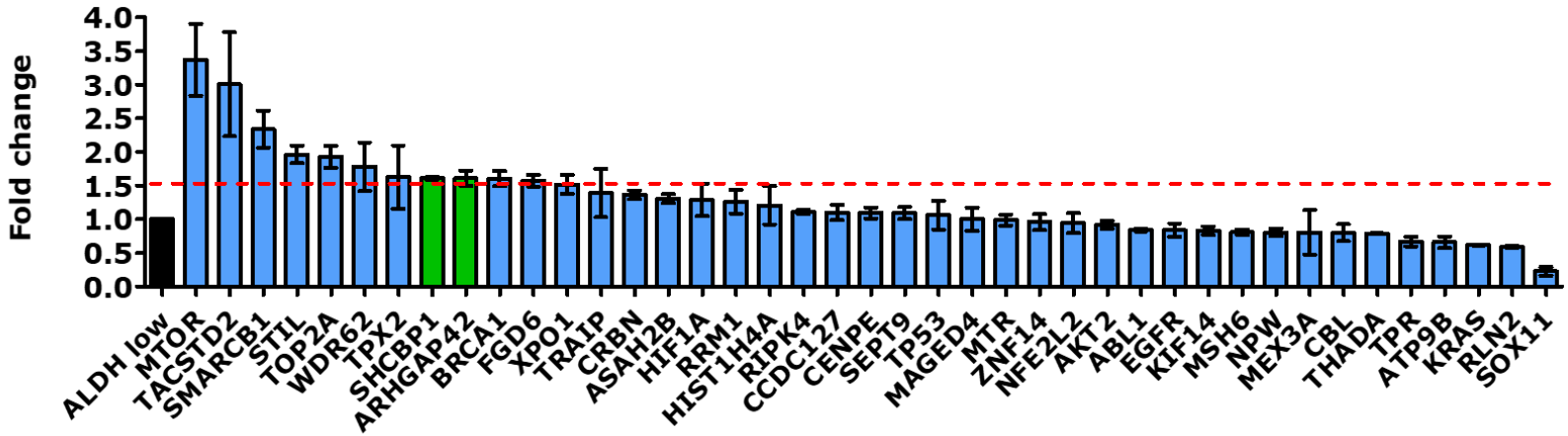
Fold change
4.0
3.5
3.0
2.5
2.0
1.5
1.0
0.5
0.0
ALDH low
MTOR
TACSTD2
SMARCB1
STIL
TOP2A
WDR62
TPX2
SHCBP1
ARHGAP42
BRCA1
FGD6
XPO1
TRAIP
CRBN
ASAH2B
HIF1A
RRM1
HIST1H4A
RIPK4
CCDC127
CENPE
SEPT9
TP53
MAGED4
MTR
ZNF14
NFE2L2
AKT2
ABL1
EGFR
KIF14
MSH6
NPW
MEX3A
CBL
THADA
TPR
ATP9B
KRAS
RLN2
SOX11

B

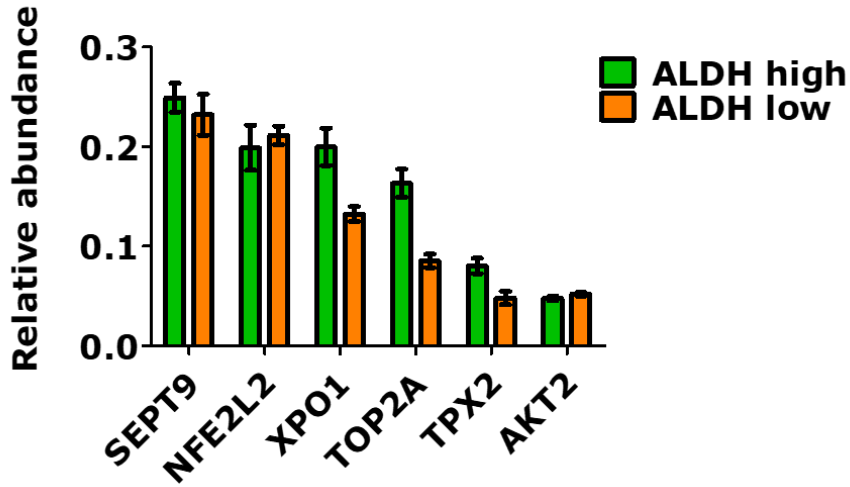
Relative abundance
0.3
0.2
0.1
0.0
ALDH high
ALDH low
SEPT9
NFE2L2
XPO1
TOP2A
TPX2
AKT2

Table 5.1. Fold change and statistical testing of gene expression in ALDH high and ALDH low DU145 cells.

	Fold change n= 1	p value n=1	Fold change n=2	p value n=2	Fold change n=3	p value n=3
ABL1	1.114	0.226	1.207	0.108	0.962	0.592
AKT2	0.732	0.159	0.919	0.523	1.232	0.603
ARHGAP42	**1.760**	**0.237**	**1.611**	**0.036**	**2.634**	**0.002**
ASAH2B	1.188	0.226	1.304	0.071	1.240	0.044
ATP9B	0.577	0.255	0.660	0.062	1.210	0.288
BRCA1	3.018	0.097	1.604	0.231	1.103	0.683
CBL	1.841	0.042	0.799	0.486	0.693	0.135
CCDC127	0.598	0.204	0.988	0.574	0.873	0.176
CENPE	2.102	0.026	1.094	0.485	0.525	0.122
CRBN	0.684	0.047	1.363	0.084	0.833	0.032
EGFR	0.751	0.115	0.836	0.515	0.679	0.248
FGD6	1.068	0.322	1.572	0.057	1.307	0.200
HIF1A	0.884	0.630	1.286	0.620	0.752	0.090
HIST1H4A	1.702	0.536	1.626	0.544	1.055	0.853
KIF14	2.761	0.032	0.829	0.176	0.664	0.005
KRAS	3.601	0.176	0.617	0.063	1.328	0.349
MAGED4	1.833	0.188	1.001	0.698	1.057	0.966
MEX3A	0.612	0.134	0.804	0.641	0.592	0.017
MSH6	0.735	0.421	0.808	0.264	1.109	0.349
MTOR	0.788	0.250	0.838	0.011	0.928	0.242
NFE2L2	1.374	0.542	0.944	0.576	0.621	0.095

NPW	0.895	0.593	0.806	0.099	1.412	0.167
RIPK4	1.431	0.085	3.005	0.090	2.045	0.038
RLN2	1.566	0.082	0.589	0.001	2.245	0.100
RRM1	1.297	0.427	1.261	0.023	1.169	0.201
SEPT9	0.935	0.533	1.091	0.658	0.939	0.292
SHCBP1	**2.828**	**0.022**	**1.612**	**0.042**	**1.229**	**0.128**
SMARCB1	1.184	0.427	2.340	0.023	1.384	0.201
SOX11	0.311	0.004	0.229	0.036	1.817	0.757
STIL	1.585	0.097	1.962	0.100	1.194	0.030
TACSTD2	0.598	0.146	1.101	0.044	0.651	0.090
THADA	0.700	0.085	0.790	0.032	1.333	0.346
TOP2A	1.327	0.430	1.925	0.019	1.328	0.093
TP53	2.616	0.027	1.060	0.951	1.112	0.600
TPR	1.461	0.236	0.701	0.378	0.797	0.348
TPR	0.736	0.838	3.371	0.132	1.579	0.733
TPX2	1.639	0.020	1.107	0.177	2.037	0.598
TRAIP	0.412	0.064	1.389	0.621	1.392	0.058
WDR62	1.053	0.042	1.779	0.225	1.535	0.039
XPO1	0.624	0.071	1.515	0.110	1.069	0.617
ZNF14	0.842	0.071	0.959	0.110	0.904	0.617

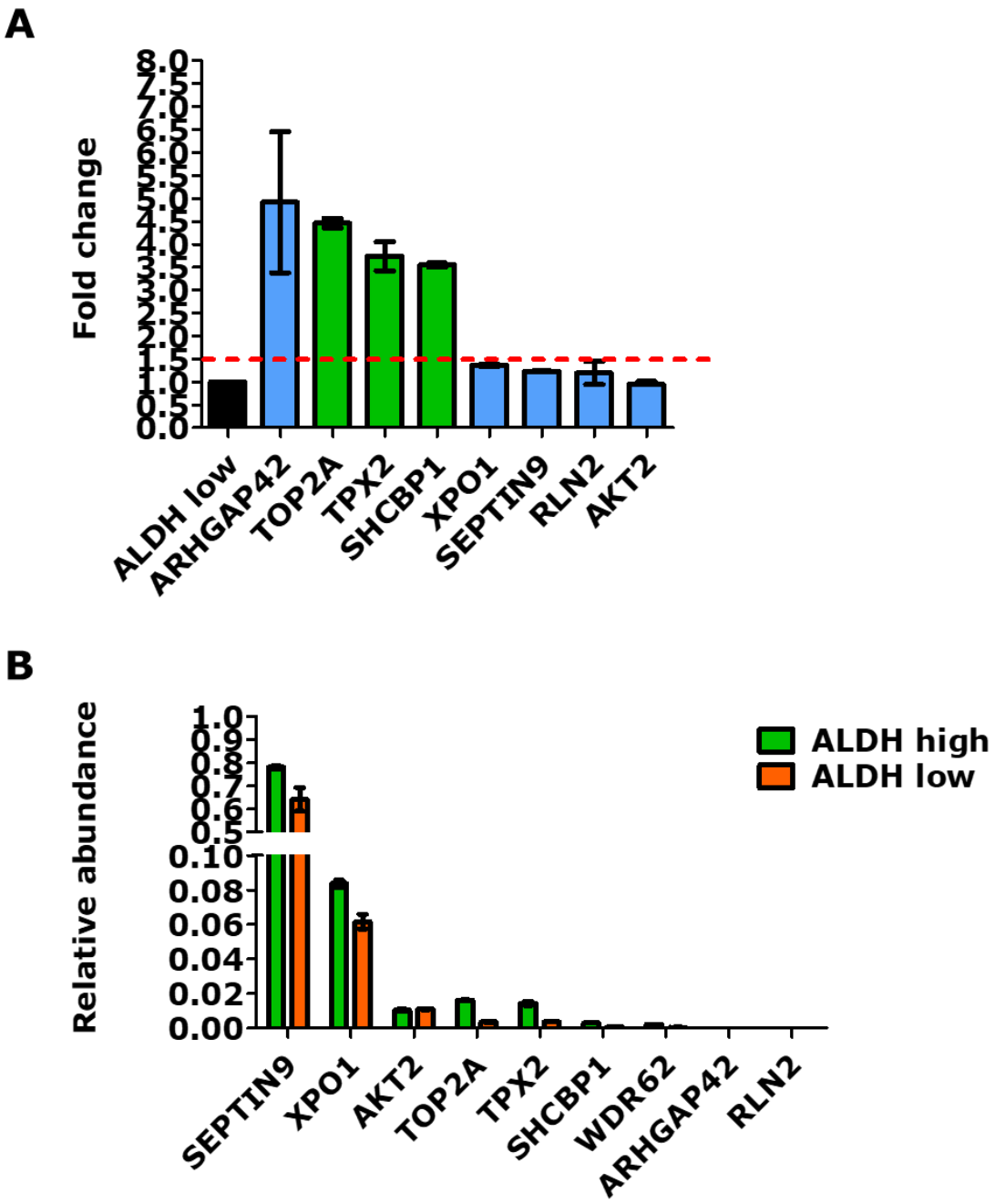

Figure 5.2. Expression of selected antigens in primary PCa cells. (A) Gene expression in ALDH high compared to ALDH low primary PCa cells. Statistical analysis of the gene expression was by paired T test; the genes coloured green were * $p<0.05$ in 2 out of 3 primary samples. Statistical significance is not shown for genes that did not meet this criterion. (B) Gene transcript abundance in ALDH high and ALDH low primary PCa cells. Gene expression data shown is from PCR reactions for sorted ALDH high and low DU145 cells shown in (A). Error bars represent mean ±SEM of technical replicates from one PCR reaction.

Protein expression of the antigens of interest was confirmed by fluorescence microscopy using unsorted DU145 cells. This was due to the lack of an optimised protocol for the culture of ALDH high and ALDH low cells for microscopy following sorting. Protein expression in the DU145 cells was confirmed by fluorescence microscopy (Figure 5.3A-D). ARHGAP42 was detected in the cytosol but not in the nucleus, the latter of which is in contrast to the expected staining pattern described in the Human Protein Atlas (www.proteinatlas.org) (Uhlén et al., 2015, 2005). TPX2, which is a microtubule nucleation factor involved in regulation of mitotic spindle formation, was only detected in cells undergoing mitosis. WDR62, which is also associated with mitotic spindle formation, was widely expressed; these are both in agreement with expected staining patterns from the Human Protein Atlas (www.proteinatlas.org) (Uhlén et al., 2015, 2005). The expression of AKT2 and XPO1 was mainly localised in the cytosol, although has been described throughout the cell in the Human Protein Atlas. Some of these differences may be attributable to the different cell lines used for validation of the antibodies used in the Human Protein Atlas project; additionally, the antibodies used were not all the same as those endorsed by the Human Protein Atlas. The appearance of SEPT9 staining is similar to that depicted in Human Protein Atlas entry for this protein; localised to actin filaments, however, requires confirmation by co-staining for actin e.g. using phalloidin. Data on the protein expression localisation of RLN2 is not currently available from the Human Protein Atlas. Cytosolic expression of RLN2 has been described by immunohistochemistry in endometrial cancer, however in the DU145 cells it was detected in the cytosol and nucleus by immunofluorescence (Fue et al., 2018). Despite abundant gene transcript levels, NFE2L2 protein was not detected, therefore this target was not further investigated. Protein expression of the antigens was not confirmed in the primary PCa cells due to technical issues in microscopy staining (described in Chapter 3).

Expression of CSC antigens in the DU145 cells, which were not sorted into ALDH high and low populations, suggests that peptides from these antigens could also be presented by non-CSC (ALDH low), as these would be expected to be the most frequent population present in unsorted samples. Expression in non-CSC was expected, as there were no genes for which gene expression was not detected by PCR in either of the ALDH high or ALDH low DU145 cells. This was the case even for ARHGAP42, which was defined as a candidate CSC antigen based on differential gene expression in ALHD high cells vs. ALDH low cells (Table 5.1). ARHGAP42 was clearly detected in all DU145 cells by immunofluorescence (Figure 5.3A). The selection of shared antigens identified by qRT-PCR for further investigation of immune responses was also aided by testing the protein expression as NFE2L2 was eliminated owing to the lack of protein expression. The antigens selected as a result of gene and protein expression analysis, which were further investigated for the capacity to elicit an immune response, were: ARHGAP42, TOP2A, XPO1, SEPT9, RLN2, TPX2 and AKT2. The peptides associated with these antigens, the predicted HLA allele binding specificity and the selection criteria for the antigen of interest, 'CSC specific,' 'Shared CSC and non-CSC' or 'Prostate specific' is detailed in Table 5.2.

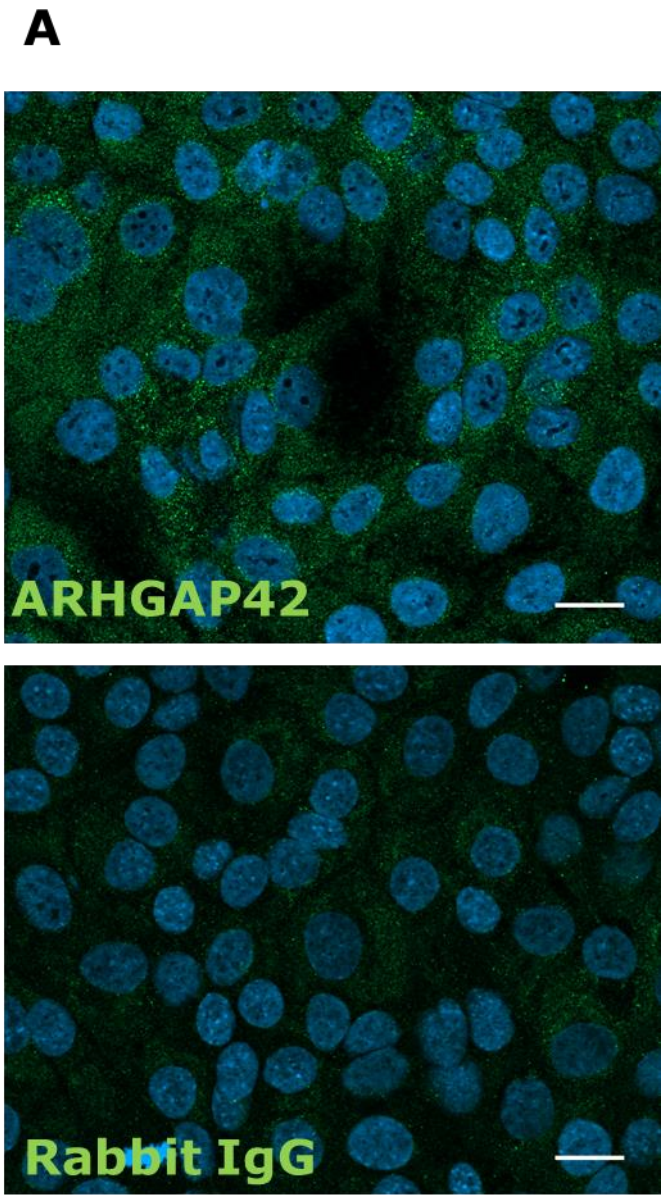

Figure 5.3 Protein expression of CSC and shared antigens in DU145 cells. (A) Fluorescence microscopy of CSC antigens ARHGAP42 with corresponding isotype controls in DU145 cells, imaged on a Zeiss axio observer z1 microscope. 10^4 cells were plated per well of a 96 well glass bottomed plate and the cells were fixed and stained when 90% confluent. The fixation methods were selected per the manufacturer's recommendation for each antibody or both 4% PFA and methanol: acetone 1:1 solutions were tested. A suitable monoclonal antibody for the detection of SCHBP1 was not available, therefore protein expression of this antigen was not confirmed, and this target was not further investigated. Scale bar represents 20μm. Positive staining was determined at the same exposure as the isotype control stained cells. Images are representative of three replicates in which at least 5 random fields of view were imaged.

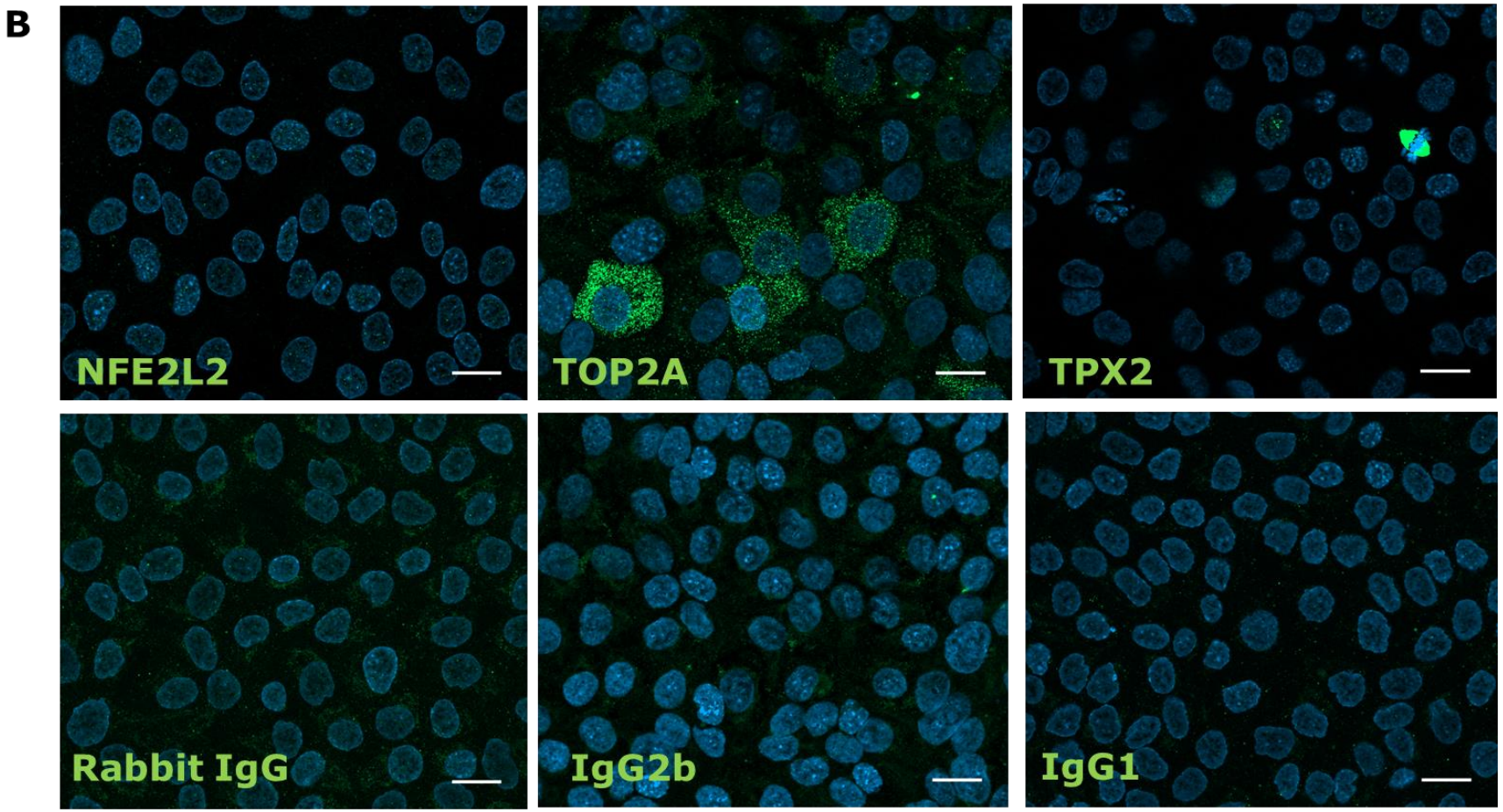

Figure 5.3 (continued) Protein expression of shared antigens in DU145 cells. (B) Fluorescence microscopy of shared antigens NFE2L2 TOP2A, and TPX2 under the same conditions as described in (A).

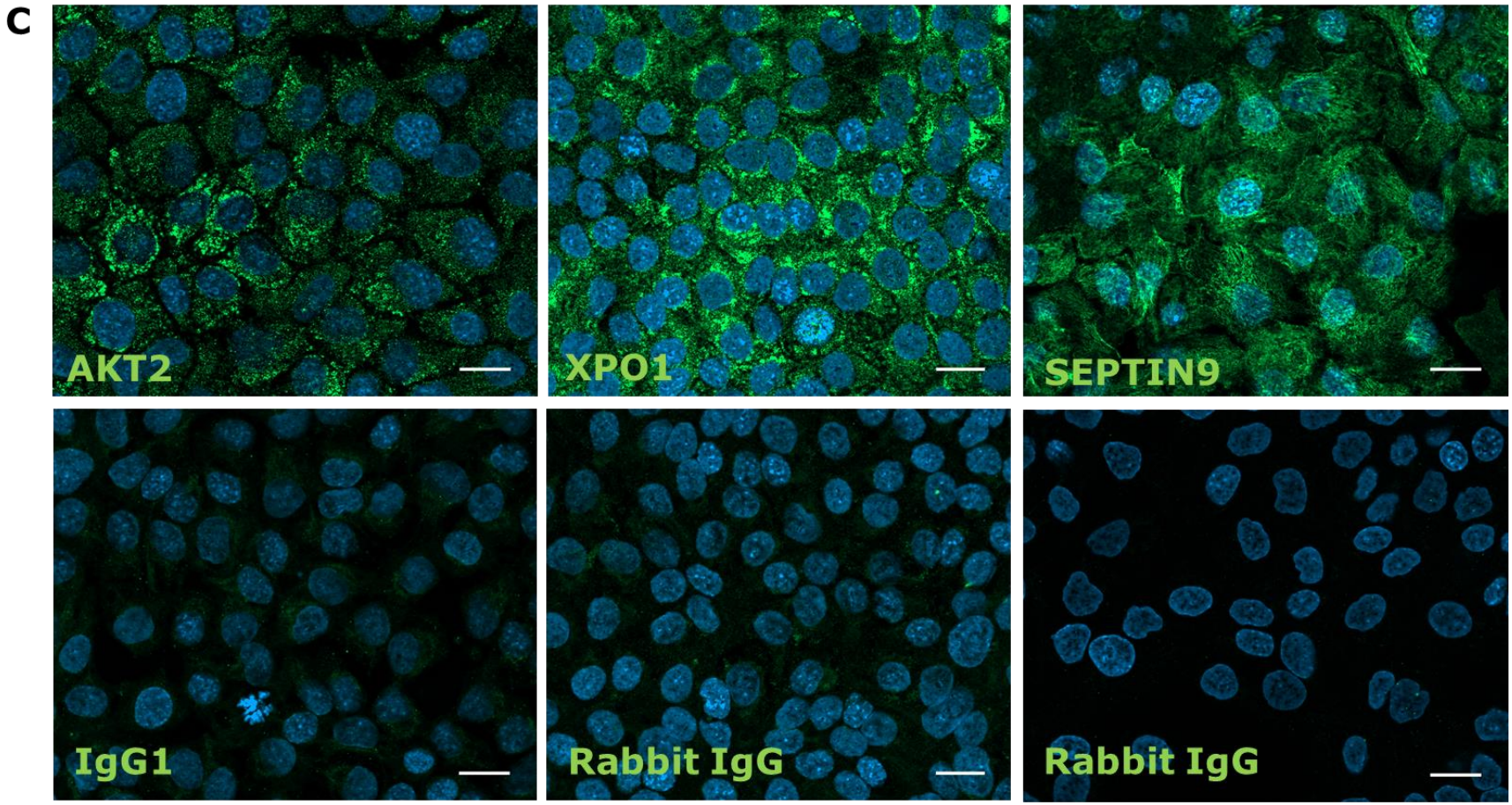

Figure 5.3 (continued) Protein expression of shared antigens in DU145 cells. (C) Fluorescence microscopy of shared antigens AKT2, XPO1 and SEPTIN9 under the same conditions as described in (A).

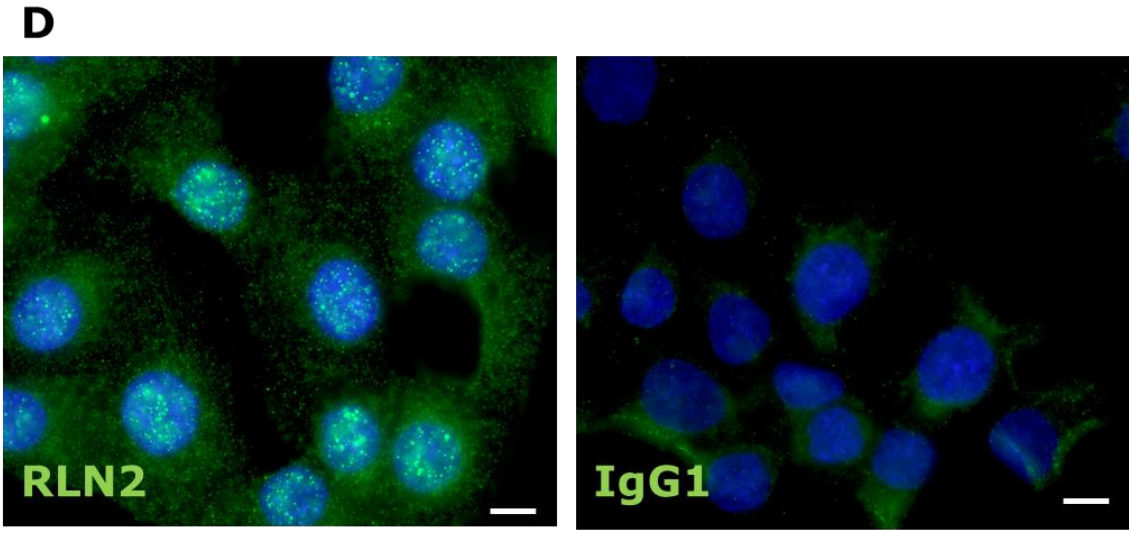

Figure 5.3 (continued) Protein expression of prostate tissue specific antigen RLN2 in DU145 cells. (D) Fluorescence microscopy of RLN2 with corresponding isotype controls in DU145 cells, imaged on a Zeiss axio observer z1 microscope (using a different camera and resolution to the images in A-C). Scale bar represents 10μm. Positive staining was determined at the same exposure as the isotype control stained cells. Images are representative of three replicates in which at least 3 random fields of view were imaged.

Table 5.2: Details of the peptides selected for further immunological analysis from the DU145 HLA ligandome. The peptide sequence, antigen it is derived from, HLA allele binding specificity (predicted by the IEDB, Chapter 4) and the characteristic of interest; CSC specific expression, shared expression in both CSC and non-CSC (determined by PCR of ALDH high and ALDH low cells) or Prostate Specific (based on gene expression data from the GTEX portal, is given.

Peptide	Antigen	HLA binding allele	Specific or shared
AETEFFSKA	STIL	HLA-B*50:01	Shared CSC and non-CSC
REHQNFYEA	ARHGAP42	HLA-B*50:01	CSC specific
EFKKLIRNR	RLN2	HLA-A*33:03	Prostate specific
DFHFRTDER	TPX2	HLA-A*33:03	Shared CSC and non-CSC
EYIKTWRPR	AKT2	HLA-A*33:03	Shared CSC and non-CSC
EYFADMKRHR	TOP2A	HLA-A*33:03	Shared CSC and non-CSC
RESPFSTSA	XPO1	HLA-B*50:01	Shared CSC and non-CSC
REMIPFAVV	SEPTIN9	HLA-B*50:01	Shared CSC and non-CSC

5.3 Isolation of T cells that recognise peptides presented by prostate CSC

5.3.1 Screening of donor T cell responses to peptides

Three HLA matched healthy donors were screened for $CD8^+$ T cell cytokine responses to the selected peptides. The aim of this was to determine which donor had the strongest T cell response (to any of the selected peptides) to inform the optimal donor for generation of T cell lines. Not unexpectedly, there were few available HLA-B*50 or HLA-A*33 donors to test for peptide recognition and responsiveness, as these occur at 1.56% and 0.72% respectively in the Welsh population (Darke et al., 1998). The haplotyping performed by the Welsh Blood Transfusion Service was low resolution, therefore the allele subtype was not known. The HLA types of the donors tested are shown in Table 5.3.

Table 5.3. The HLA Class-I alleles expressed by donors used in this study in which at least one HLA- Class I allele matches that expressed by the DU145 cell line. HLA typing was carried out by PCR by the Wales Blood Transfusion service.

Donor ID	HLA type
Donor A	A2, A68, **B50**, B27
Donor B	A2, **A33**, **B50**, B14
Donor C	A32, **A33**, B44, B14(65)

The T cell response to the relevant peptides by each donor is shown in Figure 5.4; Donor 1 (Figure 5.4A), Donor 2 (Figure 5.4B) and Donor 3 (Figure 5.4C). The donors did not have a high frequency of TNFα producing T cells. However the response to these tumour peptides was not conclusive, as the donors additionally did not respond to the positive control peptide pool (viral peptides) from CMV, EBV and Influenza (CEF) (Currier et al., 2002; Li et al., 2012). This was unexpected as the donors were each positive for at least one

HLA allele that could present in the positive control pool (Donor A: HLA-A*02, HLA-A*68 and HLA-B*27, Donor B: HLA-A*02 and Donor C: HLA-B*44), and the HLA type of the donor has been shown to correlate to responsiveness to this peptide pool (Currier et al., 2002). Since the response to tumour antigens was not detectable in bulk PBMC, which could also have been due to a possible low frequency of responsive T cells within the total number of bulk PBMC tested (10^6 per each replicate), isolation and enrichment of T cells that recognised the peptides was necessary to detect the activated T cell responses. This required the production of tetramers, to use for peptide-specific T cell isolation. A tetramer is a soluble fluorophore conjugated complex of 4 HLA-peptide monomers that has the capacity to bind peptide specific TCR on T cells. These fluorescent complexes allow the detection and isolation of peptide specific T cells using flow cytometry.

Figure 5.4. Screening of responses to the peptides identified in the DU145 HLA ligandome in HLA matched healthy donors. T cell responses to individual peptides from the CSC and shared antigens were tested by incubating the individual peptides (or viral peptide pool) with healthy donor PBMC (plated at 16^6 per well in a 48 well plate) for 6 days, followed by measurement of the TNFα cytokine response from CD8 T cells (i.e. T cells within the bulk PBMC, identified by flow cytometry staining) upon peptide restimulation, by flow cytometry. The graphs are labelled with the antigen from which the peptide is derived, for clarity. (A) Cytokine release by CD8+ T cells from an HLA-B*50 positive donor. (B) Cytokine release by CD8+ T cells from an HLA-B*50, HLA-A*33 positive donor. (C) Cytokine release by CD8+ T cells from an HLA-A*33 positive donor. PBMC were incubated with DMSO (10ul/ 2ml media) as a negative control.

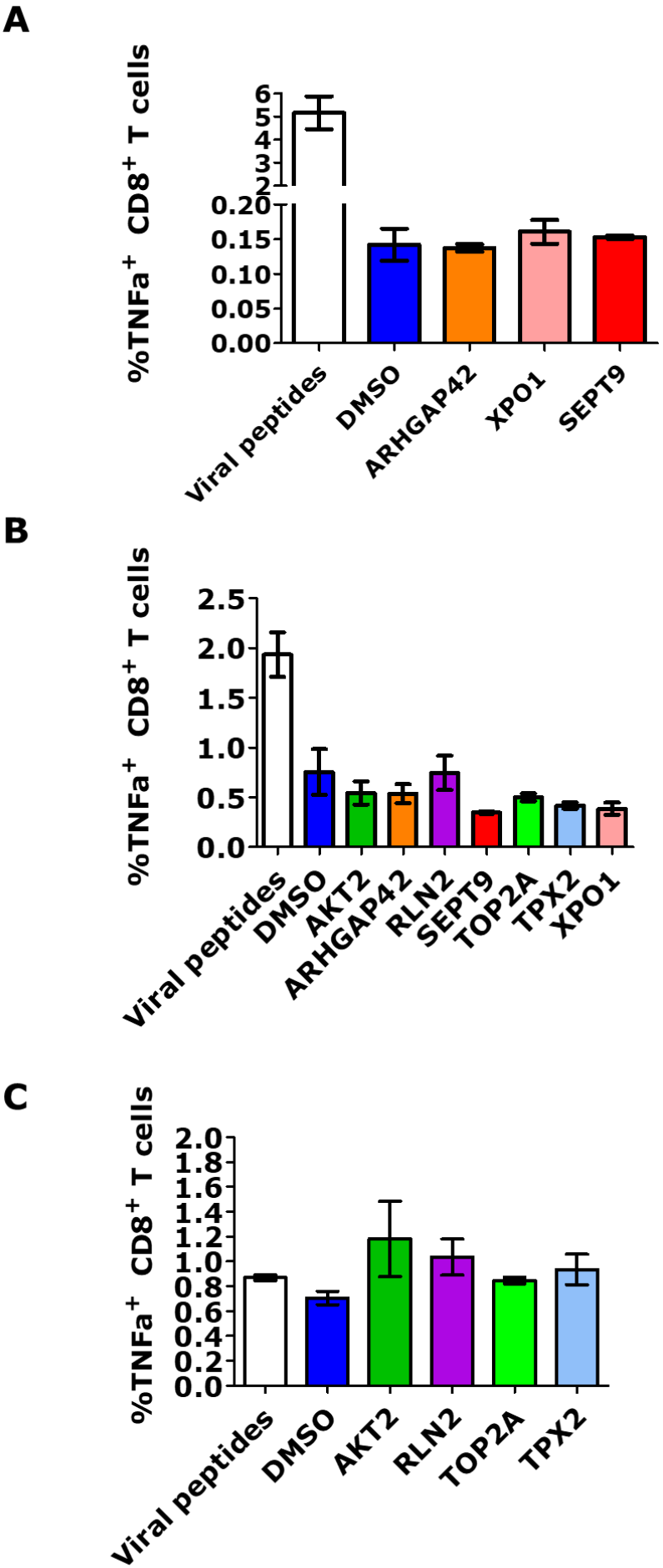
A
%TNFa+ CD8+ T cells
6
5
4
3
2
0.20
0.15
0.10
0.05
0.00
Viral peptides
DMSO
ARHGAP42
XPO1
SEPT9
B
%TNFa+ CD8+ T cells
2.5
2.0
1.5
1.0
0.5
0.0
Viral peptides
DMSO
AKT2
ARHGAP42
RLN2
SEPT9
TOP2A
TPX2
XPO1
C
%TNFa+ CD8+ T cells
2.0
1.8
1.6
1.4
1.2
1.0
0.8
0.6
0.4
0.2
0.0
Viral peptides
DMSO
AKT2
RLN2
TOP2A
TPX2

5.3.2 Homology modelling of the HLA-peptide binding interaction for selection of optimal peptides for production of HLA-peptide tetramers

Thus far there was not a strongly immunogenic CSC or shared peptide/ antigen candidate that directed the isolation of peptide-specific T cells. It would be of interest to isolate and test the responses of enriched or clonal T cell populations that recognised each peptide, however this was not possible, owing to time and financial constraints. The limited number of HLA Class I matched donors from which to isolate T cells also motivated the downsizing of the planned T cell isolation experiments. Therefore HLA Class I-peptide tetramer production for T cell isolation was limited to a small number of peptides.

Monomeric soluble HLA-peptide complexes have low affinity for TCR, therefore tetramers are produced to increase the total affinity of the TCR-HLA complex binding interaction, which is required to isolate peptide specific T cells *in vitro* (Wooldridge et al., 2009). Owing to limited time remaining in the project, it was not possible to investigate T cells that recognised each of the peptides of interest and monomers of each HLA-peptide combination for the peptides of interest identified by gene and protein expression could not be produced. Therefore, the peptide-HLA binding interaction for each HLA-peptide combination was further investigated, to select optimal combinations for monomer (and tetramer) production. The question was which peptide was predicted to interact most favourably with the cognate HLA allele, which would increase the changes of a successful HLA monomer-peptide refold to produce tetramers. The peptide-HLA binding interactions were analysed by a homology modelling approach. This approach to ranking peptides is distinct from previous studies, for example, those in which immune responses to peptide pools were tested in ELISPOT assays using AML patient PBMC (Berlin et al., 2015; Kowalewski et al., 2015). These and other studies may also have benefited from analysing more HLA alleles which have a higher population frequency, enabling screening and isolation of T cells from a greater number of donors.

Pymol and Coot software were used to produce homology models of HLA-A*33:03 and HLA-B*50, from experimentally resolved structures of HLA-A*02 and HLA-B*15 respectively (deposited in the Protein Databank) (Emsley et al., 2010; Schrödinger, LLC, 2015). The HLA-A*33:03- and the HLA-B*50:01-peptide interactions are shown in Figure 5.5 (apart from the XPO1 peptide; discussed below). The structural interactions were quantified using Protein Interfaces, Surfaces and Assemblies (PISA) software (Krissinel and Henrick, 2007). The interface parameters are shown for each complex; the p value (indicating probability of a specific interaction) was used to rank the interactions to determine the optimal peptides for tetramer production (Figure 5.6).

Concurrent to my study, collaborators produced novel HLA ligandome datasets from colon cancer, gastric cancer and AML cell lines. In the SW480 cell line (colon cancer) ligandome, HLA-A*02:01 binding peptides from XPO1 were identified. I had confirmed that XPO1 was expressed in both ALDH high and low DU145 cells and primary PCa cells, and an HLA-B*50 binding peptide from XPO1 was present in the HLA-ligandome of DU145 cells. Since the HLA-A*02 allele is more frequent in the European population than HLA-B*50, it could facilitate proof of concept testing and represent a potential immunological target applicable to a wider patient population. The HLA affinity binding percentile rank for each of the HLA-A*02:01 binding peptides was 0.5 (the percentile rank for the HLA*B50:01 XPO1 peptide was 0.2). The structural interactions were modelled and quantified in the same way as for the HLA-A*33 and HLA-B*50 HLA-peptide interactions (Figure 5.7A-C). The PISA p values comparing the two HLA-A*02:01 and the HLA-B*50:01 peptide interactions, respectively, are shown in Figure 5.7D. Both HLA-A*02:01 binding peptides are predicted to have a more favourable interface interaction with the cognate HLA allele than the HLA-B*50:01 peptide with its cognate allele. Therefore, either of these peptides would be predicted to have a stronger binding to HLA Class I and would have a greater likelihood of successfully producing a monomer.

Since all of the HLA-peptide interactions modelled were derived from elution of the peptides from the surface of the cells, all could be considered biologically occurring structures. However, quantification of the interface interactions allowed selection of the optimal peptides for production of monomers based on best predicted peptide: HLA binding interactions. The top 3 ranked peptides from the DU145 HLA ligandome, AKT2 (shared antigen), RLN2 (prostate tissue specific antigen) and ARHGAP42 (CSC antigen) in addition to the HLA-A*02 XPO1 peptide KLFEFMHET (Hongo et al., 2019) were selected for the production of tetramers for T cell isolation.

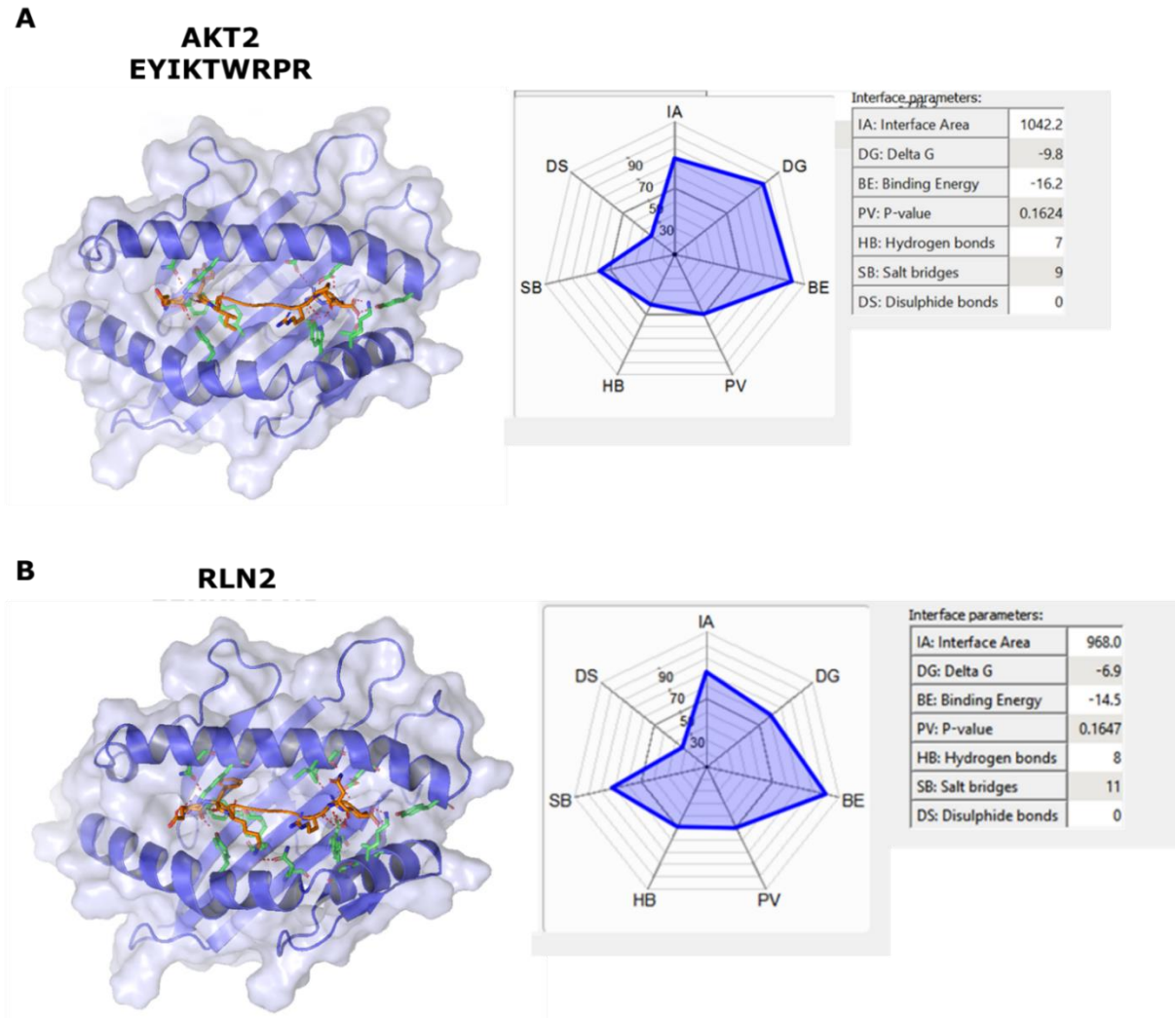

Figure 5.5. Homology modelling and quantification of HLA-peptide interactions. Images of the HLA-peptide interactions and interface interactions were generated in Pymol and PISA respectively. (A-D) HLA-A*33:03 is shown in blue and peptides are shown in orange. Specific amino acid residues which determine the interactions are shown in green and orange from the HLA protein (HLA-A*33:03 or HLAB*50:01) and the peptide respectively. Polar contacts between the HLA protein and the peptide are shown in red dashed lines. The larger the 'interface radar' area, which is based on the combination of the interface parameters, the greater the likelihood the interface is to occur as part of a biological assembly (rather than a crystal packing artefact). Homology modelling was performed in collaboration with Dr Pierre Rizkallah (Cardiff University).

C

TPX2
DFHFRTDER

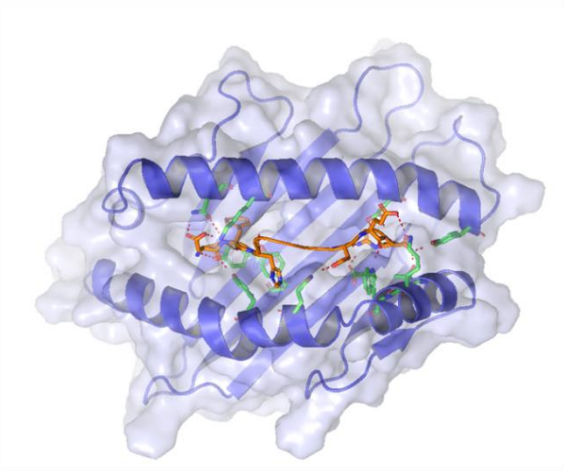

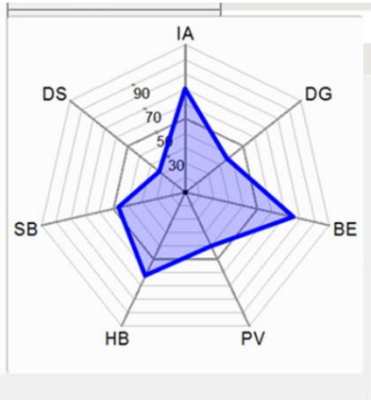

Interface parameters:

IA: Interface Area	999.9
DG: Delta G	-4.8
BE: Binding Energy	-11.4
PV: P-value	0.2315
HB: Hydrogen bonds	10
SB: Salt bridges	6
DS: Disulphide bonds	0

D

TOP2A
EYFADMKRHR

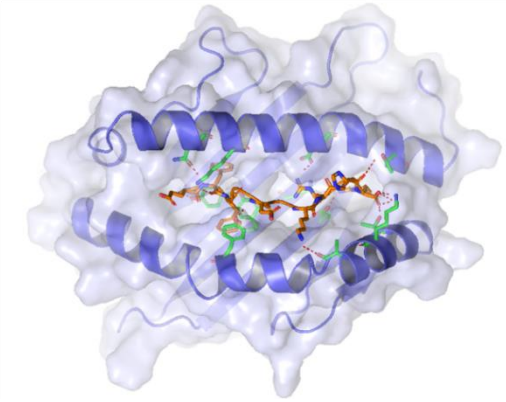

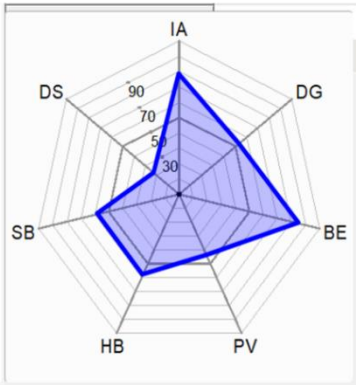

Interface parameters:

IA: Interface Area	1143.7
DG: Delta G	-6.6
BE: Binding Energy	-13.5
PV: P-value	0.1988
HB: Hydrogen bonds	9
SB: Salt bridges	8
DS: Disulphide bonds	0

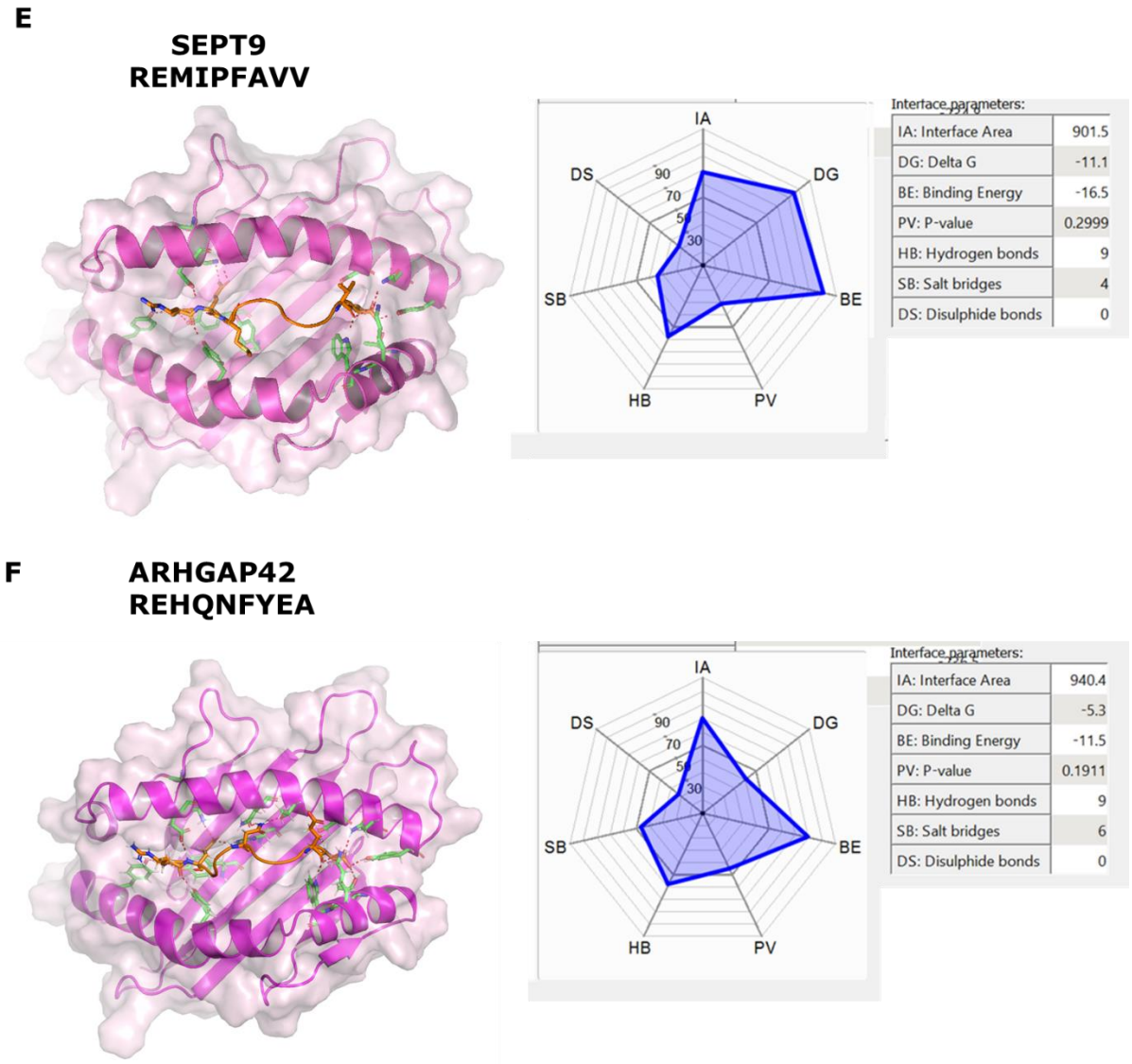

Figure 5.5. Continued homology modelling and quantification of HLA-peptide interactions. Images of the HLA-peptide interactions and interface interactions were generated in Pymol and PISA respectively. (E-F) HLA-B*50:01 is shown in magenta and peptides are shown in orange. Specific amino acid residues which determine the interactions are shown in green and orange from the HLA protein (HLA-A*33:03 or HLAB*50:01) and the peptide respectively. Polar contacts between the HLA protein and the peptide are shown in red dashed lines. The larger the 'interface radar' area, which is based on the combination of the interface parameters, the greater the likelihood the interface is to occur as part of a biological assembly (rather than a crystal packing artefact). Homology modelling was performed in collaboration with Dr Pierre Rizkallah (Cardiff University).

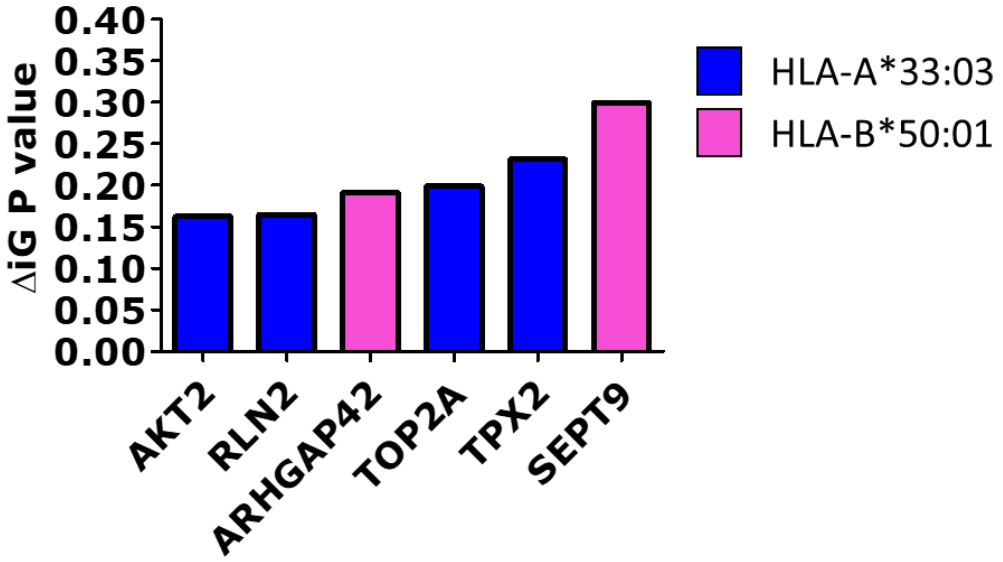

Figure 5.6 PISA p values indicating the specificity of the interaction. The ΔiG value is the solvation free energy gain i.e. the energy difference between the bound and unbound states of the monomeric unit. A positive solvation energy gain value means that energy is required for binding to occur and the unit protein is hydrophobic. The ΔiG P value is a measure of how 'surprising' an interaction is; how likely the structure is to occur randomly in solution. The lower the value the more surprising the interaction, which is an indicator that this structure is not likely to randomly occur in solution.

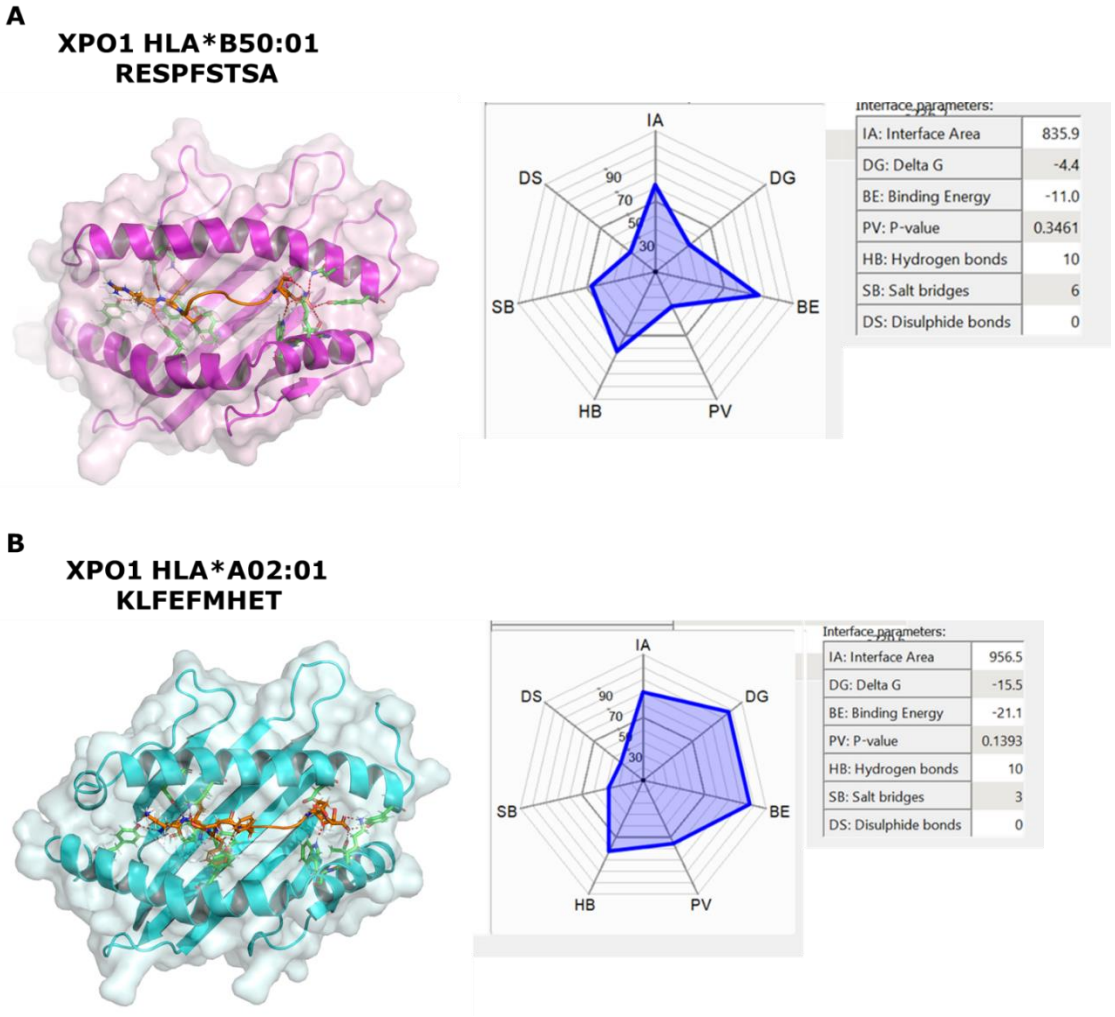

Figure 5.7 Homology modelling and quantification of HLA-peptide interactions for different peptide and cognate HLA alleles for sequences derived from the XPO1 protein. Images of the HLA-peptide interactions and interface interactions were generated in Pymol and PISA respectively. (A) HLA-B*50:01 is shown in magenta and the peptide is shown in orange. (B, C) HLA-A*02:01 is shown in cyan and the peptides are shown in orange. (A-C) Specific amino acid residues which determine the interactions are shown in green and orange from the HLA protein (HLA-B*50:01 or HLA-A*02:01) and the peptide respectively. Polar contacts between the HLA protein and the peptide are shown in red dashed lines. The larger the 'interface radar' area, which is based on the combination of the interface parameters, the greater the likelihood the interface is to occur as part of a biological assembly (rather than a crystal packing artefact). (D) PISA p values indicating the specificity of the interaction (the lower the value the more specific the interaction). The XPO1 HLA-B*50:01 peptide, RESPFSTSA is shown on a separate graph, in comparison to different HLA restricted peptides derived from the XPO1 protein.

C

XPO1 HLA*A02:01
VLIDYQRNV

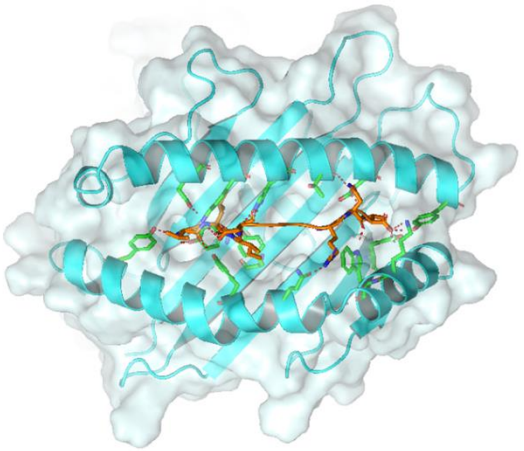

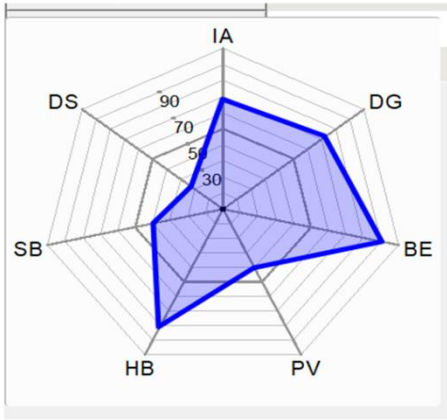

Interface parameters:

IA: Interface Area	893.4
DG: Delta G	-8.3
BE: Binding Energy	-16.0
PV: P-value	0.2498
HB: Hydrogen bonds	13
SB: Salt bridges	5
DS: Disulphide bonds	0

D

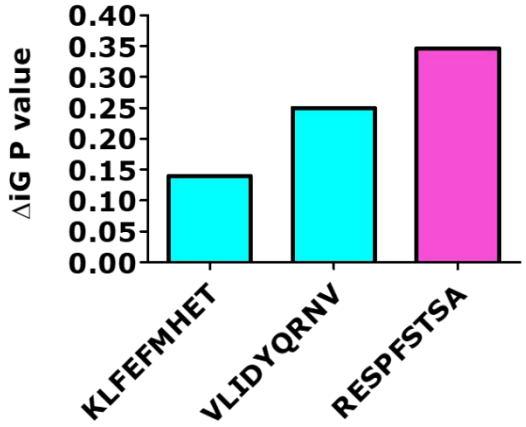

5.3.3 Production of tetramers for isolation of peptide specific T cells

Tetramers were produced firstly by making a monomer consisting of the HLA allele α-chain, which was re-folded with $\beta_2$microglobulin and the relevant peptide to produce the HLA-peptide complex. Monomer re-folding of the HLA-B*50:01-REHQNFYEA and HLA-A*02:01-KLFEFMHET complexes were confirmed by column chromatography (Figure 5.8A and B). Production of an HLA-A*33:03 α-chain was not successful due to technical difficulties in producing a correctly sequenced plasmid containing the HLA A*33:03 α-chain gene sequence. Therefore, T cell isolation was performed using only the HLA-B*50:01 tetramer (ARHGAP42 peptide: REHQNFYEA) and HLA-A*02:01 tetramer (XPO1 peptide: KLFEFMHET). The monomer complexes, which were synthesised to include a biotin tag, were incubated with streptavidin, to produce tetramers.

Figure 5.8. Production of HLA-peptide complex monomers. Elution of re-folded proteins from anion exchange; peaks indicate eluted protein complexes. Lack of protein peak indicates failure of the component parts, HLA α-chain, $\beta_2$macroglobulin and peptide in re-folding. Elution fractions containing protein are pooled for biotinylation. (A) REHQNFYEA-HLA-B*50:01 protein elution. Fractions B4-B9 were pooled. (B) KLFEFMHET-HLA-A*02:01 protein elution. Fractions 15-24 were pooled. Monomers were produced By Sian Llewellyn-Lacey (Cardiff University)

A

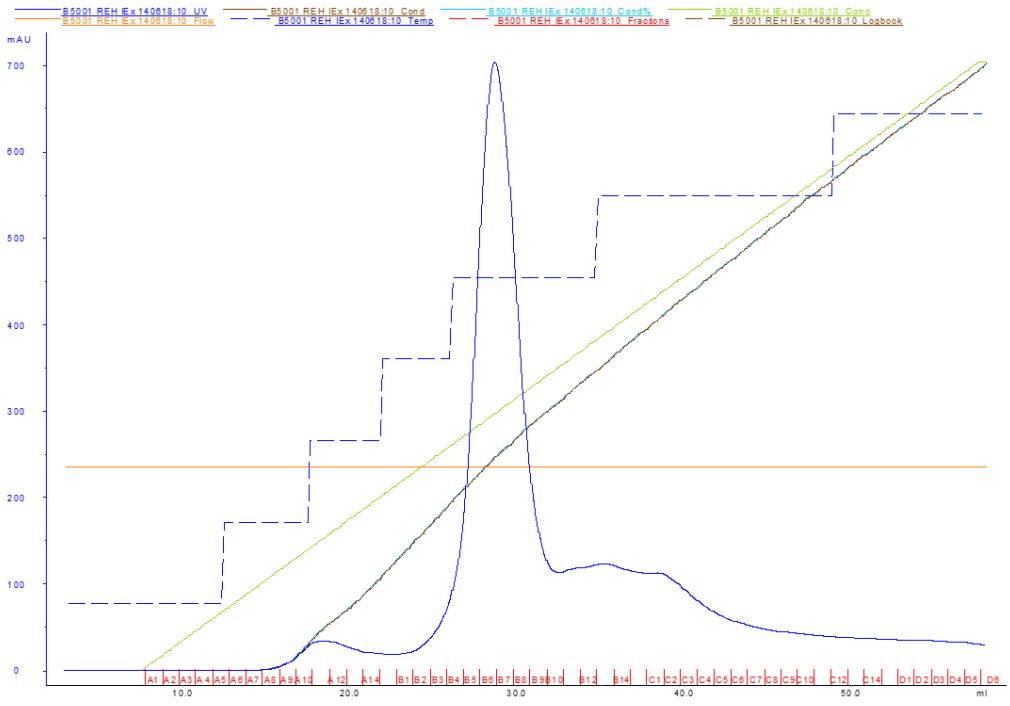
B5001 REH IEx 140618:10 UV
B5001 REH IEx 140618:10 Cond
B5001 REH IEx 140618:10 Cond%
B5001 REH IEx 140618:10 Conc
B5001 REH IEx 140618:10 Flow
B5001 REH IEx 140618:10 Temp
B5001 REH IEx 140618:10 Fractions
B5001 REH IEx 140618:10 Logbook
mAU
700
600
500
400
300
200
100
0
10.0
20.0
30.0
40.0
50.0
ml

B

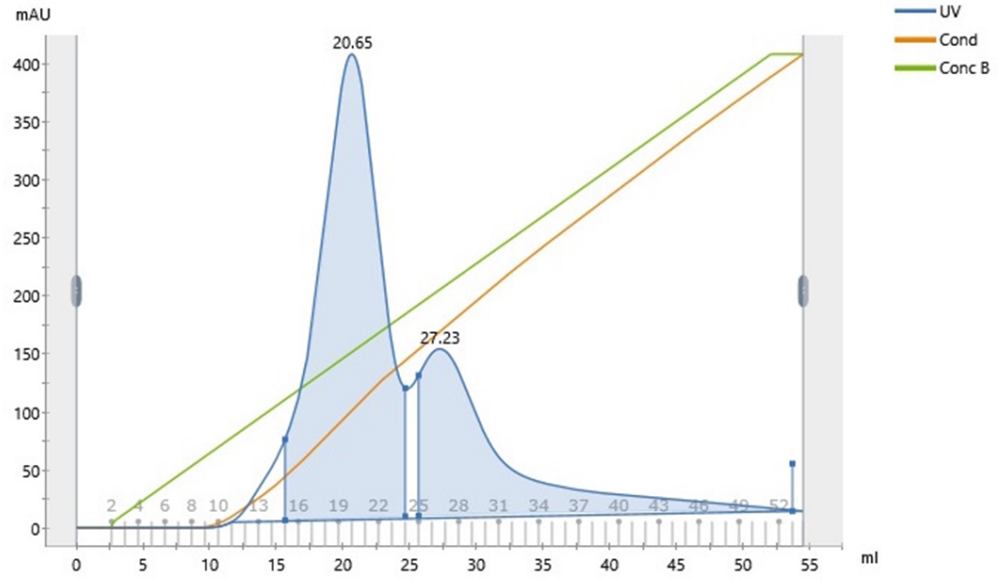
mAU
UV
Cond
Conc B
20.65
27.23
400
350
300
250
200
150
100
50
0
0
5
10
15
20
25
30
35
40
45
50
55
ml

5.3.4 T cell isolation and expansion

The REHQNFYEA-HLA-B*50:01 tetramer was used to isolate $CD8^+$ T cells from two HLA-B*50 donors (Figure 5.9A and B; these donors were tested previously in Figure 5.4 A and B respectively). The frequency of $CD8^+$ tetramer positive cells was 0.011% for Donor 1 and 0.008% for Donor 2. Development of T cell lines was not successful from these sorted populations. Possible reasons for this include the very low number of cells obtained from sorting (76 and 143 tetramer positive $CD8^+$ T cells from the sorts shown in Figure 5.9 A and B respectively). Pre-stimulation of $CD8^+$ T cells was carried out with the REHQNFYEA peptide prior to sorting the cells (Figure 5.9 C, D). This resulted in successful establishment and expansion of the HLA-B50:01 REHQNFYEA tetramer positive T cell line, from Donor 2. The frequency of $CD8^+$ cells which were tetramer positive at the time of sorting (Figure 5.9D) was 0.14% (the $CD8^+$ tetramer positive population was selected from a lower total number of $CD3^+$ cells, due to the $CD8^+$ cell selection protocol). The number of cells sorted was 191; therefore, the pre-selection of $CD8^+$ cells for sorting is suggested to be an effective way to prime peptide specific cells for sorting and successful post-sorting expansion from a frequency of peptide specific T cells in PBMC. The sorted T cells were expanded for 14 days in a co-culture with irradiated PBMC feeder cells, IL-15 and IL-2. This resulted in an increase in the frequency of $CD8^+$ cells which were tetramer positive, to 10.6% (Figure 5.9 E, F (no tetramer control)).

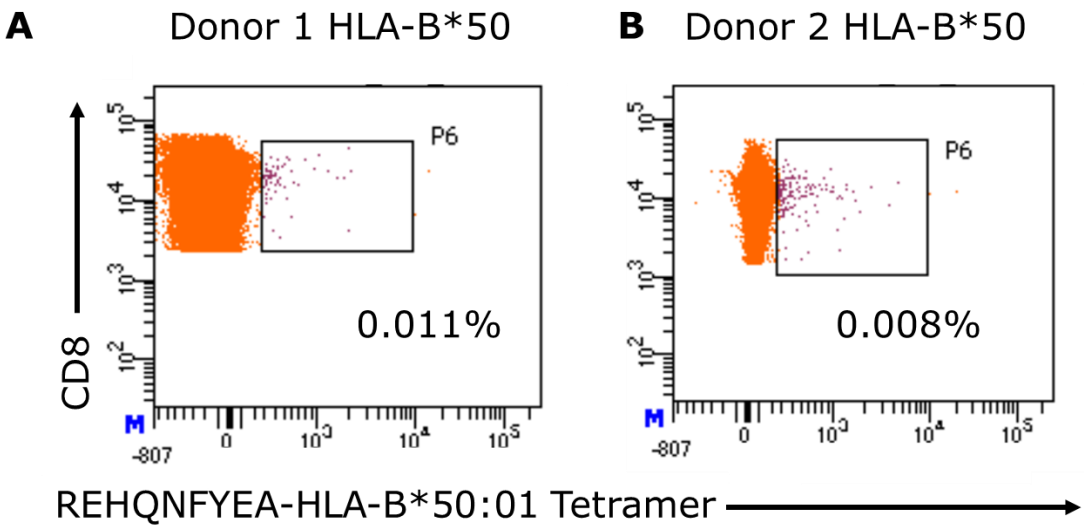

Figure 5.9. Isolation and enrichment of a T cell line recognising REHQNFYEA-HLA-B*50:01. Tetramer positive $CD8^+$ frequencies are shown on the dot plots. (A, B) FACS isolation of tetramer positive $CD8^+$ T cells. Gating was determined by comparison to a tetramer unstained control for each individual donor (data not shown). 44 million cells were analysed (with appropriate scaling up of antibodies for staining) from Donor 1 and 76 $CD8^+$ tetramer positive cells were isolated from this population and expanded as described in methods. 18 million cells were analysed from Donor 2 (with appropriate scaling up of antibodies for staining) and 142 $CD8^+$ tetramer positive cells were isolated.

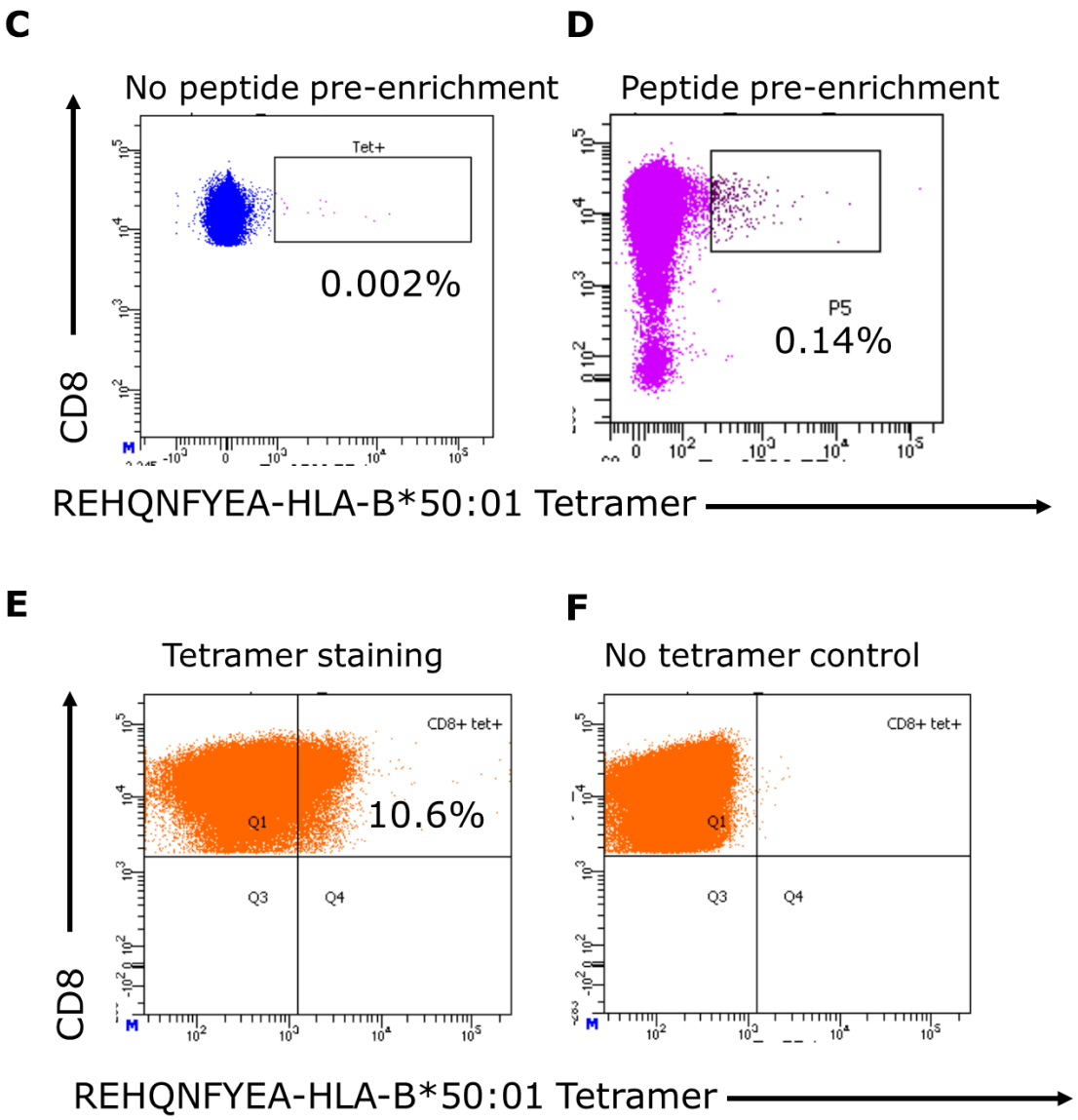

Figure 5.9. Isolation and enrichment of a T cell line recognising REHQNFYEA-HLA-B*50:01, continued. (C) Flow cytometry tetramer staining of $CD8^+$ T cells from Donor 2 without the pre-enrichment protocol. $5x10^6$ cells were stained per replicate. (D) FACS isolation of tetramer positive $CD8^+$ T cells from Donor 2, having carried out a 14-day pre-enrichment expansion. 1.3 x 10^6 cells were analysed and 191 $CD8^+$ tetramer positive cells found to be tetramer positive and viable and were expanded as detailed in Methods. (E, F) Phenotyping flow cytometry tetramer staining at day 14 of expansion $5x10^5$ cells were stained per replicate. All FACS experiments were carried out in collaboration with Professor David Price (Cardiff University), by Kelly Miners, Dr Kristin Ladell and Anzelika Rubina.

The KLFEFMHET-HLA-A*02:01 tetramer was used to isolate $CD8^+$ T cells from three HLA-A*02 donors. The HLA-A*02 population frequency is 51.25% of the Welsh population (Darke et al., 1998); therefore there was a greater availability of healthy donors, however owing to time constraints, cytokine responses to the peptide KLFEFMHET (HLA-A*02:01 peptide from the XPO1 antigen) were not tested to pre-select optimal donors prior to FACS. $CD8^+$ T cells from three HLA-A*02 healthy donors were stimulated according to the pre-enrichment protocol, followed by isolation of $CD8^+$ T cells by FACS, using the HLA-A*02:01 KLFEFMHET tetramer. The frequency of tetramer positive $CD8^+$ T cells was 0.25% (Figure 5.4 A), 0.103% (Figure 5.4 B) and 0.029% (Figure 5.4 C) respectively. The sorted T cells were expanded for 14 days in a co-culture with irradiated PBMC feeder cells, IL-15 and IL-2. This resulted in expansion of the tetramer positive T cell population from HLA-A*02 Donor 1 and Donor 2, the tetramer positive frequency after the 14-day expansion protocol was 10.6% and 4.4% respectively.

Figure 5.10. Isolation and enrichment of T cell lines recognising KLFEFMHET-HLA-A*02:01. Tetramer positive $CD8^+$ frequencies are shown on the dot plots. (A) FACS isolation of tetramer positive $CD8^+$ T cells. Gating was determined by comparison to a tetramer unstained control for each individual donor (data not shown). $2.6x10^6$ cells were analysed from Donor 1 and 2022 $CD8^+$ tetramer positive cells were isolated. $2.4x10^6$ cells were analysed from Donor 2 and 1007 $CD8^+$ tetramer positive cells were isolated. $1.8x10^6$ cells were analysed from Donor 3 and 176 $CD8^+$ tetramer positive cells were isolated. These cells were cultured in an expansion protocol described in Chapter 2: Methods. (B): Phenotyping flow cytometry tetramer staining at day 14 of expansion protocol (10^6 cells were stained); expansion of the cells from Donor 3 was not successful. All FACS experiments were carried out in collaboration with Professor David Price (Cardiff University), by Kelly Miners, Dr Kristin Ladell and Anzelika Rubina.

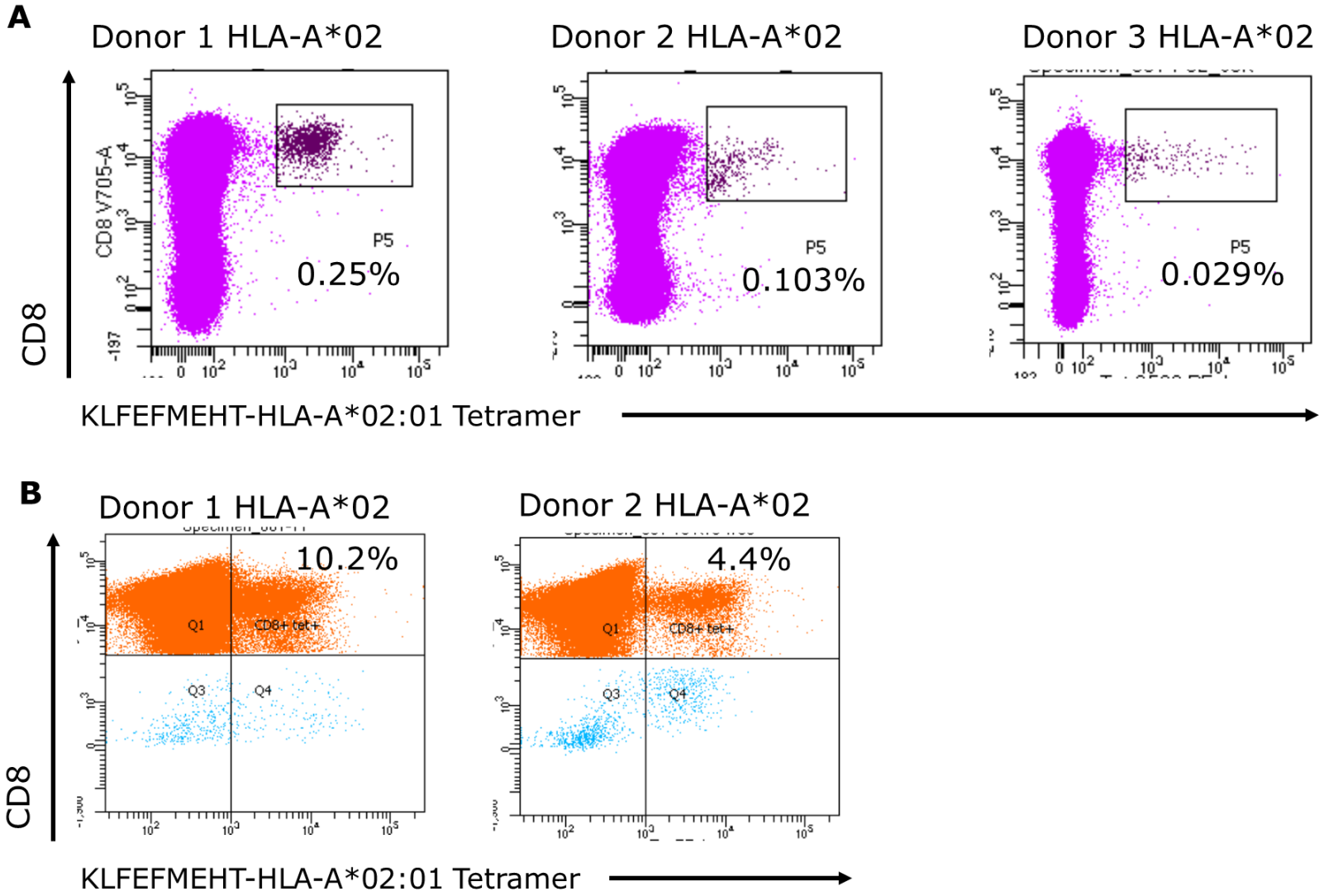
A
Donor 1 HLA-A*02
Donor 2 HLA-A*02
Donor 3 HLA-A*02
CD8
CD8 V705-A
P5
0.25%
P5
0.103%
P5
0.029%
KLFEFMEHT-HLA-A*02:01 Tetramer
B
Donor 1 HLA-A*02
Donor 2 HLA-A*02
10.2%
4.4%
Q1
CD8+ tet+
Q3
Q4
CD8
KLFEFMEHT-HLA-A*02:01 Tetramer

5.4 Testing T cell responses to peptide presenting cells

5.4.1 Characterisation of target cells

The DU145 cells, in addition to BLCL cells (autologous with the T cell line), were used to present endogenously expressed and/or exogenously added peptides to the tetramer-enriched HLA-B*50 T cell line to test peptide recognition and T cell activation. HLA-A*02 BLCL lines have previously been generated in our lab, however prostate cells were also sought to test the responses of the HLA-A*02 tetramer positive T cell lines. For this, HLA-A*02 expression of primary cell lines successfully expanded by *in vitro* culture was tested. Of the primary PCa cell lines available at the time of analysis, the primary #5042 line was found to be HLA-A*02 positive (Figure 5.11A) while the #5008 line was negative for HLA-A*02 (Figure 5.11B). Therefore, the primary PCa cell line #5042 was suitable for use in T cell assays to test the response to the HLA-A*02 peptide KLFEFMHET.

The expression of HLA Class I on the ALDH high and ALDH low DU145 cells and primary PCa cells was also tested, as it has been suggested that CSC express lower levels of HLA, as an immune protective mechanism (Di Tomaso et al., 2010; Vidal et al., 2014). The DU145 ALDH high cells expressed significantly higher HLA Class I levels than the ALDH low cells (Figure 5.12A). However, there was not a significant difference in the HLA Class I expression levels in the ALDH high compared to ALDH low primary PCa cells (Figure 5.12B). The DU145 ALDH low HLA Class I expression levels were comparable to the HLA Class I expression by primary PCa ALDH high and ALDH low cells. This highlights differences in gene expression between cells established in long term *in vitro* culture and primary cell lines. This may be due to immunological pressure (editing) *in vivo* and it may result in lower T cell responses to peptides presented by primary PCa ALDH high vs ALDH high DU145 cells.

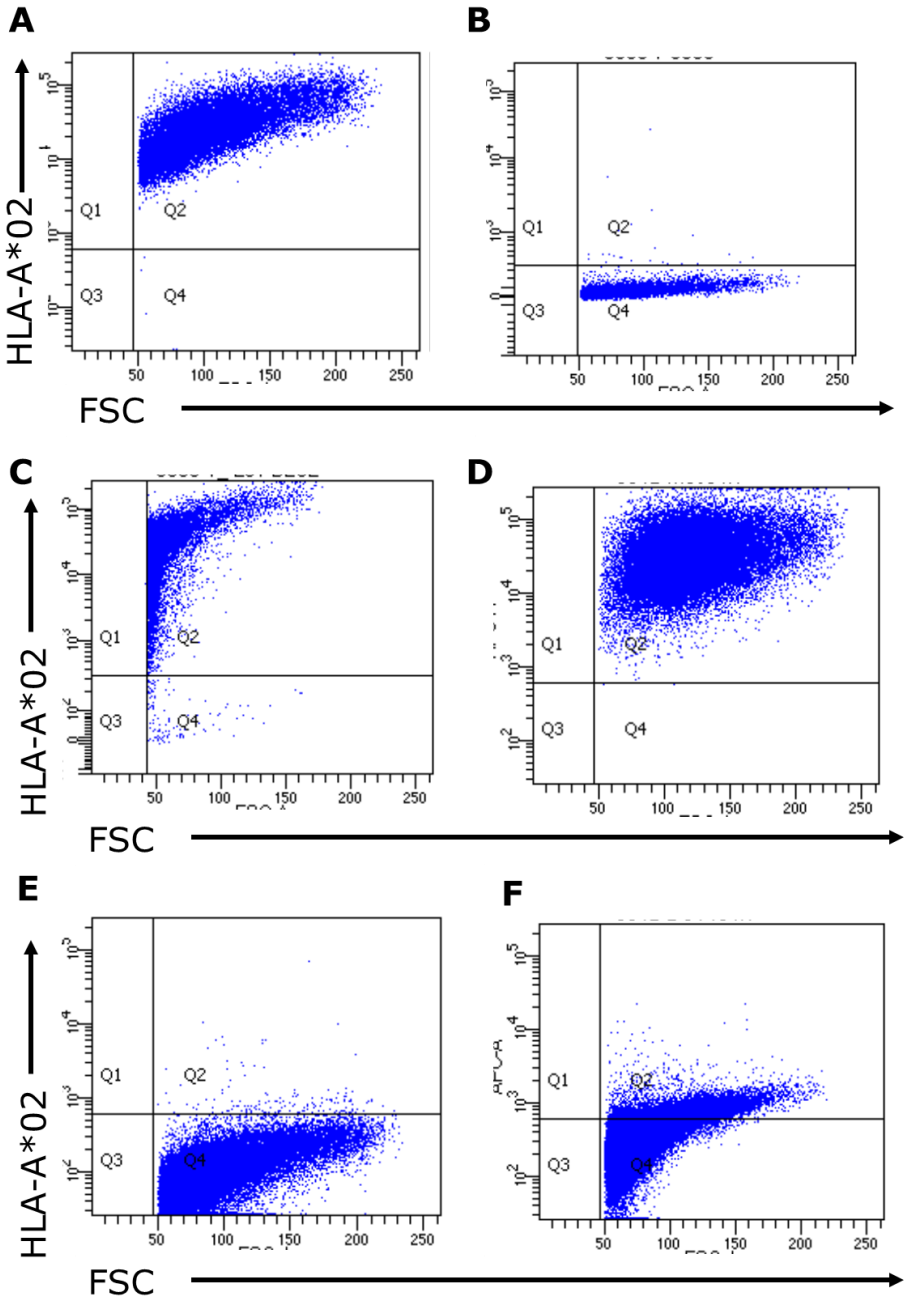

Figure 5.11 HLA-A*02 expression in primary PCa cell lines (A) HLA-A*02 antibody staining of primary PCa cell line #5042. $5x10^4$ cells were stained per replicate within the experiment. (B) HLA-A*02 antibody staining of primary PCa cell line #5008. $5x10^4$ cells were stained per replicate within the experiment (C, D) Positive control cells for HLA-A*02 expression: BLCL and mesothelioma cells, respectively, previously established in the lab for which the HLA type was determined by RT-PCR, by the Welsh Blood Transfusion service. (E) Unstained cells were used to guide gating of antibody stained cells. (F) DU145 cells were stained as a further negative control. The controls were stained or run unstained at 10^5 cells per tube.

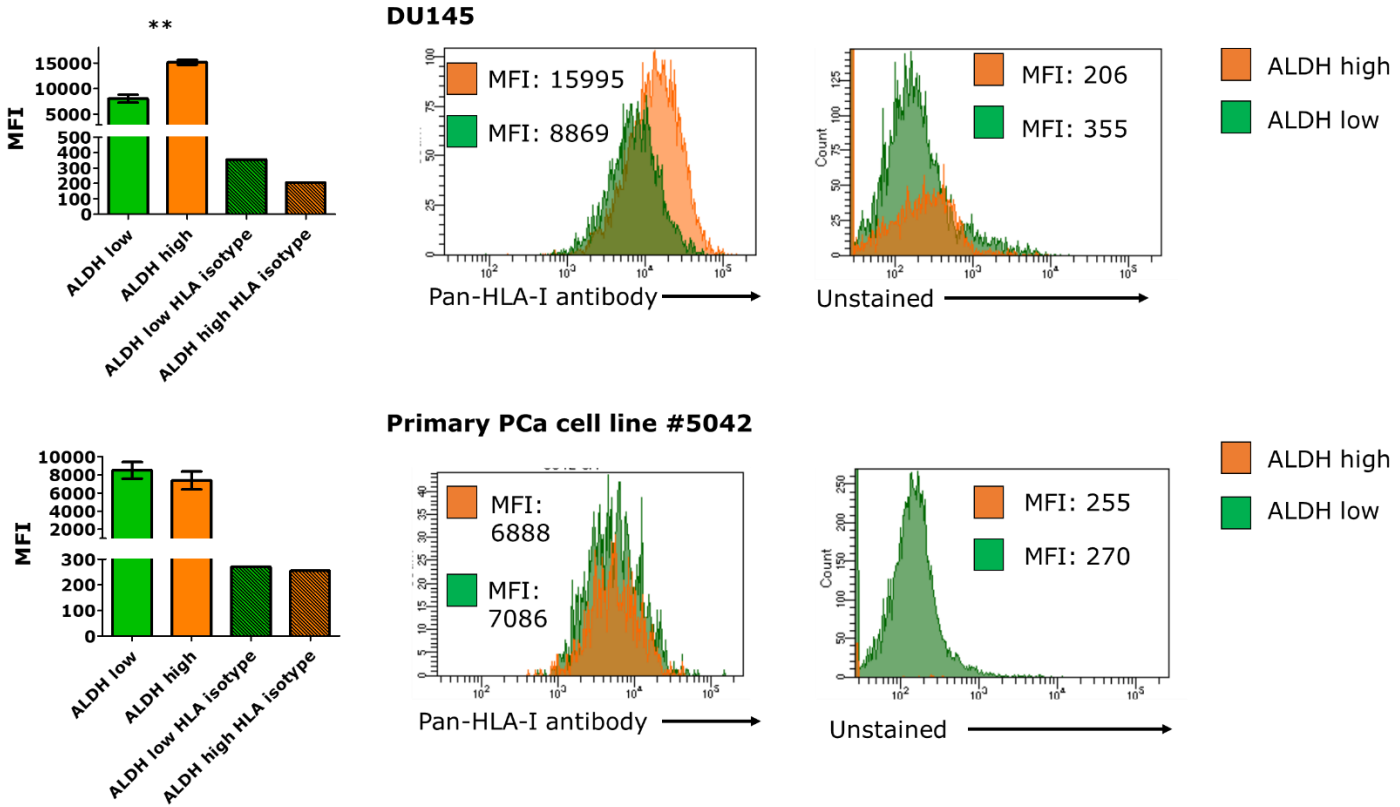

Figure 5.12. HLA expression levels of ALDH high and ALDH low DU145 and primary PCa cells. (A) MFI and histograms of HLA antibody staining in the DU145 ALDH high and ALDH low populations. (B) MFI and histograms of HLA antibody staining in the primary PCa ALDH high and ALDH low populations. For each cell line: $2x10^5$ cells were incubated with 1µl ALDH substrate and incubated according to the ALDH protocol, then stained with 50 ul HLA-ABC unconjugated primary antibody, the secondary was used at 1:200. Statistical significance was assessed by paired T test of the ALDH high and low populations; * $p<0.05$. Error bars represent three technical replicates and this experiment was repeated twice for each of the DU145 cells and primary PCa cells.

5.4.2 Phenotype of T cell lines

The expanded tetramer positive cells from HLA-B*50 Donor 1 and HLA-A*02 Donors 1 and 2 were further enriched by a tetramer sort. The REHQNFYEA-HLA-B*50:01 tetramer positive cells constituted 4% of the expanded population, potentially indicating expansion of or contamination by non-tetramer specific T cells which may have been previously sorted as false positives (Figure 5.13A). The KLFEFMEHT-HLA-A*02:01 tetramer positive cell frequency was 18.3% (Figure 5.13B) and 31.9% (Figure 5.13C) respectively, indicating expansion of the tetramer positive cells from the initial FACS sort (10.2% and 4.4% respectively).

The tetramer positive $CD8^+$ T cell lines were phenotyped for use in cytokine assays and two distinct populations were observed: $CD4^-$ $CD8^+$ tetramer positive, and $CD4^+$ $CD8^+$ tetramer positive cell (for each respective tetramer) (Figure 5.14 A-C). Exclusion of CD4 expressing CD8 cells had not been a part of the flow cytometry gating strategy for tetramer isolation, therefore some of the expansion of tetramer cells observed is attributed to growth of the $CD4^+$ $CD8^+$ T cell population. The expression of CD4 by $CD8^+$ T cells has been described in association with *in vitro* activation of naïve T cells (Flamand et al., 1998; Kitchen et al., 2005; Sullivan et al., 2001); this may account for the double positive phenotype observed following the expansion of the tetramer positive T cells in my study. Since $CD4^+$ $CD8^+$ double positive T cells have been described as having a functional cytokine production role (Overgaard et al., 2015), the peptide specific response of these T cells were also studied.

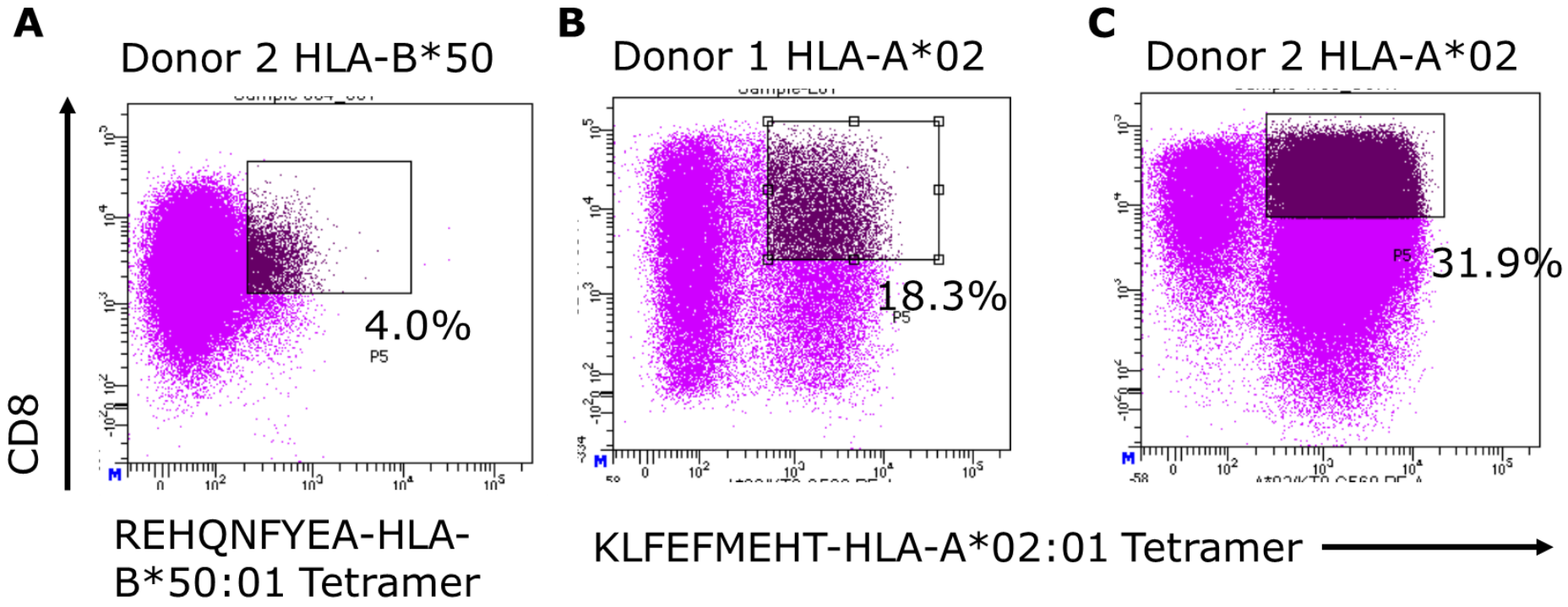

Figure 5.13 FACS isolation of tetramer positive cells from previously isolated and expanded tetramer positive T cell lines. Tetramer positive $CD8^+$ frequencies are shown on the dot plots. Gating was determined by comparison to a tetramer unstained control for each individual donor (data not shown). (A) 129926 REHQNFYEA-HLA-B*50:01 tetramer positive cells were isolated from the expanded cells ($8x10^6$) isolated previously from HLA-B*50 Donor 2. (B) 2,228,655 KLFEFMHET-HLA-A*02:01 tetramer positive cells were isolated from the expanded cells ($4.5x10^6$) isolated previously from HLA-A*02 Donor 1. (C) (2,396,152) KLFEFMHET-HLA-A*02:01 tetramer positive cells were isolated from the expanded cells isolated previously from HLA-A*02 Donor 2 ($4.2x10^6$).

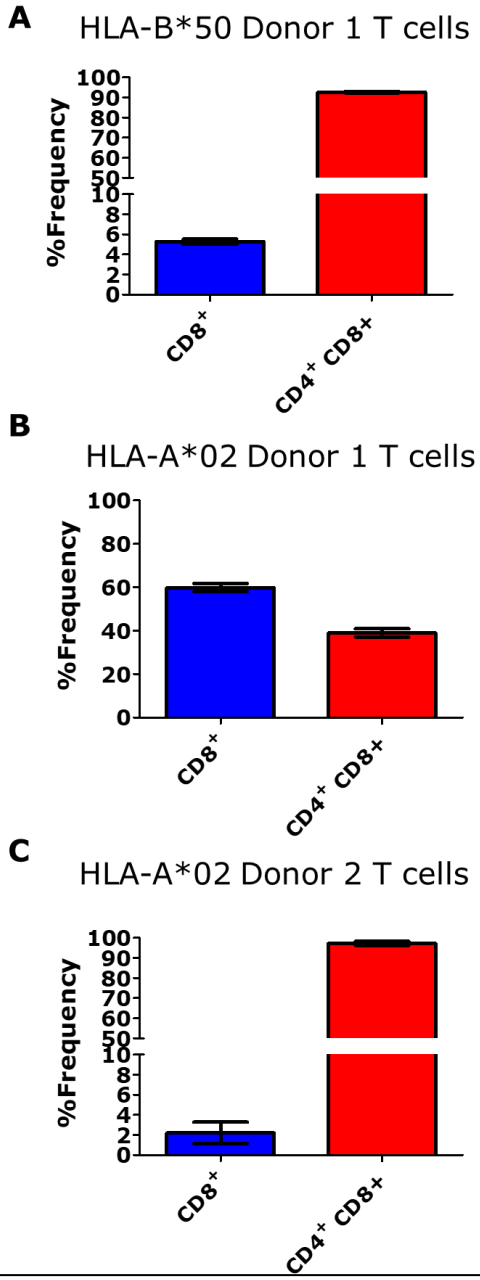

Figure 5.14 Phenotype of tetramer positive T cell lines. The tetramer positive cells from the second FACS isolation were expanded and the phenotype investigated at day 7: 10^5 cells were stained per replicate. (the reduced length of expansion was due to time constraints). (A) $CD8^+$ single positive and $CD8^+$ $CD4^+$ double positive frequencies of the expanded REHQNFYEA-HLA-B*50:01 tetramer positive population. (B) $CD8^+$ single positive and $CD8^+$ $CD4^+$ double positive frequencies of the expanded KLFEFMHET-HLA-A*02:01 tetramer positive population from HLA-A*02 Donor 1. (C) $CD8^+$ single positive and $CD8^+$ $CD4^+$ double positive frequencies of the expanded KLFEFMHET-HLA-A*02:01 tetramer positive population from HLA-A*02 Donor 2. Means and error bars were calculated from duplicates.

Due to time constraints, activation of the tetramer enriched T cell lines was tested in the absence of further enrichment or cloning. Detection of tetramer enriched T cell responses was first optimised by measuring CD107a, MIP1β, IL-2, IFNγ and TNFα production by T cells from a healthy donor (Figure 5.15). Polyfunctional antigen-specific responses, i.e. the production of more than one cytokine and/ or other functional markers, e.g. CD107a, MIP1β has been recognised as an important feature of $CD8^+$ T cells in response to both viral and tumour antigens (Lin et al., 2009; Perales et al., 2008; Precopio et al., 2007). The selected healthy donor had demonstrated a substantial cytokine response in previous experiments carried out in the course of previous studies. The donor PBMC were incubated with a custom viral peptide pool (produced by pooling custom synthesised individual viral peptides from a wide range of HLA specificities). The peptides included in this pool are detailed in Chapter 2: Materials and Methods. The HLA type of the healthy donor was: HLA-A*01, A*11, B*55, B*15(62). Thus, the healthy donor expresses some HLA Class I alleles for which there are corresponding HLA restricted peptides in the custom peptide pool (HLA-A*01 and A*11; peptides from Influenza and EBV respectively).

Of the five functional markers tested, surface upregulation of CD107a (53.1%), reflecting degranulation and T cell cytotoxicity, in response to viral peptides, was significantly higher than the other functional markers tested (Figure 5.15). The CD107a background expression (DMSO only, no peptide) was not significantly higher than that of the other functional markers, except for IL-2. The frequency of MIP1β, IFNγ and TNFα producing $CD8^+$ cells was 26.3%, 39.5% and 33.1% respectively. The production of IL-2 (1.16%) was significantly lower than all other markers. The ranking, in terms of frequency of cytokine producing $CD8^+$ T cells, was CD107a> IFNγ>MIP1β/=TNFα>IL-2 (MIP1β production was significantly lower than IFNγ, but not significantly different than TNFα and TNFα was not significantly lower than IFNγ). In a study by Lin and colleagues, detection of two functional markers was the most frequently observed T cell response, followed by three functional markers (Lin et al., 2009) whereas in my study these limited observations suggest production of four functional markers, from this particular donor. MIP1β and

IFNγ were chosen as representative functional markers to measure the tetramer positive T cell responses, as it was not possible to simultaneously assess the four functional markers in a single staining panel in combination with the T cell phenotyping markers. Simultaneous measurement of IFNγ, a cytokine, and the chemokine MIP1β has been shown to improve flow cytometry detection of antigen specific responses in HIV positive patients (Kutscher et al., 2008).

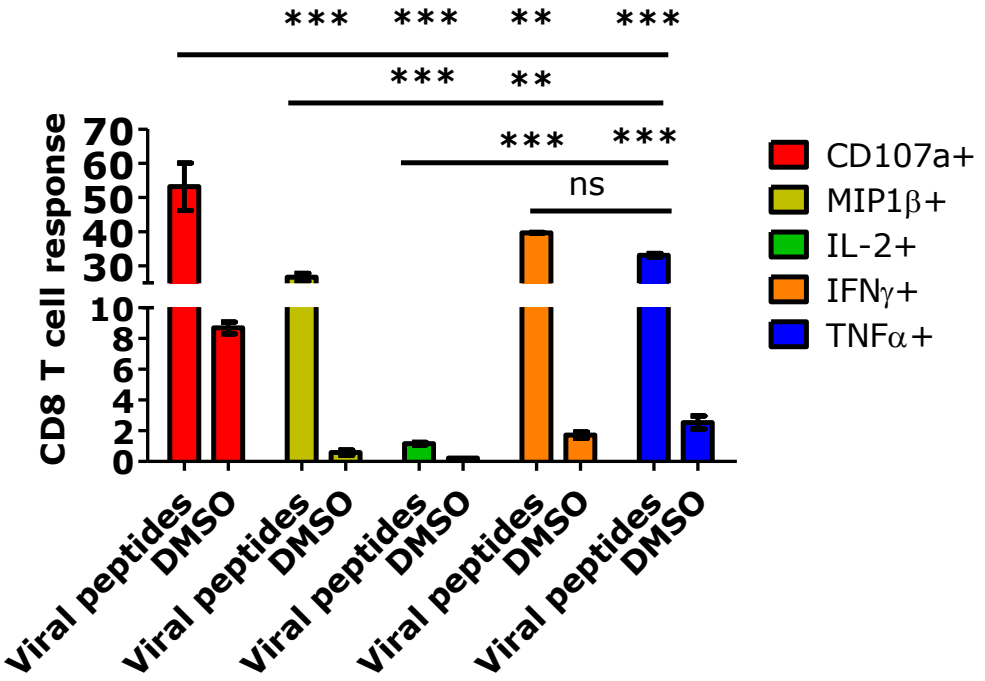

Figure 5.15. Comparison of the magnitude of different cytokine responses in a healthy donor. Following (peptide only 10μg per million cells) stimulation of 10^6 cells/ well healthy donor PBMC (plated at 10^6 cells/ well in a 48 well plate) for 7 days, the cytokine response was measured by co-incubation of PBMC with HLA matched, peptide loaded BLCL. Golgi plug and Golgi stop were added to the cells 1hr after setting up the co-incubation reaction. The CD107a antibody was also added at this stage. The cells were incubated at 37°C for 12 hr followed by staining with T cell phenotyping antibodies and intracellular cytokine staining of MIP1β, IFNγ, IL-2 and TNFα. Two separate sets of T cell and peptide presenting BLCL co-incubation reactions were carried out and stained with CD107a and MIP1β or IFNγ, IL-2 and TNFα as it was not possible to combine all markers and fluorophores into a single antibody staining panel. The reactions were carried out in parallel and the results are combined on the graph for clarity. Error bars represent duplicates. Significance was determined by 2way ANOVA with Bonferroni post-hoc tests to determine the interaction between individual groups. *** $p<0.001$, ** $p<0.01$.

5.4.3 Functional responses from peptide specific T cell lines

The tetramer enriched T cell lines were incubated with HLA matched BLCL, and DU145 or 5042 primary PCa cells, for the HLA-B*50 and HLA-A*02 T cells respectively (co-culture conditions are described in Methods). The target cells were loaded with 10 ug/ ml of peptide prior to the addition of T cells to provide a positive control of peptide presentation.

T cell responses to the REHQNFYEA peptide

The REHQNFYEA-HLA-B*50:01 $CD8^+$ T cells produced IFNγ in response to both peptide loaded (60.9% $CD8^+$ IFNγ^+), and not loaded BLCL (32.5% $CD8^+$ IFNγ^+) (Figure 5.16A). There was no significant difference in the responses. The REHQNFYEA-HLA-B*50:01 $CD8^+$ T cells produced high levels of IFNγ when co-cultured with DU145 cells in the presence (83.3%) or absence of peptide (75.1%) (Figure 5.16B). The production of MIP1β by the REHQNFYEA-HLA-B*50:01 $CD8^+$ T cells followed a similar pattern although the frequency of MIP1β producing $CD8^+$ T cells was lower than that of IFNγ producing $CD8^+$ T cells; production of MIP1β in response to peptide or absence of peptide on BLCL was 30.% and 10.6% respectively, and 35.8% and 34.2% for peptide loaded or not loaded DU145, respectively.

The IFNγ production by REHQNFYEA-HLA-B*50:01 $CD4^+$ $CD8^+$ T cells followed the same pattern as observed for the $CD8^+$ T cells. This was expected as the proportion of $CD4^+$ $CD8^+$ tetramer positive T cells was high (92%) after expanding the cells (Figure 5.14A). The $CD4^+$ $CD8^+$ T cells produced IFNγ in response to peptide loaded (83.6% $CD8^+$ IFNγ^+) and not loaded BLCL (45.7% $CD8^+$ IFNγ^+) (Figure 5.16C). The $CD4^+$ $CD8^+$ T cells similarly produced IFNγ^+ to exogenous and endogenously peptide presenting DU145 cells (Figure 5.16D). However the polyfunctional capacity of the $CD4^+$ $CD8^+$ T cells did not match that of the $CD8^+$ T cells as the production of MIP1β was lower than that of the $CD8^+$ T cells in the case of double positive T cells incubated with either of BLCL or DU145, irrespective of peptide loading.

Since this experiment was only performed once, and with tetramer-enriched rather than clonal T cells, it is not possible to draw clear conclusions. Based on the available data, the responses to BLCL could suggest lack of peptide specificity, as The ARHGAP42 antigen is not known to be expressed by BLCL (based on data from the GTEx portal: https://GTExportal.org) therefore it is unlikely to be presented endogenously. On the other hand, having been identified from the DU145 HLA ligandome, the ARHGAP42 peptide is presented endogenously by DU145, therefore responses to both peptide loaded and not loaded DU145 could be indicative of a peptide-specific response, and the responses to BLCL not loaded with peptide attributable to T cells specific for other peptides presented by BLCL, such as EBV peptides.

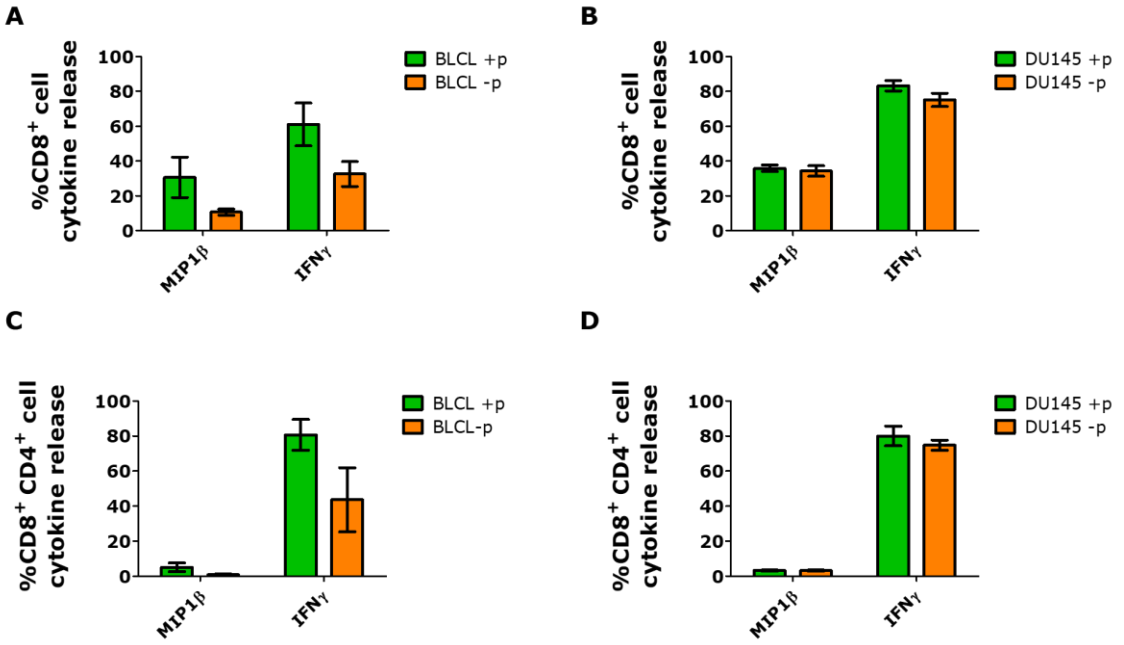

Figure 5.16. Functional responses of CD8$^+$ and CD4$^+$ CD8$^+$ T cells to target cells presenting the REHQNFYEA peptide. Cytokine responses were tested 7 days after the second tetramer-based isolation of the respective T cell lines. The expanded cells were co-incubated with either BLCL or DU145 cells at a 10:1 ratio ($1.5x10^5$ T cells: $1.5x10^4$ target cells. Golgi Stop and Golgi Plug were added for 12 hr followed by staining with T cell phenotyping antibodies and intracellular cytokine staining of MIP1β and IFNγ. The CD8$^+$ and CD4$^+$ CD8$^+$ T cell responses were measured by separate gating, from the same co-incubated population. The co-incubations set up were as follows: (A, C) HLA matched peptide-loaded/ not loaded BLCL incubated with REHQNFYEA- T cells (1:10). (B, D) peptide-loaded/ not loaded DU145 incubated with REHQNFYEA- T cells (1:10). CD8$^+$ T cell responses are measured in (A) and (B), CD4$^+$ CD8$^+$ responses are shown in (C) and (D). Means and error bars (SEM) represent triplicate measures from one experiment. Significance was determined by 2way ANOVA with Bonferroni post-hoc tests to determine the interaction between individual groups ***; $p<0.001$.

T cell responses to the KLFEFMHET peptide

The KLFEFMHET-HLA-A*02 $CD8^+$ T cells from Donor 1 produced IFNγ in response to co-culture with BLCL, and there was no significant difference in responses in the presence (55.95% IFNγ^+ $CD8^+$ T cells) or absence of peptide loading 45.45% IFNγ^+ $CD8^+$ T cells) (Figure 5.17A). The production of MIP1β was very low and might be attributable to spontaneous production (6.61% and 3.36% in the presence and absence of peptide loading respectively). The KLFEFMHET-HLA-A*02 $CD8^+$ T cells did not have an overall high response to the primary PCa cells although MIP1β production was significantly higher in the presence of peptide (14.9%) compared to cells not loaded with peptide (1.6%) (Figure 5.17B).

Donor 1 had broadly similar proportions of single positive and double positive T cells; 59% and 38% respectively (Figure 5.14B). The KLFEFMHET-HLA-A*02 $CD4^+$ $CD8^+$ T cells from Donor 1 also produced IFNγ in response to BLCL, in the presence (77.95%) and absence of peptide loading (89.9%) (Figure 5.17C). The MIP1β response to BLCL was also greater than that of the $CD8^+$ T cells (although not compared statistically); 12.8% and 14.37% $CD4^+$ $CD8^+$ MIP1β^+ T cells in the presence of peptide and absence of peptide loading respectively. The $CD4^+$ $CD8^+$ T cell response to primary PCa was similar to that of the $CD8^+$ T cells; MIP1β production in response to peptide loading was significantly higher than cells not loaded with the peptide (Figure 5.17D).

The $CD8^+$ T cell responses to BLCL by Donor 2 were lower than those of Donor 1, although a comparable pattern of response emerged; 28.7% IFNγ^+ $CD8^+$ with peptide and 23.8% IFNγ^+ $CD8^+$ without peptide (not significantly different) (figure 5.17E). The $CD8^+$ T cell responses to the primary PCa cells were significantly different in the presence of peptide loading; 23.7% and 20.9% MIP1β and IFNγ respectively, compared to 3.4% and 7.43% MIP1β and IFNγ respectively in the absence of peptide (Figure 5.17F). The $CD4^+CD8^+$ T cell population constituted the majority in this cell line; 97% (Figure 5.14C). The $CD4^+$ $CD8^+$ T cell responses to BLCL were of a greater magnitude compared to the $CD8^+$ T cells although the pattern was similar; 54.8% $CD4^+$

$CD8^+$ $IFN\gamma^+$ T cells, in the presence of and 54.9% $CD4^+$ $CD8^+$ $IFN\gamma^+$ T cells in the absence of peptide (Figure 5.17G). In contrast to the $CD8^+$ T cells from this donor, the $CD4^+$ $CD8^+$ did not have a significantly higher functional response to primary PCa cells in the presence of peptide, compared to no peptide loading (Figure 5.17H).

Due to time constraints, this experiment was performed once, using expanded T cells subject to two rounds of tetramer-based enrichment. Therefore, it is not possible to make conclusions in the absence of further data. However, based on the available data, some suggestions as to the underlying mechanism of the responses are offered. The responses of the KLFEFMEHT HLA-A*02 T cells from each of the donors may be attributable to the responses of other T cell clones present in the expanded T cell population. However, it is also possible that KLFEFMHET-HLA-A*02 $CD8^+$ T cells recognised endogenous peptide presented by the BLCL, as XPO1 expression in BLCL is reported in the GTEx portal (https://GTExportal.org) and presentation of peptides from the XPO1 protein has been previously described using BLCL as a model for peptide elution (Pearson et al., 2016).

The functional response to primary PCa cells was lower than to the BLCL, although the MIP1β and MIP1β and IFNγ production by $CD8^+$ T cells by Donors 1 and 2 respectively suggests peptide specific recognition. However, lack of recognition in the absence of peptide may indicate low levels of endogenous peptide presentation. The lower magnitude of the responses could be attributable to lower HLA levels, a common mechanism of tumour-immune evasion (Khong and Restifo, 2002), although HLA expression was not directly compared between BLCL and primary PCa cells.

These data, while preliminary, suggest that T cells can be isolated from healthy donors, that recognise peptides identified from the DU145 HLA ligandome, for which the source gene was expressed in ALDH high CSC. Further work is required to isolate peptide specific $CD8^+$ T cell clones, which

will be used to confirm the responses observed here. Therefore, both the ARHGAP42 and XPO1 peptides represent potential prostate CSC targets and the specific responses to presentation of these peptides by ALDH high and ALDH low cells will be investigated in future studies.

Figure 5.17. Functional responses of $CD8^+$ and $CD4^+$ $CD8^+$ T cells from two different donors, to target cells presenting the KLFEFMHET peptide. Cytokine responses were tested 7 days after the second tetramer-based isolation of the respective T cell lines. The expanded cells were co-incubated with either BLCL or primary PCa cells (#5042 HLA-A*02^+ cell line). The expanded cells were co-incubated with either BLCL or DU145 cells at a 10:1 ratio ($1.5x10^5$ T cells: $1.5x10^4$ target cells). Golgi Stop and Golgi Plug were added for 12 hr followed by staining with T cell phenotyping antibodies and intracellular cytokine staining of MIP1β and IFNγ. The $CD8^+$ and $CD4^+$ $CD8^+$ T cell responses were measured by separate gating, from the same co-incubated population. All co-incubations were at a 10:1 T cell: target ratio (A-D) Functional responses by KLFEFMHET HLA-A*02 T cells from Donor 1. (E-H) Functional responses by KLFEFMHET HLA-A*02 T cells from Donor 2. (A, B) $CD8^+$ T cell responses to (A) BLCL and (B) primary PCa cells loaded or not loaded with peptide. (C, D) $CD4^+$ $CD8^+$ T cell responses to (C) BLCL and (D) primary PCa cells loaded or not loaded with peptide. (E, F) $CD8^+$ T cell responses to (E) BLCL and (F) primary PCa cells loaded or not loaded with peptide. (G, H) $CD4^+$ $CD8^+$ T cell responses to (G) BLCL and (H) primary PCa cells loaded or not loaded with peptide. Means and error bars (SEM) represent triplicate measures from one experiment. Significance was determined by 2way ANOVA with Bonferroni post-hoc tests to determine the interaction between individual groups ***; $p<0.001$.

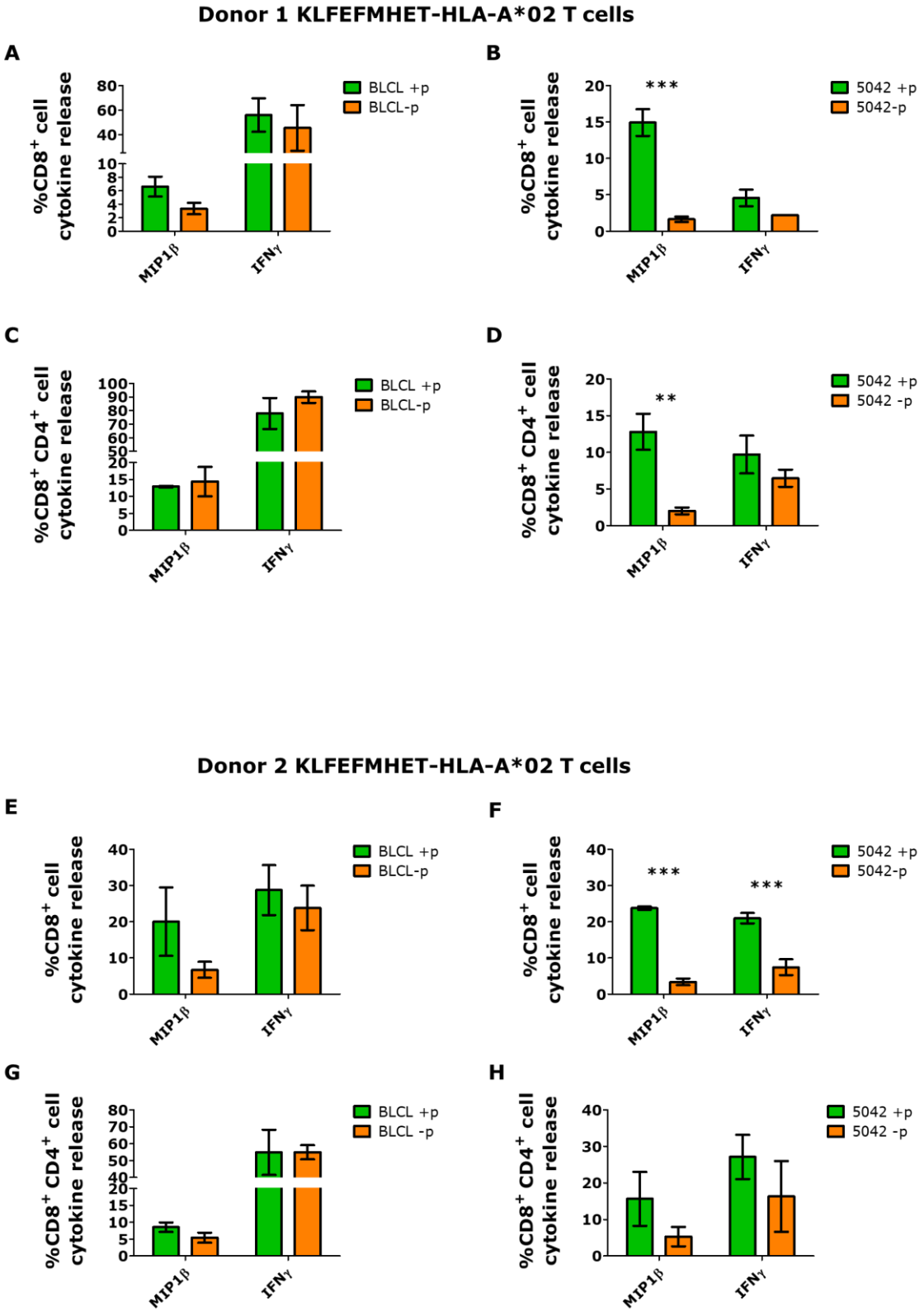
Donor 1 KLFEFMHET-HLA-A*02 T cells
A
%CD8+ cell cytokine release
BLCL +p
BLCL-p
MIP1β
IFNγ
B
***
5042 +p
5042-p
C
%CD8+ CD4+ cell cytokine release
D
**
5042 -p
Donor 2 KLFEFMHET-HLA-A*02 T cells
E
F
G
BLCL -p
H

5.5 Discussion

5.5.1 Identification of antigens from the DU145 HLA ligandome expressed in CSC

The identification of peptides uniquely presented by CSC using HLA ligandome analysis is a challenge, due to the large amount of cellular material required. There are two previous studies in which HLA ligandome analysis of CSC has been carried out (Miyamoto et al., 2018; Neidert et al., 2018). These studies used stable CSC cell lines to generate the HLA ligandome data. The cell lines were generated from single cells, by sorting the cells based on a stem cell marker, or under stem cell-selective conditions (sphere culture) (Günther et al., 2008; Takaya et al., 2016). Two separate HLA ligandomes, from the CSC and non-CSC cell lines were generated and the peptides present in each compared; thus, a peptide found only in the CSC cell line derived ligandome was identified as a CSC specific peptide/ antigen. This was not feasible in this as stable prostate CSC cell lines have not previously been described and were not generated in this project. Despite identifying ALDH as a marker for prostate CSC, the low frequency of the ALDH high and ALDH low DU145 cells (approximately 8% and 12% respectively; Figure 3.6), meant that it was not possible to obtain sufficient cell numbers for direct HLA ligandome analysis. Therefore, the expression of the genes encoding the antigens was analysed in sorted ALDH high and ALDH low populations to define the potential CSC, non-CSC and shared antigens.

This gene expression analysis confirmed ARHGAP42 and SCHBP1 were significantly upregulated in the DU145 cells; SCHBP1 was significantly upregulated in the primary PCa cells however ARHGAP42 was not significantly upregulated. It is possible that selection based on of fold change differences yielded only two candidate antigens because there is not always a clear correlation between gene expression and antigen presentation (Freudenmann et al., 2018). Therefore, further ‘shared’ antigens (expressed in both ALDH high and ALDH low DU145 cells) were selected based on gene transcript abundance. A correlation between the abundance of gene transcripts and

translated protein levels, with antigen presentation has previously been described (Bassani-Sternberg et al., 2015; Fortier et al., 2008). It has been suggested that T cells that recognise 'shared' antigens may be less effective at targeting CSC in the tumour, as the target population consists a greater proportion of the cells present, in comparison to targeting specifically the low frequency of CSC (Hirohashi et al., 2012). However, targeting multiple peptides, including those presented by CSC and shared peptides, could be a more effective therapeutic approach to overcoming the potential for epitope escape thus the combined approach of CSC and shared antigen targeting could be beneficial.

Neidert and colleagues identified 28 peptides derived from 14 antigens in the glioblastoma stem cell HLA ligandome, which were exclusively expressed in tumour tissue (Neidert et al., 2018). Miyamoto and colleagues identified 35 peptides exclusively present in the colon CSC HLA ligandome, although only one was exclusive to tumour tissues (Miyamoto et al., 2018). There were two peptides for which the respective genes were upregulated in the ALDH high compared to ALDH low cells in the DU145 HLA ligandome. The different numbers of CSC peptides identified across these studies may be attributable to differences in the study design. The GSC cell lines used by Neidert and colleagues were established as clonal sphere cultures, although the resulting CSC frequency was not defined (Günther et al., 2008), while the colon CSC cell line analysed by Miyamoto and colleagues constituted approximately 30% side population cells (Miyamoto et al., 2018). The DU145 HLA ligandome was generated from unsorted DU145 cells, while the populations in which the gene expression was analysed are taken from two 'extremes' of ALDH activity- high and low. Therefore, there is a large population of 'ALDH medium' cells, not characterised in this study, which also express antigens. Thus, the proportions of antigens expressed exclusively by ALDH high and ALDH low cells may be reflective of these populations constituting a small proportion of the bulk DU145 HLA ligandome.

Additionally, there is inherent experimental variability in isolating cells using the ALDEFLUOR assay; a large number of cells is by necessity obtained from multiple culture flasks. Multiple ALDEFLUOR reactions are carried out according to the optimal cell number for the reaction, and these tubes are sorted as different replicate tubes by FACS, which are then pooled for RNA extraction. This variability is not possible to control for, particularly in a sensitive analysis such as PCR. Variation in CSC characteristics across repeated experiments was previously noted; including variation in viability of the cells and the different appearance of colonies derived from ALDH high and ALDH low cells (Figure 3.8). Stages at which variation in the ALDEFLUOR analysis could be controlled for are discussed in Chapter 3. The gene expression was measured using RNA extracted from ALDH high and ALDH low cells from three separate FACS experiments; and each PCR reaction was performed in technical replicates, which was enough for statistical analyses. The variation could be further controlled for by increasing the number of experimental repeats or specifically performing further analysis of the selected genes of interest.

Protein expression was investigated to confirm the gene expression results, and to demonstrate the potential for translated proteins to be processed for peptide presentation. The translated protein was identified for each antigen selected based on the gene expression, except for NFE2L2. ARHGAP42 expression was widely detected in the bulk DU145 cells analysed by microscopy; it is possible that the protein staining was not sensitive enough to detect the fold change difference (>1.5 fold) shown by qRT- PCR analysis, or that post-translational regulation of ARHGAP42 protein expression occurs. As previously mentioned, the cellular localisation ARHGAP42 and TPX2 differed to that previously reported in the Human Protein Atlas (www.proteinatlas.org) (Uhlén et al., 2005). I used an antibody verified by the Human Protein Atlas project for the detection of ARHGAP42, although an antibody from a different manufacturer was used to detect TPX2. Antibody staining of TPX2 only in dividing cells additionally highlights the possibility that gene transcripts of proteins involved in specific, transient cellular processes, such as cell division, may not be detectable in genomic materials

sampled from a heterogenous cell population. The differences in cell division, observed in ALDH high and ALDH low DU145 cells and primary PCa cells (Figures 3.11 and 3.20), could also result in differences in peptide presentation from antigens derived from cell division-associated proteins. Further investigation of gene and protein expression in fast and slowly dividing ALDH high and ALDH low cells is warranted to determine if this could or identify a novel form of restricted antigen presentation in CSC compared to non-CSC.

The peptides of interest are derived from antigens which have functional roles in cellular processes, some of which may be related to carcinogenesis. Targeting of functional antigens represents an efficient therapeutic approach as it could reduce immune evasion in which cells downregulate expression of proteins the peptides are derived from. The functional role of ARHGAP42 is largely associated with the regulation of vascular tone and blood pressure (Bai et al., 2013), however has recently been associated with increased cell invasiveness *in vitro* in nasopharyngeal carcinoma, which may be mediated by the PI2K/Akt signalling pathway (Hu et al., 2018). XPO1 is a nuclear transport protein, involved in shuttling proteins out of the nucleus, including TOP2A, survivin, p53 and BRCA1. These proteins have anti-cancer functions within the nucleus, thus overexpression of XPO1, such is observed in a number of cancers, results in translocation of these proteins and a reduced tumour suppression effect (Turner et al., 2012). XPO1 is also involved in duplication of the centrosome, in the process of mitotic spindle assembly (K. T. Nguyen et al., 2012). ATK2 is a putative oncogene which is upregulated with the loss of PTEN, a commonly occurring mutation in PCa carcinogenesis (Chin et al., 2014). AKT2 has been shown to be over-expressed in PCa cell lines and is associated with the expression of CD44 (Le Page et al., 2012; Sahlberg et al., 2014). TPX2 has a functional role in mitotic spindle assembly, and is overexpressed in a number of cancers, including colon, pancreatic and lung cancer (Neumayer et al., 2014). TPX2 overexpression functionally contributes to mitotic spindle miss-segregation, resulting in chromosomal instability, including in PCa (Carter et al., 2006; Pan et al., 2017). . Further work is therefore warranted to determine the functional importance of these

proteins, e.g. by knock-out studies followed by characterisation of the cells in stemness assays, such as sphere formation and analysis of other genes associated with stemness. Some antigens have previously been identified that contributed to CSC function, including OR7C1 and DNAJB8 (Morita et al., 2016, 2014). Many of the antigens are also markers of a poor prognosis in different types of cancer; including ARHGAP42 (pancreatic cancer), TPX2 (pancreatic, liver, endometrial and lung cancer), SEPT9 (liver cancer), XPO1 (renal and liver cancer), AKT2 (prostate and endometrial cancer) TOP2A (renal, lung, liver and pancreatic cancer); all data from the Human Protein Atlas (https://www.proteinatlas.org/). Therefore T cell targeting of these antigens could be investigated in other cancer types which could lead to the development of novel immunotherapies.

5.5.2 Investigation of immune responses to CSC and shared antigens

Functional responses of bulk PBMC from HLA matched donors to the remaining peptide of interest were tested by intracellular cytokine assay, measuring TNFα production. The lack of cytokine production suggested that the tumour peptides could be poorly immunogenic, however the lack of responses to the positive control viral peptides confounded these data. While it is possible that the donors were seronegative for the peptides in the pool, it may be more probable that the particular virus to which the donor was seropositive was not represented in the pool, as peptides from each virus (CMV, EBV or Influenza) were not represented for each HLA restriction. Alternatively the donors investigated may have been low responding donors; it has been shown that the magnitude of a T cell response to the same peptide can vary between different individuals (Moldovan et al., 2016). Treating the PBMC using mitogens for example phytohemagglutinin (PHA) or phorbol myristate acetate (PMA) (Dasgupta et al., 1987; Downward et al., 1990; Ohtsuka et al., 1996) represent an additional possible control condition to rule out the possibility of technical issues such as defective antigen responsiveness of the T cell used in the assay, or poor antibody detection of TNFα. PHA and PMA activate T cells by non-antigen specific mechanisms; by binding to CD3 and activating intracellular protein kinase C, respectively

(Downward et al., 1990; Valentine et al., 1985). This could be used to determine if the donors lacked a high T cell activation response, by comparing TCR and non-TCR mediated signalling (i.e. peptide-specific or mitogen stimulation).

Since no further peptides could be eliminated based on the T cell response in bulk PBMC, homology modelling was carried out to select a limited number of peptides with which to produce HLA-peptide tetramers for T cell isolation. Homology modelling was used in the study by Kochin and colleagues, to examine sequence mediated structural differences between two different peptides of interest, in the context of the impact on engagement with the TCR (Kochin et al., 2017). However, this approach has not previously been used to investigate the structural interactions influencing binding between peptides and HLA alleles from an HLA ligandome dataset, or to select for optimal peptides with which to produce tetramers.

HLA modelling is a predictive analytical approach, similar to the HLA affinity binding analysis performed at an earlier stage of this study; however, the predictions are made based on different sources of experimental data. Novel structures are predicted on data from experimentally resolved crystal structures, rather than ligand binding data from affinity assays. Quantification of the resulting homology model produces a number of readouts including the 'p value' used in this study, which indicates how 'surprising' an interface is, in terms of the solvation free energy gain (the difference between the solvation energy of each individual structure versus the interface formed by the structures together). The homology modelling approach particularly complements the investigation of peptide interactions with rarer HLA alleles, as predictions are made based the biochemical structural interaction rules governing amino acids (e.g. polar/ non-polar and steric interactions). This is free of the assumptions regarding amino acid positioning or motifs that are made based on experimental HLA allele binding or ligand datasets. Investigation of the structural interactions between peptides and the cognate HLA molecule is complementary to predicting or measuring the binding

affinity (Antunes et al., 2018), therefore it provides a further *in silico* means of reducing the number of candidate peptides where analysis is limited by time and funding. This technique is therefore beneficial for low-throughput analysis of HLA-peptide interactions (as all models are manually generated, compared to automated ranking of binding affinity values). In the event that a clonal T cell line specifically recognising one of the CSC or shared peptides is produced as part of a future study, the production of a crystal structure of the novel TCR could be analysed using the same visualisation and quantification techniques employed for homology modelling. However, for additional comparison it would be useful to evaluate the re-folding of a poorly scoring predicted complex to determine the bearing of structural prediction on re-fold success. The HLA-peptide homology model could thus be compared to the experimentally resolved structure to determine its accuracy and inform further predictions.

5.5.3 Generation of T cell lines recognising CSC peptides

Isolation of tumour antigen specific T cells presents a number of inherent challenges. Healthy donors are expected to only possess a low frequency of naïve T cells that could recognise tumour antigens derived from self-proteins, owing to thymic deletion and a presumed lack of previous tumour challenge (Alanio et al., 2010; Starr et al., 2003). On the other hand, patient derived tumour antigen specific T cells may be dysfunctional and express inhibitory receptors, due to chronic antigen stimulation and inhibitory signalling in the TME (Finn, 2012; Reiman et al., 2007). Additionally, the affinity of self-tumour antigen TCRs is typically much lower than viral antigen specific TCR (Hebeisen et al., 2013; Stone and Kranz, 2013). The strategies used to overcome this involved peptide specific stimulation of the $CD8^+$ T cells from bulk PBMC prior to sorting, and the use of tetramers, with additional techniques to enhance tetramer binding. The cells were incubated with the protein kinase inhibitor, dasatinib, which reduces TCR internalisation following tetramer binding, followed by staining with an anti-CD8α antibody, which is also associated with improved tetramer staining (Dolton et al., 2015; Wooldridge et al., 2009).

The T cell frequency and cells yielded from FACS was particularly low in the HLA-B*50 donors (76 cells from Donor 1 and 142 cells from Donor 2; 0.011% and 0.008% of the total PBMC respectively). This was not unexpected, based on the low cytokine responses observed in the initial screening assay. The low cell yield obtained from sorting presented a challenge to expanding the tetramer positive cells. Pre-selecting and stimulating the $CD8^+$ cells with peptide did not quantitatively increase the tetramer specific cell yield from HLA-B*50 Donor 2 (191 cells; 0.14% of the $CD8^+$ population), however it did result in successful expansion when compared to previous experiments which lacked selection of the $CD8^+$ T cell population from bulk PBMC, and peptide stimulation. The underlying mechanism for this was not elucidated; however it is suggested that peptide stimulation of $CD8^+$ T cells prompted some peptide specific expansion; and peptide-activated $CD8^+$ T cells were more resistant to apoptosis as a result of activation by tetramer binding (Wooldridge et al., 2009).

The identification of a $CD4^+$ $CD8^+$ tetramer positive T cell population was an unexpected outcome of the expansion of the tetramer sorted population. Concurrent $CD4^+$ and $CD8^+$ expression occurs in the course of T cell development, prior to negative selection of responsive TCRs and maturation into single positive $CD4^+$ or $CD8^+$ T cells (Koch and Radtke, 2011). However, mature $CD4^+$ and $CD8^+$ double positive T cells have also been described (Blue et al., 1985; Overgaard et al., 2015). Previous studies have suggested that both $CD4^+$ and $CD8^+$ single positive T cells can be the source of mature double positive cells through gain of expression of CD8 or CD4 respectively (Kitchen et al., 2005; Macchia et al., 2006; Molteni et al., 2002; Sullivan et al., 2001). (Blue et al., 1985; Macchia et al., 2006; Sullivan et al., 2001). It has been suggested that expression of CD4 by $CD8^+$ T cells arises specifically in the context of *in vitro* T cell activation (Kitchen et al., 2004; Sullivan et al., 2001). Therefore, activation by the multiple rounds of tetramer-based T cell sorting carried out in my study could provide an activation signal resulting in CD4 expression by $CD8^+$ T cells. Double positive T cells appear to be functional as

they have been associated with enhanced anti-viral responses in a mouse model of HIV (Kitchen et al., 2005), and tumour specific responses in ovarian cancer (Matsuzaki et al., 2019). The TCR from a double positive T cell clone was shown to confer antigen specificity to both $CD8^+$ and $CD4^+$ single positive T cells, raising the possibility of activating a Th_1 and Th_2 functional response to the same antigen (Matsuzaki et al., 2019). Therefore, it is of interest to separately isolate the single and double positive T cells and determine the stability of the double positive populations with extended culture. Analysis of TCR from single positive and double T cells may also help determine whether they are descended from the same parental T cell.

5.5.4 Testing T cell responses to peptides

Although the T cell responses to ALDH high and ALDH low cells were not compared due to time constraints, preliminary investigation of the potential CSC-immune interactions were evaluated by measuring HLA expression by ALDH high and ALDH low DU145 and primary PCa cells. Higher HLA expression by the ALDH high DU145 cells was unexpected, as downregulation of HLA Class I by cancer cells occurs to evade the immune system (Dunn et al., 2002), and lower expression of HLA Class I by CSC, compared to non-CSC, has been demonstrated in melanoma (Maccalli et al., 2014; Schatton et al., 2010). HLA expression had a linear correlation to ALDH activity (data not shown); the bulk of the DU145 cells ('ALDH medium') expressed HLA at intermediate levels compared to higher HLA levels expressed by ALDH high DU145 and the lower HLA levels expressed by the ALDH low cells. Contrastingly, the HLA expression levels were not significantly different in the primary PCa cells investigated. This could be due to the differences in the disease stage represented by the different models, or due to *in vivo* immune interactions in the primary PCa cells. Analysis of a greater number of primary PCa cell lines is required to investigate the potential differences between established and primary PCa cells lines as it is possible that extensive *in vitro* culture of DU145 cells has resulted in genetic changes the HLA expression. Detection of any HLA Class I expression in the DU145 and primary cells is in contrast to the study by Domingo-Domenech and colleagues, in which

treatment (docetaxel) resistant DU145 did not express HLA Class I, and a rare population of HLA-I^- cells were found in primary PCa samples, with increasing frequency of the population correlating to later stage and post-treatment disease. However, since lack of HLA Class I expression also is an unexpected immune evasion mechanism, as this could lead to killing by NK cell (not tested in the study). Interestingly, in a study by Liao and colleagues, there was no significant difference in HLA Class I expression between ALDH high and ALDH low cells from HNSCC cell lines, while ALDH high ovarian cancer cells expressed lower HLA Class I (Liao et al., 2013). However, there was higher lysis of the ALDH high cells by $CD8^+$ T cells in both the ovarian cancer and HNSCC cell lines tested. Therefore, it is of interest to further evaluate the impact of the differential HLA expression by the ALDH high and ALDH low cells in my study in T cell co-culture assays. It may also be useful to compare differences in expression of proteasomal pathway proteins; e.g. TAP, ERAAP by ALDH high and ALDH low cells in established and primary PCa cells.

For pragmatic reasons, T cell responses in the tetramer enriched cell lines were initially tested against the candidate CSC associated peptides. IFNγ was the predominant functional marker produced in the T cell co-incubation experiment, against each of the HLA matched BLCL and DU145 cells, except for the $CD8^+$ T cells from Donor 1 that were co-incubated with the primary PCa cells. It is not known why MIP1β production was lower, it may suggest that that this chemokine plays a different role in the response to viral antigens compared to tumour antigens. Measurement of IFNγ and MIP1β represents a limited evaluation of polyfunctional responses, in that a cytotoxic cytokine and a chemokine are simultaneously evaluated. MIP1β is not directly involved in cell lysis, and primarily functions as a chemoattractant for CD4 T cells (O'Grady et al., 1999; Saunders et al., 2011). However, production of MIP1β by T cells has been shown to have a protective role in the immune response to HIV, and conferred increased sensitivity in detecting IFNγ mediated HIV specific T cell responses by flow cytometry (Kutscher et al., 2008; Saunders et al., 2011). Investigation of further cytokine production e.g. also comparing TNFα production, and CD107a upregulation is warranted. It is also necessary

to test the production of functional makers by T cells in a more complex model that incorporates other T cell subsets, e.g. CD4 T cells, for which MIP1β signalling may be relevant in co-ordinating the effector immune response.

The functional responses by the REHQNRYEA-HLA*B50 and KLFEFMEHT-HLA-A*02 $CD8^+$ T cells suggest peptide specificity. The REHQNRYEA-HLA*B50 appeared to respond to both exogenous and endogenous peptide presented by DU145 cells, although there may have been off target responses to non-peptide loaded BLCL. The BLCL were derived from the same donor as the T cell line, therefore an HLA mismatched response is not likely. On the other hand, responses to DU145 cells could represent non-autologous responses. It may not be possible to control for this without a cell line positive for only the HLA-B*50 allele or are HLA matched for everything except HLA*B50; the paucity of established and primary PCa cell lines and infrequency of the HLA*B50 means that this may not be feasible. Overall, the approach to confirming these observations is to produce clonal T cell lines, by further tetramer sorting experiments. Additionally, it would be beneficial to combine selection of clones with analysis of functional responses. This could be done by plating clones in limiting dilution *in vitro* culture and measuring the response to peptides, e.g. using a chromium release or other non-radiation-based lysis assay. With a clonal T cell line specific to the peptide of interest, the possibility of other clones recognising other peptides presented by the target cells, e.g. EBV epitopes by BLCL, should be minimised (Wooldridge et al., 2012). To test peptide-specific responses by KLFEFMEHT-HLA-A*02 T cell clones, a different target than EBV transformed B cells is required, owing to the possibility of endogenous presentation by these cells, for example cells deficient in endogenous peptide presentation e.g. the HLA-A*02 positive T2 cell line (Salter and Cresswell, 1986). Additionally, XPO1 gene expression and abundance was not tested in the #5042 primary PCa cell line and the HLA expression of these cells was lower than that of the ALDH high DU145 cells. Therefore, both XPO1 expression and transcript abundance, which may be indicative of antigen processing and presentation (Bassani-Sternberg et al., 2015; Fortier et al., 2008) should be tested in this cell line, and other cell lines with higher HLA-A*02 expression.

5.5.5 Conclusion

In conclusion, potential peptide targets of CSC were identified from the DU145 HLA ligandome, using ALDH high and low activity as a marker of CSC and non-CSC respectively. This approach demonstrates that bulk HLA ligandome datasets could be interrogated using CSC markers, to identify potential CSC antigens. Homology modelling was used to select optimal peptides to produce tetramers, a technical approach which has not been previously used to analyse HLA ligandome data. Due to timing limitations, tetramer-enriched polyclonal T cell lines were produced, with cloning of these T cells to form the subject of future studies. The specific T cell response to the ALDH high CSC population was not investigated and will require modifications to currently existing assays of T cell functional responses to specifically investigate CSC killing by T cells. Further work is required to confirm peptide specificity of the tetramer enriched T cell lines; functional cytokine responses were identified from the $CD8^+$ and $CD4^+$ $CD8^+$ T cells and the recognition of DU145 in the absence of exogenous peptide suggests the possibility of endogenous presentation of the ARHGAP42 peptide. Preliminary functional testing of only two of the peptide candidates was possible during this study. However, this study highlights the potential for the HLA ligandome approach as a powerful means of identifying potential immunotherapy targets for several human cancers.

Chapter 6.

General Discussion

6 General Discussion

CSC have been implicated in progression and relapse in many cancers, owing to their characteristics of treatment resistance and self-renewal. In PCa, localised disease has a high frequency of successful treatment outcomes; this contrasts with the poor prognosis associated with clinical progression. CSC, which could contribute to recurrence, thus represent an important therapeutic target. The confluence of CSC and cancer immunotherapy is an under-explored area, particularly in PCa. Therefore, in this study we aimed to isolate and characterise prostate CSC for the purpose of identifying possible target antigens for T cell immunotherapy.

6.1.1 Development of a novel primary PCa cell model *in vitro*

In this study, I established adherent *in vitro* culture conditions for primary PCa cells. There are relatively few models of primary/ localised prostate tumours, as PCa cells are difficult to successfully culture *in vitro* (Namekawa et al., 2019). Therefore, there is an ongoing need for further development of *in vitro* models of localised/ early stage PCa so that treatments aimed at reducing the frequency of disease progression, such as targeting CSC, could be investigated. It may also be more effective to test immunotherapy in a less immunosuppressive TME that occurs at an earlier stage in PCa progression (Drake, 2010). In some studies, primary PCa cells were propagated with the use of feeder cells (Frame et al., 2016; Xuefeng Liu et al., 2012). However, this method results in undefined factors within the system, which may make it difficult to replicate. The inclusion of xenobiotic feeder cells could also influence the outcome of immunology studies. I developed culture conditions for 2D *in vitro* growth of primary PCa by adapting the protocol developed by Drost and colleagues, in which primary prostate and PCa organoids were cultured in fully growth factor-defined conditions that did not include feeder cells (Drost et al., 2016). I adapted the media used for organoid culture to expand greater numbers of primary PCa cells in 2D culture, which was necessary to analyse the infrequent CSC population. The culture conditions I established did not recapitulate the prostate lineage, as the phenotype of the cells was predominantly basal.

Nevertheless, under these conditions, the adherent cells in my model displayed a different morphology to other primary PCa samples that I grew according to conditions described previously (without using feeder cells) (Frame et al., 2016), as they had 'tissue-like' morphology including regions of heterogeneity and lumen-like structures (Figure 3.15). It is of particular interest to further characterise the primary PCa cells grown under these conditions, including optimisation of a fixation and staining protocol for microscopy and genetic analysis to determine the mutational profile of individual primary PCa samples. Therefore, this culture protocol represents an important novel tissue culture development which may be useful to investigate not only CSC but localised PCa in general.

6.1.2 Comparative analysis of prostate CSC using different markers and cellular models

One of the strengths of the current study is that prostate CSC were investigated using both the DU145 cell line and primary PCa cells. It is difficult to generalise findings from one cell line model to the wider clinical course in PCa, owing to disease heterogeneity. It is also difficult to rely on results from primary PCa cells only, because of variation in cell yields and viability between patients. Therefore, a combination of cell models was used; the DU145 cells were used for reliable generation of large numbers of CSC for characterisation and assay optimisation, and primary CSC were used, in smaller numbers, to investigate markers in samples more relevant to disease. This approach is in contrast to previous studies of prostate CSC, in which either metastatic cell lines or primary PCa cells (typically derived from localised tumours) were investigated (Collins et al., 2005; Pfeiffer and Schalken, 2010). Some studies have carried out limited immunofluorescence analysis of CSC markers and clinical characteristics using primary PCa tissue (Cojoc et al., 2015b; Liu et al., 2015; Yan et al., 2014), however, the expression of CSC markers by PCa cell lines and primary PCa cells has not previously been directly compared.

Identification of prostate CSC in the DU145 and primary PCa cells was investigated using surface markers ($CD44^+$ $CD49b^{high}$ $CD133^+$) and a

functional marker (ALDH). There is evidence supporting the use of surface and/ or functional CSC markers to isolate prostate CSC (Collins et al., 2005; Liu et al., 2015; Patrawala et al., 2006, 2005; van den Hoogen et al., 2010). This suggests that there is not a singularly applicable panel of markers for systematic analysis of prostate CSC. The markers $CD44^{+}$ $CD49b^{high}$ $CD133^{+}$ are applicable to basal cells of the prostate/ prostate tumours, while ALDH is not inherently associated with a particular tissue lineage. The use of $CD44^{+}$ $CD49b^{high}$ $CD133^{+}$ is attributable to the hypothesis suggesting CSC arise from the basal compartment of the prostate, similar to prostate SC. However, a number of studies have described stemness characteristics in luminal cells in the context of healthy or cancerous prostate growth and development (Choi et al., 2012; Karthaus et al., 2014; Ousset et al., 2012; Wang et al., 2009). Additionally, differences in tumour initiating capacity of $CD44^{+}$/ $CD49b^{+}$ single positive or $CD44^{+}$ $CD49b^{high}$ double positive populations observed in the studies by Liu and colleagues and Patrawala and colleagues suggest that these markers may identify different basal CSC subpopulations, or a hierarchy of stemness characteristics associated with the expression of one or multiple CSC markers.

The concept of multiple CSC lineages or subpopulations can be accommodated by the CSC hypothesis, which has undergone updates reflecting the growing data in this area (Prager et al., 2019). It has been suggested that a tissue lineage consists of cells that possess phenotypic plasticity, which could acquire stemness characteristics (Batlle and Clevers, 2017). Therefore, while SC remain the most likely target of carcinogenesis, there exists a bidirectional, rather than unidirectional hierarchy of stemness. This adds further complexity to the analysis of CSC in cancer which is beyond the scope of this study; however, it is an important consideration for future investigations of CSC. From a therapeutic perspective, molecular treatments targeting stemness characteristics may require continued or repeated delivery if different lineages acquire CSC-like characteristics. This highlights the potential of immunotherapy as a CSC treatment, as CSC antigen specific T cells could recognise and kill the ‘new’ CSC-like population, if the same antigens are expressed by these cells.

In this study, I was unable to isolate prostate CSC using the surface markers $CD44^{+}$ $CD49b^{high}$ $CD133^{+}$ (Collins et al., 2005). The reason behind this could be attributable to investigating CD133 expression in the DU145 cell line, since its use as a prostate CSC marker was first described using primary PCa samples. However, I was additionally unable to convincingly identify $CD133^{+}$ cells in primary PCa cultures. This is in agreement with the study by Timofeeva and colleagues, using the aforementioned primary PCa model (Xuefeng Liu et al., 2012; Timofeeva et al., 2016). In another primary PCa study, CD133 expression was detected, however $CD133^{+}$ cells were not more tumorigenic than the $CD133^{-}$ cells. Expression of CD133 in PCa cell lines is not conclusive due to conflicting results from different studies describing CD133 expression or lack thereof (Dubrovska et al., 2009; Pfeiffer and Schalken, 2010; Portillo-Lara and Alvarez, 2015; van Leenders et al., 2011). As previously discussed, post-translational modification, cell culture conditions and different antibodies used for identification results in inconsistencies in the application of CD133 as a CSC marker. The different *in vitro* culture conditions in which primary PCa were successfully grown in my study could also impart differences in CD133 expression. Prostate CSC have been investigated in the absence of CD133; as $CD44^{+}$ $CD49b^{+/high}$ cells were shown to have CSC characteristics including clonogenicity and tumour initiation (Liu et al., 2015; Patrawala et al., 2007). Therefore, the general relevance of CD133 in isolating prostate CSC is unclear. Since my study was focused on identifying potential antigens of CSC for T cell targeting, it was not feasible to also compare the stemness characteristics associated with populations expressing different prostate CSC markers (e.g. $CD44^{+}$ vs $CD49b^{high}$). Therefore, the single functional marker, ALDH was investigated.

Clonogenic and self-renewal characteristics of ALDH high cells *in vitro* were demonstrated in the DU145 PCa cell line, in agreement with previous studies (Cojoc et al., 2015b; van den Hoogen et al., 2010). Additionally, *in vivo* tumorigenesis was demonstrated in a more immunocompromised model (NSG mice) than previously investigated. These functional characteristics support the use of ALDH as a prostate CSC marker. In addition to confirming

CSC characteristics in ALDH high cells, using the existing assays, novel measures were developed. The sphere formation assay was modified to incorporate a semi-quantifiable measure of sphere growth; the Orangu assay. Quantitative outputs such as this could be used to compare relative sphere formation by CSC subpopulations isolated by different combinations of CSC markers, to expand beyond the distinctions 'CSC' and 'non-CSC' and potentially investigate a spectrum of stemness reflecting a bidirectional CSC hierarchy in tumours.

Differences in cell division were identified for the first time between ALDH high and ALDH low cells in both DU145 cells and primary PCa cells, using the Cell Trace dye. This assay was particularly useful to analyse primary PCa, in which *in vitro* characterisation of sorted populations was limited due to poor viability. Previous studies have identified slow cycling cells based on label retention in glioblastoma, HNSCC and pancreatic cancer (Bragado et al., 2012; Deleyrolle et al., 2012; Dembinski and Krauss, 2009). This characteristic has also been described in prostate SC; therefore, the identification of label retaining prostate CSC in my study suggests that this stemness characteristic is common to both healthy and diseased tissue in the prostate. Cell trace dye retention could be explored as an additional marker to ALDH for the isolation of prostate CSC, or the characteristics of ALDH high/ low cells could be compared with high/ low dye retaining cells. Analysis of label-retaining cells could also be incorporated into a sphere formation assay, similar to the approach taken by others (Bragado et al., 2012; Hu et al., 2017).

Gene expression analysis has previously been carried out on PCa and healthy prostate cells. Birnie and colleagues identified markers of inflammation and adhesion in prostate CSC ($\alpha_2\beta_1$Integrin^{high} CD133^{+}) while Zhang and colleagues compared the expression profiles of basal and luminal cells, suggesting the basal phenotype had a stemness gene signature (Birnie et al., 2008; Zhang et al., 2016). I added new data to these observations on gene profiles of prostate and PCa stemness using qRT-PCR and Nanostring. These experiments showed that there was a greater number of genes differentially

expressed in primary PCa compared to DU145 cells. This may be associated with long-term *in vitro* culture conditions affecting transcriptional activity and highlights the importance of the use of primary cells for investigating prostate CSC. Pathway analysis revealed that ALDH high cells in 2 out of 3 primary PCa samples showed upregulation of genes involved in the NOTCH pathway; activation of NOTCH ligands and receptors was also described by Zhang and colleagues in primary prostate basal cells (Zhang et al., 2016), which may suggest a common stemness gene profile despite different markers being used to distinguish the populations in my study. Analysis of a larger sample size is warranted to confirm these data; additionally, the disease characteristics and gene signature could be further examined to determine a possible correlation.

The Cell Trace data and the gene expression results from the Nanostring analysis together suggest that ALDH high cells have different cell cycling characteristics to ALDH low cells. Although investigated in a limited number of samples, the Nanostring analysis showed that genes involved in cell cycling, such as CDK1, CDH1 and CCND2 were upregulated in ALDH high primary PCa cell lines and in DU145 cells. While not explored in this study, differences in cell cycling, including asynchronous DNA synthesis and quiescent subpopulations, between CSC and non-CSC is suggested to contribute to resistance to DNA damaging cancer therapies such as radiation therapy and chemotherapy (Ischenko et al., 2008). Further investigation of these characteristics in prostate CSC is warranted, particularly owing to the use of radiation therapy as a standard of care in localised PCa.

6.1.3 Development of a novel primary PCa cell model *in vitro*

In this study, HLA ligandome analysis was used to identify novel T cell target peptides which could be presented by CSC. Having established that ALDH activity could be used to identify stemness characteristics, this was applied to interrogate the DU145 HLA ligandome dataset. As previously discussed, bulk DU145 cells, rather than ALDH high and ALDH low cells, were analysed by mass spectrometry, owing to the requirement for large cell numbers in the

technique. HLA ligandome analysis provided an alternative approach to identifying CSC antigens compared to pre-selection of CSC markers as sources of potential epitopes; while some studies have investigated the targeting of such antigens e.g. ALDH and EpCAM, there remains the potential for off-target damage to tissue SC (Deng et al., 2015; Visus et al., 2011). This possibility was reduced in my study since potential target antigens were selected based on absence of or low expression in healthy tissues. In addition to functioning as potential antigens of CSC, the genes more highly expressed in the ALDH high cells could have novel functional roles in the prostate CSC phenotype.

The DU145 HLA ligandome, here used to identify potential CSC antigens, also represents the first description of a Class I ligandome for PCa. HLA ligandome analysis provides a wider snapshot of the presented peptides of a target cell population than methods based on functional responses e.g. SEREX/ T cell response measures. HLA ligandome analysis has been performed in a limited number of studies, including in ovarian cancer, a number of types of leukaemia, melanoma and colon cancer owing to the highly technical demands of the protocol (Berlin et al., 2016; Bilich et al., 2019; Gfeller et al., 2018; Pritchard et al., 2015; Schuster et al., 2017). The number of known HLA Class I ligands is increasing exponentially; while the identification of potential epitopes from these data requires an extensive undertaking, it could be a source of future therapeutic targets as the cancer immunotherapy field continues to grow. Increasing HLA Class I ligandome data derived from healthy cells will also make selection of tumour-specific targets easier. The ligands identified will also add to the understanding of antigen processing and peptide presentation, particularly in the context of the rare HLA alleles expressed by the DU145 cells.

This study demonstrated that it was possible to isolate low frequency peptide specific T cells from blood and enrich and expand them *in vitro*. T cells, recognising the novel TAAs identified in this study, could be used in further studies testing immune responses in PCa and potentially in CRC, as the peptides targeted have also previously been identified in CRC cell lines. Other

antigens, for which T cell lines were not developed, could also be investigated in different cancers (e.g. CLL) in future. The selected peptides REHQNFYEA and KLFEFMEHT were shown to be immunogenic *in vitro* and further investigation is warranted. However, due to time and funding constraints this study did not definitively demonstrate T cell recognition of these peptides as a result of natural antigen processing by CSC. Generation of T cell clones will be required to conclusively shown that peptide specific T cells recognise the CSC; within a polyclonal (tetramer-enriched) population it is possible that non-peptide specific T cells could recognise the CSC (or other tumour cells). Responses of T cell clones could be tested using the ELISPOT assay as an initial screening method as is challenging to perform T cell assays on CSC due to the low frequency in the bulk population and low cell numbers obtained from FACS sorting. This has the advantage of requiring fewer T cells and target cells, although it is limited to the detection of single cytokine responses and does not identify the specific cell population producing the cytokine. By contrast, ICCS, although requiring more cells, allows the detection of multiple cytokines (polyfunctionality) by individual cells and it may be possible to modify the method undertaken in my study, to combine tetramer staining and ICCS (Appay and Rowland-Jones, 2002).

6.1.4 Future directions

It will be necessary to develop or modify existing assays to measure T cell responses that are specific to CSC. It may be possible to use the ALDH assay to identify proportions or total numbers of ALDH high and ALDH low cells following co-incubation with CSC-peptide specific T cells. Additional co-staining may be required to distinguish ALDH activity by T cells (e.g. phenotype specific surface markers). Alternatively, the ALDH high and ALDH low populations could be sorted prior to co-incubation with T cells to measure functional activation or target cell lysis. However, the differences in viability between the ALDH high and ALDH low cells following sorting may present challenges and investigation of protocols to improve viability will be needed. Sphere formation could also be used to investigate functional T cell responses to CSC antigens, by investigating the capacity of CSC to form sphere following co-incubation with T cells. Ultimately, *in vivo* analysis of CSC-specific killing

would be necessary to determine if CSC antigen specific T cells could prevent CSC mediated tumorigenesis; alternatively the effects on tumour reduction by T cell targeting of CSC could be measured and compared to non-CSC targeting, as described previously (Miyamoto et al., 2018; Morita et al., 2016; Nishizawa et al., 2012).

There is scope for investigation of the immune response to the antigens of interest in other cancer types. In addition to the identification of a HLA-A*02:01 peptide from XPO1 in SW480 cells (Hongo et al., 2019), the HLA-B*50:01 peptide identified in my study has been previously described in the HLA ligandome of a CLL patient (Nelde et al., 2018). The REHQNFYEA peptide (ARHGAP42); was identified in the HLA ligandome of HT-116 colon cancer cells (Bassani-Sternberg et al., 2015). In this study HLA binding predictions based on the HLA type of HCT-116 cells (HLA-A* 01:01, 02:01, HLA-B*45:01, 18:01, HLA-C* 07:01, 05:01) suggest this peptide also binds HLA-B*45:01. The HLA-B*50:01 peptide identified from SEPTIN9, REMIPFAVV, has also been shown to bind HLA-B*40:02 (using HLA HLA-B*40 transfected lymphoid cells) and HLA-B*49:01 (B-LCL) (Alpízar et al., 2017; Hillen et al., 2008). This suggests that the peptides identified in the DU145 HLA ligandome could be potential therapeutic targets in other types of cancers and in patients expressing other HLA types. The HLA-A*33:03 peptides (derived from RLN2, TPX2, AKT2 and TOP2A) were not found in the IEDB database, indicating that these peptides are novel HLA ligands. Additionally, the other peptides investigated by homology modelling merit further investigation, as the structural predictions used to select optimal antigens for tetramer production do not rule out the possibility that lower scoring peptides could also produce tetramers. A more comprehensive analysis of the high affinity HLA binding antigens (N=45) could identify further targets applicable to other cancer types.

Therapeutic targeting of CSC is increasing in importance as cancer treatments improve, since longer lifespans post-treatment increase the duration during which relapse could occur, which could be driven by CSC which were not eradicated during primary treatment. As previously discussed, some form of

recurrence occurs in up to 40% of PCa patients and localised PCa represents a window in which PCa could be effectively eradicated, in contrast to incurable metastatic PCa. Clinical testing of immunotherapy for localised PCa (Parsons et al., 2018) represents a shift towards targeted therapies at an earlier disease stage, which could have more durable responses. Therefore, the work in this thesis is a timely contribution to the development of cell-specific therapies, and the expansion of immunotherapies to treat PCa.

The typical first line treatments for localised PCa (surgery, radiation therapy) are unlikely to be effective against CSC. However, there is scope to adopt a synergistic approach as exclusively targeting CSC could induce selective pressure resulting non-CSC gaining stemness features, due to cellular plasticity. Thus, despite the CSC hypothesis suggesting that targeting CSC would also lead to the death of non-CSC, a different complementary therapy to debulk the non-CSC of the tumour is also likely to be necessary. This could have the dual mechanism of action of improving immune cell infiltration of the tumour, generating damage associated immune activation signals and reducing the available pool of non-CSC that could acquire CSC characteristics due to signals in the TME (Derer et al., 2015; Kyjacova et al., 2015; Vlashi and Pajonk, 2015). HDAC inhibition is another approach that could have a synergistic effect on CSC if combined with radiation therapy, as one study found that HDAC6 inhibition increased MHC expression (in a mouse model) in NSCLC (Adeegbe et al., 2017) while HDAC inhibition has also been shown to increase radiosensitivity in CSC in PCa cells (Frame et al., 2013).

The main format of anti-CSC therapeutics currently under investigation involves targeting CSC intrinsic factors, i.e. stemness pathways. In this thesis, characterisation of ALDH high prostate cells identified NOTCH signalling and cell cycling as potential contributing factors to the CSC phenotype, and as such, represent therapeutic targets. Other stemness pathways in clinical development include targeting Wnt and Hedgehog signalling components (Clara et al., 2019; Saygin et al., 2019). Therapeutic targeting of NOTCH signalling has been investigated at different levels of the NOTCH signalling pathway, including γ-secretase inhibitors (blocking

signalling at the intracellular level) and antibodies against various NOTCH receptors and membrane bound ligands (Clara et al., 2019; Saygin et al., 2019). However, many of these agents have shown limited clinical progress, largely due to an unfavourable toxicity to efficacy ratio (Clara et al., 2019). Inhibitors of Wnt signalling include ligand (e.g. Fzd, DLL) blocking antibodies and β-catenin inhibitors, however none have yet reached phase III of clinical testing (Clara et al., 2019; Du et al., 2019; Saygin et al., 2019). In contrast, the approved anti-fungal agent Itraconazole showed preclinical efficacy in blocking Hedgehog signalling and is currently in Phase II testing against metastatic PCa (Antonarakis et al., 2013; Kim et al., 2010). Targeting pathways associated with stemness and development poses the risk of damaging healthy tissue stem cells. Therefore, further investigation of CSC markers could improve therapeutic targeting with the development of CSC marker-conjugated stemness inhibiting drugs and reduce off-target toxicities.

Some recent preclinical studies have also shown how components of the cell cycle could be targeted. T cell epitopes from cyclin E were identified in a recent study in leukaemia using a predictive algorithm (He et al., 2020). Cyclin E is upregulated in leukaemia and T cells which specifically recognised the novel epitopes preferentially lysed HLA matched leukemic cells compared to non-HLA matched cells and healthy haematological progenitor cells (He et al., 2020). Taking a different approach to targeting cell cycling, another study showed that disrupting cell cycling by CDk7 inhibition resulted in genomic stress and instability and induced TNFα and IFNγ signalling in SCLC cells (Zhang et al., 2019). The impact of cell cycle inhibition on CSC was not specifically investigated in the study by Zhang and colleagues, therefore the slower cycling observed in ALDH high cells may reduce the impact of cell cycle inhibition. Nevertheless, this supports further investigation of the mechanisms and genes involved in the disparate cell cycling found in ALDH high compared to ALDH low cells in this thesis.

While it has been suggested that CSC could also evade the immune system, for example by low HLA expression, production of immune inhibitory cytokines and upregulation of PD-L1 (Chen et al., 2015; Krishnamurthy et

al., 2014; Y. Lee et al., 2016; Vidal et al., 2014), this can be viewed in the context of an already immunosuppressive tumour microenvironment. Therefore, immunotherapies developed to eliminate tumour cells without discriminating CSC from non-CSC could also be used to target CSC. In a preclinical model of melanoma, the combined approach of PD-L1 and CLTA4 blockade and DC vaccination resulted in eradication of ALDH high CSC (Zheng et al., 2018). Approaches to specific targeting of CSC by immunotherapy include CAR-T cells or antibodies directed against CD133, CD123 or EpCAM and DC vaccines (loaded with CSC lysate) (Clara et al., 2019; Saygin et al., 2019; Turdo et al., 2019). However, these targets may present a similar risk to targeting of stemness pathways, in that the antigens could be expressed by healthy stem cells. Therefore, the antigens identified in this thesis on the basis of limited healthy tissue expression represent a viable future direction for CSC immunotherapy. Moving forward with the development of CSC specific therapies, it is also necessary to incorporate specific measures of CSC targeting into treatment outcomes. Criteria for assessing responses to immunotherapy has only recently been updated to acknowledge clinical characteristics associated with this mode of treatment (Seymour et al., 2017); therefore, it will be a challenge to gain clinical approval of CSC therapies if accurate measures of outcomes are not available. While here are many established assays to identify CSC, such as those carried out in this thesis, many of these are not suitable to be carried out clinically. Assessment of CSC specific responses are likely to fall into short- and long-term outcomes involving CSC detection post-treatment and monitoring of durable tumour elimination (lack of recurrence), respectively.

In summary, this thesis demonstrated that the functional CSC marker ALDH was superior to previously described surface markers for the identification of prostate CSC as it was applicable to both an established cell line and primary PCa cells. The suitability of ALDH for isolation of prostate CSC was supported by differences in cell division and gene expression between ALDH high and low cells in both *in vitro* models investigated; additionally, *in vivo* tumorigenesis was demonstrated using the DU145 cell line. HLA ligandome analysis of DU145 PCa cells was used to identify candidate tumour antigens,

which were further investigated in ALDH high and low cells. T cells recognising two candidate peptides were isolated using tetramers, and polyfunctional responses to the peptides were demonstrated. This study demonstrates the potential for combining HLA ligandome analysis with markers that functionally define CSC populations, to identify specific CSC targets for T cell immunotherapy.

References

Aaltomaa, S., Eskelinen, M., Lipponen, P., 1999. Expression of cyclin A and D proteins in prostate cancer and their relation to clinopathological variables and patient survival. The Prostate 38, 175–182. https://doi.org/10.1002/(SICI)1097-0045(19990215)38:3<175::AID-PROS1>3.0.CO;2-#

Adams, J., 2003. The proteasome: structure, function, and role in the cell. Cancer Treat. Rev. 29 Suppl 1, 3–9.

Adams, S., Robbins, F.-M., Chen, D., Wagage, D., Holbeck, S.L., Morse, H.C., Stroncek, D., Marincola, F.M., 2005. HLA class I and II genotype of the NCI-60 cell lines. J. Transl. Med. 3, 11. https://doi.org/10.1186/1479-5876-3-11

Adams, S.D., Barracchini, K.C., Chen, D., Robbins, F., Wang, L., Larsen, P., Luhm, R., Stroncek, D.F., 2004. Ambiguous allele combinations in HLA Class I and Class II sequence-based typing: when precise nucleotide sequencing leads to imprecise allele identification. J. Transl. Med. 2, 30. https://doi.org/10.1186/1479-5876-2-30

Adeegbe, D.O., Liu, Y., Lizotte, P.H., Kamihara, Y., Aref, A.R., Almonte, C., Dries, R., Li, Y., Liu, S., Wang, X., Warner-Hatten, T., Castrillon, J., Yuan, G.-C., Poudel-Neupane, N., Zhang, H., Guerriero, J.L., Han, S., Awad, M.M., Barbie, D.A., Ritz, J., Jones, S.S., Hammerman, P.S., Bradner, J., Quayle, S.N., Wong, K.-K., 2017. Synergistic Immunostimulatory Effects and Therapeutic Benefit of Combined Histone Deacetylase and Bromodomain Inhibition in Non-Small Cell Lung Cancer. Cancer Discov. 7, 852–867. https://doi.org/10.1158/2159-8290.CD-16-1020

Agudo, J., Park, E.S., Rose, S.A., Alibo, E., Sweeney, R., Dhainaut, M., Kobayashi, K.S., Sachidanandam, R., Baccarini, A., Merad, M., Brown, B.D., 2018. Quiescent Tissue Stem Cells Evade Immune Surveillance. Immunity 48, 271-285.e5. https://doi.org/10.1016/j.immuni.2018.02.001

Ajani, J.A., Song, S., Hochster, H.S., Steinberg, I.B., 2015. Cancer Stem Cells: The Promise and the Potential. Semin. Oncol., Cancer Stem Cells: The Promise and the Potential 42, Supplement 1, S3–S17. https://doi.org/10.1053/j.seminoncol.2015.01.001

Akram, A., Inman, R.D., 2012. Immunodominance: a pivotal principle in host response to viral infections. Clin. Immunol. Orlando Fla 143, 99–115. https://doi.org/10.1016/j.clim.2012.01.015

Alanio, C., Lemaitre, F., Law, H.K.W., Hasan, M., Albert, M.L., 2010. Enumeration of human antigen–specific naive CD8+ T cells reveals conserved precursor frequencies. Blood 115, 3718–3725. https://doi.org/10.1182/blood-2009-10-251124

Alegre, M.-L., Frauwirth, K.A., Thompson, C.B., 2001. T-cell regulation by CD28 and CTLA-4. Nat. Rev. Immunol. 1, 220–228. https://doi.org/10.1038/35105024

Alexandrov, L.B., Nik-Zainal, S., Wedge, D.C., Aparicio, S.A.J.R., Behjati, S., Biankin, A.V., Bignell, G.R., Bolli, N., Borg, A., Børresen-Dale, A.-L., Boyault, S., Burkhardt, B., Butler, A.P., Caldas, C., Davies, H.R., Desmedt, C., Eils, R., Eyfjörd, J.E., Foekens, J.A., Greaves, M., Hosoda, F., Hutter, B., Ilicic, T., Imbeaud, S., Imielinski, M., Jäger, N., Jones, D.T.W., Jones, D., Knappskog, S., Kool, M., Lakhani, S.R., López-Otín, C., Martin, S., Munshi, N.C., Nakamura, H., Northcott, P.A., Pajic, M.,

Papaemmanuil, E., Paradiso, A., Pearson, J.V., Puente, X.S., Raine, K., Ramakrishna, M., Richardson, A.L., Richter, J., Rosenstiel, P., Schlesner, M., Schumacher, T.N., Span, P.N., Teague, J.W., Totoki, Y., Tutt, A.N.J., Valdés-Mas, R., van Buuren, M.M., van 't Veer, L., Vincent-Salomon, A., Waddell, N., Yates, L.R., Australian Pancreatic Cancer Genome Initiative, ICGC Breast Cancer Consortium, ICGC MMML-Seq Consortium, Icgc PedBrain, Zucman-Rossi, J., Andrew Futreal, P., McDermott, U., Lichter, P., Meyerson, M., Grimmond, S.M., Siebert, R., Campo, E., Shibata, T., Pfister, S.M., Campbell, P.J., Stratton, M.R., 2013. Signatures of mutational processes in human cancer. Nature 500, 415–421. https://doi.org/10.1038/nature12477

Al-Hajj, M., Wicha, M.S., Benito-Hernandez, A., Morrison, S.J., Clarke, M.F., 2003. Prospective identification of tumorigenic breast cancer cells. Proc. Natl. Acad. Sci. 100, 3983–3988. https://doi.org/10.1073/pnas.0530291100

Alpízar, A., Marino, F., Ramos-Fernández, A., Lombardía, M., Jeko, A., Pazos, F., Paradela, A., Santiago, C., Heck, A.J.R., Marcilla, M., 2017. A Molecular Basis for the Presentation of Phosphorylated Peptides by HLA-B Antigens. Mol. Cell. Proteomics MCP 16, 181–193. https://doi.org/10.1074/mcp.M116.063800

Andersen, R., Donia, M., Ellebaek, E., Borch, T.H., Kongsted, P., Iversen, T.Z., Hölmich, L.R., Hendel, H.W., Met, Ö., Andersen, M.H., Straten, P. thor, Svane, I.M., 2016. Long-Lasting Complete Responses in Patients with Metastatic Melanoma after Adoptive Cell Therapy with Tumor-Infiltrating Lymphocytes and an Attenuated IL2 Regimen. Clin. Cancer Res. 22, 3734–3745. https://doi.org/10.1158/1078-0432.CCR-15-1879

Androlewicz, M.J., Anderson, K.S., Cresswell, P., 1993. Evidence that transporters associated with antigen processing translocate a major histocompatibility complex class I-binding peptide into the endoplasmic reticulum in an ATP-dependent manner. Proc. Natl. Acad. Sci. U. S. A. 90, 9130–9134. https://doi.org/10.1073/pnas.90.19.9130

Angelotti, M.L., Lazzeri, E., Lasagni, L., Romagnani, P., 2010. Only anti-CD133 antibodies recognizing the CD133/1 or the CD133/2 epitopes can identify human renal progenitors. Kidney Int. 78, 620–621. https://doi.org/10.1038/ki.2010.243

Antonarakis, E.S., Heath, E.I., Smith, D.C., Rathkopf, D., Blackford, A.L., Danila, D.C., King, S., Frost, A., Ajiboye, A.S., Zhao, M., Mendonca, J., Kachhap, S.K., Rudek, M.A., Carducci, M.A., 2013. Repurposing itraconazole as a treatment for advanced prostate cancer: a noncomparative randomized phase II trial in men with metastatic castration-resistant prostate cancer. The Oncologist 18, 163–173. https://doi.org/10.1634/theoncologist.2012-314

Antonarakis, E.S., Zahurak, M., Schaeffer, E.M., Partin, A.W., Ross, A., Allaf, M., Tosoian, J., Nirschl, T., Chapman, C., O'Neal, T.S., Cao, H., Durham, J.N., Guner, G., Del Valle, J.B., Ertunc, O., Demarzo, A., Drake, C.G., 2017. Neoadjuvant randomized trial of degarelix (Deg) ± cyclophosphamide/GVAX (Cy/GVAX) in men with high-risk prostate cancer (PCa) undergoing radical prostatectomy (RP). J. Clin. Oncol. 35, 5077–5077. https://doi.org/10.1200/JCO.2017.35.15_suppl.5077

Antunes, D.A., Abella, J.R., Devaurs, D., Rigo, M.M., Kavraki, L.E., 2018. Structure-based methods for binding mode and binding affinity prediction for peptide-MHC complexes. Curr. Top. Med. Chem. 18, 2239–2255. https://doi.org/10.2174/1568026619666181224101744

Appay, V., Rowland-Jones, S.L., 2002. The assessment of antigen-specific CD8+ T cells through the combination of MHC class I tetramer and intracellular staining. J. Immunol. Methods 268, 9–19. https://doi.org/10.1016/s0022-1759(02)00195-3

Arndt, C., Feldmann, A., Koristka, S., Cartellieri, M., Dimmel, M., Ehninger, A., Ehninger, G., Bachmann, M., 2014. Simultaneous targeting of prostate stem cell antigen and prostate-specific membrane antigen improves the killing of prostate cancer cells using a novel modular T cell-retargeting system. The Prostate 74, 1335–1346. https://doi.org/10.1002/pros.22850

Arstila, T.P., Casrouge, A., Baron, V., Even, J., Kanellopoulos, J., Kourilsky, P., 1999. A direct estimate of the human alphabeta T cell receptor diversity. Science 286, 958–961. https://doi.org/10.1126/science.286.5441.958

Artibani, W., Porcaro, A.B., De Marco, V., Cerruto, M.A., Siracusano, S., 2018. Management of Biochemical Recurrence after Primary Curative Treatment for Prostate Cancer: A Review. Urol. Int. 100, 251–262. https://doi.org/10.1159/000481438

Atsumi, T., Singh, R., Sabharwal, L., Bando, H., Meng, J., Arima, Y., Yamada, M., Harada, M., Jiang, J.-J., Kamimura, D., Ogura, H., Hirano, T., Murakami, M., 2014. Inflammation Amplifier, a New Paradigm in Cancer Biology. Cancer Res. 74, 8–14. https://doi.org/10.1158/0008-5472.CAN-13-2322

Bai, X., Lenhart, K.C., Bird, K.E., Suen, A.A., Rojas, M., Kakoki, M., Li, F., Smithies, O., Mack, C.P., Taylor, J.M., 2013. The smooth muscle-selective RhoGAP GRAF3 is a critical regulator of vascular tone and hypertension. Nat. Commun. 4, 2910. https://doi.org/10.1038/ncomms3910

Bairoch, A., 2018. The Cellosaurus, a Cell-Line Knowledge Resource. J. Biomol. Tech. JBT 29, 25–38. https://doi.org/10.7171/jbt.18-2902-002

Baniyash, M., Sade-Feldman, M., Kanterman, J., 2013. Chronic inflammation and cancer: suppressing the suppressors. Cancer Immunol. Immunother. 63, 11–20. https://doi.org/10.1007/s00262-013-1468-9

Bao, S., Wu, Q., McLendon, R.E., Hao, Y., Shi, Q., Hjelmeland, A.B., Dewhirst, M.W., Bigner, D.D., Rich, J.N., 2006. Glioma stem cells promote radioresistance by preferential activation of the DNA damage response. Nature 444, 756–760. https://doi.org/10.1038/nature05236

Barbour, A.P., Reeder, J.A., Walsh, M.D., Fawcett, J., Antalis, T.M., Gotley, D.C., 2003. Expression of the CD44v2-10 isoform confers a metastatic phenotype: importance of the heparan sulfate attachment site CD44v3. Cancer Res. 63, 887–892.

Barnea, E., Beer, I., Patoka, R., Ziv, T., Kessler, O., Tzehoval, E., Eisenbach, L., Zavazava, N., Admon, A., 2002. Analysis of endogenous peptides bound by soluble MHC class I molecules: a novel approach for identifying tumor-specific antigens. Eur. J. Immunol. 32, 213–222. https://doi.org/10.1002/1521-4141(200201)32:1<213::AID-IMMU213>3.0.CO;2-8

Barsoum, I.B., Smallwood, C.A., Siemens, D.R., Graham, C.H., 2014. A Mechanism of Hypoxia-Mediated Escape from Adaptive Immunity in Cancer Cells. Cancer Res. 74, 665–674. https://doi.org/10.1158/0008-5472.CAN-13-0992

Bassani-Sternberg, M., Bräunlein, E., Klar, R., Engleitner, T., Sinitcyn, P., Audehm, S., Straub, M., Weber, J., Slotta-Huspenina, J., Specht, K., Martignoni, M.E., Werner, A., Hein, R., H Busch, D., Peschel, C., Rad, R., Cox, J., Mann, M., Krackhardt, A.M., 2016. Direct identification of clinically relevant neoepitopes presented on native human melanoma tissue by mass spectrometry. Nat. Commun. 7, 13404. https://doi.org/10.1038/ncomms13404

Bassani-Sternberg, M., Chong, C., Guillaume, P., Solleder, M., Pak, H., Gannon, P.O., Kandalaft, L.E., Coukos, G., Gfeller, D., 2017. Deciphering HLA-I motifs across HLA peptidomes improves neo-antigen predictions and identifies allostery regulating HLA specificity. PLOS Comput. Biol. 13, e1005725. https://doi.org/10.1371/journal.pcbi.1005725

Bassani-Sternberg, M., Pletscher-Frankild, S., Jensen, L.J., Mann, M., 2015. Mass spectrometry of human leukocyte antigen class I peptidomes reveals strong effects of protein abundance and turnover on antigen presentation. Mol. Cell. Proteomics MCP 14, 658–673. https://doi.org/10.1074/mcp.M114.042812

Bassing, C.H., Swat, W., Alt, F.W., 2002. The Mechanism and Regulation of Chromosomal V(D)J Recombination. Cell 109, S45–S55. https://doi.org/10.1016/S0092-8674(02)00675-X

Batlle, E., Clevers, H., 2017. Cancer stem cells revisited. Nat. Med. 23, 1124–1134. https://doi.org/10.1038/nm.4409

Beatty, G.L., Gladney, W.L., 2015. Immune escape mechanisms as a guide for cancer immunotherapy. Clin. Cancer Res. Off. J. Am. Assoc. Cancer Res. 21, 687–692. https://doi.org/10.1158/1078-0432.CCR-14-1860

Beer, T.M., Kwon, E.D., Drake, C.G., Fizazi, K., Logothetis, C., Gravis, G., Ganju, V., Polikoff, J., Saad, F., Humanski, P., Piulats, J.M., Gonzalez Mella, P., Ng, S.S., Jaeger, D., Parnis, F.X., Franke, F.A., Puente, J., Carvajal, R., Sengeløv, L., McHenry, M.B., Varma, A., van den Eertwegh, A.J., Gerritsen, W., 2016. Randomized, Double-Blind, Phase III Trial of Ipilimumab Versus Placebo in Asymptomatic or Minimally Symptomatic Patients With Metastatic Chemotherapy-Naive Castration-Resistant Prostate Cancer. J. Clin. Oncol. 35, 40–47. https://doi.org/10.1200/JCO.2016.69.1584

Beier, D., Hau, P., Proescholdt, M., Lohmeier, A., Wischhusen, J., Oefner, P.J., Aigner, L., Brawanski, A., Bogdahn, U., Beier, C.P., 2007. CD133+ and CD133− Glioblastoma-Derived Cancer Stem Cells Show Differential Growth Characteristics and Molecular Profiles. Cancer Res. 67, 4010–4015. https://doi.org/10.1158/0008-5472.CAN-06-4180

Bendas, G., Borsig, L., 2012. . Int. J. Cell Biol. 2012, 676731. https://doi.org/10.1155/2012/676731

Bennett, S.R.M., Carbone, F.R., Karamalis, F., Miller, J.F.A.P., Heath, W.R., 1997. Induction of a CD8+ Cytotoxic T Lymphocyte Response by Cross-priming Requires Cognate CD4+ T Cell Help. J. Exp. Med. 186, 65–70. https://doi.org/10.1084/jem.186.1.65

Berlin, C., Kowalewski, D.J., Schuster, H., Mirza, N., Walz, S., Handel, M., Schmid-Horch, B., Salih, H.R., Kanz, L., Rammensee, H.-G.,

Stevanović, S., Stickel, J.S., 2016. Mapping the HLA ligandome landscape of acute myeloid leukemia: a targeted approach toward peptide-based immunotherapy. Leukemia 30, 1003–1004. https://doi.org/10.1038/leu.2016.1

Berlin, C., Kowalewski, D.J., Schuster, H., Mirza, N., Walz, S., Handel, M., Schmid-Horch, B., Salih, H.R., Kanz, L., Rammensee, H.-G., Stevanović, S., Stickel, J.S., 2015. Mapping the HLA ligandome landscape of acute myeloid leukemia: a targeted approach toward peptide-based immunotherapy. Leukemia 29, 647–659. https://doi.org/10.1038/leu.2014.233

Besser, M.J., Shapira-Frommer, R., Itzhaki, O., Treves, A.J., Zippel, D.B., Levy, D., Kubi, A., Shoshani, N., Zikich, D., Ohayon, Y., Ohayon, D., Shalmon, B., Markel, G., Yerushalmi, R., Apter, S., Ben-Nun, A., Ben-Ami, E., Shimoni, A., Nagler, A., Schachter, J., 2013. Adoptive Transfer of Tumor-Infiltrating Lymphocytes in Patients with Metastatic Melanoma: Intent-to-Treat Analysis and Efficacy after Failure to Prior Immunotherapies. Clin. Cancer Res. 19, 4792–4800. https://doi.org/10.1158/1078-0432.CCR-13-0380

Bethune, M.T., Joglekar, A.V., 2017. Personalized T cell-mediated cancer immunotherapy: progress and challenges. Curr. Opin. Biotechnol., Chemical biotechnology • Pharmaceutical biotechnology 48, 142–152. https://doi.org/10.1016/j.copbio.2017.03.024

Bhasin, M., Raghava, G.P., 2007. A hybrid approach for predicting promiscuous MHC class I restricted T cell epitopes. J. Biosci. 32, 31–42.

Bhatia, A., Kumar, Y., 2011. Cancer-Immune Equilibrium: Questions Unanswered. Cancer Microenviron. 4, 209–217. https://doi.org/10.1007/s12307-011-0065-8

Bidlingmaier, S., Zhu, X., Liu, B., 2008. The utility and limitations of glycosylated human CD133 epitopes in defining cancer stem cells. J. Mol. Med. Berl. Ger. 86, 1025–1032. https://doi.org/10.1007/s00109-008-0357-8

Bijen, H.M., van der Steen, D.M., Hagedoorn, R.S., Wouters, A.K., Wooldridge, L., Falkenburg, J.H.F., Heemskerk, M.H.M., 2018. Preclinical Strategies to Identify Off-Target Toxicity of High-Affinity TCRs. Mol. Ther. 26, 1206–1214. https://doi.org/10.1016/j.ymthe.2018.02.017

Bilich, T., Nelde, A., Bichmann, L., Roerden, M., Salih, H.R., Kowalewski, D.J., Schuster, H., Tsou, C.-C., Marcu, A., Neidert, M.C., Lübke, M., Rieth, J., Schemionek, M., Brümmendorf, T.H., Vucinic, V., Niederwieser, D., Bauer, J., Märklin, M., Peper, J.K., Klein, R., Kohlbacher, O., Kanz, L., Rammensee, H.-G., Stevanović, S., Walz, J.S., 2019. The HLA ligandome landscape of chronic myeloid leukemia delineates novel T-cell epitopes for immunotherapy. Blood 133, 550–565. https://doi.org/10.1182/blood-2018-07-866830

Bilusic, M., Madan, R.A., Gulley, J.L., 2017. Immunotherapy of Prostate Cancer: Facts and Hopes. Clin. Cancer Res. Off. J. Am. Assoc. Cancer Res. 23, 6764–6770. https://doi.org/10.1158/1078-0432.CCR-17-0019

Birnie, R., Bryce, S.D., Roome, C., Dussupt, V., Droop, A., Lang, S.H., Berry, P.A., Hyde, C.F., Lewis, J.L., Stower, M.J., Maitland, N.J., Collins, A.T., 2008. Gene expression profiling of human prostate cancer stem cells

reveals a pro-inflammatory phenotype and the importance of extracellular matrix interactions. Genome Biol. 9, R83. https://doi.org/10.1186/gb-2008-9-5-r83

Blackwood, J.K., Williamson, S.C., Greaves, L.C., Wilson, L., Rigas, A.C., Sandher, R., Pickard, R.S., Robson, C.N., Turnbull, D.M., Taylor, R.W., Heer, R., 2011. In situ lineage tracking of human prostatic epithelial stem cell fate reveals a common clonal origin for basal and luminal cells. J. Pathol. 225, 181–188. https://doi.org/10.1002/path.2965

Blue, M.L., Daley, J.F., Levine, H., Schlossman, S.F., 1985. Coexpression of T4 and T8 on peripheral blood T cells demonstrated by two-color fluorescence flow cytometry. J. Immunol. Baltim. Md 1950 134, 2281–2286.

Boegel, S., Löwer, M., Bukur, T., Sahin, U., Castle, J.C., 2014. A catalog of HLA type, HLA expression, and neo-epitope candidates in human cancer cell lines. Oncoimmunology 3. https://doi.org/10.4161/21624011.2014.954893

Boiko, A.D., Razorenova, O.V., van de Rijn, M., Swetter, S.M., Johnson, D.L., Ly, D.P., Butler, P.D., Yang, G.P., Joshua, B., Kaplan, M.J., Longaker, M.T., Weissman, I.L., 2010. Human melanoma-initiating cells express neural crest nerve growth factor receptor CD271. Nature 466, 133–137. https://doi.org/10.1038/nature09161

Boissel, N., Rea, D., Tieng, V., Dulphy, N., Brun, M., Cayuela, J.-M., Rousselot, P., Tamouza, R., Le Bouteiller, P., Mahon, F.-X., Steinle, A., Charron, D., Dombret, H., Toubert, A., 2006. BCR/ABL oncogene directly controls MHC class I chain-related molecule A expression in chronic myelogenous leukemia. J. Immunol. Baltim. Md 1950 176, 5108–5116.

Bol, K.F., Schreibelt, G., Gerritsen, W.R., Vries, I.J.M. de, Figdor, C.G., 2016. Dendritic Cell–Based Immunotherapy: State of the Art and Beyond. Clin. Cancer Res. 22, 1897–1906. https://doi.org/10.1158/1078-0432.CCR-15-1399

Bollard, C.M., Gottschalk, S., Torrano, V., Diouf, O., Ku, S., Hazrat, Y., Carrum, G., Ramos, C., Fayad, L., Shpall, E.J., Pro, B., Liu, H., Wu, M.-F., Lee, D., Sheehan, A.M., Zu, Y., Gee, A.P., Brenner, M.K., Heslop, H.E., Rooney, C.M., 2014. Sustained complete responses in patients with lymphoma receiving autologous cytotoxic T lymphocytes targeting Epstein-Barr virus latent membrane proteins. J. Clin. Oncol. Off. J. Am. Soc. Clin. Oncol. 32, 798–808. https://doi.org/10.1200/JCO.2013.51.5304

Bonnet, D., Dick, J.E., 1997. Human acute myeloid leukemia is organized as a hierarchy that originates from a primitive hematopoietic cell. Nat. Med. 3, 730–737.

Boorjian, S.A., Thompson, R.H., Tollefson, M.K., Rangel, L.J., Bergstralh, E.J., Blute, M.L., Karnes, R.J., 2011. Long-Term Risk of Clinical Progression After Biochemical Recurrence Following Radical Prostatectomy: The Impact of Time from Surgery to Recurrence. Eur. Urol. 59, 893–899. https://doi.org/10.1016/j.eururo.2011.02.026

Bosch, G.J., Joosten, A.M., Kessler, J.H., Melief, C.J., Leeksma, O.C., 1996. Recognition of BCR-ABL positive leukemic blasts by human CD4+ T cells elicited by primary in vitro immunization with a BCR-ABL breakpoint peptide. Blood 88, 3522–3527.

Bouvier, M., 2003. Accessory proteins and the assembly of human class I MHC molecules: a molecular and structural perspective. Mol. Immunol. 39, 697–706. https://doi.org/10.1016/s0161-5890(02)00261-4

Bragado, P., Estrada, Y., Sosa, M.S., Avivar-Valderas, A., Cannan, D., Genden, E., Teng, M., Ranganathan, A.C., Wen, H.-C., Kapoor, A., Bernstein, E., Aguirre-Ghiso, J.A., 2012. Analysis of Marker-Defined HNSCC Subpopulations Reveals a Dynamic Regulation of Tumor Initiating Properties. PLoS ONE 7. https://doi.org/10.1371/journal.pone.0029974

Brambilla, E., Le Teuff, G., Marguet, S., Lantuejoul, S., Dunant, A., Graziano, S., Pirker, R., Douillard, J.-Y., Le Chevalier, T., Filipits, M., Rosell, R., Kratzke, R., Popper, H., Soria, J.-C., Shepherd, F.A., Seymour, L., Tsao, M.S., 2016. Prognostic Effect of Tumor Lymphocytic Infiltration in Resectable Non–Small-Cell Lung Cancer. J. Clin. Oncol. 34, 1223–1230. https://doi.org/10.1200/JCO.2015.63.0970

Brändle, D., Müller, C., Rülicke, T., Hengartner, H., Pircher, H., 1992. Engagement of the T-cell receptor during positive selection in the thymus down-regulates RAG-1 expression. Proc. Natl. Acad. Sci. U. S. A. 89, 9529–9533.

Brentjens, R.J., Davila, M.L., Riviere, I., Park, J., Wang, X., Cowell, L.G., Bartido, S., Stefanski, J., Taylor, C., Olszewska, M., Borquez-Ojeda, O., Qu, J., Wasielewska, T., He, Q., Bernal, Y., Rijo, I.V., Hedvat, C., Kobos, R., Curran, K., Steinherz, P., Jurcic, J., Rosenblat, T., Maslak, P., Frattini, M., Sadelain, M., 2013. CD19-Targeted T Cells Rapidly Induce Molecular Remissions in Adults with Chemotherapy-Refractory Acute Lymphoblastic Leukemia. Sci. Transl. Med. 5, 177ra38-177ra38. https://doi.org/10.1126/scitranslmed.3005930

Brescia, P., Ortensi, B., Fornasari, L., Levi, D., Broggi, G., Pelicci, G., 2013. CD133 Is Essential for Glioblastoma Stem Cell Maintenance. STEM CELLS 31, 857–869. https://doi.org/10.1002/stem.1317

Bridgeman, J.S., Sewell, A.K., Miles, J.J., Price, D.A., Cole, D.K., 2012. Structural and biophysical determinants of αβ T-cell antigen recognition. Immunology 135, 9–18. https://doi.org/10.1111/j.1365-2567.2011.03515.x

Bronte, V., Kasic, T., Gri, G., Gallana, K., Borsellino, G., Marigo, I., Battistini, L., Iafrate, M., Prayer-Galetti, T., Pagano, F., Viola, A., 2005. Boosting antitumor responses of T lymphocytes infiltrating human prostate cancers. J. Exp. Med. 201, 1257–1268. https://doi.org/10.1084/jem.20042028

Bruttel, V.S., Wischhusen, J., 2014. Cancer stem cell immunology: key to understanding tumorigenesis and tumor immune escape? Front. Immunol. 5, 360. https://doi.org/10.3389/fimmu.2014.00360

Buonaguro, L., Petrizzo, A., Tornesello, M.L., Buonaguro, F.M., 2011. Translating Tumor Antigens into Cancer Vaccines. Clin. Vaccine Immunol. CVI 18, 23–34. https://doi.org/10.1128/CVI.00286-10

Burnet, F.M., 1970. The concept of immunological surveillance. Prog. Exp. Tumor Res. 13, 1–27.

Burnette, B., Weichselbaum, R.R., 2013. Radiation as an Immune Modulator. Semin. Radiat. Oncol., The Tumor as an Organ 23, 273–280. https://doi.org/10.1016/j.semradonc.2013.05.009

Cabarcas, S.M., Mathews, L.A., Farrar, W.L., 2011. The cancer stem cell niche—there goes the neighborhood? Int. J. Cancer 129, 2315–2327. https://doi.org/10.1002/ijc.26312

Calabrese, P., Tavaré, S., Shibata, D., 2004. Pretumor Progression. Am. J. Pathol. 164, 1337–1346.

Calis, J.J.A., Maybeno, M., Greenbaum, J.A., Weiskopf, D., De Silva, A.D., Sette, A., Keşmir, C., Peters, B., 2013. Properties of MHC Class I Presented Peptides That Enhance Immunogenicity. PLoS Comput. Biol. 9. https://doi.org/10.1371/journal.pcbi.1003266

Campoli, M., Ferrone, S., 2008. HLA antigen changes in malignant cells: epigenetic mechanisms and biologic significance. Oncogene 27, 5869–5885. https://doi.org/10.1038/onc.2008.273

Carlsson, B., Forsberg, O., Bengtsson, M., Tötterman, T.H., Essand, M., 2007. Characterization of human prostate and breast cancer cell lines for experimental T cell-based immunotherapy. The Prostate 67, 389–395. https://doi.org/10.1002/pros.20498

Carter, S.L., Eklund, A.C., Kohane, I.S., Harris, L.N., Szallasi, Z., 2006. A signature of chromosomal instability inferred from gene expression profiles predicts clinical outcome in multiple human cancers. Nat. Genet. 38, 1043–1048. https://doi.org/10.1038/ng1861

Cascio, P., Hilton, C., Kisselev, A.F., Rock, K.L., Goldberg, A.L., 2001. 26S proteasomes and immunoproteasomes produce mainly N-extended versions of an antigenic peptide. EMBO J. 20, 2357–2366. https://doi.org/10.1093/emboj/20.10.2357

Casucci, M., Robilant, B.N. di, Falcone, L., Camisa, B., Genovese, P., Gentner, B., Naldini, L., Savoldo, B., Ciceri, F., Bordignon, C., Dotti, G., Bonini, C., Bondanza, A., 2012. Co-Expression of a Suicide Gene in CAR-Redirected T Cells Enables the Safe Targeting of CD44v6 for Leukemia and Myeloma Eradication. Blood 120, 949–949.

Casucci, M., Robilant, B.N. di, Falcone, L., Camisa, B., Norelli, M., Genovese, P., Gentner, B., Gullotta, F., Ponzoni, M., Bernardi, M., Marcatti, M., Saudemont, A., Bordignon, C., Savoldo, B., Ciceri, F., Naldini, L., Dotti, G., Bonini, C., Bondanza, A., 2013. CD44v6-targeted T cells mediate potent antitumor effects against acute myeloid leukemia and multiple myeloma. Blood 122, 3461–3472. https://doi.org/10.1182/blood-2013-04-493361

Ceder, J.A., Jansson, L., Helczynski, L., Abrahamsson, P.-A., 2008. Delta-Like 1 (Dlk-1), a Novel Marker of Prostate Basal and Candidate Epithelial Stem Cells, Is Downregulated by Notch Signalling in Intermediate/Transit Amplifying Cells of the Human Prostate. Eur. Urol. 54, 1344–1353. https://doi.org/10.1016/j.eururo.2008.03.006

Chang, S.-C., Momburg, F., Bhutani, N., Goldberg, A.L., 2005. The ER aminopeptidase, ERAP1, trims precursors to lengths of MHC class I peptides by a "molecular ruler" mechanism. Proc. Natl. Acad. Sci. U. S. A. 102, 17107–17112. https://doi.org/10.1073/pnas.0500721102

Chapuis, A.G., Desmarais, C., Emerson, R., Schmitt, T.M., Shibuya, K., Lai, I., Wagener, F., Chou, J., Roberts, I.M., Coffey, D.G., Warren, E., Robbins, H., Greenberg, P.D., Yee, C., 2017. Tracking the Fate and Origin of Clinically Relevant Adoptively Transferred CD8+ T Cells In Vivo. Sci. Immunol. 2. https://doi.org/10.1126/sciimmunol.aal2568

Cheever, M.A., Allison, J.P., Ferris, A.S., Finn, O.J., Hastings, B.M., Hecht, T.T., Mellman, I., Prindiville, S.A., Steinman, R.M., Viner, J.L., Weiner,

L.M., Matrisian, L.M., 2009. The Prioritization of Cancer Antigens: A National Cancer Institute Pilot Project for the Acceleration of Translational Research. Clin. Cancer Res. Off. J. Am. Assoc. Cancer Res. 15, 5323–5337. https://doi.org/10.1158/1078-0432.CCR-09-0737

Chen, C., Zhao, S., Karnad, A., Freeman, J.W., 2018. The biology and role of CD44 in cancer progression: therapeutic implications. J. Hematol. Oncol.J Hematol Oncol 11, 64. https://doi.org/10.1186/s13045-018-0605-5

Chen, D.S., Mellman, I., 2013. Oncology Meets Immunology: The Cancer-Immunity Cycle. Immunity 39, 1–10. https://doi.org/10.1016/j.immuni.2013.07.012

Chen, J., Li, Y., Yu, T.-S., McKay, R.M., Burns, D.K., Kernie, S.G., Parada, L.F., 2012. A restricted cell population propagates glioblastoma growth after chemotherapy. Nature 488, 522–526. https://doi.org/10.1038/nature11287

Chen, K., Huang, Y., Chen, J., 2013. Understanding and targeting cancer stem cells: therapeutic implications and challenges. Acta Pharmacol. Sin. 34, 732–740. https://doi.org/10.1038/aps.2013.27

Chen, L., Flies, D.B., 2013. Molecular mechanisms of T cell co-stimulation and co-inhibition. Nat. Rev. Immunol. 13, 227–242. https://doi.org/10.1038/nri3405

Chen, X., Li, Q., Liu, X., Liu, C., Liu, R., Rycaj, K., Zhang, D., Liu, B., Jeter, C., Calhoun-Davis, T., Lin, K., Lu, Y., Chao, H.-P., Shen, J., Tang, D.G., 2016. Defining a Population of Stem-like Human Prostate Cancer Cells That Can Generate and Propagate Castration-Resistant Prostate Cancer. Clin. Cancer Res. 22, 4505–4516. https://doi.org/10.1158/1078-0432.CCR-15-2956

Chen, X., Liu, B., Li, Q., Honorio, S., Liu, X., Liu, C., Multani, A.S., Calhoun-Davis, T., Tang, D.G., 2013. Dissociated Primary Human Prostate Cancer Cells Coinjected with the Immortalized Hs5 Bone Marrow Stromal Cells Generate Undifferentiated Tumors in NOD/SCID-γ Mice. PLoS ONE 8. https://doi.org/10.1371/journal.pone.0056903

Chen, Y., Zhang, F., Tsai, Y., Yang, X., Yang, L., Duan, S., Wang, X., Keng, P., Lee, S.O., 2015. IL-6 signaling promotes DNA repair and prevents apoptosis in CD133+ stem-like cells of lung cancer after radiation. Radiat. Oncol. 10, 227. https://doi.org/10.1186/s13014-015-0534-1

Chen, Y.T., Scanlan, M.J., Sahin, U., Türeci, O., Gure, A.O., Tsang, S., Williamson, B., Stockert, E., Pfreundschuh, M., Old, L.J., 1997. A testicular antigen aberrantly expressed in human cancers detected by autologous antibody screening. Proc. Natl. Acad. Sci. U. S. A. 94, 1914–1918.

Chin, Y.R., Yuan, X., Balk, S.P., Toker, A., 2014. PTEN-deficient tumors depend on AKT2 for maintenance and survival. Cancer Discov. 4, 942–955. https://doi.org/10.1158/2159-8290.CD-13-0873

Choi, N., Zhang, B., Zhang, L., Ittmann, M., Xin, L., 2012. Adult murine prostate basal and luminal cells are self-sustained lineages that can both serve as targets for prostate cancer initiation. Cancer Cell 21, 253–265. https://doi.org/10.1016/j.ccr.2012.01.005

Choi, S.A., Lee, J.Y., Phi, J.H., Wang, K.-C., Park, C.-K., Park, S.-H., Kim, S.-K., 2014. Identification of brain tumour initiating cells using the stem

cell marker aldehyde dehydrogenase. Eur. J. Cancer 50, 137–149. https://doi.org/10.1016/j.ejca.2013.09.004

Chomczynski, P., 1993. A reagent for the single-step simultaneous isolation of RNA, DNA and proteins from cell and tissue samples. BioTechniques 15, 532–534, 536–537.

Chong, C., Marino, F., Pak, H., Racle, J., Daniel, R.T., Müller, M., Gfeller, D., Coukos, G., Bassani-Sternberg, M., 2018. High-throughput and Sensitive Immunopeptidomics Platform Reveals Profound Interferonγ-Mediated Remodeling of the Human Leukocyte Antigen (HLA) Ligandome. Mol. Cell. Proteomics 17, 533–548. https://doi.org/10.1074/mcp.TIR117.000383

Clara, J.A., Monge, C., Yang, Y., Takebe, N., 2019. Targeting signalling pathways and the immune microenvironment of cancer stem cells — a clinical update. Nat. Rev. Clin. Oncol. 1–29. https://doi.org/10.1038/s41571-019-0293-2

Clarke, M.F., Dick, J.E., Dirks, P.B., Eaves, C.J., Jamieson, C.H.M., Jones, D.L., Visvader, J., Weissman, I.L., Wahl, G.M., 2006. Cancer Stem Cells—Perspectives on Current Status and Future Directions: AACR Workshop on Cancer Stem Cells. Cancer Res. 66, 9339–9344. https://doi.org/10.1158/0008-5472.CAN-06-3126

Clevers, H., 2011. The cancer stem cell: premises, promises and challenges. Nat. Med. 313–319. https://doi.org/10.1038/nm.2304

Clevers, H., 2006. Wnt/β-Catenin Signaling in Development and Disease. Cell 127, 469–480. https://doi.org/10.1016/j.cell.2006.10.018

Clevers, H., Loh, K.M., Nusse, R., 2014. Stem cell signaling. An integral program for tissue renewal and regeneration: Wnt signaling and stem cell control. Science 346, 1248012. https://doi.org/10.1126/science.1248012

Codd, A.S., Kanaseki, T., Torigo, T., Tabi, Z., 2018. Cancer stem cells as targets for immunotherapy. Immunology 153, 304–314. https://doi.org/10.1111/imm.12866

Cojoc, M., Mäbert, K., Muders, M.H., Dubrovska, A., 2015a. A role for cancer stem cells in therapy resistance: cellular and molecular mechanisms. Semin. Cancer Biol. 31, 16–27. https://doi.org/10.1016/j.semcancer.2014.06.004

Cojoc, M., Peitzsch, C., Kurth, I., Trautmann, F., Kunz-Schughart, L.A., Telegeev, G.D., Stakhovsky, E.A., Walker, J.R., Simin, K., Lyle, S., Fuessel, S., Erdmann, K., Wirth, M.P., Krause, M., Baumann, M., Dubrovska, A., 2015b. Aldehyde Dehydrogenase Is Regulated by β-Catenin/TCF and Promotes Radioresistance in Prostate Cancer Progenitor Cells. Cancer Res. 75, 1482–1494. https://doi.org/10.1158/0008-5472.CAN-14-1924

Collins, A.T., Berry, P.A., Hyde, C., Stower, M.J., Maitland, N.J., 2005. Prospective identification of tumorigenic prostate cancer stem cells. Cancer Res. 65, 10946–10951. https://doi.org/10.1158/0008-5472.CAN-05-2018

Collins, A.T., Habib, F.K., Maitland, N.J., Neal, D.E., 2001. Identification and isolation of human prostate epithelial stem cells based on α2β1-integrin expression. J. Cell Sci. 114, 3865–3872.

Comiskey, M.C., Dallos, M.C., Drake, C.G., 2018. Immunotherapy in Prostate Cancer: Teaching an Old Dog New Tricks. Curr. Oncol. Rep. 20, 75. https://doi.org/10.1007/s11912-018-0712-z

Comoli, P., Chabannon, C., Koehl, U., Lanza, F., Urbano-Ispizua, A., Hudecek, M., Ruggeri, A., Secondino, S., Bonini, C., Pedrazzoli, P., 2019. Development of adaptive immune effector therapies in solid tumors. Ann. Oncol. Off. J. Eur. Soc. Med. Oncol. https://doi.org/10.1093/annonc/mdz285

Constantino, J., Gomes, C., Falcão, A., Neves, B.M., Cruz, M.T., 2017. Dendritic cell-based immunotherapy: a basic review and recent advances. Immunol. Res. 65, 798–810. https://doi.org/10.1007/s12026-017-8931-1

Conticello, C., Pedini, F., Zeuner, A., Patti, M., Zerilli, M., Stassi, G., Messina, A., Peschle, C., De Maria, R., 2004. IL-4 protects tumor cells from anti-CD95 and chemotherapeutic agents via up-regulation of antiapoptotic proteins. J. Immunol. Baltim. Md 1950 172, 5467–5477.

Cormier, J.N., Panelli, M.C., Hackett, J.A., Bettinotti, M.P., Mixon, A., Wunderlich, J., Parker, L.L., Restifo, N.P., Ferrone, S., Marincola, F.M., 1999. Natural variation of the expression of HLA and endogenous antigen modulates CTL recognition in an in vitro melanoma model. Int. J. Cancer 80, 781–790.

Corthay, A., 2014. Does the immune system naturally protect against cancer? Tumor Immun. 5, 197. https://doi.org/10.3389/fimmu.2014.00197

Cortina, C., Turon, G., Stork, D., Hernando-Momblona, X., Sevillano, M., Aguilera, M., Tosi, S., Merlos-Suárez, A., Attolini, C.S.-O., Sancho, E., Batlle, E., 2017. A genome editing approach to study cancer stem cells in human tumors. EMBO Mol. Med. e201707550. https://doi.org/10.15252/emmm.201707550

Corzo, C.A., Condamine, T., Lu, L., Cotter, M.J., Youn, J.-I., Cheng, P., Cho, H.-I., Celis, E., Quiceno, D.G., Padhya, T., McCaffrey, T.V., McCaffrey, J.C., Gabrilovich, D.I., 2010. HIF-1α regulates function and differentiation of myeloid-derived suppressor cells in the tumor microenvironment. J. Exp. Med. 207, 2439–2453. https://doi.org/10.1084/jem.20100587

Coulie, P.G., Van den Eynde, B.J., van der Bruggen, P., Boon, T., 2014. Tumour antigens recognized by T lymphocytes: at the core of cancer immunotherapy. Nat. Rev. Cancer 14, 135–146. https://doi.org/10.1038/nrc3670

Cox, A.L., Skipper, J., Chen, Y., Henderson, R.A., Darrow, T.L., Shabanowitz, J., Engelhard, V.H., Hunt, D.F., Slingluff, C.L., 1994. Identification of a peptide recognized by five melanoma-specific human cytotoxic T cell lines. Science 264, 716–719.

Cresswell, P., Bangia, N., Dick, T., Diedrich, G., 1999. The nature of the MHC class I peptide loading complex. Immunol. Rev. 172, 21–28. https://doi.org/10.1111/j.1600-065x.1999.tb01353.x

Croker, A.K., Goodale, D., Chu, J., Postenka, C., Hedley, B.D., Hess, D.A., Allan, A.L., 2009. High aldehyde dehydrogenase and expression of cancer stem cell markers selects for breast cancer cells with enhanced malignant and metastatic ability. J. Cell. Mol. Med. 13, 2236–2252. https://doi.org/10.1111/j.1582-4934.2008.00455.x

Culig, Z., Puhr, M., 2012. Interleukin-6: a multifunctional targetable cytokine in human prostate cancer. Mol. Cell. Endocrinol. 360, 52–58. https://doi.org/10.1016/j.mce.2011.05.033

Cunningham, D., You, Z., 2015. In vitro and in vivo model systems used in prostate cancer research. J. Biol. Methods 2. https://doi.org/10.14440/jbm.2015.63

Currier, J.R., Kuta, E.G., Turk, E., Earhart, L.B., Loomis-Price, L., Janetzki, S., Ferrari, G., Birx, D.L., Cox, J.H., 2002. A panel of MHC class I restricted viral peptides for use as a quality control for vaccine trial ELISPOT assays. J. Immunol. Methods 260, 157–172. https://doi.org/10.1016/S0022-1759(01)00535-X

Dalman, M.R., Deeter, A., Nimishakavi, G., Duan, Z.-H., 2012. Fold change and p-value cutoffs significantly alter microarray interpretations. BMC Bioinformatics 13, S11. https://doi.org/10.1186/1471-2105-13-S2-S11

Darke, C., Guttridge, M.G., Thompson, J., McNamara, S., Street, J., Thomas, M., 1998. HLA class I (A, B) and II (DR, DQ) gene and haplotype frequencies in blood donors from Wales. Exp. Clin. Immunogenet. 15, 69–83. https://doi.org/10.1159/000019057

Dasgupta, J.D., Cemach, K., Dubey, D.P., Yunis, E.J., Amos, D.B., 1987. The role of class I histocompatibility antigens in the regulation of T-cell activation. Proc. Natl. Acad. Sci. U. S. A. 84, 1094–1098. https://doi.org/10.1073/pnas.84.4.1094

Davidson, A.L., Dassa, E., Orelle, C., Chen, J., 2008. Structure, Function, and Evolution of Bacterial ATP-Binding Cassette Systems. Microbiol. Mol. Biol. Rev. MMBR 72, 317–364. https://doi.org/10.1128/MMBR.00031-07

Davis, M.M., Bjorkman, P.J., 1988. T-cell antigen receptor genes and T-cell recognition. Nature 334, 395–402. https://doi.org/10.1038/334395a0

Deleyrolle, L.P., Rohaus, M.R., Fortin, J.M., Reynolds, B.A., Azari, H., 2012. Identification and Isolation of Slow-Dividing Cells in Human Glioblastoma Using Carboxy Fluorescein Succinimidyl Ester (CFSE). J. Vis. Exp. JoVE. https://doi.org/10.3791/3918

Dembinski, J.L., Krauss, S., 2009. Characterization and functional analysis of a slow cycling stem cell-like subpopulation in pancreas adenocarcinoma. Clin. Exp. Metastasis 26, 611–623. https://doi.org/10.1007/s10585-009-9260-0

Deng, Z., Wu, Y., Ma, W., Zhang, S., Zhang, Y.-Q., 2015. Adoptive T-cell therapy of prostate cancer targeting the cancer stem cell antigen EpCAM. BMC Immunol. 16. https://doi.org/10.1186/s12865-014-0064-x

Derbinski, J., Schulte, A., Kyewski, B., Klein, L., 2001. Promiscuous gene expression in medullary thymic epithelial cells mirrors the peripheral self. Nat. Immunol. 2, 1032.

Derer, A., Frey, B., Fietkau, R., Gaipl, U.S., 2015. Immune-modulating properties of ionizing radiation: rationale for the treatment of cancer by combination radiotherapy and immune checkpoint inhibitors. Cancer Immunol. Immunother. CII. https://doi.org/10.1007/s00262-015-1771-8

Di Tomaso, T., Mazzoleni, S., Wang, E., Sovena, G., Clavenna, D., Franzin, A., Mortini, P., Ferrone, S., Doglioni, C., Marincola, F.M., Galli, R., Parmiani, G., Maccalli, C., 2010. Immunobiological Characterization of Cancer Stem Cells Isolated from Glioblastoma Patients. Clin. Cancer Res. Off. J. Am. Assoc. Cancer Res. 16, 800–813. https://doi.org/10.1158/1078-0432.CCR-09-2730

Dick, T.P., Nussbaum, A.K., Deeg, M., Heinemeyer, W., Groll, M., Schirle, M., Keilholz, W., Stevanović, S., Wolf, D.H., Huber, R., Rammensee, H.G., Schild, H., 1998. Contribution of proteasomal beta-subunits to the cleavage of peptide substrates analyzed with yeast mutants. J. Biol. Chem. 273, 25637–25646. https://doi.org/10.1074/jbc.273.40.25637

Dighe, A.S., Richards, E., Old, L.J., Schreiber, R.D., 1994. Enhanced in vivo growth and resistance to rejection of tumor cells expressing dominant negative IFNγ receptors. Immunity 1, 447–456. https://doi.org/10.1016/1074-7613(94)90087-6

Dinter, A., Berger, E.G., 1998. Golgi-disturbing agents. Histochem. Cell Biol. 109, 571–590.

Do, K., Doroshow, J.H., Kummar, S., 2013. Wee1 kinase as a target for cancer therapy. Cell Cycle. https://doi.org/10.4161/cc.26062

Doedens, A.L., Phan, A.T., Stradner, M.H., Fujimoto, J.K., Nguyen, J.V., Yang, E., Johnson, R.S., Goldrath, A.W., 2013. Hypoxia-inducible factors enhance the effector responses of CD8+ T cells to persistent antigen. Nat. Immunol. 14, 1173–1182. https://doi.org/10.1038/ni.2714

Doherty, R.E., Haywood-Small, S.L., Sisley, K., Cross, N.A., 2011. Aldehyde dehydrogenase activity selects for the holoclone phenotype in prostate cancer cells. Biochem. Biophys. Res. Commun. 414, 801–807. https://doi.org/10.1016/j.bbrc.2011.10.010

Dollner, R., Granzow, C., Helmke, B.M., Ruess, A., Schad, A., Dietz, A., 2004. The impact of stromal cell contamination on chemosensitivity testing of head and neck carcinoma. Anticancer Res. 24, 325–331.

Dolton, G., Tungatt, K., Lloyd, A., Bianchi, V., Theaker, S.M., Trimby, A., Holland, C.J., Donia, M., Godkin, A.J., Cole, D.K., Thor Straten, P., Peakman, M., Svane, I.M., Sewell, A.K., 2015. More tricks with tetramers: a practical guide to staining T cells with peptide–MHC multimers. Immunology 146, 11–22. https://doi.org/10.1111/imm.12499

Domingo-Domenech, J., Vidal, S.J., Rodriguez-Bravo, V., Castillo-Martin, M., Quinn, S.A., Rodriguez-Barrueco, R., Bonal, D.M., Charytonowicz, E., Gladoun, N., de la Iglesia-Vicente, J., Petrylak, D.P., Benson, M.C., Silva, J.M., Cordon-Cardo, C., 2012. Suppression of Acquired Docetaxel Resistance in Prostate Cancer through Depletion of Notch- and Hedgehog-Dependent Tumor-Initiating Cells. Cancer Cell 22, 373–388. https://doi.org/10.1016/j.ccr.2012.07.016

Downward, J., Graves, J.D., Warne, P.H., Rayter, S., Cantrell, D.A., 1990. Stimulation of p21ras upon T-cell activation. Nature 346, 719.

Drake, C.G., 2010. Prostate cancer as a model for tumour immunotherapy. Nat. Rev. Immunol. 10, 580–593. https://doi.org/10.1038/nri2817

Dreesen, O., Brivanlou, A.H., 2007. Signaling Pathways in Cancer and Embryonic Stem Cells. Stem Cell Rev. 3, 7–17. https://doi.org/10.1007/s12015-007-0004-8

Driessens, G., Beck, B., Caauwe, A., Simons, B.D., Blanpain, C., 2012. Defining the mode of tumour growth by clonal analysis. Nature 488, 527–530. https://doi.org/10.1038/nature11344

Drost, J., Karthaus, W.R., Gao, D., Driehuis, E., Sawyers, C.L., Chen, Y., Clevers, H., 2016. Organoid culture systems for prostate epithelial and cancer tissue. Nat. Protoc. 11, 347–358. https://doi.org/10.1038/nprot.2016.006

Du, F.-Y., Zhou, Q.-F., Sun, W.-J., Chen, G.-L., 2019. Targeting cancer stem cells in drug discovery: Current state and future perspectives. World J. Stem Cells 11, 398–420. https://doi.org/10.4252/wjsc.v11.i7.398

Dubrovska, A., Kim, S., Salamone, R.J., Walker, J.R., Maira, S.-M., García-Echeverría, C., Schultz, P.G., Reddy, V.A., 2009. The role of PTEN/Akt/PI3K signaling in the maintenance and viability of prostate cancer stem-like cell populations. Proc. Natl. Acad. Sci. 106, 268–273. https://doi.org/10.1073/pnas.0810956106

Dunn, G.P., Bruce, A.T., Ikeda, H., Old, L.J., Schreiber, R.D., 2002. Cancer immunoediting: from immunosurveillance to tumor escape. Nat. Immunol. 3, 991–998. https://doi.org/10.1038/ni1102-991

Dunn, G.P., Koebel, C.M., Schreiber, R.D., 2006. Interferons, immunity and cancer immunoediting. Nat. Rev. Immunol. 6, 836–848. https://doi.org/10.1038/nri1961

Dunn, G.P., Old, L.J., Schreiber, R.D., 2004a. The three Es of cancer immunoediting. Annu. Rev. Immunol. 22, 329–360. https://doi.org/10.1146/annurev.immunol.22.012703.104803

Dunn, G.P., Old, L.J., Schreiber, R.D., 2004b. The Immunobiology of Cancer Immunosurveillance and Immunoediting. Immunity 21, 137–148. https://doi.org/10.1016/j.immuni.2004.07.017

DuPage, M., Dooley, A.L., Jacks, T., 2009. Conditional mouse lung cancer models using adenoviral or lentiviral delivery of Cre recombinase. Nat. Protoc. 4, 1064–1072. https://doi.org/10.1038/nprot.2009.95

Ebstein, F., Keller, M., Paschen, A., Walden, P., Seeger, M., Bürger, E., Krüger, E., Schadendorf, D., Kloetzel, P.-M., Seifert, U., 2016. Exposure to Melan-A/MART-126-35 tumor epitope specific CD8(+)T cells reveals immune escape by affecting the ubiquitin-proteasome system (UPS). Sci. Rep. 6, 25208. https://doi.org/10.1038/srep25208

Ehrlich, P., 1909. Ueber den jetzigen Stand der Karzinomforschung. Ned Tijdschr Geneeskd 273–290.

Ellyard, J.I., Simson, L., Parish, C.R., 2007. Th2-mediated anti-tumour immunity: friend or foe? Tissue Antigens 70, 1–11. https://doi.org/10.1111/j.1399-0039.2007.00869.x

Emsley, P., Cowtan, K., 2004. Coot: model-building tools for molecular graphics. Acta Crystallogr. D Biol. Crystallogr. 60, 2126–2132. https://doi.org/10.1107/S0907444904019158

Emsley, P., Lohkamp, B., Scott, W.G., Cowtan, K., 2010. Features and development of Coot. Acta Crystallogr. D Biol. Crystallogr. 66, 486–501. https://doi.org/10.1107/S0907444910007493

Endert, P.M. van, Tampé, R., Meyer, T.H., Tisch, R., Bach, J.-F., McDevitt, H.O., 1994. A sequential model for peptide binding and transport by the transporters associated with antigen processing. Immunity 1, 491–500. https://doi.org/10.1016/1074-7613(94)90091-4

English, H.F., Santen, R.J., Isaacs, J.T., 1987. Response of glandular versus basal rat ventral prostatic epithelial cells to androgen withdrawal and replacement. The Prostate 11, 229–242.

Eppert, K., Takenaka, K., Lechman, E.R., Waldron, L., Nilsson, B., van Galen, P., Metzeler, K.H., Poeppl, A., Ling, V., Beyene, J., Canty, A.J., Danska, J.S., Bohlander, S.K., Buske, C., Minden, M.D., Golub, T.R., Jurisica, I., Ebert, B.L., Dick, J.E., 2011. Stem cell gene expression programs influence clinical outcome in human leukemia. Nat. Med. 17, 1086–1093. https://doi.org/10.1038/nm.2415

Evans, M., Borysiewicz, L.K., Evans, A.S., Rowe, M., Jones, M., Gileadi, U., Cerundolo, V., Man, S., 2001. Antigen processing defects in cervical carcinomas limit the presentation of a CTL epitope from human papillomavirus 16 E6. J. Immunol. Baltim. Md 1950 167, 5420–5428.

Falk, K., Rötzschke, O., Stevanović, S., Jung, G., Rammensee, H.G., 1991. Allele-specific motifs revealed by sequencing of self-peptides eluted from MHC molecules. Nature 351, 290–296. https://doi.org/10.1038/351290a0

Fan, X., Liu, S., Su, F., Pan, Q., Lin, T., 2012. Effective enrichment of prostate cancer stem cells from spheres in a suspension culture system. Urol. Oncol. 30, 314–318. https://doi.org/10.1016/j.urolonc.2010.03.019

Fang, D., Nguyen, T.K., Leishear, K., Finko, R., Kulp, A.N., Hotz, S., Belle, P.A.V., Xu, X., Elder, D.E., Herlyn, M., 2005. A Tumorigenic Subpopulation with Stem Cell Properties in Melanomas. Cancer Res. 65, 9328–9337. https://doi.org/10.1158/0008-5472.CAN-05-1343

Fargeas, C.A., Fonseca, A.-V., Huttner, W.B., Corbeil, D., 2006. Prominin-1 (CD133): from progenitor cells to human diseases. Future Lipidol. 1, 213–225. https://doi.org/10.2217/17460875.1.2.213

Fehling, H.J., Krotkova, A., Saint-Ruf, C., von Boehmer, H., 1995. Crucial role of the pre-T-cell receptor alpha gene in development of alpha beta but not gamma delta T cells. Nature 375, 795–798. https://doi.org/10.1038/375795a0

Finlay, D.K., Rosenzweig, E., Sinclair, L.V., Feijoo-Carnero, C., Hukelmann, J.L., Rolf, J., Panteleyev, A.A., Okkenhaug, K., Cantrell, D.A., 2012. PDK1 regulation of mTOR and hypoxia-inducible factor 1 integrate metabolism and migration of CD8+ T cells. J. Exp. Med. 209, 2441–2453. https://doi.org/10.1084/jem.20112607

Finn, O.J., 2017. Human Tumor Antigens Yesterday, Today, and Tomorrow. Cancer Immunol. Res. 5, 347–354. https://doi.org/10.1158/2326-6066.CIR-17-0112

Finn, O.J., 2012. Immuno-oncology: understanding the function and dysfunction of the immune system in cancer. Ann. Oncol. Off. J. Eur. Soc. Med. Oncol. ESMO 23 Suppl 8, viii6-9. https://doi.org/10.1093/annonc/mds256

Flamand, L., Crowley, R.W., Lusso, P., Colombini-Hatch, S., Margolis, D.M., Gallo, R.C., 1998. Activation of CD8+ T lymphocytes through the T cell receptor turns on CD4 gene expression: implications for HIV pathogenesis. Proc. Natl. Acad. Sci. U. S. A. 95, 3111–3116. https://doi.org/10.1073/pnas.95.6.3111

Fortier, M.-H., Caron, É., Hardy, M.-P., Voisin, G., Lemieux, S., Perreault, C., Thibault, P., 2008. The MHC class I peptide repertoire is molded by the transcriptome. J. Exp. Med. 205, 595–610. https://doi.org/10.1084/jem.20071985

Frame, F.M., Pellacani, D., Collins, A.T., Maitland, N.J., 2016. Harvesting Human Prostate Tissue Material and Culturing Primary Prostate Epithelial Cells, in: McEwan, PhD, I.J. (Ed.), The Nuclear Receptor Superfamily. Springer New York, New York, NY, pp. 181–201. https://doi.org/10.1007/978-1-4939-3724-0_12

Frame, F.M., Pellacani, D., Collins, A.T., Simms, M.S., Mann, V.M., Jones, G.D.D., Meuth, M., Bristow, R.G., Maitland, N.J., 2013. HDAC inhibitor confers radiosensitivity to prostate stem-like cells. Br. J. Cancer 109, 3023–3033. https://doi.org/10.1038/bjc.2013.691

Franken, N.A.P., Rodermond, H.M., Stap, J., Haveman, J., Bree, C. van, 2006. Clonogenic assay of cells in vitro. Nat. Protoc. 1, 2315–2319. https://doi.org/10.1038/nprot.2006.339

Freedland, S.J., Humphreys, E.B., Mangold, L.A., Eisenberger, M., Dorey, F.J., Walsh, P.C., Partin, A.W., 2005. Risk of Prostate Cancer–Specific Mortality Following Biochemical Recurrence After Radical Prostatectomy. JAMA 294, 433–439. https://doi.org/10.1001/jama.294.4.433

Freudenmann, L.K., Marcu, A., Stevanović, S., 2018. Mapping the tumour human leukocyte antigen (HLA) ligandome by mass spectrometry. Immunology 154, 331–345. https://doi.org/10.1111/imm.12936

Fridman, W.H., Pagès, F., Sautès-Fridman, C., Galon, J., 2012. The immune contexture in human tumours: impact on clinical outcome. Nat. Rev. Cancer 12, 298–306. https://doi.org/10.1038/nrc3245

Fue, M., Miki, Y., Takagi, K., Hashimoto, C., Yaegashi, N., Suzuki, T., Ito, K., 2018. Relaxin 2/RXFP1 Signaling Induces Cell Invasion via the β-Catenin Pathway in Endometrial Cancer. Int. J. Mol. Sci. 19. https://doi.org/10.3390/ijms19082438

Gajewski, T.F., 2007. Failure at the effector phase: immune barriers at the level of the melanoma tumor microenvironment. Clin. Cancer Res. Off. J. Am. Assoc. Cancer Res. 13, 5256–5261. https://doi.org/10.1158/1078-0432.CCR-07-0892

Gajewski, T.F., Fuertes, M., Spaapen, R., Zheng, Y., Kline, J., 2011. Molecular profiling to identify relevant immune resistance mechanisms in the tumor microenvironment. Curr. Opin. Immunol. 23, 286–292. https://doi.org/10.1016/j.coi.2010.11.013

Gameiro, S.R., Malamas, A.S., Bernstein, M.B., Tsang, K.Y., Vassantachart, A., Sahoo, N., Tailor, R., Pidikiti, R., Guha, C.P., Hahn, S.M., Krishnan, S., Hodge, J.W., 2016. Tumor Cells Surviving Exposure to Proton or Photon Radiation Share a Common Immunogenic Modulation Signature, Rendering Them More Sensitive to T Cell-Mediated Killing. Int. J. Radiat. Oncol. Biol. Phys. 95, 120–130. https://doi.org/10.1016/j.ijrobp.2016.02.022

Gao, D., Vela, I., Sboner, A., Iaquinta, P.J., Karthaus, W.R., Gopalan, A., Dowling, C., Wanjala, J.N., Undvall, E.A., Arora, V.K., Wongvipat, J., Kossai, M., Ramazanoglu, S., Barboza, L.P., Di, W., Cao, Z., Zhang, Q.F., Sirota, I., Ran, L., MacDonald, T.Y., Beltran, H., Mosquera, J.-M., Touijer, K.A., Scardino, P.T., Laudone, V.P., Curtis, K.R., Rathkopf, D.E., Morris, M.J., Danila, D.C., Slovin, S.F., Solomon, S.B., Eastham, J.A., Chi, P., Carver, B., Rubin, M.A., Scher, H.I., Clevers, H., Sawyers, C.L., Chen, Y., 2014. Organoid Cultures Derived from Patients with Advanced Prostate Cancer. Cell 159, 176–187. https://doi.org/10.1016/j.cell.2014.08.016

Gao, Y., Yang, W., Pan, M., Scully, E., Girardi, M., Augenlicht, L.H., Craft, J., Yin, Z., 2003. Gamma delta T cells provide an early source of interferon gamma in tumor immunity. J. Exp. Med. 198, 433–442. https://doi.org/10.1084/jem.20030584

Garcia-Hernandez, M. de la L., Gray, A., Hubby, B., Klinger, O.J., Kast, W.M., 2008. Prostate Stem Cell Antigen Vaccination Induces a Long-term Protective Immune Response against Prostate Cancer in the Absence of Autoimmunity. Cancer Res. 68, 861–869. https://doi.org/10.1158/0008-5472.CAN-07-0445

Gardner, A., Ruffell, B., 2016. Dendritic Cells and Cancer Immunity. Trends Immunol. 37, 855–865. https://doi.org/10.1016/j.it.2016.09.006

Garner, J.M., Fan, M., Yang, C.H., Du, Z., Sims, M., Davidoff, A.M., Pfeffer, L.M., 2013. Constitutive activation of signal transducer and activator of transcription 3 (STAT3) and nuclear factor κB signaling in glioblastoma cancer stem cells regulates the Notch pathway. J. Biol. Chem. 288, 26167–26176. https://doi.org/10.1074/jbc.M113.477950

Garrido, F., Ruiz-Cabello, F., Cabrera, T., Pérez-Villar, J.J., López-Botet, M., Duggan-Keen, M., Stern, P.L., 1997. Implications for immunosurveillance of altered HLA class I phenotypes in human tumours. Immunol. Today 18, 89–95. https://doi.org/10.1016/S0167-5699(96)10075-X

Gascoigne, N.R.J., Rybakin, V., Acuto, O., Brzostek, J., 2016. TCR Signal Strength and T Cell Development. Annu. Rev. Cell Dev. Biol. 32, 327–348. https://doi.org/10.1146/annurev-cellbio-111315-125324

Gattinoni, L., Lugli, E., Ji, Y., Pos, Z., Paulos, C.M., Quigley, M.F., Almeida, J.R., Gostick, E., Yu, Z., Carpenito, C., Wang, E., Douek, D.C., Price, D.A., June, C.H., Marincola, F.M., Roederer, M., Restifo, N.P., 2011. A human memory T-cell subset with stem cell-like properties. Nat. Med. 17, 1290–1297. https://doi.org/10.1038/nm.2446

Gee, M.H., Han, A., Lofgren, S.M., Beausang, J.F., Mendoza, J.L., Birnbaum, M.E., Bethune, M.T., Fischer, S., Yang, X., Gomez-Eerland, R., Bingham, D.B., Sibener, L.V., Fernandes, R.A., Velasco, A., Baltimore, D., Schumacher, T.N., Khatri, P., Quake, S.R., Davis, M.M., Garcia, K.C., 2018. Antigen identification for orphan T cell receptors expressed on tumor-infiltrating lymphocytes. Cell 172, 549-563.e16. https://doi.org/10.1016/j.cell.2017.11.043

Geiss, G.K., Bumgarner, R.E., Birditt, B., Dahl, T., Dowidar, N., Dunaway, D.L., Fell, H.P., Ferree, S., George, R.D., Grogan, T., James, J.J., Maysuria, M., Mitton, J.D., Oliveri, P., Osborn, J.L., Peng, T., Ratcliffe, A.L., Webster, P.J., Davidson, E.H., Hood, L., Dimitrov, K., 2008. Direct multiplexed measurement of gene expression with color-coded probe pairs. Nat. Biotechnol. 26, 317–325. https://doi.org/10.1038/nbt1385

Genetic effects on gene expression across human tissues, 2017. . Nature 550, 204–213. https://doi.org/10.1038/nature24277

Genitsch, V., Zlobec, I., Thalmann, G.N., Fleischmann, A., 2016. MUC1 is upregulated in advanced prostate cancer and is an independent prognostic factor. Prostate Cancer Prostatic Dis. 19, 242–247. https://doi.org/10.1038/pcan.2016.11

Gerdemann, U., Katari, U., Christin, A.S., Cruz, C.R., Tripic, T., Rousseau, A., Gottschalk, S.M., Savoldo, B., Vera, J.F., Heslop, H.E., Brenner, M.K., Bollard, C.M., Rooney, C.M., Leen, A.M., 2011. Cytotoxic T Lymphocytes Simultaneously Targeting Multiple Tumor-associated Antigens to Treat EBV Negative Lymphoma. Mol. Ther. 19, 2258–2268. https://doi.org/10.1038/mt.2011.167

Germain, R.N., 2002. T-cell development and the CD4–CD8 lineage decision. Nat. Rev. Immunol. 2, 309–322. https://doi.org/10.1038/nri798

Gfeller, D., Bassani-Sternberg, M., 2018. Predicting Antigen Presentation-What Could We Learn From a Million Peptides? Front. Immunol. 9, 1716. https://doi.org/10.3389/fimmu.2018.01716

Gfeller, D., Guillaume, P., Michaux, J., Pak, H.-S., Daniel, R.T., Racle, J., Coukos, G., Bassani-Sternberg, M., 2018. The Length Distribution and

Multiple Specificity of Naturally Presented HLA-I Ligands. J. Immunol. Baltim. Md 1950 201, 3705–3716. https://doi.org/10.4049/jimmunol.1800914

Ghiringhelli, F., Menard, C., Puig, P.E., Ladoire, S., Roux, S., Martin, F., Solary, E., Le Cesne, A., Zitvogel, L., Chauffert, B., 2007. Metronomic cyclophosphamide regimen selectively depletes CD4+CD25+ regulatory T cells and restores T and NK effector functions in end stage cancer patients. Cancer Immunol. Immunother. CII 56, 641–648. https://doi.org/10.1007/s00262-006-0225-8

Gielis, S., Moris, P., Bittremieux, W., Neuter, N.D., Ogunjimi, B., Laukens, K., Meysman, P., 2019. TCRex: detection of enriched T cell epitope specificity in full T cell receptor sequence repertoires. bioRxiv 373472. https://doi.org/10.1101/373472

Ginestier, C., Hur, M.H., Charafe-Jauffret, E., Monville, F., Dutcher, J., Brown, M., Jacquemier, J., Viens, P., Kleer, C., Liu, S., Schott, A., Hayes, D., Birnbaum, D., Wicha, M.S., Dontu, G., 2007. ALDH1 is a marker of normal and malignant human mammary stem cells and a predictor of poor clinical outcome. Cell Stem Cell 1, 555–567. https://doi.org/10.1016/j.stem.2007.08.014

Gires, O., Klein, C.A., Baeuerle, P.A., 2009. On the abundance of EpCAM on cancer stem cells. Nat. Rev. Cancer 9, 143. https://doi.org/10.1038/nrc2499-c1

Glumac, P.M., LeBeau, A.M., 2018. The role of CD133 in cancer: a concise review. Clin. Transl. Med. 7. https://doi.org/10.1186/s40169-018-0198-1

Gnjatic, S., Nishikawa, H., Jungbluth, A.A., Güre, A.O., Ritter, G., Jäger, E., Knuth, A., Chen, Y.-T., Old, L.J., 2006. NY-ESO-1: review of an immunogenic tumor antigen. Adv. Cancer Res. 95, 1–30. https://doi.org/10.1016/S0065-230X(06)95001-5

Gomes-Silva, D., Ramos, C.A., 2018. Cancer immunotherapy using CAR-T cells: from the research bench to the assembly line. Biotechnol. J. 13. https://doi.org/10.1002/biot.201700097

Gonzalez-Galarza, F.F., Christmas, S., Middleton, D., Jones, A.R., 2011. Allele frequency net: a database and online repository for immune gene frequencies in worldwide populations. Nucleic Acids Res. 39, D913-919. https://doi.org/10.1093/nar/gkq1128

Gopinathan, L., Tan, S.L.W., Padmakumar, V.C., Coppola, V., Tessarollo, L., Kaldis, P., 2014. Loss of Cdk2 and cyclin A2 impairs cell proliferation and tumorigenesis. Cancer Res. 74, 3870–3879. https://doi.org/10.1158/0008-5472.CAN-13-3440

Grandea, A.G., Van Kaer, L., 2001. Tapasin: an ER chaperone that controls MHC class I assembly with peptide. Trends Immunol. 22, 194–199. https://doi.org/10.1016/s1471-4906(01)01861-0

Gravis, G., Boher, J.-M., Joly, F., Soulié, M., Albiges, L., Priou, F., Latorzeff, I., Delva, R., Krakowski, I., Laguerre, B., Rolland, F., Théodore, C., Deplanque, G., Ferrero, J.-M., Culine, S., Mourey, L., Beuzeboc, P., Habibian, M., Oudard, S., Fizazi, K., 2016. Androgen Deprivation Therapy (ADT) Plus Docetaxel Versus ADT Alone in Metastatic Non castrate Prostate Cancer: Impact of Metastatic Burden and Long-term Survival Analysis of the Randomized Phase 3 GETUG-AFU15 Trial. Eur. Urol. 70, 256–262. https://doi.org/10.1016/j.eururo.2015.11.005

Greaves, M., Maley, C.C., 2012. Clonal evolution in cancer. Nature 481, 306–313. https://doi.org/10.1038/nature10762

Groh, V., Rhinehart, R., Secrist, H., Bauer, S., Grabstein, K.H., Spies, T., 1999. Broad tumor-associated expression and recognition by tumor-derived γδ T cells of MICA and MICB. Proc. Natl. Acad. Sci. 96, 6879–6884. https://doi.org/10.1073/pnas.96.12.6879

Grosse-Gehling, P., Fargeas, C.A., Dittfeld, C., Garbe, Y., Alison, M.R., Corbeil, D., Kunz-Schughart, L.A., 2013. CD133 as a biomarker for putative cancer stem cells in solid tumours: limitations, problems and challenges: CD133 in human cancers. J. Pathol. 229, 355–378. https://doi.org/10.1002/path.4086

Grudzien, P., Lo, S., Albain, K.S., Robinson, P., Rajan, P., Strack, P.R., Golde, T.E., Miele, L., Foreman, K.E., 2010. Inhibition of Notch signaling reduces the stem-like population of breast cancer cells and prevents mammosphere formation. Anticancer Res. 30, 3853–3867.

Gu, H., Wu, X.-Y., Fan, R.-T., Wang, X., Guo, Y.-Z., Wang, R., 2016. Side population cells from long-term passage non-small cell lung cancer cells display loss of cancer stem cell-like properties and chemoradioresistance. Oncol. Lett. 12, 2886–2893. https://doi.org/10.3892/ol.2016.4934

Guan, P., Doytchinova, I.A., Zygouri, C., Flower, D.R., 2003. MHCPred: a server for quantitative prediction of peptide–MHC binding. Nucleic Acids Res. 31, 3621–3624.

Guillaume, B., Chapiro, J., Stroobant, V., Colau, D., Van Holle, B., Parvizi, G., Bousquet-Dubouch, M.-P., Théate, I., Parmentier, N., Van den Eynde, B.J., 2010. Two abundant proteasome subtypes that uniquely process some antigens presented by HLA class I molecules. Proc. Natl. Acad. Sci. U. S. A. 107, 18599–18604. https://doi.org/10.1073/pnas.1009778107

Gulley, J.L., Arlen, P.M., Bastian, A., Morin, S., Marte, J., Beetham, P., Tsang, K.-Y., Yokokawa, J., Hodge, J.W., Ménard, C., Camphausen, K., Coleman, C.N., Sullivan, F., Steinberg, S.M., Schlom, J., Dahut, W., 2005. Combining a recombinant cancer vaccine with standard definitive radiotherapy in patients with localized prostate cancer. Clin. Cancer Res. Off. J. Am. Assoc. Cancer Res. 11, 3353–3362. https://doi.org/10.1158/1078-0432.CCR-04-2062

Gulley, J.L., Arlen, P.M., Madan, R.A., Tsang, K.-Y., Pazdur, M.P., Skarupa, L., Jones, J.L., Poole, D.J., Higgins, J.P., Hodge, J.W., Cereda, V., Vergati, M., Steinberg, S.M., Halabi, S., Jones, E., Chen, C., Parnes, H., Wright, J.J., Dahut, W.L., Schlom, J., 2010. Immunologic and prognostic factors associated with overall survival employing a poxviral-based PSA vaccine in metastatic castrate-resistant prostate cancer. Cancer Immunol. Immunother. CII 59, 663–674. https://doi.org/10.1007/s00262-009-0782-8

Gulley, J.L., Borre, M., Vogelzang, N.J., Ng, S., Agarwal, N., Parker, C.C., Pook, D.W., Rathenborg, P., Flaig, T.W., Carles, J., Shore, N.D., Chen, L., Heery, C.R., Gerritsen, W.R., Priou, F., Kantoff, P.W., 2018. Results of PROSPECT: A randomized phase 3 trial of PROSTVAC-V/F (PRO) in men with asymptomatic or minimally symptomatic metastatic, castration-resistant prostate cancer. J. Clin. Oncol. 36, 5006–5006. https://doi.org/10.1200/JCO.2018.36.15_suppl.5006

Günther, H.S., Schmidt, N.O., Phillips, H.S., Kemming, D., Kharbanda, S., Soriano, R., Modrusan, Z., Meissner, H., Westphal, M., Lamszus, K., 2008. Glioblastoma-derived stem cell-enriched cultures form distinct subgroups according to molecular and phenotypic criteria. Oncogene 27, 2897–2909. https://doi.org/10.1038/sj.onc.1210949

Guzel, E., Karatas, O.F., Duz, M.B., Solak, M., Ittmann, M., Ozen, M., 2014. Differential expression of stem cell markers and ABCG2 in recurrent prostate cancer. The Prostate 74, 1498–1505. https://doi.org/10.1002/pros.22867

Guzmán, C., Bagga, M., Kaur, A., Westermarck, J., Abankwa, D., 2014. ColonyArea: An ImageJ Plugin to Automatically Quantify Colony Formation in Clonogenic Assays. PLOS ONE 9, e92444. https://doi.org/10.1371/journal.pone.0092444

Guzman, M.L., Neering, S.J., Upchurch, D., Grimes, B., Howard, D.S., Rizzieri, D.A., Luger, S.M., Jordan, C.T., 2001. Nuclear factor-kappaB is constitutively activated in primitive human acute myelogenous leukemia cells. Blood 98, 2301–2307.

Hamdy, F.C., Donovan, J.L., Lane, J.A., Mason, M., Metcalfe, C., Holding, P., Davis, M., Peters, T.J., Turner, E.L., Martin, R.M., Oxley, J., Robinson, M., Staffurth, J., Walsh, E., Bollina, P., Catto, J., Doble, A., Doherty, A., Gillatt, D., Kockelbergh, R., Kynaston, H., Paul, A., Powell, P., Prescott, S., Rosario, D.J., Rowe, E., Neal, D.E., 2016. 10-Year Outcomes after Monitoring, Surgery, or Radiotherapy for Localized Prostate Cancer. N. Engl. J. Med. 375, 1415–1424. https://doi.org/10.1056/NEJMoa1606220

Han, M., Partin, A.W., Pound, C.R., Epstein, J.I., Walsh, P.C., 2001. Long-term biochemical disease-free and cancer-specific survival following anatomic radical retropubic prostatectomy. The 15-year Johns Hopkins experience. Urol. Clin. North Am. 28, 555–565.

Han, Z., Wang, X., Ma, L., Chen, L., Xiao, M., Huang, L., Cao, Y., Bai, J., Ma, D., Zhou, J., Hong, Z., 2014. Inhibition of STAT3 signaling targets both tumor-initiating and differentiated cell populations in prostate cancer. Oncotarget 5, 8416–8428.

Hanrahan, K., O'Neill, A., Prencipe, M., Bugler, J., Murphy, L., Fabre, A., Puhr, M., Culig, Z., Murphy, K., Watson, R.W., 2017. The role of epithelial-mesenchymal transition drivers ZEB1 and ZEB2 in mediating docetaxel-resistant prostate cancer. Mol. Oncol. 11, 251–265. https://doi.org/10.1002/1878-0261.12030

Hargadon, K.M., Johnson, C.E., Williams, C.J., 2018. Immune checkpoint blockade therapy for cancer: An overview of FDA-approved immune checkpoint inhibitors. Int. Immunopharmacol. 62, 29–39. https://doi.org/10.1016/j.intimp.2018.06.001

Harndahl, M., Rasmussen, M., Roder, G., Pedersen, I.D., Sørensen, M., Nielsen, M., Buus, S., 2012. Peptide-MHC class I stability is a better predictor than peptide affinity of CTL immunogenicity. Eur. J. Immunol. 42, 1405–1416. https://doi.org/10.1002/eji.201141774

Harris, D.T., Kranz, D.M., 2016. Adoptive T Cell Therapies: A Comparison of T Cell Receptors and Chimeric Antigen Receptors. Trends Pharmacol. Sci. 37, 220–230. https://doi.org/10.1016/j.tips.2015.11.004

He, H., Kondo, Y., Ishiyama, K., Alatrash, G., Lu, S., Cox, K., Qiao, N., Clise-Dwyer, K., St John, L., Sukhumalchandra, P., Ma, Q., Molldrem, J.J., 2020. Two unique HLA-A*0201 restricted peptides derived from cyclin

E as immunotherapeutic targets in leukemia. Leukemia. https://doi.org/10.1038/s41375-019-0698-z

Hebeisen, M., Oberle, S., Presotto, D., Speiser, D.E., Zehn, D., Rufer, N., 2013. Molecular Insights for Optimizing T Cell Receptor Specificity Against Cancer. Front. Immunol. 4. https://doi.org/10.3389/fimmu.2013.00154

Heidenreich, A., Bastian, P.J., Bellmunt, J., Bolla, M., Joniau, S., van der Kwast, T., Mason, M., Matveev, V., Wiegel, T., Zattoni, F., Mottet, N., 2014. EAU Guidelines on Prostate Cancer. Part 1: Screening, Diagnosis, and Local Treatment with Curative Intent?Update 2013. Eur. Urol. 65, 124–137. https://doi.org/10.1016/j.eururo.2013.09.046

Hellsten, R., Johansson, M., Dahlman, A., Sterner, O., Bjartell, A., 2011. Galiellalactone Inhibits Stem Cell-Like ALDH-Positive Prostate Cancer Cells. PLoS ONE 6, e22118. https://doi.org/10.1371/journal.pone.0022118

Hempelmann, J.A., Lockwood, C.M., Konnick, E.Q., Schweizer, M.T., Antonarakis, E.S., Lotan, T.L., Montgomery, B., Nelson, P.S., Klemfuss, N., Salipante, S.J., Pritchard, C.C., 2018. Microsatellite instability in prostate cancer by PCR or next-generation sequencing. J. Immunother. Cancer 6. https://doi.org/10.1186/s40425-018-0341-y

Herlyn, D., Herlyn, M., Steplewski, Z., Koprowski, H., 1979. Monoclonal antibodies in cell-mediated cytotoxicity against human melanoma and colorectal carcinoma. Eur. J. Immunol. 9, 657–659.

Hermann, P.C., Huber, S.L., Herrler, T., Aicher, A., Ellwart, J.W., Guba, M., Bruns, C.J., Heeschen, C., 2007. Distinct Populations of Cancer Stem Cells Determine Tumor Growth and Metastatic Activity in Human Pancreatic Cancer. Cell Stem Cell 1, 313–323. https://doi.org/10.1016/j.stem.2007.06.002

Hermansen, S.K., Christensen, K.G., Jensen, S.S., Kristensen, B.W., 2011. Inconsistent Immunohistochemical Expression Patterns of Four Different CD133 Antibody Clones in Glioblastoma. J. Histochem. Cytochem. 59, 391. https://doi.org/10.1369/0022155411400867

Hernandez, C., Huebener, P., Schwabe, R.F., 2016. Damage-associated molecular patterns in cancer: A double-edged sword. Oncogene 35, 5931–5941. https://doi.org/10.1038/onc.2016.104

Hillen, N., Mester, G., Lemmel, C., Weinzierl, A.O., Müller, M., Wernet, D., Hennenlotter, J., Stenzl, A., Rammensee, H.-G., Stevanović, S., 2008. Essential differences in ligand presentation and T cell epitope recognition among HLA molecules of the HLA-B44 supertype. Eur. J. Immunol. 38, 2993–3003. https://doi.org/10.1002/eji.200838632

Hinrichs, C.S., Restifo, N.P., 2013. Reassessing target antigens for adoptive T cell therapy. Nat. Biotechnol. 31, 999–1008. https://doi.org/10.1038/nbt.2725

Hirohashi, Y., Torigoe, T., Inoda, S., Morita, R., Kochin, V., Sato, N., 2012. Cytotoxic T lymphocytes: Sniping cancer stem cells. OncoImmunology 1, 123–125. https://doi.org/10.4161/onci.1.1.18075

Hobisch, A., Rogatsch, H., Hittmair, A., Fuchs, D., Bartsch, G., Klocker, H., Bartsch, G., Culig, Z., 2000. Immunohistochemical localization of interleukin-6 and its receptor in benign, premalignant and malignant prostate tissue. J. Pathol. 191, 239–244. https://doi.org/10.1002/1096-9896(2000)9999:9999<::AID-PATH633>3.0.CO;2-X

Hodi, F.S., O'Day, S.J., McDermott, D.F., Weber, R.W., Sosman, J.A., Haanen, J.B., Gonzalez, R., Robert, C., Schadendorf, D., Hassel, J.C., Akerley, W., van den Eertwegh, A.J.M., Lutzky, J., Lorigan, P., Vaubel, J.M., Linette, G.P., Hogg, D., Ottensmeier, C.H., Lebbé, C., Peschel, C., Quirt, I., Clark, J.I., Wolchok, J.D., Weber, J.S., Tian, J., Yellin, M.J., Nichol, G.M., Hoos, A., Urba, W.J., 2010. Improved survival with ipilimumab in patients with metastatic melanoma. N. Engl. J. Med. 363, 711–723. https://doi.org/10.1056/NEJMoa1003466

Höfner, T., Eisen, C., Klein, C., Rigo-Watermeier, T., Goeppinger, S.M., Jauch, A., Schoell, B., Vogel, V., Noll, E., Weichert, W., Baccelli, I., Schillert, A., Wagner, S., Pahernik, S., Sprick, M.R., Trumpp, A., 2015. Defined conditions for the isolation and expansion of basal prostate progenitor cells of mouse and human origin. Stem Cell Rep. 4, 503–518. https://doi.org/10.1016/j.stemcr.2015.01.015

Holah, N.S., Aiad, H.A.-E.-S., Asaad, N.Y., Elkhouly, E.A., Lasheen, A.G., 2017. Evaluation of the Role of ALDH1 as Cancer Stem Cell Marker in Colorectal Carcinoma: An Immunohistochemical Study. J. Clin. Diagn. Res. JCDR 11, EC17–EC23. https://doi.org/10.7860/JCDR/2017/22671.9291

Holler, P.D., Chlewicki, L.K., Kranz, D.M., 2003. TCRs with high affinity for foreign pMHC show self-reactivity. Nat. Immunol. 4, 55–62. https://doi.org/10.1038/ni863

Hongo, A., Kanaseki, T., Tokita, S., Kochin, V., Miyamoto, S., Hashino, Y., Codd, A., Kawai, N., Nakatsugawa, M., Hirohashi, Y., Sato, N., Torigoe, T., 2019. Upstream Position of Proline Defines Peptide–HLA Class I Repertoire Formation and CD8+ T Cell Responses. J. Immunol. ji1900029. https://doi.org/10.4049/jimmunol.1900029

Hoof, I., Peters, B., Sidney, J., Pedersen, L.E., Sette, A., Lund, O., Buus, S., Nielsen, M., 2009. NetMHCpan, a method for MHC class I binding prediction beyond humans. Immunogenetics 61, 1.

Horoszewicz, J.S., Leong, S.S., Kawinski, E., Karr, J.P., Rosenthal, H., Chu, T.M., Mirand, E.A., Murphy, G.P., 1983. LNCaP Model of Human Prostatic Carcinoma. Cancer Res. 43, 1809–1818.

Houghton, A.N., Guevara-Patiño, J.A., 2004. Immune recognition of self in immunity against cancer. J. Clin. Invest. 114, 468–471. https://doi.org/10.1172/JCI200422685

Houot, R., Schultz, L.M., Marabelle, A., Kohrt, H., 2015. T-cell-based Immunotherapy: Adoptive Cell Transfer and Checkpoint Inhibition. Cancer Immunol. Res. 3, 1115–1122. https://doi.org/10.1158/2326-6066.CIR-15-0190

Hu, Q., Lin, X., Ding, L., Zeng, Y., Pang, D., Ouyang, N., Xiang, Y., Yao, H., 2018. ARHGAP42 promotes cell migration and invasion involving PI3K/Akt signaling pathway in nasopharyngeal carcinoma. Cancer Med. 7, 3862–3874. https://doi.org/10.1002/cam4.1552

Hu, W.-Y., Hu, D.-P., Xie, L., Li, Y., Majumdar, S., Nonn, L., Hu, H., Shioda, T., Prins, G.S., 2017. Isolation and Functional Interrogation of Adult Human Prostate Epithelial Stem Cells at Single Cell Resolution. Stem Cell Res. 23, 1–12. https://doi.org/10.1016/j.scr.2017.06.009

Hu, Y., Lu, L., Xia, Y., Chen, X., Chang, A.E., Hollingsworth, R.E., Hurt, E., Owen, J., Moyer, J.S., Prince, M.E.P., Dai, F., Bao, Y., Wang, Y., Whitfield, J., Xia, J.-C., Huang, S., Wicha, M.S., Li, Q., 2016. Therapeutic Efficacy of Cancer Stem Cell Vaccines in the Adjuvant

Setting. Cancer Res. 76, 4661–4672. https://doi.org/10.1158/0008-5472.CAN-15-2664

Huang, D.W., Sherman, B.T., Lempicki, R.A., 2009a. Bioinformatics enrichment tools: paths toward the comprehensive functional analysis of large gene lists. Nucleic Acids Res. 37, 1–13. https://doi.org/10.1093/nar/gkn923

Huang, D.W., Sherman, B.T., Lempicki, R.A., 2009b. Systematic and integrative analysis of large gene lists using DAVID bioinformatics resources. Nat. Protoc. 4, 44–57. https://doi.org/10.1038/nprot.2008.211

Huels, D.J., Sansom, O.J., 2015. Stem vs non-stem cell origin of colorectal cancer. Br. J. Cancer 113, 1–5. https://doi.org/10.1038/bjc.2015.214

Huggins, C.E., Domenighetti, A.A., Ritchie, M.E., Khalil, N., Favaloro, J.M., Proietto, J., Smyth, G.K., Pepe, S., Delbridge, L.M.D., 2008. Functional and metabolic remodelling in GLUT4-deficient hearts confers hyper-responsiveness to substrate intervention. J. Mol. Cell. Cardiol. 44, 270–280. https://doi.org/10.1016/j.yjmcc.2007.11.020

Hunder, N.N., Wallen, H., Cao, J., Hendricks, D.W., Reilly, J.Z., Rodmyre, R., Jungbluth, A., Gnjatic, S., Thompson, J.A., Yee, C., 2008. Treatment of Metastatic Melanoma with Autologous CD4+ T Cells against NY-ESO-1. N. Engl. J. Med. 358, 2698–2703. https://doi.org/10.1056/NEJMoa0800251

Hunt, D.F., Henderson, R.A., Shabanowitz, J., Sakaguchi, K., Michel, H., Sevilir, N., Cox, A.L., Appella, E., Engelhard, V.H., 1992. Characterization of peptides bound to the class I MHC molecule HLA-A2.1 by mass spectrometry. Science 255, 1261–1263.

Hurt, E.M., Kawasaki, B.T., Klarmann, G.J., Thomas, S.B., Farrar, W.L., 2008. CD44+CD24− prostate cells are early cancer progenitor/stem cells that provide a model for patients with poor prognosis. Br. J. Cancer 98, 756–765. https://doi.org/10.1038/sj.bjc.6604242

Huss, W.J., Gray, D.R., Greenberg, N.M., Mohler, J.L., Smith, G.J., 2005. Breast Cancer Resistance Protein–Mediated Efflux of Androgen in Putative Benign and Malignant Prostate Stem Cells. Cancer Res. 65, 6640–6650. https://doi.org/10.1158/0008-5472.CAN-04-2548

Ilyas, S., Yang, J.C., 2015. Landscape of Tumor Antigens in T-Cell Immunotherapy. J. Immunol. Baltim. Md 1950 195, 5117–5122. https://doi.org/10.4049/jimmunol.1501657

Imrich, S., Hachmeister, M., Gires, O., 2012. EpCAM and its potential role in tumor-initiating cells. Cell Adhes. Migr. 6, 30–38. https://doi.org/10.4161/cam.18953

Isaacs, J.T., 1987. Control of cell proliferation and cell death in the normal and neoplastic prostate: a stem cell model., in: Benign Prostatic Hyperplasia. NIH US Department of Health and Human Services., Washington DC, pp. 85–94.

Ischenko, I., Seeliger, H., Schaffer, M., Jauch, K.-W., Bruns, C.J., 2008. Cancer stem cells: how can we target them? Curr. Med. Chem. 15, 3171–3184.

Islam, F., Gopalan, V., Smith, R.A., Lam, A.K.-Y., 2015. Translational potential of cancer stem cells: A review of the detection of cancer stem cells and their roles in cancer recurrence and cancer treatment. Exp. Cell Res. 335, 135–147. https://doi.org/10.1016/j.yexcr.2015.04.018

Jachetti, E., Mazzoleni, S., Grioni, M., Ricupito, A., Brambillasca, C., Generoso, L., Calcinotto, A., Freschi, M., Mondino, A., Galli, R., Bellone, M., 2013. Prostate cancer stem cells are targets of both innate and adaptive immunity and elicit tumor-specific immune responses. Oncoimmunology 2. https://doi.org/10.4161/onci.24520

Jackson, E.B., Brues, A.M., 1941. Studies on a Transplantable Embryoma of the Mouse. Cancer Res. 1, 494–498.

Jäger, E., Chen, Y.-T., Drijfhout, J.W., Karbach, J., Ringhoffer, M., Jäger, D., Arand, M., Wada, H., Noguchi, Y., Stockert, E., Old, L.J., Knuth, A., 1998. Simultaneous Humoral and Cellular Immune Response against Cancer–Testis Antigen NY-ESO-1: Definition of Human Histocompatibility Leukocyte Antigen (HLA)-A2–binding Peptide Epitopes. J. Exp. Med. 187, 265–270.

Jäger, E., Jäger, D., Karbach, J., Chen, Y.T., Ritter, G., Nagata, Y., Gnjatic, S., Stockert, E., Arand, M., Old, L.J., Knuth, A., 2000. Identification of NY-ESO-1 epitopes presented by human histocompatibility antigen (HLA)-DRB4*0101-0103 and recognized by CD4(+) T lymphocytes of patients with NY-ESO-1-expressing melanoma. J. Exp. Med. 191, 625–630. https://doi.org/10.1084/jem.191.4.625

Jaggupilli, A., Elkord, E., Jaggupilli, A., Elkord, E., 2012. Significance of CD44 and CD24 as Cancer Stem Cell Markers: An Enduring Ambiguity, Significance of CD44 and CD24 as Cancer Stem Cell Markers: An Enduring Ambiguity. J. Immunol. Res. J. Immunol. Res. 2012, 2012, e708036. https://doi.org/10.1155/2012/708036, 10.1155/2012/708036

Jaiswal, S., Chao, M.P., Majeti, R., Weissman, I.L., 2010. Macrophages as mediators of tumor immunosurveillance. Trends Immunol. 31, 212–219. https://doi.org/10.1016/j.it.2010.04.001

Jan, M., Snyder, T.M., Corces-Zimmerman, M.R., Vyas, P., Weissman, I.L., Quake, S.R., Majeti, R., 2012. Clonal Evolution of Preleukemic Hematopoietic Stem Cells Precedes Human Acute Myeloid Leukemia. Sci. Transl. Med. 4, 149ra118-149ra118. https://doi.org/10.1126/scitranslmed.3004315

Janssen, E.M., Lemmens, E.E., Wolfe, T., Christen, U., Herrath, M.G. von, Schoenberger, S.P., 2003. CD4 + T cells are required for secondary expansion and memory in CD8 + T lymphocytes. Nature 421, 852–856. https://doi.org/10.1038/nature01441

Ji, J., Judkowski, V.A., Liu, G., Wang, H., Bunying, A., Li, Z., Xu, M., Bender, J., Pinilla, C., Yu, J.S., 2014. Identification of novel human leukocyte antigen-A*0201-restricted, cytotoxic T lymphocyte epitopes on CD133 for cancer stem cell immunotherapy. Stem Cells Transl. Med. 3, 356–364. https://doi.org/10.5966/sctm.2013-0135

Junghans, R.P., Ma, Q., Rathore, R., Gomes, E.M., Bais, A.J., Lo, A.S.Y., Abedi, M., Davies, R.A., Cabral, H.J., Al-Homsi, A.S., Cohen, S.I., 2016. Phase I Trial of Anti-PSMA Designer CAR-T Cells in Prostate Cancer: Possible Role for Interacting Interleukin 2-T Cell Pharmacodynamics as a Determinant of Clinical Response. The Prostate 76, 1257–1270. https://doi.org/10.1002/pros.23214

Kachikwu, E.L., Iwamoto, K.S., Liao, Y.-P., DeMarco, J.J., Agazaryan, N., Economou, J.S., McBride, W.H., Schaue, D., 2011. Radiation Enhances Regulatory T Cell Representation. Int. J. Radiat. Oncol. Biol. Phys. 81.

Kalaora, S., Samuels, Y., 2019. Cancer Exome-Based Identification of Tumor Neo-Antigens Using Mass Spectrometry, in: López-Soto, A., Folgueras, A.R. (Eds.), Cancer Immunosurveillance: Methods and Protocols, Methods in Molecular Biology. Springer New York, New York, NY, pp. 203–214. https://doi.org/10.1007/978-1-4939-8885-3_14

Kalaora, S., Wolf, Y., Feferman, T., Barnea, E., Greenstein, E., Reshef, D., Tirosh, I., Reuben, A., Patkar, S., Levy, R., Quinkhardt, J., Omokoko, T., Qutob, N., Golani, O., Zhang, J., Mao, X., Song, X., Bernatchez, C., Haymaker, C., Forget, M.-A., Creasy, C., Greenberg, P., Carter, B.W., Cooper, Z.A., Rosenberg, S.A., Lotem, M., Sahin, U., Shakhar, G., Ruppin, E., Wargo, J.A., Friedman, N., Admon, A., Samuels, Y., 2018. Combined Analysis of Antigen Presentation and T-cell Recognition Reveals Restricted Immune Responses in Melanoma. Cancer Discov. 8, 1366–1375. https://doi.org/10.1158/2159-8290.CD-17-1418

Kallifatidis, G., Labsch, S., Rausch, V., Mattern, J., Gladkich, J., Moldenhauer, G., Büchler, M.W., Salnikov, A.V., Herr, I., 2011. Sulforaphane Increases Drug-mediated Cytotoxicity Toward Cancer Stem-like Cells of Pancreas and Prostate. Mol. Ther. 19, 188–195. https://doi.org/10.1038/mt.2010.216

Kamata, Y., Kuhara, A., Iwamoto, T., Hayashi, K., Koido, S., Kimura, T., Egawa, S., Homma, S., 2013. Identification of HLA Class I-binding Peptides Derived from Unique Cancer-associated Proteins by Mass Spectrometric Analysis. Anticancer Res. 33, 1853–1859.

Kanaseki, T., Blanchard, N., Hammer, G.E., Gonzalez, F., Shastri, N., 2006. ERAAP synergizes with MHC class I molecules to make the final cut in the antigenic peptide precursors in the endoplasmic reticulum. Immunity 25, 795–806. https://doi.org/10.1016/j.immuni.2006.09.012

Kantoff, P.W., Schuetz, T.J., Blumenstein, B.A., Glode, L.M., Bilhartz, D.L., Wyand, M., Manson, K., Panicali, D.L., Laus, R., Schlom, J., 2010. Overall Survival Analysis of a Phase II Randomized Controlled Trial of a Poxviral-Based PSA-Targeted Immunotherapy in Metastatic Castration-Resistant Prostate Cancer. J. Clin. Oncol. 28, 1099–1105.

Kaplan, D.H., Shankaran, V., Dighe, A.S., Stockert, E., Aguet, M., Old, L.J., Schreiber, R.D., 1998. Demonstration of an interferon gamma-dependent tumor surveillance system in immunocompetent mice. Proc. Natl. Acad. Sci. U. S. A. 95, 7556–7561.

Karantanos, T., Evans, C.P., Tombal, B., Thompson, T.C., Montironi, R., Isaacs, W.B., 2015. Understanding the Mechanisms of Androgen Deprivation Resistance in Prostate Cancer at the Molecular Level. Eur. Urol. 67, 470–479. https://doi.org/10.1016/j.eururo.2014.09.049

Karbach, J., Neumann, A., Atmaca, A., Wahle, C., Brand, K., von Boehmer, L., Knuth, A., Bender, A., Ritter, G., Old, L.J., Jäger, E., 2011. Efficient in vivo priming by vaccination with recombinant NY-ESO-1 protein and CpG in antigen naive prostate cancer patients. Clin. Cancer Res. Off. J. Am. Assoc. Cancer Res. 17, 861–870. https://doi.org/10.1158/1078-0432.CCR-10-1811

Karthaus, W.R., Iaquinta, P.J., Drost, J., Gracanin, A., van Boxtel, R., Wongvipat, J., Dowling, C.M., Gao, D., Begthel, H., Sachs, N., Vries, R.G.J., Cuppen, E., Chen, Y., Sawyers, C.L., Clevers, H.C., 2014. Identification of multipotent luminal progenitor cells in human prostate

organoid cultures. Cell 159, 163–175. https://doi.org/10.1016/j.cell.2014.08.017

Kawasaki, B.T., Mistree, T., Hurt, E.M., Kalathur, M., Farrar, W.L., 2007. Co-expression of the toleragenic glycoprotein, CD200, with markers for cancer stem cells. Biochem. Biophys. Res. Commun. 364, 778–782. https://doi.org/10.1016/j.bbrc.2007.10.067

Keeney, M., Gratama, J.W., Chin-Yee, I.H., Sutherland, D.R., 1998. Isotype controls in the analysis of lymphocytes and CD34+ stem and progenitor cells by flow cytometry—time to let go? Cytometry 34, 280–283. https://doi.org/10.1002/(SICI)1097-0320(19981215)34:6<280::AID-CYTO6>3.0.CO;2-H

Kemper, K., Sprick, M.R., Bree, M. de, Scopelliti, A., Vermeulen, L., Hoek, M., Zeilstra, J., Pals, S.T., Mehmet, H., Stassi, G., Medema, J.P., 2010. The AC133 Epitope, but not the CD133 Protein, Is Lost upon Cancer Stem Cell Differentiation. Cancer Res. 70, 719–729. https://doi.org/10.1158/0008-5472.CAN-09-1820

Kerr, C.L., Hussain, A., 2014. Regulators of prostate cancer stem cells. Curr. Opin. Oncol. 26, 328–333. https://doi.org/10.1097/CCO.0000000000000080

Khong, H.T., Restifo, N.P., 2002. Natural selection of tumor variants in the generation of "tumor escape" phenotypes. Nat. Immunol. 3, 999–1005. https://doi.org/10.1038/ni1102-999

Kiessling, A., Schmitz, M., Stevanovic, S., Weigle, B., Hölig, K., Füssel, M., Füssel, S., Meye, A., Wirth, M.P., Rieber, E.P., 2002. Prostate stem cell antigen: Identification of immunogenic peptides and assessment of reactive CD8+ T cells in prostate cancer patients. Int. J. Cancer 102, 390–397. https://doi.org/10.1002/ijc.10713

Kiessling, A., Wehner, R., Füssel, S., Bachmann, M., Wirth, M.P., Schmitz, M., 2012. Tumor-Associated Antigens for Specific Immunotherapy of Prostate Cancer. Cancers 4, 193. https://doi.org/10.3390/cancers4010193

Kim, James, Tang, J.Y., Gong, R., Kim, Jynho, Lee, J.J., Clemons, K.V., Chong, C.R., Chang, K.S., Fereshteh, M., Gardner, D., Reya, T., Liu, J.O., Epstein, E.H., Stevens, D.A., Beachy, P.A., 2010. Itraconazole, a commonly used antifungal that inhibits Hedgehog pathway activity and cancer growth. Cancer Cell 17, 388–399. https://doi.org/10.1016/j.ccr.2010.02.027

Kim, R.-J., Park, J.-R., Roh, K.-J., Choi, A.-R., Kim, S.-R., Kim, P.-H., Yu, J.H., Lee, J.W., Ahn, S.-H., Gong, G., Hwang, J.-W., Kang, K.-S., Kong, G., Sheen, Y.Y., Nam, J.-S., 2013. High aldehyde dehydrogenase activity enhances stem cell features in breast cancer cells by activating hypoxia-inducible factor-2α. Cancer Lett. 333, 18–31. https://doi.org/10.1016/j.canlet.2012.11.026

Kim, S.-Y., Cho, H.-S., Yang, S.-H., Shin, J.-Y., Kim, J.-S., Lee, S.-T., Chu, K., Roh, J.-K., Kim, S.U., Park, C.-G., 2009. Soluble mediators from human neural stem cells play a critical role in suppression of T-cell activation and proliferation. J. Neurosci. Res. 87, 2264–2272. https://doi.org/10.1002/jnr.22050

Kise, K., Kinugasa-Katayama, Y., Takakura, N., 2016. Tumor microenvironment for cancer stem cells. Adv. Drug Deliv. Rev. 99, 197–205. https://doi.org/10.1016/j.addr.2015.08.005

Kisselev, A.F., Akopian, T.N., Woo, K.M., Goldberg, A.L., 1999. The sizes of peptides generated from protein by mammalian 26 and 20 S proteasomes. Implications for understanding the degradative mechanism and antigen presentation. J. Biol. Chem. 274, 3363–3371. https://doi.org/10.1074/jbc.274.6.3363

Kitchen, S.G., Jones, N.R., LaForge, S., Whitmire, J.K., Vu, B.-A., Galic, Z., Brooks, D.G., Brown, S.J., Kitchen, C.M.R., Zack, J.A., 2004. CD4 on CD8+ T cells directly enhances effector function and is a target for HIV infection. Proc. Natl. Acad. Sci. U. S. A. 101, 8727–8732. https://doi.org/10.1073/pnas.0401500101

Kitchen, S.G., Whitmire, J.K., Jones, N.R., Galic, Z., Kitchen, C.M.R., Ahmed, R., Zack, J.A., 2005. The CD4 molecule on CD8+ T lymphocytes directly enhances the immune response to viral and cellular antigens. Proc. Natl. Acad. Sci. U. S. A. 102, 3794–3799. https://doi.org/10.1073/pnas.0406603102

Klebanoff, C.A., Gattinoni, L., Restifo, N.P., 2012. Sorting through subsets: Which T cell populations mediate highly effective adoptive immunotherapy? J. Immunother. Hagerstown Md 1997 35, 651–660. https://doi.org/10.1097/CJI.0b013e31827806e6

Klein, L., Hinterberger, M., Wirnsberger, G., Kyewski, B., 2009. Antigen presentation in the thymus for positive selection and central tolerance induction. Nat. Rev. Immunol. 9, 833–844. https://doi.org/10.1038/nri2669

Klein, L., Kyewski, B., Allen, P.M., Hogquist, K.A., 2014. Positive and negative selection of the T cell repertoire: what thymocytes see (and don't see). Nat. Rev. Immunol. 14, 377–391. https://doi.org/10.1038/nri3667

Klonisch, T., Wiechec, E., Hombach-Klonisch, S., Ande, S.R., Wesselborg, S., Schulze-Osthoff, K., Los, M., 2008. Cancer stem cell markers in common cancers – therapeutic implications. Trends Mol. Med. 14, 450–460. https://doi.org/10.1016/j.molmed.2008.08.003

Klotz, L., Zhang, L., Lam, A., Nam, R., Mamedov, A., Loblaw, A., 2010. Clinical results of long-term follow-up of a large, active surveillance cohort with localized prostate cancer. J. Clin. Oncol. Off. J. Am. Soc. Clin. Oncol. 28, 126–131. https://doi.org/10.1200/JCO.2009.24.2180

Koch, U., Radtke, F., 2011. Mechanisms of T cell development and transformation. Annu. Rev. Cell Dev. Biol. 27, 539–562. https://doi.org/10.1146/annurev-cellbio-092910-154008

Kochin, V., Kanaseki, T., Tokita, S., Miyamoto, S., Shionoya, Y., Kikuchi, Y., Morooka, D., Hirohashi, Y., Tsukahara, T., Watanabe, K., Toji, S., Kokai, Y., Sato, N., Torigoe, T., 2017. HLA-A24 ligandome analysis of colon and lung cancer cells identifies a novel cancer-testis antigen and a neoantigen that elicits specific and strong CTL responses. Oncoimmunology 6. https://doi.org/10.1080/2162402X.2017.1293214

Koebel, C.M., Vermi, W., Swann, J.B., Zerafa, N., Rodig, S.J., Old, L.J., Smyth, M.J., Schreiber, R.D., 2007. Adaptive immunity maintains occult cancer in an equilibrium state. Nature 450, 903–907. https://doi.org/10.1038/nature06309

Koh, Y.T., Gray, A., Higgins, S.A., Hubby, B., Kast, W.M., 2009. Androgen Ablation Augments Prostate Cancer Vaccine Immunogenicity Only When Applied After Immunization. The Prostate 69, 571–584. https://doi.org/10.1002/pros.20906

Kohga, K., Tatsumi, T., Takehara, T., Tsunematsu, H., Shimizu, S., Yamamoto, M., Sasakawa, A., Miyagi, T., Hayashi, N., 2010. Expression of CD133 confers malignant potential by regulating metalloproteinases in human hepatocellular carcinoma. J. Hepatol. 52, 872–879. https://doi.org/10.1016/j.jhep.2009.12.030

Kondo, E., Maecker, B., Draube, A., Klein-Gonzalez, N., Shimabukuro-Vornhagen, A., Schultze, J.L., von Bergwelt-Baildon, M.S., 2009. The shared tumor associated antigen cyclin-A2 is recognized by high-avidity T-cells. Int. J. Cancer 125, 2474–2478. https://doi.org/10.1002/ijc.24629

Kowalewski, D.J., Schuster, H., Backert, L., Berlin, C., Kahn, S., Kanz, L., Salih, H.R., Rammensee, H.-G., Stevanovic, S., Stickel, J.S., 2015. HLA ligandome analysis identifies the underlying specificities of spontaneous antileukemia immune responses in chronic lymphocytic leukemia (CLL). Proc. Natl. Acad. Sci. U. S. A. 112, E166-175. https://doi.org/10.1073/pnas.1416389112

Kowalewski, D.J., Stevanovic, S., 2013. Biochemical Large-Scale Identification of MHC Class I Ligands, in: Antigen Processing Methods and Protocols, Methods in Molecular Biology. Humana Press, Totowa, NJ. https://doi.org/10.1007/978-1-62703-218-6

Krampera, M., Cosmi, L., Angeli, R., Pasini, A., Liotta, F., Andreini, A., Santarlasci, V., Mazzinghi, B., Pizzolo, G., Vinante, F., Romagnani, P., Maggi, E., Romagnani, S., Annunziato, F., 2006. Role for interferon-gamma in the immunomodulatory activity of human bone marrow mesenchymal stem cells. Stem Cells Dayt. Ohio 24, 386–398. https://doi.org/10.1634/stemcells.2005-0008

Krangel, M.S., Hernandez-Munain, C., Lauzurica, P., McMurry, M., Roberts, J.L., Zhong, X.-P., 1998. Developmental regulation of V(D)J recombination at the TCR a/5 locus. Immunol. Rev. 165, 131–147. https://doi.org/10.1111/j.1600-065X.1998.tb01236.x

Kreso, A., Dick, J.E., 2014. Evolution of the Cancer Stem Cell Model. Cell Stem Cell 14, 275–291. https://doi.org/10.1016/j.stem.2014.02.006

Krieger, E., Joo, K., Lee, Jinwoo, Lee, Jooyoung, Raman, S., Thompson, J., Tyka, M., Baker, D., Karplus, K., 2009. Improving physical realism, stereochemistry, and side-chain accuracy in homology modeling: Four approaches that performed well in CASP8. Proteins Struct. Funct. Bioinforma. 77, 114–122. https://doi.org/10.1002/prot.22570

Krishnamurthy, S., Warner, K.A., Dong, Z., Imai, A., Nör, C., Ward, B.B., Helman, J.I., Taichman, R.S., Bellile, E.L., McCauley, L.K., Polverini, P.J., Prince, M.E., Wicha, M.S., Nör, J.E., 2014. Endothelial Interleukin-6 defines the tumorigenic potential of primary human cancer stem cells. Stem Cells Dayt. Ohio 32, 2845–2857. https://doi.org/10.1002/stem.1793

Krissinel, E., Henrick, K., 2007. Inference of macromolecular assemblies from crystalline state. J. Mol. Biol. 372, 774–797. https://doi.org/10.1016/j.jmb.2007.05.022

Kristiansen, G., Sammar, M., Altevogt, P., 2004. Tumour biological aspects of CD24, a mucin-like adhesion molecule. J. Mol. Histol. 35, 255–262. https://doi.org/10.1023/b:hijo.0000032357.16261.c5

Kroon, P., Berry, P.A., Stower, M.J., Rodrigues, G., Mann, V.M., Simms, M., Bhasin, D., Chettiar, S., Li, C., Li, P.-K., Maitland, N.J., Collins, A.T., 2013. JAK-STAT blockade inhibits tumor initiation and clonogenic

recovery of prostate cancer stem-like cells. Cancer Res. 73, 5288–5298. https://doi.org/10.1158/0008-5472.CAN-13-0874

Kryczek, I., Liu, S., Roh, M., Vatan, L., Szeliga, W., Wei, S., Banerjee, M., Mao, Y., Kotarski, J., Wicha, M.S., Liu, R., Zou, W., 2012. Expression of aldehyde dehydrogenase and CD133 defines ovarian cancer stem cells. Int. J. Cancer 130, 29–39. https://doi.org/10.1002/ijc.25967

Kryuchkova-Mostacci, N., Robinson-Rechavi, M., 2017. A benchmark of gene expression tissue-specificity metrics. Brief. Bioinform. 18, 205–214. https://doi.org/10.1093/bib/bbw008

Kuefer, R., Day, K.C., Kleer, C.G., Sabel, M.S., Hofer, M.D., Varambally, S., Zorn, C.S., Chinnaiyan, A.M., Rubin, M.A., Day, M.L., 2006. ADAM15 Disintegrin Is Associated with Aggressive Prostate and Breast Cancer Disease. Neoplasia N. Y. N 8, 319–329.

Kumar, B.V., Connors, T.J., Farber, D.L., 2018. Human T Cell Development, Localization, and Function throughout Life. Immunity 48, 202–213. https://doi.org/10.1016/j.immuni.2018.01.007

Kutscher, S., Dembek, C.J., Allgayer, S., Heltai, S., Stadlbauer, B., Biswas, P., Nozza, S., Tambussi, G., Bogner, J.R., Stellbrink, H.J., Goebel, F.D., Lusso, P., Tinelli, M., Poli, G., Erfle, V., Pohla, H., Malnati, M., Cosma, A., 2008. The intracellular detection of MIP-1beta enhances the capacity to detect IFN-gamma mediated HIV-1-specific CD8 T-cell responses in a flow cytometric setting providing a sensitive alternative to the ELISPOT. AIDS Res. Ther. 5, 22. https://doi.org/10.1186/1742-6405-5-22

Kwon, E.D., Drake, C.G., Scher, H.I., Fizazi, K., Bossi, A., van den Eertwegh, A.J.M., Krainer, M., Houede, N., Santos, R., Mahammedi, H., Ng, S., Maio, M., Franke, F.A., Sundar, S., Agarwal, N., Bergman, A.M., Ciuleanu, T.E., Korbenfeld, E., Sengeløv, L., Hansen, S., Logothetis, C., Beer, T.M., McHenry, M.B., Gagnier, P., Liu, D., Gerritsen, W.R., 2014. Ipilimumab versus placebo after radiotherapy in patients with metastatic castration-resistant prostate cancer that had progressed after docetaxel chemotherapy (CA184-043): a multicentre, randomised, double-blind, phase 3 trial. Lancet Oncol. 15, 700–712. https://doi.org/10.1016/S1470-2045(14)70189-5

Kyewski, B., Klein, L., 2006. A CENTRAL ROLE FOR CENTRAL TOLERANCE. Annu. Rev. Immunol. 24, 571–606. https://doi.org/10.1146/annurev.immunol.23.021704.115601

Kyjacova, L., Hubackova, S., Krejcikova, K., Strauss, R., Hanzlikova, H., Dzijak, R., Imrichova, T., Simova, J., Reinis, M., Bartek, J., Hodny, Z., 2015. Radiotherapy-induced plasticity of prostate cancer mobilizes stem-like non-adherent, Erk signaling-dependent cells. Cell Death Differ. 22, 898–911. https://doi.org/10.1038/cdd.2014.97

Lang, S.H., Stark, M., Collins, A., Paul, A.B., Stower, M.J., Maitland, N.J., 2001. Experimental Prostate Epithelial Morphogenesis in Response to Stroma and Three-Dimensional Matrigel Culture. Cell Growth Differ. 12, 631.

Lanzarotti, E., Marcatili, P., Nielsen, M., 2019. T-Cell Receptor Cognate Target Prediction Based on Paired α and β Chain Sequence and Structural CDR Loop Similarities. Front. Immunol. 10. https://doi.org/10.3389/fimmu.2019.02080

Lapidot, T., Sirard, C., Vormoor, J., Murdoch, B., Hoang, T., Caceres-Cortes, J., Minden, M., Paterson, B., Caligiuri, M.A., Dick, J.E., 1994. A cell

initiating human acute myeloid leukaemia after transplantation into SCID mice. Nature 367, 645–648. https://doi.org/10.1038/367645a0

Le Blanc, K., Tammik, C., Rosendahl, K., Zetterberg, E., Ringdén, O., 2003. HLA expression and immunologic properties of differentiated and undifferentiated mesenchymal stem cells. Exp. Hematol. 31, 890–896.

Le Page, C., Koumakpayi, I.H., Péant, B., Delvoye, N., Saad, F., Mes-Masson, A.-M., 2012. ErbB2/Her-2 regulates the expression of Akt2 in prostate cancer cells. The Prostate 72, 777–788. https://doi.org/10.1002/pros.21483

Lee, D.W., Kochenderfer, J.N., Stetler-Stevenson, M., Cui, Y.K., Delbrook, C., Feldman, S.A., Fry, T.J., Orentas, R., Sabatino, M., Shah, N.N., Steinberg, S.M., Stroncek, D., Tschernia, N., Yuan, C., Zhang, H., Zhang, L., Rosenberg, S.A., Wayne, A.S., Mackall, C.L., 2015. T cells expressing CD19 chimeric antigen receptors for acute lymphoblastic leukaemia in children and young adults: a phase 1 dose-escalation trial. The Lancet 385, 517–528. https://doi.org/10.1016/S0140-6736(14)61403-3

Lee, J., Kotliarova, S., Kotliarov, Y., Li, A., Su, Q., Donin, N.M., Pastorino, S., Purow, B.W., Christopher, N., Zhang, W., Park, J.K., Fine, H.A., 2006. Tumor stem cells derived from glioblastomas cultured in bFGF and EGF more closely mirror the phenotype and genotype of primary tumors than do serum-cultured cell lines. Cancer Cell 9, 391–403. https://doi.org/10.1016/j.ccr.2006.03.030

Lee, S.O., Yang, X., Duan, S., Tsai, Y., Strojny, L.R., Keng, P., Chen, Y., 2016. IL-6 promotes growth and epithelial-mesenchymal transition of CD133+ cells of non-small cell lung cancer. Oncotarget 7, 6626–6638. https://doi.org/10.18632/oncotarget.6570

Lee, Y., Auh, S.L., Wang, Yugang, Burnette, B., Wang, Yang, Meng, Y., Beckett, M., Sharma, R., Chin, R., Tu, T., Weichselbaum, R.R., Fu, Y.-X., 2009. Therapeutic effects of ablative radiation on local tumor require CD8+ T cells: changing strategies for cancer treatment. Blood 114, 589–595. https://doi.org/10.1182/blood-2009-02-206870

Lee, Y., Shin, J.H., Longmire, M., Wang, H., Kohrt, H.E., Chang, H.Y., Sunwoo, J.B., 2016. CD44+ Cells in Head and Neck Squamous Cell Carcinoma Suppress T-Cell-Mediated Immunity by Selective Constitutive and Inducible Expression of PD-L1. Clin. Cancer Res. Off. J. Am. Assoc. Cancer Res. 22, 3571–3581. https://doi.org/10.1158/1078-0432.CCR-15-2665

Leung, W., Heslop, H.E., 2019. Adoptive Immunotherapy with Antigen-Specific T Cells Expressing a Native TCR. Cancer Immunol. Res. 7, 528–533. https://doi.org/10.1158/2326-6066.CIR-18-0888

Li, K., Liu, C., Zhou, B., Bi, L., Huang, H., Lin, T., Xu, K., 2013. Role of EZH2 in the Growth of Prostate Cancer Stem Cells Isolated from LNCaP Cells. Int. J. Mol. Sci. 14, 11981–11993. https://doi.org/10.3390/ijms140611981

Li, S., Roberts, S., Plebanski, M., Gouillou, M., Spelman, T., Latour, P., Jackson, D., Brown, L., Sparrow, R.L., Prince, H.M., Hart, D., Loveland, B.E., Gowans, E.J., 2012. Induction of Multi-Functional T Cells in a Phase I Clinical Trial of Dendritic Cell Immunotherapy in Hepatitis C Virus Infected Individuals. PLOS ONE 7, e39368. https://doi.org/10.1371/journal.pone.0039368

Li, T., Su, Y., Mei, Y., Leng, Q., Leng, B., Liu, Z., Stass, S.A., Jiang, F., 2010. ALDH1A1 Is a Marker for Malignant Prostate Stem Cells and Predictor of Prostate Cancer Patients' Outcome. Lab. Investig. J. Tech. Methods Pathol. 90, 234–244. https://doi.org/10.1038/labinvest.2009.127

Li, Z., 2013. CD133: a stem cell biomarker and beyond. Exp. Hematol. Oncol. 2, 17. https://doi.org/10.1186/2162-3619-2-17

Liao, T., Kaufmann, A.M., Qian, X., Sangvatanakul, V., Chen, C., Kube, T., Zhang, G., Albers, A.E., 2013. Susceptibility to cytotoxic T cell lysis of cancer stem cells derived from cervical and head and neck tumor cell lines. J. Cancer Res. Clin. Oncol. 139, 159–170.

Liepe, J., Marino, F., Sidney, J., Jeko, A., Bunting, D.E., Sette, A., Kloetzel, P.M., Stumpf, M.P.H., Heck, A.J.R., Mishto, M., 2016. A large fraction of HLA class I ligands are proteasome-generated spliced peptides. Science 354, 354–358. https://doi.org/10.1126/science.aaf4384

Lim, S., Kaldis, P., 2013. Cdks, cyclins and CKIs: roles beyond cell cycle regulation. Development 140, 3079–3093. https://doi.org/10.1242/dev.091744

Lin, P., Sun, X., Feng, T., Zou, H., Jiang, Y., Liu, Z., Zhao, D., Yu, X., 2012. ADAM17 regulates prostate cancer cell proliferation through mediating cell cycle progression by EGFR/PI3K/AKT pathway. Mol. Cell. Biochem. 359, 235–243. https://doi.org/10.1007/s11010-011-1018-8

Lin, Y., Gallardo, H.F., Ku, G.Y., Li, H., Manukian, G., Rasalan, T.S., Xu, Y., Terzulli, S.L., Old, L.J., Allison, J.P., Houghton, A.N., Wolchok, J.D., Yuan, J., 2009. Optimization and validation of a robust human T cell culture method for monitoring phenotypic and polyfunctional antigen-specific CD4 and CD8 T-cell responses. Cytotherapy 11, 912–922. https://doi.org/10.3109/14653240903136987

Linette, G.P., Stadtmauer, E.A., Maus, M.V., Rapoport, A.P., Levine, B.L., Emery, L., Litzky, L., Bagg, A., Carreno, B.M., Cimino, P.J., Binder-Scholl, G.K., Smethurst, D.P., Gerry, A.B., Pumphrey, N.J., Bennett, A.D., Brewer, J.E., Dukes, J., Harper, J., Tayton-Martin, H.K., Jakobsen, B.K., Hassan, N.J., Kalos, M., June, C.H., 2013. Cardiovascular toxicity and titin cross-reactivity of affinity-enhanced T cells in myeloma and melanoma. Blood 122, 863–871. https://doi.org/10.1182/blood-2013-03-490565

Linsley, P.S., Greene, J.L., Brady, W., Bajorath, J., Ledbetter, J.A., Peach, R., 1994. Human B7-1 (CD80) and B7-2 (CD86) bind with similar avidities but distinct kinetics to CD28 and CTLA-4 receptors. Immunity 1, 793–801. https://doi.org/10.1016/s1074-7613(94)80021-9

Lissina, A., McLaren, J.E., Ilander, M., Andersson, E.I., Lewis, C.S., Clement, M., Herman, A., Ladell, K., Llewellyn-Lacey, S., Miners, K.L., Gostick, E., Melenhorst, J.J., Barrett, A.J., Price, D.A., Mustjoki, S., Wooldridge, L., 2018. Divergent roles for antigenic drive in the aetiology of primary versus dasatinib-associated CD8+ TCR-Vβ+ expansions. Sci. Rep. 8. https://doi.org/10.1038/s41598-017-18062-x

Littera, R., Piredda, G., Argiolas, D., Lai, S., Congeddu, E., Ragatzu, P., Melis, M., Carta, E., Michittu, M.B., Valentini, D., Cappai, L., Porcella, R., Alba, F., Serra, M., Loi, V., Maddi, R., Orrù, S., La Nasa, G., Caocci, G., Cusano, R., Arras, M., Frongia, M., Pani, A., Carcassi, C., 2017. KIR and their HLA Class I ligands: Two more pieces towards completing the puzzle of chronic rejection and graft loss in kidney transplantation. PLoS ONE 12. https://doi.org/10.1371/journal.pone.0180831

Litvinov, I.V., Griend, D.J.V., Xu, Y., Antony, L., Dalrymple, S.L., Isaacs, J.T., 2006. Low-Calcium Serum-Free Defined Medium Selects for Growth of Normal Prostatic Epithelial Stem Cells. Cancer Res. 66, 8598–8607. https://doi.org/10.1158/0008-5472.CAN-06-1228

Liu, A.Y., 2000. Differential Expression of Cell Surface Molecules in Prostate Cancer Cells. Cancer Res. 60, 3429–3434.

Liu, A.Y., True, L.D., LaTray, L., Ellis, W.J., Vessella, R.L., Lange, P.H., Higano, C.S., Hood, L., Engh, G. van den, 1999. Analysis and sorting of prostate cancer cell types by flow cytometry. The Prostate 40, 192–199. https://doi.org/10.1002/(SICI)1097-0045(19990801)40:3<192::AID-PROS7>3.0.CO;2-F

Liu, S., Ginestier, C., Ou, S.J., Clouthier, S.G., Patel, S.H., Monville, F., Korkaya, H., Heath, A., Dutcher, J., Kleer, C.G., Jung, Y., Dontu, G., Taichman, R., Wicha, M.S., 2011. Breast cancer stem cells are regulated by mesenchymal stem cells through cytokine networks. Cancer Res. 71, 614–624. https://doi.org/10.1158/0008-5472.CAN-10-0538

Liu, X., Chen, X., Rycaj, K., Chao, H.-P., Deng, Q., Jeter, C., Liu, C., Honorio, S., Li, H., Davis, T., Suraneni, M., Laffin, B., Qin, J., Li, Q., Yang, T., Whitney, P., Shen, J., Huang, J., Tang, D.G., 2015. Systematic dissection of phenotypic, functional, and tumorigenic heterogeneity of human prostate cancer cells. Oncotarget 6, 23959–23986.

Liu, Xingyan, He, Z., Li, C.-H., Huang, G., Ding, C., Liu, H., 2012. Correlation analysis of JAK-STAT pathway components on prognosis of patients with prostate cancer. Pathol. Oncol. Res. POR 18, 17–23. https://doi.org/10.1007/s12253-011-9410-y

Liu, Xuefeng, Ory, V., Chapman, S., Yuan, H., Albanese, C., Kallakury, B., Timofeeva, O.A., Nealon, C., Dakic, A., Simic, V., Haddad, B.R., Rhim, J.S., Dritschilo, A., Riegel, A., McBride, A., Schlegel, R., 2012. ROCK Inhibitor and Feeder Cells Induce the Conditional Reprogramming of Epithelial Cells. Am. J. Pathol. 180, 599–607. https://doi.org/10.1016/j.ajpath.2011.10.036

Liu, X.V., Ho, S.S.W., Tan, J.J., Kamran, N., Gasser, S., 2012. Ras activation induces expression of Raet1 family NK receptor ligands. J. Immunol. Baltim. Md 1950 189, 1826–1834. https://doi.org/10.4049/jimmunol.1200965

Livák, F., Tourigny, M., Schatz, D.G., Petrie, H.T., 1999. Characterization of TCR gene rearrangements during adult murine T cell development. J. Immunol. Baltim. Md 1950 162, 2575–2580.

Löffler, M.W., Kowalewski, D.J., Backert, L., Bernhardt, J., Adam, P., Schuster, H., Dengler, F., Backes, D., Kopp, H.-G., Beckert, S., Wagner, S., Königsrainer, I., Kohlbacher, O., Kanz, L., Königsrainer, A., Rammensee, H.-G., Stevanović, S., Haen, S.P., 2018. Mapping the HLA-ligandome of Colorectal Cancer Reveals an Imprint of Malignant Cell Transformation. Cancer Res. 78, 4627–4641. https://doi.org/10.1158/0008-5472.CAN-17-1745

Long, H., Xie, R., Xiang, T., Zhao, Z., Lin, S., Liang, Z., Chen, Z., Zhu, B., 2012. Autocrine CCL5 signaling promotes invasion and migration of CD133+ ovarian cancer stem-like cells via NF-κB-mediated MMP-9 upregulation. Stem Cells Dayt. Ohio 30, 2309–2319. https://doi.org/10.1002/stem.1194

Louie, L.G., King, M.C., 1991. A novel approach to establishing permanent lymphoblastoid cell lines: Epstein-Barr virus transformation of cryopreserved lymphocytes. Am. J. Hum. Genet. 48, 637–638.

Lundholm, M., Hägglöf, C., Wikberg, M.L., Stattin, P., Egevad, L., Bergh, A., Wikström, P., Palmqvist, R., Edin, S., 2015. Secreted Factors from Colorectal and Prostate Cancer Cells Skew the Immune Response in Opposite Directions. Sci. Rep. 5, 15651. https://doi.org/10.1038/srep15651

Luo, S., Sun, M., Jiang, R., Wang, G., Zhang, X., 2011. Establishment of primary mouse lung adenocarcinoma cell culture. Oncol. Lett. 2, 629–632. https://doi.org/10.3892/ol.2011.301

Luo, Y., Dallaglio, K., Chen, Y., Robinson, W.A., Robinson, S.E., McCarter, M.D., Wang, J., Gonzalez, R., Thompson, D.C., Norris, D.A., Roop, D.R., Vasiliou, V., Fujita, M., 2012. ALDH1A isozymes are markers of human melanoma stem cells and potential therapeutic targets. Stem Cells Dayt. Ohio 30, 2100–2113. https://doi.org/10.1002/stem.1193

Lyons, A.B., 2000. Analysing cell division in vivo and in vitro using flow cytometric measurement of CFSE dye dilution. J. Immunol. Methods 243, 147–154. https://doi.org/10.1016/S0022-1759(00)00231-3

Lyons, A.B., Parish, C.R., 1994. Determination of lymphocyte division by flow cytometry. J. Immunol. Methods 171, 131–137.

Ma, I., Allan, A.L., 2011. The role of human aldehyde dehydrogenase in normal and cancer stem cells. Stem Cell Rev. 7, 292–306. https://doi.org/10.1007/s12015-010-9208-4

Ma, R., Minsky, N., Morshed, S.A., Davies, T.F., 2014. Stemness in human thyroid cancers and derived cell lines: the role of asymmetrically dividing cancer stem cells resistant to chemotherapy. J. Clin. Endocrinol. Metab. 99, E400-409. https://doi.org/10.1210/jc.2013-3545

Maccalli, C., Volontè, A., Cimminiello, C., Parmiani, G., 2014. Immunology of cancer stem cells in solid tumours. A review. Eur. J. Cancer 50, 649–655. https://doi.org/10.1016/j.ejca.2013.11.014

Macchia, I., Gauduin, M.-C., Kaur, A., Johnson, R.P., 2006. Expression of CD8alpha identifies a distinct subset of effector memory CD4+ T lymphocytes. Immunology 119, 232–242. https://doi.org/10.1111/j.1365-2567.2006.02428.x

Madeira, F., Park, Y.M., Lee, J., Buso, N., Gur, T., Madhusoodanan, N., Basutkar, P., Tivey, A.R.N., Potter, S.C., Finn, R.D., Lopez, R., 2019. The EMBL-EBI search and sequence analysis tools APIs in 2019. Nucleic Acids Res. 47, W636–W641. https://doi.org/10.1093/nar/gkz268

Magnen, C.L., Bubendorf, L., Rentsch, C.A., Mengus, C., Gsponer, J., Zellweger, T., Rieken, M., Thalmann, G.N., Cecchini, M.G., Germann, M., Bachmann, A., Wyler, S., Heberer, M., Spagnoli, G.C., 2013. Characterization and clinical relevance of ALDHbright populations in prostate cancer. Clin. Cancer Res. 19, 5361–5371. https://doi.org/10.1158/1078-0432.CCR-12-2857

Maitland, N.J., Frame, F.M., Polson, E.S., Lewis, J.L., Collins, A.T., 2011. Prostate cancer stem cells: do they have a basal or luminal phenotype? Horm. Cancer 2, 47–61. https://doi.org/10.1007/s12672-010-0058-y

Mandelcorn-Monson, R.L., Shear, N.H., Yau, E., Sambhara, S., Barber, B.H., Spaner, D., DeBenedette, M.A., 2003. Cytotoxic T lymphocyte reactivity to gp100, MelanA/MART-1, and tyrosinase, in HLA-A2-

positive vitiligo patients. J. Invest. Dermatol. 121, 550–556. https://doi.org/10.1046/j.1523-1747.2003.12413.x

Marchitti, S.A., Brocker, C., Stagos, D., Vasiliou, V., 2008. Non-P450 aldehyde oxidizing enzymes: the aldehyde dehydrogenase superfamily. Expert Opin. Drug Metab. Toxicol. 4, 697–720. https://doi.org/10.1517/17425250802102627

Marcu, A., Bichmann, L., Kuchenbecker, L., Backert, L., Kowalewski, D.J., Freudenmann, L.K., Löffler, M.W., Lübke, M., Walz, J.S., Velz, J., Moch, H., Regli, L., Silginer, M., Weller, M., Schlosser, A., Kohlbacher, O., Stevanović, S., Rammensee, H.-G., Neidert, M.C., 2019. The HLA Ligand Atlas. A resource of natural HLA ligands presented on benign tissues (preprint). Immunology. https://doi.org/10.1101/778944

Marhold, M., Tomasich, E., El-Gazzar, A., Heller, G., Spittler, A., Horvat, R., Krainer, M., Horak, P., 2015. HIF1 Regulates mTOR Signaling and Viability of Prostate Cancer Stem Cells. Mol. Cancer Res. 13, 556–564. https://doi.org/10.1158/1541-7786.MCR-14-0153-T

Marincola, F.M., Jaffee, E.M., Hicklin, D.J., Ferrone, S., 2000. Escape of human solid tumors from T-cell recognition: molecular mechanisms and functional significance. Adv. Immunol. 74, 181–273.

Martínez-Lostao, L., Anel, A., Pardo, J., 2015. How Do Cytotoxic Lymphocytes Kill Cancer Cells? Clin. Cancer Res. 21, 5047–5056. https://doi.org/10.1158/1078-0432.CCR-15-0685

Mashita, N., Yamada, S., Nakayama, G., Tanaka, C., Iwata, N., Kanda, M., Kobayashi, D., Fujii, T., Sugimoto, H., Koike, M., Nomoto, S., Fujiwara, M., Kodera, Y., 2014. Epithelial to mesenchymal transition might be induced via CD44 isoform switching in colorectal cancer. J. Surg. Oncol. 110, 745–751. https://doi.org/10.1002/jso.23705

Mason, D., 1998. A very high level of crossreactivity is an essential feature of the T-cell receptor. Immunol. Today 19, 395–404. https://doi.org/10.1016/s0167-5699(98)01299-7

Mateo, J., Carreira, S., Sandhu, S., Miranda, S., Mossop, H., Perez-Lopez, R., Nava Rodrigues, D., Robinson, D., Omlin, A., Tunariu, N., Boysen, G., Porta, N., Flohr, P., Gillman, A., Figueiredo, I., Paulding, C., Seed, G., Jain, S., Ralph, C., Protheroe, A., Hussain, S., Jones, R., Elliott, T., McGovern, U., Bianchini, D., Goodall, J., Zafeiriou, Z., Williamson, C.T., Ferraldeschi, R., Riisnaes, R., Ebbs, B., Fowler, G., Roda, D., Yuan, W., Wu, Y.-M., Cao, X., Brough, R., Pemberton, H., A'Hern, R., Swain, A., Kunju, L.P., Eeles, R., Attard, G., Lord, C.J., Ashworth, A., Rubin, M.A., Knudsen, K.E., Feng, F.Y., Chinnaiyan, A.M., Hall, E., de Bono, J.S., 2015. DNA-Repair Defects and Olaparib in Metastatic Prostate Cancer. N. Engl. J. Med. 373, 1697–1708. https://doi.org/10.1056/NEJMoa1506859

Mathew, G., Timm, E.A., Jr, Sotomayor, P., Godoy, A., Montecinos, V.P., Smith, G.J., Huss, W.J., 2009. ABCG2-mediated dyecycle violet efflux defined side population in benign and malignant prostate. Cell Cycle Georget. Tex 8, 1053. https://doi.org/10.4161/cc.8.7.8043

Matsui, W.H., 2016. Cancer stem cell signaling pathways. Medicine (Baltimore) 95. https://doi.org/10.1097/MD.0000000000004765

Matsushita, H., Vesely, M.D., Koboldt, D.C., Rickert, C.G., Uppaluri, R., Magrini, V.J., Arthur, C.D., White, J.M., Chen, Y.-S., Shea, L.K., Hundal, J., Wendl, M.C., Demeter, R., Wylie, T., Allison, J.P., Smyth, M.J., Old, L.J., Mardis, E.R., Schreiber, R.D., 2012. Cancer exome

analysis reveals a T-cell-dependent mechanism of cancer immunoediting. Nature 482, 400–404. https://doi.org/10.1038/nature10755

Matsuzaki, J., Tsuji, T., Chodon, T., Ryan, C., Koya, R.C., Odunsi, K., 2019. A rare population of tumor antigen-specific CD4+CD8+ double-positive αβ T lymphocytes uniquely provide CD8-independent TCR genes for engineering therapeutic T cells. J. Immunother. Cancer 7, 7. https://doi.org/10.1186/s40425-018-0467-y

Matzinger, P., 1994. Tolerance, danger, and the extended family. Annu. Rev. Immunol. 12, 991–1045. https://doi.org/10.1146/annurev.iy.12.040194.005015

Mazzoleni, S., Jachetti, E., Morosini, S., Grioni, M., Piras, I.S., Pala, M., Bulfone, A., Freschi, M., Bellone, M., Galli, R., 2013. Gene Signatures Distinguish Stage-Specific Prostate Cancer Stem Cells Isolated From Transgenic Adenocarcinoma of the Mouse Prostate Lesions and Predict the Malignancy of Human Tumors. Stem Cells Transl. Med. 2, 678–689. https://doi.org/10.5966/sctm.2013-0041

McKeown, S.R., 2014. Defining normoxia, physoxia and hypoxia in tumours—implications for treatment response. Br. J. Radiol. 87. https://doi.org/10.1259/bjr.20130676

McPhail, S., Johnson, S., Greenberg, D., Peake, M., Rous, B., 2015. Stage at diagnosis and early mortality from cancer in England. Br. J. Cancer 112, S108–S115. https://doi.org/10.1038/bjc.2015.49

Melero, I., Gaudernack, G., Gerritsen, W., Huber, C., Parmiani, G., Scholl, S., Thatcher, N., Wagstaff, J., Zielinski, C., Faulkner, I., Mellstedt, H., 2014. Therapeutic vaccines for cancer: an overview of clinical trials. Nat. Rev. Clin. Oncol. 11, 509–524. https://doi.org/10.1038/nrclinonc.2014.111

Meng, E., Long, B., Sullivan, P., McClellan, S., Finan, M.A., Reed, E., Shevde, L., Rocconi, R.P., 2012. CD44+/CD24- ovarian cancer cells demonstrate cancer stem cell properties and correlate to survival. Clin. Exp. Metastasis 29, 939–948. https://doi.org/10.1007/s10585-012-9482-4

Mercader, M., Bodner, B.K., Moser, M.T., Kwon, P.S., Park, E.S., Manecke, R.G., Ellis, T.M., Wojcik, E.M., Yang, D., Flanigan, R.C., Waters, W.B., Kast, W.M., Kwon, E.D., 2001. T cell infiltration of the prostate induced by androgen withdrawal in patients with prostate cancer. Proc. Natl. Acad. Sci. U. S. A. 98, 14565–14570. https://doi.org/10.1073/pnas.251140998

Merchant, A.A., Matsui, W., 2010. Targeting Hedgehog -- a Cancer Stem Cell Pathway. Clin. Cancer Res. 16, 3130–3140. https://doi.org/10.1158/1078-0432.CCR-09-2846

Merseburger, A.S., Alcaraz, A., von Klot, C.A., 2016. Androgen deprivation therapy as backbone therapy in the management of prostate cancer. OncoTargets Ther. 9, 7263–7274. https://doi.org/10.2147/OTT.S117176

Merseburger, A.S., Hammerer, P., Rozet, F., Roumeguère, T., Caffo, O., da Silva, F.C., Alcaraz, A., 2015. Androgen deprivation therapy in castrate-resistant prostate cancer: how important is GnRH agonist backbone therapy? World J. Urol. 33, 1079–1085. https://doi.org/10.1007/s00345-014-1406-2

Mescher, M.F., Curtsinger, J.M., Agarwal, P., Casey, K.A., Gerner, M., Hammerbeck, C.D., Popescu, F., Xiao, Z., 2006. Signals required for programming effector and memory development by CD8+ T cells. Immunol. Rev. 211, 81–92. https://doi.org/10.1111/j.0105-2896.2006.00382.x

Mester, G., Hoffmann, V., Stevanović, S., 2011. Insights into MHC class I antigen processing gained from large-scale analysis of class I ligands. Cell. Mol. Life Sci. CMLS 68, 1521–1532. https://doi.org/10.1007/s00018-011-0659-9

Meyer, B., Papasotiriou, D.G., Karas, M., 2011. 100% protein sequence coverage: a modern form of surrealism in proteomics. Amino Acids 41, 291–310. https://doi.org/10.1007/s00726-010-0680-6

Mi, H., Thomas, P., 2009. PANTHER Pathway: an ontology-based pathway database coupled with data analysis tools. Methods Mol. Biol. Clifton NJ 563, 123–140. https://doi.org/10.1007/978-1-60761-175-2_7

Miles, J.J., Douek, D.C., Price, D.A., 2011. Bias in the αβ T-cell repertoire: implications for disease pathogenesis and vaccination. Immunol. Cell Biol. 89, 375–387. https://doi.org/10.1038/icb.2010.139

Mittal, D., Gubin, M.M., Schreiber, R.D., Smyth, M.J., 2014. New insights into cancer immunoediting and its three component phases--elimination, equilibrium and escape. Curr. Opin. Immunol. 27, 16–25. https://doi.org/10.1016/j.coi.2014.01.004

Miyamoto, S., Kochin, V., Kanaseki, T., Hongo, A., Tokita, S., Kikuchi, Y., Takaya, A., Hirohashi, Y., Tsukahara, T., Terui, T., Ishitani, K., Hata, F., Takemasa, I., Miyazaki, A., Hiratsuka, H., Sato, N., Torigoe, T., 2018. The Antigen ASB4 on Cancer Stem Cells Serves as a Target for CTL Immunotherapy of Colorectal Cancer. Cancer Immunol. Res. 6, 358–369. https://doi.org/10.1158/2326-6066.CIR-17-0518

Miyata, T., Oyama, T., Yoshimatsu, T., Higa, H., Kawano, D., Sekimura, A., Yamashita, N., So, T., Gotoh, A., 2017. The Clinical Significance of Cancer Stem Cell Markers ALDH1A1 and CD133 in Lung Adenocarcinoma. Anticancer Res. 37, 2541–2547. https://doi.org/10.21873/anticanres.11597

Miyazawa, K., Tanaka, T., Nakai, D., Morita, N., Suzuki, K., 2014. Immunohistochemical expression of four different stem cell markers in prostate cancer: High expression of NANOG in conjunction with hypoxia-inducible factor-1α expression is involved in prostate epithelial malignancy. Oncol. Lett. 8, 985. https://doi.org/10.3892/ol.2014.2274

Moad, M., Hannezo, E., Buczacki, S.J., Wilson, L., El-Sherif, A., Sims, D., Pickard, R., Wright, N.A., Williamson, S.C., Turnbull, D.M., Taylor, R.W., Greaves, L., Robson, C.N., Simons, B.D., Heer, R., 2017. Multipotent Basal Stem Cells, Maintained in Localized Proximal Niches, Support Directed Long-Ranging Epithelial Flows in Human Prostates. Cell Rep. 20, 1609–1622. https://doi.org/10.1016/j.celrep.2017.07.061

Mobbs, J.I., Illing, P.T., Dudek, N.L., Brooks, A.G., Baker, D.G., Purcell, A.W., Rossjohn, J., Vivian, J.P., 2017. The molecular basis for peptide repertoire selection in the human leukocyte antigen (HLA) C*06:02 molecule. J. Biol. Chem. 292, 17203–17215. https://doi.org/10.1074/jbc.M117.806976

Mochizuki, S., Okada, Y., 2007. ADAMs in cancer cell proliferation and progression. Cancer Sci. 98, 621–628.

Moeller, M., Haynes, N.M., Kershaw, M.H., Jackson, J.T., Teng, M.W.L., Street, S.E., Cerutti, L., Jane, S.M., Trapani, J.A., Smyth, M.J., Darcy, P.K., 2005. Adoptive transfer of gene-engineered CD4+ helper T cells induces potent primary and secondary tumor rejection. Blood 106, 2995–3003. https://doi.org/10.1182/blood-2004-12-4906

Moldovan, I., Targoni, O., Zhang, W., Sundararaman, S., Lehmann, P.V., 2016. How frequently are predicted peptides actually recognized by CD8 cells? Cancer Immunol. Immunother. 65, 847. https://doi.org/10.1007/s00262-016-1840-7

Mollenhauer, H.H., Morré, D.J., Rowe, L.D., 1990. Alteration of intracellular traffic by monensin; mechanism, specificity and relationship to toxicity. Biochim. Biophys. Acta 1031, 225–246. https://doi.org/10.1016/0304-4157(90)90008-z

Molteni, M., Kohn, L.D., Rossetti, C., Scrofani, S., Bonara, P., Scorza, R., 2002. Co-expression of the CD8 receptor in a human CD4+ T-cell clone influences proliferation, cytosolic Ca2+ release and cytokine production. Immunol. Lett. 83, 111–117.

Moore, N., Houghton, J., Lyle, S., 2012. Slow-Cycling Therapy-Resistant Cancer Cells. Stem Cells Dev. 21, 1822–1830. https://doi.org/10.1089/scd.2011.0477

Moreb, J.S., Zucali, J.R., Ostmark, B., Benson, N.A., 2007. Heterogeneity of aldehyde dehydrogenase expression in lung cancer cell lines is revealed by Aldefluor flow cytometry-based assay. Cytometry B Clin. Cytom. 72B, 281–289. https://doi.org/10.1002/cyto.b.20161

Morgan, C.A., Parajuli, B., Buchman, C.D., Dria, K., Hurley, T.D., 2015. N,N-diethylaminobenzaldehyde (DEAB) as a substrate and mechanism-based inhibitor for human ALDH isoenzymes. Chem. Biol. Interact. 234, 18–28. https://doi.org/10.1016/j.cbi.2014.12.008

Morita, R., Hirohashi, Y., Torigoe, T., Ito-Inoda, S., Takahashi, A., Mariya, T., Asanuma, H., Tamura, Y., Tsukahara, T., Kanaseki, T., Kubo, T., Kutomi, G., Mizuguchi, T., Terui, T., Ishitani, K., Hashino, S., Kondo, T., Minagawa, N., Takahashi, N., Taketomi, A., Todo, S., Asaka, M., Sato, N., 2016. Olfactory Receptor Family 7 Subfamily C Member 1 Is a Novel Marker of Colon Cancer-Initiating Cells and Is a Potent Target of Immunotherapy. Clin. Cancer Res. Off. J. Am. Assoc. Cancer Res. 22, 3298–3309. https://doi.org/10.1158/1078-0432.CCR-15-1709

Morita, R., Nishizawa, S., Torigoe, T., Takahashi, A., Tamura, Y., Tsukahara, T., Kanaseki, T., Sokolovskaya, A., Kochin, V., Kondo, T., Hashino, S., Asaka, M., Hara, I., Hirohashi, Y., Sato, N., 2014. Heat shock protein DNAJB8 is a novel target for immunotherapy of colon cancer-initiating cells. Cancer Sci. 105, 389–395. https://doi.org/10.1111/cas.12362

Morris, G.P., Allen, P.M., 2012. How the TCR balances sensitivity and specificity for the recognition of self and pathogens. Nat. Immunol. 13, 121–128. https://doi.org/10.1038/ni.2190

Mottet, N., Bellmunt, J., Bolla, M., Briers, E., Cumberbatch, M.G., Santis, M.D., Fossati, N., Gross, T., Henry, A.M., Joniau, S., Lam, T.B., Mason, M.D., Matveev, V.B., Moldovan, P.C., Bergh, R.C.N. van den, Broeck, T.V. den, Poel, H.G. van der, Kwast, T.H. van der, Rouvière, O., Schoots, I.G., Wiegel, T., Cornford, P., 2017. EAU-ESTRO-SIOG Guidelines on Prostate Cancer. Part 1: Screening, Diagnosis, and Local

Treatment with Curative Intent. Eur. Urol. 71, 618–629. https://doi.org/10.1016/j.eururo.2016.08.003

Motz, G.T., Coukos, G., 2013. Deciphering and Reversing Tumor Immune Suppression. Immunity 39, 61–73. https://doi.org/10.1016/j.immuni.2013.07.005

Moy, J.D., Moskovitz, J.M., Ferris, R.L., 2017. Biological mechanisms of immune escape and implications for immunotherapy in head and neck squamous cell carcinoma. Eur. J. Cancer Oxf. Engl. 1990 76, 152–166. https://doi.org/10.1016/j.ejca.2016.12.035

Mukherjee, S., Kong, J., Brat, D.J., 2015. Cancer Stem Cell Division: When the Rules of Asymmetry Are Broken. Stem Cells Dev. 24, 405–416. https://doi.org/10.1089/scd.2014.0442

Müller, M., Gfeller, D., Coukos, G., Bassani-Sternberg, M., 2017. 'Hotspots' of Antigen Presentation Revealed by Human Leukocyte Antigen Ligandomics for Neoantigen Prioritization. Front. Immunol. 8. https://doi.org/10.3389/fimmu.2017.01367

Müller-Hermelink, N., Braumüller, H., Pichler, B., Wieder, T., Mailhammer, R., Schaak, K., Ghoreschi, K., Yazdi, A., Haubner, R., Sander, C.A., Mocikat, R., Schwaiger, M., Förster, I., Huss, R., Weber, W.A., Kneilling, M., Röcken, M., 2008. TNFR1 Signaling and IFN-γ Signaling Determine whether T Cells Induce Tumor Dormancy or Promote Multistage Carcinogenesis. Cancer Cell 13, 507–518. https://doi.org/10.1016/j.ccr.2008.04.001

Munz, M., Baeuerle, P.A., Gires, O., 2009. The Emerging Role of EpCAM in Cancer and Stem Cell Signaling. Cancer Res. 69, 5627–5629. https://doi.org/10.1158/0008-5472.CAN-09-0654

Munz, M., Kieu, C., Mack, B., Schmitt, B., Zeidler, R., Gires, O., 2004. The carcinoma-associated antigen EpCAM upregulates c-myc and induces cell proliferation. Oncogene 23, 5748–5748.

Murata, S., Sasaki, K., Kishimoto, T., Niwa, S.-I., Hayashi, H., Takahama, Y., Tanaka, K., 2007. Regulation of CD8+ T cell development by thymus-specific proteasomes. Science 316, 1349–1353. https://doi.org/10.1126/science.1141915

Murillo-Garzón, V., Kypta, R., 2017. WNT signalling in prostate cancer. Nat. Rev. Urol. 14, 683–696. https://doi.org/10.1038/nrurol.2017.144

Murohashi, M., Hinohara, K., Kuroda, M., Isagawa, T., Tsuji, S., Kobayashi, S., Umezawa, K., Tojo, A., Aburatani, H., Gotoh, N., 2010. Gene set enrichment analysis provides insight into novel signalling pathways in breast cancer stem cells. Br. J. Cancer 102, 206–212. https://doi.org/10.1038/sj.bjc.6605468

Namekawa, T., Ikeda, K., Horie-Inoue, K., Inoue, S., 2019. Application of Prostate Cancer Models for Preclinical Study: Advantages and Limitations of Cell Lines, Patient-Derived Xenografts, and Three-Dimensional Culture of Patient-Derived Cells. Cells 8. https://doi.org/10.3390/cells8010074

Narayan, V., Gladney, W., Plesa, G., Vapiwala, N., Carpenter, E., Maude, S.L., Lal, P., Lacey, S.F., Melenhorst, J.J., Sebro, R., Farwell, M., Hwang, W.-T., Moniak, M., Gilmore, J., Lledo, L., Dengel, K., Marshall, A., Coughlin, C.M., June, C.H., Haas, N.B., 2019. A phase I clinical trial of PSMA-directed/TGFβ-insensitive CAR-T cells in metastatic castration-resistant prostate cancer. J. Clin. Oncol. 37, TPS347–TPS347. https://doi.org/10.1200/JCO.2019.37.7_suppl.TPS347

Nath, S., Mukherjee, P., 2014. MUC1: a multifaceted oncoprotein with a key role in cancer progression. Trends Mol. Med. 20, 332–342. https://doi.org/10.1016/j.molmed.2014.02.007

Neidert, M.C., Kowalewski, D.J., Silginer, M., Kapolou, K., Backert, L., Freudenmann, L.K., Peper, J.K., Marcu, A., Wang, S.S.-Y., Walz, J.S., Wolpert, F., Rammensee, H.-G., Henschler, R., Lamszus, K., Westphal, M., Roth, P., Regli, L., Stevanović, S., Weller, M., Eisele, G., 2018. The natural HLA ligandome of glioblastoma stem-like cells: antigen discovery for T cell-based immunotherapy. Acta Neuropathol. (Berl.) 135, 923–938. https://doi.org/10.1007/s00401-018-1836-9

Nelde, A., Kowalewski, D.J., Backert, L., Schuster, H., Werner, J.-O., Klein, R., Kohlbacher, O., Kanz, L., Salih, H.R., Rammensee, H.-G., Stevanović, S., Walz, J.S., 2018. HLA ligandome analysis of primary chronic lymphocytic leukemia (CLL) cells under lenalidomide treatment confirms the suitability of lenalidomide for combination with T-cell-based immunotherapy. Oncoimmunology 7. https://doi.org/10.1080/2162402X.2017.1316438

Neumayer, G., Belzil, C., Gruss, O.J., Nguyen, M.D., 2014. TPX2: of spindle assembly, DNA damage response, and cancer. Cell. Mol. Life Sci. 71, 3027–3047. https://doi.org/10.1007/s00018-014-1582-7

Newell, E.W., Becht, E., 2018. High-Dimensional Profiling of Tumor-Specific Immune Responses: Asking T Cells about What They "See" in Cancer. Cancer Immunol. Res. 6, 2–9. https://doi.org/10.1158/2326-6066.CIR-17-0519

Nguyen, K.T., Holloway, M.P., Altura, R.A., 2012. The CRM1 nuclear export protein in normal development and disease. Int. J. Biochem. Mol. Biol. 3, 137–151.

Nguyen, L.V., Vanner, R., Dirks, P., Eaves, C.J., 2012. Cancer stem cells: an evolving concept. Nat. Rev. Cancer 12, 133–143.

Ni, J., Cozzi, P., Beretov, J., Duan, W., Bucci, J., Graham, P., Li, Y., 2018. Epithelial cell adhesion molecule (EpCAM) is involved in prostate cancer chemotherapy/radiotherapy response in vivo. BMC Cancer 18, 1092. https://doi.org/10.1186/s12885-018-5010-5

Nielsen, M., Lundegaard, C., Blicher, T., Lamberth, K., Harndahl, M., Justesen, S., Røder, G., Peters, B., Sette, A., Lund, O., Buus, S., 2007. NetMHCpan, a Method for Quantitative Predictions of Peptide Binding to Any HLA-A and -B Locus Protein of Known Sequence. PLOS ONE 2, e796. https://doi.org/10.1371/journal.pone.0000796

Nielsen, M., Lundegaard, C., Worning, P., Lauemøller, S.L., Lamberth, K., Buus, S., Brunak, S., Lund, O., 2003. Reliable prediction of T-cell epitopes using neural networks with novel sequence representations. Protein Sci. Publ. Protein Soc. 12, 1007–1017.

Ning, N., Pan, Q., Zheng, F., Teitz-Tennenbaum, S., Egenti, M., Yet, J., Li, M., Ginestier, C., Wicha, M.S., Moyer, J.S., E.P.Prince, M., Xu, Y., Zhang, X.-L., Huang, S., Chang, A.E., Li, Q., 2012. Cancer stem cell vaccination confers significant anti-tumor immunity. Cancer Res. 72, 1853–1864. https://doi.org/10.1158/0008-5472.CAN-11-1400

Niranjan, B., Lawrence, M.G., Papargiris, M.M., Richards, M.G., Hussain, S., Frydenberg, M., Pedersen, J., Taylor, R.A., Risbridger, G.P., 2013. Primary culture and propagation of human prostate epithelial cells. Methods Mol. Biol. Clifton NJ 945, 365–382. https://doi.org/10.1007/978-1-62703-125-7_22

Niranjan, B., Lawrence, M.G., Papargiris, M.M., Richards, M.G., Hussain, S., Frydenberg, M., Pedersen, J., Taylor, R.A., Risbridger, G.P., 2012. Primary Culture and Propagation of Human Prostate Epithelial Cells, in: Randell, S.H., Fulcher, M.L. (Eds.), Epithelial Cell Culture Protocols. Humana Press, Totowa, NJ, pp. 365–382.

Nishida, S., Hirohashi, Y., Torigoe, T., Kitamura, H., Takahashi, A., Masumori, N., Tsukamoto, T., Sato, N., 2012. Gene Expression Profiles of Prostate Cancer Stem Cells Isolated by Aldehyde Dehydrogenase Activity Assay. J. Urol. 188, 294–299. https://doi.org/10.1016/j.juro.2012.02.2555

Nishizawa, S., Hirohashi, Y., Torigoe, T., Takahashi, A., Tamura, Y., Mori, T., Kanaseki, T., Kamiguchi, K., Asanuma, H., Morita, R., Sokolovskaya, A., Matsuzaki, J., Yamada, R., Fujii, R., Kampinga, H.H., Kondo, T., Hasegawa, T., Hara, I., Sato, N., 2012. HSP DNAJB8 Controls Tumor-Initiating Ability in Renal Cancer Stem-like Cells. Cancer Res. 72, 2844–2854. https://doi.org/10.1158/0008-5472.CAN-11-3062

Nowell, P., 1976. The clonal evolution of tumor cell populations. Science 194, 23–28. https://doi.org/10.1126/science.959840

Nuhn, P., De Bono, J.S., Fizazi, K., Freedland, S.J., Grilli, M., Kantoff, P.W., Sonpavde, G., Sternberg, C.N., Yegnasubramanian, S., Antonarakis, E.S., 2019. Update on Systemic Prostate Cancer Therapies: Management of Metastatic Castration-resistant Prostate Cancer in the Era of Precision Oncology. Eur. Urol. 75, 88–99. https://doi.org/10.1016/j.eururo.2018.03.028

O'Connor, J.C., Julian, J., Lim, S.D., Carson, D.D., 2005. MUC1 expression in human prostate cancer cell lines and primary tumors. Prostate Cancer Prostatic Dis. 8, 36–44. https://doi.org/10.1038/sj.pcan.4500762

Ogawa, K., Yoshioka, Y., Isohashi, F., Seo, Y., Yoshida, K., Yamazaki, H., 2013. Radiotherapy targeting cancer stem cells: current views and future perspectives. Anticancer Res. 33, 747–754.

Ogishi, M., Yotsuyanagi, H., 2019. Quantitative Prediction of the Landscape of T Cell Epitope Immunogenicity in Sequence Space. Front. Immunol. 10. https://doi.org/10.3389/fimmu.2019.00827

O'Grady, N.P., Tropea, M., Preas, H.L., Reda, D., Vandivier, R.W., Banks, S.M., Suffredini, A.F., 1999. Detection of Macrophage Inflammatory Protein (MIP)-1α and MIP-β during Experimental Endotoxemia and Human Sepsis. J. Infect. Dis. 179, 136–141. https://doi.org/10.1086/314559

Ohtsuka, T., Kaziro, Y., Satoh, T., 1996. Analysis of the T-cell activation signaling pathway mediated by tyrosine kinases, protein kinase C, and Ras protein, which is modulated by intracellular cyclic AMP. Biochim. Biophys. Acta BBA - Mol. Cell Res. 1310, 223–232. https://doi.org/10.1016/0167-4889(95)00172-7

Olsen, L.R., Tongchusak, S., Lin, H., Reinherz, E.L., Brusic, V., Zhang, G.L., 2017. TANTIGEN: a comprehensive database of tumor T cell antigens. Cancer Immunol. Immunother. CII 66, 731–735. https://doi.org/10.1007/s00262-017-1978-y

Olsson, E., Honeth, G., Bendahl, P.-O., Saal, L.H., Gruvberger-Saal, S., Ringnér, M., Vallon-Christersson, J., Jönsson, G., Holm, K., Lövgren, K., Fernö, M., Grabau, D., Borg, A., Hegardt, C., 2011. CD44 isoforms are heterogeneously expressed in breast cancer and correlate with tumor subtypes and cancer stem cell markers. BMC Cancer 11, 418. https://doi.org/10.1186/1471-2407-11-418

O'Neil-Andersen, N.J., Lawrence, D.A., 2002. Differential Modulation of Surface and Intracellular Protein Expression by T Cells after Stimulation in the Presence of Monensin or Brefeldin A. Clin. Diagn. Lab. Immunol. 9, 243–250. https://doi.org/10.1128/CDLI.9.2.243-250.2001

Opdenaker, L.M., Modarai, S.R., Boman, B.M., 2015. The Proportion of ALDEFLUOR-Positive Cancer Stem Cells Changes with Cell Culture Density Due to the Expression of Different ALDH Isoforms. Cancer Stud. Mol. Med. Open J. 2, 87–95. https://doi.org/10.17140/CSMMOJ-2-113

O'Shea, J.J., Schwartz, D.M., Villarino, A.V., Gadina, M., McInnes, I.B., Laurence, A., 2015. The JAK-STAT pathway: impact on human disease and therapeutic intervention. Annu. Rev. Med. 66, 311–328.

Ostrand-Rosenberg, S., 2008. Immune Surveillance: A Balance Between Pro- and Anti-tumor Immunity. Curr. Opin. Genet. Dev. 18, 11–18. https://doi.org/10.1016/j.gde.2007.12.007

Ousset, M., Van Keymeulen, A., Bouvencourt, G., Sharma, N., Achouri, Y., Simons, B.D., Blanpain, C., 2012. Multipotent and unipotent progenitors contribute to prostate postnatal development. Nat. Cell Biol. 14, 1131–1138. https://doi.org/10.1038/ncb2600

Overgaard, N.H., Jung, J.-W., Steptoe, R.J., Wells, J.W., 2015. CD4+/CD8+ double-positive T cells: more than just a developmental stage? J. Leukoc. Biol. 97, 31–38. https://doi.org/10.1189/jlb.1RU0814-382

Packer, J.R., Maitland, N.J., 2016. The molecular and cellular origin of human prostate cancer. Biochim. Biophys. Acta BBA - Mol. Cell Res. 1863, 1238–1260. https://doi.org/10.1016/j.bbamcr.2016.02.016

Paller, C.J., Antonarakis, E.S., 2013. Management of Biochemically Recurrent Prostate Cancer After Local Therapy: Evolving Standards of Care and New Directions. Clin. Adv. Hematol. Oncol. HO 11, 14–23.

Palmer, E., 2003. Negative selection — clearing out the bad apples from the T-cell repertoire. Nat. Rev. Immunol. 3, 383–391. https://doi.org/10.1038/nri1085

Palucka, K., Banchereau, J., 2013. Dendritic-Cell-Based Therapeutic Cancer Vaccines. Immunity 39, 38–48. https://doi.org/10.1016/j.immuni.2013.07.004

Pan, H.-W., Su, H.-H., Hsu, C.-W., Huang, G.-J., Wu, T.T.-L., 2017. Targeted TPX2 increases chromosome missegregation and suppresses tumor cell growth in human prostate cancer. OncoTargets Ther. 10, 3531–3543. https://doi.org/10.2147/OTT.S136491

Pan, Q., Li, Q., Liu, S., Ning, N., Zhang, X., Xu, Y., Chang, A.E., Wicha, M.S., 2015. Concise Review: Targeting Cancer Stem Cells Using Immunologic Approaches. Stem Cells Dayt. Ohio 33, 2085–2092. https://doi.org/10.1002/stem.2039

Park, B., Yee, C., Lee, K.-M., 2014. The Effect of Radiation on the Immune Response to Cancers. Int. J. Mol. Sci. 15, 927–943. https://doi.org/10.3390/ijms15010927

Parsons, J.K., Pinto, P.A., Pavlovich, C.P., Uchio, E., Kim, H.L., Nguyen, M.N., Gulley, J.L., Jamieson, C., Hsu, P., Wojtowicz, M., Parnes, H., Schlom, J., Dahut, W.L., Madan, R.A., Donahue, R.N., Chow, H.-H.S., 2018. A Randomized, Double-blind, Phase II Trial of PSA-TRICOM (PROSTVAC) in Patients with Localized Prostate Cancer: The Immunotherapy to Prevent Progression on Active Surveillance Study. Eur. Urol. Focus 4, 636–638. https://doi.org/10.1016/j.euf.2018.08.016

Pastrana, E., Silva-Vargas, V., Doetsch, F., 2011. Eyes Wide Open: A Critical Review of Sphere-Formation as an Assay For Stem Cells. Cell Stem Cell 8, 486–498. https://doi.org/10.1016/j.stem.2011.04.007

Patrawala, L., Calhoun, T., Schneider-Broussard, R., Li, H., Bhatia, B., Tang, S., Reilly, J.G., Chandra, D., Zhou, J., Claypool, K., Coghlan, L., Tang, D.G., 2006. Highly purified CD44 + prostate cancer cells from xenograft human tumors are enriched in tumorigenic and metastatic progenitor cells. Oncogene 25, 1696. https://doi.org/10.1038/sj.onc.1209327

Patrawala, L., Calhoun, T., Schneider-Broussard, R., Zhou, J., Claypool, K., Tang, D.G., 2005. Side Population Is Enriched in Tumorigenic, Stem-Like Cancer Cells, whereas ABCG2+ and ABCG2− Cancer Cells Are Similarly Tumorigenic. Cancer Res. 65, 6207–6219. https://doi.org/10.1158/0008-5472.CAN-05-0592

Patrawala, L., Calhoun-Davis, T., Schneider-Broussard, R., Tang, D.G., 2007. Hierarchical Organization of Prostate Cancer Cells in Xenograft Tumors: The CD44+α2β1+ Cell Population Is Enriched in Tumor-Initiating Cells. Cancer Res. 67, 6796–6805. https://doi.org/10.1158/0008-5472.CAN-07-0490

Pearson, H., Daouda, T., Granados, D.P., Durette, C., Bonneil, E., Courcelles, M., Rodenbrock, A., Laverdure, J.-P., Côté, C., Mader, S., Lemieux, S., Thibault, P., Perreault, C., 2016. MHC class I-associated peptides derive from selective regions of the human genome. J. Clin. Invest. 126, 4690–4701. https://doi.org/10.1172/JCI88590

Peart, M.J., Smyth, G.K., van Laar, R.K., Bowtell, D.D., Richon, V.M., Marks, P.A., Holloway, A.J., Johnstone, R.W., 2005. Identification and functional significance of genes regulated by structurally different histone deacetylase inhibitors. Proc. Natl. Acad. Sci. U. S. A. 102, 3697–3702. https://doi.org/10.1073/pnas.0500369102

Pellacani, D., Oldridge, E.E., Collins, A.T., Maitland, N.J., 2013. Prominin-1 (CD133) Expression in the Prostate and Prostate Cancer: A Marker for Quiescent Stem Cells. Adv. Exp. Med. Biol. 777, 167–184. https://doi.org/10.1007/978-1-4614-5894-4_11

Pellacani, D., Packer, R.J., Frame, F.M., Oldridge, E.E., Berry, P.A., Labarthe, M.-C., Stower, M.J., Simms, M.S., Collins, A.T., Maitland, N.J., 2011. Regulation of the stem cell marker CD133 is independent of promoter hypermethylation in human epithelial differentiation and cancer. Mol. Cancer 10, 94. https://doi.org/10.1186/1476-4598-10-94

Peng, G., Liu, Y., 2015. Hypoxia-inducible factors in cancer stem cells and inflammation. Trends Pharmacol. Sci. 36, 374–383. https://doi.org/10.1016/j.tips.2015.03.003

Perales, M.-A., Yuan, J., Powel, S., Gallardo, H.F., Rasalan, T.S., Gonzalez, C., Manukian, G., Wang, J., Zhang, Y., Chapman, P.B., Krown, S.E., Livingston, P.O., Ejadi, S., Panageas, K.S., Engelhorn, M.E., Terzulli, S.L., Houghton, A.N., Wolchok, J.D., 2008. Phase I/II study of GM-CSF DNA as an adjuvant for a multipeptide cancer vaccine in patients with advanced melanoma. Mol. Ther. J. Am. Soc. Gene Ther. 16, 2022–2029. https://doi.org/10.1038/mt.2008.196

Pernar, C.H., Ebot, E.M., Wilson, K.M., Mucci, L.A., 2018. The Epidemiology of Prostate Cancer. Cold Spring Harb. Perspect. Med. 8, a030361. https://doi.org/10.1101/cshperspect.a030361

Peters, B., Tong, W., Sidney, J., Sette, A., Weng, Z., 2003. Examining the independent binding assumption for binding of peptide epitopes to MHC-I molecules. Bioinforma. Oxf. Engl. 19, 1765–1772. https://doi.org/10.1093/bioinformatics/btg247

Peterson, P., Org, T., Rebane, A., 2008. Transcriptional regulation by AIRE: molecular mechanisms of central tolerance. Nat. Rev. Immunol. 8, 948–957. https://doi.org/10.1038/nri2450

Pfeiffer, M.J., Schalken, J.A., 2010. Stem Cell Characteristics in Prostate Cancer Cell Lines. Eur. Urol. 57, 246–255. https://doi.org/10.1016/j.eururo.2009.01.015

Phelps, R.A., Chidester, S., Dehghanizadeh, S., Phelps, J., Sandoval, I.T., Rai, K., Broadbent, T., Sarkar, S., Burt, R.W., Jones, D.A., 2009. A Two-Step Model for Colon Adenoma Initiation and Progression Caused by APC Loss. Cell 137, 623–634. https://doi.org/10.1016/j.cell.2009.02.037

Pinc, A., Somasundaram, R., Wagner, C., Hörmann, M., Karanikas, G., Jalili, A., Bauer, W., Brunner, P., Grabmeier-Pfistershammer, K., Gschaider, M., Lai, C.-Y., Hsu, M.-Y., Herlyn, M., Stingl, G., Wagner, S.N., 2012. Targeting CD20 in Melanoma Patients at High Risk of Disease Recurrence. Mol. Ther. 20, 1056–1062. https://doi.org/10.1038/mt.2012.27

Pitt, J.M., Vétizou, M., Daillère, R., Roberti, M.P., Yamazaki, T., Routy, B., Lepage, P., Boneca, I.G., Chamaillard, M., Kroemer, G., Zitvogel, L., 2016. Resistance Mechanisms to Immune-Checkpoint Blockade in Cancer: Tumor-Intrinsic and -Extrinsic Factors. Immunity 44, 1255–1269. https://doi.org/10.1016/j.immuni.2016.06.001

Plaks, V., Kong, N., Werb, Z., 2015. The Cancer Stem Cell Niche: How Essential Is the Niche in Regulating Stemness of Tumor Cells? Cell Stem Cell 16, 225–238. https://doi.org/10.1016/j.stem.2015.02.015

Pors, K., Moreb, J.S., 2014. Aldehyde dehydrogenases in cancer: an opportunity for biomarker and drug development? Drug Discov. Today 19, 1953–1963. https://doi.org/10.1016/j.drudis.2014.09.009

Portillo-Lara, R., Alvarez, M.M., 2015. Enrichment of the Cancer Stem Phenotype in Sphere Cultures of Prostate Cancer Cell Lines Occurs through Activation of Developmental Pathways Mediated by the Transcriptional Regulator ΔNp63α. PLoS ONE 10, e0130118. https://doi.org/10.1371/journal.pone.0130118

Poschke, I., Faryna, M., Bergmann, F., Flossdorf, M., Lauenstein, C., Hermes, J., Hinz, U., Hank, T., Ehrenberg, R., Volkmar, M., Loewer, M., Glimm, H., Hackert, T., Sprick, M.R., Höfer, T., Trumpp, A., Halama, N., Hassel, J.C., Strobel, O., Büchler, M., Sahin, U., Offringa, R., 2016. Identification of a tumor-reactive T-cell repertoire in the immune infiltrate of patients with resectable pancreatic ductal adenocarcinoma. Oncoimmunology 5, e1240859. https://doi.org/10.1080/2162402X.2016.1240859

Präbst, K., Engelhardt, H., Ringgeler, S., Hübner, H., 2017. Basic colorimetric proliferation assays: MTT, WST, and resazurin. Cell Viability Assays Methods Protoc. 1–17.

Prager, B.C., Xie, Q., Bao, S., Rich, J.N., 2019. Cancer Stem Cells: The Architects of the Tumor Ecosystem. Cell Stem Cell 24, 41–53. https://doi.org/10.1016/j.stem.2018.12.009

Precopio, M.L., Betts, M.R., Parrino, J., Price, D.A., Gostick, E., Ambrozak, D.R., Asher, T.E., Douek, D.C., Harari, A., Pantaleo, G., Bailer, R., Graham, B.S., Roederer, M., Koup, R.A., 2007. Immunization with vaccinia virus induces polyfunctional and phenotypically distinctive CD8(+) T cell responses. J. Exp. Med. 204, 1405–1416. https://doi.org/10.1084/jem.20062363

Pritchard, A.L., Hastie, M.L., Neller, M., Gorman, J.J., Schmidt, C.W., Hayward, N.K., 2015. Exploration of peptides bound to MHC class I molecules in melanoma. Pigment Cell Melanoma Res. 28, 281–294. https://doi.org/10.1111/pcmr.12357

Prochazka, L., Tesarik, R., Turanek, J., 2014. Regulation of alternative splicing of CD44 in cancer. Cell. Signal. 26, 2234–2239. https://doi.org/10.1016/j.cellsig.2014.07.011

Prokopec, S.D., Watson, J.D., Waggott, D.M., Smith, A.B., Wu, A.H., Okey, A.B., Pohjanvirta, R., Boutros, P.C., 2013. Systematic evaluation of medium-throughput mRNA abundance platforms. RNA 19, 51–62. https://doi.org/10.1261/rna.034710.112

Prostate cancer incidence statistics [WWW Document], 2015. . Cancer Res. UK. URL https://www.cancerresearchuk.org/health-professional/cancer-statistics/statistics-by-cancer-type/prostate-cancer/incidence (accessed 1.10.19).

Prostate cancer mortality statistics [WWW Document], 2015. . Cancer Res. UK. URL https://www.cancerresearchuk.org/health-professional/cancer-statistics/statistics-by-cancer-type/prostate-cancer/mortality (accessed 1.10.19).

Punt, C.J., Nagy, A., Douillard, J.-Y., Figer, A., Skovsgaard, T., Monson, J., Barone, C., Fountzilas, G., Riess, H., Moylan, E., 2002. Edrecolomab alone or in combination with fluorouracil and folinic acid in the adjuvant treatment of stage III colon cancer: a randomised study. The Lancet 360, 671–677.

Qin, J., Liu, X., Laffin, B., Chen, X., Choy, G., Jeter, C., Calhoun-Davis, T., Li, H., Palapattu, G.S., Pang, S., Lin, K., Huang, J., Ivanov, I., Li, W., Suraneni, M.V., Tang, D.G., 2012. The PSA−/lo prostate cancer cell population harbors self-renewing long-term tumor-propagating cells that resist castration. Cell Stem Cell 10, 556–569. https://doi.org/10.1016/j.stem.2012.03.009

Qiu, Z.-Y., Shen, W.-Y., Fan, L., Wang, L., Yu, H., Qiao, C., Wu, Y.-J., Lu, R.-N., Qian, J., He, G.-S., Xu, W., Li, J.-Y., 2015. Assessment of clonality in T-cell large granular lymphocytic leukemia: flow cytometric T cell receptor Vβ repertoire and T cell receptor gene rearrangement. Leuk. Lymphoma 56, 324–331. https://doi.org/10.3109/10428194.2014.921297

Quah, B.J.C., Parish, C.R., 2012. New and improved methods for measuring lymphocyte proliferation in vitro and in vivo using CFSE-like fluorescent dyes. J. Immunol. Methods 379, 1–14. https://doi.org/10.1016/j.jim.2012.02.012

Quail, D.F., Taylor, M.J., Postovit, L.-M., 2012. Microenvironmental regulation of cancer stem cell phenotypes. Curr. Stem Cell Res. Ther. 7, 197–216.

Quintás-Cardama, A., Verstovsek, S., 2013. MOLECULAR PATHWAYS: JAK/STAT PATHWAY: MUTATIONS, INHIBITORS, AND RESISTANCE. Clin. Cancer Res. Off. J. Am. Assoc. Cancer Res. 19, 1933–1940. https://doi.org/10.1158/1078-0432.CCR-12-0284

Rajasekhar, V.K., Studer, L., Gerald, W., Socci, N.D., Scher, H.I., 2011. Tumour-initiating stem-like cells in human prostate cancer exhibit increased NF-κB signalling. Nat. Commun. 2, 162. https://doi.org/10.1038/ncomms1159

Raman, M.C.C., Rizkallah, P.J., Simmons, R., Donnellan, Z., Dukes, J., Bossi, G., Le Provost, G.S., Todorov, P., Baston, E., Hickman, E., Mahon, T., Hassan, N., Vuidepot, A., Sami, M., Cole, D.K., Jakobsen, B.K., 2016. Direct molecular mimicry enables off-target cardiovascular toxicity by an enhanced affinity TCR designed for cancer immunotherapy. Sci. Rep. 6. https://doi.org/10.1038/srep18851

Rammensee, H.-G., Bachmann, J., Emmerich, N.P.N., Bachor, O.A., Stevanović, S., 1999. SYFPEITHI: database for MHC ligands and peptide motifs. Immunogenetics 50, 213–219. https://doi.org/10.1007/s002510050595

Ranganathan, P., Weaver, K.L., Capobianco, A.J., 2011. Notch signalling in solid tumours: a little bit of everything but not all the time. Nat. Rev. Cancer 11, 338–351. https://doi.org/10.1038/nrc3035

Raouf, A., Zhao, Y., To, K., Stingl, J., Delaney, A., Barbara, M., Iscove, N., Jones, S., McKinney, S., Emerman, J., Aparicio, S., Marra, M., Eaves, C., 2008. Transcriptome analysis of the normal human mammary cell commitment and differentiation process. Cell Stem Cell 3, 109–118. https://doi.org/10.1016/j.stem.2008.05.018

Rapoport, A.P., Aqui, N.A., Stadtmauer, E.A., Vogl, D.T., Fang, H.-B., Cai, L., Janofsky, S., Chew, A., Storek, J., Akpek, G., Badros, A., Yanovich, S., Tan, M.T., Veloso, E., Pasetti, M.F., Cross, A., Philip, S., Murphy, H., Bhagat, R., Zheng, Z., Milliron, T., Cotte, J., Cannon, A., Levine, B.L., Vonderheide, R.H., June, C.H., 2011. Combination immunotherapy using adoptive T-cell transfer and tumor antigen vaccination on the basis of hTERT and survivin after ASCT for myeloma. Blood 117, 788–797. https://doi.org/10.1182/blood-2010-08-299396

Raulet, D.H., Guerra, N., 2009. Oncogenic stress sensed by the immune system: role of natural killer cell receptors. Nat. Rev. Immunol. 9, 568–580. https://doi.org/10.1038/nri2604

Reichstetter, S., Kwok, W.W., Kochik, S., Koelle, D.M., Beaty, J.S., Nepom, G.T., 1999. MHC-peptide ligand interactions establish a functional threshold for antigen-specific T cell recognition. Hum. Immunol. 60, 608–618.

Reiman, J.M., Kmieciak, M., Manjili, M.H., Knutson, K.L., 2007. Tumor immunoediting and immunosculpting pathways to cancer progression. Semin. Cancer Biol., Making the Tumor-Specific Effectors Ineffective 17, 275–287. https://doi.org/10.1016/j.semcancer.2007.06.009

Reya, T., Clevers, H., 2005. Wnt signalling in stem cells and cancer. Nature 434, 843–850. https://doi.org/10.1038/nature03319

Reya, T., Duncan, A.W., Ailles, L., Domen, J., Scherer, D.C., Willert, K., Hintz, L., Nusse, R., Weissman, I.L., 2003. A role for Wnt signalling in self-renewal of haematopoietic stem cells. Nature 423, 409–414. https://doi.org/10.1038/nature01593

Reya, T., Morrison, S.J., Clarke, M.F., Weissman, I.L., 2001. Stem cells, cancer, and cancer stem cells. Nature 414, 105–111. https://doi.org/10.1038/35102167

Ricci-Vitiani, L., Lombardi, D.G., Pilozzi, E., Biffoni, M., Todaro, M., Peschle, C., De Maria, R., 2007. Identification and expansion of human colon-

cancer-initiating cells. Nature 445, 111–115. https://doi.org/10.1038/nature05384

Richardson, G.D., Robson, C.N., Lang, S.H., Neal, D.E., Maitland, N.J., Collins, A.T., 2004. CD133, a novel marker for human prostatic epithelial stem cells. J. Cell Sci. 117, 3539–3545. https://doi.org/10.1242/jcs.01222

Riechelmann, H., Sauter, A., Golze, W., Hanft, G., Schroen, C., Hoermann, K., Erhardt, T., Gronau, S., 2008. Phase I trial with the CD44v6-targeting immunoconjugate bivatuzumab mertansine in head and neck squamous cell carcinoma. Oral Oncol. 44, 823–829. https://doi.org/10.1016/j.oraloncology.2007.10.009

Rincón, M., Anguita, J., Nakamura, T., Fikrig, E., Flavell, R.A., 1997. Interleukin (IL)-6 directs the differentiation of IL-4-producing CD4+ T cells. J. Exp. Med. 185, 461–469.

Rinkenbaugh, A.L., Baldwin, A.S., 2016. The NF-κB Pathway and Cancer Stem Cells. Cells 5. https://doi.org/10.3390/cells5020016

Robey, E., Fowlkes, B.J., 1994. Selective events in T cell development. Annu. Rev. Immunol. 12, 675–705.

Roehl Kimberly A., Han Misop, Ramos Christian G., Antenor Jo Ann V., Catalona William J., 2004. Cancer progression and survival rates following anatomical radical retropubic prostatectomy in 3,478 consecutive patients: long-term results. J. Urol. 172, 910–914. https://doi.org/10.1097/01.ju.0000134888.22332.bb

Rooney, C.M., Leen, A.M., Vera, J.F., Heslop, H.E., 2014. T LYMPHOCYTES TARGETING NATIVE RECEPTORS. Immunol. Rev. 257. https://doi.org/10.1111/imr.12133

Rooney, C.M., Smith, C.A., Ng, C.Y., Loftin, S., Li, C., Krance, R.A., Brenner, M.K., Heslop, H.E., 1995. Use of gene-modified virus-specific T lymphocytes to control Epstein-Barr-virus-related lymphoproliferation. Lancet Lond. Engl. 345, 9–13. https://doi.org/10.1016/s0140-6736(95)91150-2

Rosati, E., Dowds, C.M., Liaskou, E., Henriksen, E.K.K., Karlsen, T.H., Franke, A., 2017. Overview of methodologies for T-cell receptor repertoire analysis. BMC Biotechnol. 17. https://doi.org/10.1186/s12896-017-0379-9

Rosenberg, S.A., Yang, J.C., Sherry, R.M., Kammula, U.S., Hughes, M.S., Phan, G.Q., Citrin, D.E., Restifo, N.P., Robbins, P.F., Wunderlich, J.R., Morton, K.E., Laurencot, C.M., Steinberg, S.M., White, D.E., Dudley, M.E., 2011. Durable Complete Responses in Heavily Pretreated Patients with Metastatic Melanoma Using T-Cell Transfer Immunotherapy. Clin. Cancer Res. 17, 4550–4557. https://doi.org/10.1158/1078-0432.CCR-11-0116

Rötzschke, O., Falk, K., Deres, K., Schild, H., Norda, M., Metzger, J., Jung, G., Rammensee, H.G., 1990. Isolation and analysis of naturally processed viral peptides as recognized by cytotoxic T cells. Nature 348, 252–254. https://doi.org/10.1038/348252a0

Russell, J.H., Ley, T.J., 2002. Lymphocyte-Mediated Cytotoxicity. Annu. Rev. Immunol. 20, 323–370. https://doi.org/10.1146/annurev.immunol.20.100201.131730

Rybak, A.P., Bristow, R.G., Kapoor, A., 2014. Prostate cancer stem cells: deciphering the origins and pathways involved in prostate tumorigenesis and aggression. Oncotarget 6, 1900–1919.

Rybak, A.P., He, L., Kapoor, A., Cutz, J.-C., Tang, D., 2011. Characterization of sphere-propagating cells with stem-like properties from DU145 prostate cancer cells. Biochim. Biophys. Acta 1813, 683–694. https://doi.org/10.1016/j.bbamcr.2011.01.018

Sabnis, N.G., Miller, A., Titus, M.A., Huss, W.J., 2017. The Efflux Transporter ABCG2 Maintains Prostate Stem Cells. Mol. Cancer Res. MCR 15, 128–140. https://doi.org/10.1158/1541-7786.MCR-16-0270-T

Sackstein, R., Schatton, T., Barthel, S.R., 2017. T-lymphocyte homing: an underappreciated yet critical hurdle for successful cancer immunotherapy. Lab. Invest. https://doi.org/10.1038/labinvest.2017.25

Sadelain, M., Brentjens, R., Riviere, I., 2013. The basic principles of chimeric antigen receptor (CAR) design. Cancer Discov. 3, 388–398. https://doi.org/10.1158/2159-8290.CD-12-0548

Sahlberg, S.H., Spiegelberg, D., Glimelius, B., Stenerlöw, B., Nestor, M., 2014. Evaluation of cancer stem cell markers CD133, CD44, CD24: association with AKT isoforms and radiation resistance in colon cancer cells. PloS One 9, e94621. https://doi.org/10.1371/journal.pone.0094621

Salimu, J., Spary, L.K., Al-Taei, S., Clayton, A., Mason, M.D., Staffurth, J., Tabi, Z., 2015. Cross-Presentation of the Oncofetal Tumor Antigen 5T4 from Irradiated Prostate Cancer Cells--A Key Role for Heat-Shock Protein 70 and Receptor CD91. Cancer Immunol. Res. 3, 678–688. https://doi.org/10.1158/2326-6066.CIR-14-0079

Sallusto, F., Lenig, D., Förster, R., Lipp, M., Lanzavecchia, A., 1999. Two subsets of memory T lymphocytes with distinct homing potentials and effector functions. Nature 401, 708–712. https://doi.org/10.1038/44385

Salter, R.D., Cresswell, P., 1986. Impaired assembly and transport of HLA-A and -B antigens in a mutant TxB cell hybrid. EMBO J. 5, 943–949.

Sanchez, C., Chan, R., Bajgain, P., Rambally, S., Palapattu, G., Mims, M., Rooney, C.M., Leen, A.M., Brenner, M.K., Vera, J.F., 2013. Combining T-cell immunotherapy and anti-androgen therapy for prostate cancer. Prostate Cancer Prostatic Dis. 16, 123–131, S1. https://doi.org/10.1038/pcan.2012.49

Sato, T., Stange, D.E., Ferrante, M., Vries, R.G.J., Van Es, J.H., Van den Brink, S., Van Houdt, W.J., Pronk, A., Van Gorp, J., Siersema, P.D., Clevers, H., 2011. Long-term expansion of epithelial organoids from human colon, adenoma, adenocarcinoma, and Barrett's epithelium. Gastroenterology 141, 1762–1772. https://doi.org/10.1053/j.gastro.2011.07.050

Saunders, K.O., Ward-Caviness, C., Schutte, R.J., Freel, S.A., Overman, R.G., Thielman, N.M., Cunningham, C.K., Kepler, T.B., Tomaras, G.D., 2011. Secretion of MIP-1β and MIP-1α by CD8+ T-lymphocytes Correlates with HIV-1 Inhibition Independent of Coreceptor Usage. Cell. Immunol. 266, 154–164. https://doi.org/10.1016/j.cellimm.2010.09.011

Savage, P.A., Vosseller, K., Kang, C., Larimore, K., Riedel, E., Wojnoonski, K., Jungbluth, A.A., Allison, J.P., 2008. Recognition of a ubiquitous self antigen by prostate cancer-infiltrating CD8+ T lymphocytes. Science 319, 215–220. https://doi.org/10.1126/science.1148886

Saygin, C., Matei, D., Majeti, R., Reizes, O., Lathia, J.D., 2019. Targeting Cancer Stemness in the Clinic: From Hype to Hope. Cell Stem Cell 24, 25–40. https://doi.org/10.1016/j.stem.2018.11.017

Schatton, T., Schütte, U., Frank, N.Y., Zhan, Q., Hoerning, A., Robles, S.C., Zhou, J., Hodi, F.S., Spagnoli, G.C., Murphy, G.F., Frank, M.H., 2010. Modulation of T-Cell Activation by Malignant Melanoma Initiating Cells. Cancer Res. 70, 697–708. https://doi.org/10.1158/0008-5472.CAN-09-1592

Schatz, D.G., 2004. Antigen receptor genes and the evolution of a recombinase. Semin. Immunol., The Evolution of Rearranging Receptor Families 16, 245–256. https://doi.org/10.1016/j.smim.2004.08.004

Schaue, D., Ratikan, J.A., Iwamoto, K.S., McBride, W.H., 2012. Maximizing Tumor Immunity With Fractionated Radiation. Int. J. Radiat. Oncol. Biol. Phys. 83, 1306–1310. https://doi.org/10.1016/j.ijrobp.2011.09.049

Scheid, E., Major, P., Bergeron, A., Finn, O.J., Salter, R.D., Eady, R., Yassine-Diab, B., Favre, D., Peretz, Y., Landry, C., Hotte, S., Mukherjee, S.D., Dekaban, G.A., Fink, C., Foster, P.J., Gaudet, J., Gariepy, J., Sekaly, R.-P., Lacombe, L., Fradet, Y., Foley, R., 2016. Tn-MUC1 DC Vaccination of Rhesus Macaques and a Phase I/II Trial in Patients with Nonmetastatic Castrate-Resistant Prostate Cancer. Cancer Immunol. Res. 4, 881–892. https://doi.org/10.1158/2326-6066.CIR-15-0189

Schepers, A.G., Snippert, H.J., Stange, D.E., Born, M. van den, Es, J.H. van, Wetering, M. van de, Clevers, H., 2012. Lineage Tracing Reveals Lgr5+ Stem Cell Activity in Mouse Intestinal Adenomas. Science 337, 730–735. https://doi.org/10.1126/science.1224676

Schmitt, M., Metzger, M., Gradl, D., Davidson, G., Orian-Rousseau, V., 2015. CD44 functions in Wnt signaling by regulating LRP6 localization and activation. Cell Death Differ. 22, 677–689. https://doi.org/10.1038/cdd.2014.156

Schmittgen, T.D., Livak, K.J., 2008. Analyzing real-time PCR data by the comparative C_T method. Nat. Protoc. 3, 1101–1108. https://doi.org/10.1038/nprot.2008.73

Schmitz, M., Temme, A., Senner, V., Ebner, R., Schwind, S., Stevanovic, S., Wehner, R., Schackert, G., Schackert, H.K., Fussel, M., Bachmann, M., Rieber, E.P., Weigle, B., 2007. Identification of SOX2 as a novel glioma-associated antigen and potential target for T cell-based immunotherapy. Br. J. Cancer 96, 1293–1301. https://doi.org/10.1038/sj.bjc.6603696

Schnell, U., Cirulli, V., Giepmans, B.N.G., 2013. EpCAM: Structure and function in health and disease. Biochim. Biophys. Acta BBA - Biomembr. 1828, 1989–2001. https://doi.org/10.1016/j.bbamem.2013.04.018

Scholtalbers, J., Boegel, S., Bukur, T., Byl, M., Goerges, S., Sorn, P., Loewer, M., Sahin, U., Castle, J.C., 2015. TCLP: an online cancer cell line catalogue integrating HLA type, predicted neo-epitopes, virus and gene expression. Genome Med. 7, 118. https://doi.org/10.1186/s13073-015-0240-5

Schrama, D., Ritter, C., Becker, J.C., 2017. T cell receptor repertoire usage in cancer as a surrogate marker for immune responses. Semin.

Immunopathol. 39, 255–268. https://doi.org/10.1007/s00281-016-0614-9

Schreiber, R.D., Old, L.J., Smyth, M.J., 2011. Cancer Immunoediting: Integrating Immunity's Roles in Cancer Suppression and Promotion. Science 331, 1565–1570. https://doi.org/10.1126/science.1203486

Schrödinger, LLC, 2015. The PyMOL Molecular Graphics System.

Schroeder, A., Herrmann, A., Cherryholmes, G., Kowolik, C., Buettner, R., Pal, S., Yu, H., Müller-Newen, G., Jove, R., 2014. Loss of androgen receptor expression promotes a stem-like cell phenotype in prostate cancer through STAT3 signaling. Cancer Res. 74, 1227–1237. https://doi.org/10.1158/0008-5472.CAN-13-0594

Schumacher, T.N., Schreiber, R.D., 2015. Neoantigens in cancer immunotherapy. Science 348, 69–74. https://doi.org/10.1126/science.aaa4971

Schuster, H., Peper, J.K., Bösmüller, H.-C., Röhle, K., Backert, L., Bilich, T., Ney, B., Löffler, M.W., Kowalewski, D.J., Trautwein, N., Rabsteyn, A., Engler, T., Braun, S., Haen, S.P., Walz, J.S., Schmid-Horch, B., Brucker, S.Y., Wallwiener, D., Kohlbacher, O., Fend, F., Rammensee, H.-G., Stevanović, S., Staebler, A., Wagner, P., 2017. The immunopeptidomic landscape of ovarian carcinomas. Proc. Natl. Acad. Sci. U. S. A. 114, E9942–E9951. https://doi.org/10.1073/pnas.1707658114

Schwartzberg, L.S., 2001. Clinical experience with edrecolomab: a monoclonal antibody therapy for colorectal carcinoma. Crit. Rev. Oncol. Hematol. 40, 17–24.

Seder, R.A., Darrah, P.A., Roederer, M., 2008. T-cell quality in memory and protection: implications for vaccine design. Nat. Rev. Immunol. 8, 247–258. https://doi.org/10.1038/nri2274

Seliger, B., Maeurer, M.J., Ferrone, S., 2000. Antigen-processing machinery breakdown and tumor growth. Immunol. Today 21, 455–464.

Semenza, G.L., 2003. Targeting HIF-1 for cancer therapy. Nat. Rev. Cancer 3, 721–732. https://doi.org/10.1038/nrc1187

Senbanjo, L.T., Chellaiah, M.A., 2017. CD44: A Multifunctional Cell Surface Adhesion Receptor Is a Regulator of Progression and Metastasis of Cancer Cells. Front. Cell Dev. Biol. 5. https://doi.org/10.3389/fcell.2017.00018

Serrano-Gomez, S.J., Maziveyi, M., Alahari, S.K., 2016. Regulation of epithelial-mesenchymal transition through epigenetic and post-translational modifications. Mol. Cancer 15. https://doi.org/10.1186/s12943-016-0502-x

Serwold, T., Gonzalez, F., Kim, J., Jacob, R., Shastri, N., 2002. ERAAP customizes peptides for MHC class I molecules in the endoplasmic reticulum. Nature 419, 480–483. https://doi.org/10.1038/nature01074

Sette, A., Sidney, J., del Guercio, M.F., Southwood, S., Ruppert, J., Dahlberg, C., Grey, H.M., Kubo, R.T., 1994. Peptide binding to the most frequent HLA-A class I alleles measured by quantitative molecular binding assays. Mol. Immunol. 31, 813–822.

Seymour, L., Bogaerts, J., Perrone, A., Ford, R., Schwartz, L.H., Mandrekar, S., Lin, N.U., Litière, S., Dancey, J., Chen, A., Hodi, F.S., Therasse, P., Hoekstra, O.S., Shankar, L.K., Wolchok, J.D., Ballinger, M., Caramella, C., de Vries, E.G.E., RECIST working group, 2017. iRECIST: guidelines

for response criteria for use in trials testing immunotherapeutics. Lancet Oncol. 18, e143–e152. https://doi.org/10.1016/S1470-2045(17)30074-8

Sfanos, K.S., Bruno, T.C., Meeker, A.K., De Marzo, A.M., Isaacs, W.B., Drake, C.G., 2009. Human prostate-infiltrating CD8+ T lymphocytes are oligoclonal and PD-1+. The Prostate 69, 1694–1703. https://doi.org/10.1002/pros.21020

Shackleton, M., Quintana, E., Fearon, E.R., Morrison, S.J., 2009. Heterogeneity in Cancer: Cancer Stem Cells versus Clonal Evolution. Cell 138, 822–829. https://doi.org/10.1016/j.cell.2009.08.017

Shahmarvand, N., Nagy, A., Shahryari, J., Ohgami, R.S., 2018. Mutations in the signal transducer and activator of transcription family of genes in cancer. Cancer Sci. 109, 926–933. https://doi.org/10.1111/cas.13525

Shankaran, V., Ikeda, H., Bruce, A.T., White, J.M., Swanson, P.E., Old, L.J., Schreiber, R.D., 2001. IFNγ and lymphocytes prevent primary tumour development and shape tumour immunogenicity. Nature 410, 1107–1111. https://doi.org/10.1038/35074122

Sheikh, N.A., Petrylak, D., Kantoff, P.W., Dela Rosa, C., Stewart, F.P., Kuan, L.-Y., Whitmore, J.B., Trager, J.B., Poehlein, C.H., Frohlich, M.W., Urdal, D.L., 2013. Sipuleucel-T immune parameters correlate with survival: an analysis of the randomized phase 3 clinical trials in men with castration-resistant prostate cancer. Cancer Immunol. Immunother. CII 62, 137–147. https://doi.org/10.1007/s00262-012-1317-2

Shen, M.M., Abate-Shen, C., 2010. Molecular genetics of prostate cancer: new prospects for old challenges. Genes Dev. 24, 1967–2000. https://doi.org/10.1101/gad.1965810

Shi, F.-D., Zhang, J.-Y., Liu, D., Rearden, A., Elliot, M., Nachtsheim, D., Daniels, T., Casiano, C.A., Heeb, M.J., Chan, E.K.L., Tan, E.M., 2005. Preferential humoral immune response in prostate cancer to cellular proteins p90 and p62 in a panel of tumor-associated antigens. The Prostate 63, 252–258. https://doi.org/10.1002/pros.20181

Shmelkov, S.V., Butler, J.M., Hooper, A.T., Hormigo, A., Kushner, J., Milde, T., St Clair, R., Baljevic, M., White, I., Jin, D.K., Chadburn, A., Murphy, A.J., Valenzuela, D.M., Gale, N.W., Thurston, G., Yancopoulos, G.D., D'Angelica, M., Kemeny, N., Lyden, D., Rafii, S., 2008. CD133 expression is not restricted to stem cells, and both CD133+ and CD133- metastatic colon cancer cells initiate tumors. J. Clin. Invest. 118, 2111–2120. https://doi.org/10.1172/JCI34401

Shugay, M., Bagaev, D.V., Zvyagin, I.V., Vroomans, R.M., Crawford, J.C., Dolton, G., Komech, E.A., Sycheva, A.L., Koneva, A.E., Egorov, E.S., Eliseev, A.V., Van Dyk, E., Dash, P., Attaf, M., Rius, C., Ladell, K., McLaren, J.E., Matthews, K.K., Clemens, E.B., Douek, D.C., Luciani, F., van Baarle, D., Kedzierska, K., Kesmir, C., Thomas, P.G., Price, D.A., Sewell, A.K., Chudakov, D.M., 2018. VDJdb: a curated database of T-cell receptor sequences with known antigen specificity. Nucleic Acids Res. 46, D419–D427. https://doi.org/10.1093/nar/gkx760

Shultz, L.D., Lyons, B.L., Burzenski, L.M., Gott, B., Chen, X., Chaleff, S., Kotb, M., Gillies, S.D., King, M., Mangada, J., Greiner, D.L., Handgretinger, R., 2005. Human lymphoid and myeloid cell development in NOD/LtSz-scid IL2R gamma null mice engrafted with

mobilized human hemopoietic stem cells. J. Immunol. Baltim. Md 1950 174, 6477–6489.

Shvartsur, A., Bonavida, B., 2015. Trop2 and its overexpression in cancers: regulation and clinical/therapeutic implications. Genes Cancer 6, 84–105.

Siegel, A.M., Heimall, J., Freeman, A.F., Hsu, A.P., Brittain, E., Brenchley, J.M., Douek, D.C., Fahle, G.H., Cohen, J.I., Holland, S.M., Milner, J.D., 2011. A critical role for STAT3 transcription factor signaling in the development and maintenance of human T cell memory. Immunity 35, 806–818. https://doi.org/10.1016/j.immuni.2011.09.016

Simons, J.W., Sacks, N., 2006. Granulocyte-macrophage colony-stimulating factor-transduced allogeneic cancer cellular immunotherapy: the GVAX vaccine for prostate cancer. Urol. Oncol. 24, 419–424. https://doi.org/10.1016/j.urolonc.2005.08.021

Singer, A., Adoro, S., Park, J.-H., 2008. Lineage fate and intense debate: myths, models and mechanisms of CD4/CD8 lineage choice. Nat. Rev. Immunol. 8, 788–801. https://doi.org/10.1038/nri2416

Small, E.J., Schellhammer, P.F., Higano, C.S., Redfern, C.H., Nemunaitis, J.J., Valone, F.H., Verjee, S.S., Jones, L.A., Hershberg, R.M., 2006. Placebo-Controlled Phase III Trial of Immunologic Therapy with Sipuleucel-T (APC8015) in Patients with Metastatic, Asymptomatic Hormone Refractory Prostate Cancer. J. Clin. Oncol. 24, 3089–3094.

Smalley, M.J., Clarke, R.B., 2005. The Mammary Gland "Side Population": A Putative Stem/Progenitor Cell Marker? J. Mammary Gland Biol. Neoplasia 10, 37–47. https://doi.org/10.1007/s10911-005-2539-0

Smith, B.A., Sokolov, A., Uzunangelov, V., Baertsch, R., Newton, Y., Graim, K., Mathis, C., Cheng, D., Stuart, J.M., Witte, O.N., 2015. A basal stem cell signature identifies aggressive prostate cancer phenotypes. Proc. Natl. Acad. Sci. 112, E6544–E6552. https://doi.org/10.1073/pnas.1518007112

Smith, P.C., Hobisch, A., Lin, D.-L., Culig, Z., Keller, E.T., 2001. Interleukin-6 and prostate cancer progression. Cytokine Growth Factor Rev. 12, 33–40. https://doi.org/10.1016/S1359-6101(00)00021-6

Smith, S.N., Harris, D.T., Kranz, D.M., 2015. T Cell Receptor Engineering and Analysis Using the Yeast Display Platform. Methods Mol. Biol. Clifton NJ 1319, 95–141. https://doi.org/10.1007/978-1-4939-2748-7_6

Smyth, M.J., Crowe, N.Y., Godfrey, D.I., 2001. NK cells and NKT cells collaborate in host protection from methylcholanthrene-induced fibrosarcoma. Int. Immunol. 13, 459–463. https://doi.org/10.1093/intimm/13.4.459

Sobel, R., Sadar, M., 2005. CELL LINES USED IN PROSTATE CANCER RESEARCH: A COMPENDIUM OF OLD AND NEW LINES—PART 1. J. Urol. 173, 342–359. https://doi.org/10.1097/01.ju.0000141580.30910.57

Soeda, A., Park, M., Lee, D., Mintz, A., Androutsellis-Theotokis, A., McKay, R.D., Engh, J., Iwama, T., Kunisada, T., Kassam, A.B., Pollack, I.F., Park, D.M., 2009. Hypoxia promotes expansion of the CD133-positive glioma stem cells through activation of HIF-1alpha. Oncogene 28, 3949–3959. https://doi.org/10.1038/onc.2009.252

SONER, B.C., AKTUG, H., ACIKGOZ, E., DUZAGAC, F., GUVEN, U., AYLA, S., CAL, C., OKTEM, G., 2014. Induced growth inhibition, cell cycle arrest and apoptosis in CD133+/CD44+ prostate cancer stem cells by

flavopiridol. Int. J. Mol. Med. 34, 1249–1256. https://doi.org/10.3892/ijmm.2014.1930

Soria-Guerra, R.E., Nieto-Gomez, R., Govea-Alonso, D.O., Rosales-Mendoza, S., 2015. An overview of bioinformatics tools for epitope prediction: Implications on vaccine development. J. Biomed. Inform. 53, 405–414. https://doi.org/10.1016/j.jbi.2014.11.003

Spary, L.K., Al-Taei, S., Salimu, J., Cook, A.D., Ager, A., Watson, H.A., Clayton, A., Staffurth, J., Mason, M.D., Tabi, Z., 2014a. Enhancement of T Cell Responses as a Result of Synergy between Lower Doses of Radiation and T Cell Stimulation. J. Immunol. 192, 3101–3110. https://doi.org/10.4049/jimmunol.1302736

Spary, L.K., Salimu, J., Webber, J.P., Clayton, A., Mason, M.D., Tabi, Z., 2014b. Tumor stroma-derived factors skew monocyte to dendritic cell differentiation toward a suppressive CD14+ PD-L1+ phenotype in prostate cancer. Oncoimmunology 3, e955331. https://doi.org/10.4161/21624011.2014.955331

Speetjens, F.M., de Bruin, E.C., Morreau, H., Zeestraten, E.C.M., Putter, H., van Krieken, J.H., van Buren, M.M., van Velzen, M., Dekker-Ensink, N.G., van de Velde, C.J.H., Kuppen, P.J.K., 2008. Clinical impact of HLA class I expression in rectal cancer. Cancer Immunol. Immunother. 57, 601–609. https://doi.org/10.1007/s00262-007-0396-y

Spranger, S., Spaapen, R.M., Zha, Y., Williams, J., Meng, Y., Ha, T.T., Gajewski, T.F., 2013. Up-Regulation of PD-L1, IDO, and Tregs in the Melanoma Tumor Microenvironment Is Driven by CD8+ T Cells. Sci. Transl. Med. 5, 200ra116. https://doi.org/10.1126/scitranslmed.3006504

Starr, T.K., Jameson, S.C., Hogquist, K.A., 2003. Positive and negative selection of T cells. Annu. Rev. Immunol. 21, 139–176. https://doi.org/10.1146/annurev.immunol.21.120601.141107

Stassi, G., Todaro, M., Zerilli, M., Ricci-Vitiani, L., Liberto, D.D., Patti, M., Florena, A., Gaudio, F.D., Gesù, G.D., Maria, R.D., 2003. Thyroid Cancer Resistance to Chemotherapeutic Drugs via Autocrine Production of Interleukin-4 and Interleukin-10. Cancer Res. 63, 6784–6790.

Stewart, B.W., Kleihues, P., 2003. World cancer report.

Stewart, J.M., Shaw, P.A., Gedye, C., Bernardini, M.Q., Neel, B.G., Ailles, L.E., 2011. Phenotypic heterogeneity and instability of human ovarian tumor-initiating cells. Proc. Natl. Acad. Sci. 108, 6468–6473. https://doi.org/10.1073/pnas.1005529108

Stickel, J.S., Weinzierl, A.O., Hillen, N., Drews, O., Schuler, M.M., Hennenlotter, J., Wernet, D., Müller, C.A., Stenzl, A., Rammensee, H.-G., Stevanović, S., 2009. HLA ligand profiles of primary renal cell carcinoma maintained in metastases. Cancer Immunol. Immunother. 58, 1407–1417. https://doi.org/10.1007/s00262-008-0655-6

Stone, J.D., Harris, D.T., Kranz, D.M., 2015. TCR affinity for p/MHC formed by tumor antigens that are self-proteins: impact on efficacy and toxicity. Curr. Opin. Immunol. 33, 16–22. https://doi.org/10.1016/j.coi.2015.01.003

Stone, J.D., Kranz, D., 2013. Role of T Cell Receptor Affinity in the Efficacy and Specificity of Adoptive T Cell Therapies. Front. Immunol. 4. https://doi.org/10.3389/fimmu.2013.00244

Stone, K.R., Mickey, D.D., Wunderli, H., Mickey, G.H., Paulson, D.F., 1978. Isolation of a human prostate carcinoma cell line (DU 145). Int. J. Cancer 21, 274–281.

Strand, D.W., Goldstein, A.S., 2015. The many ways to make a luminal cell and a prostate cancer cell. Endocr. Relat. Cancer 22, T187–T197. https://doi.org/10.1530/ERC-15-0195

Strasner, A., Karin, M., 2015. Immune Infiltration and Prostate Cancer. Front. Oncol. 5. https://doi.org/10.3389/fonc.2015.00128

Street, S.E., Cretney, E., Smyth, M.J., 2001. Perforin and interferon-gamma activities independently control tumor initiation, growth, and metastasis. Blood 97, 192–197.

Stutman, O., 1979. Chemical carcinogenesis in nude mice: comparison between nude mice from homozygous matings and heterozygous matings and effect of age and carcinogen dose. J. Natl. Cancer Inst. 62, 353–358.

Stutman, O., 1974. Tumor development after 3-methylcholanthrene in immunologically deficient athymic-nude mice. Science 183, 534–536.

Sullivan, Y.B., Landay, A.L., Zack, J.A., Kitchen, S.G., Al-Harthi, L., 2001. Upregulation of CD4 on CD8+ T cells: CD4dimCD8bright T cells constitute an activated phenotype of CD8+ T cells. Immunology 103, 270–280. https://doi.org/10.1046/j.1365-2567.2001.01243.x

Sun, Y., Kong, W., Falk, A., Hu, J., Zhou, L., Pollard, S., Smith, A., 2009. CD133 (Prominin) negative human neural stem cells are clonogenic and tripotent. PloS One 4, e5498. https://doi.org/10.1371/journal.pone.0005498

Sundberg, M., Jansson, L., Ketolainen, J., Pihlajamäki, H., Suuronen, R., Skottman, H., Inzunza, J., Hovatta, O., Narkilahti, S., 2009. CD marker expression profiles of human embryonic stem cells and their neural derivatives, determined using flow-cytometric analysis, reveal a novel CD marker for exclusion of pluripotent stem cells. Stem Cell Res. 2, 113–124. https://doi.org/10.1016/j.scr.2008.08.001

Sutkowski, D.M., Fong, C.-J., Sensibar, J.A., Rademaker, A.W., Sherwood, E.R., Kozlowski, J.M., Lee, C., 1992. Interaction of epidermal growth factor and transforming growth factor beta in human prostatic epithelial cells in culture. The Prostate 21, 133–143. https://doi.org/10.1002/pros.2990210206

Takaya, A., Hirohashi, Y., Murai, A., Morita, R., Saijo, H., Yamamoto, E., Kubo, T., Nakatsugawa, M., Kanaseki, T., Tsukahara, T., Tamura, Y., Takemasa, I., Kondo, T., Sato, N., Torigoe, T., 2016. Establishment and Analysis of Cancer Stem-Like and Non-Cancer Stem-Like Clone Cells from the Human Colon Cancer Cell Line SW480. PloS One 11, e0158903. https://doi.org/10.1371/journal.pone.0158903

Tannock, I.F., de Wit, R., Berry, W.R., Horti, J., Pluzanska, A., Chi, K.N., Oudard, S., Théodore, C., James, N.D., Turesson, I., Rosenthal, M.A., Eisenberger, M.A., 2004. Docetaxel plus Prednisone or Mitoxantrone plus Prednisone for Advanced Prostate Cancer. N. Engl. J. Med. 351, 1502–1512. https://doi.org/10.1056/NEJMoa040720

Taylor, R.A., Toivanen, R., Frydenberg, M., Pedersen, J., Harewood, L., Australian Prostate Cancer Bioresource, null, Collins, A.T., Maitland, N.J., Risbridger, G.P., 2012. Human epithelial basal cells are cells of origin of prostate cancer, independent of CD133 status. Stem Cells Dayt. Ohio 30, 1087–1096. https://doi.org/10.1002/stem.1094

Teramo, A., Barilà, G., Calabretto, G., Ercolin, C., Lamy, T., Moignet, A., Roussel, M., Pastoret, C., Leoncin, M., Gattazzo, C., Cabrelle, A., Boscaro, E., Teolato, S., Pagnin, E., Berno, T., De March, E., Facco, M., Piazza, F., Trentin, L., Semenzato, G., Zambello, R., 2017. STAT3 mutation impacts biological and clinical features of T-LGL leukemia. Oncotarget 8, 61876–61889. https://doi.org/10.18632/oncotarget.18711

Termeer, C., Benedix, F., Sleeman, J., Fieber, C., Voith, U., Ahrens, T., Miyake, K., Freudenberg, M., Galanos, C., Simon, J.C., 2002. Oligosaccharides of Hyaluronan activate dendritic cells via toll-like receptor 4. J. Exp. Med. 195, 99–111.

Thapa, R., Wilson, G.D., 2016. The Importance of CD44 as a Stem Cell Biomarker and Therapeutic Target in Cancer. Stem Cells Int. 2016, e2087204. https://doi.org/10.1155/2016/2087204

The Genotype-Tissue Expression (GTEx) project, 2013. . Nat. Genet. 45, 580–585. https://doi.org/10.1038/ng.2653

Thomas, L., 1982. On immunosurveillance in human cancer. Yale J. Biol. Med. 55, 329–333.

Timofeeva, O.A., Palechor-Ceron, N., Li, G., Yuan, H., Krawczyk, E., Zhong, X., Liu, G., Upadhyay, G., Dakic, A., Yu, S., Fang, S., Choudhury, S., Zhang, X., Ju, A., Lee, M.-S., Dan, H.C., Ji, Y., Hou, Y., Zheng, Y.-L., Albanese, C., Rhim, J., Schlegel, R., Dritschilo, A., Liu, X., 2016. Conditionally reprogrammed normal and primary tumor prostate epithelial cells: a novel patient-derived cell model for studies of human prostate cancer. Oncotarget 8, 22741–22758. https://doi.org/10.18632/oncotarget.13937

Tirino, V., Desiderio, V., d'Aquino, R., De Francesco, F., Pirozzi, G., Galderisi, U., Cavaliere, C., De Rosa, A., Papaccio, G., 2008. Detection and Characterization of CD133+ Cancer Stem Cells in Human Solid Tumours. PLoS ONE 3. https://doi.org/10.1371/journal.pone.0003469

Todaro, M., Alea, M.P., Stefano, A.B.D., Cammareri, P., Vermeulen, L., Iovino, F., Tripodo, C., Russo, A., Gulotta, G., Medema, J.P., Stassi, G., 2007. Colon Cancer Stem Cells Dictate Tumor Growth and Resist Cell Death by Production of Interleukin-4. Cell Stem Cell 1, 389–402. https://doi.org/10.1016/j.stem.2007.08.001

Todaro, M., Gaggianesi, M., Catalano, V., Benfante, A., Iovino, F., Biffoni, M., Apuzzo, T., Sperduti, I., Volpe, S., Cocorullo, G., Gulotta, G., Dieli, F., De Maria, R., Stassi, G., 2014. CD44v6 is a marker of constitutive and reprogrammed cancer stem cells driving colon cancer metastasis. Cell Stem Cell 14, 342–356. https://doi.org/10.1016/j.stem.2014.01.009

Tomita, H., Tanaka, K., Hisamatsu, K., Hara, A., 2015. The role of aldehyde dehydrogenase 1A1 in stem cells and cancer stem cells. Cancer Cell Microenviron. 2.

Topalian, S.L., Drake, C.G., Pardoll, D.M., 2015. Immune Checkpoint Blockade: A Common Denominator Approach to Cancer Therapy. Cancer Cell 4, 450–461.

Tran, C., Ouk, S., Clegg, N.J., Chen, Y., Watson, P.A., Arora, V., Wongvipat, J., Smith-Jones, P.M., Yoo, D., Kwon, A., Wasielewska, T., Welsbie, D., Chen, C.D., Higano, C.S., Beer, T.M., Hung, D.T., Scher, H.I., Jung, M.E., Sawyers, C.L., 2009. Development of a Second-Generation Antiandrogen for Treatment of Advanced Prostate Cancer. Science 324, 787–790. https://doi.org/10.1126/science.1168175

Trock, B.J., Han, M., Freedland, S.J., Humphreys, E.B., DeWeese, T.L., Partin, A.W., Walsh, P.C., 2008. Prostate cancer-specific survival following salvage radiotherapy vs observation in men with biochemical recurrence after radical prostatectomy. JAMA 299, 2760–2769. https://doi.org/10.1001/jama.299.23.2760

Tsuneki, M., Madri, J.A., 2016. CD44 Influences Fibroblast Behaviors Via Modulation of Cell-Cell and Cell-Matrix Interactions, Affecting Survivin and Hippo Pathways. J. Cell. Physiol. 231, 731–743. https://doi.org/10.1002/jcp.25123

Tumban, E., Muttil, P., Escobar, C.A.A., Peabody, J., Wafula, D., Peabody, D.S., Chackerian, B., 2015. Preclinical refinements of a broadly protective VLP-based HPV vaccine targeting the minor capsid protein, L2. Vaccine 33, 3346–3353. https://doi.org/10.1016/j.vaccine.2015.05.016

Turdo, A., Veschi, V., Gaggianesi, M., Chinnici, A., Bianca, P., Todaro, M., Stassi, G., 2019. Meeting the Challenge of Targeting Cancer Stem Cells. Front. Cell Dev. Biol. 7. https://doi.org/10.3389/fcell.2019.00016

Turner, J.G., Dawson, J., Sullivan, D.M., 2012. Nuclear export of proteins and drug resistance in cancer. Biochem. Pharmacol. 83, 1021–1032. https://doi.org/10.1016/j.bcp.2011.12.016

Twardowski, P., Wong, J.Y.C., Pal, S.K., Maughan, B.L., Frankel, P.H., Franklin, K., Junqueira, M., Prajapati, M.R., Nachaegari, G., Harwood, D., Agarwal, N., 2018. Randomized phase II trial of sipuleucel-T immunotherapy preceded by sensitizing radiation therapy and sipuleucel-T alone in patients with metastatic castrate resistant prostate cancer. Cancer Treat. Res. Commun. 19, 100116. https://doi.org/10.1016/j.ctarc.2018.100116

Ucar, D., Cogle, C.R., Zucali, J.R., Ostmark, B., Scott, E.W., Zori, R., Gray, B.A., Moreb, J.S., 2009. Aldehyde dehydrogenase activity as a functional marker for lung cancer. Chem. Biol. Interact. 178, 48–55. https://doi.org/10.1016/j.cbi.2008.09.029

Uhlén, M., Björling, E., Agaton, C., Szigyarto, C.A.-K., Amini, B., Andersen, E., Andersson, A.-C., Angelidou, P., Asplund, A., Asplund, C., Berglund, L., Bergström, K., Brumer, H., Cerjan, D., Ekström, M., Elobeid, A., Eriksson, C., Fagerberg, L., Falk, R., Fall, J., Forsberg, M., Björklund, M.G., Gumbel, K., Halimi, A., Hallin, I., Hamsten, C., Hansson, M., Hedhammar, M., Hercules, G., Kampf, C., Larsson, K., Lindskog, M., Lodewyckx, W., Lund, J., Lundeberg, J., Magnusson, K., Malm, E., Nilsson, P., Odling, J., Oksvold, P., Olsson, I., Oster, E., Ottosson, J., Paavilainen, L., Persson, A., Rimini, R., Rockberg, J., Runeson, M., Sivertsson, A., Sköllermo, A., Steen, J., Stenvall, M., Sterky, F., Strömberg, S., Sundberg, M., Tegel, H., Tourle, S., Wahlund, E., Waldén, A., Wan, J., Wernérus, H., Westberg, J., Wester, K., Wrethagen, U., Xu, L.L., Hober, S., Pontén, F., 2005. A human protein atlas for normal and cancer tissues based on antibody proteomics. Mol. Cell. Proteomics MCP 4, 1920–1932. https://doi.org/10.1074/mcp.M500279-MCP200

Uhlén, M., Fagerberg, L., Hallström, B.M., Lindskog, C., Oksvold, P., Mardinoglu, A., Sivertsson, Å., Kampf, C., Sjöstedt, E., Asplund, A., Olsson, I., Edlund, K., Lundberg, E., Navani, S., Szigyarto, C.A.-K., Odeberg, J., Djureinovic, D., Takanen, J.O., Hober, S., Alm, T.,

Edqvist, P.-H., Berling, H., Tegel, H., Mulder, J., Rockberg, J., Nilsson, P., Schwenk, J.M., Hamsten, M., von Feilitzen, K., Forsberg, M., Persson, L., Johansson, F., Zwahlen, M., von Heijne, G., Nielsen, J., Pontén, F., 2015. Proteomics. Tissue-based map of the human proteome. Science 347, 1260419. https://doi.org/10.1126/science.1260419

Urban, J.L., Waes, C. van, Schreiber, H., 1984. Pecking order among tumor-specific antigens. Eur. J. Immunol. 14, 181–187. https://doi.org/10.1002/eji.1830140214

Valent, P., Bonnet, D., De Maria, R., Lapidot, T., Copland, M., Melo, J.V., Chomienne, C., Ishikawa, F., Schuringa, J.J., Stassi, G., others, 2012. Cancer stem cell definitions and terminology: the devil is in the details. Nat. Rev. Cancer 12, 767–775.

Valentine, M.A., Tsoukas, C.D., Rhodes, G., Vaughan, J.H., Carson, D.A., 1985. Phytohemagglutinin binds to the 20-kDa molecule of the T3 complex. Eur. J. Immunol. 15, 851–854. https://doi.org/10.1002/eji.1830150821

Van Bleek, G.M., Nathenson, S.G., 1990. Isolation of an endogenously processed immunodominant viral peptide from the class I H-2Kb molecule. Nature 348, 213–216. https://doi.org/10.1038/348213a0

van Bokhoven, A., Varella-Garcia, M., Korch, C., Johannes, W.U., Smith, E.E., Miller, H.L., Nordeen, S.K., Miller, G.J., Lucia, M.S., 2003. Molecular characterization of human prostate carcinoma cell lines. The Prostate 57, 205–225.

Van den Broeck, T., van den Bergh, R.C.N., Arfi, N., Gross, T., Moris, L., Briers, E., Cumberbatch, M., De Santis, M., Tilki, D., Fanti, S., Fossati, N., Gillessen, S., Grummet, J.P., Henry, A.M., Lardas, M., Liew, M., Rouvière, O., Pecanka, J., Mason, M.D., Schoots, I.G., van Der Kwast, T.H., van Der Poel, H.G., Wiegel, T., Willemse, P.-P.M., Yuan, Y., Lam, T.B., Cornford, P., Mottet, N., 2018. Prognostic Value of Biochemical Recurrence Following Treatment with Curative Intent for Prostate Cancer: A Systematic Review. Eur. Urol. https://doi.org/10.1016/j.eururo.2018.10.011

van den Hoogen, C., van der Horst, G., Cheung, H., Buijs, J.T., Lippitt, J.M., Guzmán-Ramírez, N., Hamdy, F.C., Eaton, C.L., Thalmann, G.N., Cecchini, M.G., Pelger, R.C.M., Pluijm, G. van der, 2010. High Aldehyde Dehydrogenase Activity Identifies Tumor-Initiating and Metastasis-Initiating Cells in Human Prostate Cancer. Cancer Res. 70, 5163–5173. https://doi.org/10.1158/0008-5472.CAN-09-3806

van den Hoogen, C., van der Horst, G., Cheung, H., Buijs, J.T., Pelger, R.C.M., van der Pluijm, G., 2011. The aldehyde dehydrogenase enzyme 7A1 is functionally involved in prostate cancer bone metastasis. Clin. Exp. Metastasis 28, 615–625. https://doi.org/10.1007/s10585-011-9395-7

van der Bruggen, P., Bastin, J., Gajewski, T., Coulie, P.G., Boël, P., De Smet, C., Traversari, C., Townsend, A., Boon, T., 1994. A peptide encoded by human gene MAGE-3 and presented by HLA-A2 induces cytolytic T lymphocytes that recognize tumor cells expressing MAGE-3. Eur. J. Immunol. 24, 3038–3043. https://doi.org/10.1002/eji.1830241218

van der Bruggen, P., Traversari, C., Chomez, P., Lurquin, C., De Plaen, E., Van den Eynde, B., Knuth, A., Boon, T., 1991. A gene encoding an antigen recognized by cytolytic T lymphocytes on a human melanoma. Science 254, 1643–1647.

van Leenders, G.J., Aalders, T.W., Hulsbergen-van de Kaa, C.A., Ruiter, D.J., Schalken, J.A., 2001. Expression of basal cell keratins in human prostate cancer metastases and cell lines. J. Pathol. 195, 563–570. https://doi.org/10.1002/path.993

van Leenders, G.J.L.H., Sookhlall, R., Teubel, W.J., de Ridder, C.M.A., Reneman, S., Sacchetti, A., Vissers, K.J., van Weerden, W., Jenster, G., 2011. Activation of c-MET Induces a Stem-Like Phenotype in Human Prostate Cancer. PLoS ONE 6. https://doi.org/10.1371/journal.pone.0026753

Vantourout, P., Willcox, C., Turner, A., Swanson, C.M., Haque, Y., Sobolev, O., Grigoriadis, A., Tutt, A., Hayday, A., 2014. Immunological visibility: posttranscriptional regulation of human NKG2D ligands by the EGF receptor pathway. Sci. Transl. Med. 6, 231ra49. https://doi.org/10.1126/scitranslmed.3007579

Vaupel, P., Harrison, L., 2004. Tumor Hypoxia: Causative Factors, Compensatory Mechanisms, and Cellular Response. The Oncologist 9, 4–9. https://doi.org/10.1634/theoncologist.9-90005-4

Vazquez-Santillan, K., Melendez-Zajgla, J., Jimenez-Hernandez, L., Martínez-Ruiz, G., Maldonado, V., 2015. NF-κB signaling in cancer stem cells: a promising therapeutic target? Cell. Oncol. 38, 327–339. https://doi.org/10.1007/s13402-015-0236-6

Veldman-Jones, M.H., Brant, R., Rooney, C., Geh, C., Emery, H., Harbron, C.G., Wappett, M., Sharpe, A., Dymond, M., Barrett, J.C., Harrington, E.A., Marshall, G., 2015. Evaluating Robustness and Sensitivity of the NanoString Technologies nCounter Platform to Enable Multiplexed Gene Expression Analysis of Clinical Samples. Cancer Res. 75, 2587–2593. https://doi.org/10.1158/0008-5472.CAN-15-0262

Vence, L., Palucka, A.K., Fay, J.W., Ito, T., Liu, Y.-J., Banchereau, J., Ueno, H., 2007. Circulating tumor antigen-specific regulatory T cells in patients with metastatic melanoma. Proc. Natl. Acad. Sci. U. S. A. 104, 20884–20889. https://doi.org/10.1073/pnas.0710557105

Venturi, V., Price, D.A., Douek, D.C., Davenport, M.P., 2008. The molecular basis for public T-cell responses? Nat. Rev. Immunol. 8, 231–238. https://doi.org/10.1038/nri2260

Vermeulen, K., Bockstaele, D.R.V., Berneman, Z.N., 2003. The cell cycle: a review of regulation, deregulation and therapeutic targets in cancer. Cell Prolif. 36, 131–149. https://doi.org/10.1046/j.1365-2184.2003.00266.x

Viani, G.A., Viana, B.S., Martin, J.E.C., Rossi, B.T., Zuliani, G., Stefano, E.J., 2016. Intensity-modulated radiotherapy reduces toxicity with similar biochemical control compared with 3-dimensional conformal radiotherapy for prostate cancer: A randomized clinical trial. Cancer 122, 2004–2011. https://doi.org/10.1002/cncr.29983

Vidal, S.J., Quinn, S.A., de la Iglesia-Vicente, J., Bonal, D.M., Rodriguez-Bravo, V., Firpo-Betancourt, A., Cordon-Cardo, C., Domingo-Domenech, J., 2014. Isolation of Cancer Stem Cells From Human Prostate Cancer Samples. J. Vis. Exp. JoVE. https://doi.org/10.3791/51332

Vigneron, N., Stroobant, V., Chapiro, J., Ooms, A., Degiovanni, G., Morel, S., van der Bruggen, P., Boon, T., Van den Eynde, B.J., 2004. An antigenic peptide produced by peptide splicing in the proteasome. Science 304, 587–590. https://doi.org/10.1126/science.1095522

Visus, C., Ito, D., Amoscato, A., Maciejewska-Franczak, M., Abdelsalem, A., Dhir, R., Shin, D.M., Donnenberg, V.S., Whiteside, T.L., DeLeo, A.B., 2007. Identification of Human Aldehyde Dehydrogenase 1 Family Member A1 as a Novel CD8+ T-Cell–Defined Tumor Antigen in Squamous Cell Carcinoma of the Head and Neck. Cancer Res. 67, 10538–10545. https://doi.org/10.1158/0008-5472.CAN-07-1346

Visus, C., Wang, Y., Lozano-Leon, A., Ferris, R.L., Silver, S., Szczepanski, M.J., Brand, R.E., Ferrone, C.R., Whiteside, T.L., Ferrone, S., DeLeo, A.B., Wang, X., 2011. Targeting ALDHbright human carcinoma initiating cells with ALDH1A1- specific CD8+ T cells. Clin. Cancer Res. Off. J. Am. Assoc. Cancer Res. 17, 6174–6184. https://doi.org/10.1158/1078-0432.CCR-11-1111

Visvader, J.E., 2009. Keeping abreast of the mammary epithelial hierarchy and breast tumorigenesis. Genes Dev. 23, 2563–2577. https://doi.org/10.1101/gad.1849509

Visvader, J.E., Lindeman, G.J., 2008. Cancer stem cells in solid tumours: accumulating evidence and unresolved questions. Nat. Rev. Cancer 8, 755–768. https://doi.org/10.1038/nrc2499

Vita, R., Mahajan, S., Overton, J.A., Dhanda, S.K., Martini, S., Cantrell, J.R., Wheeler, D.K., Sette, A., Peters, B., 2019. The Immune Epitope Database (IEDB): 2018 update. Nucleic Acids Res. 47, D339–D343. https://doi.org/10.1093/nar/gky1006

Vitkin, N., Nersesian, S., Siemens, D.R., Koti, M., 2019. The Tumor Immune Contexture of Prostate Cancer. Front. Immunol. 10. https://doi.org/10.3389/fimmu.2019.00603

Vlashi, E., Pajonk, F., 2015. Cancer Stem Cells, Cancer Cell Plasticity and Radiation Therapy. Semin. Cancer Biol. 0, 28–35. https://doi.org/10.1016/j.semcancer.2014.07.001

Vogelstein, B., Papadopoulos, N., Velculescu, V.E., Zhou, S., Diaz, L.A., Kinzler, K.W., 2013. Cancer Genome Landscapes. Science 339, 1546–1558. https://doi.org/10.1126/science.1235122

Voog, J., Jones, D.L., 2010. Stem Cells and the Niche: A Dynamic Duo. Cell Stem Cell 6, 103–115. https://doi.org/10.1016/j.stem.2010.01.011

Walz, S., Stickel, J.S., Kowalewski, D.J., Schuster, H., Weisel, K., Backert, L., Kahn, S., Nelde, A., Stroh, T., Handel, M., Kohlbacher, O., Kanz, L., Salih, H.R., Rammensee, H.-G., Stevanović, S., 2015. The antigenic landscape of multiple myeloma: mass spectrometry (re)defines targets for T-cell-based immunotherapy. Blood 126, 1203–1213. https://doi.org/10.1182/blood-2015-04-640532

WANG, D., GUO, Y., LI, Y., LI, W., ZHENG, X., XIA, H., MAO, Q., 2015. Detection of CD133 expression in U87 glioblastoma cells using a novel anti-CD133 monoclonal antibody. Oncol. Lett. 9, 2603–2608. https://doi.org/10.3892/ol.2015.3079

Wang, J., Sullenger, B.A., Rich, J.N., 2012. Notch signaling in cancer stem cells. Adv. Exp. Med. Biol. 727, 174–185. https://doi.org/10.1007/978-1-4614-0899-4_13

Wang, J.C.Y., Dick, J.E., 2005. Cancer stem cells: lessons from leukemia. Trends Cell Biol. 15, 494–501. https://doi.org/10.1016/j.tcb.2005.07.004

Wang, S., Huang, S., Zhao, X., Zhang, Q., Wu, M., Sun, F., Han, G., Wu, D., 2013. Enrichment of prostate cancer stem cells from primary prostate

cancer cultures of biopsy samples. Int. J. Clin. Exp. Pathol. 7, 184–193.

Wang, T., Niu, G., Kortylewski, M., Burdelya, L., Shain, K., Zhang, S., Bhattacharya, R., Gabrilovich, D., Heller, R., Coppola, D., Dalton, W., Jove, R., Pardoll, D., Yu, H., 2004. Regulation of the innate and adaptive immune responses by Stat-3 signaling in tumor cells. Nat. Med. 10, 48–54. https://doi.org/10.1038/nm976

Wang, X., Julio, M.K., Economides, K.D., Walker, D., Yu, H., Halili, M.V., Hu, Y.-P., Price, S.M., Abate-Shen, C., Shen, M.M., 2009. A luminal epithelial stem cell that is a cell of origin for prostate cancer. Nature 461, 495–500. https://doi.org/10.1038/nature08361

Wei, C., Guomin, W., Yujun, L., Ruizhe, Q., 2007. Cancer stem-like cells in human prostate carcinoma cells DU145: The seeds of the cell line? Cancer Biol. Ther. 6, 763–768. https://doi.org/10.4161/cbt.6.5.3996

Wei, S.C., Levine, J.H., Cogdill, A.P., Zhao, Y., Anang, N.-A.A.S., Andrews, M.C., Sharma, P., Wang, J., Wargo, J.A., Pe'er, D., Allison, J.P., 2017. Distinct Cellular Mechanisms Underlie Anti-CTLA-4 and Anti-PD-1 Checkpoint Blockade. Cell 170, 1120-1133.e17. https://doi.org/10.1016/j.cell.2017.07.024

Wei, Y., Jiang, Y., Zou, F., Liu, Yingchao, Wang, S., Xu, N., Xu, W., Cui, C., Xing, Y., Liu, Ying, Cao, B., Liu, C., Wu, G., Ao, H., Zhang, X., Jiang, J., 2013. Activation of PI3K/Akt pathway by CD133-p85 interaction promotes tumorigenic capacity of glioma stem cells. Proc. Natl. Acad. Sci. U. S. A. 110, 6829–6834. https://doi.org/10.1073/pnas.1217002110

Welch, J.S., Ley, T.J., Link, D.C., Miller, C.A., Larson, D.E., Koboldt, D.C., Wartman, L.D., Lamprecht, T.L., Liu, F., Xia, J., Kandoth, C., Fulton, R.S., McLellan, M.D., Dooling, D.J., Wallis, J.W., Chen, K., Harris, C.C., Schmidt, H.K., Kalicki-Veizer, J.M., Lu, C., Zhang, Q., Lin, L., O'Laughlin, M.D., McMichael, J.F., Delehaunty, K.D., Fulton, L.A., Magrini, V.J., McGrath, S.D., Demeter, R.T., Vickery, T.L., Hundal, J., Cook, L.L., Swift, G.W., Reed, J.P., Alldredge, P.A., Wylie, T.N., Walker, J.R., Watson, M.A., Heath, S.E., Shannon, W.D., Varghese, N., Nagarajan, R., Payton, J.E., Baty, J.D., Kulkarni, S., Klco, J.M., Tomasson, M.H., Westervelt, P., Walter, M.J., Graubert, T.A., DiPersio, J.F., Ding, L., Mardis, E.R., Wilson, R.K., 2012. The origin and evolution of mutations in acute myeloid leukemia. Cell 150, 264–278. https://doi.org/10.1016/j.cell.2012.06.023

Went, P.T.H., Lugli, A., Meier, S., Bundi, M., Mirlacher, M., Sauter, G., Dirnhofer, S., 2004. Frequent EpCam protein expression in human carcinomas. Hum. Pathol. 35, 122–128. https://doi.org/10.1016/j.humpath.2003.08.026

Wetering, M. van de, Sancho, E., Verweij, C., Lau, W. de, Oving, I., Hurlstone, A., Horn, K. van der, Batlle, E., Coudreuse, D., Haramis, A.-P., Tjon-Pon-Fong, M., Moerer, P., Born, M. van den, Soete, G., Pals, S., Eilers, M., Medema, R., Clevers, H., 2002. The β-Catenin/TCF-4 Complex Imposes a Crypt Progenitor Phenotype on Colorectal Cancer Cells. Cell 111, 241–250. https://doi.org/10.1016/S0092-8674(02)01014-0

Wheelock, M.J., Shintani, Y., Maeda, M., Fukumoto, Y., Johnson, K.R., 2008. Cadherin switching. J. Cell Sci. 121, 727–735. https://doi.org/10.1242/jcs.000455

Wherry, E.J., Teichgräber, V., Becker, T.C., Masopust, D., Kaech, S.M., Antia, R., Andrian, U.H. von, Ahmed, R., 2003. Lineage relationship and protective immunity of memory CD8 T cell subsets. Nat. Immunol. 4, 225–234. https://doi.org/10.1038/ni889

White, J., Dalton, S., 2005. Cell cycle control of embryonic stem cells. Stem Cell Rev. 1, 131–138. https://doi.org/10.1385/SCR:1:2:131

Williams, A., Peh, C.A., Elliott, T., 2002. The cell biology of MHC class I antigen presentation. Tissue Antigens 59, 3–17. https://doi.org/10.1034/j.1399-0039.2002.590103.x

Willinger, T., Freeman, T., Hasegawa, H., McMichael, A.J., Callan, M.F.C., 2005. Molecular signatures distinguish human central memory from effector memory CD8 T cell subsets. J. Immunol. Baltim. Md 1950 175, 5895–5903. https://doi.org/10.4049/jimmunol.175.9.5895

Woo, E.Y., Chu, C.S., Goletz, T.J., Schlienger, K., Yeh, H., Coukos, G., Rubin, S.C., Kaiser, L.R., June, C.H., 2001. Regulatory CD4+CD25+ T Cells in Tumors from Patients with Early-Stage Non-Small Cell Lung Cancer and Late-Stage Ovarian Cancer. Cancer Res. 61, 4766–4772.

Wooldridge, L., Ekeruche-Makinde, J., van den Berg, H.A., Skowera, A., Miles, J.J., Tan, M.P., Dolton, G., Clement, M., Llewellyn-Lacey, S., Price, D.A., Peakman, M., Sewell, A.K., 2012. A single autoimmune T cell receptor recognizes more than a million different peptides. J. Biol. Chem. 287, 1168–1177. https://doi.org/10.1074/jbc.M111.289488

Wooldridge, L., Lissina, A., Cole, D.K., van den Berg, H.A., Price, D.A., Sewell, A.K., 2009. Tricks with tetramers: how to get the most from multimeric peptide-MHC. Immunology 126, 147–164. https://doi.org/10.1111/j.1365-2567.2008.02848.x

Wu, X., Peng, M., Huang, Bingqing, Zhang, H., Wang, H., Huang, Biao, Xue, Z., Zhang, L., Da, Y., Yang, D., Yao, Z., Zhang, R., 2013. Immune microenvironment profiles of tumor immune equilibrium and immune escape states of mouse sarcoma. Cancer Lett. 340, 124–133. https://doi.org/10.1016/j.canlet.2013.07.038

Wu, Y., Wu, P.Y., 2009. CD133 as a Marker for Cancer Stem Cells: Progresses and Concerns. Stem Cells Dev. 18, 1127–1134. https://doi.org/10.1089/scd.2008.0338

Xin, L., Lukacs, R.U., Lawson, D.A., Cheng, D., Witte, O.N., 2007. Self-renewal and multilineage differentiation in vitro from murine prostate stem cells. Stem Cells Dayt. Ohio 25, 2760–2769. https://doi.org/10.1634/stemcells.2007-0355

Xu, X., Chai, S., Wang, P., Zhang, C., Yang, Yiming, Yang, Ying, Wang, K., 2015. Aldehyde dehydrogenases and cancer stem cells. Cancer Lett. 369, 50–57. https://doi.org/10.1016/j.canlet.2015.08.018

Yam, C.H., Fung, T.K., Poon, R.Y.C., 2002. Cyclin A in cell cycle control and cancer. Cell. Mol. Life Sci. CMLS 59, 1317–1326. https://doi.org/10.1007/s00018-002-8510-y

Yamada, R., Takahashi, A., Torigoe, T., Morita, R., Tamura, Y., Tsukahara, T., Kanaseki, T., Kubo, T., Watarai, K., Kondo, T., Hirohashi, Y., Sato, N., 2013. Preferential expression of cancer/testis genes in cancer stem-like cells: proposal of a novel sub-category, cancer/testis/stem gene. Tissue Antigens 81, 428–434. https://doi.org/10.1111/tan.12113

Yan, J., De Melo, J., Cutz, J.-C., Aziz, T., Tang, D., 2014. Aldehyde dehydrogenase 3A1 associates with prostate tumorigenesis. Br. J. Cancer 110, 2593–2603. https://doi.org/10.1038/bjc.2014.201

Yang, I., Tihan, T., Han, S.J., Wrensch, M.R., Wiencke, J., Sughrue, M.E., Parsa, A.T., 2010. CD8+ T-cell infiltrate in newly diagnosed glioblastoma is associated with long-term survival. J. Clin. Neurosci. Off. J. Neurosurg. Soc. Australas. 17, 1381–1385. https://doi.org/10.1016/j.jocn.2010.03.031

Yasuda, K., Torigoe, T., Morita, R., Kuroda, T., Takahashi, A., Matsuzaki, J., Kochin, V., Asanuma, H., Hasegawa, T., Saito, T., Hirohashi, Y., Sato, N., 2013. Ovarian Cancer Stem Cells Are Enriched in Side Population and Aldehyde Dehydrogenase Bright Overlapping Population. PLoS ONE 8, e68187. https://doi.org/10.1371/journal.pone.0068187

Ying, J., Tsujii, M., Kondo, J., Hayashi, Y., Kato, M., Akasaka, T., Inoue, Takuta, Shiraishi, E., Inoue, Tahahiro, Hiyama, S., Tsujii, Y., Maekawa, A., Kawai, S., Fujinaga, T., Araki, M., Shinzaki, S., Watabe, K., Nishida, T., Iijima, H., Takehara, T., 2015. The effectiveness of an anti-human IL-6 receptor monoclonal antibody combined with chemotherapy to target colon cancer stem-like cells. Int. J. Oncol. https://doi.org/10.3892/ijo.2015.2851

Zakaria, N., Yusoff, N.M., Zakaria, Z., Lim, M.N., Baharuddin, P.J.N., Fakiruddin, K.S., Yahaya, B., 2015. Human non-small cell lung cancer expresses putative cancer stem cell markers and exhibits the transcriptomic profile of multipotent cells. BMC Cancer 15, 84. https://doi.org/10.1186/s12885-015-1086-3

Zanoni, M., Piccinini, F., Arienti, C., Zamagni, A., Santi, S., Polico, R., Bevilacqua, A., Tesei, A., 2016. 3D tumor spheroid models for *in vitro* therapeutic screening: a systematic approach to enhance the biological relevance of data obtained. Sci. Rep. 6, 19103. https://doi.org/10.1038/srep19103

Zelefsky, M.J., Fuks, Z., Hunt, M., Yamada, Y., Marion, C., Ling, C.C., Amols, H., Venkatraman, E.S., Leibel, S.A., 2002. High-dose intensity modulated radiation therapy for prostate cancer: early toxicity and biochemical outcome in 772 patients. Int. J. Radiat. Oncol. Biol. Phys. 53, 1111–1116.

Zhang, D., Park, D., Zhong, Y., Lu, Y., Rycaj, K., Gong, S., Chen, X., Liu, X., Chao, H.-P., Whitney, P., Calhoun-Davis, T., Takata, Y., Shen, J., Iyer, V.R., Tang, D.G., 2016. Stem cell and neurogenic gene-expression profiles link prostate basal cells to aggressive prostate cancer. Nat. Commun. 7, 10798. https://doi.org/10.1038/ncomms10798

Zhang, H., Christensen, C.L., Dries, R., Oser, M.G., Deng, J., Diskin, B., Li, F., Pan, Y., Zhang, X., Yin, Y., Papadopoulos, E., Pyon, V., Thakurdin, C., Kwiatkowski, N., Jani, K., Rabin, A.R., Castro, D.M., Chen, T., Silver, H., Huang, Q., Bulatovic, M., Dowling, C.M., Sundberg, B., Leggett, A., Ranieri, M., Han, H., Li, S., Yang, A., Labbe, K.E., Almonte, C., Sviderskiy, V.O., Quinn, M., Donaghue, J., Wang, E.S., Zhang, T., He, Z., Velcheti, V., Hammerman, P.S., Freeman, G.J., Bonneau, R., Kaelin, W.G., Sutherland, K.D., Kersbergen, A., Aguirre, A.J., Yuan, G.-C., Rothenberg, E., Miller, G., Gray, N.S., Wong, K.-K., 2019. CDK7 Inhibition Potentiates Genome Instability Triggering Anti-tumor Immunity in Small Cell Lung Cancer. Cancer Cell. https://doi.org/10.1016/j.ccell.2019.11.003

Zhao, S., Wehner, R., Bornhäuser, M., Wassmuth, R., Bachmann, M., Schmitz, M., 2010. Immunomodulatory properties of mesenchymal stromal cells and their therapeutic consequences for immune-mediated disorders. Stem Cells Dev. 19, 607–614. https://doi.org/10.1089/scd.2009.0345

Zheng, F., Dang, J., Zhang, H., Xu, F., Ba, D., Zhang, B., Cheng, F., Chang, A.E., Wicha, M.S., Li, Q., 2018. Cancer stem cell vaccination with PD-L1 and CTLA-4 blockades enhances the eradication of melanoma stem cells in a mouse tumor model. J. Immunother. Hagerstown Md 1997 41, 361–368. https://doi.org/10.1097/CJI.0000000000000242

Zheng, Y., Zha, Y., Spaapen, R.M., Mathew, R., Barr, K., Bendelac, A., Gajewski, T.F., 2013. Egr2-dependent gene expression profiling and ChIP-Seq reveal novel biologic targets in T cell anergy. Mol. Immunol. 55, 283–291. https://doi.org/10.1016/j.molimm.2013.03.006

Zhou, J., Wang, H., Cannon, V., Wolcott, K.M., Song, H., Yates, C., 2011. Side population rather than CD133+ cells distinguishes enriched tumorigenicity in hTERT-immortalized primary prostate cancer cells. Mol. Cancer 10, 112. https://doi.org/10.1186/1476-4598-10-112

Zhou, L., Sheng, D., Wang, D., Ma, W., Deng, Q., Deng, L., Liu, S., 2019. Identification of cancer-type specific expression patterns for active aldehyde dehydrogenase (ALDH) isoforms in ALDEFLUOR assay. Cell Biol. Toxicol. 35, 161–177. https://doi.org/10.1007/s10565-018-9444-y

Zhu, L., Finkelstein, D., Gao, C., Shi, L., Wang, Y., López-Terrada, D., Wang, K., Utley, S., Pounds, S., Neale, G., Ellison, D., Onar-Thomas, A., Gilbertson, R.J., 2016. Multi-organ Mapping of Cancer Risk. Cell 166, 1132-1146.e7. https://doi.org/10.1016/j.cell.2016.07.045

Zhu, S., Van den Eynde, B.J., Coulie, P.G., Li, Y.F., El-Gamil, M., Rosenberg, S.A., Robbins, P.F., 2012. Characterization of T-cell receptors directed against HLA-A*01-restricted and C*07-restricted epitopes of MAGE-A3 and MAGE-A12. J. Immunother. Hagerstown Md 1997 35, 680–688. https://doi.org/10.1097/CJI.0b013e31827338ea

Ziegler, A., Müller, C.A., Böckmann, R.A., Uchanska-Ziegler, B., 2009. Low-affinity peptides and T-cell selection. Trends Immunol. 30, 53–60. https://doi.org/10.1016/j.it.2008.11.004

Zitvogel, L., Tesniere, A., Kroemer, G., 2006. Cancer despite immunosurveillance: immunoselection and immunosubversion. Nat. Rev. Immunol. 6, 715–727. https://doi.org/10.1038/nri1936